BS 7910:2019



BSI Standards Publication

Guide to methods for assessing the acceptability of flaws in metallic structures

bsi.

Publishing and copyright information
The BSI copyright notice displayed in this document indicates when the document was last issued.

© The British Standards Institution 2019
Published by BSI Standards Limited 2019

ISBN 978 0 580 52086 0

ICS 25.160.40

The following BSI references relate to the work on this standard:

Committee reference WEE/37

Draft for comment 19/30369477 DC

Publication history
First published December 1999
Second edition, July 2005
Third edition, December 2013
Fourth (present) edition, December 2019

Amendments issued since publication	
Date	**Text affected**

Contents

Foreword *ix*

0 Introduction *0/1*

1 Scope *1/1*

2 Normative references *1/1*

3 Symbols and definitions *1/1*

4 Types of flaw *4/1*

5 General guidance on assessment *5/1*
5.1 Modes of failure and material damage mechanisms *5/1*
5.2 Sequence of assessment *5/2*
5.3 Fracture assessment options *5/3*

6 Information required for assessment *6/1*
6.0 Symbols and definitions *6/1*
6.1 General *6/1*
6.2 Essential data *6/2*
6.3 Non-destructive testing *6/2*
6.4 Stresses to be considered *6/4*

7 Assessment for fracture resistance *7/1*
7.0 Symbols and definitions *7/1*
7.1 Background *7/4*
7.2 Procedure *7/32*
7.3 Assessment (Options 1 to 3) *7/34*
7.4 Further points *7/39*

8 Assessment for fatigue *8/1*
8.0 Symbols and definitions *8/1*
8.1 Assessment procedures *8/3*
8.2 Data required for assessment *8/7*
8.3 Probability of survival *8/14*
8.4 General procedure for fracture mechanics assessment of planar flaws *8/15*
8.5 Basis of procedure for assessing flaws using quality categories *8/16*
8.6 Assessment of planar flaws using quality categories *8/19*
8.7 Assessment of embedded non-planar flaws using quality categories *8/37*
8.8 Assessment of shape imperfections using quality categories *8/39*
8.9 Estimation of tolerable sizes of flaws *8/41*

9 Assessment of flaws under creep and creep/fatigue conditions *9/1*
9.0 Symbols and definitions *9/1*
9.1 General *9/3*
9.2 Background to methods *9/4*
9.3 Background to assessments *9/4*
9.4 Factors involved in the safe use of the procedure *9/5*
9.5 Creep exemption criteria *9/5*
9.6 Creep-fatigue exemption criteria *9/8*
9.7 Crack behaviour at high temperature *9/9*
9.8 Assessment of components containing a known or postulated defect *9/11*
9.9 Further guidance on the assessment procedure *9/15*
9.10 Basic calculations *9/17*
9.11 Material data for predicting crack initiation and growth under creep and creep/fatigue *9/19*
9.12 Guidance on performing assessment calculations *9/20*
9.13 Assess significance of results *9/22*

10 Assessment for other modes of failure *10/1*
10.0 Symbols and definitions *10/1*
10.1 Yielding due to overloading of remaining cross-section *10/1*
10.2 Leakage in pressure, liquid or vacuum containing equipment *10/2*

10.3 Environmental effects *10/2*
10.4 Instability (buckling) *10/7*

Annexes
Annex A (informative) Evaluation under mode I, II and III loads *A/1*
Annex B (informative) Assessment procedures for tubular joints in offshore structures *B/1*
Annex C (informative) Assessment procedures for pressure vessels and pipelines *C/1*
Annex D (informative) Stress due to misalignment *D/1*
Annex E (informative) Flaw recharacterization *E/1*
Annex F (informative) Procedure for leak-before-break (LbB) assessment *F/1*
Annex G (informative) The assessment of locally thinned areas (LTAs) *G/1*
Annex H (informative) Reporting of assessments *H/1*
Annex I (informative) The significance of strength mismatch on the fracture behaviour of welded joints *I/1*
Annex J (informative) Use of Charpy V-notch impact tests to estimate fracture toughness *J/1*
Annex K (informative) Probabilistic assessment *K/1*
Annex L (informative) Fracture toughness determination for welds *L/1*
Annex M (informative) Stress intensity factor solutions *M/1*
Annex N (informative) Allowance for constraint effects *N/1*
Annex O (informative) Consideration of proof testing and warm prestressing *O/1*
Annex P (informative) Compendium of reference stress and limit load solutions for homogeneous and strength mismatched structures *P/1*
Annex Q (informative) Residual stress distributions in as-welded joints *Q/1*
Annex R (informative) Determination of plasticity interaction effects with combined primary and secondary loading *R/1*
Annex S (informative) Information for making high temperature crack growth assessments *S/1*
Annex T (informative) Guidance on the use of NDT with ECA *T/1*
Annex U (informative) Worked examples in fatigue assessment using the quality category approach *U/1*
Annex V (informative) Strain-based assessment (SBA) *V/1*

List of figures
Figure 0.1 – Example of integrity management procedure for flaws *0/2*
Figure 6.1 – Linearization of stress distributions *6/5*
Figure 6.2 – Procedure for resolving flaws normal to principal stress *6/8*
Figure 7.1 – General flowchart for fracture assessment *7/5*
Figure 7.2 – Flowchart for Option 1 fracture assessment *7/6*
Figure 7.3 – Flowchart for Option 2 fracture assessment *7/7*
Figure 7.4 – Flowchart for Option 3 fracture assessment *7/8*
Figure 7.5 – Flowchart for flaw characterization *7/10*
Figure 7.6 – Definitions of flaw dimensions *7/11*
Figure 7.7 – Flaw alignment rules for non-coplanar flaws *7/12*
Figure 7.8 – Flaw interaction rules for coplanar flaws *7/13*
Figure 7.9 – Definition of terms used in tensile testing *7/15*
Figure 7.10 – De-rating values for yield/proof strength and tensile strength at temperatures above room temperature in C-Mn steels and duplex stainless steels *7/17*
Figure 7.11 – Treatment of sets of between three and five tests *7/25*
Figure 7.12 – Treatment of sets of more than six tests *7/26*
Figure 7.13 – Example of a Failure Assessment Diagram *7/34*
Figure 7.14 – Ductile tearing assessment *7/38*
Figure 7.15 – Example of non-unique solutions *7/40*
Figure 8.1 – Schematic crack growth relationships *8/6*
Figure 8.2 – Recommended fatigue crack growth laws *8/11*
Figure 8.3 – Quality category *S-N* curves *8/17*

Figure 8.4 – Quality category approach: assessment of surface flaws in plates under axial loading *8/22*
Figure 8.5 – Quality category approach: assessment of surface flaws in plates (no weld toe or other stress raiser) in bending *8/24*
Figure 8.6 – Quality category approach: assessment of embedded flaws in axially loaded joints *8/26*
Figure 8.7 – Quality category approach: assessment of weld toe flaws in axially loaded joints *8/28*
Figure 8.8 – Quality category approach: assessment of weld toe flaws in joints loaded in bending *8/34*
Figure 9.1 – Determination of temperature T_c at which 0.2% creep strain is accumulated at a stress level equal to the proof strength *9/7*
Figure 9.2 – Insignificant creep curves for austenitic steels *9/8*
Figure 9.3 – Insignificant creep curves for ferritic steels *9/8*
Figure 9.4 – Schematic behaviour of crack subjected to steady loading at elevated temperature *9/10*
Figure 9.5 – Schematic representation of crack propagation and failure conditions *9/11*
Figure 9.6 – Flowchart for overall creep assessment procedure described in 9.8.2 *9/12*
Figure 10.1 – Schematic diagrams of typical relationships between crack velocity and stress intensity factor during SCC *10/4*
Figure 10.2 – Types of corrosion fatigue crack growth behaviour *10/6*
Figure A.1 – Definitions of loading modes *A/2*
Figure B.1 – Assessment method for fatigue crack growth in tubular joints *B/4*
Figure E.1 – Flowchart for recharacterization of flaws *E/2*
Figure E.2 – Rules for recharacterization of flaws *E/3*
Figure F.1 – The leak-before-break diagram *F/4*
Figure F.2 – Flow chart for LbB procedure *F/6*
Figure G.1 – Flow chart of assessment procedure *G/4*
Figure G.2 – Dimensions of an LTA *G/5*
Figure G.3 – Dimensions of a bend *G/6*
Figure G.4 – Dimensions of a sphere and vessel end *G/7*
Figure G.5 – Interaction between LTAs *G/9*
Figure I.1 – Idealized weld geometry – the parent and weld metals have yield strengths of σ_Y^W and σ_Y^P respectively *I/4*
Figure I.2 – Idealized definition of mismatch ratio, *M*, and construction of the equivalent stress-strain curve (weighted average of the other two curves) *I/5*
Figure J.1 – Flowchart for selecting an appropriate correlation for estimating fracture toughness from Charpy data *J/3*
Figure M.1 – Through-thickness flaw geometry *M/5*
Figure M.2 – Edge flaw geometry *M/5*
Figure M.3 – Surface flaw *M/6*
Figure M.4 – Stress intensity magnification factor M_m for surface flaws in tension *M/8*
Figure M.5 – Stress intensity magnification factor M_b for surface flaws in bending *M/10*
Figure M.6 – Finite surface flaw in an infinite width plate *M/11*
Figure M.7 – Extended flaw geometry *M/15*
Figure M.8 – Extended surface flaw in an infinite width plate *M/16*
Figure M.9 – Embedded flaw *M/17*
Figure M.10 – Stress intensity magnification factor M_m for embedded flaws in tension (at point nearest material surface) *M/18*
Figure M.11 – Stress intensity magnification factor M_b for embedded flaws in bending *M/20*
Figure M.12 – Corner flaw geometry *M/21*
Figure M.13 – Corner flaw at hole geometry *M/23*
Figure M.14 – Through-thickness flaw in cylinder oriented axially *M/27*
Figure M.15 – Internal surface flaw in cylinder oriented axially *M/32*

Figure M.16 – Extended internal surface flaw in cylinder orientated axially *M/34*
Figure M.17 – External surface flaw in cylinder oriented axially *M/35*
Figure M.18 – Extended axial external surface flaw in cylinder *M/36*
Figure M.19 – Through-thickness flaw in cylinder oriented circumferentially *M/38*
Figure M.20 – Internal surface flaw in cylinder oriented circumferentially *M/43*
Figure M.21 – Extended internal surface flaw in cylinder *M/45*
Figure M.22 – Extended external surface flaw in cylinder *M/46*
Figure M.23 – Through-thickness flaw in spherical shell *M/49*
Figure M.24 – Flaws in bars and bolts *M/50*
Figure M.25 – Fully circumferential flaw in a round bar *M/54*
Figure M.26 – Welded joint geometries *M/55*
Figure M.27 – Transverse load-carrying cruciform joint *M/56*
Figure N.1 – Schematic showing curve fitting of low constraint test data to obtain α and k *N/9*
Figure N.2 – Modifications to the Option 1 failure assessment curve (continuous yielding) for various values of the material parameter, α, and constraint levels, β (< 0) *N/11*
Figure N.3 – FAD analysis for (a) fracture initiation and (b) ductile tearing *N/12*
Figure O.1 – Schematic illustration of a proof test argument *O/4*
Figure O.2 – Typical warm prestress cycles *O/6*
Figure P.1 – Double edge cracked plate under tension *P/8*
Figure P.2 – Extended embedded flaw in a plate *P/10*
Figure P.3 – Circumferential internal and external surface flaws in thick-walled cylinders under combined tension and bending *P/19*
Figure P.4 – Classification of plasticity deformation patterns for mismatched structures *P/22*
Figure P.5 – Centre cracked plate under tension *P/26*
Figure P.6 – Double edge cracked plate under tension *P/29*
Figure P.7 – Single edge cracked plate under in-plane bending *P/33*
Figure P.8 – Fully circumferential internal flaw in thin-walled pipe/cylinder under tension *P/35*
Figure P.9 – Centre through-thickness crack in a clad plate under tension *P/36*
Figure Q.1 – Components of longitudinal residual stress distribution for plate butt welds and pipe axial seam welds (austenitic steel) *Q/4*
Figure Q.2 – Components of transverse stress distribution for plate butt welds and axial seam welds (austenitic and ferritic steels) *Q/5*
Figure Q.3 – Components of longitudinal stress distribution for pipe butt welds (ferritic and austenitic steels) *Q/6*
Figure Q.4 – Components of transverse stress distribution for pipe butt welds (ferritic steels) *Q/7*
Figure Q.5 – Components of longitudinal stress distribution for plate to plate T-butt welds (ferritic steels) *Q/10*
Figure Q.6 – Components of transverse stress distribution for plate to plate T-butt welds (austenitic and ferritic steels) *Q/12*
Figure Q.7 – Components of longitudinal stress distribution for tubular T-butt welds (ferritic steels) *Q/13*
Figure Q.8 – Components of transverse stress distribution for tubular T-butt welds (ferritic steels) *Q/14*
Figure Q.9 – Residual stress profile for repair welds (transverse and longitudinal) *Q/15*
Figure S.1 – General form of a creep curve defining the average and secondary creep strain rates *S/2*
Figure S.2 – General form of a creep curve defining the average and secondary creep strain rates *S/3*
Figure T.1 – Assessment of flaw tolerance using ECA *T/5*
Figure T.2 – Assessment of detected flaw *T/6*
Figure U.1 – Butt weld containing embedded flaw *U/2*
Figure U.2 – Derivation of actual quality category for a flaw *U/3*

Figure U.3 – Fillet weld containing a surface flaw *U/4*
Figure U.4 – Derivation of actual quality category for a flaw *U/5*
Figure U.5 – Obtaining the quality category for the flaw *U/6*
Figure V.1 – Flow chart for a strain-based assessment (SBA) using the methods of Annex V *V/7*
Figure V.2 – Distribution of stress and strain across the location of the flaw being assessed from an uncracked stress analysis *V/8*
Figure V.3 – Derivation of the reference stress, σ_{ref}, and the reference strain, ε_{ref}, from the applied nominal strain, ε_{nom}, and the material true stress-true strain curve *V/8*
Figure V.4 – Derivation of the flow strain, ε_f, from the material flow strength, σ_f, using the true stress-true strain curve *V/9*
Figure V.5 – Single edge-notched tension (SENT) specimen *V/10*
Figure V.6 – SBA FAL together with tearing lines used to determine the instability load level for a 0.4 mm deep flaw in a SENT specimen loaded in tension. *V/12*

List of tables

Table 7.1 – Engineering definitions of yield and tensile strengths for Options 1, 2, 3 *7/14*
Table 7.2 – Coefficient of variation (COV) for tensile properties for ferritic steels *7/16*
Table 7.3 – Elastic modulus *7/16*
Table 7.4 – Guidance for determining whether yielding is continuous or discontinuous in rolled steel plate *7/19*
Table 7.5 – Minimum of three equivalent (MOTE) *7/27*
Table 7.6 – Values of $k_{0.90}$ at the lower 20th percentile for the one-sided tolerance limit for a normal distribution *7/28*
Table 7.7 – Limits for slag inclusions and porosity *7/40*
Table 8.1 – Procedure for assessment of known flaws *8/4*
Table 8.2 – Stress ranges used in fatigue assessments *8/8*
Table 8.3 – Recommended fatigue crack growth laws for steels in air *8/10*
Table 8.4 – Recommended fatigue crack growth laws for steels in a marine environment *8/12*
Table 8.5 – Recommended fatigue crack growth threshold, ΔK_0, values for assessing welded joints *8/14*
Table 8.6 – Details of quality category *S-N* curves *8/17*
Table 8.7 – Minimum values of $\Delta\sigma_j$ for assessing non-planar flaws and shape imperfections *8/38*
Table 8.8 – Limits for non-planar flaws in as welded steel and aluminium alloy weldments *8/39*
Table 8.9 – Limits for non-planar flaws in steel weldments stress-relieved by PWHT *8/39*
Table 8.10 – Acceptance levels for misalignment expressed in terms of stress magnification factor, k_m *8/40*
Table 8.11 – Acceptance levels for weld toe undercut in material thicknesses from 10 mm to 40 mm *8/40*
Table 9.1 – Temperature below which creep is negligible in 200,000 h for carbon manganese and ferritic steels *9/6*
Table D.1 – Formulae for calculating the bending stress due to misalignment in butt joints *D/4*
Table D.2 – Formulae for calculating the bending stress due to misalignment in cruciform joints *D/7*
Table F.1 – Guidance on selection of assessment sites around a pipe system *F/5*
Table F.2 – Crack opening area methods for simple geometries and loading *F/8*
Table F.3 – Summary of short wave length surface roughness values *F/12*
Table F.4 – Particulates in primary system water *F/16*
Table K.1 – Examples of target reliabilities specified by codes and standards *K/6*
Table K.2 – Paris Law parameters including uncertainty in *A* for a one-stage model (*N*, mm) *K/12*

Table K.3 – Paris Law parameters including uncertainty in *A* for a two-stage model (*N*, mm) *K/13*
Table M.1 – Geometry functions for a finite surface flaw in an infinite width plate – deepest point of flaw *M/13*
Table M.2 – Geometry functions for a finite surface flaw in an infinite width plate – intersection of flaw with free surface *M/14*
Table M.3 – Geometry functions for an extended surface flaw in an infinite width plate *M/16*
Table M.4a) – M_1 for axial through-thickness in cylinders: membrane loading *M/28*
Table M.4b) – M_2 for axial through-thickness in cylinders: membrane loading *M/29*
Table M.4c) – M_3 for axial through-thickness in cylinders: bending loading *M/30*
Table M.4d) – M_4 for axial through-thickness in cylinders: membrane loading *M/31*
Table M.5 – M_m and M_b for axial internal surface flaw in cylinder *M/33*
Table M.6 – M_m and M_b for extended axial internal surface flaw in cylinder *M/34*
Table M.7 – M_m and M_b for axial external surface flaw in cylinder *M/35*
Table M.8 – M_m and M_b for extended axial external surface flaw in cylinder *M/36*
Table M.9a) – M_1 for circumferential through-thickness in cylinders: membrane loading *M/39*
Table M.9b) – M_2 for circumferential through-thickness flaws in cylinders: membrane loading *M/40*
Table M.9c) – M_3 for circumferential through-thickness flaws in cylinders: bending loading *M/41*
Table M.9d) – M_4 for circumferential through-thickness flaws in cylinders: bending loading *M/42*
Table M.10 – M_m and M_b for circumferential internal surface flaw in cylinder *M/44*
Table M.11 – M_m and M_b for extended circumferential internal surface flaw in cylindrical shell *M/45*
Table M.12 – Influence coefficients at points A and B for an equatorial through-thickness flaw in a sphere *M/47*
Table M.13 – M_m for semi-elliptical flaw in a round bar under tension loading *M/51*
Table M.14 – M_b for semi-elliptical flaw in a round bar under bending loading *M/51*
Table M.15 – Values of *v* and *w* for axial and bending loading *M/56*
Table N.1 – Polynomial coefficients defining β_T for CCP *N/13*
Table N.2 – Polynomial coefficients defining β_T for CCPB *N/14*
Table N.3 – Polynomial coefficients defining β_T for DENT *N/14*
Table N.4 – Polynomial coefficients defining β_T for SENT *N/15*
Table N.5 – Polynomial coefficients defining β_T for SEB *N/15*
Table N.6 – Polynomial coefficients defining β_T for SENB *N/16*
Table N.7 – Polynomial coefficients defining β_T for CT *N/16*
Table N.8 – Polynomial coefficients defining β_T for SCP: uniaxial tension *N/17*
Table N.9 – Polynomial coefficients defining β_T for SCPB *N/18*
Table N.10 – Polynomial coefficients defining β_T for extended internal circumferential surface flaw in a cylinder *N/19*
Table N.11 – Polynomial coefficients defining β_T for internal circumferential surface flaw in a cylinder (biaxial tension) *N/20*
Table N.12 – Polynomial coefficients defining β_T for internal circumferential surface flaw in a cylinder (uniaxial tension) *N/21*
Table N.13 – α and *k* defined with respect to T/σ_Y for $n = 5$ *N/23*
Table N.14 – α and *k* defined with respect to T/σ_Y for $n = 6$ *N/24*
Table N.15 – α and *k* defined with respect to T/σ_Y for $n = 7$ *N/25*
Table N.16 – α and *k* defined with respect to T/σ_Y for $n = 8$ *N/26*

Table N.17 – α and k defined with respect to T/σ_Y for n = 9 *N/27*
Table N.18 – α and k defined with respect to T/σ_Y for n = 10 *N/28*
Table N.19 – α and k defined with respect to T/σ_Y for n = 11 *N/29*
Table N.20 – α and k defined with respect to T/σ_Y for n = 12 *N/30*
Table N.21 – α and k defined with respect to T/σ_Y for n = 13 *N/31*
Table N.22 – α and k defined with respect to T/σ_Y for n = 14 *N/32*
Table N.23 – α and k defined with respect to T/σ_Y for n = 15 *N/33*
Table N.24 – α and k defined with respect to T/σ_Y for n = 16 *N/34*
Table N.25 – α and k defined with respect to T/σ_Y for n = 17 *N/35*
Table N.26 – α and k defined with respect to T/σ_Y for n = 18 *N/36*
Table N.27 – α and k defined with respect to T/σ_Y for n = 19 *N/37*
Table N.28 – α and k defined with respect to T/σ_Y for n = 20 *N/38*
Table P.1 – Calculation of bending stresses as functions of moments *P/5*
Table P.2 – Values of χ for bending loading *P/21*
Table Q.1 – Assessment ranges for as-welded residual stress distributions in ferritic steels *Q/2*
Table Q.2 – Assessment ranges for as-welded residual stress distributions in austenitic stainless steels (pipe butt welds only) *Q/2*
Table Q.3 – Components of longitudinal stress and K_{sb}^{max} for plate butt welds and pipe axial seam welds (austenitic steel) *Q/4*
Table Q.4 – Components of transverse stress and K_{sb}^{max} for plate butt welds and axial seam welds (austenitic and ferritic steel) *Q/5*
Table Q.5 – Components of longitudinal stress and K_{sb}^{max} for pipe butt welds (ferritic and austenitic steels) *Q/6*
Table Q.6 – Components of transverse stress and K_{sb}^{max} for pipe butt welds (ferritic steel) *Q/9*
Table Q.7 – Components of transverse stress and K_{sb}^{max} for pipe butt welds (austenitic steel) *Q/9*
Table Q.8 – Components of longitudinal stress and K_{sb}^{max} for plate to plate T-butt welds (ferritic steels) *Q/11*
Table Q.9 – Components of transverse stress and K_{sb}^{max} for plate to plate T-butt welds (ferritic and austenitic steels) and longitudinal stress and K_{sb}^{max} for plate to plate T-butt welds (austenitic steels) *Q/12*
Table Q.10 – Components of longitudinal stress and K_{sb}^{max} for tubular T-butt welds (ferritic steels) *Q/13*
Table Q.11 – Components of transverse stress and K_{sb}^{max} for tubular T-butt welds (ferritic steels) *Q/14*
Table Q.12 – Components of transverse and longitudinal stress distribution for repair welds (ferritic and austenitic steels) *Q/15*
Table S.1 – Mean uniaxial creep properties for different steels for short (<10 000 h) and long term tests *S/5*
Table S.2 – Mean uniaxial creep properties for different steels for short (<10 000 h) and long term tests *S/7*
Table T.1 – Examples of inspection capabilities for sub-surface flaws *T/8*
Table T.2 – Examples of inspection capabilities for back surface flaws *T/8*
Table T.3 – Examples of inspection capabilities for flaws at the accessible surface *T/9*
Table T.4 – Capabilities for detection and length measurement of surface-breaking flaws by MPI *T/15*
Table T.5 – Flaw detection capability for liquid penetrant testing *T/16*

Summary of pages

This document comprises a front cover, an inside front cover, pages i to x, pages 0/1 to V/14, an inside back cover and a back cover.

This page deliberately left blank

Foreword

Publishing information

This British Standard is published by BSI Standards Limited, under licence from The British Standards Institution, and came into effect on 31 December 2019. It was prepared by Technical Committee WEE/37, *Acceptance levels for flaws in welds*. A list of organizations represented on this committee can be obtained on request to its secretary.

Supersession

This British Standard supersedes BS 7910:2013+A1:2015, which is withdrawn.

Information about this document

This is a full revision of the standard. It introduces the following principal changes, which reflect both advances in structural integrity technology and feedback from users.

- Annex A to Annex U are now all designated as "informative" (in earlier editions they were classified as either "informative" or "normative". This minor change reflects the nature of the document, i.e. it provides guidance rather than prescribing a particular set of rules.
- A new Annex V has been added, addressing strain-based assessment and design.
- The document has been broken down into self-contained clauses and annexes, each with its own bibliography, tables, equations, figures and symbols. This has inevitably introduced an element of repetition, e.g. of key reference documents, but is intended to improve the flexibility and agility of the document in years to come.
- New bibliographic references have been added, in particular to a series of papers published in a special BS 7910-focussed issue of the *International Journal of Pressure Vessels and Piping*. These cover the major damage/failure mechanisms covered by BS 7910 (fracture, fatigue, creep, corrosion), plus specific topics related to the annexes (residual stress, constraint, reliability, NDT, strain-based assessment) and the application of BS 7910 to pipelines. Whilst the background papers are based mainly on BS 7910:2013, the information is equally applicable to BS 7910:2019 in most cases.
- New rules for flaw interaction criteria and some new materials property clauses have been introduced in Clause **7**.
- Annex F (Procedure for leak-before-break (LbB) assessment) has been simplified; the detectable leakage procedure has been retained and the full LbB removed.
- In Annex J (Use of Charpy V-notch impact tests), a new subclause addresses interpretation of incomplete transition curves and gives more guidance on use of the Master Curve approach.
- Annex K (Probabilistic assessment) has been updated; the tables of generic partial safety factors (PSFs) for use with fracture assessment have been removed.
- Annex M (Stress intensity factor solutions) contains solutions for finite and extended surface-breaking flaws in plates subjected to non-linear stress fields. These were previously included in Annex Q (Residual stress distributions in as-welded joints) but have been moved to Annex M in the interests of consistency and to underline their potential use with primary, as well as secondary, stresses.

- Annex N (Allowance for constraint effects) has been simplified by removing the look-up tables based on the *Q* parameter.
- Annex P (Compendium of reference stress and limit load solutions) includes additional information on the source of the solutions, in particular on the distinction between global and local solutions. Limit load solutions for offshore tubular joints and clad plates containing a repair weld have been removed. As a result of this change, Equation (P.31) has been removed; however, in order to maintain continuity with the 2013 edition, subsequent equations have not been renumbered.
- Annex R (Determination of plasticity interaction effects) has been simplified. In the interests of continuity with earlier revisions, both plasticity interaction factors (ρ and *V*) have been retained; the simplified approach has been kept and the alternative approaches described in the 2013 edition have been removed. Moreover, the simplified approach to the calculation of *V* has been revised to reflect the most recent amendments to the R6 procedure.

This publication can be withdrawn, revised, partially superseded or superseded. Information regarding the status of this publication can be found in the Standards Catalogue on the BSI website at bsigroup.com/standards, or by contacting the Customer Services team.

Where websites and webpages have been cited, they are provided for ease of reference and are correct at the time of publication. The location of a webpage or website, or its contents, cannot be guaranteed.

Use of this document

It has been assumed in the preparation of this British Standard that the execution of its provisions will be entrusted to appropriately qualified and experienced people, for whose use it has been produced.

As a guide this British Standard takes the form of guidance and recommendations. It should not be quoted as if it were a specification or a code of practice and claims of compliance cannot be made to it.

Presentational conventions

The guidance in this standard is presented in roman (i.e. upright) type. Any recommendations are expressed in sentences in which the principal auxiliary verb is "should".

Commentary, explanation and general informative material is presented in smaller italic type, and does not constitute a normative element.

Where words have alternative spellings, the preferred spelling of the Shorter Oxford English Dictionary is used (e.g. "organization" rather than "organisation").

Contractual and legal considerations

This publication does not purport to include all the necessary provisions of a contract. Users are responsible for its correct application.

Compliance with a British Standard cannot confer immunity from legal obligations.

0 Introduction

The background to the development of BS 7910 is given in reference [0.1].

Where it is necessary to examine critically the integrity of new or existing structures by the use of non-destructive testing (NDT) methods, acceptance levels are required for any flaws that might be revealed. These often already exist as quality control levels (for example in a construction code); however, in this British Standard the derivation of acceptance levels for flaws is based upon the principle of fitness-for-service.

By this principle a structure is considered to be adequate for its purpose, provided the conditions to cause failure are not reached. A distinction has to be made between acceptance based on quality control and acceptance based on fitness-for-service.

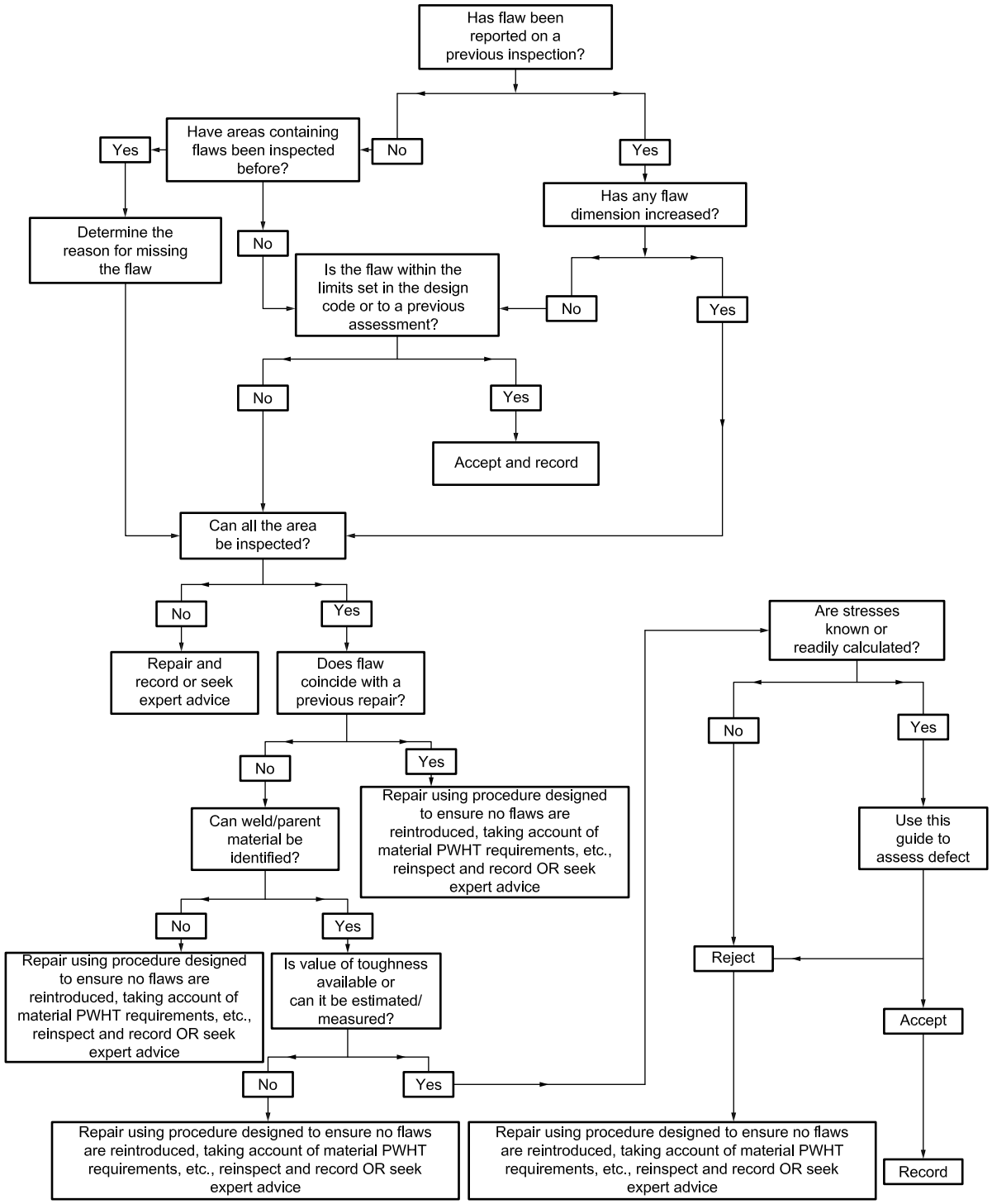
Quality control levels are usually both arbitrary and conservative, but are of considerable value in the monitoring and maintenance of quality during production. Flaws that are less severe than such quality control levels as given, for example, in current construction codes, are acceptable without further consideration. If flaws are more severe than the quality control levels, rejection is not necessarily automatic. Decisions on whether rejection, down rating and/or repairs are required may be based on fitness-for-service, either in the light of previously documented experience with similar material, stress and environmental combinations or on the basis of an engineering critical assessment (ECA) (see Figure 0.1). It is with the latter that this document is concerned. It is emphasized, however, that a proliferation of flaws, even if shown to be acceptable by an ECA, is regarded as indicating that quality is in need of improvement. The use of an ECA is not intended to be viewed as an alternative to good workmanship. The response to flaws not conforming to workmanship criteria needs to be the correction of the fault in the process causing the non-conformity. The methods covered by this British Standard are complementary to, and not a replacement for, good quality workmanship.

A procedure for an ECA is described throughout whereby the significance of flaws under a particular set of circumstances can be determined. All parties need to agree to its use.

It is impossible to provide a single list of flaws that are known not to cause premature failure, as a large number of variables are involved as enumerated in this British Standard. Where relevant experience and data already exist it is possible to dispense with the full ECA procedure and to use authenticated previous assessments as a basis for the establishment of acceptability limits. An ECA may also be used as a basis for deferring necessary repairs to a time mutually agreeable to the contracting parties. Unsatisfactory repair of innocuous flaws can result in the substitution of more harmful and/or less readily detectable flaws.

Flaw assessment on a fitness-for-service basis requires thorough examination by non-destructive testing (NDT) using techniques capable of locating and sizing flaws in critical areas. This British Standard may be used to identify such areas and to assist in optimizing the NDT procedures by identifying those aspects of flaw characterization, size and position that need to be determined. Such NDT is normally carried out after any post-weld heat treatment (PWHT) and/or proof test. However, since a major objective of this British Standard is to reduce costs by eliminating unnecessary repair, careful consideration needs to be given to the level of inspection required to implement this British Standard, and to the limitations of NDT methods.

Figure 0.1 **Example of integrity management procedure for flaws**



NOTE If a component is rejected on the basis of a fitness-for-service analysis, downrating or retirement of the component may be considered as well as repair. Alternatively, the more advanced methods of this British Standard may be used, e.g. analyses based on leak-before-break (see Annex F) or recharacterization of flaws (see Annex E).

Where NDT has revealed the presence of flaws, the following options apply.

- If the flaws do not exceed the quality control levels in the appropriate application standard, no further action is required.
- If acceptance limits have already been established on the basis of an ECA for the appropriate combination of materials, fabrication procedure, welding

consumables, stress and environmental factors, flaws need to be assessed on that basis.

- If no relevant documented experience exists, then an ECA based on the guidance given in this document may be carried out.

An ECA helps to identify the limiting conditions for failure or the limiting design conditions. It is emphasized that some aspects of an ECA are based on new concepts that could be subject to review.

The application of ECA principles means that "safe" results are obtained. The option of using appropriate safety factors has been incorporated or is inherent throughout the standard. If the accuracy of the input information employed (e.g. stress levels, materials properties at the appropriate temperature, flaw size determination) is in question, appropriate additional safety factors need to be agreed. Equally a flaw is not necessarily unacceptable when it is found initially to exceed the acceptance levels that are derived from this standard. A further assessment may be made following the principles given in this standard incorporating more precise input data or analysis methods or by testing structurally relevant components.

This British Standard also gives guidance on the use of probabilistic methods. These factors and methods do not constitute a full risk analysis of the component undergoing assessment as they do not quantify the consequences of a failure. Where failure of the structure under assessment could pose an unjustifiable or intolerable risk to the surrounding environment or population, a full risk analysis might be needed, with due recognition of both individual and societal risk [0.2].

The assessment methods given in this British Standard provide a quantitative measure of the acceptability of a flaw in a structure. They are not to be used in isolation but are to be used as part of an overall process for the management of flaws. The management of flaws is part of a wider integrity management plan for the structure or system. The management processes for flaws address factors such as:

- the cause of the flaw and remedial action to prevent further occurrences or growth;
- whether a previous inspection failed to detect this flaw. If so, the reasons for not detecting the flaw need to be determined. The inspection technique or assumptions about sub-critical crack growth rates might need to be reviewed;
- the previous history of the structure and whether it is consistent with the nature, location and size of the flaw;
- whether an inspection suggests that the flaw has grown and the observed growth is consistent with assumptions about loading and sub-critical crack growth rates after allowing for uncertainty in the inspection results;
- the implications for other structures of the same or similar design and whether modifications to the structure or a change in the service conditions might be required;
- whether there is a pattern of this flaw being detected in other structures of the same design.

An example algorithm for managing the assessment of flaws is shown in Figure 0.1. Alternative approaches may be developed.

Bibliography for Introduction

Standards publications

There are no standards publications in the Introduction.

Other documents

[0.1] HADLEY, I. BS 7910:2013 in brief. *In: International Journal of Pressure Vessels and Piping*, August 2018, 165, 263–269. <https://doi.org/10.1016/j.ijpvp.2018.07.010>

[0.2] ROYAL SOCIETY. *Risk analysis, perception, management*. London: The Royal Society, 1992.

 © The British Standards Institution 2019

1 Scope

This British Standard gives guidance and recommendations for assessing the acceptability of flaws in all types of structures and components. Although emphasis is placed on welded fabrications in ferritic and austenitic steels and aluminium alloys, the procedures can be used for analysing flaws in structures made from other metallic materials and in non-welded components or structures. The methods described are applicable at the design, fabrication and operational phases of the life of a structure.

Specific applications include:

- assessing a known flaw in order to determine the fitness-for-service of a flawed structure;
- calculating the defect-tolerance of a structure in order to inform materials selection, load capacity or inspection requirements;
- justifying waiver of post-weld heat-treatment in thick-walled steel structures.

2 Normative references

There are no normative references in this document.

NOTE Informative references are listed in individual clauses and annexes.

3 Symbols and definitions

For the purposes of this British Standard, the symbols, definitions and units given in individual clauses and annexes apply.

© The British Standards Institution 2019

This page deliberately left blank

4 Types of flaw

The effects of the following flaws may be assessed using methods given in this British Standard:

a) planar flaws:
   1) cracks;
   2) lack of fusion or penetration;
   3) undercut, root undercut, concavity and overlap (on some occasions, undercut and root undercut in welds are treated as shape imperfections);

b) non-planar flaws:
   1) cavities;
   2) solid inclusions (on some occasions cavities and solid inclusions are treated as planar flaws);
   3) local thinning (e.g. due to corrosion);
   4) porosity;

c) shape imperfections:
   1) misalignment;
   2) imperfect profile.

Flaws of the type given in c) include some that may be treated as planar flaws, which are listed in a), and others that give rise to stress concentration effects. A comprehensive classification of the various types of weld flaw which can be encountered is given in BS EN ISO 6520-1.

Bibliography for Clause 4

Standards publications

For dated references, only the edition cited applies. For undated references, the latest edition of the referenced document (including any amendments) applies.

BS EN ISO 6520-1, *Welding and allied processes – Classification of geometric imperfections in metallic materials*

Other documents

There are no other references in this clause.

This page deliberately left blank

5 General guidance on assessment

5.1 Modes of failure and material damage mechanisms

The influence of the flaws listed in Clause **4** may be assessed, using methods given in this British Standard, for the following modes of failure and damage mechanisms:

a) failure by fracture and plastic collapse (see Clause **7**);

b) damage by fatigue (see Clause **8**);

c) damage by creep and creep fatigue (see Clause **9**);

d) failure by leakage of containment vessels (see **10.2**);

e) damage by corrosion and/or erosion (see **10.3.2**);

f) damage by environmentally assisted cracking (see **10.3.3**);

g) failure by instability (buckling) (see **10.4**).

For each flaw or flaw type the following points should be assessed:

1) the potential modes of final failure; and

2) any possible material damage mechanisms leading to property degradation or sub-critical flaw growth.

NOTE Material damage and sub-critical flaw growth can be affected by the material itself, design features, stress levels, time, cyclic loading, composition and concentration of process fluids and additives, flow rates, operating temperatures, external environment, etc., though not all these considerations apply to any given material damage mechanism.

The following are examples of some of the most common material damage mechanisms.

i) Embrittlement: this type of damage can be caused in some materials by irradiation, temper embrittlement, or by caustic, hydrogen or hydrogen sulfide rich environments.

ii) Fatigue: this is a damage process whereby embedded or surface cracks can initiate and grow under fluctuating stress (e.g. due to applied loads, thermal stress variations and vibrations). Members containing stress concentrations (e.g. flaws, geometric discontinuities) are particularly susceptible. For these reasons, welded components can give much lower fatigue lives than plain material under the same loading.

iii) Corrosion fatigue: this is a type of damage similar to fatigue, but the onset of cracking and crack growth rates are accelerated by the corrosive medium.

iv) Creep cracking: this is internal and/or external cracking due to operating temperatures greater than the creep threshold temperature, which is a function of the material. Components subjected to creep conditions have a finite life and the damage rate is a function of temperature, stress and time. For this reason, the finite life of highly stressed components and welds within a structure can be much lower than the plain areas subject to membrane stress alone.

v) Internal corrosion: material loss can take many forms, such as pitting corrosion, crevice corrosion, localized corrosion, general corrosion, etc., and is mainly due to the contents of the system, including any impurities.

vi) External corrosion and under lagging corrosion: depending on the material, its loss from exposed areas can be similar to internal corrosion. This damage mechanism is mainly caused by a wet and dry environmental sequence such

as exposure to rain or the local environment surrounding the component (e.g. leaking fluids, emissions from surrounding plant).

vii) Stress corrosion cracking (SCC): in some materials internal and/or external cracking can occur due to chemical action on a stressed component. Generally as-welded components are more susceptible than those that have been post-weld heat-treated. Crack initiation and propagation rates are a function of material, stress, temperature, and the concentration of the corrosive medium.

viii) Hydrogen and hydrogen sulfide related cracking: the damage rate is a function of material, pressure, temperature, concentration of H_2 or H_2S, etc.

ix) Erosion: the internal loss of material is mainly due to rapid flow of process fluid and to abrupt changes in fluid flow direction or the presence of other liquid or solid impurities.

x) Cavitation: the most common areas affected are pump impellers and components where high flow rates occur with significant pressure drop, such as might occur across control valves in process fluid piping or pipelines.

These failure modes and damage mechanisms are not relevant in all applications. At the outset all operating conditions should be taken into account, including start-up, shut-down, process upset and external environment, to establish which are relevant to the particular component under consideration. Possible interaction between the various damage mechanisms should also be taken into account. The detailed assessment of the various modes of failure and material damage mechanisms is given in Clause **7**, Clause **8**, Clause **9** and Clause **10**.

The likelihood of failure from the operation of these failure modes and damage mechanisms can be predicted with varying degrees of confidence and accuracy. The behaviour of components subject to fatigue loading, creep, brittle fracture and general volumetric corrosion forming locally thinned areas (LTAs) is well understood. It is not practical to attempt to provide treatments for the other mechanisms listed in the same depth and generality as is provided for failure by fracture, fatigue, creep or corrosion, but they should all be addressed in an ECA, since failure can arise through their operation. Brief guidelines are offered in Clause **10** for the assessment of these mechanisms. If it is established that a risk of failure from these mechanisms exists, a specific assessment should be undertaken. This should incorporate the assumptions and approaches used, which should be fully documented and agreed by all parties.

5.2 Sequence of assessment

The following is the recommended sequence of operations for carrying out an assessment for a known flaw.

a) Identify the flaw type, i.e. planar, non-planar or shape (Clause **4**).

b) Establish the cause of the flaw.

c) Establish the essential data, relevant to the particular structure (see **6.2**).

d) Determine the size of the flaw.

e) Assess possible material damage mechanisms and damage rates.

f) Determine the limiting size for the final modes of failure.

g) Based on the damage rate, assess whether the flaw would grow to this final size within the remaining life of the structure or the in-service inspection interval, by sub-critical crack growth.

h) Assess the consequences of failure.

i) Carry out sensitivity analysis.

 © The British Standards Institution 2019

j) If the flaw would not grow to the limiting size, including appropriate factors of safety, it is acceptable. The safety factors should take account both of the confidence in the assessment and of the consequences of failure.

Estimation of tolerable planar flaw sizes may be made by starting from a series of limiting flaw sizes as determined in f) and determining the initial flaw sizes that would grow to these within the remaining life as in g). Procedures for calculating such tolerable final flaw sizes are given in Clause **7**, Clause **8**, Clause **9** and Clause **10**.

5.3 Fracture assessment options

Several levels of treatment of flaws are possible, depending on the application and materials data available. Three options for dealing with fracture are included in Clause **7**.

- Option 1 is a conservative procedure that is relatively simple to employ and does not require detailed stress/strain data for the materials being analysed.
- Option 2 is based on the use of a material-specific stress-strain curve.
- Option 3 uses numerical analysis to generate a failure assessment diagram (FAD).

Procedures are given in Clause **8** and Clause **9** for estimating fatigue and creep crack growth respectively, when specific materials data is provided. Guidance is also given in these clauses on making assessments when specific information is not available. Where appropriate, guidance is included on the probability of survival and on the desirability of conducting a sensitivity analysis.

Bibliography for Clause 5

There are no references in this clause.

This page deliberately left blank

6 Information required for assessment

6.0 Symbols and definitions

For the purposes of this clause, the following symbols, definitions and units apply, unless otherwise indicated at the point of use.

Symbol	Definition	Units
a	Half flaw length for through-thickness flaw, flaw height for surface flaw or half height for embedded flaw	mm
B	Section thickness in plane of flaw	mm
c	Half flaw length for surface and embedded flaws	mm
K_I	Applied tensile (mode I) stress intensity factor (SIF)	$N/mm^{3/2}$
K_{Ic}	Plane strain fracture toughness	$N/mm^{3/2}$
K_{ISCC}	Critical stress intensity factor for stress corrosion cracking	$N/mm^{3/2}$
k_m	Stress concentration factor due to misalignment	—
k_t	Stress concentration factor due to local structural discontinuities (e.g. holes, notches, sharp corners)	—
k_{tb}	Bending stress concentration factor	—
k_{tm}	Membrane stress concentration factor	—
P_b	Primary bending stress	N/mm^2
P_m	Primary membrane stress	N/mm^2
Q	Secondary stress	N/mm^2
Q_b	Secondary bending stress	N/mm^2
Q_m	Secondary membrane stress	N/mm^2
R	Stress ratio, i.e. ratio of minimum to maximum stress (or stress intensity factor) during fatigue cycling	—
ΔK_I	Cyclic range of K_I	$N/mm^{3/2}$
$\Delta\sigma$	Applied stress range	N/mm^2
$\Delta\sigma_b$	Bending component of stress range	N/mm^2
$\Delta\sigma_m$	Membrane component of stress range	N/mm^2
$\Delta\sigma_1$, $\Delta\sigma_2$	Linearized values of primary or secondary stress ranges	N/mm^2
σ	Stress	N/mm^2
σ_{max}	Maximum value of stress distribution across a section	N/mm^2
σ_1, σ_2	Linearized values of primary or secondary stresses	N/mm^2

6.1 General

The ECA requires assumptions to be made about input parameters. Therefore, if there is any likelihood that an ECA will be required during the life of a structure, relevant materials properties should be generated at the construction stage, or appropriate materials should be retained for later testing. Accurate fracture toughness data are particularly important, and tests on weld procedure qualification samples are advisable. Similarly, fatigue crack growth, creep and SCC data may be obtained from the actual materials of construction. Any such tests should be performed in accordance with the appropriate standard from the following list:

- BS ISO 12108 for fatigue crack growth;
- BS ISO 12108 for fatigue crack growth threshold;
- BS 7448, BS EN ISO 15653 and ISO 12135 for fracture toughness;

- BS 8571 for low-constraint fracture toughness;
- BS EN ISO 7539 for SCC.

The information should take account of the material strain and thermal history and the appropriate environment. The assessment should cover all loadings, including, as appropriate, those arising during transport, construction, installation and testing, and, where necessary, take account of fault and accident conditions. The effects of local loads and misalignment should also be taken into account. Any assumptions should be justified to the satisfaction of all parties and appropriate documentation, including material specification and details of actual material used, should be appended to the ECA.

6.2 Essential data

Relevant data from the following list should be obtained:

a) nature, position and orientation of flaw;

b) structural and weld geometry, fabrication procedure;

c) stresses (pressure, thermal, residual or resulting from any other type of mechanical loading) and temperatures including transients;

d) yield or 0.2% proof strength, tensile strength and elastic modulus (in certain cases, a complete engineering stress/strain curve is required);

e) fatigue/corrosion fatigue *S–N* and crack propagation data;

f) fracture toughness (K_{Ic} or values of *J*-integral or CTOD) data [in certain cases fracture toughness may be estimated from relevant Charpy V-notch data (see Annex J)];

g) creep rupture, creep crack propagation and creep fatigue data; and

h) bulk corrosion and SCC (K_{ISCC}) data.

6.3 Non-destructive testing

6.3.1 General

NDT is an essential aspect of a fitness-for-service assessment. The NDT technique(s) used for flaw evaluation should be chosen to provide the type of information required to an acceptable degree of accuracy. Such information should include some or all of the following items:

a) flaw length;

b) flaw height;

c) flaw position;

d) flaw orientation with respect to the principal stress direction; and

e) whether the flaw cross-section is planar or non-planar.

6.3.2 Methods for surface-breaking flaws

The following methods (in no order of preference) may be used for the detection of surface-breaking flaws:

a) visual;

b) liquid penetrant;

c) magnetic particle (for ferromagnetic materials);

d) eddy current [including AC field measurement (ACFM)];

e) electrical potential drop (AC or DC);

f) radiography; and

g) ultrasonics.

These methods are also suitable for measuring the surface length of such flaws, but only ultrasonic, eddy current (including ACFM) and potential drop methods are capable of providing a measurement of their height. Further guidance on the use of NDT is given in Annex T.

6.3.3 Methods for embedded flaws

The following methods (in no order of preference) may be used for the detection of embedded flaws:

a) radiography;

b) ultrasonics;

c) eddy current (including ACFM); and

d) electrical potential drop (DC only).

Radiography and ultrasonics are both capable of providing a measurement of flaw length, but ultrasonic testing is the only NDT method that is routinely used to measure flaw height. Eddy current, ACFM and potential drop methods tend to provide a measurement of the cross-sectional area of the flaw.

6.3.4 Applicable standards and treatment of uncertainties

NDT should be carried out in accordance with the appropriate standards from the following list:

- ultrasonics, including Time of Flight Diffraction (TOFD): BS EN 17640, BS EN ISO 22825, BS EN ISO 10863, BS EN ISO 13588, BS EN ISO 11666, BS EN ISO 15626 and BS EN ISO 19285;
- radiography: BS EN ISO 10675, BS EN ISO 17636-1 and BS EN ISO 17636-2;
- magnetic particle: BS EN ISO 17638 and BS EN ISO 23278;
- liquid penetrant: BS EN ISO 3452 and BS EN ISO 23277;
- eddy current: BS EN ISO 15548, BS EN ISO 15549 and BS EN ISO 17643;
- visual: BS EN ISO 17637 and BS EN 1370.

Any inspection procedure which deviates from or is not covered by an appropriate standard should be appended to the ECA. Suitable allowances should be incorporated in the assessment of flaw sizes to cover intrinsic and measurement errors involved and thereby ensure conservative assessment of flaw severity. These allowances and their bases should be quoted in the ECA. Guidance on the measurement error and reliability of commonly used inspection methods is given in Annex T.

Standard inspection techniques, which are suitable and economically viable for examining long lengths of weld, are not necessarily appropriate for the accurate flaw measurement required for an ECA. In such cases, supplementary techniques or additional test methods should be employed.

6.3.5 Treatment of uninspectable areas

Where a region of a structure cannot be inspected, the size of flaw that could exist in the uninspectable region should be estimated based on flaw distributions in areas of the structure which could be inspected. When assessing the likelihood of the presence of such flaws, account may be taken of

knowledge of the weld preparations, the welding process and procedures, and the general quality of welding attained. Account may also be taken of the operating applied loads, process fluid parameters and any significant external environment relevant to the region.

6.4 Stresses to be considered

6.4.1 General

Stresses used in the ECA should be justified and tabulated and form an integral part of the assessment. When complete stress information is not available, the basis for any estimate should be agreed with all parties and included in the assessment. The methods in this British Standard relate predominantly to stress-based assessment, i.e. when the nominal stress is lower than the yield strength of the flawed section. A method for strain-based assessment is given in Annex V.

The stresses to be considered in the assessment are those which would be calculated by a stress analysis of the unflawed structure. The actual stress distributions may be used, or the stresses (or stress ranges) may be linearized, as shown in Figure 6.1. Linearization may be carried out across the flaw [Figure 6.1a)] or across the section containing the flaw [Figure 6.1b)]. The latter method normally provides overestimates, but has the advantage that linearization does not need to be repeated with crack growth. Account should be taken of the primary membrane and bending stresses, the secondary stresses and the magnification of the primary stresses caused by local or gross discontinuities or by misalignment, as described in **6.4.2**, **6.4.3** and **6.4.4**. Typical schematic representations of these are given in Figure 6.1. In an assessment of the effect of a single or steady state applied load, it is important to distinguish between primary and secondary stresses, as only the former contribute to plastic collapse. In a fatigue assessment, the important distinction is between static and fluctuating stresses and all fluctuating stresses are treated in the same way as primary stresses. In the special case when allowance is made for R (**8.2.1.4**), steady state primary stresses and secondary stresses should also be taken into account, in order to determine the actual values of the maximum and minimum applied stresses. The stress categories described below do not necessarily coincide with those used in other documents (for example, PD 5500). In the fracture assessment routes described in Clause **7**, shear stresses are not included. If shear stresses are significant, the guidance in Annex A may be used.

6.4.2 Primary stress *(P)*

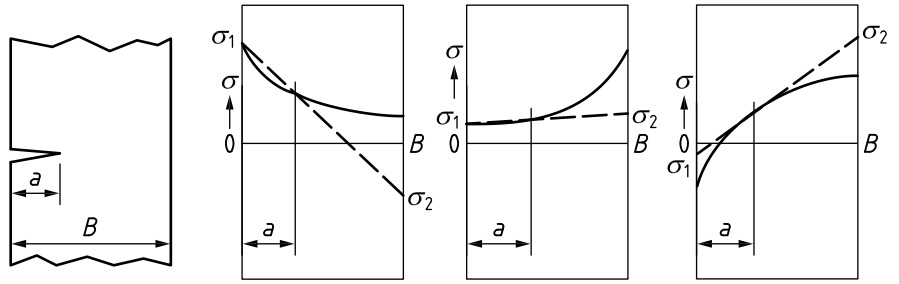
Primary stresses are stresses that can, if sufficiently high, contribute to plastic collapse (secondary stresses do not) (see **6.4.3**). They can also contribute to failure by fracture, fatigue, creep or SCC. They include all stresses arising from internal pressure and external loads. Some stresses classified as secondary by design codes and guidance documents, e.g. ASME Boiler and Pressure Vessel Code, Section III, and PD 5500, are regarded as primary in this British Standard, e.g. certain thermal and residual stresses (see **7.1.6**). The primary stresses are divided into membrane, P_m, and bending, P_b, components as follows.

- Membrane stress (P_m) is the mean stress through the section thickness that is necessary to ensure the equilibrium of the component or structure.
- Bending stress (P_b) is the component of stress due to imposed loading that varies linearly across the section thickness. The bending stresses are in equilibrium with the local bending moment applied to the component. For the purpose of this British Standard, P_b is regarded as a stress superimposed upon P_m.

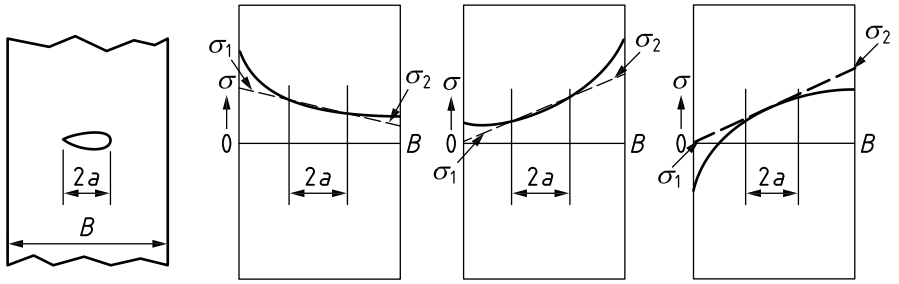
 © The British Standards Institution 2019

Figure 6.1 **Linearization of stress distributions**

a) Linearization of stress distributions across flaw



1) Examples of linearization of primary or secondary stress distributions for surface flaws



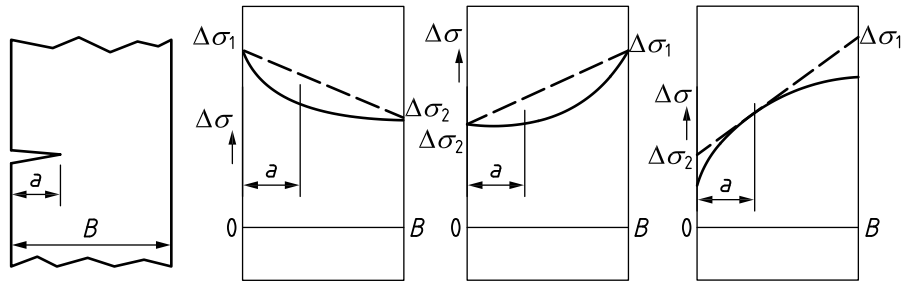
2) Examples of linearization of primary or secondary stress distributions for embedded flaws

P_m,Q_m and P_b,Q_b can be determined from the distributions in a)1) and a)2) using the following equations:

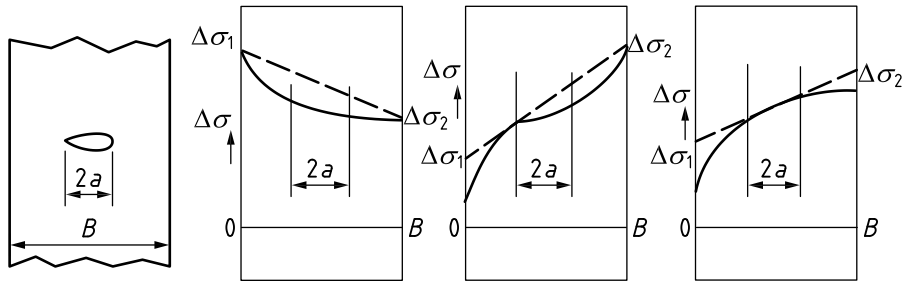
$$P_m,Q_m = \frac{\sigma_1 + \sigma_2}{2} \quad \text{and} \quad P_b,Q_b = \frac{\sigma_1 - \sigma_2}{2}$$

NOTE Any linearized distribution of stress is acceptable provided that it is greater than or equal to the magnitude of the real distribution over the flaw surface.

b) Linearization of stress range distributions across section



1) Examples of linearization of stress range distributions for surface flaws



2) Examples of linearization of stress range distributions for embedded flaws

$\Delta\sigma_m$ and $\Delta\sigma_b$ can be determined from the distributions in b)1) and b)2) using the following equations:

$$\Delta\sigma_m = \frac{\Delta\sigma_1 + \Delta\sigma_2}{2} \quad \text{and} \quad \Delta\sigma_b = \frac{\Delta\sigma_1 - \Delta\sigma_2}{2}$$

6.4.3 Secondary stress *(Q)*

The secondary stresses, Q, are self-equilibrating stresses necessary to satisfy compatibility in the structure. An alternative description is that they can be relieved by local yielding, heat treatment, etc.

Thermal and residual stresses are usually secondary.

NOTE Fluctuating thermal stresses are treated as primary in a fatigue assessment.

Secondary stresses do not cause plastic collapse as they arise from strain/displacement limited phenomena. They do however contribute to the severity of local conditions at a crack tip, and, when it is necessary to include them in an assessment, they should be included in calculations of K_I and ΔK_I. Thermal stresses (primary and secondary) should also be multiplied by appropriate stress concentration and misalignment factors, k_t and k_m.

The secondary stresses may be divided into membrane, Q_m, and bending, Q_b, components as for primary stresses (see **7.1.8**).

6.4.4 Stresses at structural discontinuities

6.4.4.1 General

Stress concentrations occur at structural discontinuities under applied primary or thermal stresses. Secondary stresses are not influenced by structural discontinuities except that thermal stresses, when considered primary (see **7.1.8**), are affected by structural discontinuities. Their effects are quantified by calculating peak stresses at the discontinuities, as described in **6.4.4.2** to **6.4.4.4**. The bending component may be obtained by subtracting the membrane component from the peak stress.

6.4.4.2 Gross structural discontinuities

Typical gross structural discontinuities are those occurring at pressure vessel nozzles and at the major intersections in tubular structures. For such situations, the stress at the discontinuity is calculated by multiplying the applied stress by the appropriate stress concentration factor, for the purposes of calculating crack driving force, K_I. For nominal stress, membrane stress and bending stress, the stress concentration factors are k_t, k_{tm}, and k_{tb}, respectively. Where stress information is available in the form of membrane and bending stresses, separate stress concentration factors, k_{tm} and k_{tb}, should be applied to each. Further guidance for tubular joints and for pressure vessel nozzles is given in Annex B and Annex C respectively. This type of stress concentration usually decays over distances greater than the section thickness, and can lead to a plastic hinge across the full section thickness over local regions.

6.4.4.3 Discontinuities due to misalignment or deviation from intended shape

Discontinuities due to misalignment or deviation from intended shape cause bending stresses. This is calculated by multiplying the applied membrane stress by a stress magnification factor k_m (see Annex D). This type of stress magnification also decays over distances greater than the section thickness and can lead to a plastic hinge across the full thickness over local regions. If additional bending stresses due to misalignment occur within a region of stress concentration due to a gross structural discontinuity, both effects should be taken into account.

 © The British Standards Institution 2019

6.4.4.4 Local structural discontinuities

Stress concentrations due to local structural discontinuities (e.g. holes, notches, sharp corners) usually decay over distances less than the hole or notch radius, which might be a small proportion of the wall thickness. If the flaw lies within this region, then the effect of the stress concentrations on both fracture/fatigue and plastic collapse should be taken into account and the peak stress may be calculated by multiplying the applied stress by k_t.

Stress concentration effects due to weld toes do not contribute to plastic collapse. However, they increase the stress intensity factor (see Annex M). For sharp corners, the theoretical stress concentration factor is infinite, and cracks at such regions should be treated by a stress intensity magnification factor. Local structural discontinuities can be located within zones of stress concentration caused by gross discontinuities and/or by misalignment, and all these effects should be taken into account in the stress analysis.

Different methods of incorporating peak stresses are used in various different assessment methods within this British Standard, as detailed in **7.1.6**, **7.2.3**, Clause **8** and Clause **9**.

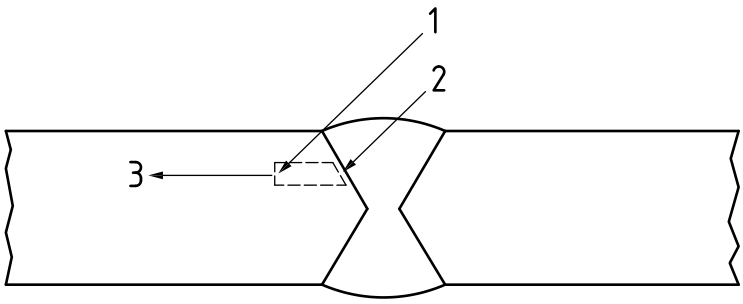
6.4.5 Treatment of flaws not aligned with a plane of principal stress

Where the plane of the flaw is not aligned with a plane of principal stress, further consideration is needed. The first step is to project the flaw on to each of the three planes normal to the principal stresses and to evaluate each of the three projected flaws. One of these projections often leads to a stress intensity factor and a reference stress that are both significantly higher than those for the other two projections. In this case, the assessment should be carried out, taking a and $2c$ as the projected dimensions on that plane. This method is often applicable to near circumferential flaws in the wall of a pipe, where the flaw is projected on to the circumferential plane (see Figure 6.2). There are however restrictions on proceeding in this way. Specialist advice (for example, alternative detailed advice is given in R6, **11.3** [6.1]) should be sought in the following situations.

- There is a large angle (greater than about 20°) between the plane of the actual flaw and the principal plane on which the stress intensity factor and reference stress are greatest.
- There is only a small difference between the stress intensity factors on two or more planes of projection.
- The maximum stress intensity factor occurs for the flaw projected onto one plane and the maximum reference stress occurs for the flaw projected onto another plane.
- One of the principal stresses is significantly compressive, i.e. of a similar magnitude to the maximum principal tensile stress.

In these circumstances significant mode II and/or III loading could be present. Annex A provides guidance on the treatment of these modes of loading.

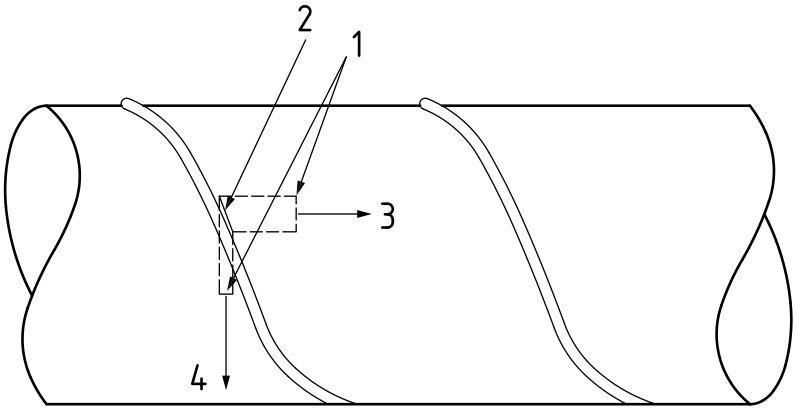
Figure 6.2 **Procedure for resolving flaws normal to principal stress**



a) Butt weld example

Key

1 Resolved flaw (normal to principal stress)
2 Actual flaw
3 Principal stress



b) Spirally-welded pipe example

Key

1 Resolved flaw (resolved to maximize significance)
2 Actual flaw
3 Principal axial stress
4 Principal hoop stress

Bibliography for Clause 6

Standards publications

For dated references, only the edition cited applies. For undated references, the latest edition of the referenced document (including any amendments) applies.

ASME Boiler and Pressure Vessel Code, Section III*: Rules for construction of nuclear power plant components*

BS 7448, *Fracture mechanics toughness tests*

BS 8571, *Method of test for determination of fracture toughness in metallic materials using single edge notched tension (SENT) specimens*

BS EN 1370, *Founding – Examination of surface condition*

BS EN 17640, *Non-destructive testing of welds – Ultrasonic testing – Techniques, testing levels, and assessment*

BS EN ISO 3452, *Non-destructive testing*

BS EN ISO 7539, *Corrosion of metals and alloys*

BS EN ISO 10675, *Non-destructive testing of weld – Acceptance levels for radiographic testing*

BS EN ISO 10863, *Non-destructive testing of welds – Time-of-flight diffraction technique (TOFD) – Acceptance levels*

BS EN ISO 11666, *Non-destructive testing of welds – Ultrasonic testing – Acceptance levels*

BS EN ISO 13588, *Non-destructive testing of welds – Ultrasonic testing – Use of automated phased array technology*

BS EN ISO 15548, *Non-destructive testing of welds – Eddy current examination of welds by complex plane analysis*

BS EN ISO 15549, *Non-destructive testing – Eddy current testing – General principles*

BS EN ISO 15626, *Non-destructive testing of welds – Time-of-flight diffraction technique (TOFD) – Acceptance levels*

BS EN ISO 15653, *Metallic materials – Method of test for the determination of quasistatic fracture toughness of welds*

BS EN ISO 17636-1, *Non-destructive testing of welds – Radiographic testing – X- and gamma-ray techniques with film*

BS EN ISO 17636-2, *Non-destructive testing of welds – Radiographic testing – X- and gamma-ray techniques with digital detectors*

BS EN ISO 17637, *Non-destructive testing of welds – Visual testing of fusion-welded joints*

BS EN ISO 17638, *Non-destructive testing of welds – Magnetic particle testing*

BS EN ISO 17643, *Non-destructive testing of welds – Eddy current examination of welds by complex plane analysis*

BS EN ISO 19285, *Non-destructive testing of welds – Phased array ultrasonic testing (PAUT) – Acceptance levels*

BS EN ISO 23277, *Non-destructive testing of welds – Penetrant testing – Acceptance levels*

BS EN ISO 23278, *Non-destructive testing of welds – Magnetic particle testing – Acceptance levels*

BS EN ISO 22825, *Non-destructive testing of welds – Ultrasonic testing – Testing of welds in austenitic steels and nickel-based alloys*

BS ISO 12108, *Metallic materials – Fatigue testing – Fatigue crack growth method*

ISO 12135, *Metallic materials – Unified method of test for the determination of quasistatic fracture toughness*

PD 5500, *Specification for unfired fusion welded pressure vessels*

Other documents

[6.1] R6 PANEL. *R6: Assessment of the integrity of structures containing defects.* Revision 4, as amended. Gloucester: EDF Energy, 2001.

This page deliberately left blank

7 Assessment for fracture resistance

7.0 Symbols and definitions

For the purposes of this clause, the following symbols, definitions and units apply, unless otherwise indicated at the point of use.

Symbol	Definition	Units
A_r	Coefficient used in deriving stress-strain curve for ferritic steels from yield/proof strength, tensile strength and uniform elongation [see Equation (7.4) and Equation (7.5)]	—
a	Half flaw length for through-thickness flaw, flaw height for surface flaw or half height for embedded flaw (original or recharacterized)	mm
a_j	Flaw size after ductile crack growth Δa_j	mm
a_{pl}	Measure of the extent of Irwin's plastic zone	mm
a_0	Initial flaw size	mm
a_1, a_2	Heights of non-planar or coplanar surface flaws in close proximity when considering flaw interaction	mm
$2a_1$, $2a_2$	Heights of non-planar or coplanar embedded flaws in close proximity when considering flaw interaction	mm
B	Section thickness in plane of flaw	mm
b	Thickness of sub-sized fracture toughness specimen	mm
b_0	Size of the un-notched ligament, equal to $(W - a_0)$	m
C_V	Lower bound Charpy V-notch impact energy at the service temperature (for which fracture toughness is required)	J
c	Half flaw length for surface or embedded flaw	mm
$2c$	Recharacterized flaw length when considering flaw interaction	mm
$2c_1$, $2c_2$	Heights of non-planar or coplanar flaws in close proximity when considering flaw interaction	mm
E	Elastic modulus	N/mm^2
E'	Elastic modulus corrected for constraint conditions $E' = E$ for plane stress, $E' = E/(1 - \nu^2)$ for plane strain	N/mm^2
HV_{10}	Vicker's hardness, determined using a 10 kg load	—
J	Line or surface integral that encloses the crack front from one crack surface to the other, used to characterize the local stress-strain field around the crack tip	N/mm
J_c	Value of J at either: a) unstable fracture; or b) onset of arrested brittle crack or pop-in *NOTE This term applies only where $\Delta a < 0.2$ mm.*	N/mm
J_e	Value of J determined using an elastic analysis	N/mm
J_m	Value of J at first attainment of a maximum force plateau	N/mm
J_{mat}	Material fracture toughness measured by J-methods	N/mm
J_u	Value of J at either: a) unstable fracture; or b) onset of arrested brittle crack or pop-in *NOTE This term applies only where $\Delta a > 0.2$ mm offset to the blunting line.*	N/mm

(continued)

Symbol	Definition	Units
$J_{0.2BL}$	Size insensitive fracture resistance J at 0.2 mm stable crack extension offset from the construction (blunting) line	N/mm
K	Stress intensity factor (SIF)	$N/mm^{3/2}$
K_B	Fracture toughness for the equivalent full thickness of the component (determined from K_b)	$MPa\sqrt{m}$
K_b	Fracture toughness determined from sub-sized specimen of thickness b	$MPa\sqrt{m}$
K_c	Value of K at either: a) unstable fracture; or b) onset of arrested brittle crack or pop-in *NOTE This term applies only where $\Delta a < 0.2$ mm.*	$N/mm^{3/2}$
K_I	Applied tensile (mode I) stress intensity factor	$N/mm^{3/2}$
K_I^p	Stress intensity factor due to primary stress	$N/mm^{3/2}$
K_I^s	Stress intensity factor due to secondary stress	$N/mm^{3/2}$
K_i	Individual data points in statistical treatment of fracture toughness data	$N/mm^{3/2}$
$\bar{K}_i$	Mean value of fracture toughness (see **7.1.7**)	$N/mm^{3/2}$
K_J	Value of fracture toughness derived from J-integral	$N/mm^{3/2}$
$K_{Jc(limit)}$	Limiting value of K_b	$N/mm^{3/2}$
K_{Jm}	Fracture toughness derived from J_m	$N/mm^{3/2}$
K_m	Fracture toughness at maximum load	$N/mm^{3/2}$
K_{mat}	Characteristic material fracture toughness determined in terms of stress intensity factor	$N/mm^{3/2}$
K_r	Fracture ratio	—
K_u	Value of K at either: a) unstable fracture; or b) onset of arrested brittle crack or pop-in *NOTE This term applies only where $\Delta a > 0.2$ mm.*	$N/mm^{3/2}$
$K_{0.2mm}$	Initiation of tearing fracture toughness	$N/mm^{3/2}$
K_δ	Fracture toughness estimated from CTOD	$N/mm^{3/2}$
K_{1mm}, K_{2mm}	K_{mat} corresponding to the postulated amount of tearing, typically up to 1 mm or 2 mm	$N/mm^{3/2}$
k_{tb}	Bending stress concentration factor	—
$k_{0.90}$	Value of the one-sided tolerance limit for a normal distribution	—
L	Attachment length	mm
L_r	Ratio of reference stress to yield strength (or applied load to limit load)	—
$L_{r,max}$	Maximum permitted limit of L_r	—
M_k, M_{km}, M_{kb}	Stress intensity magnification factors for a flaw at the weld toe	—
M_m, M_b	Stress intensity magnification factors for flaw shape	—
m	Parameter as a function of yield strength and tensile strength, used in converting K_{mat} to δ_{mat} and vice versa; see Equation (7.16) and Equation (7.17)	—

(continued)

Symbol	Definition	Units
n	Strain-hardening exponent, see Equations (7.4), (7.6) and (7.7)	—
P	Applied load	N
P_b	Primary bending stress	N/mm^2
P_L	Limit load	N
P_m	Primary membrane stress	N/mm^2
p	Shortest distance from surface to embedded flaw	mm
Q	Secondary stress	N/mm^2
Q_b	Secondary bending stress	N/mm^2
Q_m	Secondary membrane stress	N/mm^2
R	Ratio of minimum to maximum load in fatigue	—
R_{eH}	Upper yield strength of material	N/mm^2
R_{eL}	Lower yield strength of discontinuously yielding material	N/mm^2
R_m	Ultimate tensile strength of material	N/mm^2
$R_{p0.2}$	0.2% proof strength	N/mm^2
$R_{p1.0}$	1% proof strength	N/mm^2
$R_{t0.5}$	Yield strength associated with a total elongation (strain) of 0.5%	N/mm^2
S^2	Variance	—
s, s_1, s_2	Distance between potentially interacting flaws	mm
T	Assessment temperature	°C
T_0	Temperature for a median toughness of 100 MPa$\sqrt{}$m in 25 mm thick specimens	°C
V	Plasticity correction factor	—
W	Specimen or structural width	mm
Y	Stress intensity correction factor	—
z	Number of samples in a set of fracture toughness data	—
Δa	Increment in a or ductile tearing	mm
Δa_f	Crack growth due to fatigue loading	mm
Δa_j	Intermediate value of tearing flaw extension	mm
Δa_t	Crack growth due to tearing	mm
Δa_{tot}	Total crack growth	mm
$\Delta\varepsilon$	Extent of Lüders strain as in Equation (7.8)	—
$\Delta\varepsilon$	Increase in strain as in Equation (7.33)	—
δ	Crack tip opening displacement (CTOD) or crack opening displacement (COD)	mm
δ_c	CTOD for test specimens that fail by cleavage fracture after <0.2 mm of ductile tearing	mm
δ_{mat}	Material toughness determined by CTOD method	mm
δ_u	CTOD for tests that fail by cleavage fracture after ductile tearing of at least 0.2 mm	mm
$\delta_{0.2BL}$	Resistance to crack extension expressed in terms of CTOD at 0.2 mm crack extension offset to the blunting line	mm
ε	Strain	—
ε_{ref}	Reference strain; the true strain at the true stress $\sigma_{ref} = L_r\sigma_Y$	—
ε_t	True strain	—

(continued)

Symbol	Definition	Units
ε_u	Uniform elongation strain at ultimate tensile strength	—
ε_Y	Yield strain, i.e. strain at σ_Y	—
λ	Parameter used in constructing Option 1 FAD	—
μ	Parameter used in constructing FAD line, taken as the minimum value of either $0.001(E/\sigma_Y)$ or 0.6	—
ν	Poisson's ratio	—
ρ	Plasticity interaction factor	—
σ	Stress	N/mm^2
σ_f	Flow strength (assumed to be the average of the yield and the tensile strengths)	N/mm^2
σ'_f	Value of flow strength (assumed to be the average of yield and tensile strengths) of the "appropriate" material at the assessment temperature	N/mm^2
σ^p	Stress arising from primary loads	N/mm^2
σ_{ref}	Reference stress used for creep and plastic consideration; it is sometimes calculated from plane strain von Mises limit load as in Annex N	N/mm^2
σ^s	Stress arising from secondary loads	N/mm^2
σ_t	True stress	N/mm^2
σ_U	Tensile strength	N/mm^2
σ_Y	Lower yield strength or 0.2% proof strength	N/mm^2
σ'_Y	Yield strength of "appropriate" material at the assessment temperature	N/mm^2
σ'_{YRT}	Yield strength of the "appropriate" material at room temperature in Equation (7.24a)	N/mm^2

7.1 Background

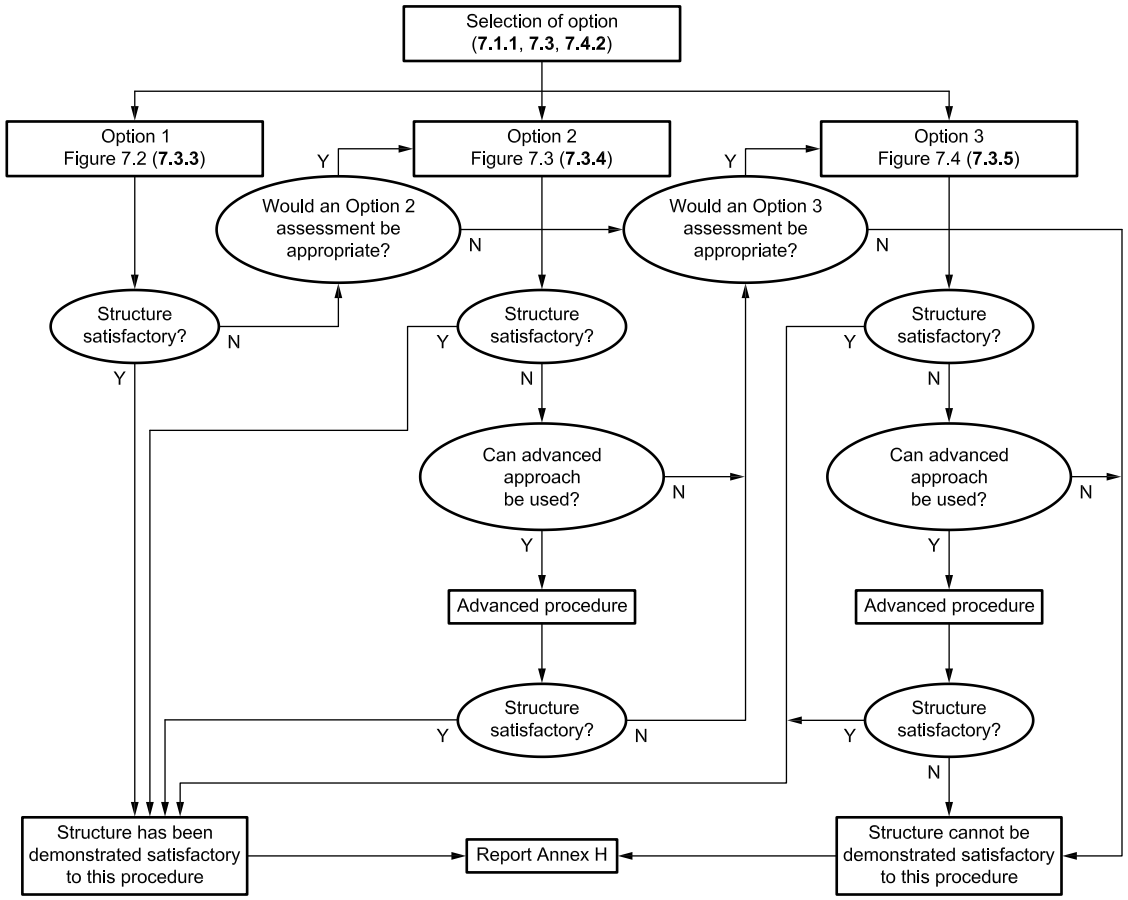
7.1.1 General

The background to this clause is given in references [7.1], [7.2], [7.3] and [7.4].

There are three options for fracture assessment in this clause, Options 1, 2 and 3, which use similar methods (**7.3**). Which one is used depends on the available materials properties and the level of conservatism required. A flowchart describing the various options is given in Figure 7.1.

NOTE The methods presented in this clause are based on the assumption that the primary stresses acting on the uncracked body are predominantly in the elastic range, i.e. below the yield strength of the material (so-called stress-based assessment). A method for strain-based assessment is given in Annex V.

Figure 7.1 **General flowchart for fracture assessment**



NOTE Advanced procedure could include consideration of weld strength mismatch, crack tip constraint, leak-before-break, etc.

Assessment is generally made by means of a failure assessment diagram (FAD) based on the principles of fracture mechanics. The vertical axis of the FAD compares the applied loading, in terms of the corresponding stress intensity factors, to the fracture toughness of the material. The horizontal axis is the ratio of the applied primary load to that required for plastic collapse. A failure assessment line (FAL) is plotted on the diagram. Calculations for a flaw provide either the co-ordinates of an assessment point or, in the case of crack growth, a locus of points. The positions of these are compared with the FAL to determine the acceptability of the flaw. Options 1 to 3 are shown in Figure 7.2 to Figure 7.4.

Figure 7.2 **Flowchart for Option 1 fracture assessment**

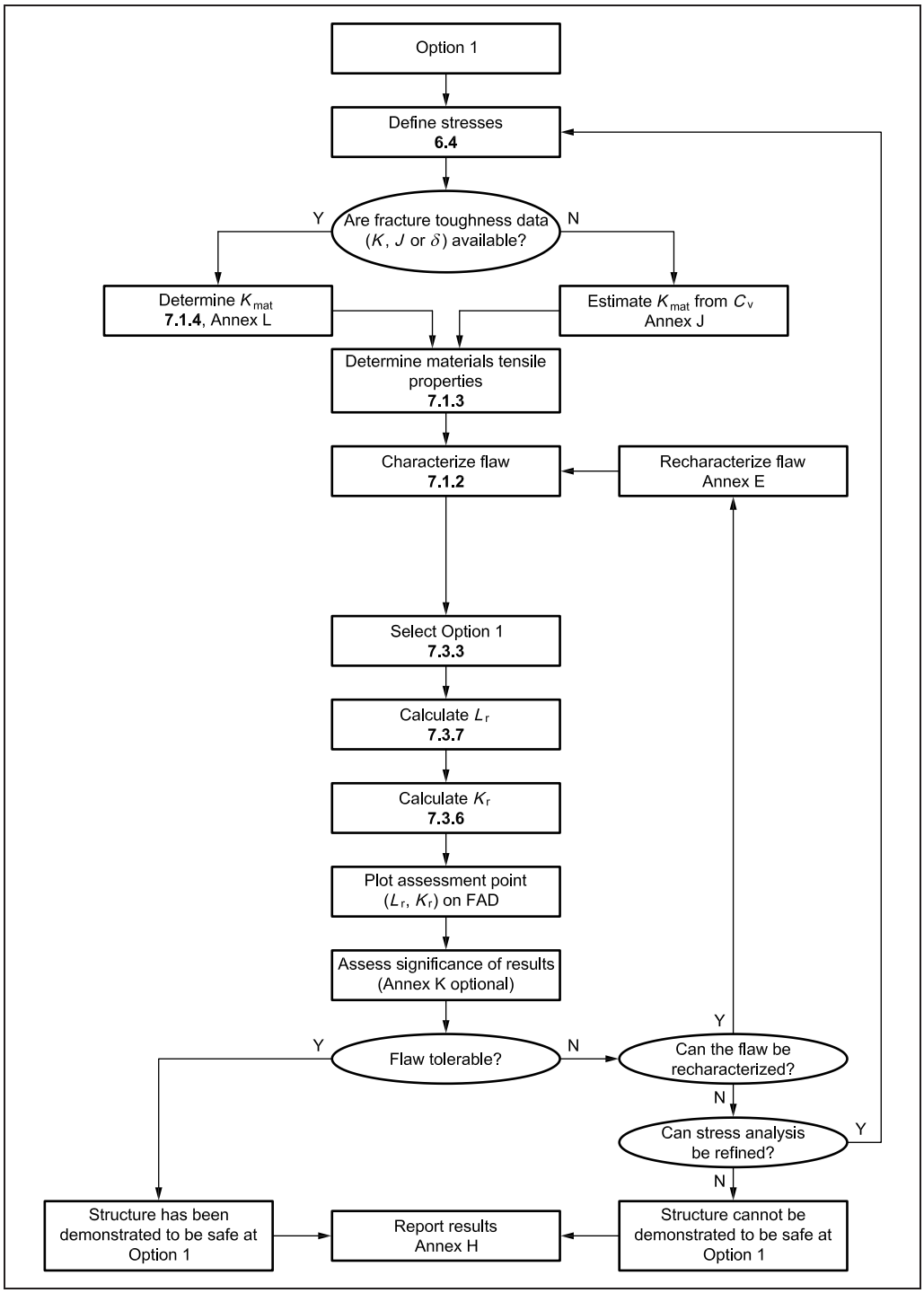


Figure 7.3 **Flowchart for Option 2 fracture assessment**

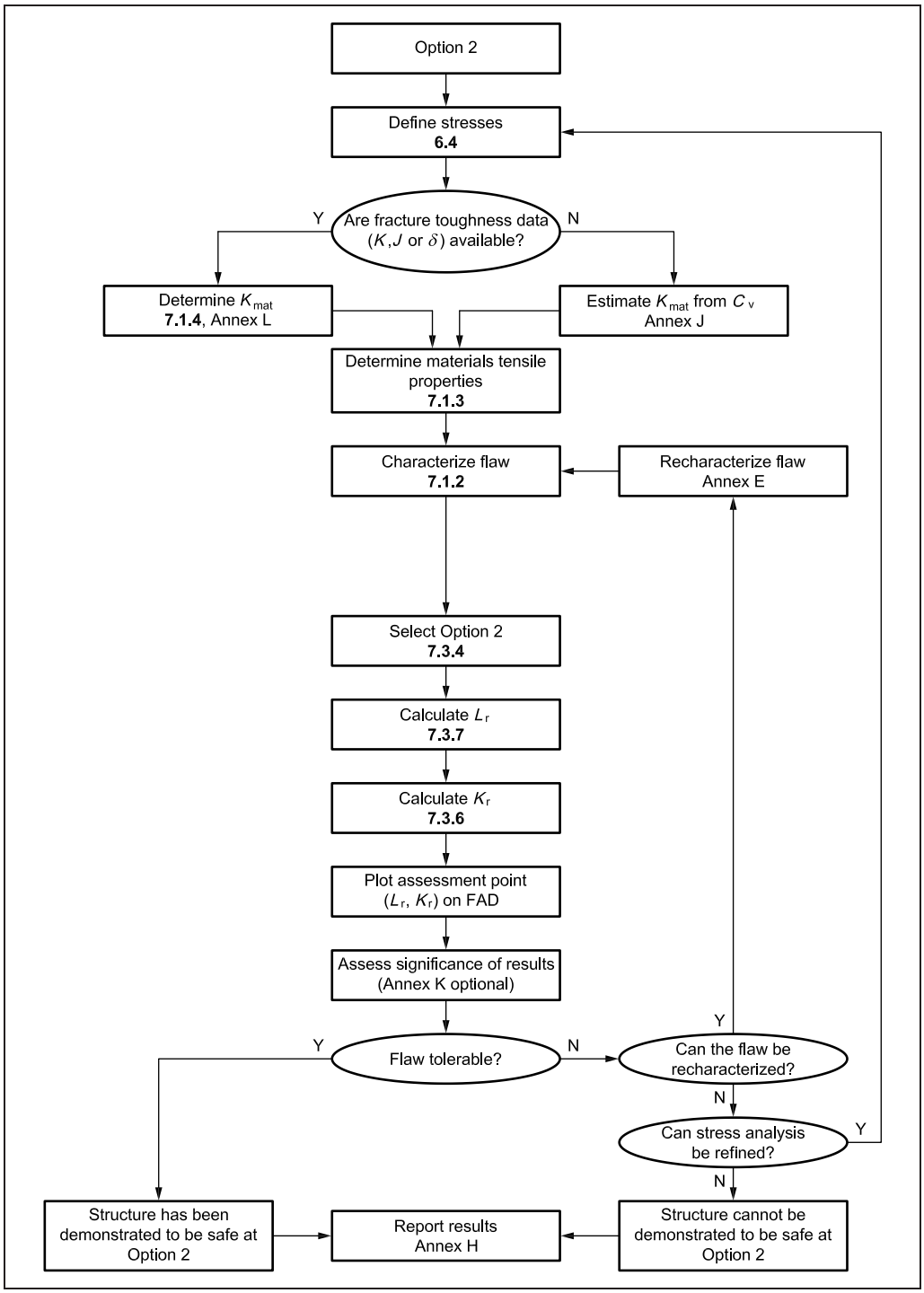
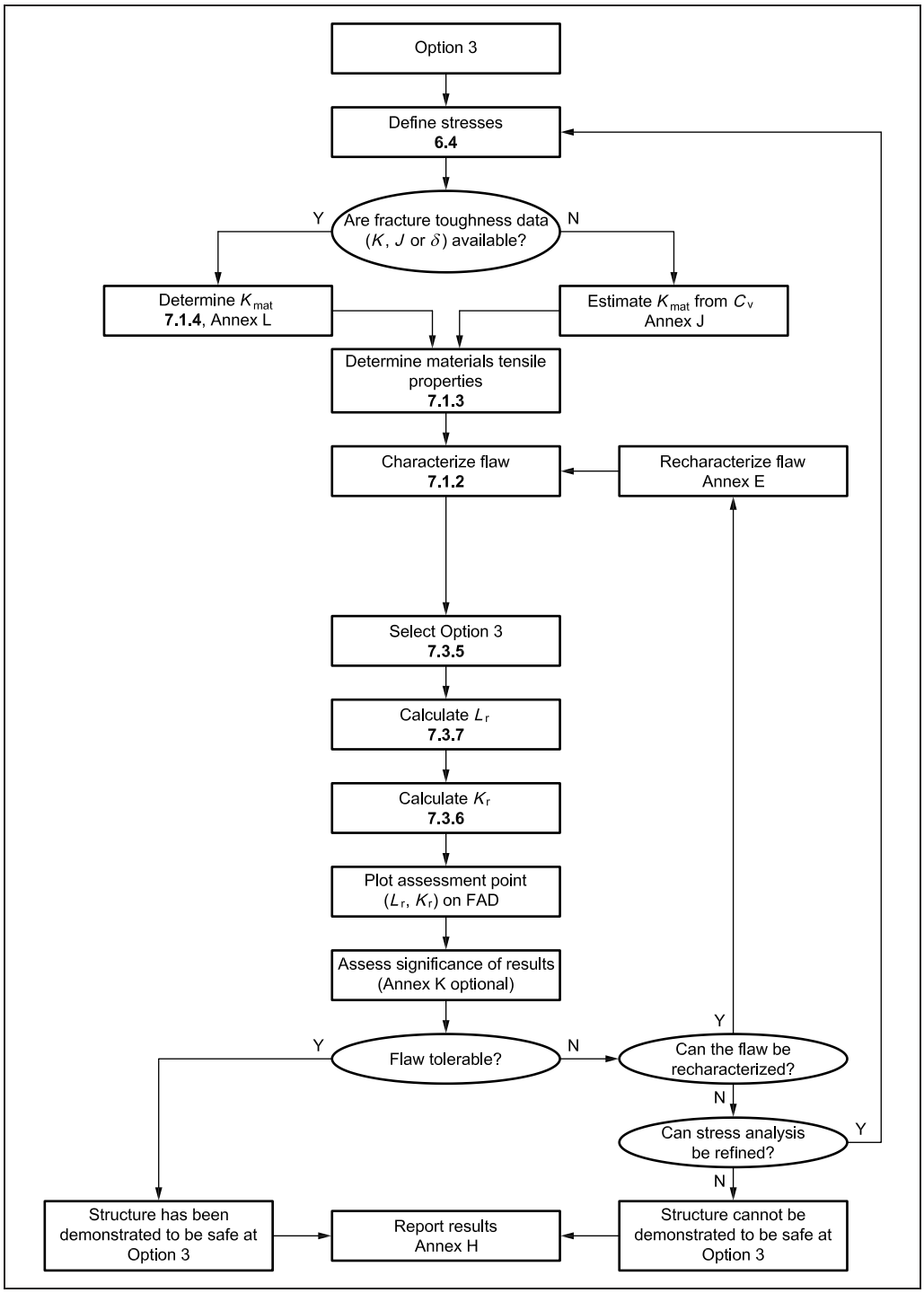


Figure 7.4 **Flowchart for Option 3 fracture assessment**



The acceptability of a flaw may be assessed directly or the calculation may be iterated in order to determine the limiting value of a parameter such as flaw size, applied load or fracture toughness.

The assessments using the FAD relate to planar flaws. Guidance on the assessment of other anomalies is given in **7.4.4**.

The assessments in this clause refer to tensile mode I loading only. Mixed mode loading is addressed in Annex A.

In some cases acceptability can be demonstrated when an initial assessment shows a flaw to be unacceptable. This can require improving the quality of the

input data, and/or applying a higher assessment option, or accounting for ductile tearing under increasing load.

In some cases, surface-breaking or embedded flaws are initially found to be unacceptable due to predicted ligament failure, but this might not be limiting. The flaw may then be re-characterized as a through-thickness or surface-breaking flaw and reassessed. The procedure for flaw re-characterization is given in Annex E.

For pressurized applications, a leak-before-break analysis might show that a stable leak would occur rather than a break (see Annex F).

The procedures in this clause assume that the region affected by the flaw consists of a single material. Advice on the appropriate materials properties in the case of a welded component is given in **7.1.3** to **7.1.7**, for tensile and fracture toughness properties. A procedure for performing a strength mismatch assessment which takes benefit from materials of higher strength in the vicinity of the flaw is given in Annex I.

The fracture toughness used in this clause is obtained following the advice in **7.1.4** to **7.1.7** and assumes conditions of high constraint at the crack tip. Low constraint conditions, as promoted for example by shallow flaws and predominantly tensile loading (e.g. when the through-wall bending stress is much smaller than membrane stress, as in a pipe), can lead to increased fracture toughness and hence increased margins in the assessment. A procedure that allows for conditions of low in-plane structural constraint is given in Annex N. Annex N should not be used in conjunction with Annex I.

7.1.2 Flaw dimensions and interaction

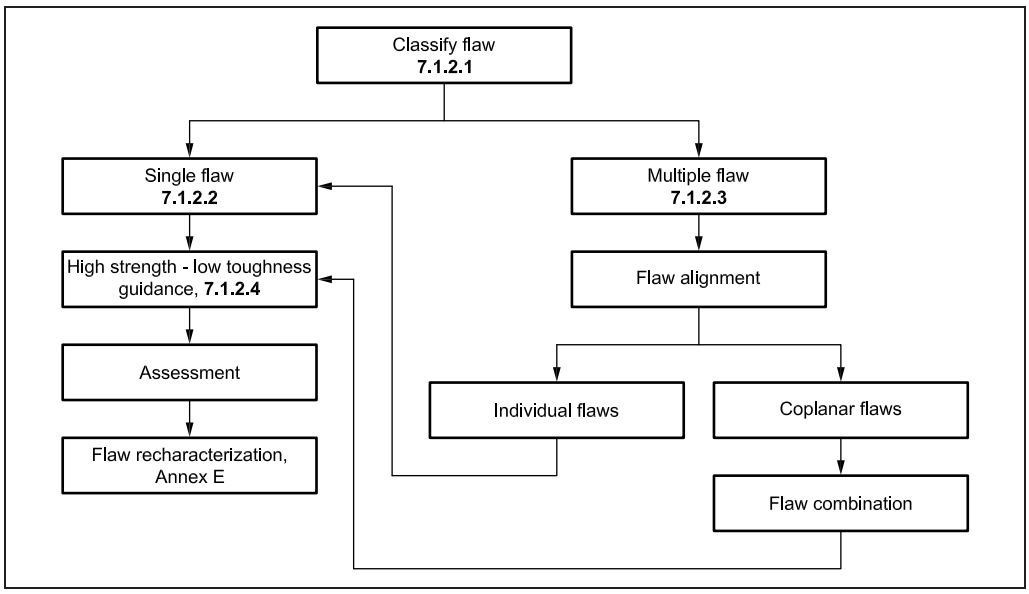
7.1.2.1 This subclause provides guidance on determining the flaw dimensions from non-destructive or other means of flaw detection. The guidance is given for individual flaws (single flaws) in **7.1.2.2** and for multiple flaws in **7.1.2.3**, where the interaction effects between neighbouring flaws in close proximity might require multiple flaws to be combined into a virtual larger flaw for the purpose of flaw assessment. Flaw interaction is normally assessed at the start and at the end of the evaluation interval incorporating any sub-critical crack growth during that interval. For cases of high strength/low toughness steels where cleavage is a concern, special consideration is required, as detailed in **7.1.2.4**. In cases where ligament failure might not be critical to the overall integrity of the component, flaw recharacterization may be performed as described in Annex E. A flowchart of the overall process of flaw characterization is given in Figure 7.5.

7.1.2.2 Single planar flaws should be characterized by the height and length of their containment rectangles. These dimensions are defined in Figure 7.6 as follows: 2*a* for through-thickness flaws; *a* and 2*c* for surface flaws; and 2*a* and 2*c* for embedded flaws. One side for the case of a surface flaw, and two (parallel) sides for the case of embedded flaws, should be aligned with the free surface nearest to the flaw and denoted as 2*c*. The remaining two sides should be orthogonal to the same free surface and denoted as *a* for surface flaws or 2*a* for embedded flaws. When it is demonstrated that it is conservative to do so and the appropriate stress intensity factor and reference stress solutions are used, it is permissible to construct a containment rectangle not aligned with the free surface.

7.1.2.3 Multiple planar flaws in close proximity can lead to an interaction and to more severe effects than single flaws alone. Simple criteria for interaction are given in Figure 7.7 and Figure 7.8, with the dimensions of the effective flaws after interaction. If multiple flaws exist, each flaw should be checked for interaction with each of its neighbouring flaws using the original flaw dimensions. Flaws on different cross-section planes should first be checked for alignment using the flaw alignment criteria in Figure 7.7. Aligned flaws or flaws that occur on the

same plane (coplanar flaws) should then be checked against the flaw combination criteria of Figure 7.8 and combined into a single flaw if necessary. It is not normally necessary to consider further interaction of a combined flaw with the neighbouring flaws. It is not necessary to apply flaw interaction criteria for fatigue assessment. However, if there is any uncertainty as to whether flaws are separate, they should be combined or specific calculations carried out.

Figure 7.5 **Flowchart for flaw characterization**



7.1.2.4 In high strength/low toughness materials the bounding flaw might not provide sufficient conservatism [7.5]. In such cases the maximum height of the flaw for surface flaws (actual or calculated tolerable flaw) or the larger of the two orthogonal flaw dimensions for embedded flaws (actual or calculated tolerable flaw) should be compared with the simplified calculation of Irwin's plastic zone size given by Equation (7.1):

$$a_{pl} = \frac{1}{\pi}\left(\frac{K_{mat}}{\sigma_Y}\right)^2 \quad (7.1)$$

where:

K_{mat} is determined in accordance with **7.1.4**;

σ_Y is determined in accordance with **7.1.3**.

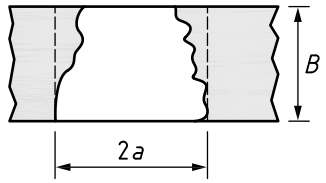
If the maximum flaw height or the larger of the two orthogonal flaw dimensions is less than the value from Equation (7.1), the normal assessment route is followed. Conversely, if the maximum flaw height or the larger of the two orthogonal flaw dimensions is greater than the value from Equation (7.1), one of the following routes should be followed:

a) actual flaws should be characterized as normal and the stress intensity factor(s) for the characterized flaw increased by 10%; or

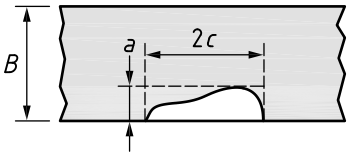
b) the actual flaws should be characterized so that the characterized flaw is increased by 20%, both in length and height.

The two approaches above provide a conservative characterization, but they do not necessarily produce the same assessment results. A sensitivity study should be undertaken. The acceptability of the flaws should normally be based on the more conservative assessment.

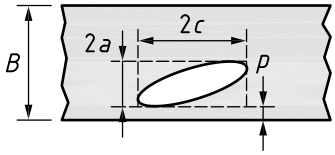
Figure 7.6 **Definitions of flaw dimensions**



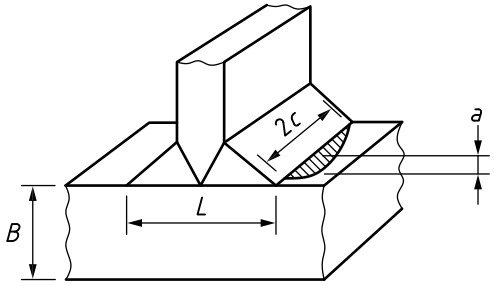
a) Through thickness flaw
(Required dimensions: *2a*, *B*)



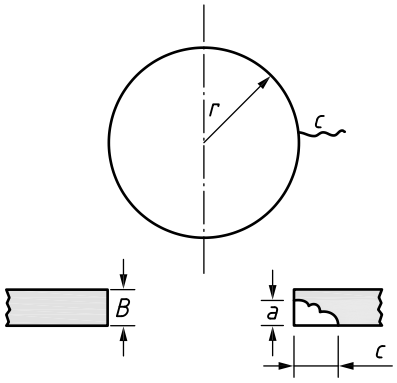
b) Surface flaw
(Required dimensions: *a*, *2c*, *B*)



c) Embedded flaw
(Required dimensions: *2c*, *p*, *2a*, *B*)



d) Flaw at toe of fillet weld
(Required dimensions: *2c*, *a*, *B*, *L*)



e) Flaw at hole
(Required dimensions: *c*, *a*, *B*, *r*)

Figure 7.7 **Flaw alignment rules for non-coplanar flaws**

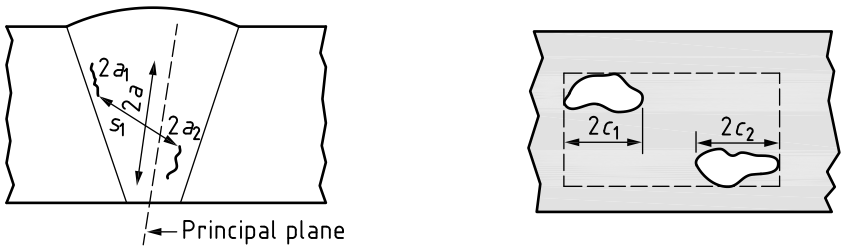
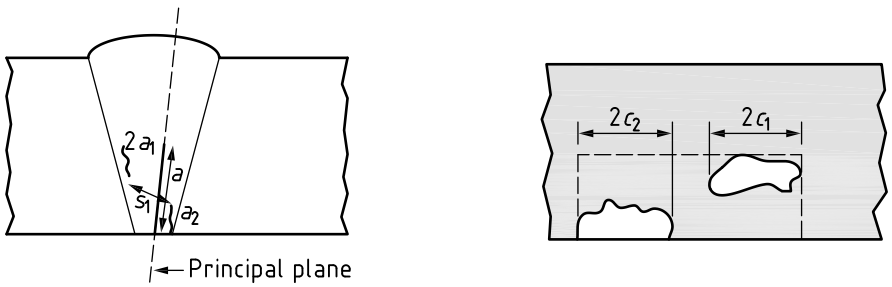
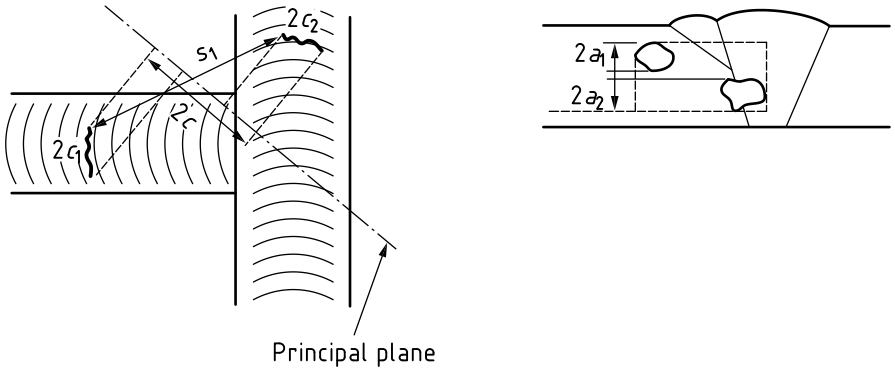
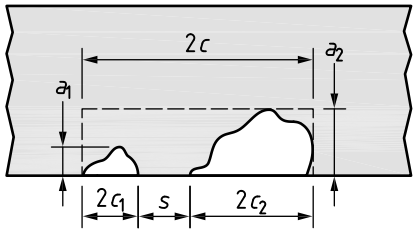
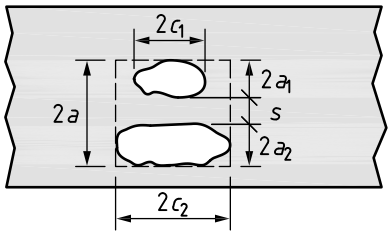
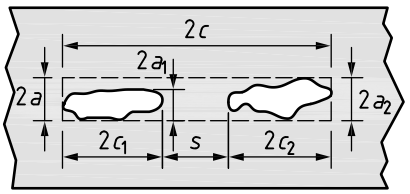
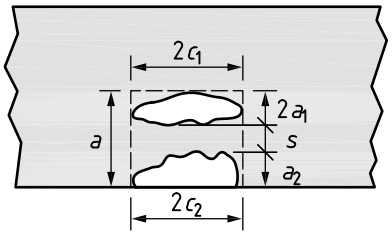
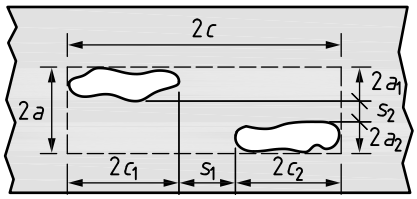
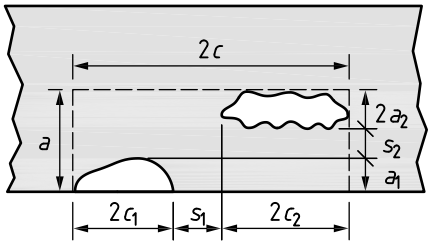
Schematic flaws	Criteria for alignment
 1) Principal plane normal to the maximum principal stress in weld 2) Projection of flaws onto the principal plane a) Adjacent non-coplanar	$s_1 \leq a_1 + a_2$
 1) Principal plane normal to the maximum principal stress in weld 2) Projection of flaws onto the principal plane b) Adjacent non-coplanar surface and embedded flaws	$s_1 \leq a_1 + a_2$
 c) Adjacent non-coplanar embedded flaws in intersecting welds	$s_1 \leq a_1 + a_2$

Figure 7.8 **Flaw interaction rules for coplanar flaws**

Schematic flaws	Criteria for interaction	Effective dimensions after interaction
 a) Coplanar surface flaws	$s \leq$ max. ($0.5a_1$, $0.5a_2$) for all flaws except a_1/B and a_2/B > 0.5 $s \leq$ max. (a_1, a_2) for flaws with a_1/B and a_2/B > 0.5	a = max. (a_1, a_2) $2c = 2c_1 + 2c_2 + s$
 b) Coplanar embedded flaws (interaction in thickness direction)	$s_1 \leq a_1 + a_2$	$2a = 2a_1 + 2a_2 + s$ $2c$ = max. ($2c_1$, $2c_2$)
 c) Coplanar embedded flaws (interaction in width direction)	$s \leq$ max. (a_1, a_2) for all flaws	$2a$ = max. ($2a_1$, $2a_2$) $2c = 2c_1 + 2c_2 + s$
 d) Coplanar surface and embedded flaws (interaction in thickness direction)	$s_1 \leq a_1 + a_2$	$a = 2a_1 + a_2 + s$ $2c$ = max. ($2c_1$, $2c_2$)
 e) Coplanar embedded flaws (interaction in thickness and width direction)	$s_1 \leq$ max. (a_1, a_2) for all flaws and $s_2 \leq a_1 + a_2$	$2c = 2c_1 + 2c_2 + s_1$ $2a = 2a_1 + 2a_2 + s_2$
 f) Coplanar surface and embedded flaws (interaction in both thickness and width direction)	$s_1 \leq$ max. ($0.5a_1$, a_2) for all flaws and $s_2 \leq a_1 + a_2$	$a = a_1 + 2a_2 + s_2$ $2c = 2c_1 + 2c_2 + s_1$

7.1.3 Tensile properties

7.1.3.1 Tensile test properties

The material yield strength, σ_Y, tensile strength, σ_U, and modulus of elasticity, E, are required for assessment of fracture resistance. They should be determined in accordance with BS EN ISO 6892-1, BS EN ISO 6892-2 or BS EN ISO 6892-3 at the appropriate temperature and strain rate. Where possible, the longitudinal axis of the tensile specimen should be normal to the plane of the flaw being assessed. However, in the case of welds, where this is impractical (because welds are generally narrow compared to the size of a tensile specimen), it is acceptable to employ tensile specimens which are parallel to the longitudinal axis of the weld. Unless specific solutions are available to assess the effect of weld strength mismatch (see Annex I and Annex P), safe assessments can be made of flaws located in welded regions (weld metal and HAZ) if the tensile properties assumed are the lower of the parent metal, weld metal or HAZ. For assessment Options 2 and 3 the full stress-strain curve is required.

NOTE 1 Unless otherwise stated, guidance given on tensile properties refers to the engineering definitions of tensile properties determined under quasi-static loading conditions. Where assessments consider dynamic loading, tensile properties need to be established for the appropriate loading rate.

NOTE 2 Materials are generally non-isotropic. Tensile properties depend on processing history and specimen orientation. Where the flaw orientation is not known, the tensile specimen orientation needs to be representative of the lowest yield strength direction.

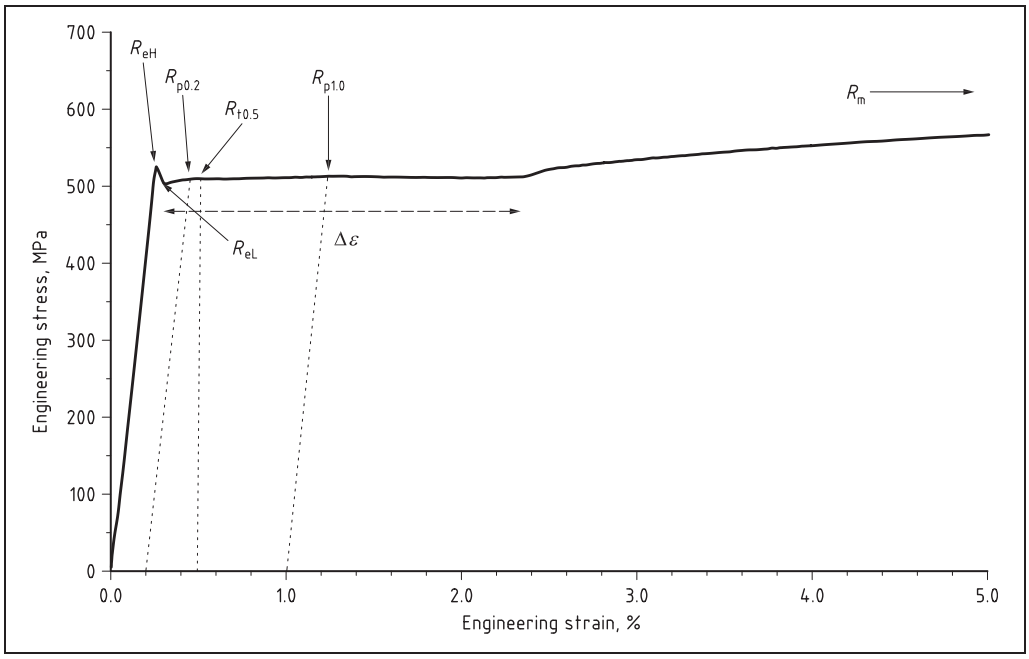
When an assessment is conducted according to the Option 1 FAD, yield strength, σ_Y, corresponds to $R_{p0.2}$, R_{eL} or $R_{t0.5}$ as described in BS EN ISO 6892-1 and in a number of material specification standards. Some steel product standards define yield strength in terms of the upper yield strength, R_{eH}. For the purposes of this British Standard, σ_Y is then to be considered as $0.95R_{eH}$. When an assessment is conducted to Options 2 or 3, yield strength corresponds to $R_{p0.2}$ or $R_{p1.0}$ for ferritic or austenitic steels, respectively. Tensile strength, σ_U, corresponds to R_m. These definitions are listed in Table 7.1 and illustrated in Figure 7.9.

Table 7.1 **Engineering definitions of yield and tensile strengths for Options 1, 2, 3**

Definition	Option 1	Option 2	Option 3
0.2% offset to elastic slope	$R_{p0.2}$	$R_{p0.2}$	$R_{p0.2}$
1% offset to elastic slope	$R_{p1.0}$	$R_{p1.0}$	$R_{p1.0}$
Lower yield strength	R_{eL}	—	—
Strength at 0.5% strain	$R_{t0.5}$	—	—
95% upper yield strength	$0.95R_{eH}$	—	—
Tensile strength	R_m	R_m	R_m

 © The British Standards Institution 2019

Figure 7.9 **Definition of terms used in tensile testing**



*NOTE 3 Unless HAZ softening is present, the yield and tensile strengths of the HAZ do not need to be determined. HAZ softening and the strength associated with this can be estimated from hardness tests (see **7.1.3.7**).*

The shape of the knee region of the FAD is critically dependent on the quality of the stress-strain data from the limit of proportionality up to approximately 2% strain. Consequently, there should be sufficient data to define this region adequately.

*NOTE 4 When it is necessary to define a strain hardening coefficient for the material, n, the slope of the plastic component of ln (σ) versus ln (ε) curve is used (see **7.1.3.5**).*

7.1.3.2 Statistical variations

Statistical variations in experimental tensile properties should be taken into account. Depending on the type of assessment being conducted, it is normally necessary to use either lower bound or mean properties. For stress-based assessments, the mean minus two standard deviation tensile properties are used in calculations of K_r and L_r for the assessment points, while the mean tensile properties are used to determine the failure assessment line of the FAD and to estimate $L_{r,max}$. For the estimation of residual stresses where direct measurements have not been made, the starting point for the calculations for Option 1 assessments is 1.1 times the specified minimum yield strength. For Option 2 and 3 assessments it is the mean yield strength.

When it is necessary to estimate lower bound tensile properties and there are insufficient data to estimate the standard deviation with confidence, the coefficient of variation (COV), which is the ratio of the standard deviation to the mean (given in Table 7.2 for ferritic steels), may be used. Here, the experimentally determined value is treated as the mean value.

NOTE When the assessment is conducted using specified minimum values defined in a material specification, these values may be considered as representing lower bounds at the temperature defined by the specification and no further correction for statistical variation is necessary (e.g. for calculation of L_r). However, residual stresses are governed by the actual yield strength of the material, and to allow for this, a 10% increase in the specified yield strength is made.

Table 7.2 **Coefficient of variation (COV) for tensile properties for ferritic steels**

Variable	COV
Elastic modulus, E	0.05
Yield/proof strength, σ_Y, $R_{p0.2}$, etc. of parent material	0.07
Tensile strength, σ_U, of parent material	0.05
Yield and tensile strength of welds	0.10

7.1.3.3 Elastic modulus and Poisson's ratio

Special testing procedures and instrumentation are required to determine elastic modulus and Poisson's ratio. If reliable information is not available, the values given in Table 7.3 may be used without any further correction for statistical variations. For steels Poisson's ratio is 0.3.

NOTE Moduli for a wide range of steels and temperature are given in the ASME Boiler and Pressure Vessel Code, Section II, Part D, and these may be used.

Table 7.3 **Elastic modulus**

Temperature °C	Ferritic steels N/mm^2	Austenitic steels N/mm^2
–200	219 000	208 000
–150	215 000	205 000
–100	212 000	203 000
–75	210 000	201 000
–50	209 000	200 000
0	206 000	197 000
25	205 000	195 000
50	203 000	193 000
100	201 000	190 000
150	198 000	187 000
200	195 000	183 000
250	191 000	179 000
300	187 000	176 000
350	182 000	172 000
400	177 000	169 000
450	171 000	165 000
500	164 000	160 000
550	156 000	156 000
600	146 000	151 000
650	135 000	146 000

7.1.3.4 Assessment temperature

When tensile properties are unavailable for the assessment temperature, the following empirical-based corrections have been found to be useful and should be applied to ferritic steels for data obtained at room temperature after correction for statistical variations (see **7.1.3.2**) where appropriate.

When the assessment temperature is below room temperature and above −196 °C:

$$\sigma_{Y(\text{at low temperature})} = \sigma_{Y(\text{at room temperature})} + \frac{10^5}{(491 + 1.8T)} - 189 \quad (7.2)$$

Tensile strength, σ_U, at temperatures below room temperature can be estimated from the room temperature value, as follows:

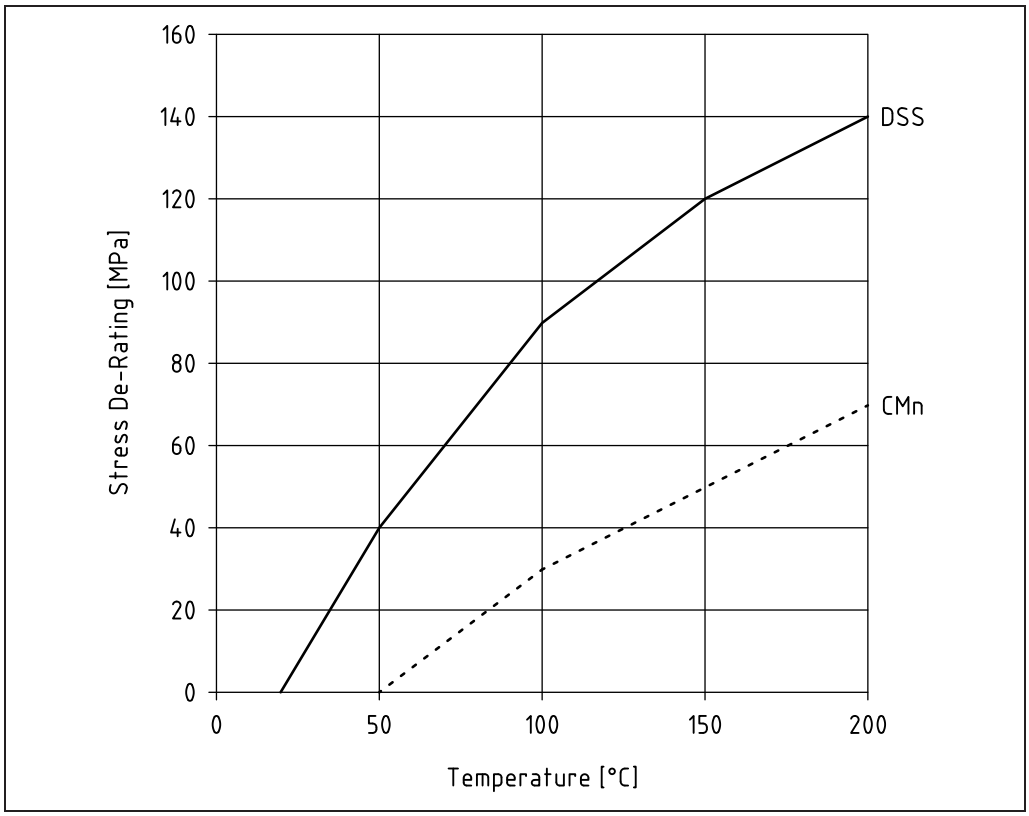
$$\sigma_{U(\text{at low temperature})} = \sigma_{U(\text{at room temperature})} \times \left[0.7857 + 0.2423 \exp\left(-\frac{T}{170.646}\right)\right] \quad (7.3)$$

NOTE 1 Equation (7.2) is from BS EN ISO 15653, whilst Equation (7.3) is based upon an unpublished statistical analysis of data from a wide range of steels. Both equations are based on empirical data and might converge at some temperature.

When the assessment temperature is above room temperature there is generally a decrease in yield or proof strength and tensile strength. For ferritic C-Mn steels (with specified minimum yield strengths in the range 245 N/mm^2 to 485 N/mm^2) and duplex stainless steels (with specified minimum yield strengths up to 550 N/mm^2), room temperature strength should be reduced or de-rated in accordance with Figure 7.10 (see DNVGL-ST-F101 [7.7]). Figure 7.10 should not be extrapolated to temperatures above 200 °C without supporting evidence.

NOTE 2 In steels that are sensitive to dynamic strain ageing, the tensile strength increases with temperature over the range shown in Figure 7.10. However, in general, the de-rating given here is conservative for the purposes of assessment.

Figure 7.10 **De-rating values for yield/proof strength and tensile strength at temperatures above room temperature in C-Mn steels and duplex stainless steels**



7.1.3.5 Stress-strain curve

When an engineering stress-strain curve is unavailable, the following approach may be used as an alternative to that implied by the Option 1 FAD. The stress-strain curve up to the tensile strength for ferritic steels is derived from yield/proof strength, tensile strength and uniform elongation using the following method:

$$\varepsilon = \frac{\sigma}{E} + \frac{A_r \sigma_Y}{E}\left(\frac{\sigma}{\sigma_Y}\right)^n \tag{7.4}$$

$$A_r = \frac{E\varepsilon_Y}{\sigma_Y} - 1 \tag{7.5}$$

$$n = \frac{\log_{10}[(E\varepsilon_u/\sigma_U) - 1] - \log_{10}[(E\varepsilon_Y/\sigma_Y) - 1]}{\log_{10}(\sigma_U/\sigma_Y)} + 1 \tag{7.6}$$

If ε_U is not available, a value of 5% can be assumed.

An alternative to Equation (7.6) (see references [7.8] and [7.9]) is to derive the strain hardening exponent from the following equation:

$$n = \frac{1}{0.3\left[1 - \left(\frac{\sigma_Y}{\sigma_U}\right)\right]} \tag{7.7}$$

*NOTE 1 Equations (7.4) to (7.6) are modifications to the Ramberg-Osgood equation for steels showing continuous yielding behaviour. Equation (7.7) was derived from ferritic steels with yield/proof strengths in the range 300 MPa to 1 000 MPa and $0.65 < \sigma_Y/\sigma_U < 0.95$. This is a lower bound estimate of strain, and so it overestimates the true hardening behaviour of the material, i.e. underestimates n. Discontinuous yielding is addressed in **7.1.3.6**.*

NOTE 2 With the appropriate choice of variables, these equations have been found to be useful in providing smooth mean stress-strain curves fitted to experimental data for generating failure assessment lines for Option 2 and Option 3 FADs.

7.1.3.6 Yield discontinuity/Lüders strain

C-Mn steels can exhibit a yield discontinuity (Lüders strain or yield plateau) in the stress-strain curve, as illustrated in Figure 7.9. Guidance on susceptibility to Lüders strain for rolled steel plates is given in Table 7.4, for cases where data are not available. Owing to the wide range of factors affecting the shape of the stress-strain curves in pipelines, such as processing history, coating heat treatment and installation strains, it is recommended that unless a large data set of similarly-processed pipes exists on which to base the assumption of type of stress-strain curve, testing should be carried out on pipe samples in the same condition and relevant orientation in which the assessment is to be made. If there is uncertainty or data are not available, a Lüders plateau should be assumed for $L_r \geq 1$ and no yield plateau for $L_r < 1$.

 © The British Standards Institution 2019

Table 7.4 **Guidance for determining whether yielding is continuous or discontinuous in rolled steel plate**

Yield strength range, N/mm^2	Process route	Composition aspects	Heat treatment aspects	Assume yield plateau (discontinuous yielding) [A]
$R_{eH} \leq 350$	As-rolled	Conventional steels, e.g. BS EN 10025-2 [B] grades without microalloy additions	NA	Yes
		Mo, Cr, Nb, Al or Ti present	NA	(No)
	Normalized	BS EN 10025-2 type compositions without microalloy additions	Conventional normalizing	Yes
		BS EN 10025-3 type compositions with microalloy additions	Conventional normalizing	Yes
	Controlled rolled	BS EN 10025-3 and BS EN 10025-4 compositions	—	Yes
$R_{eH} > 350$	Controlled rolled	BS EN 10025-3 and BS EN 10025-4 compositions	Light TMCR schedules ($R_{eH} < 400$)	Yes
			Heavy TMCR schedules ($R_{eH} > 400$)	(Yes)
$R_{eH} \leq 500$	Quenched and tempered	Mo or B present with microalloy additions Cr, V, Nb or Ti	Heavy tempering favours plateau	Yes
			Light tempering favours no plateau	(Yes)
		Mo or B not present but microalloy additions Cr, V, Nb or Ti are (V has a particularly strong effect)	Heavy tempering	(Yes)
			Light tempering	(No)
$R_{p0.2}$ or $R_{eH} > 500$	Quenched and tempered	Mo or B present with microalloy additions Cr, V, Nb or Ti	Tempering to $R_{p0.2} <$ ~690	(No)
			Tempering to $R_{p0.2} >$ ~690	No
		Mo or B not present but microalloy additions Cr, V, Nb or Ti are	Tempering to $R_{p0.2} <$ ~690	Yes
			Tempering to $R_{p0.2} \geq$ ~690	(No)
$R_{p0.2} \leq 1\,000$	As-quenched	All compositions	NA	No

[A] Text in brackets indicates that there is uncertainty and a sensitivity analysis should be conducted to establish the effect the presence or absence of a yield plateau has on the assessment.

[B] Yield strength in Table 7.4 is defined as the upper yield, R_{eH}, to harmonize with the relevant standards.

The extent of the Lüders strain, $\Delta\varepsilon$, is estimated from:

$$\Delta\varepsilon = 0.037\,5(1 - 0.001\sigma_Y) \text{ for } \sigma_Y \leq 1\,000 \text{ N/mm}^2 \quad (7.8)$$

where:

σ_Y is the yield strength.

Equation (7.8) may be used in conjunction with Equation (7.4) to estimate the stress-strain curve for material which Table 7.4 indicates has a Lüders plateau. This is achieved by employing Equation (7.4) to obtain strain up to the yield strength and then adding the $\Delta\varepsilon$ increment from Equation (7.8) to the calculated strains; then Equation (7.4) is re-applied for stress equal to and exceeding the yield strength, always adding the increment from Equation (7.8) to the strain used in calculating stress from Equation (7.4), up to the tensile strength.

7.1.3.7 Tensile properties from hardness

When tensile data are not available from C-Mn steels, yield/proof strength and tensile strengths (in MPa) at room temperature can be estimated from measured Vickers hardness (HV_{10}) as follows (see BS EN ISO 15653):

Parent metal:

$$\sigma_Y = 3.28HV_{10} - 221, \text{for } 160 < HV_{10} < 495 \quad (7.9)$$

$$\sigma_U = 3.3HV_{10} - 8, \text{for } 100 < HV_{10} < 400 \quad (7.10)$$

Weld metal:

$$\sigma_Y = 2.35HV_{10} + 62, \text{for } 170 < HV_{10} < 330 \quad (7.11)$$

$$\sigma_U = 3.0HV_{10} + 22.1, \text{for } 170 < HV_{10} < 330 \quad (7.12)$$

Hardness measurement is subject to scatter, and a sufficient number of tests should be carried out to determine mean hardness with confidence for use in Equation (7.9) to Equation (7.12). The effect of scatter in the estimate of tensile properties should be taken into account (see **7.1.3.2**).

If HAZ softening is observed, Equations (7.9) and (7.10) should be used to estimate tensile properties.

7.1.3.8 Engineering and true-stress strain

True stress, σ_t, and true strain, ε_t, can be determined from engineering stress, σ, and strain, ε, as follows:

$$\sigma_t = \sigma(1 + \varepsilon) \quad (7.13)$$

$$\varepsilon_t = \ln(1 + \varepsilon) \quad (7.14)$$

7.1.4 Fracture toughness

7.1.4.1 Fracture toughness should be established in accordance with recognized national testing standards (e.g. BS 7448, ISO 12135, BS EN ISO 15653, BS 8571, ASTM E1820, ASTM E1921) and reported in terms of *J*-integral from the test record wherever possible. If only crack tip opening displacement (CTOD) values are available these are converted into *K* equivalents according to **7.1.4.6**. The results employed in assessments should fulfil the qualification requirements specified by the standards. If full qualification to a testing standard is not achieved, additional tests are advisable. If it is not possible to test additional specimens, careful consideration of the results is required to ensure that fracture toughness is not overestimated. This is particularly important when specimens fail by brittle fracture since the fracture toughness can be particularly sensitive to deviations from the qualification requirements specified by testing standards. Where possible, the crack orientation, strain rate (see **7.1.6.2**), environmental conditions [7.10] and crack tip microstructure employed in the fracture

 © The British Standards Institution 2019

toughness specimen should be representative of the flaw being assessed. If the microstructure at the flaw location is unknown, data representing the lowest toughness microstructure present in the component need to be generated. Further guidance is provided in Annex L.

NOTE The following list, by no means exhaustive, highlights some of the factors that can produce overestimates of fracture toughness:

- *minimum fatigue precrack length less than specified in the standard;*
- *uneven fatigue precrack shape (depending on the shape, this can either increase or decrease fracture toughness);*
- *fatigue precrack plane not the same as the machine notch (e.g. a twist in the plane of the fatigue precrack);*
- *fatigue precracking force exceeds the limit imposed by the standard;*
- *crack tip not in target microstructure;*
- *the test terminates in cleavage and the temperature is higher than that of the component being assessed;*
- *fracture toughness determined at a quasi-static loading rate while structure is subjected to dynamic loading. This is more likely to be a problem with ferritic/bainitic steels. Depending on the position of the result in the transition curve, this can either increase or decrease fracture toughness. Further guidance is given **7.1.6.2**.*

7.1.4.2 Particular attention is drawn to the importance of ensuring that all results in a data set represent similar microstructures. In particular, tests conducted on welds (HAZ, and weld metal) should have the crack tips in similar microstructures. Considerable variability between specimens can occur due to the crack tip being located in different microstructural regions. It might be necessary to carry out post-test metallography of a specimen testing a weld and, in particular HAZ, to determine the precise location of the crack tip. Results analysed as a set should include only data from tests in which the crack tip is confirmed to be located in microstructure of similar type.

Specimens should test the microstructure present at the flaw being assessed. However, generally, this is not known with precision. Consequently, the specimen should be targeted to test the microstructure with the lowest toughness microstructure present at the expected flaw location. Annex L provides further guidance on this.

NOTE Further information about post-test metallography conducted on weld specimens is given in BS EN ISO 15653.

7.1.4.3 For ferritic/bainitic steels it is particularly important that fracture toughness data are generated at a temperature not exceeding that of the structural component being assessed.

7.1.4.4 It is common practice to use fracture toughness specimens that are representative of the thickness of the component being assessed and at least three full-thickness specimens are tested. However, the number of tests required depends on fracture behaviour, the assessment option chosen, and the confidence required in the assessment and this is addressed in **7.1.6.1** and **7.1.7**.

7.1.4.5 When fracture toughness has been determined using specimen geometries other than deeply notched bend (SENB) or compact tension (CT) defined in the standards referred to in **7.1.4.1**, care should be taken to ensure that the crack tip constraint generated in the specimen is not less than that generated by the flaw in the component to be assessed.

NOTE 1 Low constraint specimens, such as shallow notched bend (BS EN ISO 15653) or tension (SENT, BS 8571) specimens are sometimes used in order to achieve a closer approximation to the crack tip constraint in the structural component and/or to test weld regions that are relevant to the location of the flaw. Crack tip constraint (as well as fracture toughness and failure mode) can change with increases in crack depth in such specimens. A common use of the SENT specimen is for the determination of fracture toughness used in the assessment of steel pipeline girth welds (see BS 8571, DNVGL-RP-F108 [7.6]).

NOTE 2 Annex N gives further information on the calculation and application of crack tip constraint conditions.

7.1.4.6 Fracture toughness is required to be converted into a critical stress intensity factor, K_{mat}. When fracture toughness has been determined using *J*-integral:

$$K_J = \sqrt{\frac{EJ}{1-\nu^2}} \tag{7.15}$$

When fracture toughness has been obtained in terms of crack tip opening displacement (CTOD or δ) using deeply-notched, high constraint bend specimens:

$$K_\delta = \sqrt{\frac{m\sigma_Y \delta E}{1-\nu^2}} \tag{7.16}$$

$$m = 1.517\left(\frac{\sigma_Y}{\sigma_U}\right)^{-0.3188} \quad \text{for } 0.3 < \sigma_Y/\sigma_U < 0.98 \tag{7.17}$$

E and σ_Y are required at the same temperature as the fracture toughness test.

If Equation (7.17) cannot be used, m should be set to a value of 1.5.

NOTE 1 This conversion from CTOD is intended to be applied when historical data are available and it is not possible to determine the J-integral from the test record (fracture toughness testing standards such as BS 7448, BS EN ISO 15653, ISO 12135 and ASTM E1820 describe appropriate procedures for determining J-integral).

NOTE 2 Equation (7.17) was derived from experimental tests conducted on deeply notched bend specimens. It is considered that conservative results will be obtained if the equation is applied to CTOD results obtained from SENT specimens. However, SENT tests conducted to BS 8571 enable J to be determined directly.

*NOTE 3 If tensile properties are not available at the fracture toughness test temperature, information on the variation of E, σ_Y and σ_U with temperature is given in **7.1.3.3** and **7.1.3.4**.*

The mean values of tensile properties (σ_Y and σ_U) should be used for the appropriate crack tip location employed in the fracture toughness test. However, if specific tensile data are not available for tests on the weld heat affected zone, the lesser of the weld metal or parent material tensile properties should be assumed.

7.1.4.7 Normally fracture toughness data would be generated using full thickness specimens (see **7.1.4.4**). However, fracture toughness can be established using sub-sized specimens provided that certain conditions are met (see **7.1.5**).

7.1.4.8 When the material is ductile, or steel is on the upper shelf, K_{mat} is obtained for the same crack extension (e.g. $J_{0.2BL}$) or K_{mat} is related to crack extension by a *J* resistance curve. In both cases a resistance curve is derived in accordance with the testing standard (e.g. BS 7448-4, BS 8751, ISO 12135, ASTM E1820). A lower bound to the experimental data should be employed to ensure conservatism.

NOTE 1 The lower bound can be a curve parallel to the mean curve derived from a best fit to the data, transposed to pass through the lowest experimental result for the range of crack extension for which the assessment is to be conducted.

NOTE 2 When the material is fully ductile, the recommendation is to derive a resistance curve rather than to use values of fracture toughness at maximum load (K_m, J_m). Use of a resistance curve provides the best descriptor of fracture toughness and enables greater flexibility when conducting the ECA.

7.1.4.9 If any of the resistance curve tests terminate in unstable fracture, either by cleavage in ferritic/bainitic steels or by ductile instability, the reason for this should be investigated. Post-test metallography might be necessary to establish whether or not the amount of prior stable crack extension was a result of a favourable positioning of the crack tip with respect to the microstructures present. A different crack tip position might result in less stable crack extension before fracture and lower fracture toughness. This is more likely to be a problem in inhomogeneous materials such as welds.

7.1.4.10 The resistance curve should not be used in the integrity assessment beyond the limit of crack extension defined by the testing standard, or beyond the lowest crack extension prior to unstable fracture observed in any of the test specimens, without justification.

7.1.5 Treatment of results from sub-sized fracture toughness specimens

7.1.5.1 Fracture toughness may be determined using specimens thinner than the component thickness provided that results from steels which terminate in cleavage fracture (termed δ_c, δ_u, or J_c, J_u) are corrected for size effects as described in **7.1.5.2**. When material behaves in a fully ductile manner (on the upper shelf), initiation fracture toughness (termed $\delta_{0.2BL}$, or $J_{0.2BL}$) or resistance curve data (see BS 7448-4) are used in the assessment. In this case, no size correction is necessary, provided that the data are not applied beyond the qualification limitations imposed by the testing standard (i.e. limitations on amount of crack extension permitted and maximum J/δ values).

7.1.5.2 When fracture toughness has been determined using sub-sized specimens (i.e. less than the component thickness) and the tests terminate in cleavage fracture, the following correction is applied to each test result to provide fracture toughness, K_B, for the equivalent full-thickness of the component.

$$K_B = 20 + (K_b - 20) \times \left(\frac{b}{B}\right)^{0.25} \tag{7.18}$$

NOTE Units for K_B and K_b are MPa$\sqrt{m}$.

7.1.5.3 Equation (7.18) is used if both of the following conditions are met:

a) there is limited ductile crack extension prior to cleavage and Δa does not exceed the lesser of $0.05(W - a_0)$ or 1 mm; and

b) fracture takes place under small scale yielding conditions defined as:

$$K_b < K_{Jc(limit)} \tag{7.19}$$

$$K_{Jc(limit)} = \left[\frac{Eb_0\sigma_Y}{(1 - \nu^2)30}\right]^{0.5} \tag{7.20}$$

NOTE 1 In this equation, units for $K_{Jc(limit)}$ are MPa$\sqrt{m}$, and units for b_0 are m.

*NOTE 2 Note 2 of **7.1.4.6** is applicable here.*

7.1.5.4 If condition **7.1.5.3**a) is not met, K_b is replaced by the highest K_b achieved in the set of tests conducted where the condition is achieved. If condition **7.1.5.3**b) is not met, K_b is set equal to $K_{Jc(limit)}$. If neither condition is met, the lower of the two is used.

*NOTE As an alternative, the Master Curve approach described in **7.1.7.6** and Annex L may be used.*

7.1.6 Number of tests

7.1.6.1 Assessments conducted to Option 1, or Option 2 where advantage is not taken of constraint loss according to Annex N, have, historically, been based on K_{mat} derived from the minimum of three similar test results (i.e. the minimum of three values based on K_J or K_B). This has been considered appropriate when the specimen thickness is representative of the component thickness, all specimens test the same microstructure, all fail by brittle fracture (e.g. J_c, J_u), all represent ductile behaviour for the same crack extension (e.g. $J_{0.2BL}$), or all are ductile giving maximum load behaviour (J_m). When there is mixed fracture behaviour, i.e. J_c, J_u mixed with J_m, or all are maximum load values, i.e J_m, then J_m results are treated as virtual fractures and replaced by the $K_{Jc(limit)}$ defined by Equation (7.20). If the minimum individual value of fracture toughness is less than 70% of the average of the three censored data, or if the maximum is more than 140% of the average of the three censored data, scatter is considered excessive and additional test data are necessary. If these criteria are met then the minimum value represents K_{mat} for the flaw assessment.

Higher confidence in the assessment can be obtained if more than three tests are conducted (see Note 1) and the statistical analysis procedures in **7.1.7** are employed. Further information is given in reference [7.11]. Flowcharts summarizing the procedures to be followed when there are between three and five results, and six and more results, are given in Figure 7.11 and Figure 7.12, respectively. More than three tests are necessary when advantage is taken of constraint loss (according to Annex N), and the statistical analysis procedures in **7.1.7.3** should be employed.

*NOTE 1 With reference to Figure 7.11 and Figure 7.12, when there are fewer than six tests and the relevant criteria are achieved, the minimum value represents K_{mat} for the flaw assessment. However, when there are six or more results the statistical treatment described in **7.1.7** is available for the selection of K_{mat}.*

NOTE 2 The minimum of three nominally identical tests represents the median (50th percentile) of the fracture toughness distribution with 87.5% confidence. In other words, the minimum of three represents the median fracture toughness with high confidence; there is 12.5% chance that it can be lower. Another way of interpreting the minimum of three is that it represents the 20th percentile of the distribution with 50% confidence. Hence there is a 50% chance that the 20th percentile is overestimated when only three tests are conducted. To achieve higher confidence (say 90%) that the minimum value from a set of tests corresponds to the 20th percentile, more tests are required; in this case the set would have to include at least ten results.

NOTE 3 The limits on scatter from three tests are more likely to be achieved in test specimens that behave in a ductile manner than those that fail by cleavage. The limits are likely to be exceeded when testing ferritic/bainitic steels in the ductile to brittle transition region. In these circumstances, additional test data and more advanced statistical treatment of the data are necessary to establish confidence in the choice of K_{mat}.

NOTE 4 Post-test metallography can assist in reducing scatter in data by excluding results from the set which do not test the target microstructure.

 © The British Standards Institution 2019

Figure 7.11 **Treatment of sets of between three and five tests**

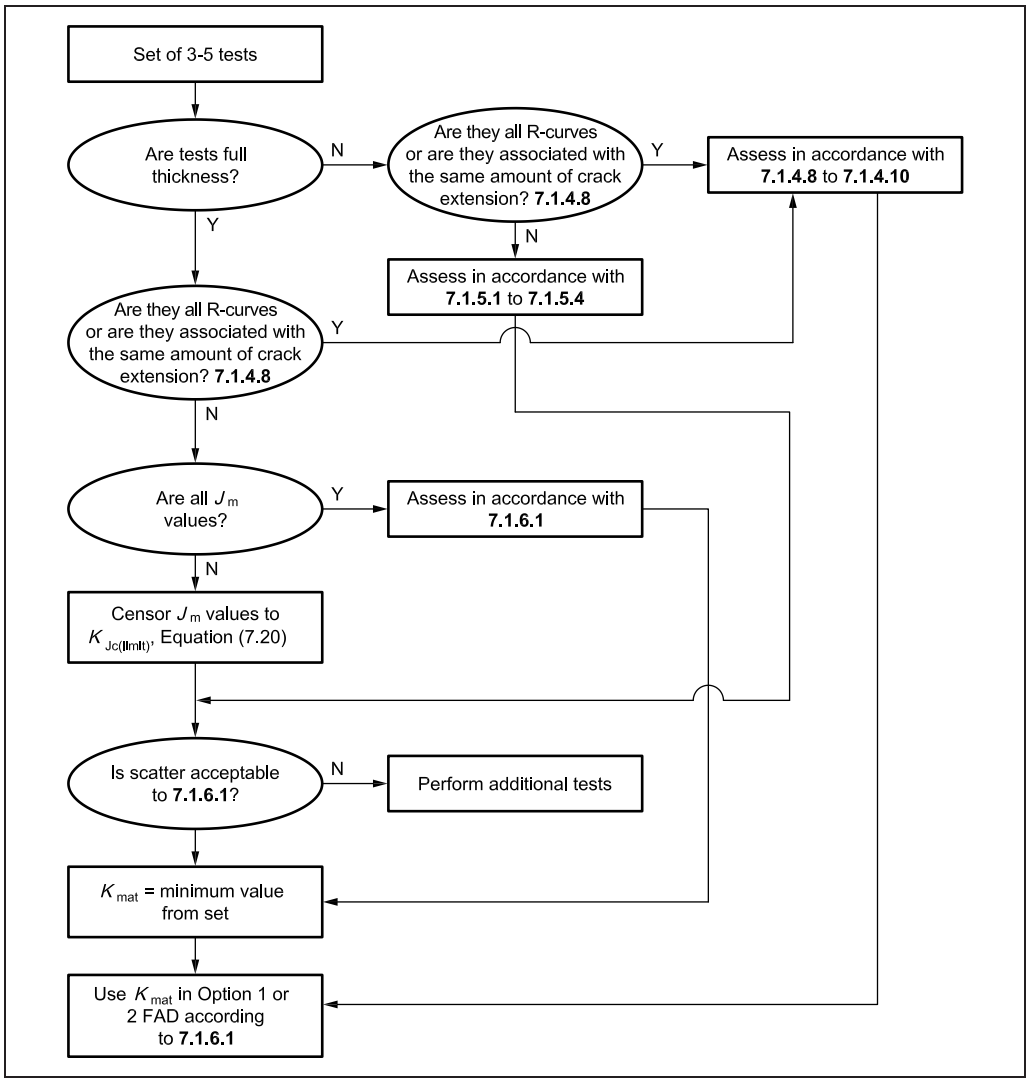
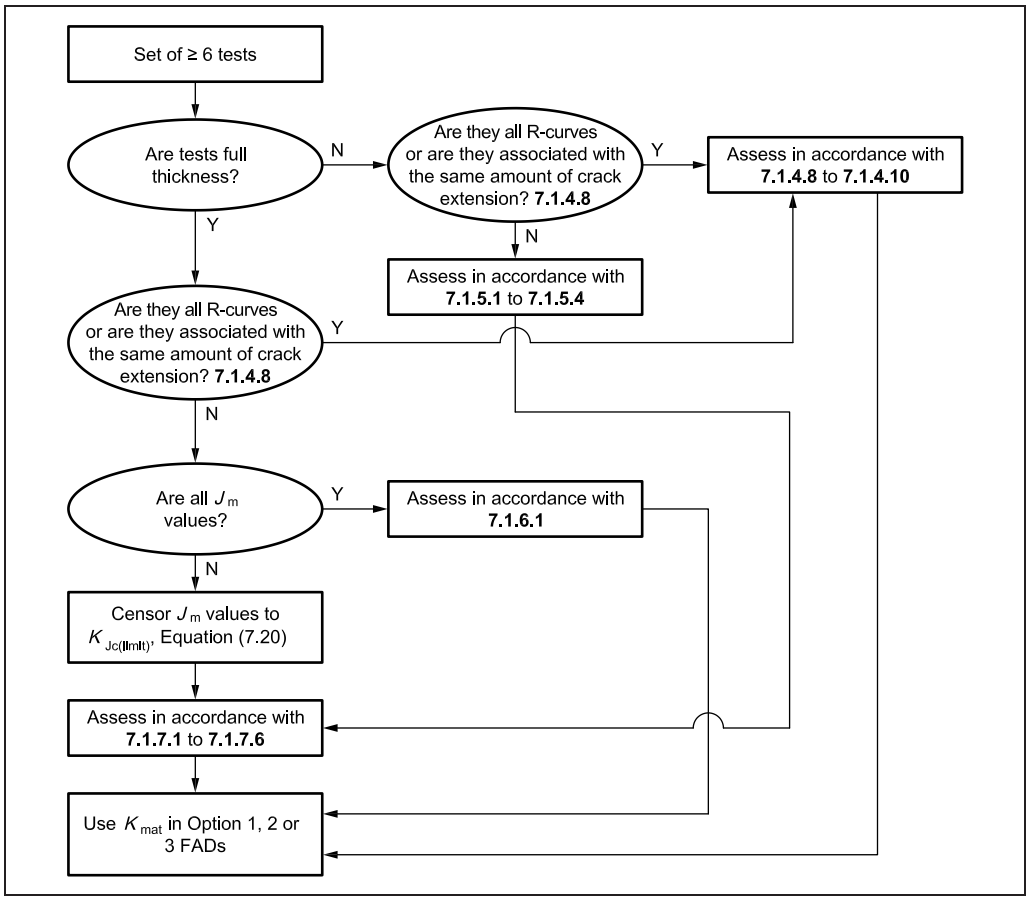


Figure 7.12 **Treatment of sets of more than six tests**



7.1.6.2 Tests are normally performed at slow or quasi-static loading rates, typically less than 3 MPa$\sqrt{m}$ s^{-1}. The quasi-static assessment procedures are then modified by evaluating the materials properties at the appropriate loading rate. The effect of increasing loading rate on the fracture toughness properties of ferritic steels, in the absence of dynamic strain ageing, is to increase both the brittle-to-ductile transition temperature and the upper shelf fracture toughness. There is no effect on the lower shelf fracture toughness. Therefore, in the absence of data at the appropriate loading rate, it is permissible to use quasi-static fracture toughness data, provided that an allowance is made for the increase in the transition temperature. A procedure for making this temperature correction based on the Master Curve method, where the transition curve is indexed by T_0, is described in Annex L.

NOTE Further guidance on dynamic fracture toughness testing can be found in BS 7448-3, ASTM E1820 and ASTM E1921.

7.1.6.3 When direct determination of fracture toughness is not possible, estimates may be made using Charpy correlations as described in Annex J. Alternatively, generic data (e.g. obtained from literature) may be used provided that they are demonstrated to be fully representative of the material used in the structure being assessed and that the fracture toughness chosen represents a lower bound to the data.

7.1.7 Statistical treatment of fracture toughness data

7.1.7.1 Statistical treatment of data, for cases in which fracture toughness test specimens exhibit ductile failure, is described in **7.1.4.8**. For specimens that fracture, or exhibit mixed fracture behaviour, the following treatment of data should be taken into account. For assessments conducted to Options 1 or 2

where there are more than three results in a set of data, two options are possible. If the data meet the criteria in **7.1.5.3** with the exception of scatter limits based on three tests, the minimum of three equivalent (MOTE) may be employed as described in **7.1.7.2**. For other situations the statistical treatments of fracture toughness data described in **7.1.7.3**, **7.1.7.4** and Annex L may be employed. When there is mixed fracture behaviour, i.e. J_c, J_u mixed with J_m, J_m, results are treated as virtual fractures and replaced by the $K_{Jc(limit)}$ defined by Equation (7.20). If sub-sized specimens are used, the fracture toughness requires size correction as described in **7.1.5.2**.

7.1.7.2 If more than three results are available and the recommendations in **7.1.6** (with the exception of the scatter limits) and **7.1.4.2** are met, to ensure that the data represent a homogeneous group, the minimum of three equivalent (MOTE) value defines K_{mat} as described in Table 7.5. When there are more than 15 results it is recommended that the procedures in **7.1.7.3**, **7.1.7.4** or Annex L are employed.

Table 7.5 **Minimum of three equivalent (MOTE)**

Number of fracture toughness results	MOTE value
3 to 5	Lowest
6 to 10	Second lowest
11 to 15	Third lowest

7.1.7.3 The following simple statistical treatment of data can be applied to determine a lower bound estimate of fracture toughness with high confidence. This statistical treatment or that described in Annex L is applicable to all assessment options and is particularly recommended when advantage is taken of constraint loss according to Annex N. The data set should represent the same microstructural region, as described in **7.1.4.2**. In a data set comprising z data points, evaluate K_{mat} as follows.

a) Evaluate the mean fracture toughness from:

$$\bar{K}_i = \frac{\left[\sum_{i=1}^{z} K_i\right]}{z} \tag{7.21}$$

where K_i are the individual data points.

b) Evaluate the variance S^2 from:

$$S^2 = \frac{\left[\sum_{i=1}^{z} \left(K_i - \bar{K}_i\right)^2\right]}{z - 1} \tag{7.22}$$

c) Specify the percentile of the distribution for which K_{mat} is required with a given confidence. Typically, the 20th lower percentile is used and K_{mat} is evaluated as:

$$K_{mat} = \bar{K}_i - Sk_{0.90} \tag{7.23}$$

Values of k for the lower 20th percentile for 90% confidence are given in Table 7.6 for test sample sizes (z) up to 20.

Table 7.6 **Values of $k_{0.90}$ at the lower 20th percentile for the one-sided tolerance limit for a normal distribution**

z	$k_{0.90}$
3	3.039
4	2.295
5	1.976
6	1.794
7	1.675
8	1.590
9	1.525
10	1.474
11	1.432
12	1.397
13	1.368
14	1.342
15	1.320
16	1.307
17	1.283
18	1.268
19	1.253
20	1.240

This table is derived from reference [7.12].

7.1.7.4 For cleavage data in the brittle-to-ductile transition region of ferritic/bainitic steels, it is preferable to use $\ln(K_i)$ rather than K_i in Equation (7.21) to Equation (7.23). A log-normal distribution is more appropriate than a normal distribution for such data as the latter distribution can lead to over-conservative or even negative lower bound values.

NOTE 1 Equation (7.23) used in conjunction with Table 7.6 defines the proportion of the population that is expected to be greater than K_{mat}, 80% in this case with 90% confidence. Other percentiles can be used depending on the application, but the 20th percentile has been found to be useful in many applications.

NOTE 2 Table 7.6 includes $k_{0.90}$ values for $z < 6$. These are included for completeness and would not normally be used, because the statistical analysis described in this clause would normally be applied only to $z \geq 6$.

7.1.7.5 K_{mat} determined according to these procedures (or those in Annex L) may be used directly in integrity assessments or after corrections have been applied to allow for differences in crack tip constraint between the specimen and structure in accordance with Annex N.

7.1.7.6 An alternative treatment of data to that provided in **7.1.7.3** is given by the Master Curve approach described in ASTM E1921 for homogeneous steels and the Master Curve maximum likelihood (MML) method for inhomogeneous materials, such as welds, as described in Annex L. Both procedures are designed to be applied to fracture toughness data generated on ferritic and bainitic steels at temperatures in the lower shelf and transition region.

7.1.8 Stresses

The assessments take account of the actual distributions of stress in the vicinity of the flaw, where they are known. The stresses are classified as primary and secondary in accordance with **6.4**.

In some situations, thermal and residual stresses, which can be self-balancing throughout a structure, can act as primary stresses on an individual component (see Annex Q). This occurs when the flaw is small compared with the zone of influence of the thermal or residual stress, for example in the case of large elastic follow-up (see **7.1.11**). In these circumstances, such thermal and residual stresses should be treated as primary and incorporated in the K_r and L_r calculations.

The direct stress component perpendicular to the plane of the flaw should be used in the calculation of the stress intensity factor K_I. However, if the flaw is aligned such that its plane is not perpendicular to the maximum principal stress direction, the procedures described in Clause **6** and Annex A should be followed.

For the calculation of the plastic collapse parameter, L_r, the appropriate stress depends on the geometry, applied loading and the yield criterion employed. The relevant stress is not necessarily the perpendicular stress as used to determine K_I; for example, the limit pressure for a plain cylinder containing a fully circumferential surface crack of depth less than about half the wall thickness and under internal pressure loading alone is controlled by the hoop stress in the plane of the flaw. Advice on calculation of the appropriate reference stress/limit load is given in Annex P.

7.1.9 Peak stress at weld toe

There is no simple upper bound limit for the peak stress at a shallow surface flaw ($a/B < 0.2$) located within the stress concentration zone at the toe of a weld. Such flaws may be assessed in one of two ways. The preferred methods for most situations are:

a) the stress intensity factor is calculated for the equivalent geometry without the presence of the weld toe, and multiplied by the stress intensity magnification parameter, M_k, as defined in Annex M; or

b) the stress distribution is calculated so as to include the effect of the weld toe, e.g. by finite element analysis, and the stress intensity factor is then calculated directly using weight function methods.

Flaws at the toe of a fillet or T-butt weld, which is itself in a geometric stress concentration (e.g. a nozzle/pad combination), should be assumed to lie in the combined geometric and fillet weld stress concentration fields for a depth up to $0.15B$.

7.1.10 Residual stresses

7.1.10.1 General

Residual stresses may be assumed to be uniform or non-uniform. Uniform (membrane) stress distributions are considered in this subclause, while non-uniform distributions are described in Annex Q.

7.1.10.2 As-welded structures

For a structure in the as-welded condition, with a flaw lying in a plane parallel to the welding direction (i.e. the stresses to be considered are perpendicular to the weld), the tensile residual stress (Q_m) should initially be assumed to be equal to the lesser of the room temperature yield strengths of the weld or parent metal. This is termed the "appropriate" material yield strength (σ'_Y) for the case of a flaw parallel to the weld.

For a structure in the as-welded condition, with a flaw lying in a plane transverse to the welding direction (i.e. the stresses to be considered are parallel to the weld), the tensile residual stress should initially be assumed to be equal to

the room temperature yield strength of the material in which the flaw is located. This is termed the "appropriate" material yield strength (σ'_Y) for the case of a flaw perpendicular to the weld. If the flaw lies partly in weld metal and partly in parent metal, the residual stress should be assumed to be equal to the greater of the room temperature yield strengths of the weld or parent metal.

Some global relief of residual stresses may be assumed as a result of the primary loading applied to the as-welded structure. The membrane residual stress may then be assumed as the lower of Equation (7.24a) and Equation (7.24b):

$$Q_m = \sigma'_Y \tag{7.24a}$$

$$Q_m = \left(1.4 - \frac{\sigma_{ref}}{\sigma'_f}\right)\sigma'_Y \tag{7.24b}$$

where:

σ'_Y is the yield strength (see **7.1.3.1**) of the "appropriate" material at the assessment temperature [except that, for assessment temperatures below ambient, it is the room temperature value, i.e. σ'_{YRT}, in Equation (7.24a)];

σ'_f is the flow strength (average of yield and ultimate strengths) of the "appropriate" material at the assessment temperature.

The upper limit for σ_{ref} should be σ'_f and the lower limit $0.4\sigma'_f$.

The effects of proof testing and warm prestressing on residual stress are given in Annex O.

NOTE 1 The equations above were derived from uniaxial loading ([7.13], [7.14]) and the extent of residual stress relief might be lower in biaxially loaded structures ([7.15], [7.16], [7.17]).

*NOTE 2 The information on residual stresses given in **7.1.10.2** may be used as the basis to waive post-weld heat-treatment (PWHT) of thick ferritic steel weldments. If the structure can be demonstrated to be sufficiently defect-tolerant in the as-welded condition, then the omission of PWHT might be justified.*

7.1.10.3 Post-weld heat-treated (PWHT) structures

In a structure subject to PWHT, the residual stress is not generally reduced to zero. The level of residual stress remaining in welds after PWHT may be estimated on the basis of stress relaxation tests for all-weld or parent metal specimens, as appropriate. Where these data are not available, it may be assumed, for carbon manganese and 2¼Cr1Mo steels, that the stresses after heat treatment in an enclosed furnace within the range 580 °C to 620 °C are as follows [7.18].

a) For a flaw lying in a plane parallel to the welding direction (i.e. the stresses to be considered are perpendicular to the weld), the residual stress (Q_m) should be assumed to be 20% of the lesser of the yield strengths of the weld or parent metal.

b) For a flaw lying in a plane transverse to the welding direction (i.e. the stresses to be considered are parallel to the weld), the residual stress (Q_m) should be assumed to be equal to 30% of the room temperature yield strength of the material in which the flaw is located, or 30% of the greater of the yield strengths of the weld or parent metal for the case of a flaw which lies partly in weld metal and partly in parent metal.

For heat treatment at temperatures below 580 °C, but above 550 °C, the stresses are as follows [7.19].

1) For a flaw in a plane parallel to the weld (residual stresses are perpendicular to the weld), the value Q_m should be assumed to be 20% of the lesser of

the yield strengths of the weld or parent metal, i.e. the same as for heat treatment at 580 °C to 620 °C.

2) For a flaw in a plane perpendicular to the weld (residual stresses are parallel to the weld), Q_m should be assumed to be equal to 40% of the room temperature yield strength of the material in which the flaw is located, or 40% of the greater of the yield strengths of the weld or parent metal for the case of a flaw which lies partly in weld metal and partly in parent metal.

If the PWHT temperature is below 550 °C, seek specialist advice.

If secondary stresses are treated as primary in the above derivation of residual stresses, they should be treated as primary in the overall assessment.

When local PWHT is carried out, the level of residual stress might be higher than that recommended for heat treatment carried out in an enclosed furnace. The level of residual stress depends on factors such as the temperature attained, the width of the heated band and the width of the insulated region. However, because of the wide range of variables, no general recommendations can be made and expert advice should be sought; otherwise conservative assumptions should be made [7.20].

7.1.11 Elastic follow-up

Elastic follow-up should be considered in several instances when applying this standard, particularly in relation to the classification of stresses into primary and secondary. The concept of elastic follow-up originated from a model for creep deformation of a piping system where the possibility for self-springing being accompanied by excessive creep in localized regions of high stress was noted. In the context of creep stress relaxation, elastic follow-up is the argument that the elastic action of the least strained component of a structure restricts the stress in the most highly strained component from relaxing.

The concept of elastic follow-up is closely related to the proximity of the structure to a load-controlled or displacement-controlled situation (i.e. the locality of the displacements).

For a load-controlled situation, elastic follow-up is very high and the corresponding stresses have a primary effect on failure of the structure, hence they should be classified as primary. In contrast, for a displacement-controlled situation, elastic follow-up is insignificant and the corresponding stresses are classified as secondary. Identifying whether elastic follow-up is present in a structure is not straightforward and in some instances lies between these two extremes.

In stress-strain space, a purely load-controlled situation is when strain increases with constant stress when converting from an idealized elastic stress-strain curve to a realistic elastic-plastic stress-strain curve. A purely displacement-controlled situation is when stress decreases with constant strain for the same conversion. Such considerations usually necessitate detailed finite element calculations. In the absence of these, or when their outcome is inconclusive, the loading under consideration should be classified as load-controlled and hence primary.

7.1.12 Sensitivity analysis

A sensitivity analysis, determining the sensitivity of the results to credible variations in input parameters, should normally be performed as part of an engineering critical assessment, especially where the results are marginal.

In general, confidence in assessments performed according to the procedures described in this standard is gained in two stages. The use of lower bound material data and limit load solutions, together with upper bound loads,

reference stresses, defect sizes and stress intensity factor values, provides the initial confidence. This should then be reinforced by investigating the sensitivity of the assessment point to variations of appropriate input parameters.

7.2 Procedure

7.2.1 General

Subclauses **7.2.2** to **7.2.14** set out the procedure for the assessment of fracture resistance.

7.2.2 Definition and categorization of all loads and stresses

*NOTE See **6.4** and **7.1.8** to **7.1.11**.*

The most onerous loading conditions for the flawed structure should be evaluated. This is not always self-evident and several loading conditions, and flaw locations in the case of postulated flaws, might need to be compared. In categorizing the loading, a distinction is made between loads which contribute to plastic collapse and loads which do not (see **6.4** and **7.1.8**). Stresses arising from these loads are labelled σ^P and σ^S, respectively, and are treated differently in the calculations of **7.3**. A simplified analysis is obtained if all loads are assumed to result in σ^P stresses. Such an analysis leads to an underestimate of margins on load provided that σ^S stresses are tensile.

7.2.3 Definition of fracture toughness

The fracture toughness data required are influenced by the type of analysis. Details of the fracture toughness properties are given in **7.1.4** to **7.1.7**. In practice, the availability of fracture toughness data might also influence the selection of the type of analysis (**7.3.1** and **7.3.8**).

The fracture toughness should correspond to the material containing the crack tip.

7.2.4 Determination of material tensile properties

The tensile properties (see **7.1.3**) should be those of the weakest material in the vicinity of the flaw; this is not necessarily the material containing the crack tip. The alternative is to perform a strength mismatch assessment using the procedures in Annex I.

7.2.5 Characterization of the size and shape of the flaw

Where the selected type of analysis includes ductile crack growth it is necessary to characterize not only the initial flaw size, a_0, but also the flaw size, a_j, after some ductile crack growth, Δa_j.

7.2.6 Selection and definition of the FAD

The selection and definition of the FAD should be carried out in accordance with **7.3**.

7.2.7 Selection of the type of analysis

Subclauses **7.3.1** and **7.3.8** give information on the types of analysis and the selection procedure.

7.2.8 Calculation of L_r

L_r should be calculated in accordance with **7.3.7**.

 © The British Standards Institution 2019

7.2.9 Calculation of K_r

K_r should be calculated in accordance with **7.3.6**.

7.2.10 FAD

All points should be plotted on the FAD.

7.2.11 Estimation of the flaw growth in service

It is necessary to determine whether sub-critical crack growth occurs under service conditions when performing a fitness-for-service assessment. If a mechanism, such as fatigue (see Clause **8**), creep (see Clause **9**) or environmentally-assisted crack growth (see Clause **10**), exists for such sub-critical growth, then it is necessary to quantify the extent of such growth.

7.2.12 Assessment of the significance of the results

Assessment points should be judged against the failure assessment line. In making this judgement the following criteria should be satisfied for each type of analysis.

a) Limiting loading conditions for initiation analysis. The analysis is performed at a specific flaw size and a single assessment point is obtained. The limiting condition occurs when this lies on the failure assessment line.

b) Limiting loading conditions for tearing analysis. In the analysis it is necessary to postulate various amounts of ductile crack growth and to evaluate assessment points (L_r, K_r) for each one. This produces a locus of assessment points on the FAD. The limiting condition occurs when the locus touches the failure assessment line at one point only with all other points on the locus lying outside the area bounded by the axes and the line. Where ductile tearing data are sufficiently extensive, this corresponds to a tangency condition between the locus of assessment points and the failure assessment line. More commonly, however, ductile tearing data are only available for small amounts of crack growth (~2 mm). The limiting condition then often corresponds to the failure assessment point, evaluated for the maximum extent of the crack growth data, being on the failure assessment curve.

The potential for failure in other regions of the structure, whether cracked or uncracked, should also be assessed.

A margin between the specified loading conditions and the limiting loading condition confers confidence in the result. The necessary margin should be judged by performing a sensitivity analysis on the results (see **7.1.12**).

7.2.13 Further refinements

Failure to obtain satisfactory margins for a particular analysis does not necessarily mean that safety cannot be demonstrated. It might be possible to refine the stress analysis or to re-analyse the structure using a tearing analysis, a re-characterized flaw or an alternative FAD, as indicated in the flowcharts, Figure 7.2 to Figure 7.4. It might be possible to use an alternative approach; for example, to invoke constraint (Annex N), weld mismatch (Annex I), proof test or warm pre-stressing arguments (Annex O), or for pressurized components to make a leak-before-break case (Annex F).

7.2.14 Reporting of results

Results should be reported in accordance with Annex H.

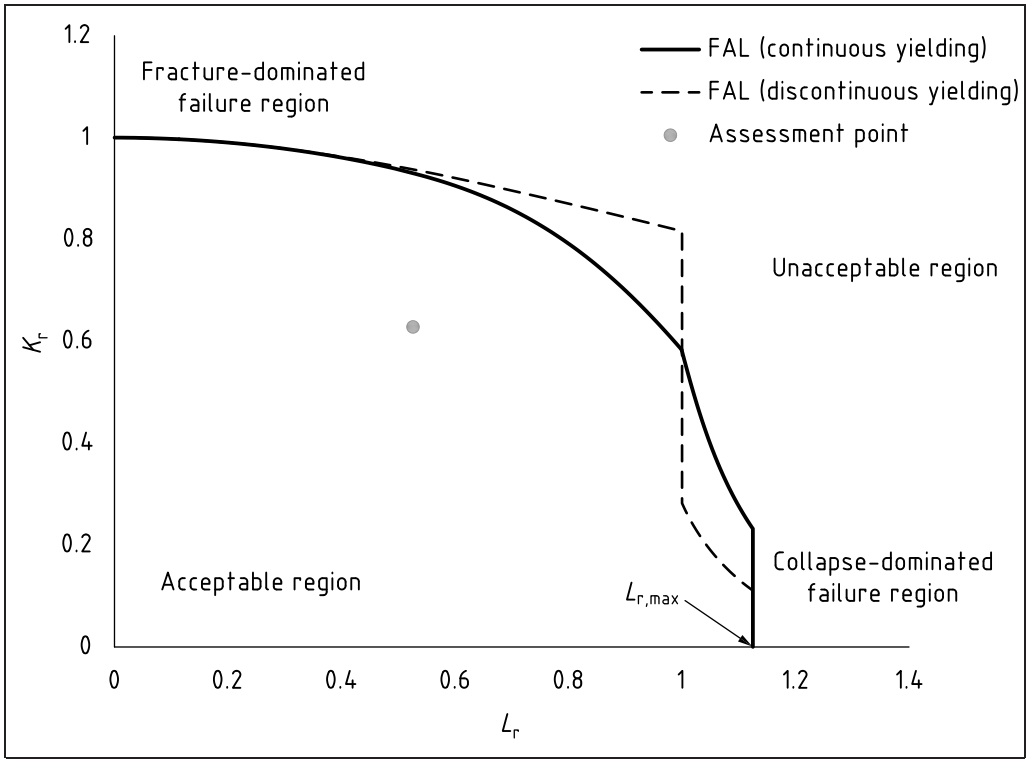
7.3 Assessment (Options 1 to 3)

7.3.1 Main features

This is the normal assessment route for general applications. It has three alternative approaches: Options 1, 2 and 3. These are of increasing complexity in terms of the required material and stress analysis data but provide results of increasing accuracy.

Each approach has a failure assessment line (FAL) given by the equation of a curve, $K_r = f(L_r)$, and a cut-off value of L_r, $L_{r,max}$. An example of such a failure assessment diagram (FAD) is shown in Figure 7.13. If the calculated assessment point (L_r, K_r) lies within the area bounded by the axes, the FAL and the vertical line corresponding to $L_{r,max}$, the flaw is acceptable; if it lies on or outside the line, the flaw is unacceptable. However, in the case of an unacceptable flaw, it might be possible to refine the analysis, in terms of the analysis option employed (**7.3.3** to **7.3.5**), the input data used including the materials properties, or to take account of ductile tearing (**7.3.8**), before conceding that an acceptable case cannot be made.

Figure 7.13 **Example of a Failure Assessment Diagram**



The assessment route includes an argument based on initiation of crack growth and the case of stable tearing under increasing load, where the material and temperature are such that a ductile tearing mechanism might occur. Assessments are based on a single value of toughness. This can be a value associated with limited ductile tearing. For ductile crack growth, the value of toughness used as a measure of initiation typically corresponds to 0.2 mm of crack extension, including blunting, in accordance with the fracture toughness testing standard used (see **7.1.4** to **7.1.7**) so ductile tearing assessment should not be performed for crack growth below that figure.

No inherent safety factors are included. Sensitivity studies taking account of realistic variations in input parameters should be employed to assess the effect on margins.

 © The British Standards Institution 2019

7.3.2 The cut-off value of L_r

The cut-off is to prevent plastic collapse. It is set at the point at which $L_r = L_{r,max}$, where:

$$L_{r,max} = \frac{\sigma_Y + \sigma_U}{2\sigma_Y} \quad (7.25)$$

For the purposes of defining the cut-off, mean rather than minimum tensile properties should be used. The tensile properties are based on the engineering values of yield and tensile strength as defined in **7.1.3**.

7.3.3 Option 1

This option does not require detailed stress-strain data. The equations describing the FAL are:

$$f(L_r) = \left(1 + \frac{1}{2}L_r^2\right)^{-0.5}\left[0.3 + 0.7\exp\left(-\mu L_r^6\right)\right] \text{for } L_r \leq 1 \quad (7.26)$$

$$f(L_r) = f(L_r = 1)L_r^{(N-1)/(2N)} \text{ for } 1 < L_r < L_{r,max} \quad (7.27)$$

and:

$$f(L_r) = 0 \text{ for } L_r \geq L_{r,max} \quad (7.28)$$

where:

$$\mu = \min\left(0.001\frac{E}{\sigma_Y}, 0.6\right)$$

$$N = 0.3\left(1 - \frac{\sigma_Y}{\sigma_U}\right)$$

This curve is suitable for materials that do not exhibit a yield discontinuity. Advice on whether a material displays a yield discontinuity is given in **7.1.3.6**.

For materials which exhibit or are characterized as exhibiting discontinuous yielding, Equation (7.26) to Equation (7.28) should be replaced by Equation (7.29) to Equation (7.32).

$$f(L_r) = \left(1 + \tfrac{1}{2}L_r^2\right)^{-0.5} \quad \text{for} \quad L_r < 1 \quad (7.29)$$

$$f(L_r) = \left(\lambda + \tfrac{1}{2\lambda}\right)^{-0.5} \quad \text{for} \quad L_r = 1 \quad (7.30)$$

$$f(L_r) = f(L_r = 1)L_r^{(N-1)/(2N)} \quad \text{for} \quad 1 < L_r < L_{r,max} \quad (7.31)$$

$$f(L_r) = 0 \quad \text{for} \quad 1 < L_r < L_{r,max} \quad (7.32)$$

The quantity $\lambda > 1$ in Equation (7.30) is defined in terms of elastic modulus, E, the yield strength, R_{eL}, and the increase in strain, $\Delta\varepsilon$, at stress R_{eL} (in MPa), without any increase in stress, by:

$$\lambda = 1 + \frac{E\Delta\varepsilon}{R_{eL}} \quad (7.33)$$

In the absence of detailed stress-strain data enabling Equation (7.30) and Equation (7.31) to be evaluated, $\Delta\varepsilon$ may be estimated from Equation (7.8) for materials where σ_Y <1 000 N/mm^2.

Equation (7.8) then leads to an estimated $\Delta\varepsilon > 0.2\%$. The strain hardening exponent n is given by Equation (7.7).

The failure assessment line for discontinuous materials defined by Equation (7.29) to Equation (7.32) exhibits a discontinuity at $L_r = 1$ as $\Delta\varepsilon > 0$ and a vertical line joins the points defined by Equation (7.29) and Equation (7.30) at $L_r = 1$ as shown in Figure 7.13.

7.3.4 Option 2

The Option 2 failure assessment curve is defined by Equation (7.34) and Equation (7.35). It requires the mean uniaxial tensile true stress-strain curve at the assessment temperature for stresses up to the engineering value of tensile strength and is suitable for all metals regardless of the stress-strain behaviour. Where there is a discontinuity in the stress-strain curve at the lower yield strength, there is a discontinuity in the Option 2 curve at the corresponding value of L_r which is often $L_r = 1$.

In order to derive the Option 2 curve, detailed stress-strain data are needed, especially at strains below 1%. As a minimum it should be calculated at values $L_r = 0.7$, 0.9, 0.98, 1.0, 1.02 and 1.1, and then at a sufficient number of points to define the curve up to $L_{r,max}$.

$$f(L_r) = \left(\frac{E\varepsilon_{ref}}{L_r\sigma_Y} + \frac{L_r^3\sigma_Y}{2E\varepsilon_{ref}}\right)^{-0.5} \text{ for } L_r < L_{r,max} \tag{7.34}$$

and:

$$f(L_r) = 0 \text{ for } L_r \geq L_{r,max} \tag{7.35}$$

*NOTE Yield strength in Equation (7.34) is the engineering value as defined in **7.1.3**.*

7.3.5 Option 3

A failure assessment curve specific to a particular material, geometry and loading type may be determined using both elastic and elastic-plastic analyses of the flawed structure as a function of the loads giving rise to primary stresses, i.e. those which contribute to the evaluation of L_r. It is given by:

$$f(L_r) = \sqrt{\frac{J_e}{J}} \text{ for } L_r < L_{r,max} \tag{7.36}$$

$$f(L_r) = 0 \text{ for } L_r \geq L_{r,max} \tag{7.37}$$

where:

J_e is the value from the J-integral from the elastic analysis at the load corresponding to the value L_r;

J is the value from the J-integral from the elastic-plastic analysis at the load corresponding to the value L_r.

This curve is not suitable for general use. It is useful only for specific cases as an alternative approach to Options 1 and 2.

7.3.6 The fracture ratio, K_r

The fracture ratio, K_r, is determined by either Equation (7.38) or Equation (7.39):

$$K_r = \frac{K_I^p + VK_I^s}{K_{mat}} \tag{7.38}$$

$$K_r = \frac{K_I^p + K_I^s}{K_{mat}} + \rho \tag{7.39}$$

where:

K_{mat} is the fracture toughness taking account of any ductile tearing following initiation (see **7.1.4**).

The terms V and ρ are defined in Annex R as functions of both the primary and secondary loads and account for plasticity interaction effects.

If K_I^s is negative then K_I^s and ρ should be set to zero in Equation (7.38) and Equation (7.39); this is conservative for the purposes of assessment.

 © The British Standards Institution 2019

The fracture toughness used in Equation (7.38) and Equation (7.39) is normally the high constraint toughness as determined from testing standards using deeply-cracked bend specimens such as the compact tension or edge-cracked bend specimens (see **7.1.4** to **7.1.7**). This is assumed to represent a lower bound to the toughness for assessments. However, for conditions of low in-plane structural constraint and where the material fracture toughness at the assessment temperature exhibits a significant dependence on constraint, it is possible to take account of the increased value of toughness in the assessment. Advice on performing a constraint assessment is given in Annex N. For brittle fracture of ferritic materials a constraint analysis is likely to be of most benefit in the lower transition, where the initiation toughness is likely to be sensitive to constraint conditions. In the ductile regime, while materials data suggests that initiation is relatively insensitive to constraint, an increase in tearing resistance is likely to be seen in a ductile tearing assessment (see **7.3.8**).

7.3.7 The load ratio, L_r

The load ratio, L_r, is determined from the primary loads acting on the component via:

$$L_r = \frac{P}{P_L(a,\sigma_Y)} = \frac{\sigma_{ref}}{\sigma_Y} \quad (7.40)$$

where:

$P_L(a, \sigma_Y)$ is the elastic perfectly plastic limit load for flaw size a and yield strength σ_Y;

a is the flaw size, including any ductile tearing.

Structural collapse is considered in this British Standard to be governed by failure of the section containing the flaw. The possibility of premature collapse elsewhere in the structure should be separately investigated. The use of a limit load corresponding to such a remote failure mechanism in an assessment of the section containing the flaw might be overly conservative.

*NOTE Yield strength in Equation (7.40) is the engineering value as defined in **7.1.3**.*

7.3.8 Ductile tearing

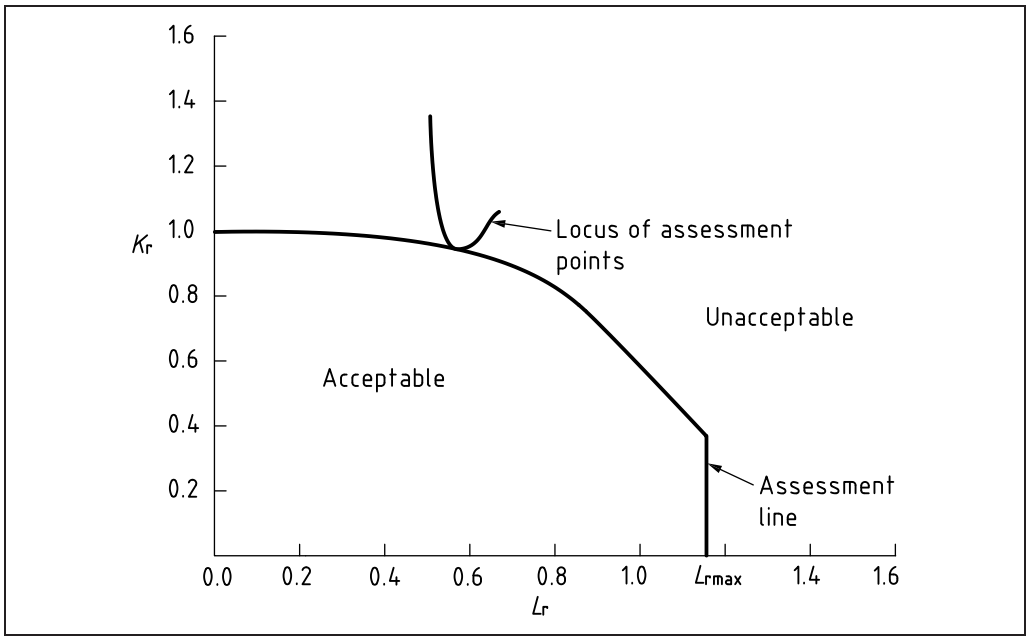
The procedure in this subclause is appropriate for ductile materials that exhibit stable tearing under increasing load, e.g. austenitic materials, and ferritic materials on the upper shelf, where an initiation assessment does not lead to an acceptable flaw or where a better estimate of reserve factor and margins is required. The ductile tearing assessment can then use any of the Option 1, 2 or 3 approaches. Various amounts of ductile tearing are postulated and the fracture ratio, K_r, and the load ratio, L_r, are evaluated at a flaw size equal to the current flaw plus the postulated amount of crack growth and the assessed load level in accordance with **7.3.6** and **7.3.7**, respectively.

In addition, fracture ratio K_r is evaluated using an enhanced value of fracture toughness, K_{mat}, corresponding to the postulated amount of tearing, typically up to 1 mm or 2 mm, in a fracture assessment. In such assessments, K_{mat} is set to K_{1mm}, or K_{2mm} for example, rather than being based on the initiation of tearing fracture toughness, $K_{0.2mm}$. In some situations, it is appropriate to consider the amount of tearing up to instability. When carrying out a fracture assessment involving ductile tearing, the instability conditions should be evaluated in order to ensure that the crack growth being allowed for is in the stable tearing regime. The evaluation of the instability conditions for a given size of flaw for a given load is described below.

Plot all pairs (L_r, K_r) as coordinate points on the FAD, as a function of increasing flaw size (i.e. initial flaw size, based on initiation of tearing fracture toughness,

$K_{0.2mm}$, followed by flaw size based on various postulated amounts of tearing), at a fixed load (or fixed combination of primary and secondary loading), to derive the locus of assessment points (see Figure 7.14). If the locus lies completely outside the FAD, then the flaw is unacceptable. If it crosses the FAL into the region bounded by the failure assessment curve and the cut-off, some ductile tearing could occur. However, this is predicted to stabilize and the flaw is deemed acceptable. In practice, the ductile tearing assessment can be limited by the range of validity of the tearing resistance data (see **7.1.4** to **7.1.7**) and the tearing locus on Figure 7.14 might not extend sufficiently far as to cross into the acceptable region on the FAD. A condition of tangency between the locus of assessment points and the failure assessment line (see Figure 7.14) corresponds to the condition of unstable ductile crack growth, for the given loading, at the relevant crack size.

Figure 7.14 **Ductile tearing assessment**



7.3.9 Interaction of ductile tearing and fatigue crack growth

This subclause provides advice on the interaction of fatigue crack growth and stable ductile tearing. Ductile tearing can contribute to crack extension under fatigue if the value of the *J*-integral at maximum load exceeds the value for initiation of tearing, $J_{0.2BL}$ (see **7.1.4**).

The total crack growth, Δa_{tot}, is given by adding the cyclic and static contributions, Δa_f, Δa_t, respectively, that is:

$$\Delta a_{tot} = \Delta a_f + \Delta a_t \quad (7.41)$$

Fatigue crack growth, Δa_f, should be calculated in accordance with Clause **8**. The details of the calculation of tearing, Δa_t, depend on the load history.

a) For tearing due to load applications, due to fault or overload conditions for example, where the corresponding value of *J* exceeds the maximum during the fatigue cycles, Δa_t is determined from a single ductile tearing analysis (see **7.3.8**) performed for the maximum load in the history and a flaw size equal to the initial flaw size plus the total crack growth of Equation (7.41).

b) In some cases, it might be necessary to assess ductile tearing under conditions where tearing occurs in each fatigue cycle. Ductile tearing and fatigue crack growth are then calculated on a cycle-by-cycle basis. The

procedure is based on method a) with the fatigue crack growth in Equation (7.41) based on the number of cycles to date.

This approach is considered to be conservative. It neglects any re-sharpening of the tip of the flaw due to fatigue crack growth through the zone of ductile damage ahead of the torn flaw. This re-sharpening would act to increase the tearing resistance of the material and should be considered for cases of significant fatigue crack growth where the flaw might grow outside the ductile damage zone.

There are conditions where Equation (7.41) might not be valid. These include cases of significant crack closure in the fatigue cycle leading to load ratios $R < 0$ and for ductile crack extension in excess of fracture toughness testing validity limits (see **7.1.4**). It is considered that interaction effects for cases of variable load amplitude and variable temperature are covered by Equation (7.41). However, to cover uncertainties, sensitivity studies should be performed in general when taking account of the interaction of stable ductile tearing and fatigue (see **7.1.12**).

Further description of this approach, including examples, is set out in Section II.8 of the R6 procedure [7.21].

7.4 Further points

7.4.1 Environmental effects

Environmental effects on fracture are addressed in **10.3**.

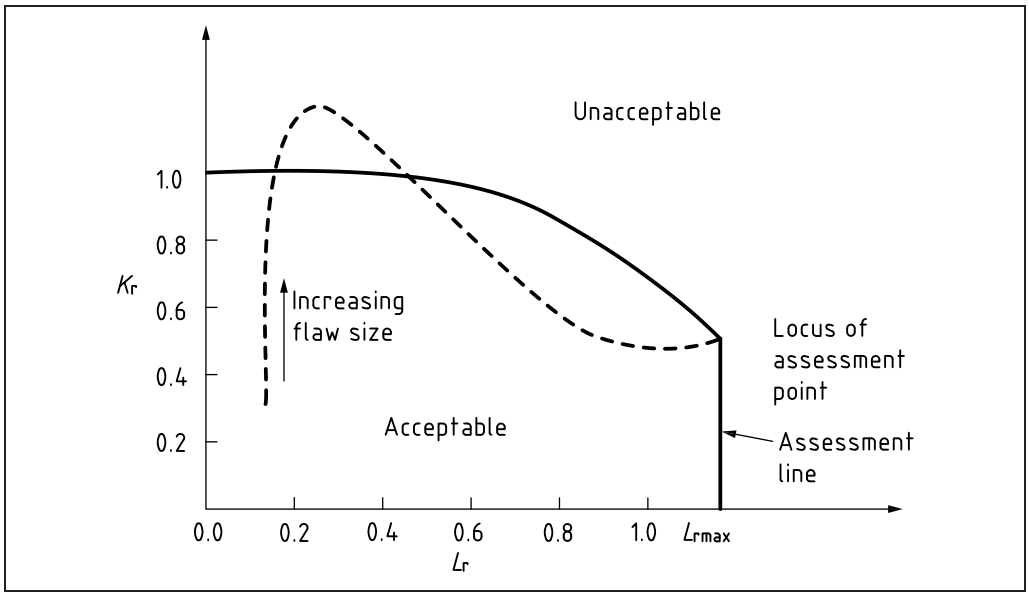
7.4.2 Comparison of the options

Conservatism usually reduces with increasing analysis option but there are situations where this does not occur. For example, the Option 1 curve for continuous yielding materials is an approximate lower bound for a range of materials; for some low strain hardening materials, the Option 2 line can lie inside the general Option 1 line.

7.4.3 Non-unique solutions

Because of the mathematical form of solutions used in the procedures and the interaction of input data, it is possible that a flaw of one size is acceptable but a flaw of smaller size is unacceptable (see Figure 7.15). Such conditions [7.22] are most likely to occur when stress distributions decrease through the section (e.g. due to bending stresses or the stress raising effect of weld toes), or where increasing primary stresses result in increased relaxation of assumed residual stresses. Sensitivity analyses should be employed to check for possible non-unique solutions (see **7.1.12**).

Figure 7.15 **Example of non-unique solutions**



7.4.4 Fracture assessment for non-planar flaws, imperfect shape, locally thinned regions and fillet welds

7.4.4.1 Non-planar flaws

It is conservative to treat non-planar flaws as if they are planar, using **7.1.2** to determine the appropriate dimensions and the relevant solution in Annex M to determine the stress intensity factor. Otherwise, the limits of Table 7.7 are acceptable for non-planar flaws in steels that meet the following criteria:

- the specified minimum yield strength is <450 N/mm^2;
- the average of three Charpy V-notch energy absorption at the minimum service temperature is ≥40 J;
- the minimum individual Charpy V-notch energy absorption at the minimum service temperature is 27 J;
- the applied stress (membrane plus bending) at the flaw location is <80% of the specified minimum yield strength.

For other materials, the limits of Table 7.7 are acceptable provided that the fracture toughness (K_{mat}) of the material in which the flaw lies exceeds 1 250 N/mm$^{3/2}$ (40 MPa$\sqrt{}$m) at minimum service temperature. For materials of lower toughness, these flaws should be assessed on the basis of their dimensions as planar flaws.

Table 7.7 **Limits for slag inclusions and porosity**

Slag inclusions	**Porosity**	
	Percentage of projected area on radiograph %	**Individual pore diameter**
No limit on length; maximum height or width *B*/8 or 3 mm, whichever is smaller	5	*B*/4 or 6 mm, whichever is smaller

7.4.4.2 Imperfect shape (including undercut)

Variations in weld profile from that specified, which could give a weld throat dimension below that needed to carry the maximum allowable design stresses, are unacceptable.

Undercut can prevent detection of other flaws by non-destructive testing. If it can be shown that no planar flaws exist other than undercut, then undercut is acceptable to a maximum depth of 1 mm or 10% of the thickness, whichever is the lesser, under the following circumstances:

a) the structure or component is made of steel;

b) the specified minimum yield strength is <450 N/mm^2;

c) the average for three tests of the Charpy V-notch energy absorption at the minimum service temperature is ≥40 J;

d) the minimum individual value Charpy V-notch energy absorption at the minimum service temperature is ≥27 J;

e) the applied stress (membrane plus bending) at the flaw location is <80% of the specified minimum yield strength;

All other cases of undercut should be assessed as planar flaws.

7.4.4.3 Locally-thinned regions (corrosion/erosion/pits)

It is conservative to assess local thinning, due for example to corrosion or erosion, as a planar flaw of the same depth and shape. However, if the thinning does not create a sharp discontinuity, the likelihood of failure is expected to be controlled by plastic collapse considerations (see Annex G).

7.4.4.4 Fillet welds

A flaw located at the root of a fillet weld, even when made in accordance with good workmanship principles, is not readily amenable to analysis by ECA. Fillet welds contain an inherent flaw in the form of the unfused land, making them potentially sensitive to fatigue failure through the weld throat (see Clause **8**), and fracture at low temperature and/or under impact loading. Volumetric inspection of fillet welds is also problematic.

It is possible, in principle, to calculate stress intensity factors for the particular geometry represented by a fillet weld, and apply the general methods of the fracture assessment clauses.

Flaws in the weld metal of fillet welds, e.g. in the weld throat, might affect the static strength of the weld through their effect on the cross-sectional area. The real stressing situation in fillet welds is complex, particularly under combined loading situations. It is recommended that the maximum shear stress should be calculated on the net minimum throat area, by combining the normal, parallel shear and perpendicular shear components as in the IIW method ([7.23], [7.24]) This maximum shear stress should not exceed 0.58 times the minimum tensile yield strength of the weld metal used.

Bibliography for Clause 7

Standards publications

For dated references, only the edition cited applies. For undated references, the latest edition of the referenced document (including any amendments) applies.

ASME Boiler and Pressure Vessel Code, Section II, Part D: *Materials – Properties*

ASTM E1820, *Standard test method for measurement of fracture toughness*

ASTM E1921, *Standard test method for determination of reference temperature, T_o, for ferritic steels in transition range*

BS 7448 (all parts), *Fracture mechanics toughness tests*

BS 8571, *Method of test for determination of fracture toughness in metallic materials using single edge notched tension (SENT) specimens*

BS EN 10025-2, *Hot rolled products of structural steels – Part 2: Technical delivery conditions for non-alloy structural steels*

BS EN 10025-3, *Hot rolled products of structural steels – Part 3: Technical delivery conditions for normalized/normalized rolled weldable fine grain structural steels*

BS EN 10025-4, *Hot rolled products of structural steels – Part 4: Technical delivery conditions for thermomechanical rolled weldable fine grain structural steels*

BS EN ISO 15653, *Metallic materials – Method of test for the determination of quasistatic fracture toughness of welds*

BS EN ISO 6892-1, *Metallic materials – Tensile testing – Part 1: Method of test at room temperature*

BS EN ISO 6892-2, *Metallic materials – Tensile testing – Part 2: Method of test at elevated temperature*

BS EN ISO 6892-3, *Metallic materials – Tensile testing – Part 3: Method of test at low temperature*

ISO 12135, *Metallic materials – Unified method of test for the determination of quasistatic fracture toughness*

Other documents

[7.1] HADLEY, I. and LEI, Y. Outline of the fracture clauses of BS 7910:2013. *In: International Journal of Pressure Vessels and Piping (IJPVP)*, 2018, 168, 289–300. <https://doi.org/10.1016/j.ijpvp.2018.11.004>

[7.2] BEZENSEK, B. and SHARPLES, J. Flaw interaction rules given in BS 7910:2013 – The history and the way forward. *In: International Journal of Pressure Vessels and Piping (IJPVP)*, December 2018, 168, 225–232. <https://doi.org/10.1016/j.ijpvp.2018.11.003>

[7.3] HADLEY, I. and PISARSKI, H.G. Materials properties for engineering critical assessment: Background to the advice given in BS 7910:2013. *In: International Journal of Pressure Vessels and Piping (IJPVP)*, December 2018, 168, 191–199. <https://doi.org/10.1016/j.ijpvp.2018.10.016>

[7.4] SHARPLES, J. and HADLEY, I. Treatment of residual stress in fracture assessment: background to the advice given in BS 7910:2013. *In: International Journal of Pressure Vessels and Piping (IJPVP)*, December 2018, 168, 323–334. <https://doi.org/10.1016/j.ijpvp.2018.11.005>

[7.5] BEZENSEK, B., SHARPLES, J. K. and WILKES, M. A. An engineering approach to characterization of twin flaws in cleavage. *In: Proceedings of ASME Pressure Vessel and Piping Conference, Paper No. PVP2010-25134*. Bellevue, WA, USA, July 2010.

[7.6] DNVGL-RP-F108, *Assessment of flaws in pipeline and riser girth welds*. 2019. <https://www.dnvgl.com/oilgas/download/dnvgl-rp-f108-assessment-of-flaws-in-pipeline-and-riser-girth-welds.html>

[7.7] DNVGL-ST-F101. *Submarine pipeline systems*. October 2017. <https://www.dnvgl.com/oilgas/download/dnvgl-st-f101-submarine-pipeline-systems.html>

[7.8] BANNISTER, A.C, RUIZ OCEJO, J. and GUTIERREZ-SOLANA, F. Implications of the yield stress/tensile stress ratio to the SINTAP failure assessment diagrams for homogeneous materials, *In: Engineering Fracture Mechanics*, 67(6), 1 December 2000, 547–562. <https://doi.org/10.1016/S0013-7944(00)00073-4>

[7.9] BANNISTER, A.C. and TRAIL, S.J. *Structural Integrity Assessment Procedures for European Industry (SINTAP)*. Sub-Task 2.1 Report: The Significance of the Yield Stress/Tensile Stress Ratio to Structural Integrity. <http://www.eurofitnet.org/sintap_BRITISH_STEEL_The_Significance_of_y-t_ratio.pdf>

[7.10] CHEAITANI, M.J., and PARGETER, R.J. Fracture mechanics techniques for assessing the effects of hydrogen on steel properties. *In: Proceedings of International Steel and Hydrogen Conference*, 28 September 2011.

[7.11] PISARSKI, H. Treatment of fracture toughness data for engineering critical assessment (ECA). *In: Welding in the World*, 2017, 61(4), 723–732.

[7.12] OWEN, D. B. *Handbook of statistical tables*. Reading, Massachusetts: Addison-Wesley, 1962.

[7.13] HADLEY, I. and SMITH, S.D. Effects of mechanical loading on residual stress and fracture: Part I: Background to the BS 7910:2013 Rules, PVP2014-28152. *In: Proceedings of the ASME 2014 Pressure Vessels and Piping Conference*, July 20–24, 2014, Anaheim, California, USA.

[7.14] HADLEY, I. and SMITH, S.D. Effects of mechanical loading on residual stress and fracture: Part II: Validation of the BS 7910:2013 Rules, PVP2014-28092. *In: Proceedings of the ASME 2014 Pressure Vessels and Piping Conference*, July 20–24, 2014, Anaheim, California, USA.

[7.15] HADLEY, I. *Effects of warm prestress on residual stress and fracture in uniaxially loaded welded joints*. TWI Industrial Member report 1093/2017. Cambridge: TWI, 2017.

[7.16] HADLEY, I. *Effects of biaxiality on residual stress relief and fracture in welded joints*. TWI Industrial Member report 1094/2017. Cambridge: TWI, 2017.

[7.17] HADLEY, I. and LONDON, T. Optimising fracture assessment of welded structures using BS 7910, R6 and FEA, OMAE2019-95934. *In: Proceedings of the ASME 2019 Conference on Ocean, Offshore and Arctic Engineering*, OMAE2019, June 9–14, 2019, Glasgow, Scotland.

[7.18] WEI, L. and NOWAK, M. *A review of post weld heat treatment effects on welding residual stresses*. TWI Industrial Member Report 1071/2016. Cambridge: TWI, 2016.

[7.19] PISARSKI, H.G., Implications of changes in the post-weld heat treatment requirement on properties of steels and welds for offshore structure. *In: Proceedings of the 15th International Offshore Mechanics and Arctic Engineering (OMAE) Conference*, Florence, Italy, 16–20 June 1996.

[7.20] REN, Y., PARADOWSKA, A.M., WANG, B. and EREN, E. Residual stress state of X65 pipeline girth welds before and after local and global PWHT, PVP2016-63378. *In: Proceedings of the ASME 2016 Pressure Vessels and Piping Conference*. Vancouver, BC, Canada, 17–21 July 2016.

[7.21] R6 PANEL. *R6: Assessment of the integrity of structures containing defects*. Revision 4, as amended. Gloucester: EDF Energy, 2001.

[7.22] PHAAL, R. Non-unique solutions in PD 6493:1991 fracture assessment procedures. In: H.S. MEHTA, ed. Fracture mechanics: applications and new materials. *In: Proceedings of the Pressure Vessels and Piping conference*, Denver, Co., 25–29 July, 1993. New York: ASME, 1991. PVP-260 149–155. ISBN 0791809870.

[7.23] HICKS, J.G. *Welded joint design*. 2nd edition. Cambridge: Woodhead Publishing, 1997. ISBN 1 85573 337 4.

[7.24] INTERNATIONAL INSTITUTE OF WELDING. Commission XV: Calculation formulae for welded connections subject to static loads. *In: Welding in the World*, 1964, 2(4), 168–197.

8 Assessment for fatigue

8.0 Symbols and definitions

For the purposes of this clause, the following symbols, definitions and units apply, unless otherwise indicated at the point of use.

Symbol	Definition	Units
A	Constant in fatigue growth relation that depends on material and the applied conditions, including environment and cyclic frequency	see footnote 8.1)
A^1	Other values of A used in quality category method	—
a	Half flaw length for through-thickness flaw, flaw height for surface flaw or half height for embedded flaw	mm
a_f	Final flaw size	mm
a_i	Initial flaw size	mm
$\bar{a}_i$	Initial value of effective flaw parameter for fatigue analysis	mm
$\bar{a}_{max}$	Maximum permitted value of effective flaw parameter for fatigue analysis (quality category method)	mm
B	Section thickness in plane of flaw	mm
B'	Effective section thickness ($2a + 2p$)	mm
c	Half flaw length for surface or embedded flaw	mm
da/dN	Flaw growth rate with cycles	mm/cycle
E	Elastic modulus	N/mm^2
E_{steel}	Elastic modulus of steel	N/mm^2
E_{ET}	Elastic modulus at elevated temperature	N/mm^2
E_{RT}	Elastic modulus at room temperature	N/mm^2
K	Stress intensity factor (SIF)	N/mm$^{3/2}$
K_c	Critical stress intensity factor for failure under static load	N/mm$^{3/2}$
K_{max}	Maximum stress intensity factor	N/mm$^{3/2}$
K_{min}	Minimum stress intensity factor	N/mm$^{3/2}$
k_m	Stress concentration factor due to misalignment	—
k_{tb}	Bending stress concentration factor	—
k_{tm}	Membrane stress concentration factor	—
L	Attachment length	mm

8.1) The units and value of A depend on those used to measure da/dN and ΔK, and on the value of the exponent, m. If A is known in one set of units, A_a, the corresponding value for another set of units, A_b, is given by:

$$A_b = A_a \frac{f_a}{f_b{}^m}$$

where:

f_a is the conversion factor for da/dN from the first to the second unit system; and

f_b is the conversion factor for ΔK from the first to the second unit system.

(continued)

Symbol	Definition	Units
M_k	Stress intensity magnification factor for flaws at a weld toe	—
m	Constant in flaw growth law that depends on material and the applied conditions, including environment and cyclic frequency	—
N	Fatigue life	cycles
n_j	Number of cycles in stress spectrum at stress range $\Delta\sigma_j$	cycles
P	Primary stress	N/mm^2
P_b	Primary bending stress	N/mm^2
P_m	Primary membrane stress	N/mm^2
$P_{max} + Q_{max}$	Maximum algebraic values of the primary plus secondary stress	N/mm^2
$P_{min} + Q_{min}$	Minimum algebraic values of the primary plus secondary stress	N/mm^2
p	Shortest distance from material surface to embedded flaw	mm
Q	Secondary stress	N/mm^2
Q_b	Secondary bending stress	N/mm^2
Q_m	Secondary membrane stress	N/mm^2
R	Stress ratio (or effective stress ratio, for welded joints)	—
S	Stress range or, for variable amplitude, the equivalent constant amplitude stress range	N/mm^2
S_i	Value of S for $\bar{a}_i$	N/mm^2
S_m	Value of S for $\bar{a}_{max}$	N/mm^2
S^1	Stress ranges corresponding to constant A^1	N/mm^2
Y	Stress intensity correction factor	—
Δa	Crack growth	mm
Δc	Increment in c	mm
ΔK	Stress intensity factor range	N/mm$^{3/2}$
ΔK_{eff}	Effective stress intensity range	N/mm$^{3/2}$
ΔK_0	Threshold stress intensity factor range below which fatigue crack growth (or corrosion fatigue crack growth) does not occur	N/mm$^{3/2}$
$\Delta K_{0,steel}$	Threshold stress intensity factor range for steel	N/mm$^{3/2}$
ΔN	Increment in N	cycles
ΔP_b	Primary bending stress range	N/mm^2
ΔP_m	Primary membrane stress range	N/mm^2
ΔQ_b	Secondary bending stress range	N/mm^2
ΔQ_m	Secondary membrane stress range	N/mm^2
$\Delta\sigma$	Applied stress range	N/mm^2
$\Delta\sigma_b$	Bending component of stress range	N/mm^2
$\Delta\sigma'_b$	Bending stress range excluding the effects of misalignment	N/mm^2
$\Delta\sigma_j$	Stress range in variable amplitude fatigue spectrum which is applied n_i times	N/mm^2

 © The British Standards Institution 2019

(continued)

Symbol	Definition	Units
$\Delta\sigma_m$	Membrane component of stress range	N/mm^2
$\Delta\sigma_s$	Bending stress range due to misalignment	N/mm^2
$\Delta\sigma_1$, $\Delta\sigma_2$ .... $\Delta\sigma_j$	Applied stress ranges used in calculating constant amplitude stress range S (Miner's rule)	N/mm^2
σ'_b	Bending stress excluding effect of misalignment	N/mm^2
σ_m	Membrane stress	N/mm^2

8.1 Assessment procedures

8.1.1 General

The background to this clause is given in reference [8.1].

Procedures are given for assessing the acceptability of flaws found in service in relation to their effects on fatigue strength, both in welded and unwelded parts (see **8.4** to **8.8**), or for the estimation of tolerable flaw sizes based on fitness-for-service (see **8.9**). Planar and non-planar flaws are considered in a fatigue assessment. Fracture mechanics principles are used to describe the behaviour of planar flaws (see **8.1.2**) while the assessment of non-planar flaws is based on experimental *S-N* data (see **8.1.3**). Guidance is also given on the assessment of shape imperfections (see **8.1.4**). The assessment methods are summarized in Table 8.1. Results should be reported in accordance with Annex H.

The presence of a weld reduces the fatigue strength to levels below the fatigue strength of unwelded parent material due to the geometric stress concentration it introduces. The reduction depends on the weld detail under consideration. Fatigue *S-N* curves for typical weld details are given in BS 7608. When considering the acceptance level for a weld flaw in a fatigue-loaded structure, the flaw is significant only if it causes a greater reduction in fatigue strength than that caused by the weld detail.

Table 8.1 **Procedure for assessment of known flaws**

Step		Relevant clause references	Relevant figure(s) and table(s)
1	Determine cyclic stress range from P_m, k_{tm}, P_b, k_{tb}, Q	**6.4.1**, **6.4.5**, **8.2.1**	Figure 6.1b), Figure 6.2 and Table 8.2
2	Resolve flaw normal to maximum principal stress	**6.4.5**	Figure 6.2
3	Define flaw dimensions	**7.1.2**	Figure 7.6
4	Assess uninspectable regions	**6.3.5**	—
5	Define limit to crack growth:	—	—
a)	for unstable fracture	—	—
	Option 1	**7.3.3**	Figure 7.2
	Option 2	**7.3.4**	Figure 7.3
	Option 3	**7.3.5**	Figure 7.4
b)	other failure modes	Clause **10**	—
Planar flaws (general procedure)		—	—
6	Select values of A, m and ΔK_0	**8.2.3**	Table 8.3 to Table 8.5
7	Determine ΔK for cyclic stress range and flaw height and shape	**8.4.3**, Annex M	—
8	Calculate crack growth increments Δa and Δc for one stress cycle	**8.4.4**	—
9	Repeat steps 7 and 8 for crack height $a + \Delta a$ and continue until the limit to crack growth (step 5) or the specified design life is reached. The flaw is acceptable if the limit to crack growth is not exceeded in the design life.	**8.4.4**, **8.4.5**, **8.4.6**	—
Planar flaws (using quality categories)		—	—
10	Select quality category required	**8.5.3.1** or **8.5.3.2**	Figure 8.3 and Table 8.6
11	Calculate k_m for misalignment	**8.8.1**, Annex D	Table D.1 and Table D.2
12	From flaw dimensions, determine initial flaw parameter $\bar{a}_i$	**8.6.2**	Figure 8.4 to Figure 8.8
13	Determine limit to crack growth (step 5)	**8.6.2**	—
14	Determine S_i and S_m and $\bar{a}_i$ and $\bar{a}_m$	**8.6.2**	Figure 8.4 to Figure 8.8
15	Determine quality category for flaw under consideration from $S = (S_i^3 - S_m^3)^{1/3}$. If this is equal to or better than the quality required, flaw is acceptable.	**8.6.2**	Figure 8.3
Non-planar and shape imperfections		—	—
16	Confirm that flaw does not need to be treated as planar	Clause **4**, **8.2.2**	—
17	Calculate k_m for misalignment	**8.8.1**, Annex D	Table D.1 and Table D.2
18	Determine required quality category	**8.5.3**	Figure 8.3
19	Determine allowable flaw sizes of shape imperfections	**8.7, 8.8**	Table 8.7 to Table 8.11
20	Compare detected with allowable flaws or imperfections	**8.7**, **8.8**	—

 © The British Standards Institution 2019

8.1.2 Fracture mechanics analysis of planar flaws

Two methods are outlined for assessing planar flaws. A general procedure is given in **8.4**, while a so-called "quality category" procedure related to *S-N* curves is given in **8.5**. Both methods are based on the fracture mechanics analysis of cracks under fatigue loading and estimate the fatigue life by integrating the crack growth law. The general procedure permits the use of accurate expressions for the cyclic stress intensity factor and specific fatigue crack growth data. The quality category procedure entails the use of the results of fracture mechanics calculations already performed and presented graphically.

In a fracture mechanics assessment it is usual to adopt conservative estimates of the various parameters required. Recommendations in this clause are based on this. However, another approach is to use reliability methods to allow for uncertainties in the parameters.

The fracture mechanics approach assumes that a flaw can be idealized as a sharp tipped crack which propagates in accordance with the law relating the crack growth rate, da/dN, and the range of stress intensity factor, ΔK, for the material containing the flaw. The crack growth law is determined experimentally, and might be generated specifically for the ECA (see BS ISO 12108). However, crack growth laws are recommended in **8.2.3**, and the use of appropriate published data is also permitted. The overall relationship between da/dN and ΔK is normally observed to be a sigmoidal curve in a log(da/dN) versus log(ΔK) plot. There is a central portion for which it can be reasonable to assume a linear relationship (i.e. the Paris law) or, for greater precision, to represent the data by two or more straight lines (see Figure 8.1). At low values of ΔK, the rate of growth falls off rapidly, such that, below a threshold stress intensity factor range, ΔK_0, crack growth is insignificant. At high values of ΔK, when the maximum stress intensity factor in the cycle, K_{max}, approaches the critical stress intensity factor for failure under static load, K_c, the rate of crack growth accelerates rapidly. A number of crack growth laws are available which describe the entire sigmoidal relationship [8.2] and [8.3]. However, it is often sufficient to assume that the central portion applies for all values of ΔK from ΔK_0 up to failure. See, for example, references [8.4], [8.5], [8.6] and [8.7]. Assuming, for illustration purposes, the Paris law, the relevant equation is as follows:

$$\frac{da}{dN} = A(\Delta K)^m \tag{8.1}$$

For $\Delta K < \Delta K_0$, da/dN is assumed to be 0.

The stress intensity factor range, ΔK, is a function of structural geometry, stress range and instantaneous crack size and is calculated from the following equation:

$$\Delta K = Y(\Delta\sigma)\sqrt{\pi a} \tag{8.2}$$

The overall life is calculated by substituting Equation (8.2) into Equation (8.1) and integrating the following equation:

$$\int_{a_i}^{a_f} \frac{da}{Y^m(\pi a)^{m/2}} = A(\Delta\sigma)^m N \tag{8.3}$$

The acceptability of a crack of initial size a_i then depends on whether the calculated cyclic life, N, is greater or less than the required life.

*NOTE When Equation (8.3) is used to assess variable amplitude loading (see **8.2.1.5**), it is equivalent to the use of Miner's rule (see also BS 7608).*

For situations in which crack growth near the threshold is significant, a less conservative form of Equation (8.1) based on the effective value of ΔK, ΔK_{eff}, might be justified. In these circumstances, the relevant equation is the following:

$$\frac{da}{dN} = A(\Delta K_{eff})^m \tag{8.4}$$

where the default value of ΔK_{eff} is ΔK.

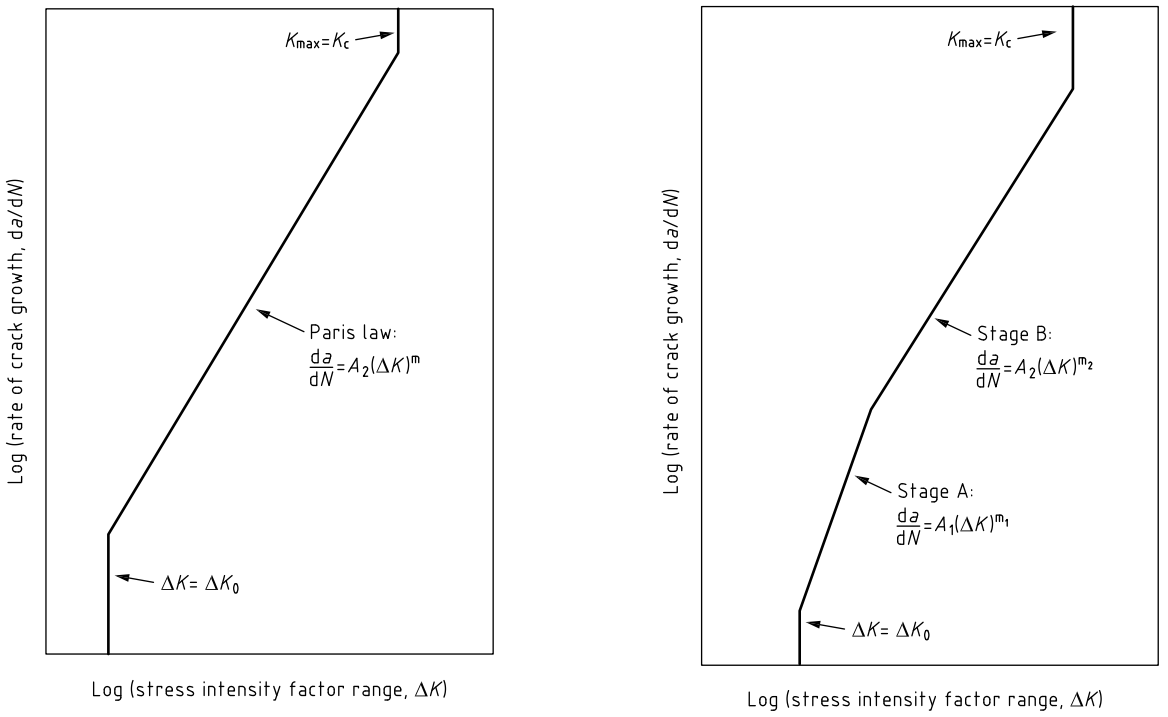
At temperatures up to 100 °C, the proximity to the threshold, ΔK_0, means that for $\Delta K < \Delta K_0/R$:

$$\Delta K_{eff} = \frac{(\Delta K - \Delta K_0)}{(1 - R)} \tag{8.5}$$

The values of the material constants m and A in Equation (8.4) are usually different from those in Equation (8.1). Substituting ΔK_{eff}, Equation (8.3) becomes:

$$\int_{a_i}^{a_f} \left[\frac{1 - R}{Y\sqrt{(\pi a)} - \Delta K_0/\Delta\sigma}\right]^m da = A(\Delta\sigma)^m N \tag{8.6}$$

Figure 8.1 **Schematic crack growth relationships**



a) Simple Paris law crack growth relationship

b) Two stage crack growth relationship

8.1.3 Assessment of non-planar flaws

It is conservative to treat non-planar flaws as if they are planar and to assess them using fracture mechanics (see **8.1.1**). However, in some cases (see **8.5**) they can be assessed as standard weld details in terms of *S-N* curves obtained by statistical analysis of test data. The resulting acceptance limits, given in **8.7**, are founded on fatigue test results obtained from specimens containing naturally and artificially flawed butt welds.

8.1.4 Assessment of shape imperfections

8.1.4.1 General

Shape imperfections increase the severity of existing regions of stress concentration in the welded joint, chiefly at the weld toe.

Guidance is given in **8.8** on the assessment of the two shape imperfections that are most significant for fatigue, namely misalignment and weld toe undercut.

8.1.4.2 Misalignment

Misalignment in a joint subjected to nominally membrane loading introduces bending stresses, increasing the total stress range near the joint. Fatigue test results from aligned and misaligned butt welded and cruciform joints are correlated in terms of the sum of the applied axial stress and the induced bending stress in the region of crack initiation. Thus, the bending stress due to misalignment is added to the applied stress when calculating the total stress in the fatigue assessment (see **6.4** and Annex D). This stress may be used in conjunction with the design *S-N* curve for the (aligned) joint to assess the effect of misalignment.

Alternatively, it may be used in the assessment of a planar or non-planar flaw in a misaligned joint.

8.1.4.3 Undercut

The acceptance limits for weld toe undercut in **8.8.2** are based on fatigue test results from butt and fillet-welded joints containing natural undercut or undercut artificially manufactured for the purposes of the fatigue test programme, often by machining [8.8]. Thus, as in the case of non-planar flaws, they relate directly to the design *S-N* curves.

8.1.4.4 Local thinned areas

It is conservative to assess local thinned areas, due for example to corrosion pitting or erosion, as a planar flaw of the same depth and shape (see **8.1.2**). Alternatively, within the limits prescribed in **8.8.2**, the acceptance levels for undercut in butt welds may be used.

8.2 Data required for assessment

8.2.1 Stress

8.2.1.1 Fluctuating stresses

Assessments use the nominal applied stress range acting on the section containing the flaw, resulting from the fluctuating components of load. Thus, residual stresses are not included, but fluctuating thermal stresses are. The stresses may be treated either directly or after resolution into the components described in **6.4.1**.

8.2.1.2 Stress concentrations

Only stress concentrations due to gross structural discontinuities and misalignment are included when calculating the applied stress. The stress concentration effect of a local structural discontinuity, due for example to welded joint geometry, is only taken into account in a fracture mechanics assessment as part of the calculation of the stress intensity factor (see **8.4.3**).

The peak stress due to misalignment depends only on the membrane component of applied stress. If a misaligned joint is within the stress concentration field due

to a gross structural discontinuity, this membrane stress has to include the effect of the gross structural discontinuity.

8.2.1.3 Determination of stress ranges when resolved into components *P* and *Q*

The procedure for determining the stress ranges when resolved into components *P* and *Q* is as follows.

a) Identify the extreme maximum and minimum algebraic values of the primary plus secondary stresses [$(P + Q)_{max}$ and $(P + Q)_{min}$], and their through-thickness distributions if possible, throughout the loading cycle under consideration. Applied tensile and compressive stresses are considered to be positive and negative respectively.

b) Calculate the peak stress, taking into account any gross structural discontinuities.

c) At the two extremes in the loading cycle, determine $k_{tm}(P_m + Q_m) + k_{tb}(P_b + Q_b)$. Separate the membrane and bending stress components σ_m and σ'_b, if necessary, by linearizing the through-thickness stress distribution in a conservative way. In particular, linearization should not underestimate the surface stresses or, as far as possible, the stress acting in the region of the flaw being assessed (see Figure 6.1).

d) Calculate the maximum changes in σ_m and σ'_b, to give stress ranges $\Delta\sigma_m$ and $\Delta\sigma'_b$.

e) Calculate the additional stress range due to misalignment under the membrane stress range, $\Delta\sigma_m$ [$(k_m - 1)\ \Delta\sigma_m$]. Add this to $\Delta\sigma'_b$ to give the total bending stress range, $\Delta\sigma_b = \Delta\sigma'_b + (k_m - 1)\ \Delta\sigma_m$.

f) If misalignment alone is being assessed, it is neglected at this stage ($k_m = 1$), so that $\Delta\sigma_b = \Delta\sigma'_b$. The effect of misalignment is then assessed using **8.8.1**.

g) Membrane or bending stress ranges may be used separately or together, depending on the type of assessment being performed (see Table 8.2).

Table 8.2 **Stress ranges used in fatigue assessments**

Application		Stress	Comments
1	Assessment of embedded non-planar flaws (see **8.7**) or undercut (see **8.8.2**) using quality category *S-N* curves	$(\Delta\sigma_m + \Delta\sigma_b)$	*S-N* curves do not distinguish between membrane and bending stresses
2	Assessment of misalignment	$(\Delta\sigma_m + \Delta\sigma_b)$ with $k_m = 1$	*S-N* curves do not distinguish between membrane and bending stresses
3	Assessment of planar flaws using quality category *S-N* curves (see **8.6**)	$(\Delta\sigma_m + \Delta\sigma_b)$	Used with Figure 8.4, Figure 8.6 or Figure 8.7, or, $\leq 0.25\ \Delta\sigma_b$, Figure 8.5 or Figure 8.8
4	Assessment of planar flaws using fracture mechanics	$\Delta\sigma_m$ and $\Delta\sigma_b$ (or $\Delta\sigma_m + \Delta\sigma_b$)	Used separately if stress intensity factor (*K*) solution differentiates between membrane and bending stress (see Annex M), otherwise sum used

8.2.1.4 Effect of applied stress ratio

The use of the full stress range regardless of applied stress ratio (*R*) is the established approach to the fatigue design of welded joints, whether in the as-welded or PWHT condition (see BS 7608). It is based on the fact that yield

strength magnitude tensile residual stresses usually exist in weld regions [8.9], so the effective stress ratio (typically $R \geq 0.5$) may exceed the applied stress ratio (see also **8.2.3.3** and **8.2.3.4**).

If it is required to take account of stress ratio (e.g. when considering unwelded components or using **8.2.3.6**), the effective value obtained by superimposing applied and residual stresses should be used.

8.2.1.5 Variable amplitude loading

Where the stress range varies during the life of the structure, knowledge of these variations is required. A stress spectrum should be converted to identifiable stress ranges using a cycle counting method (e.g. rainflow or reservoir). The stress spectrum should then be represented as a distribution of stress ranges versus numbers of occurrences. If this is further reduced to a histogram, any convenient number of stress intervals can be used, but, for conservatism, each block of cycles should be assumed to experience the maximum stress range in that block.

Under variable amplitude loading, the use of Equation (8.3) might overestimate fatigue life and for critical conditions the calculated fatigue life should be halved ([8.10], [8.11], [8.12]) (see BS 7608).

8.2.2 Flaw type and dimensions

The flaw type (see Clause **4**) should be established. The following should be assessed as planar flaws:

a) surface breaking non-planar flaws;

b) weld toe undercut deeper than 1 mm;

c) embedded flaws that cannot be positively identified as non-planar;

d) any flaw, if it is necessary to assess fatigue crack growth from the flaw (e.g. to estimate inspection intervals).

The definitions of flaw dimensions are given in **7.1.2**. It is not usually necessary to apply the flaw interaction criteria in **7.1.2.2** in a fatigue assessment. However, if there is any doubt that multiple flaws are separate (for example, due to the limitations of NDT), they should be assumed to be combined. Embedded planar flaws should be idealized as having an elliptical shape and surface planar flaws a semi-elliptical shape.

8.2.3 Fatigue crack growth law

8.2.3.1 General

The rate of fatigue crack growth assumed in this subclause is given by Equation (8.1) for values of ΔK above a threshold value, ΔK_0. For $\Delta K < \Delta K_0$, da/dN is assumed to be zero. Values of A and m depend on material and applied conditions.

Recommendations [8.13] are available in the form of simple laws [see Figure 8.1a)] and more precise two-stage relationships [Figure 8.1b)]. For the latter, both the mean and mean plus two standard deviations (mean + 2SD) of $\log(da/dN)$ versus $\log(\Delta K)$ relationships for $R < 0.5$ and $R \geq 0.5$ are given. However, for conservatism (see Table 8.3) and to allow for the influence of residual stresses, the mean + 2SD laws for $R \geq 0.5$ should normally be used to assess welded components.

8.2.3.2 Specific fatigue crack growth and crack growth threshold data

Where specific fatigue crack growth and, if applicable, threshold data are available for the material and service conditions, they may be used in the general procedure for planar flaw assessment given in **8.4**.

NOTE A number of reviews are available of published fatigue crack growth data for a range of materials and environments ([8.14] to [8.23]), and of threshold data ([8.17], [8.18], and [8.23] to [8.26]). Marine environments have received particular attention ([8.19], [8.20], [8.21]).

For CMn pipeline steels subjected to production fluids, there have been a number of studies of "sweet" (oxygen-free brine with CO_2) [8.27] and "sour" (oxygen-free brine with H_2S) conditions. References [8.28] and [8.29] give data for sweet conditions, and references [8.28], [8.30], [8.31], [8.32] and [8.33] for sour conditions. Some data for corrosion resistant alloys in production environments are available in reference [8.30]. Fatigue crack growth rates are strongly dependent on the precise environmental composition, temperature and pressure. Particular care is needed for the assessment of flaws in aggressive environments, particularly with respect to the effects of crack depth, testing frequency and waveform on the rate of crack growth ([8.28], [8.34], [8.35]). Near-threshold fatigue crack growth rates are difficult to determine accurately in environments that give rise to significant scale formation and special test techniques might be required [8.36].

Where any uncertainty exists concerning the relevance of available data for the particular assessment being performed, specific data should be obtained using the methods given in BS ISO 12108 (see also **10.3.3.3**).

8.2.3.3 Recommended fatigue crack growth laws for steels in air

Values of the constants A and m in Equation (8.1), given in Table 8.3, should be used for:

- steels (ferritic, austenitic or duplex ferritic-austenitic) with yield or 0.2% proof strengths $\leq$700 N/mm^2;
- operation in air or other non-aggressive environments at temperatures up to 100 °C.

Unless justification for using different values is provided, the upper bound (mean + 2SD) values for $R \geq 0.5$ should be used for all assessments of flaws in welded joints. These laws are shown in Figure 8.2a).

Table 8.3 **Recommended fatigue crack growth laws for steels in air** [A)]

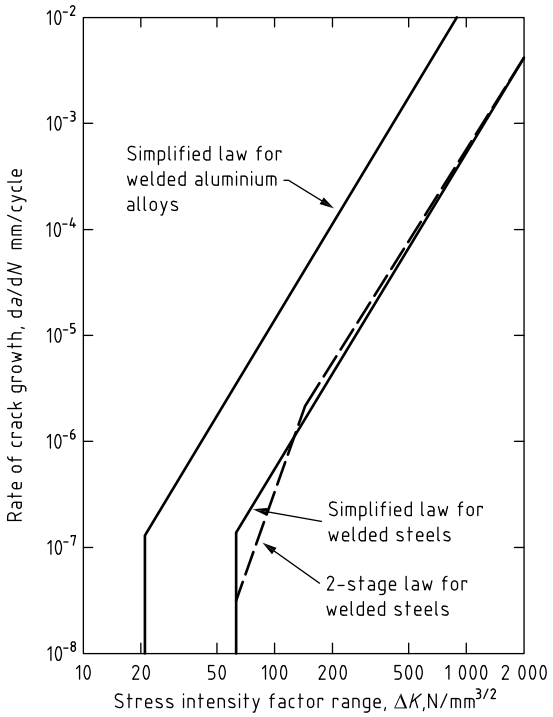
R	Stage A				Stage B				Stage A/ Stage B transition point ΔK, N/mm$^{3/2}$	
	Mean curve		Mean + 2SD		Mean curve		Mean + 2SD			
	A [B)]	m	A [B)]	m	A [B)]	m	A [B)]	m	Mean curve	Mean + 2SD
<0.5	1.21×10^{-26}	8.16	4.37×10^{-26}	8.16	3.98×10^{-13}	2.88	6.77×10^{-13}	2.88	363	315
≥0.5	4.80×10^{-18}	5.10	2.10×10^{-17}	5.10	5.86×10^{-13}	2.88	1.29×10^{-12}	2.88	196	144

[A)] Mean + 2SD for $R \geq 0.5$ values recommended for assessing welded joints.

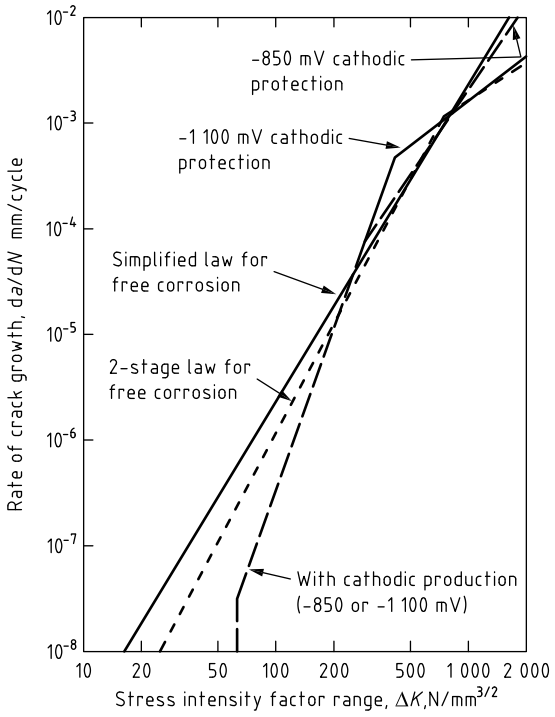
[B)] For da/dN in mm/cycle and ΔK in N/mm$^{3/2}$.

 © The British Standards Institution 2019

Figure 8.2 **Recommended fatigue crack growth laws**



a) Operation in air and other non-aggressive environments



b) Welded steels (including austenitics) in marine environments

8.2.3.4 Recommended fatigue crack growth laws for steels, excluding austenitic and duplex stainless steels, in a marine environment

Values of the constants A and m in Equation (8.1) given in Table 8.4 should be used for assessing low strength steels. They are applicable:

- to steels (excluding austenitic and duplex stainless steels) with yield or 0.2% proof strengths $\leq$600 N/mm^2;
- when operating in marine environments at temperatures up to 20 °C.

These laws are shown in Figure 8.2b).

Table 8.4 **Recommended fatigue crack growth laws for steels in a marine environment** [A)]

R	Stage A				Stage B				Stage A/Stage B transition point ΔK, N/mm$^{3/2}$	
	Mean curve		Mean + 2SD		Mean curve		Mean + 2SD			
	A [B)]	m	A [B)]	m	A [B)]	m	A [B)]	m	Mean curve	Mean + 2SD
Steel freely corroding in a marine environment										
<0.5	3.0×10^{-14}	3.42	8.55×10^{-14}	3.42	1.27×10^{-7}	1.30	1.93×10^{-7}	1.30	1 336	993
≥0.5	5.37×10^{-14}	3.42	1.72×10^{-13}	3.42	5.67×10^{-7}	1.11	7.48×10^{-7}	1.11	1 098	748
Steel in a marine environment with cathodic protection at –850 mV (Ag/AgCl)										
<0.5	1.21×10^{-26}	8.16	4.37×10^{-26}	8.16	5.16×10^{-12}	2.67	1.32×10^{-11}	2.67	462	434
≥0.5	4.80×10^{-18}	5.10	2.10×10^{-17}	5.10	6.0×10^{-12}	2.67	2.02×10^{-11}	2.67	323	290
Steel in a marine environment with cathodic protection at –1 100 mV (Ag/AgCl)										
<0.5	1.21×10^{-26}	8.16	4.37×10^{-26}	8.16	5.51×10^{-8}	1.40	9.24×10^{-8}	1.40	576	514
≥0.5	4.80×10^{-18}	5.10	2.10×10^{-17}	5.10	5.25×10^{-8}	1.40	1.02×10^{-7}	1.40	517	415

[A)] Mean + 2SD values for $R \geq 0.5$ recommended for assessing welded joints.

[B)] For da/dN in mm/cycle and ΔK in N/mm$^{3/2}$.

The values in Table 8.4 are based on data obtained either in artificial seawater or in 3% NaCl solution at temperatures from 5 °C to 20 °C and cyclic frequencies from 0.17 Hz to 0.5 Hz [8.13]. Use of the recommended crack growth laws for operating conditions outside these ranges requires justification. Significantly higher crack growth rates have been observed in certain steel HAZ microstructures tested in seawater with cathodic protection under long duration loading cycles due to combined fatigue and stress corrosion [8.37].

NOTE The fatigue crack growth laws given in this standard for steels in a marine environment (with or without cathodic protection) are derived from data obtained at wave motion frequencies in the range 0.17 Hz to 0.5 Hz. Fatigue crack growth rates in a corrosive environment are affected by the loading frequency and it is recognised that fatigue crack growth may accelerate under lower frequency loading under such environmental conditions. Significantly higher fatigue crack growth rates have been observed at (very) low frequencies [8.38].

8.2.3.5 Simplified fatigue crack growth laws for steels

For preliminary screening assessments, hand-calculations or assessments that can be compared directly with calculations based on fatigue design rules for welded steels (see BS 7608), simple and conservative laws are recommended for steels with yield or 0.2% proof strengths up to 600 N/mm^2. These correspond to the upper bounds to the data used to derive the crack growth laws presented in **8.2.3.3** drawn with a slope of $m = 3$, consistent with the slope of the design *S-N* curves.

For steels, including austenitics, operating in air or other non-aggressive environments at temperatures up to 100 °C, the recommended values of the constants m and A in Equation (8.1) are as follows:

$m = 3$

$A = 5.21 \times 10^{-13}$

for da/dN in mm/cycle and ΔK in N/mm$^{3/2}$. This law is included in Figure 8.2.

For elevated temperatures, up to 600 °C, the following values are recommended:

$m = 3$

$$A = 5.21 \times 10^{-13} \left(\frac{E_{RT}}{E_{ET}}\right)^3$$

where:

E_{RT} is the elastic modulus at room temperature (say 20 °C);

E_{ET} is the elastic modulus at the elevated temperature.

For steels (including austenitic stainless steels) operating in marine environments at temperatures up to 20 °C, with or without cathodic protection, the following values are recommended:

$m = 3$

$A = 2.3 \times 10^{-12}$

This law is included in Figure 8.2.

8.2.3.6 Recommended fatigue crack growth thresholds for steels

Threshold stress intensity factor, ΔK_0, values are strongly dependent on environment and R ([8.17], [8.18], [8.24], [8.25], [8.26]). ΔK_0 is found to increase as R decreases. Recommended values for some conditions are given in Table 8.5. The lower bound value obtained at high R values in the relevant environment should be adopted for all assessments of flaws in welded joints.

The values of ΔK_0 in Table 8.5 for austenitic steels and unprotected steels operating in a marine environment are also applicable for assessing unwelded components. However, for unwelded steel components, account may be taken of R. Based on published data for steels (excluding austenitic) in air and with cathodic protection in marine environments at temperatures up to 20 °C, the following values of ΔK_0 (in N/mm$^{3/2}$) are recommended:

$$\Delta K_0 = 63 \text{ for } R \geq 0.5 \quad (8.7a)$$

$$\Delta K_0 = 170 - 214R \text{ for } 0 \leq R < 0.5 \quad (8.7b)$$

$$\Delta K_0 = 170 \text{ for } R < 0 \quad (8.7c)$$

However, the value used should not exceed 63 N/mm$^{3/2}$ (2 MPa$\sqrt{}$m) for assessments of surface-breaking flaws less than 1 mm deep.

Table 8.5 **Recommended fatigue crack growth threshold, ΔK_0, values for assessing welded joints**

Material	Environment	ΔK_0, N/mm$^{3/2}$ (MPa$\sqrt{}$m)
Steels, including austenitic	Air or other non-aggressive environments, up to 100 °C	63 (2)
Steels, excluding austenitic	Marine with cathodic protection, up to 20 °C	63 (2)
Steels, including austenitic	Marine, unprotected	0 (0)
Aluminium alloys	Air or other non-aggressive environments, up to 20 °C	21 (0.7)

8.2.3.7 Fatigue crack growth and crack growth threshold in nonferrous metals

Whenever possible, specific crack growth data for the material being considered should be used. For aluminium alloys, multi-branch crack growth relationships for a range of alloys are given in BS EN 1999-1-3. However, for approximate assessments ([8.15], [8.39], [8.40], [8.41]), the recommended crack growth constants of m = 3 and $A = 5.21 \times 10^{-13}$ for steels could be applied to another material with elastic modulus E by using m = 3 and the following value for A:

$$A = 5.21 \times 10^{-13} \left(\frac{E_{\text{steel}}}{E} \right)^3 \quad (8.8)$$

Similarly, the threshold stress intensity factor can be obtained from Equation (8.9) as follows:

$$\Delta K_0 = \Delta K_{0,\text{steel}} \left(\frac{E}{E_{\text{steel}}} \right) \quad (8.9)$$

8.2.4 Limits to crack propagation

In the fatigue assessment of planar flaws, an upper limit should be set to the extent of crack propagation that may be allowed without failure occurring during operation by any of the modes listed in Clause **5**. The maximum total stress should be used to determine the maximum acceptable crack size as referred to in Clause **5**.

8.3 Probability of survival

The simplified procedure outlined in **8.5** and the procedures for non-planar flaws and undercut given in **8.7** and **8.8**, respectively, are based on the results of large numbers of laboratory fatigue tests. These were analysed statistically assuming a

 © The British Standards Institution 2019

lognormal distribution of fatigue life to obtain the lower 95% confidence limit, corresponding to 97.7% probability of survival.

Similarly, use of the recommended (mean + 2SD) fatigue crack growth rate laws and crack growth thresholds (see **8.2.3**) corresponds to this probability of survival in fatigue life calculations. Other survival probabilities could be adopted from the information given in Table 8.3 and Table 8.4 or from the original data [8.13]. Alternatively, if the assessment is related to the quality categories (see **8.5**), use may be made of the fact that differences in fatigue life between the categories are approximately equivalent to one standard deviation.

8.4 General procedure for fracture mechanics assessment of planar flaws

8.4.1 The crack propagation relationship and relevant value of ΔK_0 should be determined as described in **8.2.3**. For elliptical flaws, it may normally be assumed that the same relationship applies for crack growth in both the *a* and *c* directions.

8.4.2 The relevant stress range should be determined (see **8.2.1**). For spectrum loading, unless the order of application of cycles is known, cycles, or blocks of cycles should be assumed to occur in the most damaging order. It is not always clear what the most damaging order is, and therefore it might be necessary to perform the calculations for various orders to determine the worst case.

8.4.3 For the actual or assumed flaw dimensions and position (see **8.2.2**), the stress intensity factor range, ΔK, corresponding to the applied stress range should be estimated. Stress intensity factor solutions are provided in Annex M. Alternatively, published solutions (e.g. references [8.42], [8.43], [8.44], [8.45]), numerical analysis methods or weight function techniques [8.45] may be used, but the basis of the method and the results should be documented. For partial-thickness surface or embedded flaws, ΔK should be determined at the ends of both the minor and major axes of the elliptical idealization of the flaw (see **8.2.2**).

8.4.4 The growth of the crack, Δa, should be estimated for one cycle from the value of ΔK calculated in **8.4.3** using the crack growth relationship determined in **8.4.1**. The dimension, *a*, should be increased by Δa. Similarly, the growth, Δc, at the ends of a part wall surface breaking or embedded flaw should be estimated for one cycle from the value of ΔK calculated for those flaw ends. The length of the flaw $2c$ should be increased by $2\Delta c$.

8.4.5 Taking the peak value of the tensile stress in the stress cycle, the stress intensity factor corresponding to the new size and shape should be estimated using **8.4.3**. For fatigue loading, the solutions in **8.4.3** can still be assumed to be applicable for stresses exceeding yield.

8.4.6 The incremented crack dimension obtained in **8.4.4** and the peak value of the stress intensity factor calculated in **8.4.5** should be compared with the limiting values with regard to other failure modes (see **8.2.4** and Annex E).

8.4.7 If acceptable, the next stress cycle should be considered and the procedure from **8.4.2** repeated. If the specified fatigue design life is reached and the limit to growth is not exceeded, the flaw should be regarded as acceptable. For elliptical and semi-elliptical flaws, the crack front shape changes as *a* increases. This analysis should be continued until one of the following occurs:

a) *For embedded flaws*: when the small ligament (nearest to the free surface) is assessed as having failed in accordance with Clause **7**, the flaw should be treated as a surface-breaking flaw of length $(2c + p)$. Fatigue crack growth is then assumed to continue, unless failure is deemed to have occurred for the re-characterised surface-breaking flaw, for example by leakage caused by breakthrough (see Figure E.1).

b) *For surface-breaking flaws*: when the ligament of the surface-breaking flaw fails in accordance with Clause **7**, it should be treated as a through-thickness flaw of length ($2c + B$) and the process of fatigue crack growth is then assumed to continue unless failure is deemed to have occurred, for example by leakage.

8.4.8 Continue until reaching a_f determined from Clause **7** or reaching the end of life, whichever happens first.

8.5 Basis of procedure for assessing flaws using quality categories

8.5.1 General

In this procedure, flaws are assessed on the basis of a comparison of the *S-N* curves that represent the actual and required fatigue strengths of the flawed weld. A grid of *S-N* curves is used, each curve representing a particular quality category. The flaw is acceptable if its actual quality category is the same as or higher than the required quality category.

The required quality category is determined for the service conditions to be experienced by the flawed weld. This may be fixed on the basis of the stress ranges and the total number of cycles of fatigue loading anticipated in the life of the component (see **8.5.3.1**). Alternatively, the quality category may be selected by reference to adjacent design details. This should include the weld being assessed (e.g. the toe of a butt weld in which an embedded flaw is being assessed). The quality category *S-N* curve need be no higher than the *S-N* curve for the design detail (see **8.5.3.2**).

The actual quality category for the flaw being assessed is determined from **8.6**, **8.7** or **8.8**, as appropriate.

Examples of the use of this approach are given in Annex U.

8.5.2 Quality categories

8.5.2.1 Quality category *S-N* curves

The quality categories refer to particular fatigue design requirements or the actual fatigue strengths of flaws and are defined in terms of the ten *S-N* curves in Figure 8.3 labelled Q1 to Q10. These are described by the following equation:

$$\Delta\sigma^3 N = \text{constant} \tag{8.10}$$

Values of the constant are given in Table 8.6. It is convenient to characterize each curve in terms of the stress range, S, corresponding to a particular fatigue life and Table 8.6 includes values of S corresponding to a life of 2×10^6 cycles.

 © The British Standards Institution 2019

Figure 8.3 **Quality category *S-N* curves**

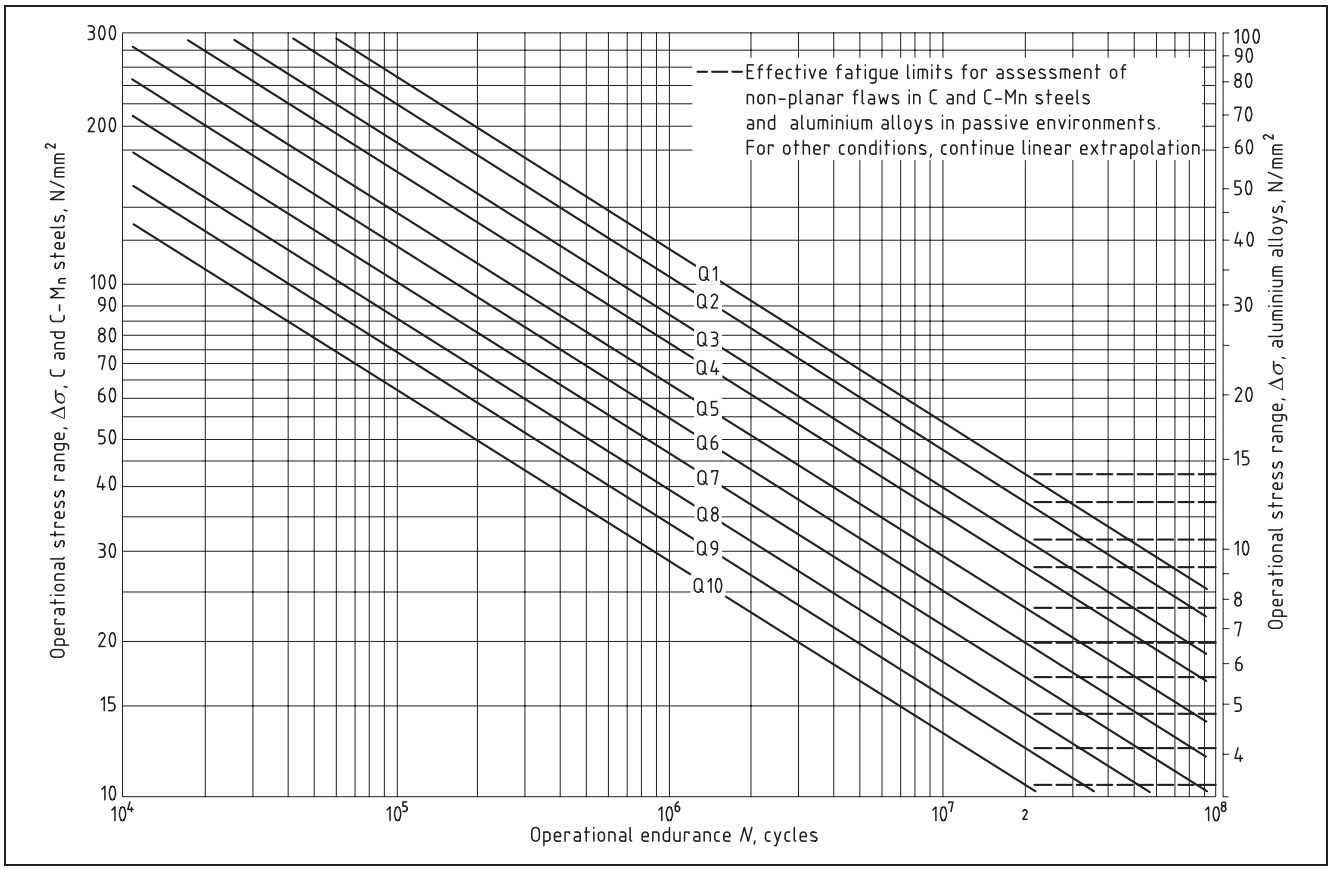


Table 8.6 **Details of quality category *S-N* curves**

Quality category	Constant in equation of curve $\Delta\sigma 3N$ = constant (values for steel)	Equivalent BS 7608 design class	Stress range, *S*, for 2×10^6 cycles	
			Steels N/mm^2	Aluminium alloys N/mm^2
Q1	1.52×10^{12}	D	91	30
Q2	1.04×10^{12}	E	80	27
Q3	6.33×10^{11}	F	68	23
Q4	4.31×10^{11}	F2	60	20
Q5	2.50×10^{11}	G	50	17
Q6	1.58×10^{11}	G2	43	14
Q7	1.00×10^{11}	—	37	12
Q8	6.14×10^{10}	—	32	10
Q9	3.89×10^{10}	—	27	9
Q10	2.38×10^{10}	—	23	8

To facilitate comparisons of the fatigue lives of flaws with those of weld design details in steels (see **8.5.3.2**), quality category *S-N* curves Q1 to Q6 are identical to the design *S-N* curves[8.2)] corresponding to 97.7% survival limits, for classes D to G2 in the fatigue design guidance document BS 7608 (see Table 8.6). Furthermore they are directly comparable with some of the design *S-N* curves in BS EN 1993-1-2 for welded steels. The flaw acceptance levels given also ensure 97.7% probability of survival when related to the quality category *S-N* curves. However, in the assessment of planar flaws, they may be adapted to

8.2) The equivalent curves BS 7608 use the notation $S_r - N$.

consider other probabilities of survival (see **8.6.4**), for example if a higher probability of survival is required for flaws than for design details.

8.5.2.2 Effect of material type

The majority of the data on which the procedures of **8.6** and **8.7** are based are from fatigue tests on welds containing flaws and from fatigue crack propagation studies on ferritic steels (some data for aluminium alloys were also analysed). It is, however, generally observed that, in dry air environments, fatigue cracks grow at closely similar rates in a wide range of steels, including austenitic stainless steels.

The curves in Figure 8.3 and the corresponding values of *S* in Table 8.6 for quality categories in aluminium alloy welds are identical to those for steel, but with the stress range divided by three. Furthermore, they are directly comparable with some of the design *S-N* curves in BS EN 1999-1-3, for welded aluminium.

For steels, the quality category *S-N* curves Q1 to Q6 in this standard are identical to those for various weld details in BS 7608. The quality category *S-N* curves for aluminium alloys do not necessarily coincide with the fatigue design *S-N* curves for welded aluminium alloys in other publications. This is particularly true for high design class details where the correlation between steel and aluminium based on their elastic moduli (see **8.2.3.7**) does not always hold, and fatigue design stresses for aluminium exceed one-third of those for steel. Account should be taken of this when selecting the required quality category by reference to adjacent design details (see **8.5.3.2**).

8.5.2.3 Stress-relieved welds

In view of the effect of residual stresses in welded joints (see **8.2.1**), the procedures for assessing flaws by reference to quality categories and the associated *S-N* curves are based on the use of the full stress range. This applies both to as-welded and to stress-relieved weldments, regardless of *R*. However, thermal stress relief has the beneficial effect of removing hydrogen from embedded slag inclusions and account is taken of this in deriving the permissible lengths of inclusions (see **8.7.3**).

8.5.3 Required quality category

8.5.3.1 Identifying the quality category by reference to service loading

The quality categories are identified as follows.

a) Constant amplitude loading

A quality category *S-N* curve lying above the point fixed by the required stress range and cyclic life.

b) Variable amplitude loading

Suppose the fatigue loading comprises k blocks with n_1 cycles at an applied stress range $\Delta\sigma_1$, n_2 cycles at $\Delta\sigma_2$, n_j cycles at $\Delta\sigma_j$, etc. Using Miner's rule, the equivalent constant amplitude stress range, S, corresponding to 2×10^6 cycles is then calculated using the following equation:

$$S = \left(\frac{\sum_{j=1}^{j=k} \Delta\sigma_j{}^3 n_j}{2 \times 10^6} \right)^{1/3} \qquad (8.11)$$

The required quality category is that corresponding to the stress range in Table 8.6 that is next above the calculated *S* value.

8.5.3.2 Identifying the quality category by comparison with design details

One rationale for the acceptance of a flaw is that its fatigue life is no lower than that of an adjacent standard detail, which is known to have an adequate life. This provides a basis for selecting the quality category required for the flaw. For example, a flaw in a transverse butt weld would be acceptable if its quality category *S-N* curve coincided with the design *S-N* curve for the (flaw-free) butt weld for failure from the weld toe. To facilitate the selection of quality category by such means for steels, Q1 to Q6 *S-N* curves coincide with those for standard weld detail classes D to G2 in BS 7608.

The presence of, for example, a nominal Class D detail, does not imply that the fatigue design stresses and lives are the maximum allowable for such a detail. This Class D detail might, for example, be adjacent to one of Class F, in which case the fatigue design would be fixed by the latter. In such a case, the quality category to which the nominal Class D weld should be inspected is Q3 and not Q1. Additional lower quality categories, Q7 to Q10, have been included to allow for those cases where fatigue loading is not the controlling criterion in determining the types of joint detail to be used in a weldment, but where fatigue cannot be ignored in an assessment of flaws. These do not relate to any specific joint classification and have been arbitrarily chosen.

The quality categories may be used where there is no detailed knowledge of the fatigue loadings. In this case, the required category may be matched to the lowest design detail in the same part of the weldment and subjected to the same stress ranges as the weld under consideration. In this case there is an equal probability of failure from the design detail as from any weld flaws assessed by these methods.

8.6 Assessment of planar flaws using quality categories

8.6.1 General

The procedure described in this subclause makes use of the results of fracture mechanics calculations already performed and presented graphically. The calculations were carried out using the general procedure given in **8.4** for selected geometries of welded joints containing planar flaws, subjected to either axial or bending loading, with the recommended Paris crack growth law for steels, i.e. $m = 3$ and $A = 5.21 \times 10^{-13}$, in Equation (8.1). Application of the graphs for other values of A is also described, using the appropriate stress intensity factor solutions from Annex M and therefore incorporating change in crack front shape as the crack propagates in the calculations.

8.6.2 Quality category for flaw

The actual quality categories for a range of planar flaws are determined using Figure 8.4 to Figure 8.8 depending on the type of flaw (surface or embedded), its location, the geometry of the weld detail containing the flaw and the loading. The first step is to convert actual flaw dimensions, a and $2c$, to an effective initial flaw parameter, $\bar{a}_i$, corresponding to a straight-fronted crack ($a/2c \rightarrow 0$), using Figure 8.4 to Figure 8.8, as appropriate.

A tolerable value of the flaw parameter, $\bar{a}_{max}$, to which fatigue crack growth is permitted, should be specified. Again, this is an equivalent straight-fronted crack. It might refer to failure (see **8.2.4**), or to some other criterion (e.g. detectability of the fatigue crack), in which case $\bar{a}_{max}$ is lower. However, if the tolerable flaw size does not refer to failure, $\bar{a}_{max}$ could be specified directly as the tolerable height of straight-fronted flaw. Alternatively, if the tolerable flaw

is specified in terms of an elliptical shape (e.g. minimum size of crack of a specified shape which is detectable in service), it could be specified as the straight-fronted flaw which is equivalent to the actual tolerable flaw in terms of the remaining fatigue life. Thus, $\bar{a}_{max}$ is obtained in the same way as $\bar{a}_i$ using Figure 8.4 to Figure 8.8, as appropriate. The corresponding quality category is found from Figure 8.4 to Figure 8.8, as appropriate, as follows.

a) Entering the figures at $\bar{a}_{max}$ on the ordinate axes and (interpolating as necessary); for the given thickness, B, a value of S should be read off, namely S_m.

b) Entering the figures at $\bar{a}_i$ on the ordinate axes and (interpolating as necessary); for the given thickness, B, a value of S should be read off, namely S_i.

Then:

$$S = \left(S_i^3 - S_m^3\right)^{1/3} \quad (8.12)$$

If $\bar{a}_{max} \gg \bar{a}_i$, then $S \approx S_i$. The actual quality category for the flaw in question is the next below S in Table 8.6. If this is the same as or higher than the required quality category, the flaw is acceptable.

8.6.3 Background to assessment of planar flaws using the quality category approach

The quality category procedure is based on the integration of the crack propagation law for a constant stress range from an initial flaw size either until the crack penetrates through the thickness or until some other failure mode intervenes. The integration was performed using Equation (8.1) with $A = 5.21 \times 10^{-13}$ and $m = 3$, which results in 97.7% probability of survival.

The method of calculation used a block size in which the number of cycles was less than 0.5% of total life. For each welded joint geometry and material thickness from 5 mm to 100 mm, calculations were performed for a range of flaw sizes and shapes ranging from straight-fronted (i.e. $a/2c \rightarrow 0$) to semicircular ($a/2c = 0.5$) surface flaws or circular ($2a/2c = 1$) buried flaws. The stress intensity factor solutions from Annex M were used. The crack front shape was automatically adjusted after each increment of crack growth. In the case of weld toe flaws, the assumption was made that, for surface crack growth, M_k was constant and corresponded to the value for a crack height $a = 0.15$ mm. Straight-fronted cracks were assumed to remain straight-fronted throughout their fatigue lives. In this way, flaw sizes corresponding to the quality category S-N curves were determined as a function of material thickness and flaw shape for each joint geometry. The results for straight-fronted flaws are presented in Figure 8.4 to Figure 8.8.

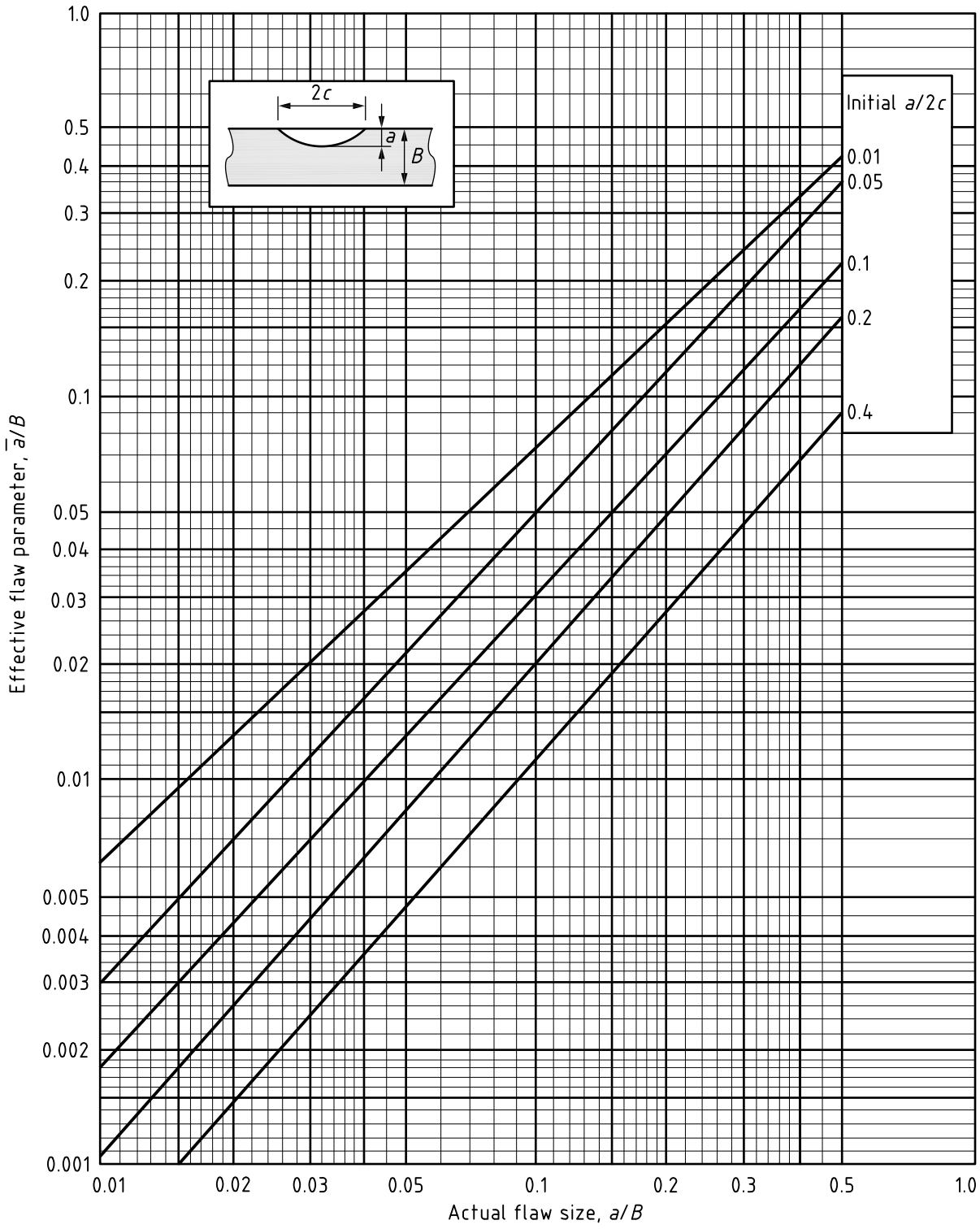
Comparison of the results for straight-fronted and elliptical flaws for each quality category enabled the height of a straight-fronted crack that was equivalent in terms of fatigue strength to an elliptical flaw to be established. This is the effective initial flaw parameter $\bar{a}_i$, which is plotted as a function of equivalent elliptical flaw shape and material thickness in Figure 8.4 to Figure 8.8. The use of these figures in conjunction with Figure 8.4 to Figure 8.8 enables any initial flaw shape to be considered.

 © The British Standards Institution 2019

The application of Equation (8.12) is equivalent to the subtraction of the integral of Equation (8.3), for crack growth from $\bar{a}_{max}$ to B, from that for growth from $\bar{a}_i$ to B, thus deducting the fatigue life lost as a result of the intervention of an alternative failure mode.[8.3)]

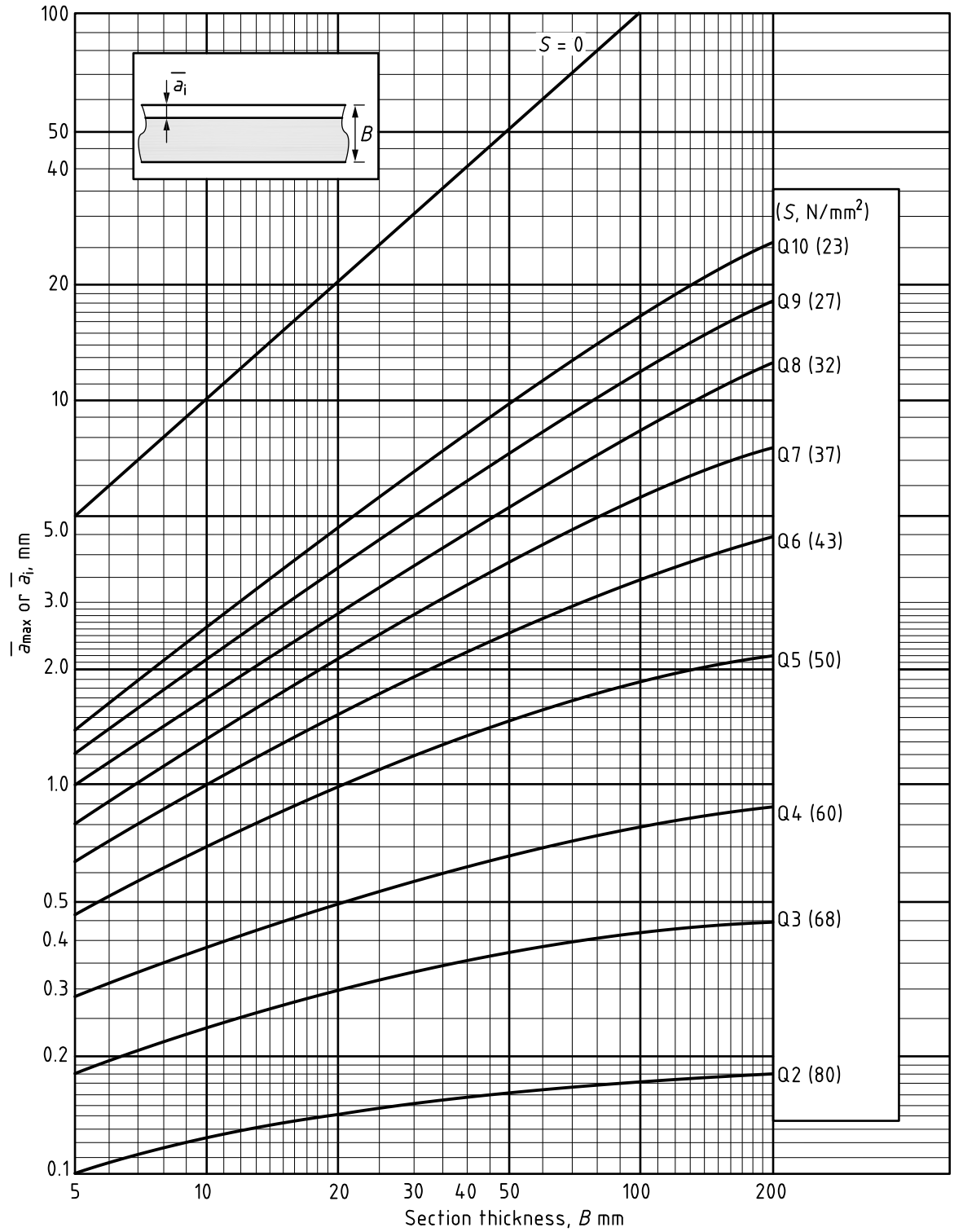
8.3) As shown by Figure 8.7, it is virtually impossible to detect the size of flaw which would be considered acceptable at the toes of fillet welds for design to Classes F or F2 (categories Q3 and Q4). The bases for the *S-N* curves for the various joint classes are test data for nominally sound welds made under laboratory conditions [8.46]. It is almost certain that none of the test welds had flaws of normally detectable size at the weld toe. However, they will have had, in this position, the small slag intrusions observed by Signes et al [8.47]. Watkinson et al [8.48] showed these to vary in size between 0.15 mm and 0.4 mm and it is interesting to observe that this range lies between quality categories Q3 and Q5 for a material thickness of about 10 mm in Figure 8.7b)iii). These are the equivalent categories to the fillet-welded details in Classes F and G.
The curves of Figure 8.7 also highlight the thickness effect [8.49] whereby, after an initial rise, the allowable initial flaw size tends to drop rapidly as thickness increases. The physical explanation for this is that the depth below the surface over which the stress concentration effect of a fillet weld is active is proportional to thickness. Thus, in thick material, the fatigue crack will be influenced over much more of its growth by this stress concentration. Almost all of the work surveyed by Gurney and Maddox [8.46] was on specimens 10 mm to 12 mm thick. Experimental work on thicker material ([8.50], [8.51]) indicates that the trend shown in Figure 8.7 is reasonable.

Figure 8.4 **Quality category approach: assessment of surface flaws in plates under axial loading**



a) Relation between actual flaw dimensions and effective flaw parameter

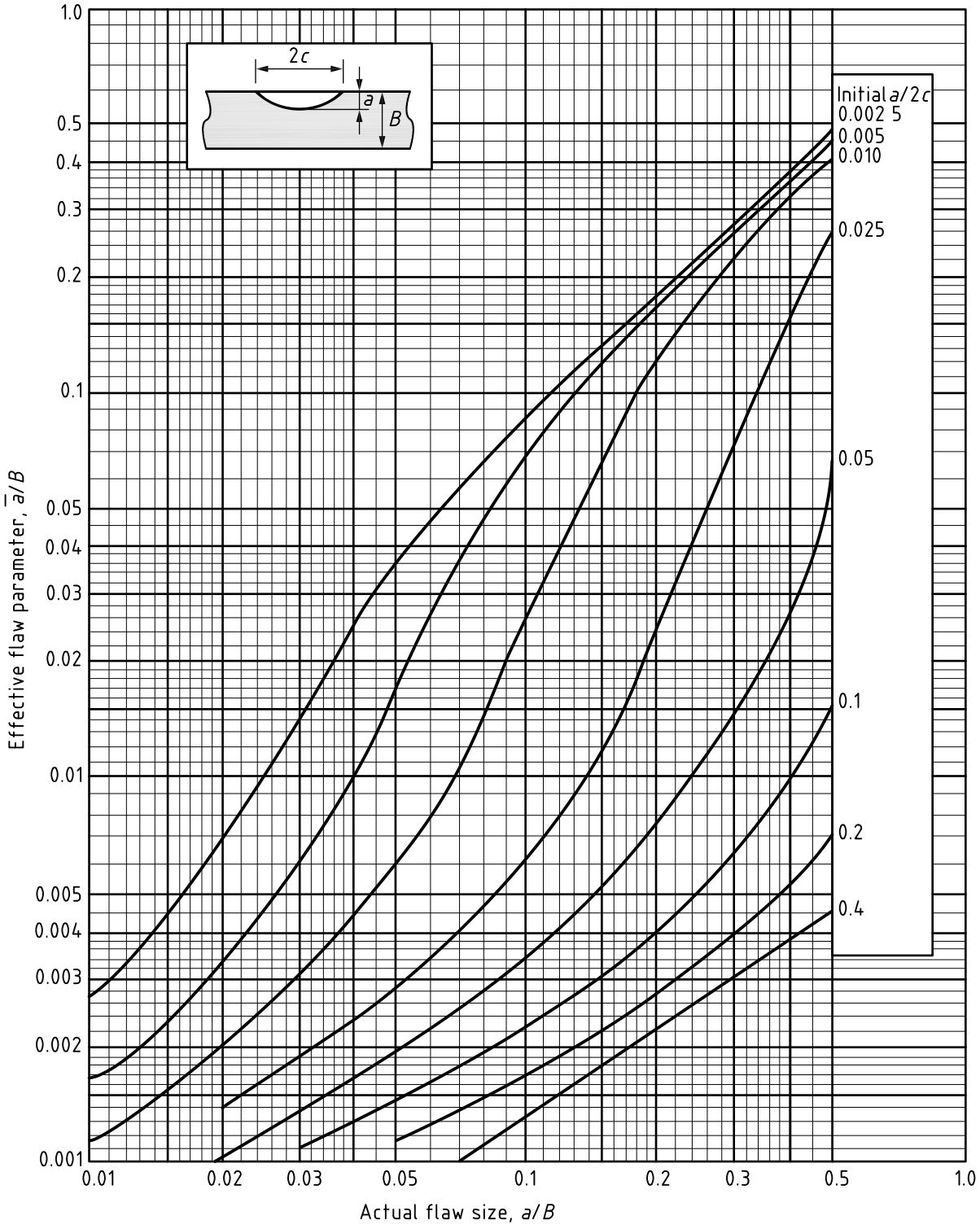
Figure 8.4 **Quality category approach: assessment of surface flaws in plates under axial loading** *(continued)*



b) Relation between effective flaw parameter, section thickness and quality category

NOTE Values of S are for steel. For aluminium alloys, divide by 3.

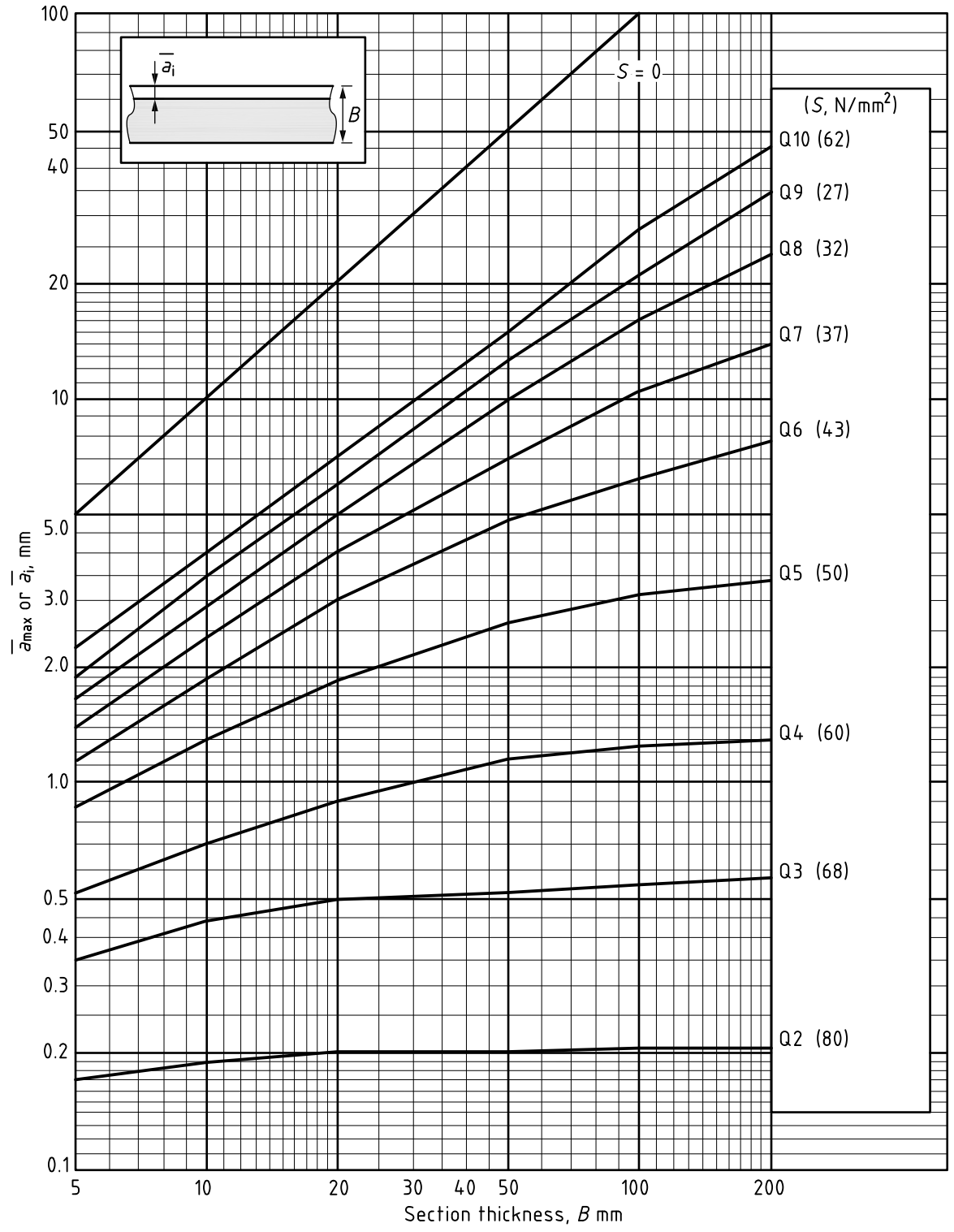
Figure 8.5 **Quality category approach: assessment of surface flaws in plates (no weld toe or other stress raiser) in bending**



a) Relation between actual flaw dimensions and effective flaw parameter

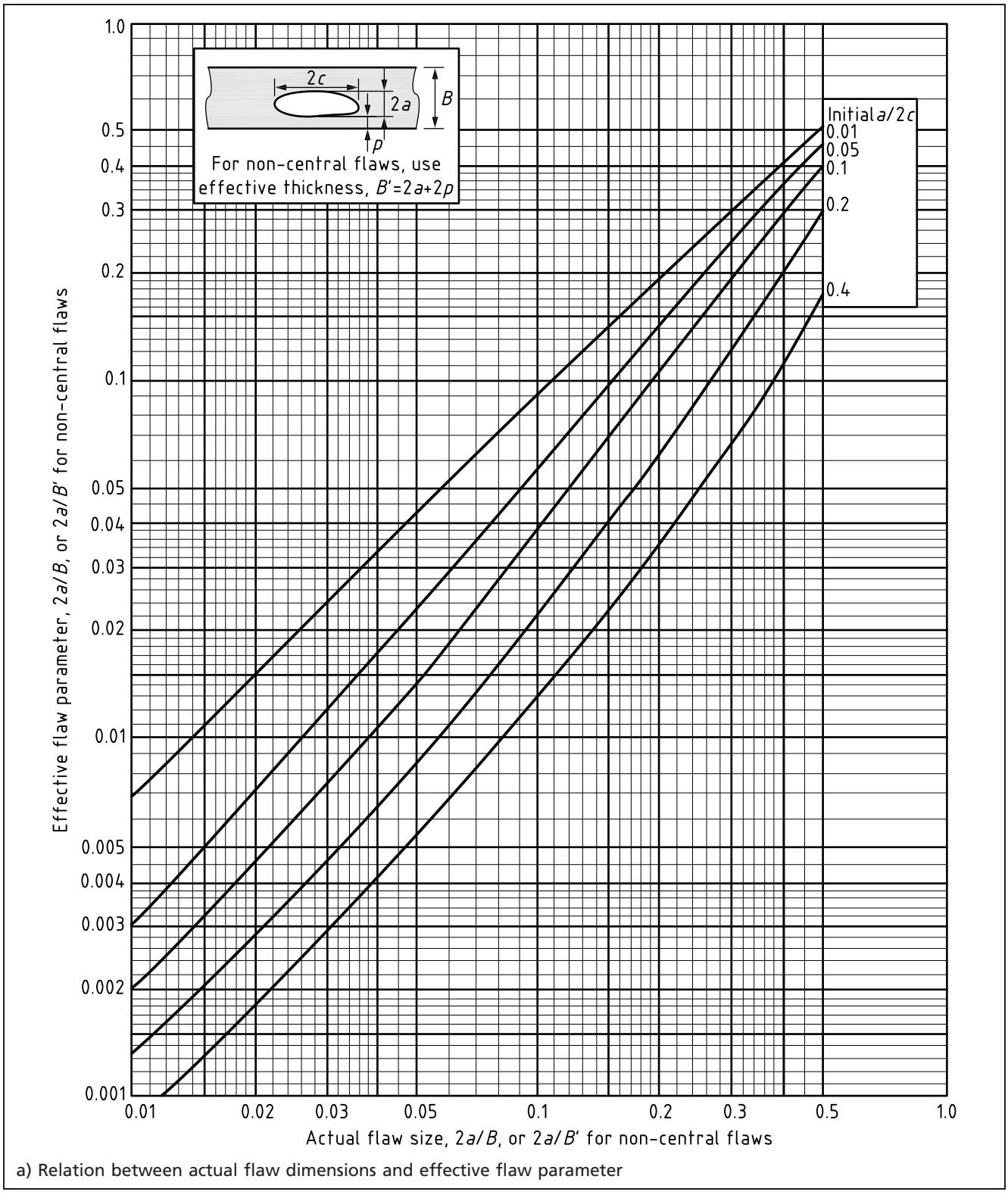
 © The British Standards Institution 2019

Figure 8.5 **Quality category approach: assessment of surface flaws in plates (no weld toe or other stress raiser) in bending** *(continued)*



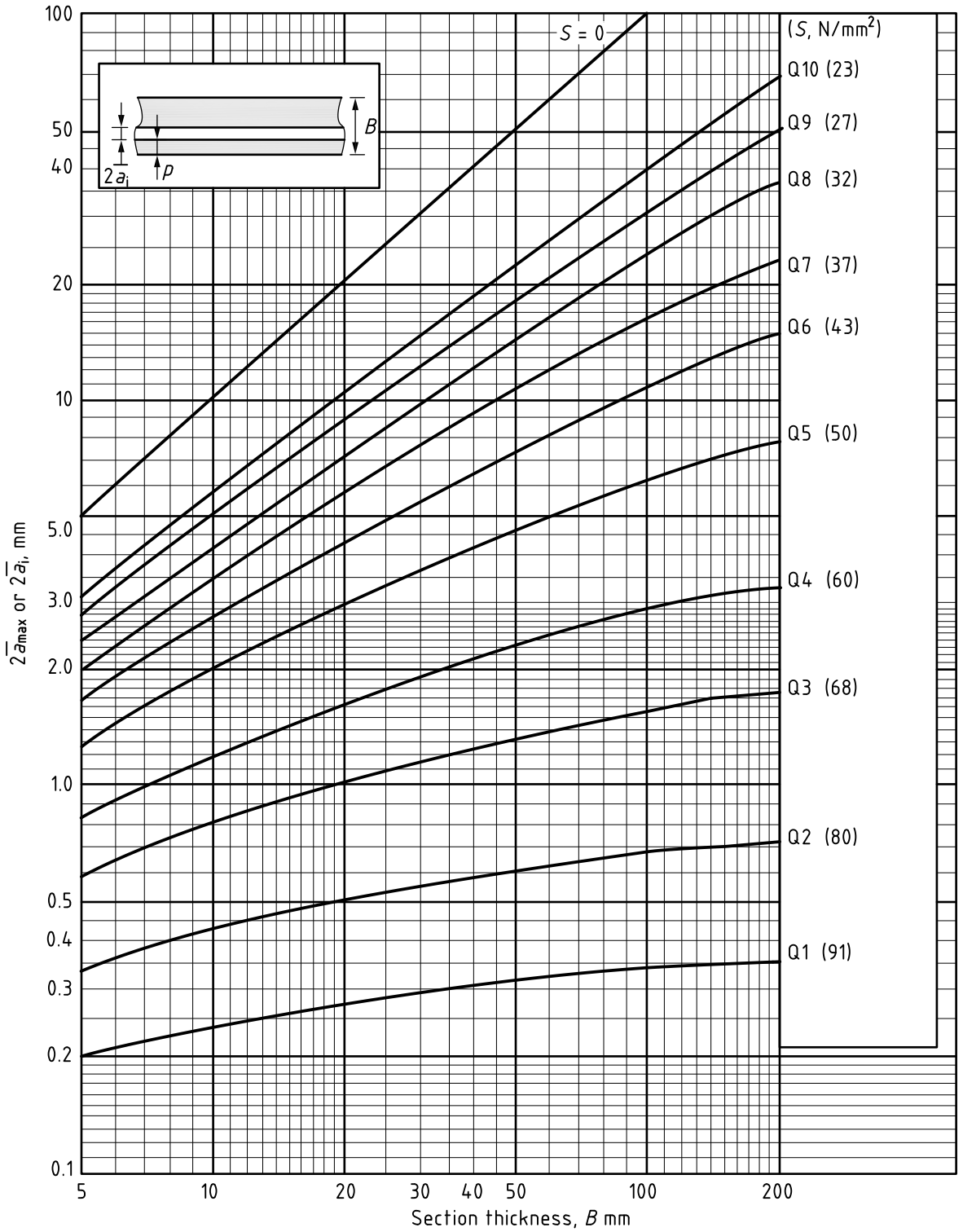
b) Relation between effective flaw parameter, section thickness and quality category

Figure 8.6 **Quality category approach: assessment of embedded flaws in axially loaded joints**



a) Relation between actual flaw dimensions and effective flaw parameter

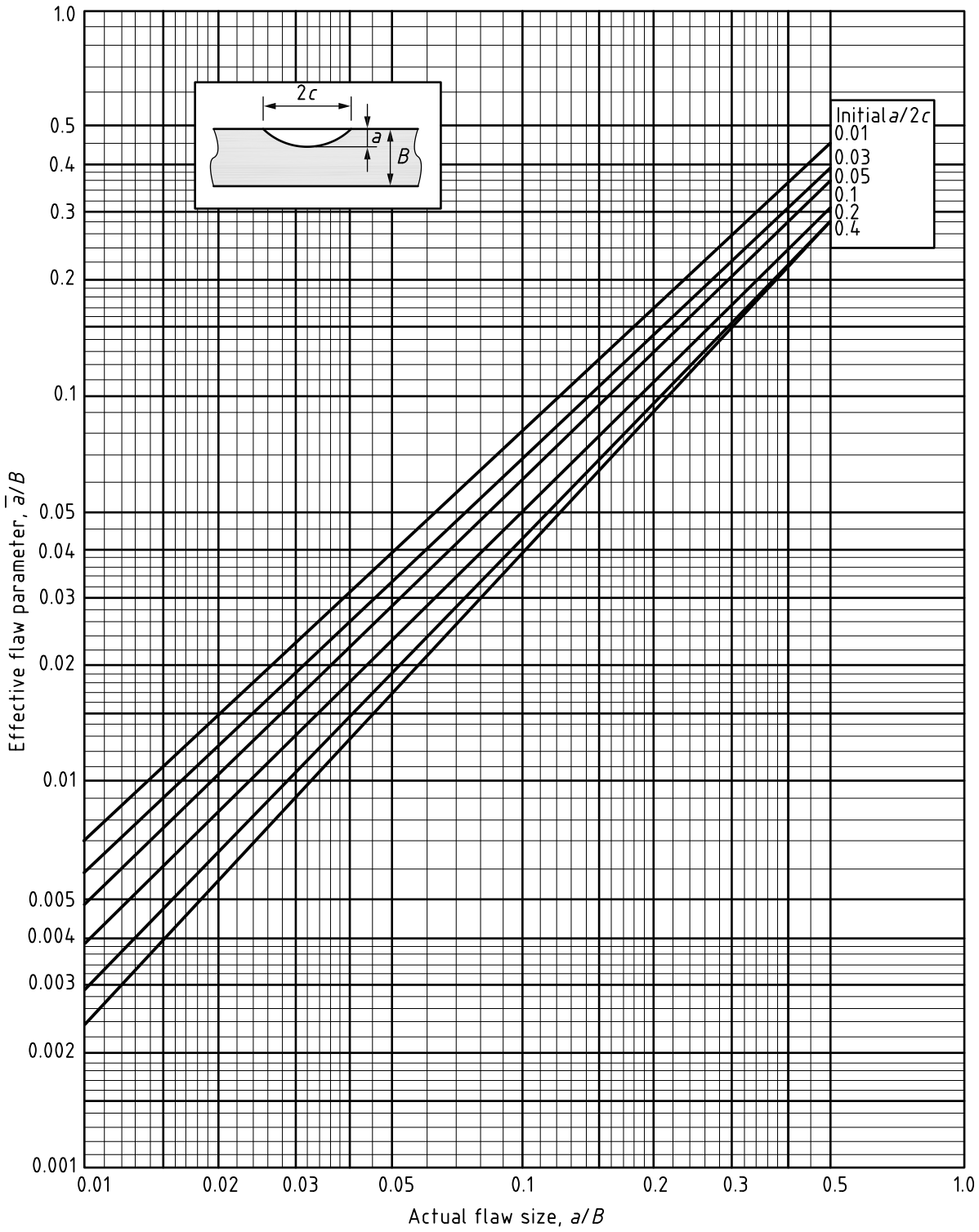
Figure 8.6 **Quality category approach: assessment of embedded flaws in axially loaded joints** *(continued)*



b) Relation between effective flaw parameter, section thickness and quality category

NOTE Values of S are for steel. For aluminium alloys, divide by 3.

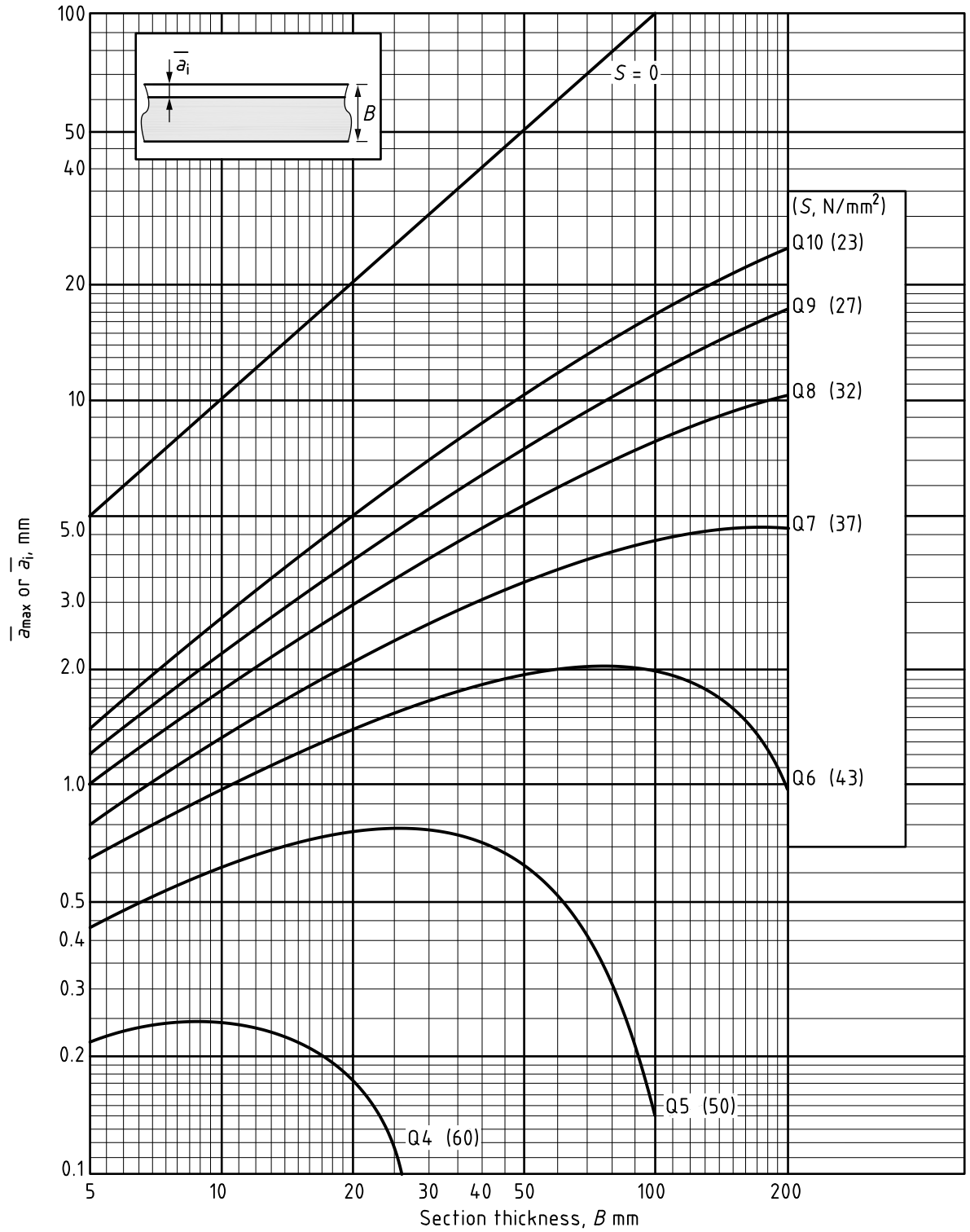
Figure 8.7 **Quality category approach: assessment of weld toe flaws in axially loaded joints**



a) Relation between actual flaw dimensions and effective flaw parameter

NOTE Values of S are for steel. For aluminium alloys, divide by 3.

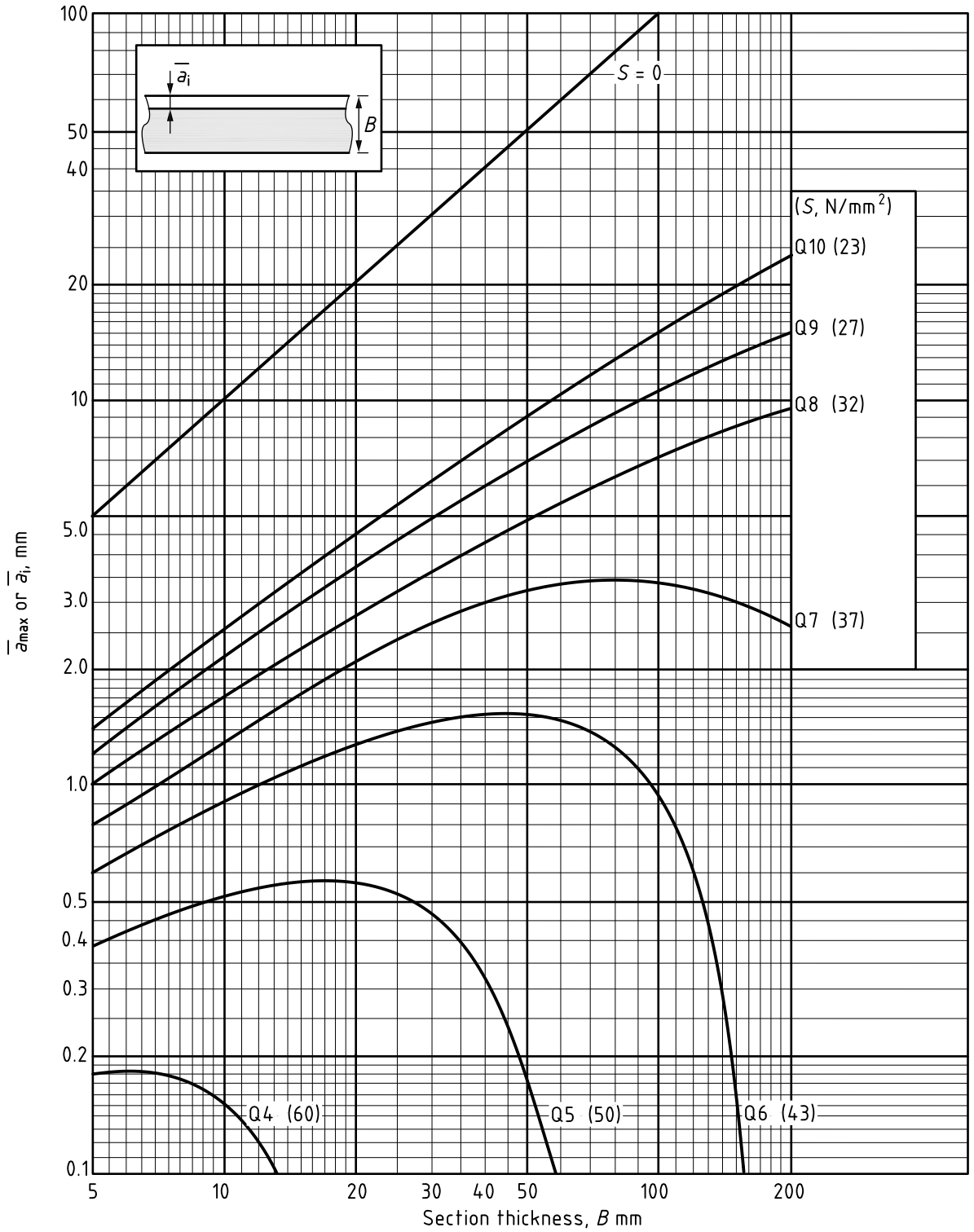
Figure 8.7 **Quality category approach: assessment of weld toe flaws in axially loaded joints** *(continued)*



b) Relation between effective flaw parameter, welded joint geometry and quality category
i) L/B = 0.5

NOTE Values of S are for steel. For aluminium alloys, divide by 3.

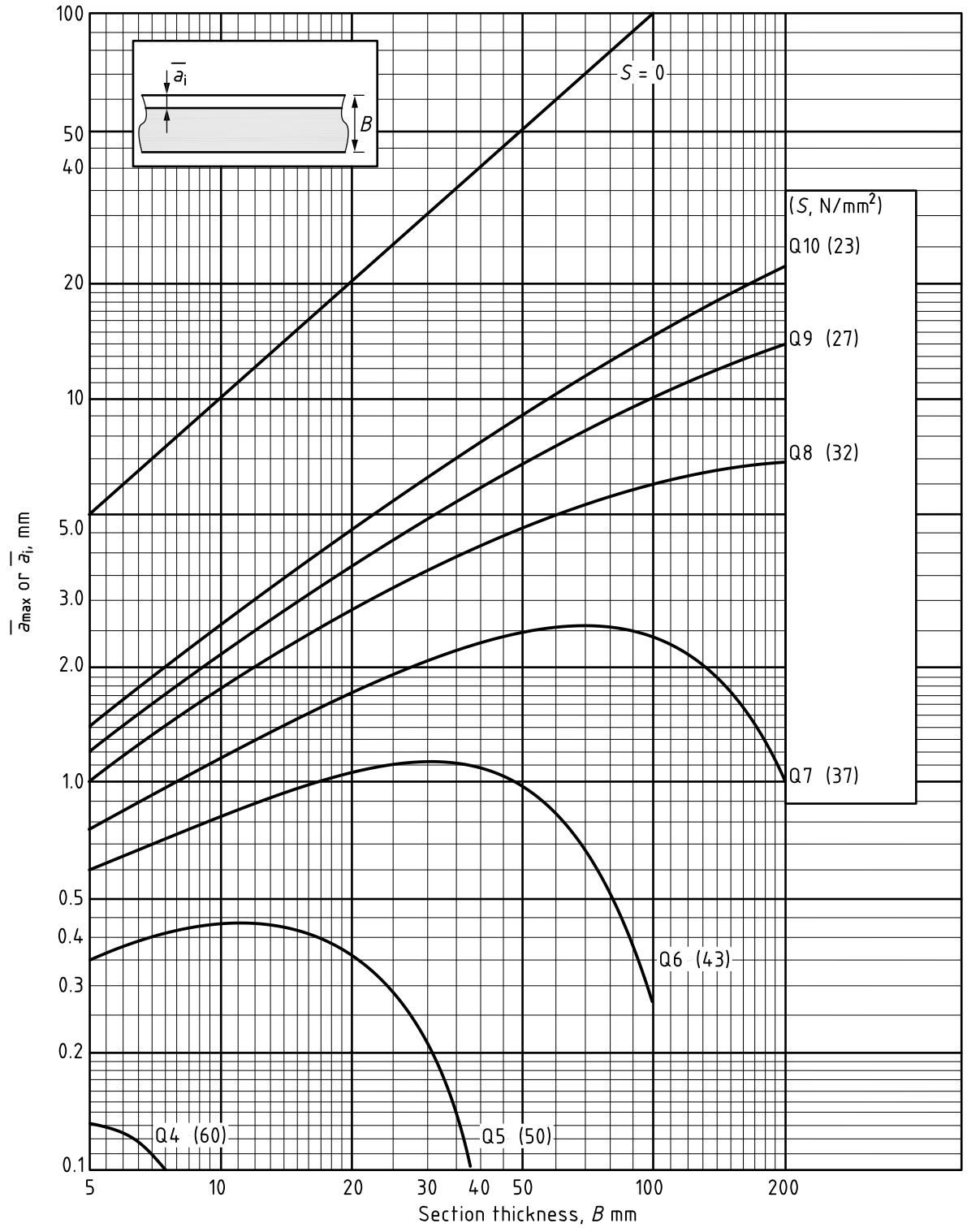
Figure 8.7 **Quality category approach: assessment of weld toe flaws in axially loaded joints** *(continued)*



b) Relation between effective flaw parameter, welded joint geometry and quality category
ii) L/B = 0.75

NOTE Values of S are for steel. For aluminium alloys, divide by 3.

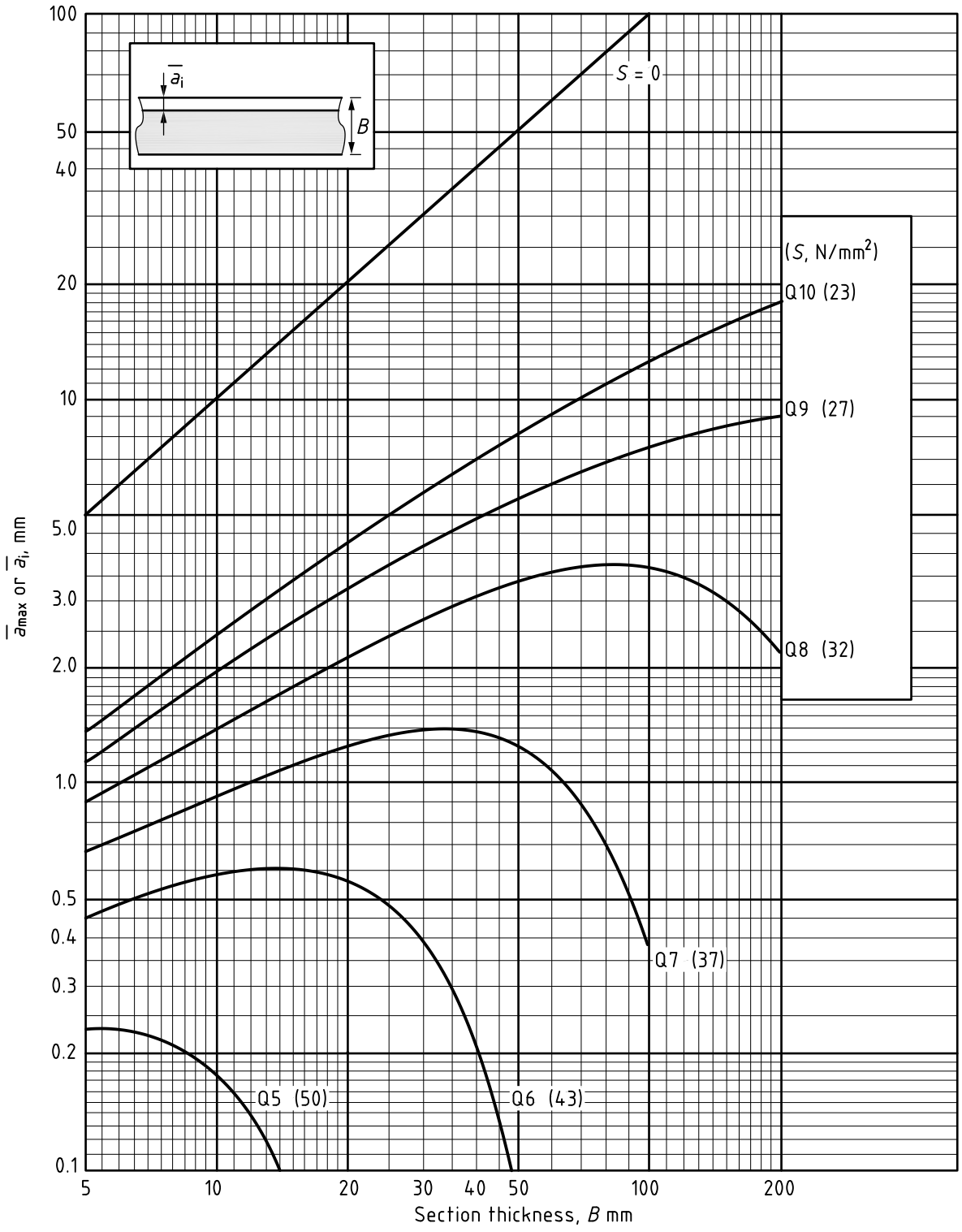
Figure 8.7 **Quality category approach: assessment of weld toe flaws in axially loaded joints** *(continued)*



b) Relation between effective flaw parameter, welded joint geometry and quality category
iii) L/B = 1.0

NOTE Values of S are for steel. For aluminium alloys, divide by 3.

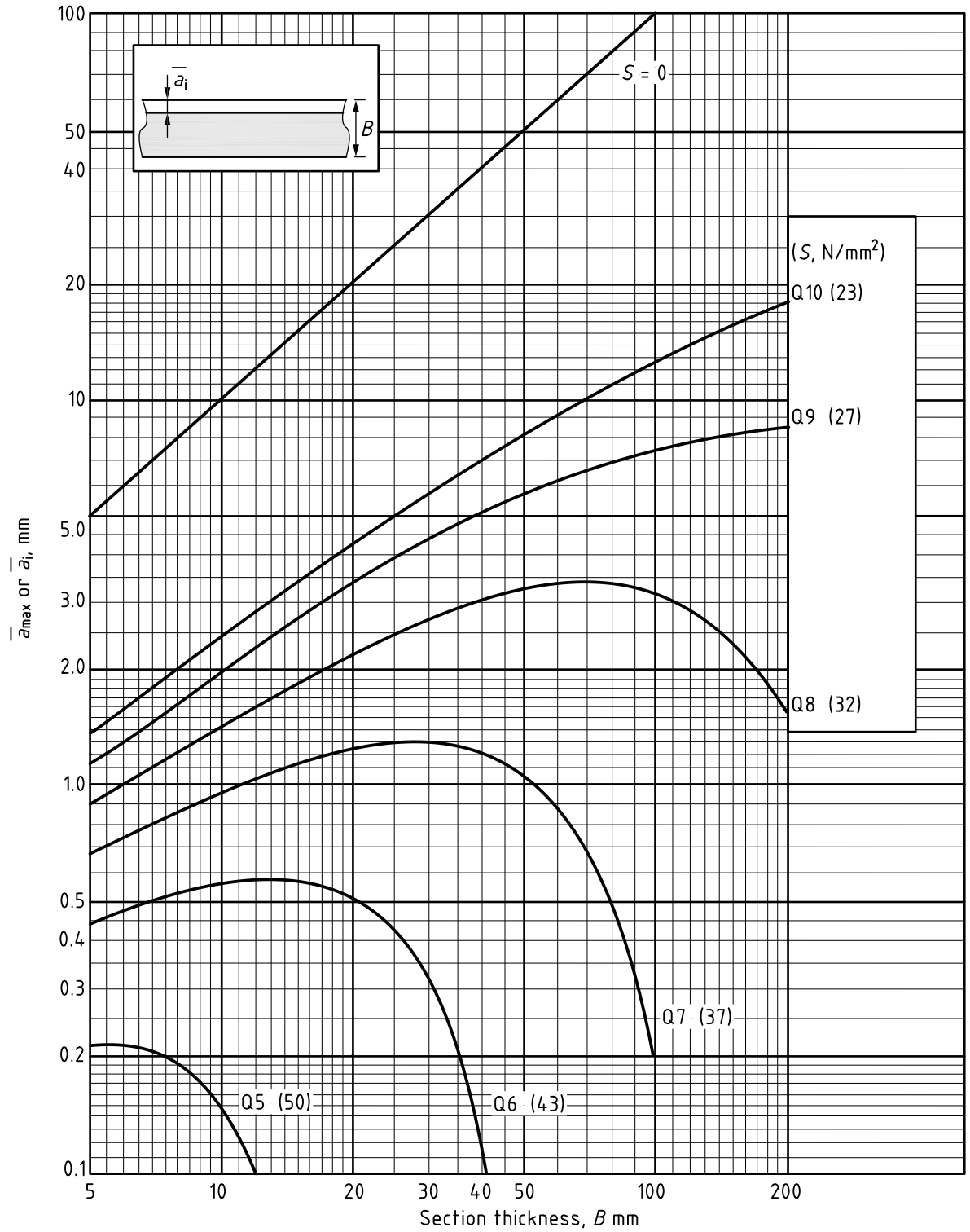
Figure 8.7 **Quality category approach: assessment of weld toe flaws in axially loaded joints** *(continued)*



b) Relation between effective flaw parameter, welded joint geometry and quality category
iv) L/B = 1.8

NOTE Values of S are for steel. For aluminium alloys, divide by 3.

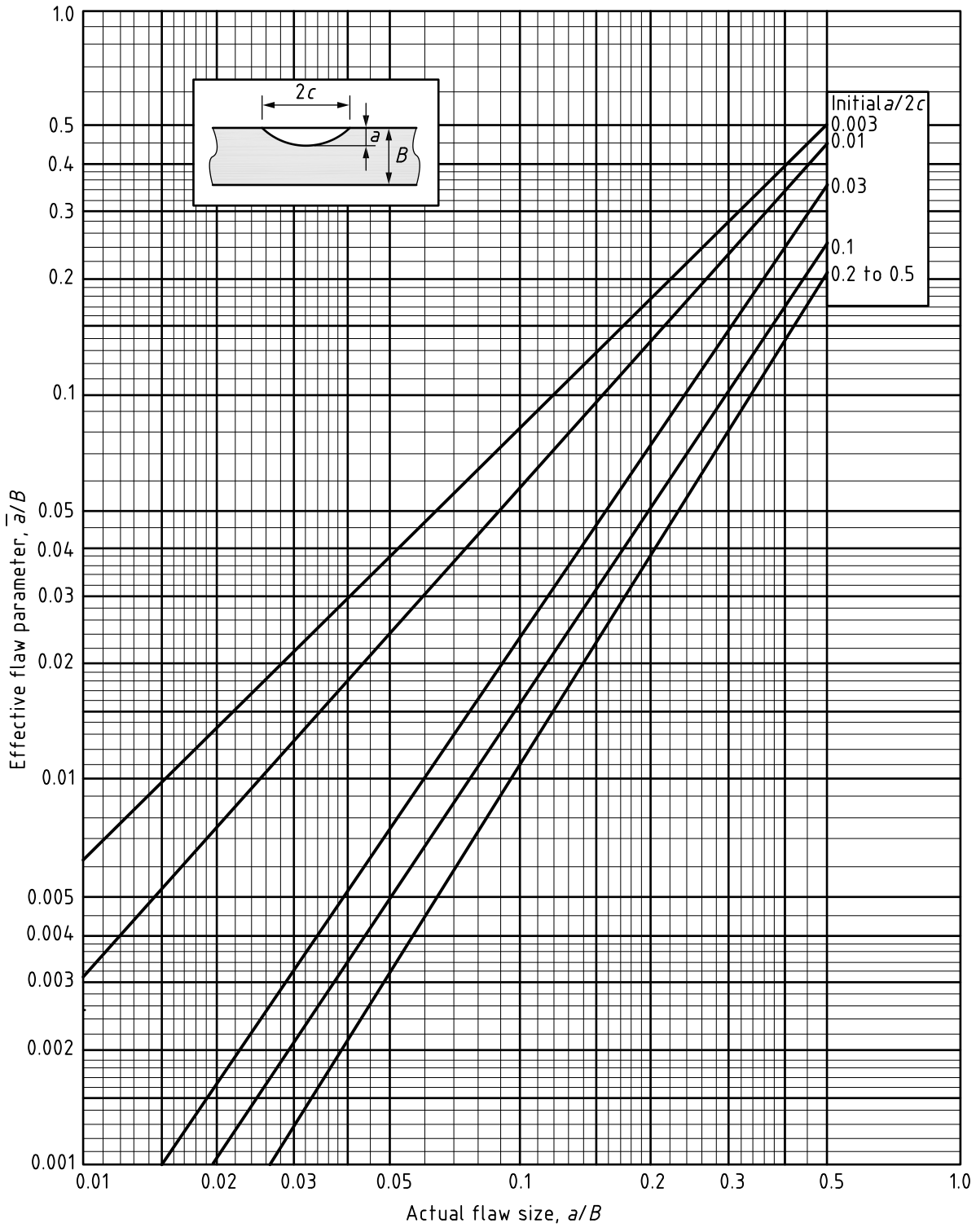
Figure 8.7 **Quality category approach: assessment of weld toe flaws in axially loaded joints** *(continued)*



b) Relation between effective flaw parameter, welded joint geometry and quality category
v) L/B = 5.3

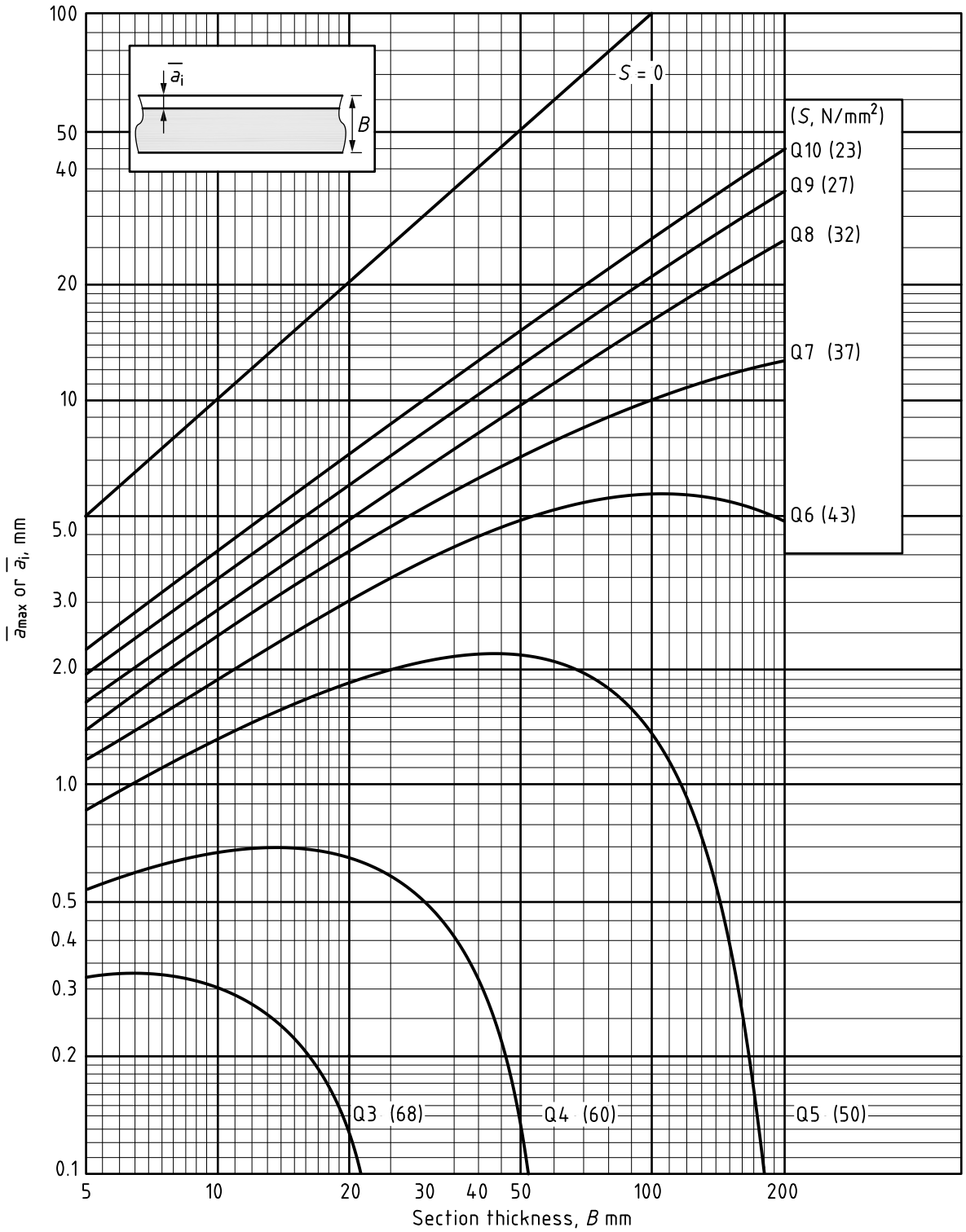
NOTE Values of S are for steel. For aluminium alloys, divide by 3.

Figure 8.8 **Quality category approach: assessment of weld toe flaws in joints loaded in bending**



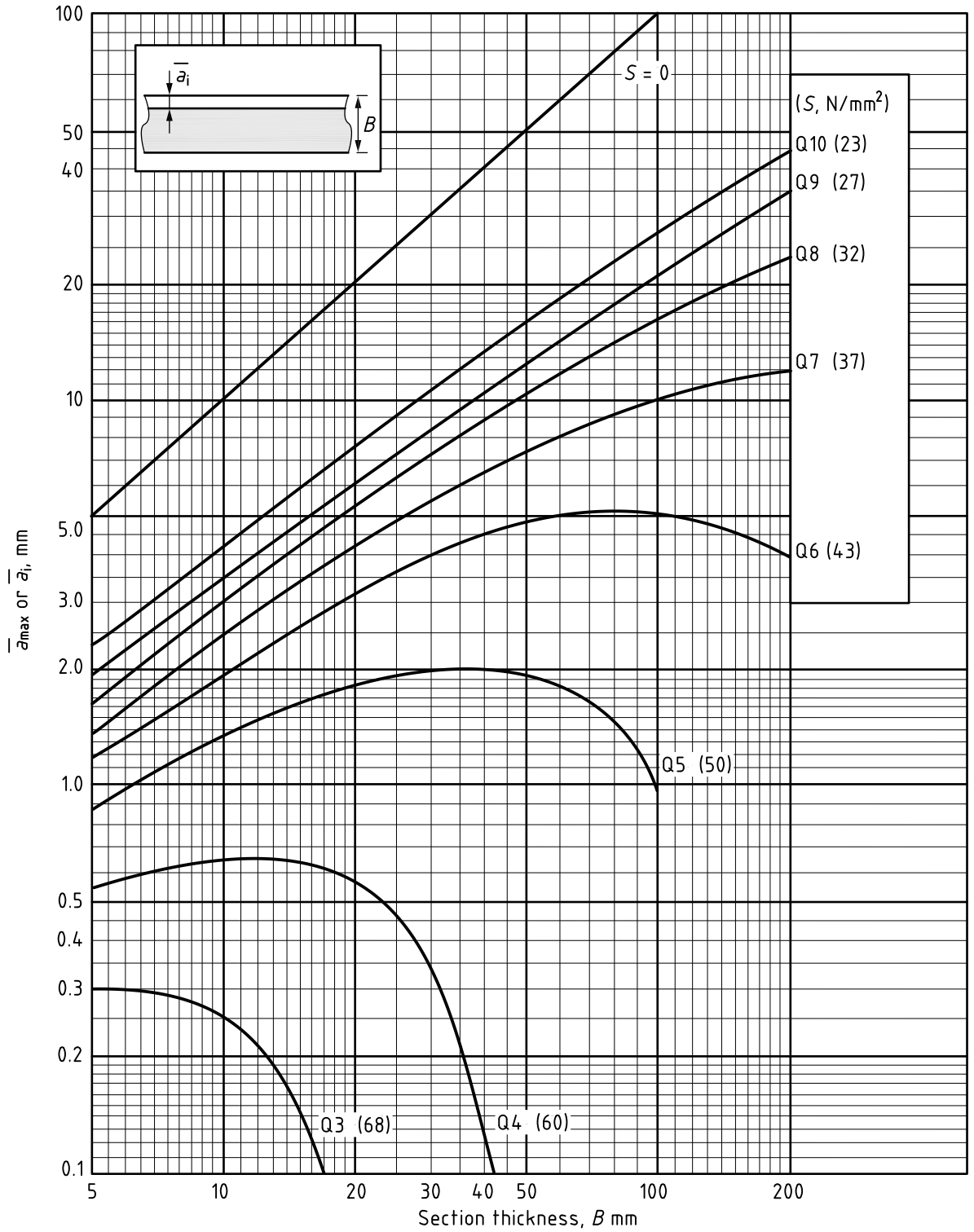
a) Relation between actual flaw dimensions and effective flaw parameter

Figure 8.8 **Quality category approach: assessment of weld toe flaws in joints loaded in bending** *(continued)*



b) Relation between effective flaw parameter, welded joint geometry and quality category
i) $L/B < 1.0$

Figure 8.8 **Quality category approach: assessment of weld toe flaws in joints loaded in bending** *(continued)*



b) Relation between effective flaw parameter, welded joint geometry and quality category
ii) $L/B \geq 1.0$

NOTE Values of S are for steel. For aluminium alloys, divide by 3.

8.6.4 Quality categories for different crack growth rate assumptions

The curves in Figure 8.4 to Figure 8.8 have been calculated using the values $m = 3$ and $A = 5.21 \times 10^{-13}$. They are only applicable for $m = 3$ but, as fatigue life is directly proportional to A, they may be used for other values of A if an effective quality category is established.

Expressed in terms of S, the stress range S^1 corresponding to this effective quality category for a crack growth constant A^1 is as follows:

$$S^1 = S\left(\frac{5.21 \times 10^{-13}}{A^1}\right)^{1/3} \tag{8.13}$$

Therefore in order to assess a surface flaw in a steel structure in seawater using the values of m and A recommended in **8.2**, the flaw is first assessed using **8.6.2** and a quality category determined. Suppose this is Q4, so that $S = 60$ N/mm^2. Then:

$$S^1 = 60\left(\frac{5.21 \times 10^{-13}}{2.3 \times 10^{-12}}\right)^{1/3} = 37\,\text{N/mm}^2 \tag{8.14}$$

giving an effective quality category of Q8. This effective quality category is compared with the required quality category to assess the acceptability of the flaw.

The same procedure could be used to consider a different probability of survival to that embodied in the curves in Figure 8.4 to Figure 8.8, that is 97.7% (approximately two standard deviations from the mean), by defining the appropriate value of A. Alternatively, one step in the quality categories is approximately equivalent to one standard deviation of log(life) or log(crack growth rate). Therefore, for 99.9% probability of survival (approximately three standard deviations from the mean) only flaws compatible with Q3 would be acceptable in order to achieve a required quality category of Q4.

8.7 Assessment of embedded non-planar flaws using quality categories

8.7.1 General

Only flaws that are shown to be embedded and non-planar as defined in Clause **4**b) should be analysed for acceptability in accordance with the criteria in this subclause. If there is any uncertainty, flaws should be assumed to be planar and assessed in accordance with the procedures in **8.5** or **8.7**.

As is the case with the *S-N* curves for design details, fatigue failure in this subclause corresponds to the attainment of through-thickness fatigue cracking. Therefore, if it is required to take into account other failure criteria (e.g. fracture from a part-through-thickness crack), the flaw should be assessed as planar.

As it is usually difficult to determine the distance between multiple slag inclusions occurring in the same cross-section, they should be treated as a single planar flaw of height 2a equal to the total height of material containing inclusions. If, however, it can be demonstrated that the separation between such flaws is >1.25 times the height of the larger flaw, they may be assessed as separate slag inclusions, in accordance with **8.7.4** (Table 8.8 or Table 8.9, as appropriate).

The treatment may be applied to carbon and carbon manganese steels and to low alloy pressure vessel steels operating at temperatures up to 375 °C. It may also be applied to austenitic stainless steels up to 430 °C and to aluminium alloys up to 100 °C, in all cases for material thicknesses of at least 10 mm.

8.7.2 Required quality category

The quality category required should be determined in accordance with **8.5.2**. However, if Equation (8.11) is used, an effective fatigue limit may be assumed, such that all values of $\Delta\sigma_j$ below those given in Table 8.7 may be ignored in deriving the equivalent constant amplitude stress range, *S*.

Table 8.7 **Minimum values of $\Delta\sigma_j$ for assessing non-planar flaws and shape imperfections**

Quality category	Minimum value of $\Delta\sigma_j$ for inclusion in calculation of *S*	
	Steels N/mm^2	**Aluminium alloys** N/mm^2
Q1	42	14
Q2	37	12
Q3	32	11
Q4	28	9
Q5	23	8
Q6	20	7
Q7	17	6
Q8	15	5
Q9	12	4
Q10	11	4

Since the stress ranges that may be ignored depend on the quality category required and this in turn depends on *S*, it is sometimes necessary to iterate to arrive at the final quality category required.

8.7.3 Quality category for non-planar flaws

If the detected non-planar flaw is smaller than that given in **8.7.4** (Table 8.8 or Table 8.9 as appropriate), it should be regarded as acceptable. In assessing porosity, the area of radiograph to be considered should be the length of weld affected by porosity times the maximum width of the weld. Individual pores larger in diameter than *B*/4 or 6 mm, whichever is the lesser, should be repaired.

8.7.4 Background to the assessment of embedded non-planar flaws

The method for assessing embedded non-planar flaws outlined in this subclause is based on a very large volume of data, giving results of fatigue tests on butt welds in steel containing slag inclusions ([8.52], [8.53]) and in steel welds containing porosity [8.54].

Table 8.8 and Table 8.9 give different limits for slag inclusions in as-welded and stress-relieved welds. Larger inclusions are tolerable in stress-relieved welds and it is believed that this is entirely due to the elimination of hydrogen from the voids as a result of PWHT. For weldments where an effective stress relief can be shown to have been achieved mechanically but where PWHT has not been performed, the limits of Table 8.8 should be applied.

The limits for porosity that could be permitted purely from a fatigue point of view are very large. The levels given in Table 8.8 and Table 8.9 are based on the density of porosity that might interfere with radiographic inspection and mask other flaws. Reasonable judgement has to be exercised in interpreting the condition given in **8.7.3** that the area of radiograph to be considered should be the length of weld affected by porosity times the maximum width of the weld. Clearly, if a small area of weld contains dense porosity with a much larger surrounding area containing sparse porosity, the area of radiograph to be

assessed should be that incorporating the dense porosity. The tolerable porosity levels for an effective ultrasonic inspection can be considerably less, particularly for thinner sections.

Table 8.8 **Limits for non-planar flaws in as welded steel and aluminium alloy weldments**

Quality category	Maximum length of slag inclusion[A)] (mm)	Limits for porosity expressed as % of area on radiograph
Q1	2.5	3
Q2	4	3
Q3	10	5
Q4	35	5
Q5 and lower	No maximum	5

[A)] Tungsten inclusions in aluminium alloy welds do not affect fatigue behaviour and need not be considered as flaws under this heading.

Table 8.9 **Limits for non-planar flaws in steel weldments stress-relieved by PWHT**

Quality category	Maximum length of slag inclusion, mm	Limits for porosity expressed as % of area on radiograph
Q1	19	3
Q2	58	3
Q3 and lower	No maximum	5

8.8 Assessment of shape imperfections using quality categories

8.8.1 Assessment of misalignment

The presence of misalignment in a welded joint can reduce the fatigue life because it leads to an increase in stress at the joint when it is loaded, due to the introduction of local bending stresses. Assessment of the effect of misalignment on fatigue life involves calculation of the bending stress (see Annex D). Secondary bending stresses are not induced as a result of misalignment in continuous welds loaded longitudinally or in joints subjected only to applied external bending. Thus, there is no limit to the allowable extent of misalignment in such cases, from a fitness-for-service viewpoint.

In the assessment of weldments in which the only imperfection is misalignment, the quality category required should be determined in accordance with **8.5.3**, or, if Equation (8.11) is used, **8.7.2**. The misalignment is acceptable if the total stress range resulting from the sum of the applied stress range, $\Delta\sigma$, and the bending stress range due to misalignment, $\Delta\sigma_s$, does not exceed S in Table 8.7 for the required quality category.

$\Delta\sigma$ is the cyclic stress range from **8.2.1**, calculated excluding the effect of misalignment. As an alternative approach, the acceptance limits are summarized in Table 8.10 in terms of the magnification factor [stress concentration factor (SCF)], k_m, where:

$$k_m = 1 + \frac{\Delta\sigma_s}{\Delta\sigma} \tag{8.15}$$

See Annex D for the calculation of k_m.

Table 8.10 **Acceptance levels for misalignment expressed in terms of stress magnification factor, k_m**

Quality category	Allowable k_m in accordance with BS 7608 class of (aligned) weld detail				
	D	E	F	F2	W
Q1	1.0	—	—	—	—
Q2	1.14	1.0	—	—	—
Q3	1.34	1.18	1.0	—	—
Q4	1.52	1.34	1.13	1.0	—
Q5	1.84	1.61	1.37	1.21	—
Q6	2.16	1.88	1.61	1.42	1.0
Q7	2.48	2.18	1.85	1.63	1.15
Q8	2.92	2.56	2.18	1.92	1.35
Q9	3.40	2.99	2.53	2.23	1.58
Q10	4.00	3.52	2.98	2.63	1.85

NOTE 1 k_m is the magnification factor due to any type of misalignment, including combinations of more than one type.

NOTE 2 Assessment of class W joints refers to possible fatigue cracking in the weld throat and is based on the stress range on the weld throat.

NOTE 3 k_m values are not given for cases in which the basic fatigue strength of the aligned joint is less than the quality category.

8.8.2 Assessment of undercut

The quality category required should be determined in accordance with **8.5.3** or, if Equation (8.11) is used, **8.7.2**.

Acceptance levels for weld toe undercut in butt and fillet welds stressed in the transverse direction for the various quality categories are given in Table 8.11. The maximum acceptable depth of undercut in any thickness of material is 1 mm. Undercut that exceeds these limits or undercut in material thicker than 40 mm should be assessed as a planar flaw using **8.4** or **8.6**.

Table 8.11 **Acceptance levels for weld toe undercut in material thicknesses from 10 mm to 40 mm**

Quality category	Depth of undercut/material thickness	
	Butt welds	Fillet welds
Q1	0.025	—
Q2	0.05	—
Q3	0.075	0.05
Q4	0.10	0.075
Q5 to Q10	0.10	0.10

NOTE Maximum depth of undercut in any thickness is 1 mm.

Undercut in continuous welds stressed in the longitudinal direction does not affect the fatigue life of the joint so there is no limit to its size in terms of fitness-for-service.

 © The British Standards Institution 2019

8.8.3 Background to assessment of shape imperfections

The method of assessing misalignment is based on the successful correlation of a large body of fatigue test data obtained from aligned and misaligned joints in terms of the local stress range equal to the sum of the applied stress and the local bending stress due to misalignment. The fatigue data considered were obtained from transversely loaded butt and cruciform joints containing axial and/or angular misalignment and from vessels with misaligned seams, mainly in steel ([8.55], [8.56], [8.57]), but supported by limited data for aluminium alloys [8.58]. For convenience, the magnification factor, k_m [see Equation (8.15)], is used to enable the influence of misalignment to be expressed as a factor on fatigue design stresses.

The acceptance limits for undercut were derived from published fatigue data for transversely-loaded steel butt and fillet welds containing either natural or artificial undercut [8.8]. By comparing these data with data for similar joints without undercut, the depths of undercut corresponding to reductions in fatigue strength equivalent to steps in the grid of quality category *S-N* curves (Figure 8.3) were determined. An alternative presentation of undercut size in terms of depth to material thickness ratio reduced the scatter in the data. The limitations on material thickness and maximum undercut depth are necessary because of the restricted database available.

8.9 Estimation of tolerable sizes of flaws

The estimation of the size of hypothetical flaws which could be present in a welded joint and grow to an appropriate limiting size (see **8.2.4**) by fatigue during the required lifetime provides a quantitative basis for specifying quality control levels. Similarly, rational acceptance levels could be based on knowledge of the type and extent of shape imperfections whose presence would not increase the stress at the weld sufficiently to reduce the fatigue life below that required. In determining a tolerable flaw level in a weld, the most severe combination of cyclic stress, flaw position and flaw orientation should be assumed. In the context of the cyclic stress to be assumed, the possible presence of misalignment might need to be considered and hence acceptance levels for both flaws and misalignment established. The degree of conservatism that should be in-built into a general estimate of tolerable flaw size results in a size below that which could be demonstrated to be acceptable as an individual flaw in accordance with **8.4** to **8.8**.

For planar flaws, the step-by-step procedure of **8.4** may be used. The tolerable initial flaw size is determined by iteration.

Tolerable flaw sizes and shape imperfection levels may also be determined using the procedure given in **8.5**. The required quality category is established from **8.5** to **8.7**, as appropriate, and the corresponding acceptance levels are determined from **8.6.2** (planar flaws), **8.7.1** (embedded non-planar flaws) or **8.8** (shape imperfections).

Bibliography for Clause 8

Standards publications

For dated references, only the edition cited applies. For undated references, the latest edition of the referenced document (including any amendments) applies.

BS 7608, *Guide to fatigue design and assessment of steel products*

BS EN 1993-1-2, *Eurocode 3 – Design of steel structures – General rules – Structural fire design*

BS EN 1999-1-3, *Eurocode 9 – Design of aluminium structures – Structures susceptible to fatigue*

BS ISO 12108, *Metallic materials – Fatigue testing – Fatigue crack growth method*

Other documents

[8.1] ZHANG, Y.-H. and DORÉ, M. Fatigue crack growth assessment using BS 7910:2013 – Background and recommended developments. *In: International Journal of Pressure Vessels and Piping*, 168, December 2018, 79–86. <https://doi.org/10.1016/j.ijpvp.2018.09.002>.

[8.2] IRVING, P.E. and MCCARTNEY, L.N. Prediction of fatigue crack growth rates: theory, mechanisms and experimental results. *In: Metal Science*, 1977, 11 (8/9), 351–36. ISSN 0306-3453.

[8.3] FORMAN, R.G. Study of fatigue crack initiation from flaws using fracture mechanics theory. *In: Engineering fracture mechanics,* 1972, 4(2), 333–345. ISSN 0013-7944.

[8.4] PARIS, P.C. and ERDOGAN, F. A. A critical analysis of crack propagation laws. *In: Journal of Basic Engineering (Trans. ASME)*, 1963, 85 D(4), 528–534.

[8.5] MADDOX, S.J. Fatigue crack propagation data obtained from parent plate, weld metal and HAZ in structural steels. *In: Welding Research International.* 1974, 4(1), 36–60. ISSN 0306-9427.

[8.6] GRIFFITHS, J.R. and RICHARDS, C.E. The influence of thickness on fatigue crack propagation rates in a low alloy steel weld metal above and below general yield. *In: Materials Science and Engineerin*g. 1973, 11(6), 305–310. ISSN 0025-5416.

[8.7] RICHARDS, C.E. and LINDLEY, T.C. The influence of stress intensity and microstructure on fatigue crack propagation in ferritic materials. *In: Engineering Fracture Mechanics.* 1973, 4(4), 951–978. ISSN 0013-7944.

[8.8] PETERSHAGEN, H. *The influence of undercut on the fatigue strength of welds – A literature survey.* IIW Document XIII-1120-84. London: International Institute of Welding, 1984.

[8.9] GURNEY, T.R. *Fatigue of welded structures*. 2nd ed. Cambridge, UK: Cambridge University Press, 1979. ISBN 0-521-22558-2.

[8.10] GURNEY, T.R. *Cumulative damage of welded joints*. Cambridge: Woodhead Publishing Ltd, 2006. ISBN 978-1-85573-938-3.

[8.11] ZHANG, Y. H., and MADDOX, S.J. Investigation of fatigue damage to welded joints under variable amplitude loading spectra. *In: International Journal of Fatigue*, 2009, 31(1), 138–152.

[8.12] ZHANG, Y.H. *Investigation of fatigue damage to welded joints under variable amplitude loading spectra*. TWI Industrial Member Report 889/2007. Cambridge: TWI, 2007.

[8.13] KING, R. *A review of fatigue crack growth rates in air and seawater.* HSE Report OTH 511. London: Health and Safety Executive Books, 1998. ISBN 0-7176-2413-7. <http://www.hse.gov.uk/research/othpdf/500-599/oth511.pdf>

[8.14] ENGINEERING SCIENCES DATA UNIT. *Fatigue crack propagation in low and medium strength low alloy steel plate, bar and forgings*. ESDU Data Sheet 81011. London: ESDU, 1981.

[8.15] FROST, N.E., MARSH, K.J. and POOK, L.P. *Metal fatigue*. Oxford: Clarendon Press, 1974. ISBN 0198561148.

[8.16] HUDSON, C.M, SEWARD, S.K. and FERRAINOLO, J.J. A compendium of sources of fracture toughness and fatigue crack growth data for metallic alloys. *In: International Journal of Fracture. Part 1 (1978):* 14(4), R151–R184; *Part 2 (1982):* 20(3), R57–R117; *Part 3 (1989)*: 39(4), R43–R63; *Part 4 (1991)*: 48(2), R19–R43. ISSN 0376-9429.

[8.17] UNDERWATER ENGINEERING GROUP. *Design of tubular joints for offshore structures.* UR33. 3 volumes. London: CIRIA, 1985. ISBN 0860172317.

[8.18] TAYLOR, D.A. *Compendium of fatigue thresholds and growth rates*. Cradley Heath, UK: Engineering Materials Advisory Services Limited, 1985. ISBN 0947817050.

[8.19] JASKE, C.E., PAYER, J.H. and BALINT, V.S. *Corrosion fatigue of metals in marine environments.* Columbus, OH: Battelle Press (for the Metals and Ceramics Information Center), 1981. ISBN 0935470077.

[8.20] AUSTEN, I.M. and WALKER, E.F. Corrosion fatigue crack growth rate information for offshore life prediction. *In:* C. NOORDHOEK and J. de BACK, eds. *Developments in marine technology – 3. Proceedings of Third ECSC offshore international conference on steel in marine structures (SIMS '87)*, Delft, The Netherlands, 15–18 June 1987. Paper SIMS TS 50: 859–870. ISBN 0444428054.

[8.21] BOOTH, G.S. and DOBBS, S. Corrosion fatigue crack growth in BS 4360 Grade 50D steel. *In: Welding Institute Research Bulletin*, 1986, 27(9), 293–297.

[8.22] McEVILLY, A.J. *Atlas of stress-corrosion and corrosion fatigue curves*. Materials Park, OH: ASM International, 1986. ISBN 0871703742.

[8.23] RUDD, W.J. *Fatigue crack growth in very high strength steels*. BSC Report SH/RPODE/EM/7389/4/79/B. British Steel Corporation, 1979.

[8.24] GARWOOD, S.J. Fatigue crack growth threshold determination; a simple estimation technique. *In: Welding Institute Research Bulletin*, 1979, 20(9), 262–265.

[8.25] ENGINEERING SCIENCES DATA. *Fatigue threshold stress intensity factors and slow crack propagation rates in low and medium strength low alloy steel*. London: ESDU, 1981. ESDU Data Sheet 81012.

[8.26] AUSTEN, I.M. *Measurement of fatigue crack growth threshold values for use in design*. BSC Report SH/EN/9708/2/83/B. British Steel Corporation, 1983.

[8.27] TOGNARELLI, M.A., THODLA, R. and SHADEMAN, S. Fatigue Crack Growth Rate and Fracture Toughness of API5L X65 in Sweet Environments. *In: Proceedings of the 32nd International Conference on Ocean, Offshore and Arctic Engineering*, OMAE2013-10216, 2013.

[8.28] BAXTER, D.P., MADDOX, S.J. and PARGETER, R.J. Corrosion fatigue behaviour of welded risers and pipelines. *In: Proceedings of 26th International conference on Offshore Mechanics and Arctic Engineering*, June 2007, San Diego, California, USA.

[8.29] PARGETER, R.J., HOLMES, B. and BAXTER, D.P. Corrosion fatigue of steel catenary risers in sweet production. *In: Proceedings of 27th International conference on Offshore Mechanics and Arctic Engineering*, June 2008, Estoril, Portugal.

[8.30] HOLTAM, C.M. and BAXTER, D.P. Fatigue performance of sour deepwater riser welds: crack growth vs. endurance. *In: Proc. of 30th International conference on Offshore Mechanics and Arctic Engineering*, June 2011, Rotterdam, The Netherlands.

[8.31] VOSIKOVSKY, O. and RIVARD, A. The effect of hydrogen sulphide in crude oil on fatigue crack growth in a pipe line steel, *In: Corrosion*. 1982, 38(1), 19–22, 2.

[8.32] EADIE, R.L. and SZKLARZ, K.E. Fatigue crack propagation and fracture in sour dilute brine, Paper No. 611. *In: Proceedings of Corrosion 99*, NACE International, Houston, TX, 1999.

[8.33] EADIE, R.L. and SZKLARZ, K.E. Fatigue initiation and crack closure of low alloy steels in sour brine environments, Paper No. 610. *In: Proceedings of Corrosion 99*, NACE International, Houston, TX, 1999.

[8.34] WOOLLIN, P., MADDOX, S.J. and BAXTER, D.P. Corrosion fatigue of welded stainless steels for deepwater riser applications. *In: Proceedings of 24th International Conference on Offshore Mechanics and Arctic Engineering*, June 2005, Halkidiki, Greece.

[8.35] HAMMOND, R.I. and BAXTER, D.P. Corrosion fatigue of simulated CMn steel HAZs. *In: Proceedings of 27th International conference on Offshore Mechanics and Arctic Engineering*, June 2008, Estoril, Portugal.

[8.36] HOLTAM, C.M. and BAXTER, D.P. Fatigue crack growth performance of sour deepwater riser welds in the nearthreshold regime. *In: Proceedings of 30th Offshore Technology Conference*, May 2011, Richardson, Texas, USA.

[8.37] WOOLLIN, P. Fatigue crack propagation in C-Mn steel HAZ microstructures tested in air and seawater. *In: Proceedings of 17th International Conference on Offshore Mechanics and Arctic Engineering*. CD-ROM. New York: ASME International, 1998. ISBN 0791819523.

[8.38] BAXTER, D.P. and TUBBY, P. SAFEBUCK JIP: Critical aspects of the fatigue limit state of pipelines designed to laterally buckle. Paper No. OTC 21510. *In: Offshore Technology Conference*. OTC 2011. Houston, Texas, USA, 2–5 May 2011.

[8.39] PEARSON, S. Fatigue crack propagation in metals. *In: Nature*. 1966, 211(5053), 1077–1078. ISSN 0028-0836.

[8.40] HARRISON, J.D. An analysis of data on non-propagating fatigue cracks on a fracture mechanics basis. *In: Metal Construction.* 1970, 2(3), 93–98. ISSN 0307-7896.

[8.41] MADDOX, S.J. Fatigue design of welded aluminium alloy structures. *In: Proceedings of 2nd International Conference on Aluminium Weldments*, Munich, 24–26 May 1982. Dusseldorf: Aluminium-Verlag, 1982. Session 3, Paper 4, 17. ISBN 387017157.

[8.42] TADA, H., PARIS, P. and IRWIN, G. *The stress analysis of cracks handbook*. Hellertown, MA: Del Research Corporation, 1973.

[8.43] MURAKAMI, Y. *Stress intensity factor handbook. Vols. 1 and 2*. Oxford: Pergamon Press, 1987. Vol. 3 Kyoto, Japan: Society of Materials Science, 1992.

[8.44] HOBBACHER, A. Stress intensity factors of welded joints. *In: Engineering Fracture Mechanics.* 1993, 46(2), 173–182 and 49(2), 323. ISSN 0013-7944.

[8.45] OORE, M. and BURNS, D.J. Estimation of stress intensity factors for irregular cracks subjected to arbitrary normal stress fields. *In: Proceedings of 4th International Conference on Pressure Vessel Technology*, Vol. 1: Materials, fracture and fatigue. London, 19–23 May 1980. London: Institution of Mechanical Engineers, 1980. Paper C25/80, 139–147. ISBN 0852984596.

[8.46] GURNEY, T.R. and MADDOX, S.J. A re-analysis of fatigue data for welded joints in steel. *In: Welding Research International*. 1973, 3(4), 1–54. ISSN 0306-9427.

[8.47] SIGNES, E.G., BAKER, R.G., HARRISON, J.D. and BURDEKIN, F.M. Factors affecting the fatigue strength of welded high strength steels. *In: British Welding Journal.* 1967, 14(3), 108–116.

[8.48] WATKINSON, F., BODGER, P.H. and HARRISON, J.D. The fatigue strength of welded joints in high strength steels and methods for its improvement. *In: Proceedings of Conference on Fatigue of Welded Structures*, Brighton, 6–9 July 1970. Abington, UK: Welding Institute, 1971. Paper 7, 97–113.

[8.49] GURNEY, T.R. The influence of thickness on the fatigue behaviour of welded joints. *In: Proceedings of the 2nd International Conference on the Behaviour of Offshore Structures (BOSS '79)*, London, 28–31 Aug. 1979. Cranfield, UK: BHRA Fluid Engineering, 1979. Vol. 1, Paper 41. ISBN 0906085357.

[8.50] MADDOX, S.J. *The effect of plate thickness on the fatigue strength of fillet welded joints.* Abington, Cambridge: The Welding Institute, 1987. ISBN 0853002088.

[8.51] BERGE, S. and WEBSTER, S.E. The size effect on the fatigue behaviour of weld joints. *In:* C. NOORDHOEK and J. de BACK, eds. *Developments in marine technology. Proceedings of 3rd International Conference on Steel in Marine Structures (SIMS '87)*, Delft, The Netherlands, 15–18 June 1987. Amsterdam: Elsevier, 1987. Paper SIMS PS8, 179–203. ISBN 0444428054.

[8.52] HARRISON, J.D. The basis for an acceptance standard for weld defects. Part 2: Slag inclusions. *In: Metal Construction and British Welding Journal*. 1972, 4(7), 262–268. ISSN 0307-7896.

[8.53] HARRISON, J.D., and DOHERTY, J. A re-analysis of fatigue data from butt welded specimens containing slag inclusions. *In: Welding Research International*. 1978, 8(2), 81–101. ISSN 0306-9427.

[8.54] HARRISON, J.D. The basis for an acceptance standard for weld defects. Part 1: Porosity. *In: Metal Construction and British Welding Journal*, 1972, 4(3), 99–107. ISSN 0307-7896.

[8.55] MADDOX, S.J. *Fitness for purpose assessment of misalignment in transverse butt welds subject to fatigue loading*. IIW Document XIII-1180-85. London: International Institute of Welding, 1985.

[8.56] MADDOX, S.J. *Fitness-for-purpose assessment of misalignment in transverse butt welds subject to fatigue loading.* TWI Industrial Member Report 279/1985. Cambridge: TWI, 1985.

[8.57] ANDREWS, R.M. The effect of misalignment on the fatigue strength of welded cruciform joints. *In: Fatigue and Fracture of Engineering Materials and Structures*. 1996, 19(6), 755–768. ISSN 8756-758X.

[8.58] GUNN, K.W. and McLESTER, R. The effect of mean stress on fatigue properties of aluminium alloy butt welded joints. *In: British Welding Journal*. 1960, 7(3), 201–208.

9 Assessment of flaws under creep and creep/fatigue conditions

9.0 Symbols and definitions

For the purposes of this clause, the following symbols, definitions and units apply, unless otherwise indicated at the point of use.

Symbol	Definition	Units
A	Temperature dependent constant in creep strain rate [Equation (9.3)]	$MPa^{-n}h^{-1}$
A	Constant in creep crack growth [Equation (9.14)]	Defined for crack growth rates in mmh^{-1} and C^* in units of $MPamh^{-1}$
a	Current crack size in creep	mm
$\dot{a}$	Crack growth rate	mm/h
a'	Arbitrary crack size (Figure 9.4)	mm
$\dot{a}_c$	Rate of crack propagation due to creep	mm/h
a_g	Crack size after growth	mm
a_{min}	Crack depth below which the crack growth rate is assumed to be constant (typically 0.2 mm)	mm
a_0	Initial flaw size	mm
B'	Parameter used in crack growth rate law	—
C	Material and temperature dependent constant in creep assessment [Equation (9.15)]	—
$C(t)$	Transient creep crack tip parameter	$MPamh^{-1}$
C^*	Steady state crack tip and crack growth parameter [Equation (9.7)]	$MPamh^{-1}$
c	Crack half-length (Figure 9.5)	mm
c_0	Initial half-length of crack (Figure 9.5)	mm
d	Small distance ahead of a crack tip in time-dependent failure assessment	μm
da/dN	Crack growth rate with loading cycles	mm/cycle
$(da/dN)_c$	Rate of crack propagation due to creep	mm/cycle
$(da/dN)_f$	Rate of crack propagation due to fatigue	mm/cycle
E	Elastic modulus	N/mm^2
K	Stress intensity factor	$MPa\sqrt{m}$
K_{max}	Maximum stress intensity factor	$MPa\sqrt{m}$
K_{min}	Minimum stress intensity factor	$MPa\sqrt{m}$
K^p	Stress intensity factor due to primary load only	$MPa\sqrt{m}$
L_r	Ratio of reference stress to yield strength, or applied load to limit load	—
N	Number of hold steps [Equation (9.1)]	—
n	Power-law creep stress exponent	—
P	Primary stress	N/mm^2
P_L	Limit load	N
$P_L(a,\sigma_Y)$	Rigid plastic limit load for flaw size a and yield strength σ_Y	N

(continued)

Symbol	Definition	Units
Q	Exponent in cyclic crack growth equation	—
q	Exponent in creep crack growth equation [Equation (9.14)]	—
q_o	Fraction of load cycle when crack is open	—
R	Ratio of minimum to stress intensity factor, K_{min}, to maximum stress intensity factor, K_{max}, in fatigue analysis	—
R'	Characteristic length used in creep crack propagation equation	m
r_p	Cyclic plastic zone size	μm
r_p^{crack}	Cyclic plastic zone size at the crack tip	μm
T	Temperature	°C
T_c	Creep exclusion temperature	°C
T_{ref}	Reference temperature in creep	°C
t	Time	hours
t	Hold time at a given temperature [Equation (9.1)]	hours
t_{CD}	Time to failure of plant by bulk creep rupture, measured from initial start-up	h
$t_{CD}(a)$	Time to creep rupture of current crack of size a, including initiation time	h
$t_{CD}(a')$	Time to creep rupture of given crack of size a' (Figure 9.4)	h
$t_{CD}(a_0)$	Time to creep rupture, including initiation time, of initial crack of size a_0	h
t_g	Time required for the crack to propagate by an amount Δa_g	h
t_h	Hold time at a given temperature or dwell period	h
t_i	Crack initiation time, prior to commencement of creep crack growth	h
t_m	Maximum allowable time at reference temperature	h
t_r	Time to rupture determined from creep rupture curve	h
$t_r(\sigma)$	Time to rupture at the appropriate temperature and at a stress, σ	h
t_{red}	Redistribution time	h
t_s	Future life required	h
t_0	Life to date	h
t_1, t_2, t_3	Arbitrary time step (Figure 9.1)	h
W	Width of cracked specimen (Figure 9.2)	mm
β	Exponent in creep crack initiation [Equation (9.13)], obtained from creep crack growth tests as specified in ASTM E1457	—
β	Factor determining stress state in the plastic zone [Equation (9.2)]	—
γ	Material constant obtained from creep crack growth tests as specified in ASTM E1457	—
Δa_g	Limit of tearing	mm

 © The British Standards Institution 2019

(continued)

Symbol	Definition	Units
ΔJ	J-integral to calculate ΔK_{eff}	MPam
ΔK	Stress intensity factor range, $K_{max} - K_{min}$	MPa$\sqrt{}$m
ΔK_{eff}	Effective stress intensity range	MPa$\sqrt{}$m
$\Delta \bar{\varepsilon}_t$	Total surface strain range	—
δ_i	Crack tip opening displacement corresponding to initiation of creep crack growth	mm
$\dot{\varepsilon}_C$	Creep strain rate	/h
$\bar{\dot{\varepsilon}}_C$	Equivalent creep strain rate	/h
ε_c	Accumulated creep strain	—
ε_e	Elastic strain at the reference stress σ_{ref}/E	—
$\bar{\varepsilon}_f$	Creep ductility	
ν	Poisson's ratio	—
σ_d	Stress at a small distance, d, ahead of the crack tip	N/mm^2
σ_f	Flow strength (assumed to be the average of the yield and the tensile strengths)	N/mm^2
σ_{ref}	Reference stress used for creep and plastic consideration; it is sometimes calculated from plane strain von Mises limit load as in Annex N	N/mm^2
σ_U	Ultimate tensile strength	N/mm^2
σ_Y	Lower yield strength or 0.2% proof strength	N/mm^2
σ_0	Start-of-dwell surface stress of an uncracked body	N/mm^2
$\sigma_{0.2}$	0.2% proof strength	N/mm^2
$\sigma_{\varepsilon 0.2}$	Stress to give 0.2% creep strain over the period of operation of the plant	N/mm^2

9.1 General

The background to this clause is given in reference [9.1].

This clause gives guidelines for assessing the significance of flaws in components that operate in the creep range. Procedures are presented for describing creep or creep/fatigue failure by net section rupture, crack growth or some combination of both processes under both static and cyclic loading conditions. The influence of fatigue and the onset of brittle or ductile fracture in determining tolerable flaw size is also considered. The calculations make use of limit analysis methods, continuum damage mechanics and fracture mechanics concepts. Several levels of complexity are discussed depending on the criticality of the problem and the availability of materials property data. Approximations are presented for dealing with cracked components when only stress rupture data are available. This clause is based on the R5 and FITNET Procedures ([9.2], [9.3], [9.4]) but simplified where appropriate. Where detailed information is needed the user is advised to review the original documents ([9.2], [9.3], [9.4]). Additional information can also be found in ASTM E2760 and references [9.5] to [9.7].

This clause has been developed for use when assessing components made in ferritic and austenitic steels as most validated information is available on these materials. The same principles are applicable to other metallic components, provided that the relevant materials data and appropriate validations are obtained.

NOTE 1 Annex H gives recommendations for reporting an assessment.

NOTE 2 Annex S gives generic material data and further recommendations.

9.2 Background to methods

References [9.2] to [9.33] provide information on the background of all or parts of the methods presented. This clause contains conservative assessment and remaining life estimation procedures that can be used at the design stage and for in-service situations. The approach allows decisions to be made depending on the accuracy and quality of information, on the operating circumstances, and on the materials properties available. However, the clause does not advise on the level of conservatism in the analysis. This is particularly important when newer higher strength steels, for which little or no long-term materials properties data are available, are being considered.

The methods proposed in this clause are those presently used by a number of industrial laboratories and research establishments that are involved in high temperature testing. Users should take into consideration for their own specific case of component, material choice and operating conditions, that the recommendations might need further validation and verification.

9.3 Background to assessments

In contrast to assessments of uncracked bodies based on earlier codes of practice, e.g. ASME Boiler and Pressure Vessel Code, Section III, or ASME Case N-47 [9.34], the assessment steps described in this clause are for assessing defects in structures operating at high temperatures and subject to creep-fatigue loading conditions. These have been derived mainly from the R5 and FITNET procedures ([9.2], [9.3], [9.4]); however, techniques in other similar codes ([9.8] to [9.10]) have also been taken into consideration. The fundamental methods are described in references [9.2], [9.3], [9.4] and [9.11].

The basic requirements for an assessment are:

a) the operating conditions and loading history;

b) the nature of the defect and its size, shape and position;

c) the appropriate materials data; and

d) appropriate structural calculations to correlate laboratory test data with the behaviour of components.

This information is then used to assess whether a defect of a given size is likely to grow to an unacceptable size by creep or creep-fatigue mechanisms in a given service life under a given loading history.

The procedure in this clause may also be applied or be adapted to consider other assessments, such as:

1) the loading history that can be tolerated for a specific defect size and a given service life;

2) the initial flaw that is likely to grow to the maximum acceptable size in a given service life (and hence the safety margin for a given flaw size); and

3) the combinations of materials properties, geometry and loadings for which crack tip behaviour has a negligible effect on lifetime.

Alternative procedures to those set out here may be followed if they have been appropriately validated. Only the basic procedures needed for flaw assessment have been included in this clause and these necessarily contain an element of conservatism.

It might be appropriate to use less conservative procedures where economic circumstances justify such a course of action. These, however, involve more

complex analysis than that described here and material testing is usually necessary. In these situations it is advisable to obtain specialist advice.

9.4 Factors involved in the safe use of the procedure

The following factors should be taken into account for appropriate use of data from laboratory tests in component failure analysis.

a) Annex S gives data for a range of materials in tables. The scatter and sensitivity in creep properties inherently produce a large variation in predictions. Upper and lower bounds are therefore introduced which can give different lifetime predictions. A sensitivity analysis should be performed to account for these variations.

b) The use of data from historical sources, and results from different batches of material, from different laboratories or with an insufficient number of test specimens, is likely to lead to increased scatter. It is advisable to carry out a sensitivity analysis to increase confidence in the results.

c) Simplified analysis procedures are intended to provide a conservative indication of the failure time, but in certain circumstances these can be over-conservative. To perform a more refined analysis, further tests or numerical analyses might be needed to derive improved predictions.

The following factors also influence assessment results.

1) The results can be sensitive to the procedures employed for estimating parameters such as stress intensity factor, K, reference stress, σ_{ref}, and steady state creep characterizing parameter, C^*. Use of non-linear FE methods can improve accuracy.

2) Significant differences can be observed between short-term and long-term laboratory tests. Therefore, where available, long-term laboratory data should be used for long-term component life predictions. However in the absence of long-term data, short-term data may be used provided an appropriate safety factor is applied. Difficulty in ascertaining the level of crack tip constraint and multiaxial stress effects in the component reduces the accuracy of crack growth predictions. Use of 3D FE modelling can assist.

3) Unknowns in modelling the actual loading history, component system stresses and lack of knowledge of past service history and residual stresses are sources of error in predictions.

4) The prediction from probabilistic assessment of data can be used to deal with data scatter and other unknowns.

9.5 Creep exemption criteria

9.5.1 General

For plant operating at high temperatures, the first factor to be established is whether the component is operating in the creep regime. Guidance is given in **9.5.2** for determining whether the component can be considered as being exempt from the possibility of creep failure. The guidelines rely on the use of the creep results for the actual material of interest or minimum property data for the alloy type. In circumstances where only mean data are available, a suitable safety factor should be adopted and/or sensitivity calculations carried out. It is particularly important to ensure that due consideration is given to the creep properties of all constituent microstructures of a welded joint. If the component/temperature/service life combination fulfils the exemption criteria of **9.5.2**, no further consideration need be given to creep. If the exemption criteria are not met, the possibility of creep failure cannot be ruled out. Provided that it can be shown by reference to previous experience that the material is not

sensitive to creep crack propagation, flaws may be assessed using calculations based on creep rupture of the remaining net section. Existing design documents (e.g. BS EN 13480 or PD 5500) might assist in this respect.

For situations where creep crack propagation is possible, the remaining procedures in **9.8.2** should be employed. If cyclic loading is involved, consideration should be given to the possibility of creep-fatigue interaction.

9.5.2 Temperature limits

The significance of creep strains should be determined for the assessed loading and temperature history. Creep can be significant for some types of loading history but not for others. For a component, or part of a component, creep may be discounted if either of the following conditions is met.

a) The maximum temperature during the total operating period is less than the temperature, T_c (T_c is specific to the material of construction and the period of operation). For materials with uniaxial creep rupture ductilities >10% in the time/temperature regime of interest, T_c is the temperature at which 0.2% creep strain is accumulated at a stress level equal to the flow strength over the period of operation of the component (see Figure 9.1). The flow strength, σ_f, is equal to $(\sigma_Y + \sigma_U)/2$ at the service temperature for fracture assessments.

   Examples of values for T_c are given in Table 9.1 for a range of steels, based on published lower bound data (see PD 6525-1, ASME Boiler and Pressure Vessel Code, Section III, ASME Case N-47, and Institution of Mechanical Engineers, the Creep of Steels Working Party [9.11]) and a lifetime of 200 000 h. It might be possible to demonstrate higher temperature limits when use of mean data can be justified or when $L_r \leq 0.2$ (see Figure 9.1).

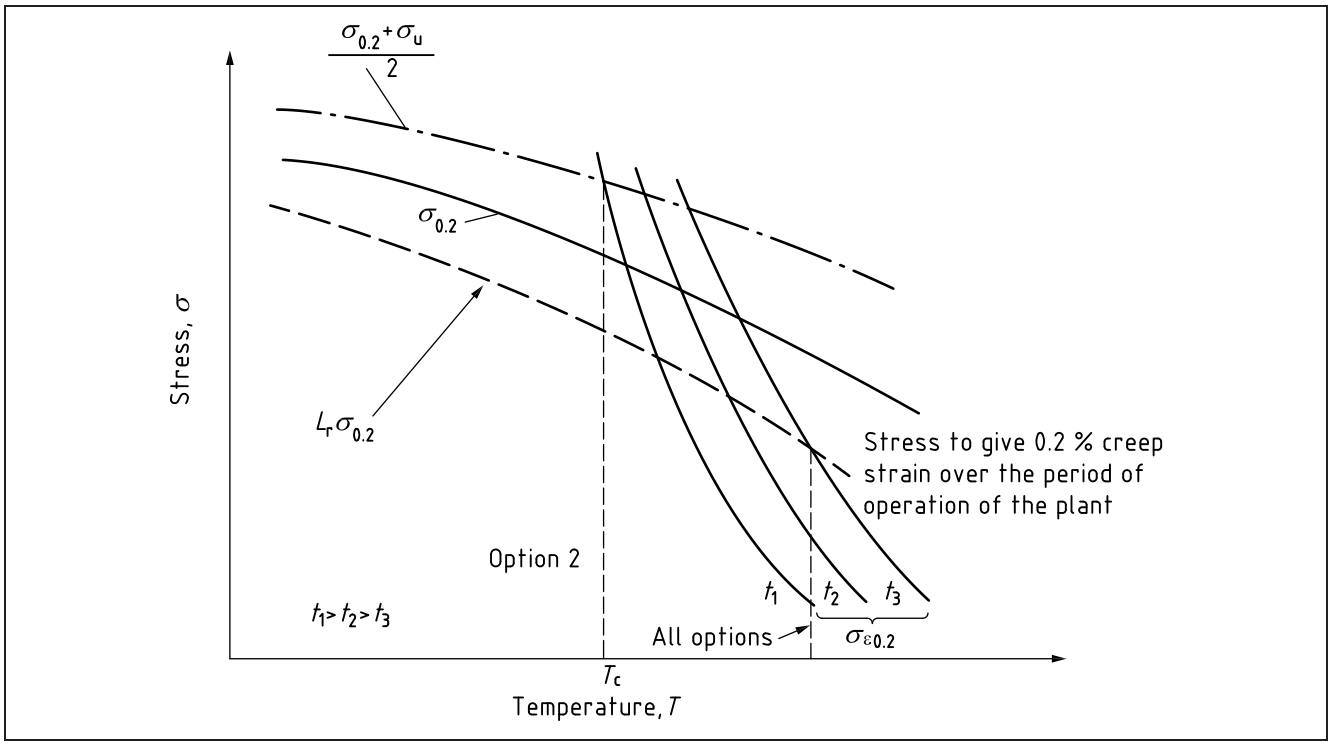
   For other steels and/or longer lifetimes, the value of T_c has to be derived from data obtained from creep tests on relevant material. For materials with uniaxial creep rupture ductilities <10% in the time/temperature regime of interest, T_c should be determined on the basis of the flow strength associated with a creep strain having a magnitude of 1/50th of the actual rupture ductility [9.13].

Table 9.1 **Temperature below which creep is negligible in 200,000 h for carbon manganese and ferritic steels**

Type of steel	T_c (°C)
Carbon manganese steel	310
Ferritic steel [A)] CrMoV, 1CrMo, 2¼Cr1Mo, 9Cr1Mo,12CrMoV(W)	400

[A)] See PD 6525-1 and [9.2].

Figure 9.1 **Determination of temperature T_c at which 0.2% creep strain is accumulated at a stress level equal to the proof strength**



b) The effects of creep may be neglected if the sum of the ratios of the hold time, t, to the maximum allowable time, t_m, at the reference temperature, T_{ref}, for the total number of hold time periods is less than one:

$$\sum_{j=1}^{N} [t/t_m(T_{ref})]_j < 1 \qquad (9.1)$$

The values of t_m depend on material, temperature and/or crack size as shown in Figure 9.2 and Figure 9.3 for austenitic and ferritic steels, respectively. T_{ref} may be taken as the maximum temperature at the chosen location, corresponding to the period during the cycle at which the loading is constant with time. The criteria used to derive these insignificant creep curves are described in **9.6.2**. Generally, t_m, for materials with creep rupture ductilities >10%, is taken as the time required to achieve an accumulated creep strain of 0.2% at a stress level equal to the flow strength. For ductilities <10%, t_m should be determined on the basis of creep strains with a magnitude equal to 1/50th of the creep rupture ductility [9.12]. However, for consistency with the tests for creep exemption for uncracked structures, values of t_m should not be greater than those allowed in design codes.

Figure 9.2 **Insignificant creep curves for austenitic steels**

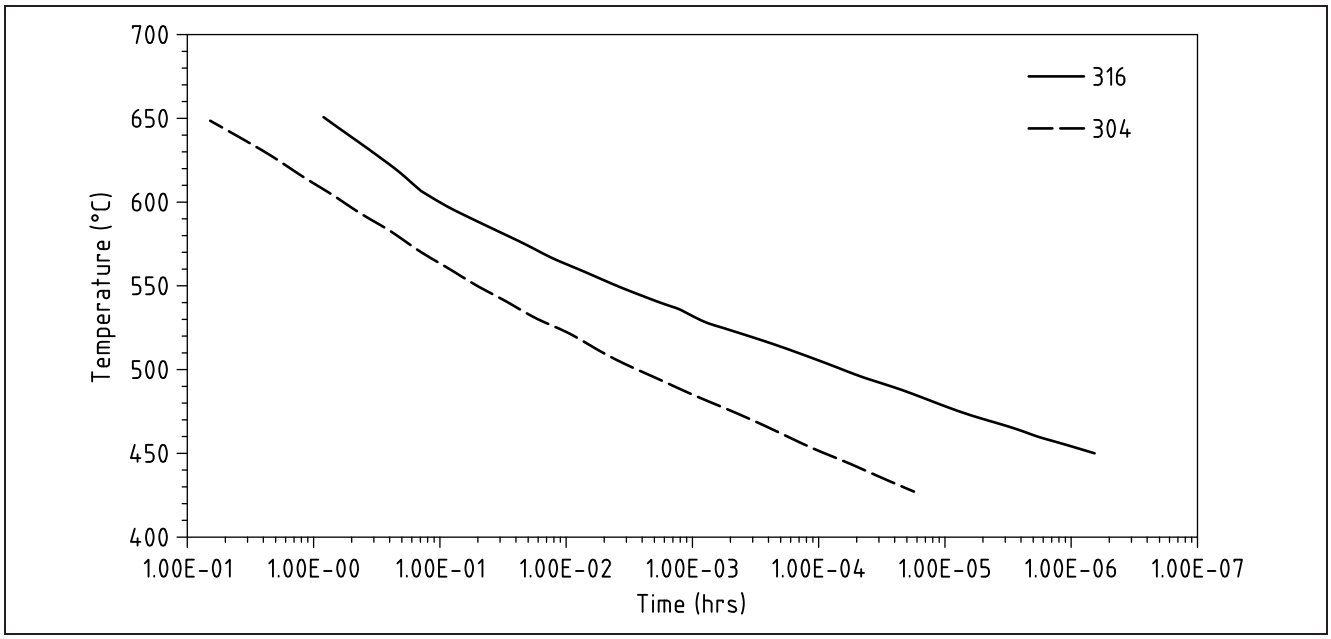
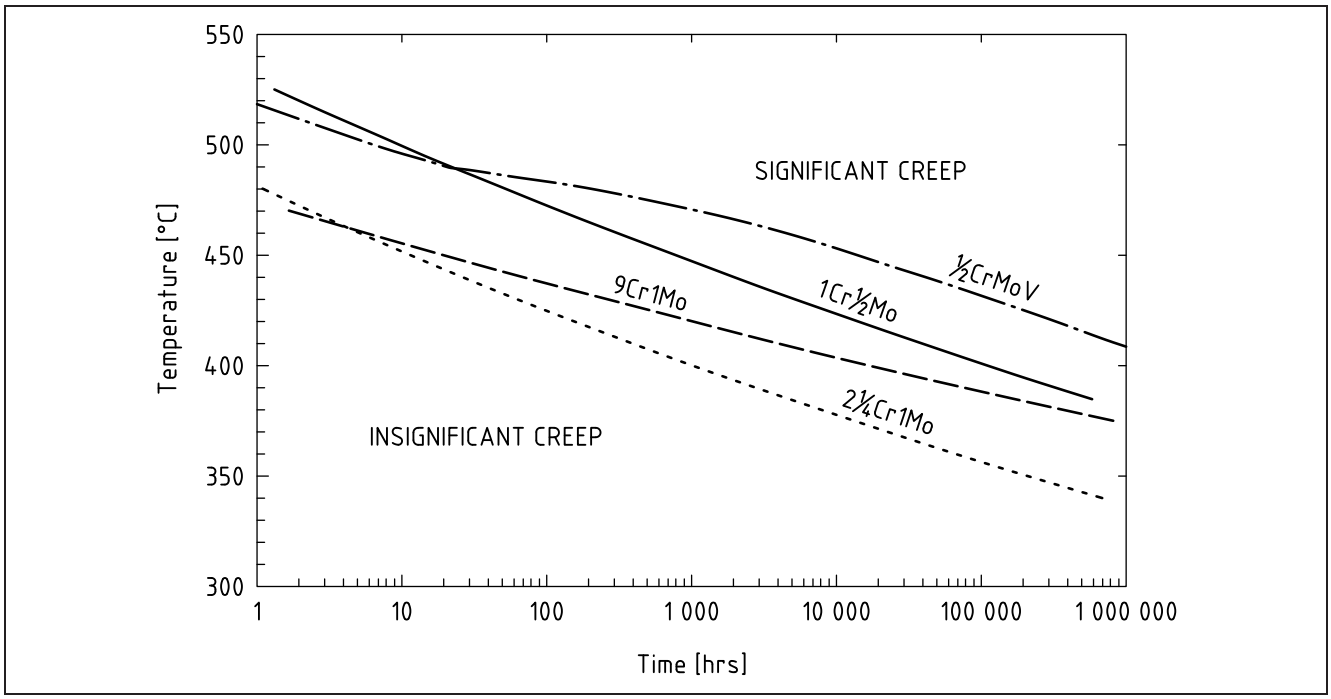


Figure 9.3 **Insignificant creep curves for ferritic steels**



9.6 Creep-fatigue exemption criteria

9.6.1 General

In some cases the complexity of a creep and creep-fatigue crack growth assessment can be avoided by performing simple calculations to demonstrate the insignificance of creep and/or fatigue. In the event of both creep and fatigue being shown to be significant, simple tests can also be used to demonstrate insignificant creep-fatigue interactions, and thus remove the onerous requirement to generate material fatigue data incorporating the effects of creep holds.

9.6.2 Insignificant creep

If temperatures are sufficiently low during periods of steady operation, creep effects can be insignificant. Refer to **9.5.2** for insignificant creep temperatures.

9.6.3 Insignificant fatigue

It should first be determined whether or not creep behaviour is unperturbed by cyclic behaviour. This should be performed both for the overall structural response and for stresses local to the crack tip. Whether the crack depth is such that the structure is not significantly affected may be demonstrated by showing that the elastic stress range does not exceed the sum of the steady state creep stress and the stress to cause yield at the other extreme of the cycle.
(See R5 [9.2] for further information.)

Insignificant fatigue is demonstrated for stresses local to the crack tip if the cyclic plastic zone at the crack tip is small for the most severe fatigue cycle. Under cyclic loading, the allowable elastic stress range is $2\sigma_Y$ in the absence of cyclic hardening or softening, and the cyclic plastic zone size at the crack tip:

$$r_p^{crack} = \beta\left(\frac{\Delta K}{2\sigma_Y}\right)^2 \quad (9.2)$$

where β is typically $1/2\pi$ in plane stress and $1/6\pi$ in plane strain. More generally, the cyclic plastic zone size at the crack tip should be calculated using the cyclic yield or 0.2% offset strength. This cyclic plastic zone size should be much less than the crack size or any other dimension characteristic of the structure, such as section thickness or remaining ligament ahead of the crack.

Cyclic loading effects on creep crack growth may be excluded if the tests in this clause demonstrate that fatigue is insignificant, provided that the estimated fatigue crack growth does not exceed 1/10th of the estimated creep crack growth.

In general at high frequencies at approximately >1 Hz, transgranular cycle-dependent fatigue cracking is more likely to dominate (see ASTM E2760), and for low frequencies at approximately <0.01 Hz, intergranular time-dependent creep cracking is likely to dominate. At intermediate frequencies, creep/fatigue interaction might need to be considered.

9.6.4 Significance of creep-fatigue interactions

When both creep and cyclic loading are shown to be significant, the significance of creep-fatigue interaction should be determined. The biggest interaction is generally found in the frequency range of 0.01 Hz to 1 Hz. However, in general it may be assumed that the effect of creep damage on fatigue crack growth rates has little influence on the total crack growth per cycle. It is adequate, therefore, in Step 9 of **9.8** to sum creep crack growth with continuous cycle fatigue crack growth estimates.

9.7 Crack behaviour at high temperature

The behaviour of a crack in a component subject to steady loading at elevated temperature is shown schematically in Figure 9.4. Following the initial loading of the component, the crack can blunt and, in these circumstances, there is a crack initiation period before crack propagation takes place. Where such blunting does not occur, crack propagation may be assumed to start immediately on loading. The crack grows, in all cases, by a fracture mechanics controlled mechanism. Crack propagation can theoretically continue until structural failure takes place. Creep damage can build up ahead of the crack, and creep rupture of the remaining material can occur at time t_{CD}, designating time for continuum damage. These conditions are shown diagrammatically in Figure 9.5. The

initiation period could be as much as 80% of life. Initiation is defined in ASTM E1457 as the period of time for an extension of 0.2 mm in crack length which has been shown to be the length over which steady state creep will prevail in laboratory specimens. However, this length can be chosen to be larger in components based on the accuracy of NDT to measure crack length. Usually a crack extension of up to 1 mm for estimating an initiation period is advisable. Also, in some circumstances, additional confidence may be obtained by demonstrating leak-before-break (Annex F). Failure could occur prior to continuum damage or creep crack growth by plastic collapse or brittle fracture, if the crack length reaches a critical value for the given load.

When a flaw has been discovered after a component has been in service, the conservative assumption should be made that the crack initiated earlier in life, unless there is strong evidence to the contrary. The assessment of a flaw in an actual component is carried out in a series of well-defined steps as follows.

a) Subclause **9.8** describes the initial work that needs to be undertaken to decide whether the procedure is applicable. It shows what needs to be done to establish service loads and temperatures, to characterize the dimensions of a flaw and to define materials properties and stress levels.

b) The calculations needed to predict flaw growth are outlined in **9.8**. These also describe the checks that are made to establish margins against creep rupture and fast fracture.

c) The materials data required for the assessment are discussed in Annex S and examples are quoted for the most commonly used materials. This annex also provides a means of estimating materials properties when test data are not available.

Figure 9.4 **Schematic behaviour of crack subjected to steady loading at elevated temperature**

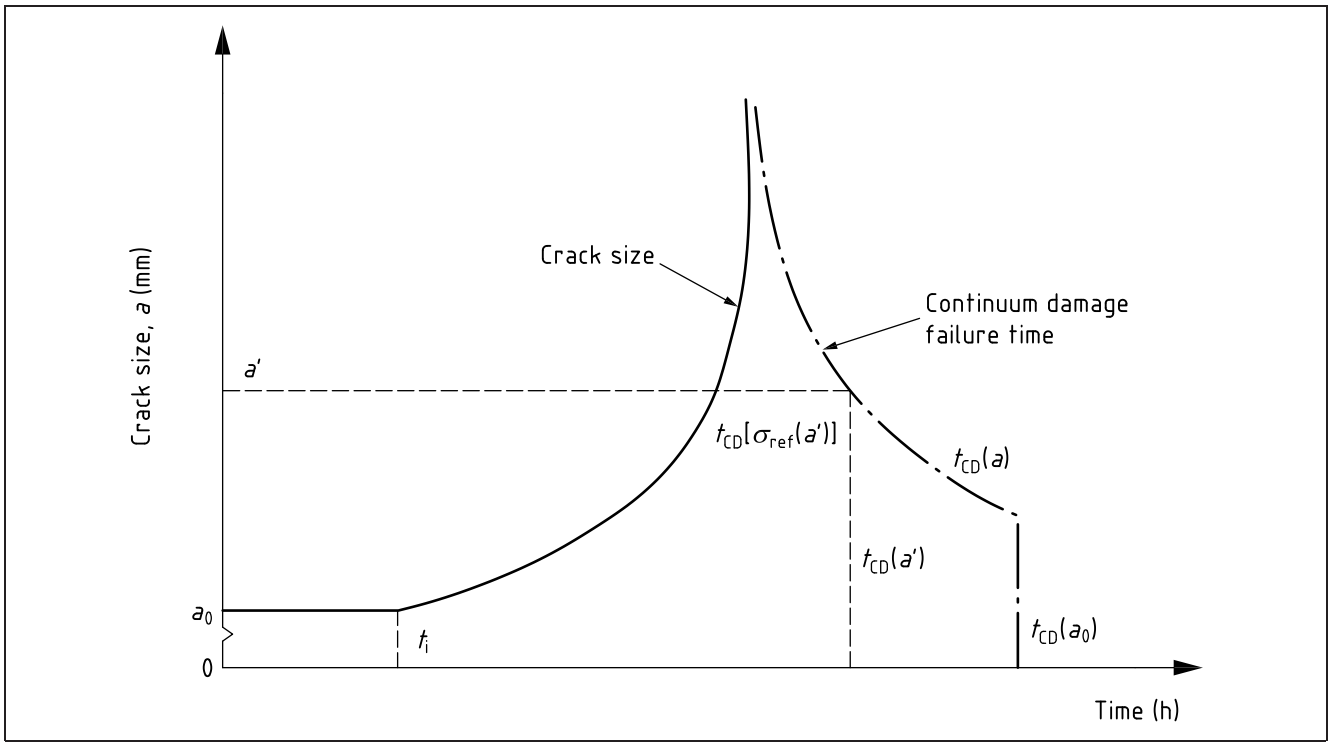
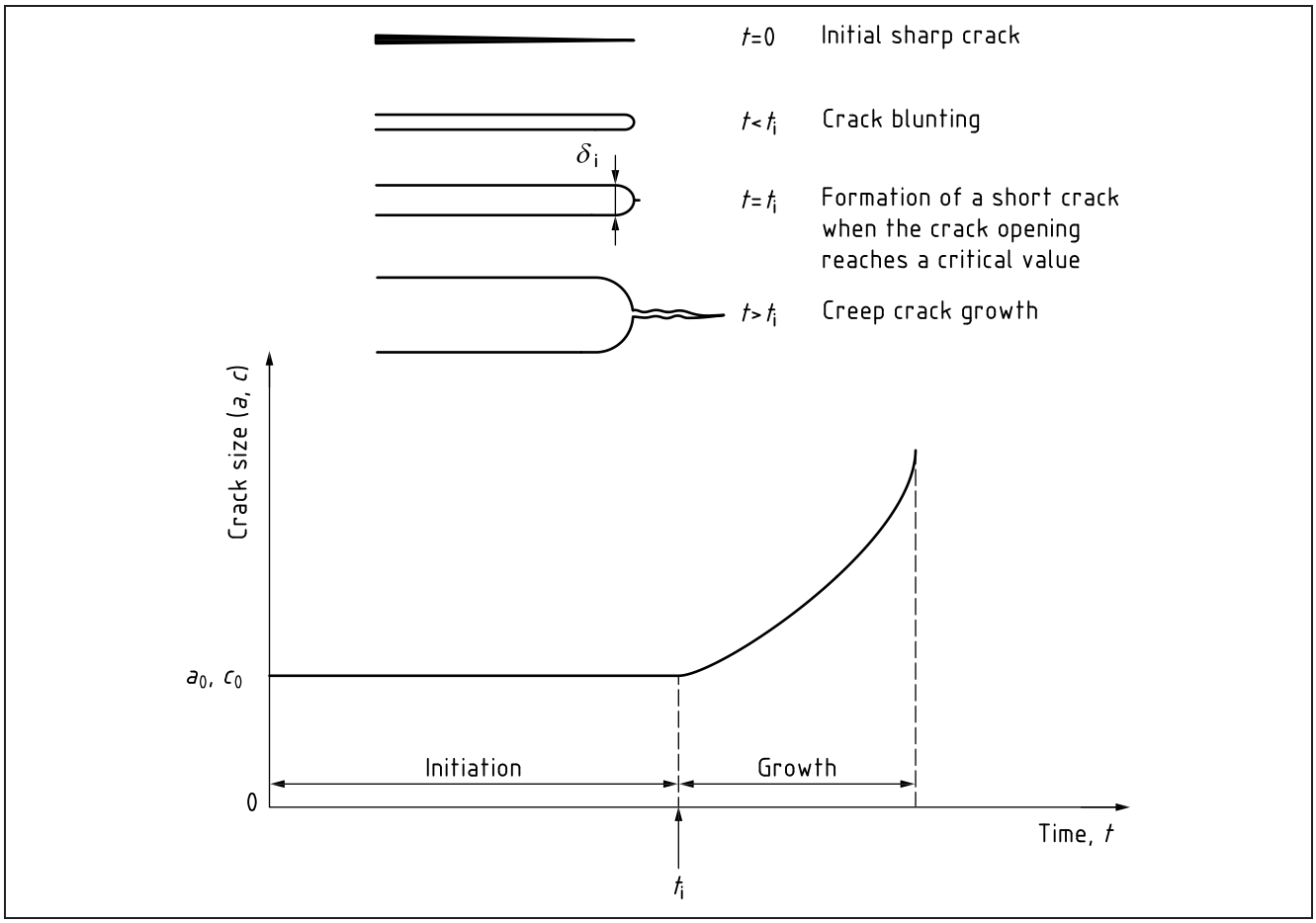


Figure 9.5 **Schematic representation of crack propagation and failure conditions**

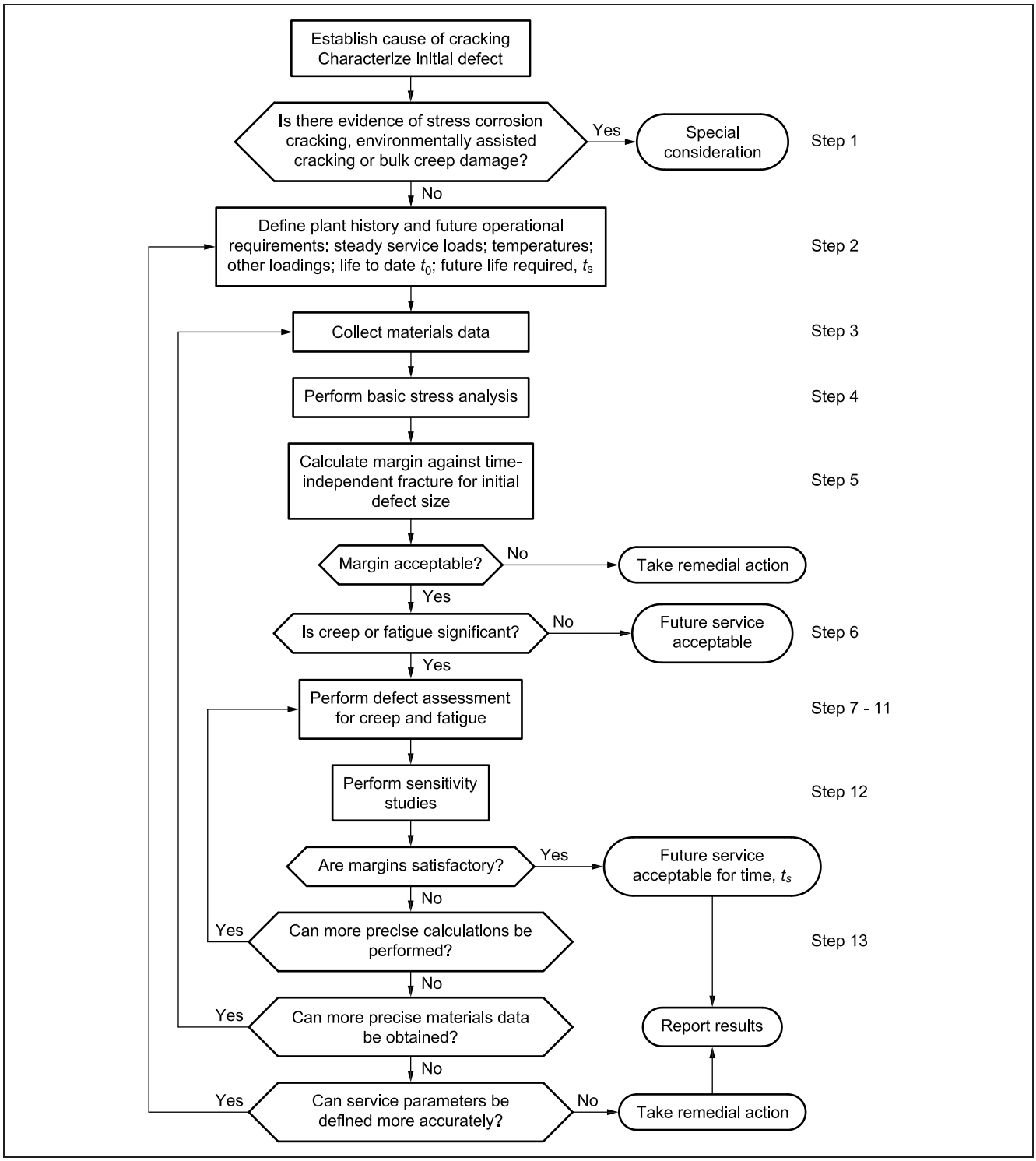


9.8 Assessment of components containing a known or postulated defect

9.8.1 General

In this subclause, a procedure is set out for assessing a component containing a known or postulated defect under creep-fatigue loading. Continuum damage accumulation and crack growth are addressed. The cases of insignificant creep and insignificant fatigue are included as special cases. The procedure may be applied to a component that has not yet seen operation at creep temperatures, or one that has already operated for a period, t_0, at high temperature. In the latter case, advice is given additionally on the effect of the time at which the defect is assumed to form. The steps in the procedure are listed in **9.8.2**. General flowcharts for the procedure are given in Figure 9.6. Further information on performing the individual steps is given in **9.9** and **9.10**.

Figure 9.6 **Flowchart for overall creep assessment procedure described in 9.8.2**



9.8.2 Assessment procedure

9.8.2.1 Establish cause of cracking and characterize initial defect (Step 1)

It is first necessary to establish the cause of the cracking to ensure that the creep procedures are applicable. This is discussed in **9.9.1**.

The defect type (Clause **4**), position and size (Clause **6**) should also be identified. For defects found in service, this process might require the advice of materials and non-destructive testing experts, particularly for the case of defects in welds. Suitable sensitivity studies should be performed to address uncertainties.

The detected defect should be characterized by a suitable bounding profile amenable to analysis. Defects which are not of simple Mode I type should be resolved into Mode I orientation. It might also be possible later to re-characterize a defect in the case that the initial assessment leads to an unacceptable result. Advice on defect characterization is given in Clause **7** and Annex E. Advice on methods for detecting and measuring defects is in Annex T and covers components operating at high temperature.

9.8.2.2 Define service conditions (Step 2)

It is necessary to resolve the load history into cycle types suitable for analysis. This includes both historical operation and the assumed future service conditions. In addition, the service life seen to date and the desired future service life should be defined.

For the case of a component that was known to be defect-free at the start of high temperature operation, an estimate of the time at which the defect formed should also be determined. Suitable sensitivity studies should be performed to address uncertainty in the time of defect formation.

9.8.2.3 Collection of materials data (Step 3)

It is first necessary to define the materials relevant to the assessed feature, including, in the case of weldments, the weld metal and heat-affected zone structures. It is then necessary to collect the materials properties appropriate to the type of assessment to be performed (cyclic, creep, etc.) over the appropriate temperature range and in the correct cyclically-conditioned state. For example, it might be necessary to consider the effects of thermal ageing and reduced ductility due to internal oxidation products leaking to preferred fracture paths. In practice, the material data requirements are influenced by the outcome of the tests for significant creep or fatigue in **9.8.2.6**. Time-independent materials properties are required for the stability analyses in **9.8.2.5** and **9.8.2.11**, noting that fracture toughness properties might be required for creep-damaged material.

9.8.2.4 Perform basic stress analysis (Step 4)

Elastic stress analyses of the uncracked feature (see **6.4** and **7.1.6**) should be performed for the extremes of the service cycles identified under **9.8.2.2**, assuming homogeneous properties. The analysis should allow for any changes from the start of operation; for example, increased stress due to loss of section by wall thinning or increased temperatures due to reduction in thermal diffusivity as a result of surface scale. In the case of cyclic loading, a shakedown assessment of the uncracked feature should then be performed. It should be determined that the feature satisfies strict or global shakedown. If shakedown cannot be demonstrated, it might be necessary to employ inelastic analysis methods. If shakedown is demonstrated, the crack depth should be such that the compliance of the structure is not significantly affected.

9.8.2.5 Check stability under time-independent loads (Step 5 and 11)

The component should be assessed against failure by time-independent mechanisms under fault or overload conditions at the initial defect size using the fracture part of this procedure. This assessment should use the initial values of any residual stresses, not those in the shakedown state. If failure is conceded at this stage, the assumptions in the analysis should be revisited or remedial action taken. Only if sufficient margins can be justified is it permissible to continue to **9.8.2.6** to justify future service life.

9.8.2.6 Check significance of creep and fatigue (Step 6)

The significance of creep should be assessed. If creep is insignificant then the assessment becomes one of cyclic loading alone using the methods in Clause **8**, and **9.8.2.7** and **9.8.2.10** are omitted. Conversely, if fatigue is judged to be insignificant, then the assessment becomes one of steady creep loading alone and further consideration of cyclic loading is not required. A further test determines whether creep-fatigue interaction is significant. If it is not, simplified summation rules for combining creep and fatigue crack growth increments may be adopted. Subclause **9.6** contains detailed advice on the significance of creep-fatigue interaction.

9.8.2.7 Calculate rupture life based on the initial defect size (Step 7 and 10)

The time to continuum damage failure (creep rupture), t_{CD}, is firstly calculated based on the initial crack size from **9.8.2.1**; if this is less than the required service life, then margins are not acceptable and it is not necessary to perform crack growth calculations. The estimate of rupture life is based on a calculated limit load/reference stress and, for predominately primary loading, the material's creep rupture data. For damage due to cyclic relaxation and due to the relaxation of welding residual stresses, ductility exhaustion methods are more appropriate. The detailed calculations are described in **9.12.1**.

9.8.2.8 Calculate initiation time (Step 8)

The initiation time is the time, t_i, from the start of the assessed period of high-temperature operation prior to which no significant crack growth occurs. Depending on the cause of cracking, its location within a weldment and the type of loading, it might be possible to calculate a non-zero initiation time. It is conservative to ignore this period and assume that crack growth occurs immediately on first loading. Calculation methods are set out in **9.11.1**.

9.8.2.9 Calculate crack size after growth (Step 9)

The crack size at the end of the assessed period of operation is calculated by integrating the appropriate creep and fatigue crack growth expressions. This integration is simplified in some cases, depending on the outcomes of the significance tests in **9.8.2.6**. Changes in reference stress due to crack growth should be included in the calculations. Calculation methods are set out in **9.11.2** and **9.11.3**.

9.8.2.10 Re-calculate rupture life after crack growth (Step 10)

The time to continuum damage failure should be re-calculated taking into account the increased crack size from **9.8.2.9**. Crack growth calculations should not be performed in practice beyond an acceptable rupture life. It is conservative to base the estimate of rupture life on the final crack size as this neglects slower accumulation of creep damage when the crack size is smaller during growth.

9.8.2.11 Check stability under time-independent loads after crack growth (Step 11)

The component should be assessed against failure by time-independent mechanisms under fault or overload conditions at the crack size after growth (**9.8.2.9**) using the fracture part of this procedure. Crack growth calculations should not be performed beyond this crack size and therefore, in practice, this step is carried out in conjunction with the crack size calculations of **9.8.2.9**.

 © The British Standards Institution 2019

9.8.2.12 Assess significance of results (Step 12)

Margins against failure are not prescribed here and are left to the user to set. The sensitivity of the results of the preceding steps to realistic variations in loads, initial flaw size and location, and materials properties should, however, be assessed as part of a sensitivity study. The various modelling assumptions made can also be revisited with a view to reducing conservatisms in the analysis if unacceptable margins are determined. If this still fails to result in an acceptable assessment, the options of reducing future service conditions, or repair or replacement of the defective component, should be considered. This is discussed in **9.13**.

9.8.2.13 Report results (Step 13)

The results of the assessment, including margins determined, and the details of the materials properties, flaw size, loads, stress analysis calculations, etc., used in the assessment, should be comprehensively reported (see Annex H). This facilitates both verification of the particular assessment and repeatability in future assessments.

9.9 Further guidance on the assessment procedure

9.9.1 Establish cause of cracking

Before performing calculations, an investigation should be carried out to determine the most likely cause of cracking. This should involve a combination of NDT, visual examination and metallurgical examination as a minimum. The mode of cracking should be identified as this can provide qualitative information on the relative contributions of creep and fatigue to the overall process; creep crack growth is generally intergranular whereas fatigue crack growth tends to be transgranular. Also, where possible, a dimensional check should be carried out to establish whether there has been any significant distortion and thinning.

Where a defect has been discovered in a component that has been in service, the conservative assumption for the calculation of continuum damage is that the crack initiated early in life. This should be assumed unless there is evidence to the contrary. Where the defect can be reliably justified to have formed after the start of high-temperature operation, then it is permissible to use an estimate of the corresponding time in the calculations of crack growth and continuum damage. The reference stress appropriate to this period is then determined on the basis of the uncracked body. Suitable sensitivity studies should be performed to address the effect of the assumption on the robustness of the assessment. Particular caution should be taken if the defect formed in service by creep mechanisms, noting the comments in the next paragraph concerning the effects of creep damage on crack growth properties.

Significant creep damage, away from the crack tip, probably indicates that there has been local over-heating or over-stressing. In these circumstances, all crack growth calculations should take account of the material in its damaged state. In addition, where cracks are discovered in material that has experienced extensive creep damage, it is essential for end-of-life assessment that material data are used which are fully representative of material in its damaged state. Data on fracture toughness and remaining creep rupture life are particularly sensitive in this respect.

Where there is evidence of environmentally assisted cracking (multiple cracking without cavitation), the methods required are discussed in Clause **10**.

9.9.2 Define service conditions

This procedure is applicable to components which operate for long periods at steady or unsteady cyclic conditions of load (stress), or displacement, and temperature. Each loading and temperature should be defined for the locations of interest. In making an assessment, it is conservative to assume that all the loading is load-controlled and ignore stress relaxation; it may also be assumed that infrequent short-term overloads do not modify the crack tip conditions significantly.

Specification of the service conditions should define the load, temperature and life seen to date. In addition to historical operation, future service conditions should be defined. The loading should include all time-independent, transient and fault loading. In many circumstances, the service load and temperature history can be broken down into a number of blocks during which stress and temperature are sensibly constant. This simplifies the analysis.

Where transient loading occurs, during either start-up or shutdown, the number of load and temperature cycles and their magnitude should be established. Conservative assumptions should be adopted.

9.9.3 Collect materials data

9.9.3.1 Creep rupture data

Creep rupture data are required to calculate the rupture life of the remaining ligament and to estimate the current continuum damage level in the ligament as the defect grows. This information can be experimentally derived using uniaxial tests or found in appropriate databases. Annex S presents generic creep rupture data for a range of alloys.

9.9.3.2 Creep deformation data

Creep deformation data are required for steady loadings to estimate the creep crack initiation time and subsequent creep crack growth rates using reference stress techniques. For cases with steady primary load or large elastic follow-up, forward creep data collected under constant load conditions are appropriate. For essentially strain-controlled conditions, in the absence of follow-up, stress relaxation data might be more appropriate than forward creep data. Reliable constitutive equations are needed to provide a smooth transition between these extremes. For creep-fatigue loadings, a description is required of the creep deformation of the material in the relevant cyclic condition in order to estimate creep crack growth rates during the dwell periods. Creep deformation data might also be required to calculate the time for failure by continuum damage using a ductility exhaustion approach or to estimate creep damage at the surface for use in a creep-fatigue crack growth law. Often a simple power law expression:

$$\dot{\varepsilon}_c = A\sigma^n \tag{9.3}$$

is used to describe creep strain rate.

More generally, creep deformation is described by three stages: primary, secondary and tertiary creep requiring more complex creep laws. Equation (9.3) is suitable when secondary creep dominates or when an average creep rate is being adopted. Examples of creep strain deformation data are given in Annex S.

 © The British Standards Institution 2019

9.9.3.3 Creep ductility data

Creep ductility data are required to calculate the time for failure by continuum damage using a ductility exhaustion approach or to estimate creep damage at the surface. These data may also be used to estimate creep crack growth rates for situations in which explicit crack growth data are not available. Generic growth rates for a range of alloys are given in Annex S.

9.10 Basic calculations

9.10.1 Stress intensity factors

The linear elastic stress intensity factor, K, depends on the loading and the crack size, and might vary with position around a crack front. For cyclic loading, the stress intensity factor range and the ratio, R, of minimum stress intensity factor, K_{min}, to maximum stress intensity factor, K_{max}, should be evaluated. The value of R should be calculated from a shakedown analysis rather than a simple elastic analysis. This is because creep during a cycle tends to lead to a cyclic stress state which gives a lower value of R than the initial elastic response. The shakedown analysis only affects the value of R and not the total stress intensity factor range, as the residual stress is independent of position in the cycle.

In the absence of cyclic plasticity in the uncracked body, the effective stress intensity factor range, ΔK_{eff}, is defined by:

$$\Delta K_{eff} = q_o \Delta K \tag{9.4}$$

q_o may be estimated conservatively from:

$$\begin{aligned} q_o &= 1 && \text{for } R \geq 0 \\ q_o &= \frac{1 - 0.5R}{1 - R} && \text{for } R < 0 \end{aligned} \tag{9.5}$$

Additional advice is given in Clause **8** where fatigue analysis is discussed.

9.10.2 Reference stress

For creep crack growth evaluation, it is necessary to evaluate the reference stress at the start of the dwell. The reference stress for simple primary loading is determined by the methods of limit analysis described in Annex P and is defined by:

$$\sigma_{ref} = \frac{P\sigma_Y}{P_L(\sigma_Y, a)} \tag{9.6}$$

In cases where cyclic loading is present, the load P is evaluated from the stress, produced by the shakedown analysis, at the time in the cycle corresponding to the creep dwell. It should be noted that this is not necessarily at the peak stress in the cycle. P_L is the value of P corresponding to plastic collapse assuming a yield strength σ_Y. The effect of the flaw should be included in evaluating the plastic collapse load. When creep crack growth is being considered, the relevant flaw size is the size of the original flaw plus the amount of crack growth. For the purposes of initial calculation of the time for failure by continuum damage mechanics and calculation of initiation time, the relevant flaw size is that of the original defect.

9.10.3 *C** parameter

For steady state creep, the crack tip stress and strain rate fields (and hence creep crack growth rates) may be characterized by the *C** parameter. This is the creep equivalent of the *J*-contour integral used to describe elastic-plastic fracture. It may be evaluated by finite element analysis but a reference stress based estimate of *C** is often used. This is given by Equation (9.6) and Equation (9.7).

$$C^* = \sigma_{\text{ref}}\dot{\varepsilon}_c[\sigma_{\text{ref}}(a),\varepsilon_c]R' \tag{9.7}$$

where:

$\dot{\varepsilon}_c$ is the creep strain rate at the current reference stress and creep strain, ε_c, accumulated under the reference stress history up to the current time, t.

NOTE Normally the strain hardening rule is used to define creep strain rates under increasing stress during the crack initiation and growth stages.

This is also applicable to complex time-varying creep law. The characteristic length, R', is defined by:

$$R' = \left(\frac{K^{\text{p}}}{\sigma_{\text{ref}}}\right)^2 \tag{9.8}$$

As both K^{p} and σ_{ref} are directly proportional to the loading, P, the value of R' is independent of the magnitude of P. However, R' does vary with crack size and, when crack growth is being considered, both K^{p} and σ_{ref} should be calculated for the defect size equal to the size of the original crack plus the amount of crack growth. The value of R' is also different at the surface and deepest points of a semi-elliptical surface defect due to differences in the values of K^{p}.

For other than simple primary loadings, estimates of *C** are given in R5 [9.2].

9.10.4 Redistribution time, t_{red}

This calculation is required only when cyclic loading is insignificant.

Time is required for stress redistribution due to creep from the initial elastic state at the start of a creep dwell. The requirement for the stress redistribution to be complete and widespread creep conditions to be established may be expressed in terms of a redistribution time, t_{red}. This may be expressed conveniently in terms of the reference stress for cases of primary load only as:

$$\varepsilon_c[\sigma_{\text{ref}}(a),t_{\text{red}}] = \frac{\sigma_{\text{ref}}(a)}{E} \tag{9.9}$$

where:

$\varepsilon_c[\sigma_{\text{ref}}(a),t]$ is the accumulated creep strain at the reference stress for time, t, and crack length, a, from uniaxial creep data.

9.10.5 *C(t)* parameter

For times less than the redistribution time, it might be necessary to calculate the transient crack tip parameter $C(t)$. An interpolation formula for $C(t)$ during the transition between initial elastic loading and steady state secondary creep is:

$$\frac{C(t)}{C^*} = \frac{(1+\varepsilon_c/\varepsilon_e)^{1/(1-q)}}{(1+\varepsilon_c/\varepsilon_e)^{1/(1-q)} - 1} \tag{9.10}$$

where:

q is the exponent in the creep crack growth law of Equation (9.14) or alternatively estimated from $q = n/(n+1)$.

For times in excess of the redistribution time, *C(t)* approaches *C**.

 © The British Standards Institution 2019

To allow for the increased amplitude of the crack tip fields at short times, it is assumed that for times less than the redistribution time ($t < t_{red}$), Equation (9.14) may be generalized to:

$$\dot{a} = A[C(t)]^q \tag{9.11}$$

However, the effects of the redistribution period can usually be allowed for approximately as follows:

$$\begin{aligned} \dot{a} &= 2A(C^*)^q \quad \text{for } t_i \le t \le t_{red} \\ \dot{a} &= A(C^*)^q \quad \text{for } t_i \ge t_{red} \end{aligned} \tag{9.12}$$

9.11 Material data for predicting crack initiation and growth under creep and creep/fatigue

9.11.1 Creep crack initiation data

For situations where fatigue is insignificant, it might be possible to take account of an initiation period prior to crack extension. For widespread creep conditions, creep crack initiation data may be expressed by a relationship of the form:

$$t_i(C^*)^\beta = \gamma \tag{9.13}$$

Alternative crack initiation methods and the properties needed to derive initiation times are given in Annex S where available.

9.11.2 Creep crack growth data

Creep crack growth data are required to calculate crack growth under steady loading conditions or to estimate the crack extension during dwell periods for creep-fatigue conditions. Creep crack growth data are generally presented as a simple relationship of the form:

$$\dot{a}_c = A(C^*)^q \tag{9.14}$$

Annex S gives some typical values of A and q for a number of materials. They are dependent on the test specimen geometry used to obtain creep crack growth data. For a conservative assessment, compact or deeply cracked bend specimens should be chosen and data should satisfy validity criteria. For specific applications, data on other geometries might be justified; for example, to allow for loss of constraint, alternative test specimens may be used (see ASTM E1457).

9.11.3 Cyclic crack growth data

The type of cyclic crack growth data required depends on the size of the defect relative to the cyclic plastic zone at the surface of the component. Here large cracks bigger than the cyclic plastic zone are considered, using a Paris law modified for crack closure.

The cyclic component of creep-fatigue crack growth is described by:

$$\left(\frac{da}{dN}\right)_f = C(\Delta K_{eff})^l \tag{9.15}$$

In situations where cyclic crack growth data have been obtained from tests with significant plasticity, it is preferable to evaluate ΔK_{eff} from experimental estimates of ΔJ. However, it is conservative to use data which have been correlated with elastically calculated ΔK_{eff} values. Further information on the use of fatigue crack growth data is given in Clause **8**, which includes alternative expressions to Equation (9.15).

9.11.4 Other data

In addition to the creep data described in **9.9.3** to **9.11** and detailed in Annex S, it might be necessary to have other information to perform an assessment; these are listed below.

a) *Elastic and physical constants*. Values for elastic modulus, E, Poisson's ratio, ν, and the instantaneous or mean coefficient of thermal expansion, are required to perform the basic stress analysis and might also be required if a detailed shakedown analysis has to be performed.

b) *Stress-strain data*. Values for the minimum 0.2% proof strength from monotonic tensile tests are required. Cyclic stress-strain data are required to determine the stress intensity factor range when cyclic plastic deformation occurs and to determine deformation stress-strain loops.

c) *Fracture toughness data.* Values of the fracture toughness are required to check crack stability for time-independent loadings. In general, data relate to materials which have experienced no prior global (ligament) or local (crack tip) creep damage. It is therefore necessary to confirm that the fracture toughness values used for assessing crack stability under time-independent loadings are appropriate for the material condition ahead of the crack tip, as discussed in Clause **7**, Annex J and Annex L.

9.12 Guidance on performing assessment calculations

9.12.1 Calculate rupture life, t_{CD}

Both time-based and ductility-based approaches may be used for assessing creep damage. For loadings which are predominantly constant and primary, the stress is well known and it is appropriate to use stress/time-to-rupture relationships for assessment. For damage due to cyclic relaxation, the strain accumulated is limited in each cycle and ductility methods are appropriate. For predominately primary loading the time, t_{CD}, for creep damage to propagate through a structure and lead to failure is taken as:

$$t_{CD} = t_r[\sigma_{ref}(a)] \tag{9.16}$$

where $t_r(\sigma)$ is the rupture time at stress, σ, from conventional stress/time-to-rupture data (Annex S) and the reference stress is calculated for the primary loads only for the current crack size, a.

Prior to crack growth the rupture time is calculated for the initial defect size, a_0. If t_{CD} is less than the remaining assessment time, then remedial action should be taken. For combined and cyclic loading, it might be necessary to evaluate t_{CD} from a ductility exhaustion approach; further details are given in R5 [9.2].

9.12.2 Calculate crack size after growth, a_g

The extent to which crack growth calculations are required depends on the relative magnitudes of the service life to date, t_0, the desired future service life, t_s, and the initiation time, t_i; this may be summarized as follows.

If $t_0 + t_s < t_i$, the crack does not incubate and $a_g = a_0$.

If the crack incubates during the assessment time, then it is necessary to calculate the crack size, a_g, after growth in time $t_0 + t_s - t_i$.

If the crack has incubated prior to the assessment, then it is necessary to calculate the crack size, a_g, after growth in time t_s.

The time required for the crack to propagate by an amount Δa_g is denoted t_g. There are a number of different regimes for calculations of crack growth and these are set out below.

 © The British Standards Institution 2019

9.12.3 Fatigue crack growth outside the cyclic plastic zone

9.12.3.1 Crack growing outside the cyclic plastic zone size, r_p, at the surface of the component

In this regime, the fatigue crack growth rate law of Equation (9.15) is used and the total crack growth per cycle, da/dN, is obtained as the simple sum of the contributions due to cyclic and creep crack growth rates:

$$\frac{da}{dN} = \left(\frac{da}{dN}\right)_f + \left(\frac{da}{dN}\right)_c \tag{9.17}$$

where:

$\left(\frac{da}{dN}\right)_f$ is given by Equation (9.15).

If creep-fatigue interactions are shown to be significant in **9.6**, the constants should be modified for hold-time effects.

If fatigue crack growth has been shown to be insignificant in **9.6**, this term is omitted.

The creep crack growth per cycle in Equation (9.17) also depends on loading regime as set out in **9.12.3.2** to **9.12.3.3**.

9.12.3.2 Steady state creep crack growth for times $t > t_{red}$, with insignificant cyclic loading

For the load controlled case and the attainment of steady state creep conditions, creep crack growth is obtained from creep crack growth data in the form of Equation (9.14).

The creep crack extension per cycle, $(da/dN)_c$, is evaluated as the integral of Equation (9.14) over the dwell period, t_h:

$$\left(\frac{da}{dN}\right)_c = \int_0^{t_h} A(C^*)^q dt \tag{9.18}$$

9.12.3.3 Non-steady state creep crack growth, $t < t_{red}$, when cyclic loading is insignificant

As discussed in **9.10.5**, a simplified treatment of transient creep given in Equation (9.12) can be employed. If the total time for the assessment does not exceed t_{red}, then the simplified treatment of transient creep given in Equation (9.12) is not adequate and it is necessary to use the parameter *C(t)* explicitly, from Equation (9.10), in estimating creep crack growth.

The creep crack extension per cycle, $(da/dN)_c$, including transient effects, is then evaluated over the dwell period, t_h, as:

$$\left(\frac{da}{dN}\right)_c = \int_0^{t_h} A[C(t)]^q dt \tag{9.19}$$

9.13 Assess significance of results

9.13.1 Guidance on assessing the significance of results and reporting

9.13.1.1 General

Application of the assessment procedures leads to one of the following results.

a) The final defect size leads to an acceptable end-of-life safety margin. In this case, a sensitivity analysis should be carried out to ensure that the safety margin is not overly sensitive to variations in the input parameters of the assessment.

b) Failure or excessive crack growth is indicated within the required service life. In these circumstances, the assessment may be revisited with a view to reducing the assumed conservatisms. In the event that acceptable end-of-life safety margins still cannot be demonstrated, remedial action should be taken, as described in **9.13.2.**

These scenarios are discussed in further detail in **9.13.1.2**.

9.13.1.2 Sensitivity analysis

The limiting conditions for a failure assessment are described elsewhere in the procedure. The limiting state is not normally acceptable for engineering purposes, and confidence in determining safe loading conditions is traditionally gained by applying safety or reserve factors in design calculations. However, the application of particular numerical factors in fracture analyses can be misleading because of the inherent but variable interdependence of the parameters contributing to fracture behaviour.

Confidence in assessments is gained in two stages. Firstly, the use of lower bound limit load solutions, together with upper bound applied loads, defect sizes and stress intensity factor values, provides confidence that the failure assessment is suitably conservative. Secondly, this should be reinforced by investigating the sensitivity of the assessment point to variations of appropriate input parameters.

For example, the sensitivity analysis could consider uncertainties in the service loading conditions, the extrapolation of materials data to service conditions, the nature, size and shape of the flaw, and the parameter inputs.

For defects found in service, the sensitivity of the assessment to any assumption about whether the crack is already growing may be tested by performing assessments both with and without the initiation stage. It is recommended that, where cast-specific data are not available, an initial assessment be performed using best-estimate, mean data. The sensitivity study should include the following combinations:

a) lower bound creep crack growth rate with upper bound creep strain data;

b) upper bound creep crack growth rate with lower bound creep strain data. It should be recognized that a sensitivity analysis which combines upper bound creep strain data, lower bound crack initiation data and upper bound creep crack growth data is likely to be overly conservative.

Confidence in an assessment is gained when it is possible to demonstrate that realistic changes in the input parameters do not lead to dramatic reductions in the end-of-life safety margin. Further confidence in the assessment and in any appropriate inspection period is gained when consideration of the end-of-life crack growth rate shows that there is not rapid crack extension leading to imminent failure. Details of the sensitivity analysis should be reported with the assessment results.

An alternative to the deterministic approach is to use probabilistic methods to directly determine failure probabilities. These methods make use of the statistical variation of the input parameters, rather than assuming that the parameters are single-valued, as in the deterministic approach. Such assessments require estimates of the statistical distributions of the variable input parameters. Advice is contained in Annex K.

The factor of safety that should be applied to predictions of crack growth and final failure is dependent on the degree of conservatism introduced into the input data and on the results of sensitivity analyses. Further guidance is given in Annex K.

9.13.1.3 Report results

When reporting the results of a structural integrity assessment, the information listed below should be included:

a) *loading conditions* – e.g. service load and temperature and service life including life seen to date; conditions considered for time independent loadings, for example transient or fault loadings; categorization of loads and stresses;

b) *materials properties* – material specification; creep rupture data, creep strain data, creep crack growth data; time-independent assessment material data (yield strength, ultimate tensile strength and fracture toughness for material with creep damage at crack tip); elastic data (elastic modulus, Poisson's ratio); whether data obtained by direct testing or indirect means; source and validity of data;

c) *definition of flaw* – flaw location, shape and size; allowance for sizing errors; whether re-characterization of flaw undertaken;

d) *reference stress* – source of limit load/reference stress solution; yield criterion; whether local and/or global collapse considered;

e) *stress intensity factor solution* – source of K solution (e.g. standardized solution, finite element analysis);

f) *C^* solutions* – from the appropriate reference stress solution and uniaxial creep properties;

g) *significance of creep and fatigue* – results of tests for insignificant creep, fatigue and creep-fatigue interactions, if applicable;

h) *time-independent assessment* – form of assessment, reserve factors;

i) *cycle-dependent assessment* – type of fatigue crack growth law; stress intensity factor range, crack closure parameter, surface strain range, creep damage; time to shake down to steady cyclic state;

j) *time-dependent assessment* – results of analysis; initiation time, redistribution time, defect size after growth, crack velocity parameter, time to rupture by continuum damage;

k) *sensitivity analysis* – input parameters against which sensitivity studies undertaken (e.g. flaw size, materials properties); results of each individual study;

l) *reporting* – nature of the quality assurance to which the analysis has been subjected.

Known conservatisms incorporated in the assessment route should be listed. All departures from the procedure should be reported and separately justified. A separate statement should be made about the significance of potential failure mechanisms remote from the defective areas.

9.13.2 Remedial action

Many design standards require or recommend periodic inspection of components under loads such as internal pressure and/or high temperature operation.

Typical re-inspection periods are every ten years or lower depending on the component. Inspections can be performed using some of the available methods and techniques described in Annex T. Inspection of components operating in the creep range uses these techniques to demonstrate integrity, but other techniques are also used to determine creep status, including the following.

- *Magnetite layer measurement*. The magnetite layer is indicative of the operational effective temperature. The layer is usually measured by ultrasonic testing, but sometimes destructive testing of samples extracted from selected points confirms ultrasonic testing results.
- *Hardness*. Hardness is not a clear indicator of remaining lifetime, but it is a cheap technique and in combination with replicas can provide useful information about creep component status.
- *Metallographic replicas*. The analysis of replicas provides information about physical and structural damage of the component. As replicas require some surface preparation, it is usual to complement these with hardness measurements. The technique is also used to analyse detected cracks, helping to determine cracking mechanisms and crack growth, for input into remaining lifetime assessment.
- *Dimensional analysis*. Creep deformation can be detected and surveyed by selected measurements.
- *X-ray diffraction*. This technique provides information on material composition, level of stress and creep status.
- *Micro-specimen destructive testing*. Some tests are available, providing information on materials properties and creep status. The most frequently used techniques are the miniature specimen creep test, the impression creep test and the small punch test.

Remedial action could involve changing the in-service parameters (such as load, temperature or desired service life) and then using the assessment procedure either to demonstrate acceptance or to estimate at what time repair is necessary. Alternatively, the defective component might be repaired or replaced.

Bibliography for Clause 9

Standards publications

For dated references, only the edition cited applies. For undated references, the latest edition of the referenced document (including any amendments) applies.

ASME Boiler and Pressure Vessel Code, Section III: *Rules for construction of nuclear power plant components*

ASTM E2760, *Standard test method for creep-fatigue crack growth testing*

ASTM E1457, *Standard test method for measurement of creep crack growth times in metals*

BS EN 13480, *Metallic industrial piping*

PD 5500, *Specification for unfired fusion welded pressure vessels*

PD 6525-1, *Elevated temperature properties for steels for pressure purposes. Stress rupture properties*

Other documents

[9.1] AINSWORTH, R.A. The creep clauses of BS 7910. *In: International Journal of Pressure Vessels and Piping*, 165, August 2018, 208–213. <https://doi.org/10.1016/j.ijpvp.2018.06.014>

[9.2] R5 PANEL. *R5 Assessment procedure for the high temperature response of structures (as amended)*. Report R5, Issue 3, UK: EDF Energy, 2003.

[9.3] KOÇAK, M., WEBSTER, S., JANOSCH, J.J., AINSWORTH, R.A. and KOERS, R. *FITNET Fitness-for-Service (FFS) – Procedure (Volume 1),* Geesthacht, Germany: GKSS Research Centre, 2008. ISBN 978-3-940923-00-4.

NOTE 1 This document is out of print and has effectively been superseded by BS 7910:2013.

[9.4] KOÇAK, M., HADLEY, I., SZAVAI, S., TKACH, Y. and TAYLOR, N. *FITNET Fitness-for-Service (FFS) – Annex (Volume 2),* Geesthacht, Germany: GKSS Research Centre, 2008. ISBN 978-3-940923-01-1.

NOTE 2 This document is out of print and has effectively been superseded by BS 7910:2013.

[9.5] WEBSTER, G.A., DAVIES, C.M., SKELTON, R.P., NIKBIN, K.M. and DEAN, D.W. Determination of creep crack growth incubation periods in type 316H stainless steel. *In: Proceedings of the 2nd International Conference on Creep and Fracture in High Temperature Components – Design and Life Assessment*, Zurich, April 21–23, 2009.

[9.6] DAVIES, C.M. Predicting creep crack initiation in austenitic and ferritic steels using the creep toughness parameter and time-dependent failure assessment diagram. *In: Fatigue and Fracture of Engineering Materials and Structures*, 2010, 33(12), 911–911. <https://onlinelibrary.wiley.com/doi/abs/10.1111/j.1460-2695.2010.01537.x>

[9.7] DAVIES, C.M., WEBSTER, G. A. and NIKBIN, K. M. Predictions of Creep Crack Initiation Periods. *In: Proceedings of ASME 2010 Pressure Vessels and Piping Division/K-PVP Conference*. July 18–22, 2010, Bellevue, Washington, USA. ASME, PVP2010-25035.

[9.8] AFCEN. *RCC-MR, Design and construction rules for mechanical components of FBR nuclear islands and high temperature applications – Appendix A16: Guide for leak before break analysis and defect assessment*. France: AFCEN, 2002.

[9.9] DRUBAY, B., MARIE, S., CHAPULIOT, S. and LACIRE, M. A16: Guide for defect assessment at elevated temperature. *In: International Journal of Pressure Vessels and Piping*, 2003, 80(7–8), 499–516.

[9.10] AMERICAN PETROLEUM INSTITUTE AND THE AMERICAN SOCIETY OF MECHANICAL ENGINEERS. *API 579-1/ASME FFS-1 Fitness-for-service*, 2016.

[9.11] INSTITUTION OF MECHANICAL ENGINEERS*, THE CREEP OF STEELS WORKING PARTY. High temperature design data for ferritic pressure vessel steels.* London: Mechanical Engineering Publications Ltd, 1983. ISBN 0 85298 526 6.

[9.12] TAN, M., CELARD, N.J.C., NIKBIN, K., and WEBSTER, G.A. Comparison of creep crack initiation and growth in four steels tested in HIDA. *In: International Journal PVP*, 2001, 737–747.

[9.13] WEBSTER, G.A. and AINSWORTH, R.A. *High temperature component life assessment*. London: Chapman & Hall, 1994. ISBN 0 412 58520.

[9.14] LINK, R. and KAMRAN, N. *Fracture and Fatigue of Structures: 35th Volume*. ASTM STP 1480. ASTM International, 2007. ISBN 978 0 8031 6247 1.

[9.15] NIKBIN, K.M., SMITH, J.J. and WEBSTER, G.A. Prediction of Creep Crack Growth from Uniaxial Data. *In: Proceedings of the Royal Society of London*, 1984, 396(1810), 183–197.

[9.16] NIKBIN, K.M., SMITH, J.J. and WEBSTER, G.A. An Engineering Approach to the Prediction of Creep Crack Growth. *In: Journal of Engineering Materials and Technology*, Trans. ASME, 1986, 108(2), 186–191.

[9.17] AINSWORTH, R.A. CEGB assessment procedure for defects in plant operating in the creep regime. *In: Fatigue and Fracture of Engineering Materials and Structures*, 1987, Vol. 10, 115–127.

[9.18] WINSTONE, M.R., NIKBIN, K.M. and WEBSTER, G.A. Modes of failure under creep/fatigue loading of a nickel-based superalloy. *In*: *Journal of Materials Science*, 1985, 20(7), 2471–2476. ISSN 0022-2461.

[9.19] WEBSTER, G.A, NIKBIN, K.M., CHORLTON, M.R., CÉLARD, N.J.C. and OBER, M. Comparison of High Temperature Defect Assessments Methods. *In: Material at High Temperature*, 1998, 15(3–4), 337–346.

[9.20] WASMER, K., NIKBIN, K.M. and WEBSTER, G.A. Creep crack initiation and growth in thick section steel pipes under internal pressure. *In: International Journal of Pressure Vessels and Piping*, 2003, 80(7–8), 489–498.

[9.21] BIGLARI, F., NIKBIN, K.M., GOODALL, I.W. and WEBSTER, G.A. Determination of fracture mechanics parameters J and C* by finite element and σ_{ref} methods for a semi-elliptical flaw in a plate. *In: International Journal of Fracture*, July 2003, Vol 8–9.

[9.22] WASMER, K., DAVIES, C.M., NIKBIN, K.M., O'DOWD, N.P. and WEBSTER, G.A. A sensitivity study of creep initiation and growth prediction. *In: Welded, Proceedings of the 2nd International Conference on Integrity of High Temperature Welds*, London, 10–12 November 2003.

[9.23] YOON, K.B., PARK, T.G. and SAXENA, A. creep crack growth analysis of elliptic surface cracks in pressure vessels. *In: International Journal of Pressure Vessels and Piping*, 80(7–8), July-August 2003, 465–479. <https://doi.org/10.1016/S0308-0161(03)00101-7>

[9.24] NEWMAN, J.C. and RAJU, I.S. An empirical stress intensity factor eqn. for the surface crack. *In: Engineering Fracture Mechanics*, 1981, 1–2(15), 185–192.

[9.25] ROOKE, D.P. and CARTWRIGHT, D.J. *Compendium of stress intensity factors*. London: The Stationery Office, 1976. ISBN 0117713368.

[9.26] ZAHOOR, A. Closed form expressions for fracture mechanics analysis of cracked pipes. *In: Journal of Pressure Vessel Technology*, 1985, 107, 203–205.

[9.27] TADA, H. *Stress analysis of cracks handbook*. 2nd edition. Paris Productions Incorporated,1985.

[9.28] KUMAR, V., GERMAN, M.D. and SHIH, C.F. estimation techniques for the prediction of elastic-plastic fracture of structural components of nuclear systems. *In: EPRI Report SRD-80-094*, EPRI, Palo Alto, CA, June 1981.

[9.29] DAVIES, C.M., KOURMPETIS, M., O'DOWD, N.P. and NIKBIN, K.M. Experimental evaluation of the J or C* parameter for a range of cracked geometries. *In: Journal of ASTM International*, 2006, 3(4). <https://doi.org/10.1520/ JAI13220>

[9.30] NIKBIN, K.M., YATOMI, M., WASMER, K. and WEBSTER, G.A. Probabilistic analysis of creep crack initiation and growth in pipe components. *In: International Journal of Pressure Vessels and Piping*, July-August 2003, 80(7–8), 565–571.

[9.31] MILLER, A.G. Review of limit loads of structures containing defects. *In: International Journal of Pressure Vessel and Piping*, 1988, 32(1–4), 197–327.

[9.32] KIM, YUN-JAE, SHIM, DO-JUN, NIKBIN, K.M., KIM, YOUNG-JIN, HWANG, SEONG-SIK and KIM, JOUNG-SOO. FE based plastic limit loads for cylinders with part-through surface cracks under combined loading. *In: International Journal of Pressure Vessels and Piping*, 2003, 80(7–8), 527–540.

[9.33] GOODALL, I.W. and WEBSTER, G.A. Theoretical determination of reference stress for partially penetrating flaws in plates. *In: International Journal of Pressure Vessels and Piping*, 2001, 78(10), 687–695.

[9.34] HUDDLESTON, R.L. and SWINDEMAN, R.W. *Materials and design bases issues in ASME Code Case N-47*. Nuclear Regulatory Commission, Washington, DC (United States). Division of Engineering; Oak Ridge National Lab., TN (United States); 1993.

This page deliberately left blank

10 Assessment for other modes of failure

10.0 Symbols and definitions

For the purposes of this clause, the following symbols, definitions and units apply, unless otherwise indicated at the point of use.

Symbol	Definition	Units
C_1	Constant in the stress corrosion crack growth equation	see footnote 10.1)
d*a*/d*N*	Flaw growth rate with cycles	mm/cycle
d*a*/d*t*	Flaw growth rate with time	mm/h
f_{scc}	Factor of safety with respect to stress corrosion cracking ($f_{scc} \geq 1.0$)	—
K	Stress intensity factor	$N/mm^{3/2}$
K_I	Applied tensile (mode I) stress intensity factor	$N/mm^{3/2}$
K_{Ic}	Plane strain fracture toughness	$N/mm^{3/2}$
K_{ISCC}	Critical stress intensity factor for stress corrosion cracking	$N/mm^{3/2}$
k_{tb}	Bending stress concentration factor	—
k_{tm}	Membrane stress concentration factor	—
n(scc)	Exponent in the stress corrosion crack growth relationship	—
P_b	Primary bending stress	N/mm^2
P_m	Primary membrane stress	N/mm^2
Q	Secondary stress	N/mm^2
R	Ratio of minimum stress to maximum stress	—
ΔK	Stress intensity factor range	$N/mm^{3/2}$
ΔK_0	Threshold stress intensity factor range below which fatigue crack growth (or corrosion fatigue crack growth) does not occur (Clause **8**)	$N/mm^{3/2}$
σ_{ref}	Reference stress	MPa

10.1 Yielding due to overloading of remaining cross-section

The need for critical assessment of this failure mode is most likely to arise in small structural sections. A detailed assessment for tensile loading may be carried out using the formulae given in Annex P to calculate reference stress σ_{ref}, and limiting the maximum value of σ_{ref} to the material flow strength. For shear loading the maximum shear stress should be calculated on the net area and this value limited to 0.58 times the material yield strength. Assessment for this

10.1) The units and value of C depend on those used to measure d*a*/d*t* and ΔK, and on the value of the exponent, *n(scc)*. If C is known in one set of units, C_a, the corresponding value for another set of units, C_b, is given by:

$$C_b = C_a \frac{f_a}{f_b^{n(scc)}}$$

where:

f_a is the conversion factor for d*a*/d*t* from the first to the second unit system; and

f_b is the conversion factor for ΔK from the first to the second unit system.

failure mode is automatically performed when using the procedures given in Clause **7**.

10.2 Leakage in pressure, liquid or vacuum containing equipment

Flaws that provide a path from the interior to the exterior in equipment used for containing fluids under pressure or vacuum should normally be regarded as unacceptable. A leak-before-break assessment might be appropriate in some circumstances (see Annex F).

10.3 Environmental effects

10.3.1 General

The effect of aggressive environments should be taken into account in an ECA. Since environmental effects are normally highly specific, it is only possible to give general guidance. However, such effects can be extremely sensitive to small variations in material and operating conditions. Any assessment or experimental measurements should take into account variations of heat treatment, chemical compositions, etc., within a given material specification. Equally, in-service conditions can change susceptibility to environmental effects due, for example, to temper embrittlement or sensitization of material and, for such cases, assessments or measurements have to be made for materials for which the appropriate in-service conditions have been simulated.

10.3.2 Locally thinned areas (LTAs)

The suitable choice of materials for the particular environment is an important factor in avoiding failure due to LTAs, such as corrosion and/or erosion. The following should also be applied:

a) for flaws not open at either surface, the recommendations of **10.1** should be followed with any corrosion/erosion allowance removed;

b) for crevices of any sort exposed at the surface to a corrosive or erosive environment, including cracks, lack of fusion or penetration, pores and pits, an estimate should be made of the maximum rate of crevice corrosion and time to grow to a size that is regarded as unacceptable.

See Annex G for guidance on the assessment of the significance of LTAs in internally pressurized pipes or pressure vessels.

An assessment should take into account the possibility of failure by yielding, leakage, fracture or other modes of failure from the increased flaw size resulting from any active corrosion or erosion mechanisms. In the absence of sufficient information where crevice corrosion is relevant, no exposed crevices should be regarded as acceptable.

10.3.3 Environmentally assisted cracking

10.3.3.1 General

When assessing the integrity of a structure containing a flaw or flaws, the likelihood of sub-critical crack growth under service conditions by environmentally assisted cracking should be assessed. Environmentally assisted cracking is a collective description for stress corrosion, corrosion fatigue, and combinations thereof. The interactions between these failure mechanisms can be complex. For example, apparent stress corrosion thresholds and growth rates can be profoundly influenced by minor cyclic forces or very slow monotonically increasing forces. The term corrosion does not necessarily imply gross surface oxidation or dissolution, but is often the very mild form of general corrosion associated with the formation of passive and largely protective oxide films.

Because of its complexity, the assessment of flaws in structures where environmentally assisted crack extension might occur should only be undertaken by engineers with a high level of appropriate knowledge.

Because of the potential complexity of these interactions and because they are specific to particular material/environment combinations, only data obtained under conditions resembling as closely as possible the practical situation should be used in the assessment of environmentally assisted cracking. Identifying the cause of cracking in terms of the mechanistic process can be difficult, hence the need for representative test conditions. General guidance on testing procedures for determining stress corrosion threshold stress intensity factors, K_{ISCC}, and crack propagation rates is given in **10.3.3.2.2**, **10.3.3.2.3** and **10.3.3.3.2**. Where necessary, tests should be conducted on representative materials (parent metals, weld metals and/or HAZs, as appropriate). Environmental chemistry and temperature should be appropriately simulated and appropriate loading conditions (e.g. loading cycle and frequency) should be used, including any possible influence of dynamic forces that invariably act on real structures. The extent and duration of chemical transients, the high probability of environmental chemistry modification in cracks and crevices and the possibility that hydrogen embrittlement processes can affect buried flaws should also be taken into account.

The procedures presented here use a linear elastic fracture mechanics approach to describe crack growth due to environmentally assisted cracking. These techniques are specific to assessing sub-critical crack growth, either from original welding flaws (which are idealized as sharp cracks) or from cracks formed in service by other mechanisms. Sub-critical growth from existing flaws or cracks is only one part of an overall assessment of susceptibility to environmentally assisted cracking. In addition to the stability of existing cracks or flaws, an assessment should always be made of the risk of crack initiation from plain surfaces or blunt stress concentrations to ensure that the total stress ($k_{tm}P_m + k_{tb}P_b + Q$) is less than the appropriate threshold stress for environmentally assisted crack initiation. Alternatively, it might be possible to demonstrate that the environment is effectively benign.

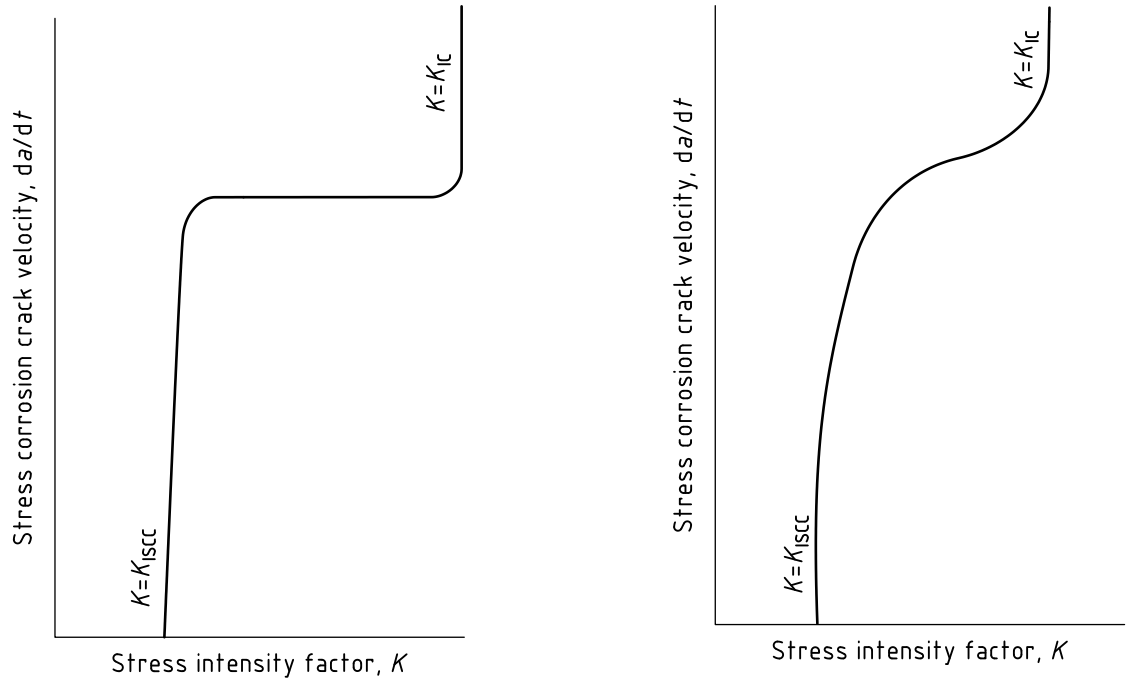
NOTE The fracture toughness at initiation of stable tearing can be defined using R-curve data obtained from tests performed using specific material-environmental combinations. However, the use of tearing resistance curves for the assessment of ductile tearing in an aggressive environment is still the subject of ongoing research.

10.3.3.2 Stress corrosion cracking (SCC)

10.3.3.2.1 General

SCC results from the conjoint action of an aggressive environment and a static applied or residual stress. It includes cracking due both to metal dissolution and to hydrogen embrittlement. An apparently benign environment can be corrosive locally due to concentrations of chemical species. Once initiated, stress corrosion cracks usually attain an approximately uniform velocity, provided that the driving force is maintained and that the local environment remains unchanged. This velocity is dependent on the particular metal and environment. Typical behaviour is shown in Figure 10.1 in terms of the crack growth rate, da/dt, plotted against the stress intensity factor, K.

Figure 10.1 **Schematic diagrams of typical relationships between crack velocity and stress intensity factor during SCC**



a) Showing distinct crack growth plateau

b) Showing a more gradual change in crack growth rate with K

In order to assess the significance of a known flaw, the applied stress intensity factor, K_I, should be estimated following procedures laid down in **7.3.6**. Residual stresses can be of overriding importance. This applied value should then be compared with the threshold stress intensity factor for susceptibility to SCC, K_{ISCC}. If K_I is less than $(1/f_{scc})K_{ISCC}$, the flaw is acceptable. The factor of safety, f_{scc} ($f_{scc} \geq 1.0$), should be agreed between the parties and documented. Under these conditions, the data required are confined to values of K_{ISCC}, which is defined as the stress intensity factor at which stress corrosion cracks initiate and grow for the specified condition (metal, environment, exposure time, loading conditions, etc.) under predominantly plane strain conditions. Advice on the determination of K_{ISCC} is given in **10.3.3.2.2.**

If the applied value of K_I exceeds $(1/f_{scc})K_{ISCC}$, the possibility of stress corrosion crack growth should be recognized. In this case, the most appropriate approach might be remedial action, such as modification of the environment, elimination of the flaw(s) or stress relief. However, an assessment may be made to determine whether the flaws would grow to an unacceptable size within the design life of the structure or within the appropriate inspection interval. This assessment should be based on available stress corrosion crack velocity data, extrapolated, where necessary, to stress intensity factors below K_{ISCC}. Extrapolation is necessary if $(1/f_{scc})K_{ISCC} < K_I < K_{ISCC}$. The method of extrapolation should be agreed between the parties. Advice on the determination of stress corrosion crack velocity is given in **10.3.3.2.3**.

10.3.3.2.2 K_{ISCC} determination

Stress corrosion processes can be very sensitive to small changes in test conditions. In particular, the environment itself is an important variable, and it should be ensured that the service conditions are adequately simulated. Detailed guidance on this topic is given in BS EN ISO 7539-1. K_{ISCC} tests are normally conducted under static load conditions, but structures are seldom subjected to purely static loading and the value of K_{ISCC} can be considerably reduced if a

cyclic component, even of very small magnitude, is superimposed on the static loading. For these reasons, it is often more appropriate to assess the significance of flaws in terms of the threshold range in stress intensity factor, ΔK_0, for the growth of fatigue cracks under the environmental and loading conditions of interest. Advice on the determination of ΔK_0 is given in **10.3.3.3.2**.

If K_{ISCC} values are appropriate, they should be determined for the materials of interest using the procedures described in BS EN ISO 7539-6. This clause describes both crack initiation and crack arrest methods using fatigue pre-cracked, fracture mechanics type specimens tested under constant load (increasing *K*) or constant displacement (decreasing *K*). For some systems, the value can vary depending on the method of measurement. For instance, in a constant load (increasing *K*) test, the onset of stress corrosion is measured as the point at which crack extension occurs from a fatigue pre-crack. In a constant displacement (decreasing *K*) test, the point at which crack extension terminates is measured, and, as this will have involved prior extension by stress corrosion (rather than fatigue), the potential difference in crack morphology could influence the result. The significance of scales or other corrosion products forming on the crack flanks during the test can also differ between the two types of test. The most appropriate test technique might depend on the material-environment system in question, and the availability of suitable testing facilities, so expert advice should be obtained. The procedure for testing under rising load or rising displacement conditions is described in BS EN ISO 7539-9. The loading or crack opening displacement rate is the critical parameter and it is preferable to test over a range of rates to obtain conservatively the minimum, lower bound, value of K_{ISCC}. This might be lower than that obtained by conventional static loading or fixed displacement test under otherwise identical test conditions.

10.3.3.2.3 Stress corrosion crack velocity determination

Data on the materials of interest may be obtained by monitoring the crack velocity during stress corrosion testing of pre-cracked fracture mechanics specimens using the procedures given in BS EN ISO 7539-6 and the crack monitoring methods, e.g. as given in R5 [10.1]. These techniques enable the stress corrosion crack velocity, d*a*/d*t*, to be determined as a function of the stress intensity factor, *K*, as illustrated in Figure 10.1. One or more expressions of the following form:

$$\frac{da}{dt} = C_1 K^{n(\mathrm{scc})} \tag{10.1}$$

can be fitted to the data, where C_1 and n(scc) are constants. However, the detailed functional relationship is system-dependent and not as simple as this power relationship.

Alternatively, in instances where a stress corrosion mechanism prevails in service, it might be possible to estimate crack velocity conservatively by appropriate inspection of the equipment at suitable intervals. This involves careful determination of the size of service flaws, either from samples taken from the equipment or in situ using suitable metallographic techniques.

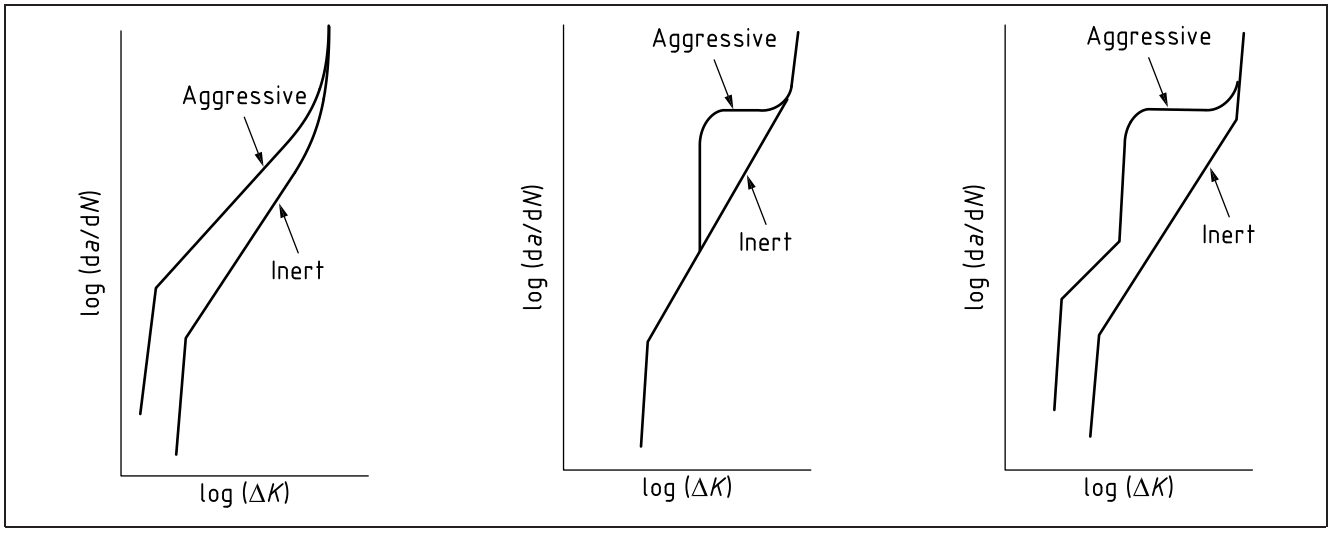
If it is necessary to assess the growth of flaws by a SCC mechanism, these expressions may be integrated numerically to predict the anticipated amount of growth during the design life of the structure or the relevant inspection period, whichever is appropriate. If, as a result of this growth, the flaws do not reach the maximum tolerable size for other failure mechanisms (brittle or ductile fracture; see Clause **7**), the flaws are acceptable. If the calculated crack size at the end of the design life or inspection interval exceeds the tolerable size for other failure mechanisms, the flaws are unacceptable.

10.3.3.3 Corrosion fatigue

10.3.3.3.1 General

Fatigue crack growth in aggressive environments can be greater than in inert ones. A number of types of corrosion fatigue relationship have been observed in different metal/environment systems, as summarized schematically in Figure 10.2. This complex behaviour means that, if reliable corrosion fatigue crack growth data are not available for the material, environment and loading conditions of interest, they should be determined in accordance with **10.3.3.3.2**. Equations describing fatigue crack growth in aggressive environments are available in only a very limited number of instances. Crack growth parameters are given in **8.2.3.4**, **8.2.3.5** and **8.2.3.6** for the special case of crack growth in ferritic steels in a marine environment.

Figure 10.2 **Types of corrosion fatigue crack growth behaviour**



10.3.3.3.2 Determination of corrosion fatigue data

The determination of corrosion fatigue data with pre-cracked specimens is similar to that described in BS ISO 12108 for normal fatigue data, but it is vital to employ environmental conditions and a loading cycle and test frequency which are representative of those encountered in service. In addition to temperature and chemical composition (including degree of aeration), factors such as flow rate, crack length and shape, and contact with dissimilar metals or electrochemical polarization can influence growth rates and should be reproduced during testing.

For the determination of threshold ΔK_0 values above which corrosion fatigue cracks initiate and grow under the specified test conditions, similar pre-cracked specimen geometries and procedures may be used as in the fatigue threshold testing to BS ISO 12108, provided that the appropriate environmental conditions are adequately simulated. However, care is needed when analysing corrosion fatigue data in the near-threshold regime, as crack arrest during laboratory testing might not be indicative of a true threshold condition being reached. Load history and/or crack depth can also have a significant influence [10.2]. Wherever possible, near-threshold data should be determined under realistic loading conditions (i.e. ΔK-increasing rather than ΔK-decreasing).

The threshold value of the stress intensity factor range ΔK_0 in corrosion fatigue is influenced by crack size and by the stress ratio. In the short crack regime, cracks can grow at ΔK values seemingly below ΔK_0, because the latter is commonly determined from long crack measurement and because linear elastic fracture mechanics (LEFM) becomes invalid. Also, in the long crack regime,

increasing the stress ratio, R, usually reduces the threshold value because of diminished impact of crack closure. For that reason a high R value for determining the threshold is a sensible conservative assumption. BS EN ISO 11782-2 provides guidance on determination of ΔK_0.

Similar specimens and methods may also be used to determine the relationship between da/dN and ΔK for corrosion fatigue. When practical applications involve random loading cycles or well-defined periodic changes in cyclic loading conditions, it is preferable to simulate service conditions, particularly with respect to stress ratio, cyclic frequency and cyclic wave form.

Environmental influences can be incorrectly estimated if the imposed cyclic frequencies are either too high and there is insufficient time for corrosion/diffusion processes to occur, or too low, allowing, for example, for re-passivation. The rise time over which the application of stress occurs during the fatigue cycle can also strongly influence the corrosion fatigue process and appropriate cyclic wave forms should be employed in any testing. Sinusoidal, triangular, saw-tooth and square wave forms are often employed to simulate service loading conditions and, where appropriate, representative hold times should be imposed during the cycle.

When the appropriate crack growth relationship has been determined, the flaw should be assessed in accordance with Clause **8**.

10.4 Instability (buckling)

10.4.1 General

In members loaded in compression, flaws should be assessed with regard to their possible effects on the buckling resistance of the component or structure. In this regard, flaws are divided into three broad categories:

a) those that reduce the effective local cross-section, i.e. planar and non-planar flaws;

b) laminations or lamellar flaws lying parallel to the component surfaces; and

c) flaws involving failure to conform to the design form (misalignment, angular and out-of-plane distortion, etc.).

In any assessment of flaws with regard to instability, account should be taken of the possibility of crack growth by fatigue, corrosion-fatigue, SCC and creep. Guidance on these aspects is given in Clause **8** and Clause **9**. The instability assessment should be performed for the flaw size at the end of design life. Some structures operate in a post-buckled mode. While a flaw might not affect the initial buckling strength, it might reduce the post-buckled deformation capacity. No specific guidance is given here on this aspect, but it should be borne in mind for structures required to operate in such conditions.

10.4.2 Flaws that reduce the local cross-section

At any cross-section, the total aggregate area and position of any flaws should be such that the buckling strength of the component is not reduced below the maximum applied loading effects. The effect on buckling of flaws that reduce the local cross-section is dependent on the loss of section area as well as on the position of the flaw, both overall within the member and within the thickness of the member. An assessment of the significance of a flaw with regard to buckling should take these aspects into account. The buckling strength should be checked using the second moment of area for the reduced cross-section in the plane perpendicular to the compressive stress ($P_m + P_b + Q$) and taking into account any eccentricity in loading due to the presence of the flaw.

If a flaw occurs parallel to the surface under the weld attaching a stiffener to a plate loaded in compression, it reduces the effective length over which the stiffener is attached to the plate. Such flaws can take the form of laminations or lamellar tears or of underbead cracks. If a flaw of this type is detected, it should be assessed assuming that the stiffener is intermittently welded to the plate and that the flaw forms a space between two welds.

10.4.3 Flaws parallel to plate surfaces

The significance of planar flaws parallel to a plate surface and in the direction of compressive stress (laminations, lamellar tears, etc.) should be assessed by checking the buckling strength of each part of the material between the flaw and the component surface. This should be done by calculation, as if the individual parts of the material are separate plates of the same area as the flaw using the distance between the flaw and the surface as an effective thickness. It should be assumed that the plate is simply supported around its boundaries defined by the boundaries of the flaw.

10.4.4 Failure to conform to the design form

Flaws involving failure to conform to the design form at welds can have serious implications with regard to the buckling strength of members or components loaded in compression. Limits for flaws of misalignment, out-of-plane, and angular distortion in pressure vessels subjected to external pressure and in structural members loaded in compression are given in PD 5500 and BS EN 1090-2. Concerning pressure vessels, guidance can also be found in PD 5500 Enquiry Case No. 5500/33, which deals with the verification of shape of vessels subject to external pressure. If the structure under consideration is not built to one or other of these standards, care should be taken in applying the allowable tolerances from these standards, to ensure that these tolerances are consistent with the assumptions inherent in the actual design method used for the structure.

Bibliography for Clause 10

Standards publications

For dated references, only the edition cited applies. For undated references, the latest edition of the referenced document (including any amendments) applies.

BS EN 1090-2, *Execution of steel structures and aluminium structures – Technical requirements for steel structures*

BS EN ISO 7539-1, *Corrosion of metals and alloys – Stress corrosion testing – Part 1: General guidance on testing procedures*

BS EN ISO 7539-6, *Corrosion of metals and alloys – Stress corrosion testing – Preparation and use of precracked specimens for tests under constant load or constant displacement*

BS EN ISO 7539-9, *Corrosion of metals and alloys – Stress corrosion testing – Preparation and use of pre-cracked specimens for tests under rising load or rising displacement*

BS EN ISO 11782-2, *Corrosion of metals and alloys – Corrosion fatigue testing – Crack propagation testing using precracked specimens*

BS ISO 12108, *Metallic materials – Fatigue testing – Fatigue crack growth method*

PD 5500, *Specification for unfired fusion welded pressure vessels*

Other documents

[10.1] R5 PANEL. *R5 assessment procedure for the high temperature response of structures (as amended)*. Report R5, Issue 3, Revision 002. UK: EDF Energy, 2014.

[10.2] HOLTAM, C. M., BAXTER, D. P., ASHCROFT, I. A., and THOMSON R. C. Effect of crack depth on fatigue crack growth rates for a C–Mn pipeline steel in a sour environment. *In: International Journal of Fatigue*, February 2010, 32(2), 288–296.

This page deliberately left blank

Annex A (informative)

Evaluation under mode I, II and III loads

A.0 Symbols and definitions

For the purposes of this annex, the following symbols, definitions and units apply, unless otherwise indicated at the point of use.

Symbol	Definition	Units
a	Half flaw length for through-thickness flaw, flaw height for surface flaw or half height for embedded flaw	mm
a_0	Initial flaw size	mm
K_{eff}	Effective linear elastic stress intensity factor in mixed mode loading	N/mm$^{3/2}$
K_{eff}^{p}	Effective linear elastic stress intensity factor due to primary load	N/mm$^{3/2}$
K_{eff}^{s}	Effective linear elastic stress intensity factor due to secondary load	N/mm$^{3/2}$
K_{I}	Applied tensile (mode I) stress intensity factor (SIF)	N/mm$^{3/2}$
K_{I}^{p}	Stress intensity factor due to primary stress	N/mm$^{3/2}$
K_{I}^{s}	Stress intensity factor due to secondary stress	N/mm$^{3/2}$
K_{II}	Mode II linear elastic stress intensity factor	N/mm$^{3/2}$
K_{IIc}	Critical value of K_{II} at onset of brittle fracture in mode II	N/mm$^{3/2}$
K_{II}^{p}, K_{II}^{s}	Values of K_{II} due to primary and secondary stresses, respectively	N/mm$^{3/2}$
K_{III}	Mode III linear elastic stress intensity factor	N/mm$^{3/2}$
K_{III}^{p}, K_{III}^{s}	Values of K_{III} due to primary and secondary stresses, respectively	N/mm$^{3/2}$
K_{mat}	Material fracture toughness measured by stress intensity factor	N/mm$^{3/2}$
K_{r}	Fracture ratio	—
K_{r}^{p}	Contribution to K_r from primary stresses	—
K_{r}^{s}	Contribution to K_r from secondary stresses	—
K_{12}	Fracture toughness at initiation of ductile tearing	N/mm$^{3/2}$
L_{r}	Ratio of applied load to yield load	—
$L_{r,max}$	Permitted limit of L_r	—
V	Plasticity correction factor	—
α	Parameter used in defining K_{eff}	—
ν	Poisson's ratio	—
ρ	Plasticity interaction factor	—
σ_Y	Lower yield strength or 0.2% proof strength	N/mm^2

A.1 General

This annex gives guidance on flaw evaluation under combinations of mode I, mode II and mode III loads (defined in Figure A.1) where shear stresses in the plane of the flaw are to be considered. The annex is based on Chapter III.4 of R6 [A.1], with minor amendments. Advice on reference planes for flaw characterization is given in **6.4.5** and, except when principal planes are used, shear stresses have to be taken into account. The definition of an effective stress intensity factor, K_{eff}, for use in defining K_r in **7.3.6** is set out and distinguishes between materials where:

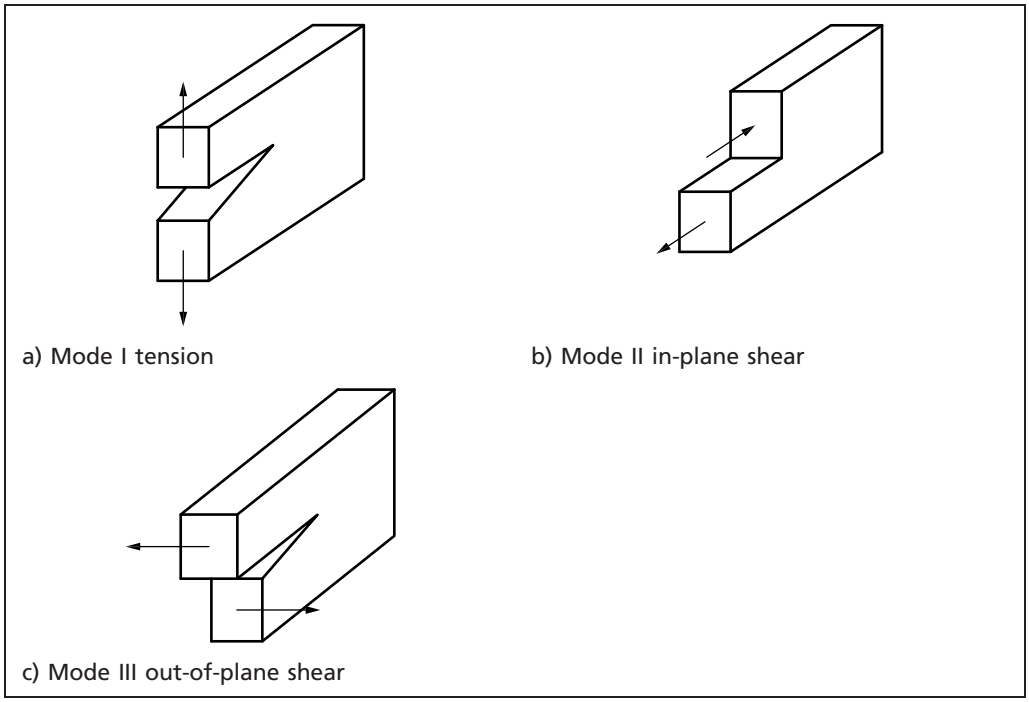
$$\frac{K_{mat}}{\sigma_Y} < 6.3\sqrt{mm} \quad \text{(A.1)}$$

and those where:

$$\frac{K_{mat}}{\sigma_Y} \geq 6.3\sqrt{mm} \quad \text{(A.2)}$$

This is considered particularly for sensitivity analyses where materials properties are varied.

Figure A.1 **Definitions of loading modes**



Shear loadings and mixed mode loadings tend to produce lower hydrostatic stresses and higher strains near the tip of the flaw than pure mode I loadings ([A.2], [A.3], [A.4], [A.5], [A.6]). A mechanistic understanding of mixed mode loading requires these stress and strain fields to be combined with a detailed knowledge of the failure micromechanism [A.3]. The assessment route in this annex is therefore based upon mode I material property values K_{mat} and σ_Y and mode I failure assessment diagrams. The mode II and mode III contributions are incorporated into the calculation of the applied stress intensity factor, K_{eff}, and the plastic limit load. The justification for this is empirical and discussed in **A.4**.

The procedures are, in principle, those outlined in Clause **7**. However, it is advised that the approach is limited to an initiation analysis only, because of uncertainty and complications about the plane of the growing flaw (see **A.4**). Advice on specific issues is contained in **A.2** to **A.4**.

A.2 Failure assessment diagrams for use in modes I, II and III

Mode I diagrams are generally representative of those derived for mode II and mode III ([A.3], [A.7], [A.8]), although theoretical evidence exists that under some circumstances these diagrams might not be conservative [A.8]. Any differences are similar to those observed between various mode I curves and therefore the curves of Clause **7** are also recommended for use in assessments under mode II and mode III loads. The Option 1 diagram in particular is recommended for use in mixed mode loading assessments.

Under mixed mode loading there is less validation for the failure assessment curves ([A.3], [A.4], [A.9], [A.10]) and therefore these curves are used only in conjunction with a sensitivity analysis.

A.3 Determination of K_r

A.3.1 General

In **6.4**, the applied stresses are resolved into primary and secondary type stresses. Under mode I loading the value of K_r is the sum of two components, K_r^p and K_r^s, corresponding to the primary and secondary stress categories. Under combined mode I, mode II and mode III loading this simple addition is no longer valid and the linear dependence of K_r on applied load is lost.

In view of the problems in the analysis of ductile crack growth under mixed mode loading (see **A.4**), advice is given only for the evaluation of K_r for an initiation analysis. Fatigue crack growth and environmentally assisted cracking are not taken into account.

A.3.2 Linear elastic stress intensity factor

Stress intensity factors may be determined using the general procedures given in Annex M. In the absence of accurate compliance functions for mixed mode loading, mode I values can be used to provide conservative estimates. When dealing with flaws subject to mixed mode loading, either the situation can be analysed directly or the flaw can be projected onto a reference plane (see **6.4.5**). In the latter case, however, unless the principal planes are chosen, shear stresses need to be taken into account in the evaluation of stress intensity factors.

In general the stress intensity factors (SIF) for tensile (mode I), in-plane shear (mode II) and out-of-plane shear (mode III) loadings are required in the calculation of K_r.

These are designated as follows:

- $K_I^p(a)$ and $K_I^s(a)$ – the linear elastic SIFs for the flaw size, a, for loads giving rise, respectively, to primary and secondary stress components which are normal to the plane of the flaw;
- $K_{II}^p(a)$ and $K_{II}^s(a)$ – the linear elastic SIFs for the flaw size, a, for loads giving rise, respectively, to primary and secondary stress components which are in-plane shear;
- $K_{III}^p(a)$ and $K_{III}^s(a)$ – the linear elastic SIFs for the flaw size, a, for loads giving rise, respectively, to primary and secondary stress components which are out-of-plane shear (torsion).

It is also necessary to evaluate the parameter ρ, which takes account of plasticity corrections required to cover interactions between primary and secondary stresses (see **7.3.6**). A method of evaluating ρ is given in **A.3.5**.

A.3.3 The effective stress intensity factor

The flaw size, a, is the size of the original flaw, a_0.

Determine the three SIF components K_I, K_{II}, and K_{III}:

$$K_I = K_I^p + K_I^s \quad (A.3)$$

$$K_{II} = K_{II}^p + K_{II}^s \quad (A.4)$$

$$K_{III} = K_{III}^p + K_{III}^s \quad (A.5)$$

Calculate the effective SIF, K_{eff}.

a) If $\frac{K_{mat}}{\sigma_Y} \geq 6.3\sqrt{mm}$

then K_{eff} is evaluated as follows:

$$K_{eff} = [K_I^2 + K_{II}^2 + \alpha K_{III}^2/(1-\nu)]^{1/2} \quad (A.6)$$

where ν is Poisson's ratio and it is conservative to set α = 1.

b) If $\frac{K_{mat}}{\sigma_Y} < 6.3\sqrt{mm}$

and there are specific material data to justify that $K_{IIc} > K_{mat}$, then Equation (A.6) is used to define K_{eff}. If $K_{IIc} < K_{mat}$, or if there is insufficient evidence to assert otherwise, then K_{eff} is evaluated as follows:

$$K_{eff} = \left[(K_{12})^2 + \alpha K_{III}^2/(1-\nu)\right]^{1/2} \quad (A.7)$$

where:

$$K_{12} = \frac{\left(2K_I + 6\sqrt{K_I^2 + 8K_{II}^2}\right)}{8}\left(\frac{K_I^2 + 12K_{II}^2 + K_I\sqrt{K_I^2 + 8K_{II}^2}}{2K_I^2 + 18K_{II}^2}\right)^{3/2} \text{ for} |K_I/K_{II}| \geq 0.466 \quad (A.8)$$

and:

$$K_{12} = \frac{|K_{II}|}{0.7} \text{ for} |K_I/K_{II}| < 0.466 \quad (A.9)$$

It is conservative to set α = 1.

For metallurgically brittle fracture it is sometimes possible to neglect the contribution of the mode III stresses. In cases where this can be justified from available experimental data, the parameter α should be set to 0 in Equation (A.6) or Equation (A.7) and the justification reported.

A.3.4 Evaluation of K_r for an initiation analysis

Subclause **7.3.6** gives routes for evaluation of K_r for the case of mode I loading, based on calculation of either of two parameters (ρ or V) to account for interaction effects on plasticity.

The approach for treating mixed mode fracture in this annex uses the ρ parameter (a method based on V, if required, is given in R6 [A.1]). Then K_r follows from:

$$K_r = \frac{K_{eff}}{K_{mat}} + \rho \quad (A.10)$$

where ρ is defined in accordance with **A.3.5** at the initial flaw size, a_0, and K_{eff} follows from **A.3.3**.

A.3.5 Determination of ρ

A.3.5.1 In the absence of firm knowledge concerning the interaction of primary and secondary stresses in different modes, the procedure in Annex R is adopted with an effective SIF replacing the mode I SIF (**A.3.5.2** to **A.3.5.4**).

A.3.5.2 For the elastically calculated secondary stresses for the flaw size of interest, define K^{s}_{eff} from Equation (A.6) or Equation (A.7), as appropriate, depending on the values of K_{mat}/σ_Y, K_I/K_{II} and K_{IIc}/K_{mat}, with K_I, K_{II} and K_{III} in Equation (A.6) to Equation (A.9) replaced by K^{s}_{I}, K^{s}_{II} and K^{s}_{III} respectively.

A.3.5.3 For the primary stresses, define K^{p}_{eff} from Equation (A.6) or Equation (A.7) as appropriate, depending on the values of K_{mat}/σ_Y, K_I/K_{II} and K_{IIc}/K_{mat}, with K_I, K_{II} and K_{III} in Equation (A.6) to Equation (A.9) replaced by K^{p}_{I}, K^{p}_{II} and K^{p}_{III} respectively.

A.3.5.4 Evaluate the ratio (K^{p}_{eff}/L_r). For multiple loading systems in which the various primary loads increase independently (non-proportionally), both K^{p}_{eff} and L_r depend on the ratios of the independent loads. Thus, the value of (K^{p}_{eff}/L_r) should be calculated for each load combination of interest when, for example, assessing individual load factors.

A.3.5.5 Evaluate $K^{s}_{eff}/(K^{p}_{eff}/L_r)$ from the results of **A.3.5.2** to **A.3.5.4**.

A.3.5.6 Evaluate ρ in accordance with Annex R, replacing K_I with K_{eff}.

A.3.6 Determination of L_r

The parameter L_r is a measure of how close the structure containing the flaw is to plastic collapse. Applied loads that give rise to primary stresses are used to evaluate L_r (**6.4.2**, **7.3.7**). L_r is defined as the ratio of the loading condition being assessed to the limit load of the structure (**7.3.7**):

$$L_r = \frac{\text{total applied load giving rise to primary stresses}}{\text{limit load of the flawed structure}} = \frac{\text{reference stress}}{\text{yield strength}} \quad \text{(A.11)}$$

For multiple loading systems, $(1/L_r)$ is the factor by which the loads of interest giving rise to primary stresses are increased to attain the limit load of the flawed structure.

The value of σ_Y used in evaluating L_r is obtained from uniaxial tensile data as indicated in **7.1.3**. The von Mises yield criterion should be used to determine the limit load or reference stress for shear or multiaxial stress fields.

The limit load review of Miller [A.11] contains a number of solutions which involve multiaxial and shear loadings. In addition, Ewing [A.12] and Ewing and Swingler [A.13] have presented a number of solutions for extended flaws under mixed mode I/mode II loadings. In other cases, values of L_r may be obtained by following the general methods described in Annex P.

A.4 Further information

There are no universally accepted methods of fracture toughness testing other than those for mode I loading. Testing methods for pure mode II loading ([A.14], [A.15]) and pure mode III loading ([A.16], [A.17]) were proposed in the early 1980s, but interpretation of the resulting load-deflection curves is difficult, and the results can generally be used only to indicate whether or not the toughness is greater than that under mode I loading. More recently, there has been extensive cracked body finite element analyses for particular mixed mode specimen designs in order to develop mixed mode *J*-integral solutions ([A.18], [A.19], [A.20], [A.21], [A.22], [A.23], [A.24]). There is no consensus on the best specimen design or test procedure, and the load and displacement boundary conditions applied to a mixed mode test specimen are more difficult to define or control than the much simpler mode I conditions ([A.22], [A.25]).

Theoretical analysis gives some indication of expected behaviour. For pure mode III loading it is difficult to achieve a brittle fracture, so the expected fracture toughness under these conditions is therefore greater than that under

mode I ([A.3], [A.26]). Under such circumstances it might be possible to neglect the mode III contribution to fracture. However, a conservative approach is adopted in this annex which generally includes the contribution from mode III, unless the user demonstrates by available experimental evidence that such a contribution can be neglected.

Similarly, for brittle fracture under mode II or mixed mode I/mode II the expected toughness is greater than that under mode I, except in circumstances where crack tip plasticity is very small ([A.3], [A.26], [A.27]). The available experimental evidence supports this and suggests that for mode II or mixed mode I/mode II the special circumstances arise only at very low temperatures (−200 °C) for common structural steels, or at ambient temperatures in very high strength/low toughness steels ([A.3], [A.7], [A.24], [A.28]). This annex adopts the use of the mode I toughness for assessment purposes in the brittle fracture region, except for in cases where $K_{mat}/\sigma_Y < 6.3\sqrt{mm}$.

Finite element studies of mixed mode I/mode II loading ([A.5], [A.6]) indicate that the introduction of shear loading causes effects similar to in-plane constraint loss in mode I, namely a reduction in the peak direct and hydrostatic stresses in the vicinity of the flaw tip. This promotes a transition from cleavage fracture near mode I to ductile fracture near mode II ([A.24], [A.27]). Mixedmode assessments performed according to this procedure on steels in the lower transition region might be considerably conservative.

The evidence from mixed mode I/mode II fracture testing of ductile materials is inconclusive. In some cases a mode II initiation toughness and crack growth resistance the same as or higher than the mode I equivalent is reported ([A.15], [A.18], [A.21], [A.29], [A.30], [A.31], [A.32], [A.33], [A.34]), and in others a lower mode II initiation toughness and crack growth resistance is reported ([A.19], [A.20], [A.23], [A.35], [A.36], [A.37], [A.38]). Some of this variability in behaviour might be due to the difficulties inherent in mixed mode fracture testing. Despite this, there is close qualitative agreement between the results of recent studies on structural steels tested using three different specimen designs ([A.19], [A.20], [A.23], [A.37]). All show a steady fall in the ductile crack growth resistance curve as the proportion of mode II loading increases, with the lowest resistance curve obtained for pure or nearly pure mode II loading. This fall in apparent fracture resistance is associated with a change in the mechanism of fracture. Near mode I the flaw blunts symmetrically and crack growth takes place by the classical void coalescence and growth mechanism; whereas near mode II the flaw blunts asymmetrically and crack growth takes place by a shear band mechanism from the sharpened side of the flaw tip. These experimental observations are supported by theoretical modelling using finite element methods [A.6].

The procedure adopted in this annex in Equation (A.6) is based on the use of the mode I fracture toughness in conjunction with a simple sum of the squares of the stress intensity factors ([A.3], [A.9], [A.10]). At first sight this might not appear to be consistent with the experimental results and theoretical modelling cited above. However, tests performed by Swankie [A.23] have been assessed using the methods of this annex [A.25], and they showed that the lower mixed mode and mode II ductile crack growth resistance curves are always associated with specimens tested at loading levels beyond the collapse cut-off, $L_{r,max}$.

This approach is limited to initiation analyses. The analytical and experimental studies of stable crack growth under combined tensile and shear loading are limited and complicated by crack growth often occurring at an angle to the direction of the original flaw. Any analysis involving ductile crack growth under these circumstances therefore requires justification of the resistance curve data adopted. It is not possible at present to recommend general methods, although successful mixed mode tearing analyses have been performed [A.25].

Using the Option 3 curve based on *J*-analysis, the failure assessment curves relevant to pure mode II and pure mode III loading have been obtained and

compared with the mode I curves of Option 1 and Option 2 ([A.7], [A.8]). On this basis the failure assessment curves originally developed for mode I loading are also recommended for other loading modes. However, the analytical evidence, particularly for small flaws, suggests that under some circumstances the mode III curves lie inside the mode I diagram. Sufficient conservatism exists in the procedures to account for these variations, but validation under mixed mode loading is very limited, and therefore a thorough sensitivity analysis is required for these forms of loading.

Bibliography for Annex A

Standards publications

There are no standards references in this annex.

Other documents

[A.1] R6 PANEL. *R6: Assessment of the integrity of structures containing defects. Revision 4, as amended*. Gloucester: EDF Energy, 2001.

[A.2] SHIH, C.F. Small-scale yielding analysis of mixed mode plane-strain crack problems. *In: Fracture Analysis*, ASTM STP 560, 1974, 187–210.

[A.3] BUDDEN, P.J. and JONES, M.R. *Mixed mode fracture*. CEGB Report RD/B/6159/R89, 1989.

[A.4] BUDDEN, P.J. and JONES, M.R. A ductile fracture model in mixed modes 1 and 2. *In: Fatigue and Fracture of Engineering Materials and Structures*, 1991, 14(4), 469–482.

[A.5] DU, Z.Z., BETEGON, C. and HANCOCK, J.W. J dominance in mixed mode loading. *In: International Journal of Fracture*, 1991, 52(3), 191–206.

[A.6] SHERRY, A.H., WILKES, M.A. and AINSWORTH, R.A. Numerical modelling of mixed-mode ductile fracture. *In: Proceedings of ASME Pressure Vessels and Piping Conference*, Seattle, 2000. ASME PVP, 2000, Vol. 412.

[A.7] BRADFORD, R.A.W. *A summary of mode II failure assessment diagrams for carbon-manganese steels*. CEGB Report SWR/SSD/0631/N/85, 1985.

[A.8] BRADFORD, R.A.W. *A discussion of failure assessment diagrams in mode III*. CEGB Memorandum SWR/SSD/S/1536/S/85, 1985.

[A.9] GREEN, G. *Monotonic fracture under mixed mode loading: a review of experimental data and the implications for structural integrity assessment*. CEGB Report SWR/SSD/0632/R/85, 1985.

[A.10] DEAN, D.W. *Analysis of mixed mode fracture data using the CEGB failure assessment procedure*. CEGB Report SER/SSD/86/0018/N, 1986.

[A.11] MILLER, A.G. Review of limit loads of structures containing defects. *In: International Journal of Pressure Vessel and Piping*, 1988, 32(1–4), 197–327.

[A.12] EWING, D.J.F. *Plastic yielding under combined tensile/shear loading*. CEGB Report TPRD/L/2360/N82, 1982.

[A.13] EWING, D.J.F. and SWINGLER, J.N. *Plastic yielding of an edge cracked section in the presence of shear*. CEGB Report TPRD/L/2770/N84, 1985.

[A.14] MILES, L. *Development of a mode II facture toughness testing procedure for an elastic-plastic material*. CEGB Report SSD/SW/R395, 1982.

[A.15] CHANT, M., GREEN, G., WHATMOUGH, I.J. and WILLIAMS, D.C. *The first large shear specimen test*. CEGB Report SWR/SSD/0250/R/83, 1983.

[A.16] TSANGARAKIS, N. Fracture behaviour of 4340 steel under mode III loading. *In: Engineering Fracture Mechanics*, 1979, 16(4), 569.

[A.17] YODA, M. The J-integral fracture criterion under opening and tearing modes and unloading effects. *In: Engineering Fracture Mechanics*, 1979, 13(3), 647–656.

[A.18] TOHGO, K. and ISHII, H. Elastic-plastic fracture toughness test under mixed mode I–II loading, *In: Engineering Fracture Mechanics*, 1992, 41(4), 529–540.

[A.19] LAUKKANEN, A., WALLIN, K. and RINTAMAA, R. Evaluation of the effects of mixed mode I–II loading on elastic-plastic ductile fracture of metallic materials. *In: Mixed-Mode Crack Behaviour*, ASTM STP 1359, 1999.

[A.20] PIRONDI, A. and DALLE DONNE, C. Mixed mode fracture of a ferritic steel: J-integral against CTOD. *In: Proceedings of 5th International Conference on Biaxial/Multiaxial Fatigue and Fracture*, Cracow, Poland, 1997.

[A.21] AOKI, S., KISHIMOTO, K., YOSHIDA, T., SAKATA, M. and RICHARD, H.A. Elastic-plastic fracture of an aluminium alloy under mixed mode loading. *In: Journal of the Mechanics and Physics of Soil*, 1990, 38(2), 195–213.

[A.22] AYATOLLAHI, M.R. *Geometry and constraint effects in mixed mode fracture*, PhD Thesis, University of Bristol, 1998.

[A.23] SWANKIE, T.D. *The role of shear and constraint in mixed mode fracture*, PhD Thesis, University of Bristol, 1999.

[A.24] SWANKIE, T.D. and SMITH, D.J. Low temperature mixed mode fracture of a pressure vessel steel subject to prior loading. *In: Engineering Fracture Mechanics*, 1998, 61(3–4), 387–405.

[A.25] SMITH, M.C. *The application of R6 appendix 7 to mixed mode fracture tests of a pressure vessel steel*, British Energy Generation Report E/REP/GEN/0022/00, 2000.

[A.26] PHILLIPS, J. *The prediction of fracture toughness for a pressure vessel steel under mode 3 loading*. CEGB Report RD/B/5224N81, 1981.

[A.27] AINSWORTH, R.A. and HARRISON, R.P. *Application of the CEGB failure assessment route in the presence of shear loading*, CEGB Report RD/B/5022N81, 1981.

[A.28] SMITH, D.J., AYATOLLAHI, M.R., DAVENPORT, J.C.W. and SWANKIE, T.D. Mixed mode brittle and ductile fracture of a high strength rotor steel at room temperature. *In: International Journal of Fracture*, 1998, 94(3), 235–250.

[A.29] COTTERELL, B., LEE, E. and MAI, Y.M. Mixed mode plane stress ductile fracture. *In: International Journal of Fracture*, 1982, 20(4), 243–250.

[A.30] CHANT, M., GREEN, G. and WILLIAMS, D.C. *The second large shear specimen test*, CEGB Report SWR/SSD/0344/N/83, 1983.

[A.31] SHI Y.W., ZHOU, N.N. and ZHANG, J.X. Comparison of mode I and mode II elastic-plastic fracture toughness for two low alloyed high strength steels. *In: International Journal of Fracture*, 1994, 68(1), 89–97.

[A.32] BANKS-SILLS, L. and SHERMAN, D. JII fracture testing of a plastically deforming material. *In: International Journal of Fracture*, 1991, 50(1), 15–26.

[A.33] YODA, J. The effect of notch root radius on the J-integral fracture toughness under mode I, II, and III loadings. *In: Engineering Fracture Mechanics*, 1987, 26(3), 425–431.

[A.34] JIANGBO, S., JUN, S., PIN, Z., ZENGJIE, D. and HUIJIU, Z. Study on the behavior of elastic-plastic fracture under mixed mode loading in aluminum Ly12 – J-integral analysis. *In: International Journal of Fracture*, 2000, 102(2), 141–154.

[A.35] MACCAGNO, T.M. and KNOTT, J.F. Mixed mode I/II fracture of lightly tempered HY130 steel at room temperature. *In: Engineering Fracture Mechanics*, 1992, 41(6), 805–820.

[A.36] BHATTACHARJEE, D. and KNOTT, J.F. Ductile fracture in HY100 steel under mixed mode I/mode II loading. *In*: *Acta Metallurgica et Materiala*, 1994, 42(5), 1747–1754.

[A.37] DAVENPORT, J.C.W. and SMITH, D.J. Mixed mode ductile tearing in a ferritic steel. *In: International Journal of Fracture*, 1998, 94(3), 235–250.

[A.38] TOHGO, K., OTSUKA, K. and GAO, H.W. Behaviour of ductile crack initiation from a crack under mixed mode loading. *In: Journal of the Society of Materials Science, Japan*, 1990, 39(443), 1089–1094 (in Japanese).

This page deliberately left blank

Annex B (informative)

Assessment procedures for tubular joints in offshore structures

B.0 Symbols and definitions

For the purposes of this annex, the following symbols, definitions and units apply, unless otherwise indicated at the point of use.

Symbol	Definition	Units
A	Constant in fatigue growth relation	see footnote B.1)
A_C	Crack area	mm^2
a	Half flaw length for through-thickness flaw, flaw height for surface flaw or half height for embedded flaw	mm
a_f	Final flaw size	mm
a_i	Initial flaw size	mm
B	Section thickness in plane of flaw	mm
c	Half flaw length for surface or embedded flaw	mm
F_{AR}	Reduction factor to allow for loss of load-bearing area due to presence of a flaw in a tubular joint	—
K_r	Fracture ratio	—
$k_{t.Ax}$	Axial, in- and out-of-plane stress concentration factor in tubular joints	—
$k_{t,HS}$	Hot-spot stress concentration factor in tubular joint	—
$k_{t.IPB}$	In-plane stress concentration factor in tubular joints	—
$k_{t.OPB}$	Out-of-plane stress concentration factor in tubular joints	—
L_r	Ratio of applied load to yield load	—
l_w	Length of weld	mm
M_{ai}	Applied in-plane moments for tubular joints	Nmm
M_{ao}	Applied out-of-plane moment for tubular joints	Nmm
M_{ci}, M_{co}	Fully plastic moments for cracked tubular joints calculated for in- and out-of-plane loads	Nmm
m	Exponent in flaw growth law	—
m_q	Exponent in the calculation of F_{AR}	—
N	Number of cycles	—
P_a	Applied axial load on tubular joint	N
P_c	Collapse load for cracked tubular joint	N

B.1) The units and value of A depend on those used to measure da/dN and ΔK, and on the value of the exponent, m. If A is known in one set of units, A_a, the corresponding value for another set of units, A_b, is given by:

$$A_b = A_a \frac{f_a}{f_b{}^m}$$

where:

f_a is the conversion factor for da/dN from the first to the second unit system; and

f_b is the conversion factor for ΔK from the first to the second unit system.

(continued)

Symbol	Definition	Units
P_L	Limit load	N
Q_β	Factor to allow for increased strength observed in tubular joints at $\beta > 0.6$	—
Y	Ratio of chord radius to chord wall thickness in a tubular joint	—
Y_m, Y_b	Stress intensity correction factors for membrane and bending stress	—
$Y_{w,m}$, $Y_{w,b}$	Stress intensity correction factors for weld location for membrane and bending stress	—
β	Ratio of brace diameter to chord diameter in a tubular joint	—
ΔK	Stress intensity factor range	$N/mm^{3/2}$
ΔK_b	Bending stress intensity factor range	$N/mm^{3/2}$
ΔK_m	Membrane stress intensity factor range	$N/mm^{3/2}$
$\Delta\sigma_{Ax}$	Axial stress range in tubular joint	N/mm^2
$\Delta\sigma_{HS}$	Hot-spot stress range	N/mm^2
$\Delta\sigma_{HS.Ax}$	Axial, in- and out-of-plane hot-spot stress ranges in tubular joint	N/mm^2
$\Delta\sigma_{HS.IPB}$	Hot-spot axial, in-plane stress range in tubular joint	N/mm^2
$\Delta\sigma_{HS.OPB}$	Hot-spot axial, out-of-plane stress range in tubular joint	N/mm^2
$\Delta\sigma_{HS.Tot}$	Total hot-spot stress range in tubular joints	N/mm^2
$\Delta\sigma_{IPB}$	In-plane bending stress range in tubular joint	N/mm^2
$\Delta\sigma_b$	Bending component of stress range	N/mm^2
$\Delta\sigma_m$	Membrane component of stress range	N/mm^2
$\Delta\sigma_{nom}$	Nominal stress range in tubular joint	N/mm^2
$\Delta\sigma_{nom.Ax}$	Axial, in- and out-of-plane nominal stress ranges in tubular joint	N/mm^2
$\Delta\sigma_{nom.IPB}$	Nominal axial, in-plane stress range in tubular joint	N/mm^2
$\Delta\sigma_{nom.OPB}$	Nominal axial, out-of-plane stress range in tubular joint	N/mm^2
$\Delta\sigma_{OPB}$	Out-of-plane bending stress range in tubular joint	N/mm^2
σ_b	Bending hot-spot stress component for the uncracked joint	N/mm^2
σ_{bc}	Bending hot-spot stress component for the cracked joint	N/mm^2
σ_f	Flow strength (assumed to be the average of the yield and the tensile strengths)	N/mm^2
σ_{ref}	Reference stress used for creep and plastic consideration; it is sometimes calculated from plane strain von Mises limit load as in Annex N	N/mm^2
σ_Y	Lower yield strength or 0.2% proof strength	N/mm^2
Ω	Degree of bending in tubular joints	—
Ω_{Ax}	Axial degree of bending in tubular joints	—
Ω_{IPB}	In-plane degree of bending in tubular joints	—
Ω_{OPB}	Out-of-plane degree of bending in tubular joints	—
Ω_{Tot}	Total degree of bending in tubular joints	—

B.1 Overview

B.1.1 Introduction

This annex presents guidance on specific procedures for the assessment of flaws in offshore structures. The assessment of fatigue crack growth and fracture in tubular joints requires specialist guidance due to the complexity of the joint geometry and the applied loading, and this annex provides supplementary guidance on the application of the procedures described in Clause **7** and Clause **8** to tubular joints. Its scope is limited to the assessment of known or assumed weld toe flaws, including fatigue cracks found in service, in brace or chord members of T, DT, X, Y, K, KT or multi planar joints between circular section tubes under axial and/or bending loads. The annex describes one specific analysis route. Others are possible, in general accordance with this British Standard.

B.1.2 General procedure

The basic components of the fatigue crack growth procedure, outlined in Figure B.1, and the fracture assessment procedure for tubular joints are as follows.

a) Global structural analysis: determination of components of brace nominal stress corresponding to fatigue and storm loads generated by wave loading.

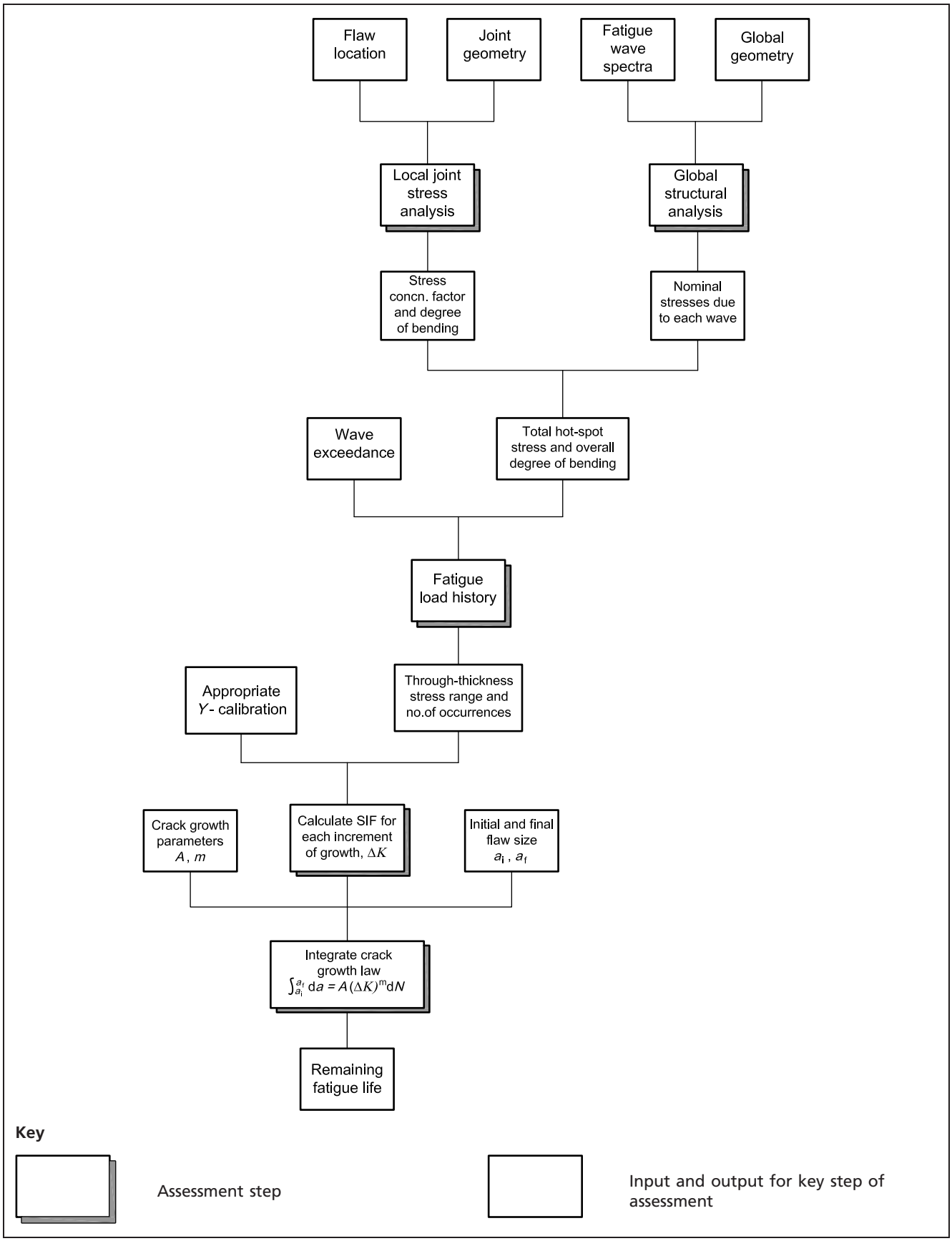
b) Local joint stress analysis: determination of the hot-spot stress concentration factors and the degree of bending, Ω, i.e. the proportion of the bending to total stress through the wall thickness, relevant to the crack location.

c) Determination of stress spectrum: generation of the hot-spot stress range histogram for the joint (see **8.2.1.5**).

d) Fatigue crack growth analysis: integration of the appropriate fatigue crack growth law (see **8.1.2**) to determine the remaining fatigue life.

e) Fracture analysis: determination of K_r and L_r after each increment of crack growth, use of failure assessment diagrams (FADs).

Figure B.1 **Assessment method for fatigue crack growth in tubular joints**



B.2 Stress analysis

B.2.1 General

Results of structural analysis of the overall frame under the chosen critical loading conditions should be available to give the forces and moments in the members in the region being assessed. These should be provided as axial force, in-plane and out-of-plane bending moments. Both maximum load and fatigue load ranges are required.

B.2.2 Global structural analysis

A global finite element analysis of the complete structure is performed to determine the stress spectrum corresponding to the wave loading at the flaw location. The wave exceedance curve is used to construct a histogram of wave height versus the number of occurrences. The stress range due to each wave height is then determined in the global structural analysis. The latter gives the nominal brace loading due to the action of the fatigue and storm wave loading. From this the axial, in-plane bending and out-of-plane bending brace stress ranges ($\Delta\sigma_{Ax}$, $\Delta\sigma_{IPB}$ and $\Delta\sigma_{OPB}$ respectively) are computed for each wave height.

Further details are given in BS EN ISO 19902, Health and Safety Executive [B.1], American Petroleum Institute Recommended Practice API RP 2A [B.2], Graff [B.3] and Barltrop and Adams [B.4].

B.2.3 Local joint stress analysis

The local joint stress ranges are generated by the nominal brace axial and bending loads, which are reacted by the chord. High secondary bending stresses are developed due to the local deformation of the tubular walls. This leads to high stress concentrations and through-thickness stress gradients at the brace/chord intersection. The variation of stress range around the joint periphery needs to be determined and stress range histograms are evaluated for a minimum of eight equally spaced positions, including the saddle and crown locations.

Each hot-spot stress range component is determined from the nominal stress range, $\Delta\sigma_{nom}$, and the appropriate stress concentration factor ([B.1], [B.5]), i.e.:

$$\Delta\sigma_{HS} = \Delta\sigma_{nom} k_{t,HS} \tag{B.1}$$

The hot-spot stress range component is subdivided into axial and bending components, thus:

$$\Delta\sigma_{m} = (1 - \Omega)\Delta\sigma_{HS} \tag{B.2}$$

$$\Delta\sigma_{b} = \Omega\Delta\sigma_{HS} \tag{B.3}$$

The local stress field can be based on published parametric equations for $k_{t,HS}$ and Ω [B.6]. Alternatively, more accurate predictions can be obtained by performing a finite element analysis.

The nominal stresses obtained from the global analysis and the stress field parameters at the crack location, $k_{t,HS}$ and Ω, obtained from the local joint stress analysis are used to calculate the total hot-spot stress and total degree of bending for each wave:

$$\begin{aligned}\Delta\sigma_{HS.Tot} &= \Delta\sigma_{HS.Ax} + \Delta\sigma_{HS.IPB} + \Delta\sigma_{HS.OPB} \\ &= \Delta\sigma_{nom.Ax} k_{t.Ax} + \Delta\sigma_{nom.IPB} k_{t.IPB} + \Delta\sigma_{nom.OPB} k_{t.OPB}\end{aligned} \tag{B.4}$$

The degree of bending for the total hot-spot stress range is determined from the following expression:

$$\Omega_{Tot} = \frac{\Omega_{Ax}\Delta\sigma_{HS.Ax} + \Omega_{IPB}\Delta\sigma_{HS.IPB} + \Omega_{OPB}\Delta\sigma_{HS.OPB}}{\Delta\sigma_{HS.Tot}} \tag{B.5}$$

B.3 Stress intensity factor solutions

B.3.1 Evaluation methods

The principal methods used to determine stress intensity factors for tubular joints are the following:

a) numerical (i.e. finite element or boundary element) analysis of tubular joints;

b) standard and analytical (e.g. weight function) solutions for semi-elliptical cracks in plates.

B.3.2 Numerical solutions for tubular joints

Numerical methods provide the most realistic predictions of stress intensity factors. However, the determination of stress intensity factors for cracks in tubular joints by numerical methods requires complex modelling and stress analysis, and consequently only a limited number of solutions are available ([B.7], [B.8], [B.9], [B.10]).

B.3.3 Plate solutions

The application of plate solutions to the assessment of tubular joints provides stress intensity factors for a very wide range of geometries. Stress intensity factors for the deepest and the surface points can be determined using the Newman and Raju ([B.11], [B.12], [B.13]) solution in conjunction with magnification factors determined either by 2-D finite element analysis (see **M.5**) or by the weight function solution for surface cracks [B.14]. The use of the 2-D magnification factor solutions tends to be conservative, particularly for the evaluation of the stress intensity factor at the surface point. The weight function solutions might be more appropriate for the surface point, though validation of these solutions is limited.

If allowance is made for load shedding resulting from the reduction of member stiffness with crack growth, more realistic estimates of the stress intensity factor in a tubular joint can be obtained from plate solutions (but see Note). The moment release model proposed by Aaghaakouchak et al. [B.15] can be used in conjunction with plate solutions to reduce the excessive conservatism inherent in the application of stress intensity factor solutions of plate joints to tubular joints. The moment release model assumes that load shedding reduces the net moment acting across the cross-section of a cracked tubular member, and hence also reduces the stress intensity factor. The linear moment release model involves the reduction of the bending stress components using the following simple expression:

$$\sigma_{bc} = \sigma_b\left(1 - \frac{a}{B}\right) \tag{B.6}$$

NOTE Limited studies have indicated that in some cases application of Equation (B.6) might lead to an underestimate of K up to 30% [B.16] and [B.17].

B.4 Fatigue assessment

B.4.1 Stress range

The variation of damage at the joint periphery should be determined and the stress range histogram corresponding to the maximum damage in the region corresponding to the crack location selected. The stress range histogram is then applied on a block by block basis.

B.4.2 Stress intensity factor range

The stress intensity factor range is calculated from the following general expression:

$$\begin{aligned}\Delta K &= \Delta K_{\mathrm{m}} + \Delta K_{\mathrm{b}} \\ &= [Y_{\mathrm{w,m}}(1 - \Omega_{\mathrm{Tot}}) + Y_{\mathrm{w,b}}\Omega_{\mathrm{Tot}}]\Delta\sigma_{\mathrm{HS}}\sqrt{\pi a}\end{aligned} \quad \text{(B.7)}$$

If the plate stress intensity factor solution is used, Equation (B.7) can be expressed as follows:

$$\Delta K = [M_{\mathrm{km}}Y_{\mathrm{m}}(1 - \Omega_{\mathrm{Tot}}) + M_{\mathrm{kb}}Y_{\mathrm{b}}\Omega_{\mathrm{Tot}}]\Delta\sigma_{\mathrm{HS}}\sqrt{\pi a} \quad \text{(B.8)}$$

B.4.3 Initial flaw dimensions

The methods given in this standard can be used to assess the integrity of a structure containing an initial hypothetical flaw. The initial flaw size should not be underestimated. The size of this assumed flaw should be the estimated maximum size, taking into account the reliability of the chosen inspection method(s) (see Annex T) and of the welding procedure applied.

B.4.4 Limit to fatigue crack propagation

For cracking in the chord, failure is generally considered to occur when the crack penetrates the wall thickness, though the possibility of brittle fracture or plastic collapse should be taken into account for cracks in the weld region. For cracking in the brace, the same considerations apply, although the final failure mode is more likely to be associated with the weldment, so the toughness of the weldment should be taken into account.

B.5 Fracture assessment

B.5.1 General

Tubular joints can be assessed using the general procedure described in **7.3**, with the modifications presented below. The fracture assessment procedure for offshore structures involves the modification of the Option 2 FAD. All loading effects should be determined in the first instance for best estimates of the maximum loading, excluding load factors prescribed by limit state design codes. Where a probabilistic assessment is required, estimates of the variability and distributions of the loading and other input parameters are necessary.

B.5.2 Primary stresses

For the selected wave, the maximum applied nominal forces and moments in the joint containing the flaw need to be determined. The maximum applied nominal forces and moments are then converted into maximum applied axial, in-plane and out-of-plane nominal stresses from which the local joint stresses are determined, as described in **B.1**.

B.5.3 Residual stresses

General guidance on the treatment of residual stresses is given in **7.1.8**. This is supplemented by recommendations on residual stress distributions in Annex Q.

B.5.4 Determination of K_{r}

The fracture parameter, K_{r}, is determined using the procedure in **7.3.6**.

B.5.5 Collapse parameter, L_r

B.5.5.1 General

General guidance and recommendations on the prediction of plastic collapse are given in Annex P. The collapse parameter, L_r, for tubular joints may be calculated using either local or global collapse analyses [B.10]. The local collapse approach is usually very conservative, whereas the use of the global approach tends to give more realistic predictions of plastic collapse in tubular joints. Further information is given in ISO 19902.

B.5.5.2 Local collapse analysis for part-thickness flaws in circumferential butt welds

For the deepest point of part-thickness flaws in circumferential butt welds, the standard solution in Annex P should be used to calculate the reference stress, σ_{ref}, across the remaining ligament, using as the effective width the length of the joint subjected to tensile stresses.

For the surface point at the ends of surface-breaking flaws in circumferential butt welds, the standard solutions in Annex P should be used to calculate the reference stress, σ_{ref}, for a through-thickness flaw having a length equal to the surface length of the part thickness flaw, $2c$. The effective width should be taken as the length of the joint subject to tensile stresses.

B.5.5.3 Global collapse analysis

B.5.5.3.1 For circumferential butt welds or tubular nodal joints containing a flaw in the brace, lower bound collapse loads should be calculated separately for axial loading, in-plane bending and out-of-plane bending for the overall cross-section of the member containing the flaw based on net area and yield strength. The net area for axial loading should be taken as the full area of the cross-section of the joint minus the area of rectangle containing the flaw. The collapse load, P_L, is the load to raise the average stress on the net area to the yield strength. The fully plastic moment of the cross-section of the joint should be calculated for in-plane or out-of-plane loads, allowing for the cross-sectional area of the rectangle containing the flaw. The net fully plastic moments, M_{ci} and M_{co}, based on the yield strength, are the collapse moments.

B.5.5.3.2 For tubular nodal joints containing a part-thickness or through-thickness flaw in the chord, parametric equations for the design strength of the uncracked geometry are available; see BS EN ISO 19902, Health and Safety Executive (HSE) [B.1] and American Petroleum Institute (API) [B.2]. The lower bound characteristic ultimate strength for the geometry concerned should be calculated using the equations for the uncracked geometry from the above references, together with the specified minimum yield strength. The ultimate strengths for axial, in-plane and out-of-plane bending loads should be calculated separately.

B.5.5.3.3 For T-joints subjected to compression or tension loading, the ultimate strength should be calculated from the HSE characteristic strength or API RP 2A [B.2] formulae for the relevant loading mode. For K-joints, the HSE characteristic strength or API RP 2A compression strength should be used, even when the flaw is located in the tension brace/chord joint.

B.5.5.3.4 The plastic collapse loads for the cracked geometry are determined by reducing the plastic collapse loads for the corresponding uncracked geometry on the basis of the net load-bearing area for axial loading and the effect of the flaw area on the plastic collapse modulus for bending loads. The correction factor for axial loading is given [B.18] by the equation:

$$F_{AR} = \left(1 - \frac{A_c}{Bl_w}\right)\left(\frac{1}{Q_\beta}\right)^{m_q} \quad \text{(B.9)}$$

B.5.5.3.5 For tubular joints containing through-thickness flaws, validation of Equation (B.9) is at present limited to joints with β ratios less than 0.8 and the following configurations:

a) K-joint with a through-thickness crack at the crown subjected to balanced axial loading;

b) tension axially loaded T and DT joint with a through-thickness crack at the saddle.

For K-joints, use either of the following:

1) the HSE characteristic compression design strength with $m_q = 1$; or

2) the API RP 2A compression design strength with $m_q = 0$.

For T and DT joints, use either of the following:

i) the HSE characteristic tension design strength with $m_q = 1$; or

ii) the API RP 2A tension design strength with $m_q = 0$.

B.5.5.3.6 For tubular nodal joints containing a part thickness or through-thickness flaw in the chord, the parameter L_r is calculated from the following:

$$L_r = \left(\frac{\sigma_f}{\sigma_Y}\right)\left[\left|\frac{P_a}{P_c}\right| + \left(\frac{M_{ai}}{M_{ci}}\right)^2 + \left|\frac{M_{ao}}{M_{co}}\right|\right] \quad \text{(B.10)}$$

The vertical lines in $\left|\frac{P_a}{P_c}\right|$ and $\left|\frac{M_{ao}}{M_{co}}\right|$ mean the absolute values (moduli) of these ratios.

P_c, M_{ci} and M_{co} are plastic collapse loads in the cracked condition for axial loading, in-plane bending and out-of-plane bending respectively. For example, P_c is equal to F_{AR} times the plastic collapse load in the uncracked condition for axial loading.

B.5.5.3.7 If conservative assumptions lead to a global collapse value of L_r being higher than the local collapse value of L_r, the local value may be used.

B.5.6 Flaw assessment

As an initial assessment, the coordinates relating to the deepest point and surface point positions should be plotted on the FAD. If the points lie within the locus, the flaw may be deemed acceptable. If any of the points lie on or outside the locus, the flaw is unacceptable.

If all points lie within the FAD, the coordinates should be re-evaluated using the partial safety factors appropriate to the required level of reliability. If all the reassessed points lie within the locus, the flaw is acceptable for the level of the reliability selected. If any of the points lie on or outside the locus, the flaw is unacceptable for the level of reliability selected.

Bibliography for Annex B

Standards publications

For dated references, only the edition cited applies. For undated references, the latest edition of the referenced document (including any amendments) applies.

ISO 19902, *Petroleum and natural gas industries – Fixed steel offshore structures*

Other documents

[B.1] HEALTH AND SAFETY EXECUTIVE. *Offshore installations: guidance on design, construction and certification*. Fourth ed. London: Health and Safety Executive, 1990 (superseded by OTO/015 (2001). <http://www.hse.gov.uk/research/otohtm/2001/oto01015.htm>

[B.2] AMERICAN PETROLEUM INSTITUTE. *Recommended practice for planning, designing and constructing fixed offshore platforms – Working stress design*. API RP 2A-WSD. 21st ed. Washington: API, 2000.

[B.3] GRAFF, W.J. *Introduction to offshore structures: Design, fabrication, installation*. Houston: Gulf Publishing Company, 1981. ISBN 0872016943.

[B.4] BARLTROP, N.D.P. and ADAMS, A.J. *Dynamics of fixed marine structures*. 3rd ed. MTD Publication 91/102. London: Marine Technology Directorate/ Butterworth-Heinemann, 1991. ISBN 0750610468.

[B.5] EFTHYMIOU, M. Development of SCF formulae and generalized influence functions for use in fatigue analysis. *In: CIRIA and J.G. WYLDE, eds. Recent developments in offshore tubular joints technology (OTJ '88). In: Proceedings of Offshore Tubular Joint Conference, Eaglefield Green, Surrey, UK, Oct. 1988*. London: CIRIA, Underwater Engineering Group, 1988.

[B.6] CONNOLLY, M.P., HELLIER, A.K., DOVER, W.D. and SUTOMO, J. A parametric study of the ratio of bending to membrane stress in tubular Y and T joints. *In: International Journal of Fatigue*, 1990, 12(1), 3–11.

[B.7] HASWELL, J.V. A general fracture mechanics model for a cracked tubular joint derived from the results of a finite element parametric study. *In: BARBAS, S.T. et al., eds. Proceedings of 11th International Conference on Offshore Mechanics and Arctic Engineering, (OMAE '92), Calgary, Canada, 7-12 June 1992*. Vol. III-B, Materials Engineering. New York: ASME, 1992, 267–274. ISBN 0791809129.

[B.8] RHEE, H.C., HAN, S., and GIBSON, G.S. Reliability of solution method and empirical formulas of stress intensity factors for weld toe cracks of tubular joints. *In: SALAMA, M.M. et al., eds. Proceedings of 10th Conference on Offshore Mechanics and Arctic Engineering (OMAE '91), Stavanger, Norway, 23-28 June 1991*. Vol. III-B, Materials Engineering. New York: ASME, 1991, 441–452. ISBN 0791807207.

[B.9] HO, C.M. and ZWERNEMAN, F.J. *Assessment of simplified methods – Report on joint industry project fracture mechanics investigation of tubular joints, Phase two*. Stillwater, OK: Oklahoma State University, 1995.

[B.10] BURDEKIN, F.M. and COWLING, M.J. *Defect assessment in offshore structures, a procedure*. Aberdeen: CMPT Publications, 1998. ISBN 1 870533 330.

[B.11] NEWMAN, J.C. and RAJU, I.S. Stress intensity factor equation for cracks in three-dimensional finite bodies. *In: Fracture Mechanics: Proceedings of 14th Symposium. Vol. I: Theory and Analysis*. STP 791. Philadelphia: ASTM, 1983: 238–265.

[B.12] RAJU, I.S. and NEWMAN, J.C. Stress intensity factors for a wide range of semi-elliptical surface cracks in finite thickness plates. *In: Engineering Fracture Mechanics*, 1979, 11(4), 817–829. ISSN 0013-7944.

[B.13] NEWMAN, J.C. and RAJU, I.S. An empirical stress intensity factor equation for the surface crack. *In: Engineering Fracture Mechanics*, 1981, 1–2(15), 185–192.

[B.14] SHEN, G. and GLINKA, G. Weight functions for a surface semi-elliptical crack in a finite thickness plate. *In: Theoretical and Applied Fracture Mechanics*, 1991,15(3), 247–255.

[B.15] AAGHAAKOUCHAK, A., GLINKA, G., and DHARMAVASAN, S.A. A load shedding model for fracture mechanics analysis of fatigue cracks in tubular joints. *In: Proceedings of OMAE 1989: 8th Conference on Offshore Mechanics and Arctic Engineering*, The Hague, The Netherlands, 19–23 March 1989. Vol. III: Materials Technology. New York: ASME, 1989.

[B.16] CHEAITANI, M.J. and BOLT, H.M. Evaluation of stress intensity factor solutions for offshore tubular joints. In: SALAMA, M.M. et al., eds. *In: Proceedings of 15th Conference on Offshore Mechanics and Arctic Engineering (OMAE '96)*, Florence, Italy, 16–20 June 1996. New York: ASME, 1996, Vol. 3, 521–532. ISBN 0791814920.

[B.17] MADDOX, S.J. Fatigue crack growth in tubular T-joints under in-plane bending. *In:* FARKAS and JARMAI, eds. *Tubular Structures VII: Miskolc, Hungary, 28-30 August, 1996*. Rotterdam: A.A. Balkema, 1996. ISBN 9054108282.

[B.18] CHEAITANI, M.J. and BURDEKIN, F.M. Ultimate strength of cracked tubular joints. In: GRUNDY, P., HOLGATE, A. and WONG, B. eds. *In: Tubular structures VI: Proceedings of 6th International Symposium, Melbourne, 14–16 Dec, 1994*. Rotterdam/Brookfield: A.A. Balkema, 1994, 607–616. ISBN 9054105208.

This page deliberately left blank

Annex C (informative)

Assessment procedures for pressure vessels and pipelines

C.0 Symbols and definitions

There are no symbols and definitions in this annex.

C.1 General

The background to this annex (in relation to pipelines) is given in reference [C.1].

Advice is given in this annex on how this British Standard should be applied to pressure vessels and pipelines as part of a fitness-for-service assessment. Many types of engineering plant can be classified as pressure vessels. These range from very thick-walled reactor vessels to thin-walled storage vessels. Transmission pipelines transport gases and liquids at high pressures and can be subjected to a variety of loads ranging from internal pressure to external ground loading. Rather than giving industry prescriptive guidelines, this annex gives guidance on the type of input data that are required and issues to be considered in the context of the integrity management plan. Annex G gives guidance on the thinning of pressure vessels and pipelines, due to, for example, corrosion.

Assessing fitness-for-service requires more than a consideration of the significance of the flaw. It is also necessary to consider the previous history of the structure in order to establish the cause of the flaw. Information about the behaviour of similar structures or flaws, if available, is valuable, as this can indicate whether the structure has a poor or good safety record.

Service-induced flaws in pressure vessels and pipelines usually take the form of corrosion, structural damage, for example a dent or a gouge, fatigue, or environmentally induced cracks.

Cracks, particularly surface breaking cracks, should be viewed with caution. They should be assessed in accordance with the procedures given in Clause **7** to Clause **9**, as appropriate.

Because of these variables, prescriptive guidelines are not presented in this annex. However, the following procedure should be followed when reviewing a pressure vessel or a pipeline.

- Establish the cause and nature of the damage/flaw.
- Establish the quality and properties of the associated material.
- Identify and calculate all stresses acting on the damaged or flawed region.
- Establish the size of the flaw or damage zone, and quantify any associated tolerances and reliabilities.
- Identify all possible failure modes, and consider the consequences of the release of the contents from the pressure vessel or pipeline.

C.2 Guidance for pressure vessels

C.2.1 General

The type of engineering critical assessment (ECA) required is dependent on the flaw in question. Most pressure vessel flaws are associated with welds. However, gouges in parent material, flaws resulting in a loss of wall thickness in the pressure vessel material and flaws in weldments may be assessed using this standard. Gouges and flaws within dents require special consideration due to the geometric stress concentration of the dent and to its potential instability (popping out). If these effects can be quantified, the techniques described in this

standard may be applied. Otherwise, specialist methods detailed in the literature should be used, e.g. Cosham et al. [C.2].

The fitness-for-service assessment requires three inputs: the flaw size, the stress field in which the flaw is located, and the materials properties relevant to the particular failure mode(s) being considered, e.g. mechanical properties, fracture toughness, fatigue crack growth properties. In some assessments, testing, stress analysis, further inspection or metallurgical work might be required to generate suitable data. Obtaining all relevant data can be difficult, particularly values of toughness for older or second-hand equipment.

The fitness-for-service assessment should take into account all possible failure modes (creep, buckling, etc.) and the effect of environment (e.g. stress corrosion) and duty (e.g. fatigue) to which the pressure vessel is subjected.

C.2.2 Toughness data

In a very limited number of cases, operators obtain representative fracture toughness data at the construction stage. Charpy impact data might be available from the original construction records, in which case the correlations given in Annex J may be used. Alternatively, cut-out material may be used or a conservative lower bound established from the literature for similar steel and weldments adopted.

C.2.3 Flaw size data

Flaw size data are obtained by NDT. It is essential that the operator and organization inspecting the vessel are thoroughly qualified and experienced to a specified level. All NDT should be conducted in accordance with recognized and appropriate standards. These standards (and any deviation) should be specified in the ECA. Guidance on the use of NDT with ECA is given in Annex T.

Ultrasonics is the major inspection method used in measuring flaw sizes for fitness-for-service assessments. This is because the flaw height (through-thickness) is the critical dimension in an assessment, with flaw length being of secondary importance. Ultrasonic inspections are prone to inaccuracies and unreliability. An ultrasonic inspection can reliably detect a weld flaw, but sizing can be subject to inaccuracy. Therefore, safety factors or allowance for errors should be applied to flaw sizes reported by ultrasonics.

C.2.4 Flaw type

C.2.4.1 Orientation

The possible extension of a crack-like flaw should be assessed by application of the total stress tending to open the crack, i.e. the stress perpendicular to the crack plane. The angle between the crack plane and the principal stress direction should be established and the projected length of the flaw in the principal stress direction should be used as the length for calculating purposes (see **6.4.5**).

C.2.4.2 Multiple flaws

Flaws classified as multiple, intermittent flaws should be assessed in accordance with **7.1.2**.

C.2.4.3 Visible cracks

Cracks can be indicative of poor design features, workmanship or inspection, or stress corrosion, fatigue or corrosion fatigue, and therefore the cause should be ascertained before proceeding with an assessment. In older vessels, surface cracks can be caused by plate laminations appearing after being opened up by the tension resulting from welds cooling down. Such cases require further

investigation of the vessel parent plate in that area in order to establish the true nature of the problem.

Some cracks can be shown to be original fabrication flaws using methods such as metallographic replicas or boat samples (shallow removal of the crack and neighbouring material). All cracks should be thoroughly investigated and their cause established before an assessment is conducted. Where the cause is poor design or excessive loading, a flaw assessment might not be appropriate; repair and redesign might be required.

C.2.4.4 Flaws removed by grinding

Any reductions in wall thickness should be assessed.

Surface breaking flaws are commonly ground out. This grinding serves the dual purpose of accurately sizing the flaw and removing it. However, the grinding groove is itself a flaw and should be assessed accordingly. Grind repairs in vessels require detailed assessment of the stress acting on the grind, particularly at stiffened regions in the vessel, which can be associated with welds and act as stress raisers.

Grind-outs are associated with large geometric discontinuities, such as saddles, and can be extensive. Grind-outs can have a significant effect on the stress levels around the discontinuity, in which case a full structural analysis might be necessary to establish realistic stress values in such areas, especially if new flaws appear adjacent to previous grind-outs.

The procedures adopted for the analysis of grind-outs caused by removal of flaws are outside the procedures given in the pressure vessel and piping codes and need individual treatment.

However, if the grind-out is smooth and free from surface breaking flaws, it may be treated as follows. For static failure (provided that there is no risk of failure by brittle fracture and that the sole potential final failure mode is plastic collapse), treat as a reduction in cross-sectional area (see Annex G). For fatigue, give consideration to the stress concentration arising as a result of the grind-out profile.

C.2.4.5 Repairs

Flaws associated with poor repairs often result in failures. Any weld repair or grind repair should be designed such that it does not crack or deteriorate during service. A repair weld or grind repair that contains cracks is unsatisfactory and indicates both poor design and unsatisfactory repair procedures. In these situations, there should be a complete reappraisal of the repaired region. Redesign of the problem area and an alternative, improved repair method could be necessary.

C.2.5 Stress analysis

In many cases, stress analysis is relatively simple, but more difficult cases arise, particularly with flaws associated with branch or fillet weld connections. Flaws in these locations are subject to stress concentrations. For the stress analysis of flaws at nozzles, the stress concentration factors given in PD 5500 and Annex G may be used for guidance. Where standard solutions are not available, numerical analysis might be required.

C.3 Guidance for oil and gas transmission pipelines

Oil and gas transmission pipelines can contain flaws in the parent material or in the weldments. These flaws can occur during fabrication or construction, or in service by mechanical damage, corrosion, etc. The significance of these flaws

may be assessed using appropriate fitness-for-service methods, including the methods in this document.

The assessment should take into account all the stresses that can act on a pipeline. These include static and cyclic stresses for internal pressure, external forces [due to work on the pipeline, ground movement, free spanning (offshore lines), etc.], construction stresses, thermal stresses, etc.

The assessment should confirm that all pipeline parent materials have adequate ductility to prevent brittle fracture initiation. Additionally, gas pipelines should be designed to avoid fracture propagation. This is generally achieved by specifying pipe body Charpy V-notch and drop-weight tear test (DWTT) requirements [C.3], which also prevent brittle fracture initiation.

The significance of flaws in the parent pipe material may be assessed using one of the following methods:

a) the methods detailed in this document;

b) another recognized standard, e.g. ASME B31G or DNVGL-RP-F101 [C.4];

c) specialist methods, e.g. Kiefner et al. [C.5] or Polasik et al. [C.6].

Gouges, flaws resulting in a loss of wall thickness in the pipe material, and flaws in weldments may be assessed using this document. Gouges and flaws within dents require special consideration due to the geometric stress concentration of the dent and to its potential instability (popping out). If these effects can be quantified, the techniques described in this guide may be applied. Otherwise, specialist methods detailed in the literature should be used, e.g. Cosham et al. [C.2]. Flaws in pipeline girth welds can be assessed using this standard, or specialist methods detailed in the literature, e.g. Andrews et al. [C.7].

Transmission pipelines are increasingly being inspected using in-line inspection tools. Some of these tools can detect and size flaws in a pipeline. Any assessment of a pipeline flaw which has been detected and sized by an in-line inspection tool should take into account the capability, reliability and accuracy of the tool's inspection technology. Additionally, the assessment should take into account any potential further growth of the flaw following the inspection.

Bibliography for Annex C

Standards publications

For dated references, only the edition cited applies. For undated references, the latest edition of the referenced document (including any amendments) applies.

ASME B31G, *Manual for determining the remaining strength of corroded pipelines*

PD 5500, *Specification for unfired fusion welded pressure vessels*

Other documents

[C.1] ANDREWS, R., COSHAM, A. and MACDONALD, K. Application of BS 7910 to high pressure pipelines. *In: International Journal of Pressure Vessels and Piping*, December 2018, 168, 148–155. <https://doi.org/10.1016/j.ijpvp.2018.09.008>

[C.2] COSHAM, A., HOPKINS, P., CURSON, N., CHUNG, A., TURNER, S. and LOCKEY, A. PDAM 2. *In: Technology for Future and Ageing Pipelines Conference*. Gent, Belgium, 11–12 April 2018. Gent, Belgium: The Lab. Soete, University of Gent & Eastleigh, UK: Tiratsoo Technical.

[C.3] COSHAM, A., ANDREWS, R.M. and SCHMIDT, T. The EPRG Recommendations for crack arrest toughness for line pipe steel (3rd ed.). *In: Proceedings of the 12th International Pipeline Conference, IPC 2018*, Paper No.: IPC 2018-78043, Calgary, Alberta, Canada, 24–28 September, 2018.

[C.4] DNV GL. *Corroded pipelines*. DNVGL-RP-F101. Norway: DNV GL, 2019.

[C.5] KIEFNER, J.F., MAXEY W.A., EIBER, R.J. and DUFFY, A.R. Failure stress levels of flaws in pressurized cylinders. *In: Proceedings of Progress in Flaw Growth and Toughness Testing*, Philadelphia, 28–30 August. ASTM STP 536, 1973, 461–481.

[C.6] POLASIK, S.J., JASKE, C.E. and BUBENIK, T.A. Review of engineering fracture mechanics model for pipeline applications. Paper No. IPC2016-64450. *In: Proceedings of the 2016 11th International Pipeline Conference*. IPC2016. Calgary, Alberta, Canada, 26–30 September 2016. New York, USA: American Society of Mechanical Engineers.

[C.7] ANDREWS, R.M., DENYS, R.M., KNAUF, G. and ZAREA, M. EPRG guidelines on the assessment of defects in transmission pipeline girth welds – Revision 2014. *In: The Journal of Pipeline Engineering*, 2015, 14(1), 9–21.

This page deliberately left blank

Annex D (informative)

Stress due to misalignment

D.0 Symbols and definitions

For the purposes of this annex, the following symbols, definitions and units apply, unless otherwise indicated at the point of use.

Symbol	Definition	Units
B	Section thickness in plane of flaw	mm
B_1, B_2	Thickness of plates in calculating bending stress due to misalignment in butt joints	mm
D	Mean diameter	mm
D_{max}, D_{min}	Maximum and minimum diameters in a vessel or pipe	mm
d	Deviation from true circle due to angular misalignment	mm
E	Elastic modulus	N/mm^2
e	Axial misalignment (eccentricity or centre line mismatch)	mm
h	Weld leg length	mm
k_m	Stress magnification factor due to misalignment	—
l	Distance from axially misaligned joint to load or extremities of region of angular misalignment (shortest distance = l_1)	mm
l_1, l_2	Plate length	mm
n	Factor used in calculating bending stress due to axial misalignment between flat plates of different thickness	—
P_m	Primary membrane stress	N/mm^2
p_m	Maximum pressure in calculation of misalignment in pressurized pipe	N/mm^2
y	Height of peaking due to angular misalignment	mm
α	Angular change at misaligned joint	Radians
β	Factor used in calculating bending stress due to angular misalignment in butt joints	—
ΔP_m	Primary membrane stress range	N/mm^2
$\Delta\sigma_s$	Bending stress range due to misalignment	N/mm^2
θ	Angle between the weld seam and the point at which the maximum diameter is observed	°
κ	Restraint parameter for butt joints or cruciform joints	—
ν	Poisson's ratio	—
$\sigma_{max,m}$	Membrane component of the maximum applied tensile stress	N/mm^2
σ_s	Maximum induced bending stress due to misalignment, which has the same sign as P_m (i.e. σ_s/P_m is positive)	N/mm^2
σ_W	Applied stress on weld throat	N/mm^2

D.1 Calculation of stress magnification factor

The presence of misalignment, axial (eccentricity) or angular, or both, at a welded joint can cause an increase or decrease in stress at the joint when it is loaded, due to the introduction of local bending stresses ([D.1] to [D.5]). These influence both stress intensity factors (Annex M) and reference stresses (Annex P) (see **6.4.4**). It is conservative to treat stresses due to misalignment as primary, although in some cases they act as secondary, i.e. in terms of the FAD they affect the calculation of K_r, but not L_r [D.6]. This applies to both butt and fillet welded joints, but only under loading which results in membrane stresses transverse to the line of misalignment. Bending stresses do not occur as a result of misalignment in continuous welds loaded longitudinally or at joints in plates subjected only to bending. However, misaligned joints in sections (e.g. beams, tubes) subjected to overall bending experience combined membrane and bending stresses, and additional bending stresses can arise due to the membrane stress component.

If more than one type of misalignment exists, the total induced bending stress is the sum of the bending stresses due to each type. Both tensile (positive) and compressive (negative) stresses arise as a result of misalignment, depending on the surface or through-thickness position being considered. Account should be taken of the relevant sign when calculating the net effect of combined misalignments (combined axial and angular misalignment might act together, e.g. both tensile, or in opposition) and when calculating the total stress due to applied and induced stresses.

The bending stress due to misalignment depends not only on its type and extent, but also on factors that influence the ability of the welded joint to rotate under the induced bending moment. These factors include loading and boundary conditions, section shape and the presence of other members which provide local stiffening. Special analysis (e.g. finite element stress analysis) is usually required to quantify their effects. Unless it can be demonstrated that restraint on the joint reduces the influence of misalignment, the induced bending stress should be calculated assuming no restraint.

Formulae for calculating the bending stress, σ_s, as a function of applied membrane stress, P_m, for a number of cases of misalignment are given in Table D.1 and Table D.2 (from references [D.1] to [D.5]). For joints that experience combined membrane and bending stresses, the formulae are used in conjunction with the membrane stress component only. Apart from the weld root in a cruciform fillet weld, all the formulae give σ_s at the weld toe.

Where the bending stress is affected by the loading due to the joint rotating under load or a circular section re-rounding under internal pressure, these formulae assume that the deviation from the ideal shape is measured at zero applied load. If the deviation is measured under load, it might be necessary to correct for any change in shape to obtain the deviation at zero load for use in the formulae. An example where such shape changes can be significant is in-line inspection of a thin-walled pressurized pipe [item g) of Table D.1] using a high-resolution geometry pig.

If the stress is required at a different position through the thickness, for example when assessing buried flaws, the bending stress due to misalignment can be assumed to vary linearly through the material thickness to zero at its neutral axis.

 © The British Standards Institution 2019

It is sometimes convenient (see **8.8.1**) to express the effect of misalignment in terms of the maximum factor by which the applied stress (P_m) or stress range (ΔP_m) is magnified as a result of its presence. This magnification factor, k_m, is defined as:

$$k_m = \frac{P_m + \sigma_s}{P_m} = 1 + \frac{\sigma_s}{P_m} \quad \text{(D.1)}$$

$$k_m = \frac{\Delta P_m + \Delta\sigma_s}{\Delta P_m} = 1 + \frac{\Delta\sigma_s}{\Delta P_m} \quad \text{(D.2)}$$

For combined misalignments (e.g. axial and angular):

$$k_m = 1 + (k_m - 1)_{axial} + (k_m - 1)_{angular} \quad \text{(D.3)}$$

The guidance given in this annex might be unduly conservative if applied to through-thickness flaws. This is because the presence of such flaws reduces local bending stresses resulting from misalignment. The magnitude of local bending due to misalignment decreases with increasing crack length for through-thickness flaws.

Table D.1 **Formulae for calculating the bending stress due to misalignment in butt joints**

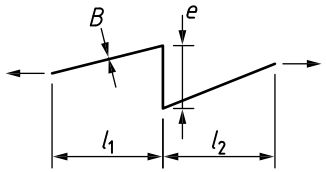
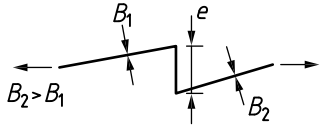
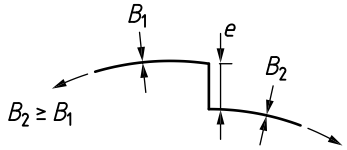
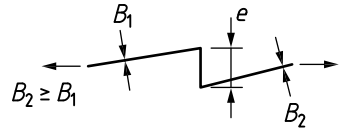
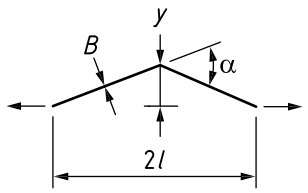
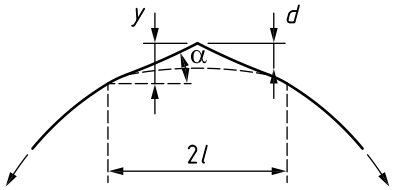
Type	Detail	Bending stress σ_s	Remarks
a) Axial misalignment between flat plates		$\frac{\sigma_s}{P_m} = \kappa\left[\frac{el_1}{B(l_1+l_2)}\right]$ where κ is a factor dependent on restraint	κ = 6 for unrestrained joint For remotely loaded joints assume $l_1 = l_2$
b) Axial misalignment between flat plates of different thickness		$\frac{\sigma_s}{P_m} = \frac{6e}{B_1}\left(\frac{B_1^n}{B_1^n + B_2^n}\right)$	Relates to remotely loaded, unrestrained joints. Use of n = 1.5 is supported by tests.
c) Axial misalignment at longitudinal seam welds in tubes, pipes and vessels, with or without thickness change		$\frac{\sigma_s}{P_m} = \frac{6e}{B_1(1-\nu^2)}\left[\frac{1}{1+(B_2/B_1)^{0.6}}\right]$	—
d) Axial misalignment at girth welds in tubes, pipes, vessels and at seams in spheres, with or without thickness changes		If $\sigma_s/P_m < 1$: $\frac{\sigma_s}{P_m} = \frac{6e}{B_1(1-\nu^2)}\left[\frac{1}{1+(B_2/B_1)^{1.5}}\right]$ If $\sigma_s/P_m \geq 1$: $\frac{\sigma_s}{P_m} = \frac{2.6e}{B_1}\left[\frac{1}{1+0.7(B_2/B_1)^{1.4}}\right]$ (Connelly and Zettlemoyer [D.7])	—

Table D.1 **Formulae for calculating the bending stress due to misalignment in butt joints** *(continued)*

Type	Detail	Bending stress σ_s	Remarks
e) Angular misalignment between flat plates	 α in radians	Assuming boundary conditions equivalent to fixed ends: $\frac{\sigma_s}{P_m} = \frac{3y}{B}\left[\frac{\tanh(\beta/2)}{\beta/2}\right]$ $= \frac{3a}{4}\frac{2l}{B}\left[\frac{\tanh(\beta/2)}{\beta/2}\right]$ pinned ends: $\frac{\sigma_s}{P_m} = \frac{6y}{B}\left[\frac{\tanh(\beta)}{\beta}\right]$ $= \frac{3a}{2}\frac{2l}{B}\left[\frac{\tanh(\beta)}{\beta}\right]$ where, in each case: $\beta = \frac{2l}{B}\left(\frac{3\sigma_{max,m}}{E}\right)^{0.5}$	The tanh correction (in square brackets) allows for reduction in angular misalignment due to straightening of joint under tensile loading. It is always ≤1 and therefore it is usually conservative to ignore it. The exception is if, when combined with axial misalignment, the angular component has the effect of reducing the overall stress. Its effect is negligible for $2l/B < 10$ and it is independent of the assumed end fixing condition for $2l/B > 100$. Note, for compressive loading, without any lateral restraint, the "tanh" term becomes a "tan" term and it is no longer conservative to ignore it.
f) Angular misalignment at longitudinal or circumferential seams in tubes or vessels		Assuming boundary conditions equivalent to fixed ends: $\frac{\sigma_s}{P_m} = \frac{3d}{B(1-\nu^2)}\left[\frac{\tanh(\beta/2)}{\beta/2}\right]$ pinned ends: $\frac{\sigma_s}{P_m} = \frac{6d}{B(1-\nu^2)}\left[\frac{\tanh(\beta)}{\beta}\right]$ where, in each case: $\beta = \frac{2l}{B}\left[\frac{3(1-\nu^2)\sigma_{max,m}}{E}\right]^{0.5}$	Assuming an idealized geometry: $d = \frac{y}{2}$ or $\frac{\alpha l}{2}$

© The British Standards Institution 2019

Table D.1 **Formulae for calculating the bending stress due to misalignment in butt joints** *(continued)*

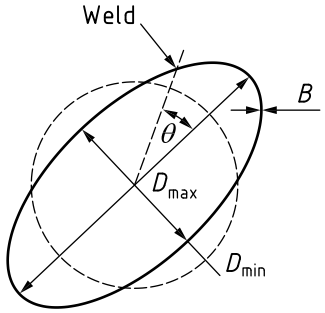
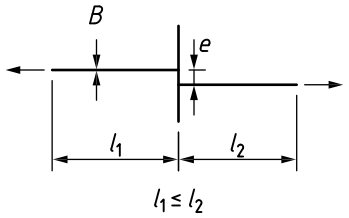
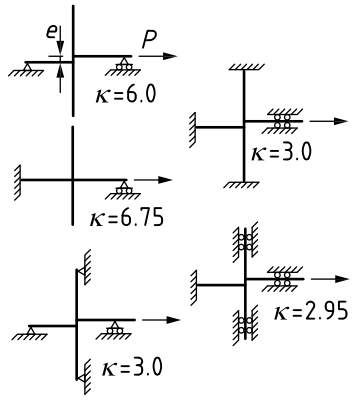
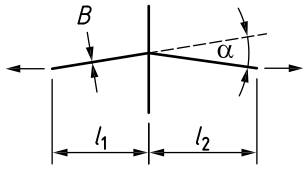
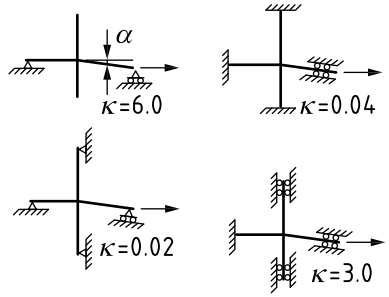
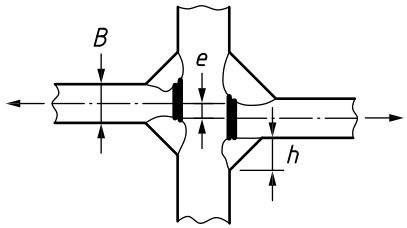
Type	Detail	Bending stress σ_s	Remarks
g) Ovality in pressurized pipes or vessels	 θ in degrees	$\frac{\sigma_s}{P_m} = \frac{1.5(D_{max} - D_{min}) \cos 2\theta}{B\left\{1 + 0.5\left[\frac{p_m(1-\nu^2)}{E}\right]\left(\frac{D}{B}\right)^3\right\}}$	Formula takes account of exact location of weld seam and beneficial change in shape of vessel due to pressurization. If, under fatigue loading, p_m varies, use the mean value during the time interval considered. A conservative estimate of σ_s is: $\frac{\sigma_s}{P_m} = \frac{1.5(D_{max} - D_{min})}{B}$

Table D.2 **Formulae for calculating the bending stress due to misalignment in cruciform joints**

Type	Detail	Bending stress σ_s	Remarks
a) Axial misalignment in butt or fillet welded joints		$\frac{\sigma_s}{P_m} = \frac{\kappa e l_1}{B(l_1 + l_2)}$ where κ is a factor dependent on restraint, e.g. 	Refers to fatigue failure in plate from toe weld. For unrestrained, remotely loaded joint, assume κ = 6 and l_1 = l_2
b) Angular misalignment in butt or fillet welded joints		$\frac{\sigma_s}{P_m} = \frac{\kappa a l_1 l_2}{B(l_1 + l_2)}$ where κ is a factor dependent on restraint, e.g. 	Refers to fatigue failure in plate from toe weld.

© The British Standards Institution 2019

Table D.2 **Formulae for calculating the bending stress due to misalignment in cruciform joints** *(continued)*

Type	Detail	Bending stress σ_s	Remarks
c) Axial misalignment in fillet welded joints		$\frac{\sigma_s}{\sigma_w} = \frac{e}{B+h}$	Refers to fatigue failure in plate from weld throat from root. This case is not for use in the calculation of the stress intensity factor for a weld root flaw in **M.11**.

Bibliography for Annex D

Standards publications

There are no standards references in this annex.

Other documents

[D.1] MADDOX, S.J. *Fitness for purpose assessment of misalignment in transverse butt welds subject to fatigue loading*. IIW document XIII-1180-85. London: International Institute of Welding, 1985.

[D.2] ANDREWS, R.M. The effect of misalignment on the fatigue strength of welded cruciform joints. *In: Fatigue and Fracture of Engineering Materials and Structures*. 1996, 19(6), 755–768. ISSN 8756-758X.

[D.3] BERGE, S. and MYHRE, H. Fatigue strength of misaligned cruciform and butt joints *In: Norwegian maritime research*. 1977, 5(1), 29–39. ISSN 0304-1743.

[D.4] JAMES, D.P., EDWARDS, D.C. and CHRISTIAN, J.R. Fatigue considerations in the design of pipelines. *In: Improving Welded Product Design*. 1971, London: The Welding Institute, 62–72.

[D.5] HAIGH, B.P. An estimate of the bending stresses Induced by pressure in a tube that is not initially quite circular. Appendix IX to the Second Report to the Welding Research Committee. *In: Proceedings of the Institution of Mechanical Engineers*, 1936, 133, 96–98.

[D.6] CHEAITANI, M.J. Axial misalignment in FAD-based fracture assessment of circumferential girth weld flaws. TWI Industrial Member Report 999/2011. Cambridge: TWI, 2011.

[D.7] CONNELLY, L.M. and ZETTLEMOYER, N. Stress concentration of girth welds of tubulars with axial wall misalignment. *In: Tubular Structures. Proceedings of the Fifth International Symposium, Nottingham, United Kingdom, 25–27 August 1993*. London: Spon Press, 1993. ISBN 0419187707.

This page deliberately left blank

Annex E (informative)

Flaw recharacterization

E.0 Symbols and definitions

For the purposes of this annex, the following symbols, definitions and units apply, unless otherwise indicated at the point of use.

Symbol	Definition	Units
a	Flaw height for surface flaw or half height for embedded flaw	mm
B	Section thickness in plane of flaw	mm
c	Half flaw length for surface or embedded flaw	mm
p	Shortest distance from surface to embedded flaw	mm

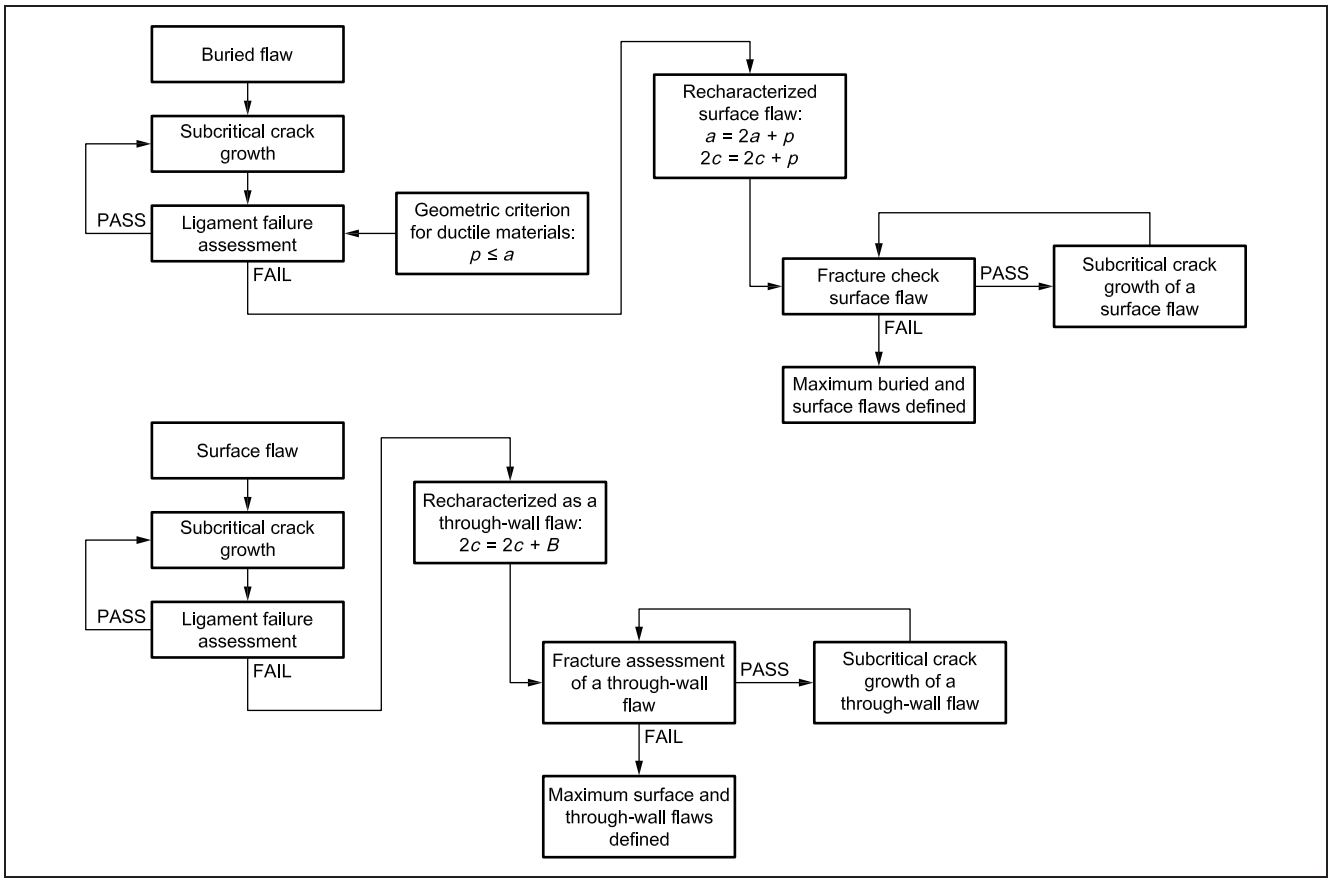
E.1 General

The background to this annex is given in reference [E.1].

When an embedded or a surface flaw is assessed as unacceptable in accordance with Clause **7**, the prediction of failure of a ligament is not always critical to the overall integrity of the structure or component. In such cases, a further assessment step may be carried out, in which the ligament concerned is assumed not to be present and the initial embedded or surface flaw is recharacterized as a surface or through-thickness flaw, respectively, as appropriate. The process is illustrated in Figure E.1. The resulting flaw might require an allowance to be made for dynamic conditions and for possible crack growth at the ends.

The guidance given in this annex is applicable to sub-critical crack growth (such as by fatigue) and ductile mechanisms of crack growth. Under conditions of unstable brittle crack growth (such as for materials on the lower shelf or the transition region), there are typically no benefits of invoking the flaw recharacterization process and it is generally not recommended.

Figure E.1 **Flowchart for recharacterization of flaws**



E.2 Procedure

The transitioning of a buried flaw to a surface flaw under ductile failure mode should be based on the ligament failure of a buried flaw assessed in accordance with Clause **7**, Annex M and Annex P, with the static initiation fracture toughness in accordance with Clause **7**.

The transitioning of a surface flaw to a through-wall flaw under a ductile failure mode should be based on the assessment of the uncracked ligament (i.e. the ligament ahead of the deepest point on the flaw front) in accordance with Clause **7**, Annex M and Annex P, with the static initiation fracture toughness in accordance with Clause **7**.

NOTE Recent studies ([E.1], [E.2]) suggest that the geometry-based criterion of $p = a$ may be conservatively used for ductile materials.

The transitioning of a buried flaw to a surface flaw under fatigue dominant sub-critical crack growth is governed by the stability of the ligament under maximum fatigue or transient loads. The guidance set out above should be used to assess the transitioning of a buried flaw under fatigue conditions.

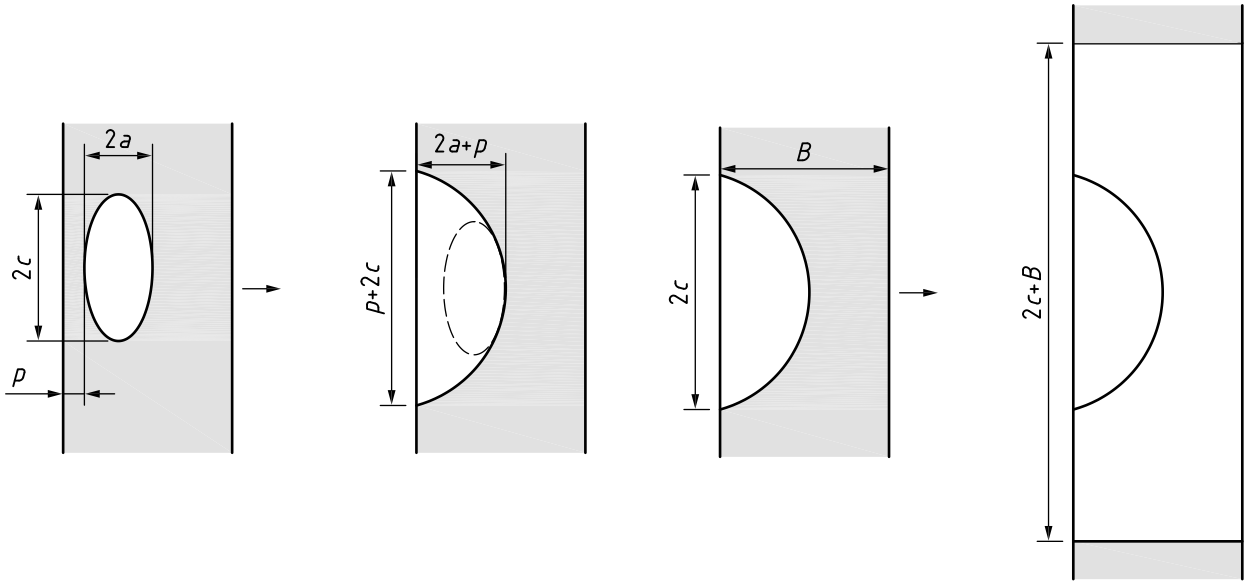
The size of the recharacterized surface flaw should allow for possible crack growth at the ends during ligament breakthrough. The size of the recharacterized flaw is calculated by increasing the total length of the original flaw, as shown in Figure E.2, as follows:

- surface flaw length: $2c + p$;
- surface flaw height: $2a + p$;
- through-wall flaw length: $2c + B$.

When ligament failure is dominated by fatigue crack growth, the recharacterized surface flaw (or through-wall flaw) should be increased in accordance with Figure E.2 for the subsequent fatigue crack growth calculations of the recharacterized flaw. The recharacterized flaw may be assessed in accordance with Clause **7**.

This annex is beneficial to the assessment only if local conditions in the ligament are more severe than those of the recharacterized flaw. If the recharacterized flaw fails the assessment, the initial flaw is not acceptable.

Figure E.2 **Rules for recharacterization of flaws**



a) Embedded flaws b) Surface flaws

Bibliography for Annex E

Standards publications

There are no standards references in this annex.

Other documents

[E.1] BEZENSEK, B., COULES, H., SHARPLES, J. and TKACH, Y. Proposed updates to the buried-to-surface flaw recharacterization rules in Annex E of BS 7910. *In: Proceedings of the ASME 2019 38th International Conference on Ocean, Offshore and Arctic Engineering*, OMAE2019, June 9–14, 2019, Glasgow, Scotland, OMAE2019-96327.

[E.2] DNVGL-RP-F108. *Assessment of flaws in pipeline and riser girth welds, recommended practice*. DNV GL AS, 2019. <https://www.dnvgl.com/oilgas/download/dnvgl-rp-f108-assessment-of-flaws-in-pipeline-and-riser-girth-welds.html>

This page deliberately left blank

Annex F (informative)

Procedure for leak-before-break (LbB) assessment

F.0 Symbols and definitions

For the purposes of this annex, the following symbols, definitions and units apply, unless otherwise indicated at the point of use.

Symbol	Definition	Units
A	Crack opening area (COA) in a LbB assessment [see Equation (F.1)]	mm^2
A_{ex}	Exit COA	mm^2
A_i	COA corresponding to the location at which $L = 12D_i$	mm^2
A_o	Entrance COA	mm^2
a	Half flaw length for through-thickness flaw, flaw height for surface flaw or half height for embedded flaw	mm
B	Section thickness in plane of flaw	mm
C_D, C_D^{I}, C_D^{II}, C_D^{III}	Discharge coefficients	—
C_v	Loss coefficient for bends and protrusions over the flaw flow path length [see Equation (F.23)]	—
C_1, C_2	Constants used in calculating in conventional friction factor	—
c	Flaw half-length in leak-before-break (LbB) assessment (see Figure F.1)	mm
c_L	Half-length of through-wall defect at limit of leak detection or half-length of detectable through wall-defect in a LbB assessment	mm
$c_L^{'}$	Enhanced value of c_L in a LbB assessment	mm
c_c	Limiting generalized flaw half-length in a LbB assessment	mm
D	Flaw height or wall thickness at flaw position [see Equation (F.12)]	mm
D_i	Hydraulic parameter of the flaw	mm
d	Ligament thickness B-a or flaw divergence parameter	mm
E'	Elastic modulus corrected for constraint conditions $E' = E$ for plane stress, $E' = E/(1 - \nu^2)$ for plane strain	N/mm^2
F, F_1, F_2	Friction loss coefficient used in determining discharge coefficients in a LbB assessment [see Equation (F.12) to Equation (F.13e)]	—
f	Fanning friction factor	—
f_{conv}	Conventional friction factor	—
f_{max}	Maximum effective friction factor, f	—
$\bar{G}$	Average flow rate per unit area in the flaw	tonne/mm^2/s
$\bar{G}T$	Average mass flux in the dispersed two-phase region ($L/D_i > 12$) of the flaw	tonne/mm^2/s
G_c	Mass flow rate per unit area at the choking (flaw exit) plane	tonne/mm^2/s
G_o	Mass flow rate per unit area at the flaw entrance plane	tonne/mm^2/s
k	Parameter used in calculating discharge coefficient	—

(continued)

Symbol	Definition	Units
L	Average of the front and back surface flaw lengths	mm
N	Ramp function in a LbB assessment [see Equation (F.14)]	—
P_m	Membrane stress	N/mm^2
p	Pressure	N/mm^2
p_a	Pressure loss due to acceleration arising from phase change [see Equation (F.21)]	N/mm^2
p_{aa}	Pressure loss due to acceleration arising from changes in area	N/mm^2
p_c	Critical pressure, i.e. pressure at the choking plane	N/mm^2
p_e	Entrance pressure loss	N/mm^2
p_{ex}	Pressure of fluid at the exit	N/mm^2
p_f	Frictional pressure loss	N/mm^2
p_k	Pressure loss due to bends and protrusions	N/mm^2
p_0	Pressure of fluid at the flaw entrance	N/mm^2
Q	Mass flow through an equivalent rectangular flaw of mean width W and length L	tonne/s F.1)
R	Mean radius	mm
R_a	Surface roughness of flaw	mm
r_m	Mean radius	mm
S	Ratio P_m/σ_f	—
S_{Lc}	Liquid entropy at choking plane	Nmm/°C/ tonne
S_{gc}	Gas entropy at choking plane	Nmm/°C/ tonne
S_o	Stagnation entropy	N/mm^2
W	Mean flaw width	mm
W_{ex}	Exit flaw width	mm
W_0	Entry flaw width	mm
$\bar{X}$	Average mixture quality in the flaw	—
X_E	Equilibrium mixture quality, i.e. volume fraction of vapour	—
X_c	Non-equilibrium mixture quality	—
$\alpha(\lambda)$	Bulging factor	—
γ_0	Isentropic exponent	—
δ	Crack tip opening displacement (CTOD) or crack opening displacement (COD)	mm
θ	Flaw half-angle	°
λ	Parameter used in LbB assessment	—
ν	Poisson's ratio	—
$\bar{v}_L$	Average specific volume of the vapour in the flaw	mm^3/ tonne
v_{Lc}	Specific volume (1/density) of liquid at the choking plane	mm^3/ tonne

F.1) The units for Q may be kg/s or g/s, but it is essential that they are consistent with those used for ρ_f. In order for fluid parameters to be consistent with units in this annex, Q should be in tonne/s and ρ_f should be tonne/m^3.

(continued)

Symbol	Definition	Units
v_{Lo}	Specific volume of liquid at the flaw entrance plane	mm^3/ tonne
$\bar{v}_g$	Average specific volume of the liquid in the flaw	mm^3/ tonne
v_{gc}	Specific volume (1/density) of vapour at the choking plane	mm^3/ tonne
ρ_0	Density of fluid at the flaw entrance	kg/mm^3 or g/mm^3
σ_f	Flow strength	N/mm^2
$\Omega(G_c, p_c)$	Pressure constraint equation, Equation (F.15)	N/mm^2

F.1 General

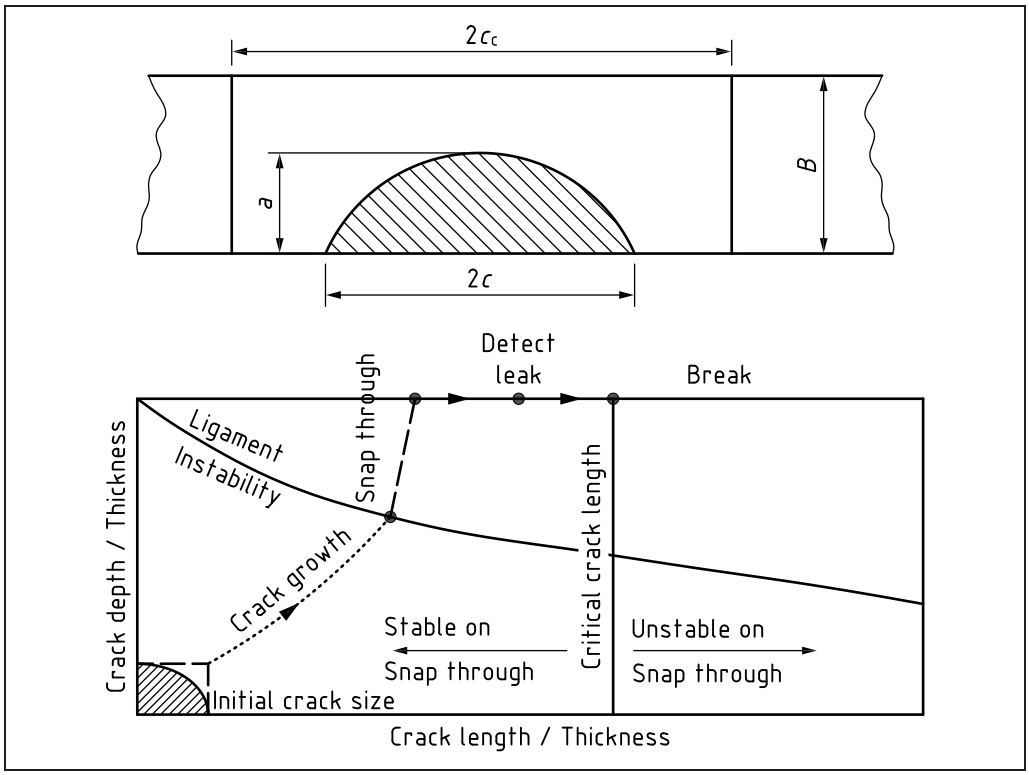
This annex is based on the detectable leakage approach given in Chapter III.11 of R6 [F.1], with minor modifications.

Clause **7** gives several options by which it might be possible to demonstrate the safety of a structure containing flaws when an initial assessment has failed to show that adequate margins exist. For pressurized components, one of these options is to make a leak-before-break (LbB) case by demonstrating that a flaw is likely to grow in such a way as to cause, in the first instance, a stable detectable leak of the pressure boundary rather than a sudden, disruptive break. It is, however, important to be aware that LbB is usually considered in safety justifications as part of a defence in depth argument as opposed to the main safety argument.

The concept of LbB can be explained with the aid of the diagram shown in Figure F.1 (from reference [F.2]). This diagram has axes of flaw height, *a*, and length, *2c*, normalized by the wall thickness, *B*. An initial part-through flaw on the front surface of the component is represented by a point on the diagram.

A flaw grows by fatigue, tearing, creep or other process until it reaches some critical height at which the remaining ligament ahead of the flaw breaks through the wall at the back surface. The flaw then continues growing in surface length until there is sufficient opening to cause a detectable leak or until it becomes unstable. A LbB argument demonstrates that leakage of fluid through a flaw in the wall of a pipe or vessel would be detected prior to the flaw attaining conditions of instability at which rapid flaw extension occurs.

Figure F.1 **The leak-before-break diagram**



This annex sets out a procedure, based on a simplified detectable leakage approach, for making a LbB argument and recommends methods for carrying out each of the steps in the procedure.

This procedure is based on evaluating the size of flaw whereby leakage can be detected and comparing this with the size of the limiting flaw.

The procedure should be strictly adhered to when developing LbB arguments. LbB should not be justified merely in a qualitative way, by arguing that, for example, "a piping system is of a ductile material and therefore any leakage from a through-wall flaw is bound to be detected prior to it growing to a critical size".

There are more rigorous and complex approaches, like the one detailed in R6 [F.1], whereby the starting point is the consideration of the growth of an initially part-penetrating flaw.

F.2 Procedure

F.2.1 General aspects

In the procedure set out in **F.2.2**, the crack opening area, the rate at which fluid leaks from the flaw and the limiting flaw length need to be evaluated.

Additional calculations should be carried out to assess the sensitivity of the results to likely variations in the input data. Guidance on this and on other aspects of the analysis is given in R6 [F.1].

Methods other than this procedure may be used if they can be justified and appropriate validation exists.

In contrast to the procedures of Clause **7**, which are concerned with failure avoidance, part of the LbB case involves failure prediction. Conservative values should be used to calculate the critical length of the through-wall flaw, in accordance with the procedures of Clause **7**. For the purpose of the LbB procedure, the critical length is therefore synonymous with, and should be taken

 © The British Standards Institution 2019

to be equal to, the limiting length. The term "limiting length" is therefore used in this annex.

LbB assessments for a pressure boundary should be conducted for locations judged to be most at risk. Some guidance on the selection of assessment sites is given in Table F.1. It might be necessary to examine several locations to demonstrate that the worst case has been found. Any postulated flaws should be orientated in the most onerous direction to ensure that they experience the highest stresses and worst materials properties at that location.

A LbB case might not be tenable in plant that is prone to damage mechanisms which can lead to very long surface flaws. Also, the risk of transient water hammer loading in piping containing high-energy fluid can preclude LbB arguments unless the peak loads can be adequately assessed and then considered in the evaluation of the limiting flaw size. Where there is significant risk of damage to piping due to impacts (e.g. missiles or dropped loads), other whipping pipes or from equipment failure, such considerations should override any LbB case.

Table F.1 **Guidance on selection of assessment sites around a pipe system**

Consideration	Influence on LbB arguments
Pipe size	For given operating conditions and operating stresses, leak rates are less for smaller pipes than for larger pipes.
Stresses	For a given geometry, material and temperature, LbB margins tend to reduce as stress levels increase.
Components (elbows, tees, valves, etc.)	Likely to have complex stress fields which complicate LbB arguments and geometric stress raisers which can promote in-service degradation.
Welds and castings	Defects are more likely to occur in these features than in straight forged pipe made to modern standards.
Materials properties	Low yield stress, low fracture toughness and poor creep ductility make it more difficult to demonstrate a LbB case.
Susceptibility to degradation	Locations should be ranked against mechanisms such as fatigue, continuum damage, ageing, etc. Other mechanisms such as SCC, erosion, corrosion, etc. might preclude a LbB case.
Leak detection	The detection system used might have to change for different potential flaw locations and leak rates.
Consequences	Acceptability of guillotine failure might determine which locations should be assessed.
Inspection	History or feasibility of future inspections might be a crucial factor in choosing locations for assessment.

F.2.2 Details of procedure

F.2.2.1 General

The starting point is to postulate a through-wall flaw and show that, if it arose in practice, fluid leakage would occur and be detectable before the flaw had grown to the limiting length. For this approach to be valid, there should be a mechanism for developing such localized cracking and no risk of the formation of long surface flaws.

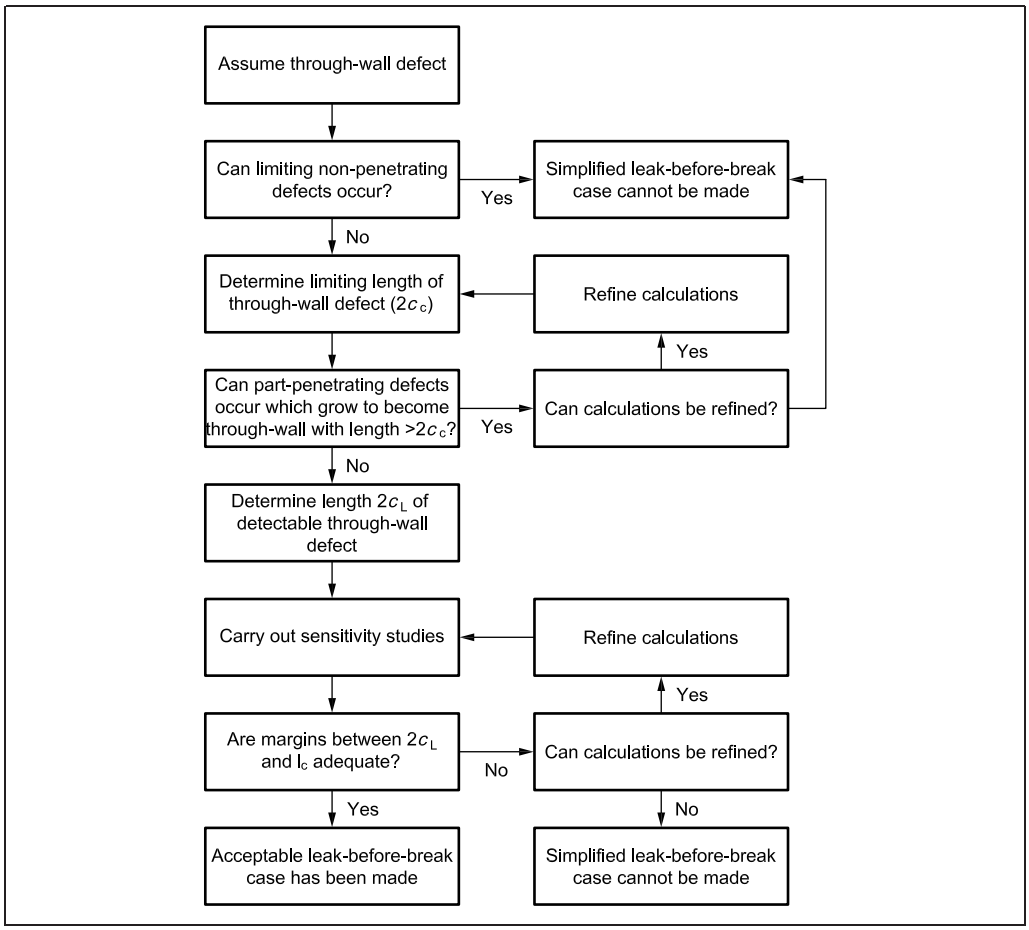
"Detectable leakage" arguments, like those used in the procedure outlined here (see Figure F.2), are increasingly being used for LbB assessments. An example is the procedure for light water reactor (LWR) pipework published by the US Nuclear Regulatory Commission in NUREG 1061 Volume 3 [F.3]. That procedure is intended for the assessment of LWR piping under extreme seismic loading; it recommends specific safety margins, defines the loads to be assessed excluding

residual and through-wall thermal stresses, and allows extended ductile flaw extension. In line with most other clauses and annexes in this British Standard, this annex does not provide guidance on margins.

A detectable leakage analysis is usually carried out in design or safety studies, where through-wall flaws are postulated in welds and other features. The flaw is generally assumed to be parallel-sided. However, care should be taken when using this strategy. The appropriate mechanisms of localized degradation should exist for the development of a detectable through-wall flaw and a long surface flaw should not arise which would lead to gross failure of the pressure boundary. For flaws in the vicinity of welds, the role of weld materials properties and welding residual stresses, in particular, should be taken into account as these influence flaw propagation, COA and limiting flaw length.

A sensitivity analysis should be carried out to determine the extent to which changes in the input data affect the results of the calculations.

Figure F.2 **Flowchart for LbB procedure**



F.2.2.2 Determine limiting length, $2c_c$, of through-wall flaw (Step 1)

The minimum limiting length, $2c_c$, is determined for the most onerous loading condition using lower bound materials properties and the procedures from Clause **7**. Where appropriate, stable tearing can be included in the calculation of $2c_c$.

F.2.2.3 Calculate the length, $2c_L$, of a through-wall flaw that leaks at the minimum detectable rate under normal operating conditions (Step 2)

The leak rate is determined from the COA as follows.

The COA of the through-wall flaw is required to estimate leakage flow rates. The COA depends on the flaw geometry (effective length, shape, orientation, etc.), the component geometry, the materials properties and the loading conditions.

A best-estimate approach should be used for calculating COA to establish the viability of a LbB case and to provide a basis for the assessment of margins. However, COA calculations are not simple and a bounding approach which minimizes flow rates is conservative and can reduce effort.

See **F.2.3** for advice on the calculation of COA for idealized flaws in flat plates, pipework components and spheres.

Approximate analytical solutions are available to predict leakage rates for single- and two-phase flows through a wide range of through-wall defects. Details of these solutions are given in **F.2.4**. Alternatively, leakage rate may be estimated from relevant experimental data if these are available.

Normal operating loads rather than peak loads should be assessed to avoid under-predicting the detectable leakage flaw length. The length of the postulated through-wall flaw is adjusted until the leak rate just becomes detectable [the minimum detectable leak rate depending on the detection apparatus (see **F.2.5**)]. An appropriate margin on leak detection should be included.

F.2.2.4 Assess results (Step 3)

The length $2c_L$ should be less than $2c_c$, with a suitable margin on length. If this is satisfied, a detectable leakage case is made. Implicit in this case is the assumption that the leak could be detected very quickly once the fluid loss exceeds a certain rate. When plant is only monitored at intervals, allowance should be made for any flaw growth that might occur between inspections. The minimum detectable flaw size $2c_L$ from Step 2 should then be replaced by an enhanced size, $2c_L'$, which includes growth over the full interval between inspections. The increment $2c_L' - 2c_L$ should be estimated using the flaw growth procedure in Clause **9**.

F.2.3 Calculation of crack opening area

COA models for plates, cylinders and spheres with through-wall flaws, and associated references, are summarized in Table F.2. Estimates of COA can vary widely depending on how the flaw is idealized, which crack opening model is used and what materials properties are assumed. This subclause provides advice on the factors that should be considered. Lower-bound COA solutions are set down for some simple geometries and loadings and references given to more detailed solutions. It also advises on whether a simplified LbB procedure where a through-wall defect is assumed should be implemented. For example, the methods for calculating COA in the presence of weld residual stress fields show the feasibility, or otherwise, of developing a detectable through-wall flaw at a weld location. In this regard, all loads, including those of weld residual stresses, should be taken into account when evaluating COA. Mean materials properties should be used to provide a best estimate of COA. It is important to consider time-dependent changes in both materials properties and loads, the latter arising from, for example, stress relaxation and stress redistribution processes. The plant loading conditions used for COA and leakage rate estimates are usually those associated with normal operation.

Estimation methods for COA can be classified into three categories:

- linear elastic models;
- elastic models incorporating a small-scale plasticity correction; and
- elastic-plastic models.

Time-dependent changes in COA due to creep effects are not within the scope of this British Standard, but guidance is provided in R6 [F.1]. Under load control and tensile through-wall stressing, plasticity leads to an increased COA compared with the elastic solution. Use of the elastic solution is then conservative in the leak detection element of a LbB argument. Conversely, under displacement control, plasticity results in a reduction in COA.

Table F.2 **Crack opening area methods for simple geometries and loading**

Geometry	**Primary loading**	**Elastic or small-scale yielding**		**Elastic-plastic**
		Elastic model	**Plastic model**	
Plates	Membrane	Westergaard [F.4] Takahashi [F.5]	Wüthrich [F.6]	—
	Membrane + through-wall bending	Miller [F.7]	—	—
Spheres	Membrane	Wüthrich [F.6] $R/B > 10$, $\lambda \leq 5$	Wüthrich [F.6]	—
	Membrane + through-wall bending	Miller [F.7]	—	—
Cylinders with axial flaws	Tension	France et al. [F.8], $3 \leq R/B \leq 100$	Wüthrich [F.6]	Kim et al. [F.9]
	Through-wall bending	France et al. [F.8], $3 \leq R/B \leq 100$	—	—
Cylinders with circumferential flaws	Tension	France et al. [F.8] $3 \leq R/B \leq 100$ Takahashi [F.5], [F.10]	Wüthrich [F.6] Rahman et al. [F.11]	Langston [F.12] Takahashi [F.5] Rahman et al. [F.11] Kim et al. [F.9]
	Global bending	France et al. [F.8], $3 \leq R/B \leq 100$ Takahashi [F.5], [F.10]	Wüthrich [F.6] Rahman et al. [F.11]	Langston [F.12] Takahashi [F.5], [F.10] Rahman et al. [F.11] Kim et al. [F.13] to [F.18]
	Tension + global bending	Add elastic components	Wüthrich [F.6] Rahman et al. [F.11]	Takahashi [F.5], [F.10] Rahman et al. [F.11] Kim et al. [F.13] to [F.18]
	Through-wall bending	France et al. [F.8] $3 \leq R/B \leq 100$	—	—

NOTE For the cylinder, "tension" is generally axial load. Some references explicitly include internal pressure. Similarly, most references give the centre COD, δ, and not the COA directly.

 © The British Standards Institution 2019

A wide range of published solutions is available for idealized slot-like flaws in simple geometries subject to basic loads such as pressure, membrane and bending loads. Their accuracy varies with the geometry and flaw size, and with the type and magnitude of the load. Generally, the models, except for results based on detailed finite element analysis, estimate the COA at the mid-thickness position; that is, they do not account for crack taper, particularly that arising from through-wall bending loads. The effect of internal pressure is often represented by the equivalent membrane load. However, within the plastic range, the stress in the plane of the flaw can influence the COA and its effect should be taken into account ([F.13], [F.19]). For circumferentially-flawed cylinders in the absence of bending restraint, for example, the COA due to a tensile load is lower than that due to the equivalent pressure load and thus its use is conservative in a LbB argument.

The COA may be calculated from explicit calculations of crack opening by integrating along the flaw. Where results are given only for the crack opening displacement (COD), δ, at the flaw centre, often an elliptical opening profile is assumed, so that the COA, $A = (\pi c\delta)/2$. A diamond-shaped profile might be more appropriate for circumferential flaws of length greater than about half the pipe circumference, so that $A = c\delta$ ([F.5] [F.10]). These simple relationships might not apply for asymmetric crack openings in complex geometries ([F.20], [F.21]). Estimates of the COA for complex-shaped flaws, for example where a fully circumferential flaw penetrates the pressure boundary along only part of its length, and for flaws at thickness transitions in pipes or at pipe/nozzle intersections, etc., may be derived using more accurate models ([F.21], [F.22], [F.23], [F.24], [F.25]). For such complex geometries and unusual flaw configurations, or for calculations requiring a high level of confidence, it might be necessary to use the finite element approach to give accurate or even conservative COA results.

A lower-bound approximation to A, for a through-wall flaw of length $2c$ in a shell with membrane stress, P_m, and ratio, $S = P_m/\sigma_f$, of membrane stress to flow strength is (see reference [F.6]):

$$A = \alpha(\lambda)\frac{\pi P_m 2c^2}{E'}\left[\left(1+\frac{S^2}{2}\right)^{3/2} - \left(\frac{S^2}{2}\right)^{3/2}\right] \quad \text{(F.1)}$$

where the term in brackets is a first-order correction for the effects of crack tip plasticity and increases with the loading level, S. The factor $\alpha(\lambda)$ is a correction to allow for bulging in terms of the shell parameter:

$$\lambda = \frac{\left[0.75\left(1-\nu^2\right)\right]^{0.25} 2c}{\left(r_m B\right)^{0.5}} \quad \text{(F.2)}$$

For axial flaws in cylinders with $\lambda \leq 8$:

$$\alpha(\lambda) = 1 + 0.1\lambda + 0.16\lambda^2 \quad \text{(F.3)}$$

For circumferential flaws in cylinders with $\lambda \leq 5$:

$$\alpha(\lambda) = \left(1 + 0.117\lambda^2\right)^{0.5} \quad \text{(F.4)}$$

For meridional flaws in spheres with $\lambda \leq 5$:

$$\alpha(\lambda) = 1 + 0.02\lambda + 0.22\lambda^2 \quad \text{(F.5)}$$

These expressions for $\alpha(\lambda)$ were derived using thin-wall, shallow-shell elasticity theory and are strictly valid only for mean radius to thickness ratios $r_m/B \geq 10$ and when flaw lengths do not exceed the least radius of curvature of the shell. Alternative small-scale yielding models use explicit flaw size corrections based on an effective flaw length or angle ([F.5], [F.10], [F.11]).

Elastic finite element results for COA for flaws subject to combined primary and secondary stress in plates and cylinders, and for through-wall self-balancing

stress distributions, enable the effect of these load types on COA to be assessed ([F.26] to [F.28]).

Background to and validation of the models in Table F.2 for circumferentially flawed cylinders is discussed in [F.29] and [F.30]. For this geometry, more accurate elastic-plastic models have been formulated. These should be used for best-estimate LbB calculations where stress levels are high enough to induce significant plasticity. Often, models require the stress-strain curve in Ramberg-Osgood form [F.11]. Reference stress methods, however, enable the material's stress-strain curve to be used directly [F.12]. Moreover, the accuracy of reference stress estimates of COD can be improved by modifying the limit load ([F.12] to [F.18], [F.31] to [F.33]). The modified limit load is defined as a geometry-, load- and flaw size-dependent multiple of the conventional rigid-plastic limit load, and is calibrated using detailed finite element analyses. The multiplying factor is given for a range of flaw angles and r_m/B ratios. Similar approximations for axially flawed cylinders have also been obtained [F.9]. This approach enabled accurate prediction of COD for a large number of pipe test data.

The modified reference stress approach has also been formulated in terms of FAD estimates of COD ([F.17], [F.18]). The simplest approach requires only the material's yield and ultimate stresses. This conservatively underestimates the COD compared with detailed finite element and experimental pipe test data for a range of pipe r_m/B values and loads. A second approach uses the full stress-strain curve and leads to more accurate and generally conservative results.

For bounding calculations of COA in cylinders, the linear elastic finite element results of [F.8] should be used. Elastic solutions, for the case of the circumferential flaw under axial tension, are also given in [F.5] and [F.10] as explicit expressions for the factor α as a function of flaw angle and r_m/B. The solution is extended to the case of global bending by multiplying the tension value of α by $(3 + \cos\theta)/4$ where θ is the flaw half-angle. The results are consistent with those in reference [F.8].

Where elastic estimates of high accuracy are required, non-linear geometric deformation effects can be important [F.34]. The solutions for plates and cylinders effectively assume that the flaws are in the centre of an infinite body, which is a reasonable approximation for many geometries. However, if the flaw is close to a significant geometric constraint, for example a pipe:nozzle intersection, local effects can influence the COA ([F.11], [F.16]). This is also true if significant through-wall bending stresses are present.

Most LbB assessments are likely to be concerned with the existence or potential existence of flaws at welds. The variation in materials properties at welds, the influence of the weld preparation angle and the presence of residual welding stresses all affect the COA ([F.15], [F.35], [F.36]). A circumferential through-wall flaw in a weld is analysed in reference [F.35]. For this situation the best estimate of COA is given by using the parent metal properties.

For pipework subjected to global transverse bending, the orientation of the resultant bending moment in respect of the through-wall flaw should be taken into account ([F.12], [F.37]). Off-centre loads can cause asymmetric and hence non-elliptical crack opening or partial closure, or complete closure if the flaw lies totally on the compressive side. Generally, finite element calculations have assumed a centred load.

For thick-walled geometries, the effect of crack-face pressure, which acts to open the flaw, is a function of crack opening; for narrow flaws, the mean pressure is lower than for wide flaws. To assess the significance of such effects, 50% of the difference between the internal and external pressures should be added to the membrane stress on the flaw face. This value should then be reassessed when undertaking the leakage flow calculations, which usually determine the exit pressure, and the results iterated if necessary.

Local through-wall bending stresses can induce elastic flaw face rotations, which reduces the effective COA. If complete flaw closure occurs, no LbB case can be made. Significant local through-wall bending stresses can be associated with weld residual stresses, geometric discontinuities, thermal gradients or primary loads (e.g. hoop stresses in a pressurized thick cylinder). References for estimating elastic crack face rotations in simple geometries are included in Table F.2.

The initial leakage rate through a flaw that has just broken through the pressure boundary could be significantly less than that predicted assuming a uniform flaw length equal to the recharacterized length. This is because the flaw might not penetrate the wall along its entire length when ligament failure first occurs, and the recharacterization rules can overestimate the actual flaw length. In general, this is not of concern, since before the flaw can grow to a limiting length it will first extend to the breakthrough length assumed in the COA calculations. However, for cases where through-wall bending stresses predominate, and development of a rectangular shape is unlikely, the COA can be minimized using the approximations in reference [F.38] by using a uniform lower-bound length based on the lesser of the two surface values.

F.2.4 Leak rate calculation

F.2.4.1 General

The calculation of the leak rate through a flaw is a complex problem involving the flaw geometry, the flow path length, friction effects and the thermodynamics of the flow. The guidance provided in the following subclauses should be adhered to for evaluating leak rates.

Subclause **F.2.4.2** deals with single-phase flow and the method is designed to calculate leakage rate for compressible gases. Consequently, the guidance can be used for any single-phase gas that can be described by the ideal gas law (superheated steam is also possible). It should not be used when there is a change of phase through the crack. Using it for water well below the saturation temperature, or other single-phase fluids, is not generally recommended as these are basically incompressible and an alternative method would be more appropriate.

Subclause **F.2.4.3** deals with two-phase flow and can account for choked flow with phase change through a flaw. The method is applicable to water, but the equations are general and applicable to other fluids. If this method is to be used for other fluids (e.g. cryogenics), then the non-equilibrium mixture quality, X_c, defined by Equation (F.16) should be carefully considered, as this was derived for water.

In all cases, fluid properties that are appropriate for the operating pressure and temperature should be used.

F.2.4.2 Single-phase flow

F.2.4.2.1 General

For single-phase flow, the following equation is recommended for calculating leak rate. Equation (F.6) calculates flow rates for equivalent rectangular flaws and includes the effects of friction. The flow rate relation used is appropriate to isothermal or polytropic flow of gases:

$$Q = C_D(p_0\rho_0)^{0.5}WL \quad \text{(F.6)}$$

Equation (F.6) has been validated to some extent for artificial flaws [F.39], with reasonable agreement observed between experiment and theory. Although measurements have also been made for real flaws ([F.40], [F.41]), the extent of validation is relatively small and the agreement with theory generally less good.

The derivation and significance of the parameters required in Equation (F.6) are now described.

F.2.4.2.2 Crack opening width and length

Entry and exit COAs, A_0 and A_{ex}, respectively, should be derived in accordance with **F.2.3**. The entry and exit flaw widths, W_0 and W_{ex}, respectively, are then given by:

$$W_0 = \frac{A_0}{L}, \quad W_{ex} = \frac{A_{ex}}{L} \tag{F.7}$$

These parameters are then used to calculate the mean flaw width:

$$W = \frac{W_0 + W_{ex}}{2} \tag{F.8}$$

and the flaw divergence parameter:

$$d = \frac{W_{ex} - W_0}{2W} \tag{F.9}$$

For a diverging ($d > 0$) or converging ($d < 0$) flaw that might occur if significant through-wall bending is present, approximations given in reference [F.42] may be used for the effect on the discharge coefficient. For this type of flaw, a lower bound to the flow rate may also be calculated using the smaller of the COAs.

F.2.4.2.3 Discharge coefficient

F.2.4.2.3.1 General

The discharge coefficient, C_D, depends on friction. Friction is related to a single surface roughness parameter, R_a, for which a value is required. In deriving R_a, expert guidance can be required in the interpretation of roughness measurements, as these measurements are dependent on a number of parameters; in particular, the measured value of R_a increases as the sampling length over which it is measured increases. This is illustrated in reference [F.43] where data for surface roughness for a number of different flaw types are represented. In the absence of specific R_a data, the lower values quoted in reference [F.43], corresponding to the shorter transverse length measurements, may be used as indicative values for the determination of the friction factor. These values, taken from reference [F.44], are reproduced in Table F.3, which includes, where appropriate, mean values and standard deviations, and can be used in sensitivity studies.

Table F.3 **Summary of short wave length surface roughness values**

Crack mechanism	Materials	R_a range (μm)	Average R_a (μm)	Standard deviation (μm)
Intergranular SCC	Stainless steel	0.64 to 10.5	4.7	3.9
Fatigue (air)	Stainless steel	8.1	—	—
Fatigue (air)	Carbon steel	3 to 8.5	6.5	3
Corrosion fatigue	Carbon steel	3 to 11	8.8	3

The Fanning friction factor, f, should be calculated from the mean flaw width, W, and R_a using a relation [F.44]:

$$f = \left[4.5\log_{10}\left(\frac{2W}{R_a}\right) - 2.5\right]^{-2} \tag{F.10}$$

as discussed in references [F.39] and [F.45]. The Fanning friction factor is equal to the conventional friction factor, f_{conv}, divided by 4.

 © The British Standards Institution 2019

The friction factor is generally bracketed by Equation (F.10) and a more conservative relation [F.44]:

$$f = \left[3.64\log_{10}\left(\frac{2W}{R_a}\right) - 2.636\right]^{-2} \quad \text{(F.11)}$$

as discussed in reference [F.46]. The friction factor can be assumed to have a relevant lower bound, corresponding to smooth flow [F.47]. There is also experimental evidence that the friction factor reaches an effective maximum, f_{max}, which is dependent on surface geometry. This is discussed more fully in reference [F.45]. A number of references, all discussed in reference [F.45], report f_{max} in the approximate range 0.2 to 1.0 ([F.40], [F.48] to [F.50]). This applies to fully developed turbulent flow.

If the calculated friction factor is greater than 0.25, then the sensitivity of the flow rate to f should be investigated by varying R_a to give values of between 0.25 and 1.0.

The friction factor is used together with the divergence parameter to calculate the discharge coefficient. The flaw height, D, is normally taken as the wall thickness at the flaw position. This is used to calculate a friction loss coefficient, F, for the flaw, from:

$$F = f\,D/W \quad \text{(F.12)}$$

The friction loss coefficient is then used with the flaw divergence parameter, d, to calculate the discharge coefficient.

The equations that can be used to determine C_D also depend on whether the flow is choked, that is the ratio, $p_0\,/p_{ex}$, of pressure inside the pipe or vessel to that outside is high enough for the flow to be sonic, which is usually the case.

F.2.4.2.3.2 When $d > 0$

For very low friction [$F < (1.5 + 2.5d)^2 / 2 \equiv F_1$] where choking occurs at entry:

$$C_D = 0.4(1-d) \equiv C_D^{I} \quad \text{(F.13a)}$$

When the flow is choked at exit {$F_1 < F < [(1 - d)(p_0/p_{ex})–1]^2 / 2 \equiv F_2$}:

$$C_D = \left[\frac{\left(1-d^2\right)}{(1+2F)^{0.5}}\right] \equiv C_D^{II} \quad \text{(F.13b)}$$

When the flow is unchoked ($F > F_2$) and p_0 / p_{ex} is too low for the flow to go sonic, C_D is given by:

$$C_D = (1-d^2)\frac{\left[1-(p_{ex}/p_o)^2\right]^{0.5}}{\left[1+(2F)^{0.5}-k\right]} \equiv C_D^{III} \quad \text{(F.13c)}$$

where:

$$k = (1-d)\left\{(p_o/p_{ex}) - \left[(p_o/p_{ex})^2 - 1\right]^{0.5}\right\} \quad \text{(F.13d)}$$

F.2.4.2.3.3 When $d < 0$

Equation (F.13c) is used when $F > F_2$.

When $F \leq F_2$, C_D is given by:

$$C_D = \min\left[0.4, 0.6(1+d), C_D^{II}\right] \quad \text{(F.13e)}$$

F.2.4.2.3.4 Pressure, temperature and fluid density and viscosity

Entrance and exit pressure and temperature are generally reasonably well defined from measurements. Fluid properties are generally taken from tabular data.

F.2.4.3 Two-phase flow

F.2.4.3.1 General

For two-phase flow of steam/water mixtures, the procedure outlined in this subclause should be followed [F.51].

The procedure has been validated by comparisons with flow through circular pipes and artificial and real flaws [F.51]; reasonable agreement was observed between measurement and theory for artificial flaws. As with single-phase flow, the agreement between measurement and theory was variable in the case of real flaws. For flaws of width ≥50 μm, calculated leak rates have been observed to differ from measured leak rates typically by a factor of 2 or less. However, for a flaw of approximate width 20 μm, discrepancies of up to a factor of 9 have been observed. Commonly, the discrepancy in leak rates for narrow flaws has been attributed to the effects of particulate plugging, though other factors, such as uncertainties in flaw dimensions, can also be significant. These are discussed in reference [F.52].

F.2.4.3.2 Procedure

The mass flow rate can be calculated using:

$$G_c^2 = \frac{1}{\left[\frac{X_c v_{gc}}{\gamma_0 p_c} - (v_{gc} - v_{Lc}) N \frac{dX_E}{dp}\right]_{choking\_plane}} \quad \text{(F.14)}$$

where N is equal to 0 at $X_E = 0$ and 1.0 for $X_E \geq 0.05$.

Equations (F.13a) to (F.13e) are solved in conjunction with the pressure constraint equation, which is:

$$\Omega(G_c, p_c) = p_c + p_e + p_f + p_a + p_{aa} + p_k - p_0 = 0 \quad \text{(F.15)}$$

The other pressure terms depend on G_c.

The non-equilibrium mixture quality, X_c, is given by:

$$X_c = N X_E \{1 - \exp[-B'(B/D_i - 12)]\} \quad \text{(F.16)}$$

where:

B' is a constant, equal to 0.0523 [F.53].

The equilibrium mixture quality is defined by:

$$X_E = \left[\frac{S_o - S_{Lc}}{S_{gc} - S_{Lc}}\right] \quad \text{(F.17)}$$

This relation comes from equating the entropy at a point upstream of the two-phase region (the stagnation entropy) with the entropies of gas and liquid where critical flow is attained. The stagnation entropy is evaluated by assuming the fluid has been brought to rest (i.e. stagnated) isentropically.

In Equation (F.15), the entrance pressure loss, p_e, is given by:

$$p_e = \frac{G_0^2 v_{Lo}}{2 C_D^2} \quad \text{(F.18)}$$

where C_D is 0.95 for flaws with CODs < 150 μm and between 0.62 and 0.95 for flaws with CODs ≥ 150 μm.

 © The British Standards Institution 2019

In Equation (F.15), the frictional pressure loss, p_f, is given by:

$$p_f = \frac{f_{conv} L}{D_i} \frac{\bar{G}^2}{2} \left[(1 - \bar{X}) \bar{v}_L + \bar{X} \bar{v}_g \right] \quad \text{(F.19)}$$

The friction factor, $f_{conv} = 4f$, is given by:

$$f_{conv} = \left[C_1 \log_{10} \left(\frac{W}{R_a} \right) + C_2 \right]^{-2} \quad \text{(F.20)}$$

where:

C_1 is 2.00 where $W/R_a > 100$, and 3.39 where $W/R_a < 100$;

C_2 is 1.74 where $W/R_a > 100$, and 0.869 where $W/R_a < 100$.

This relation [F.47] gives somewhat lower values of the friction factor than that in reference [F.54], which is commonly used for single-phase flow.

The pressure loss due to acceleration arising from phase change, p_a, is given by:

$$p_a = \bar{G}_T{}^2 \left[(1 - X_c) v_{Lc} + X_c v_{gc} - v_{Lc} \right] \quad \text{(F.21)}$$

The pressure loss due to acceleration arising from changes in area, p_{aa}, is given by:

$$p_{aa} = \frac{G_c{}^2 v_{Lo}}{2} \left[\left(\frac{A_{ex}}{A_i} \right)^2 - \left(\frac{A_{ex}}{A_o} \right)^2 \right] + \frac{G_c{}^2}{2} \left[(1 - \bar{X}) v_{LC} + \bar{X} v_{gc} \right] \left[1 - \left(\frac{A_{ex}}{A_i} \right)^2 \right] \quad \text{(F.22)}$$

The pressure loss due to bends and protrusions, p_k, is given by:

$$p_k = C_v \frac{\bar{G}^2}{2} \left[(1 - \bar{X}) \bar{v}_L + \bar{X} \bar{v}_g \right] \quad \text{(F.23)}$$

The derivation and significance of the parameters commonly required is now described.

F.2.4.3.3 Flaw shape and area dimensions

Rectangular, elliptical and diamond-shaped flaws can be relatively easily represented, and it should be determined which more closely represents the flaw in question. In all cases the COA (entry and exit) from the mid-point COD and the flaw length should be calculated.

F.2.4.3.4 Discharge coefficient

A discharge coefficient is required for the calculation of the flaw entrance pressure loss. A value of 0.95 should be used for tight flaws, i.e. with a COD of less than 150 μm [F.55]. For flaws with larger CODs, a discharge coefficient between 0.62 and 0.95 should be chosen. The figure chosen should be based on how round the entrance edges are in comparison with the COD.

F.2.4.3.5 Roughness

A surface roughness coefficient is required, and the guidelines for this are as for single-phase flow. Using the hydraulic radius and the roughness coefficient, a friction factor can be calculated using relations given in reference [F.47].

F.2.4.3.6 Flaw height

As for single-phase flow, the flaw height is normally the wall thickness at the flaw position. This is then used to calculate a friction pressure loss coefficient from the friction factor.

F.2.4.3.7 Loss coefficient for bends and protrusions

A loss coefficient for bends and protrusions is also required. There are few guidelines for this at present. However, a fit to experimental data for a fatigue crack in a girth weld has suggested a value of six velocity heads per mm of flaw flow path and a value of three velocity heads per mm of flaw flow path for an intergranular stress corrosion crack.

F.2.4.3.8 Non-equilibrium mixture quality

This is defined by default based on experiments [F.53].

F.2.4.3.9 Pressure, temperature and liquid and vapour density and viscosity

Entrance and exit pressure and temperature are generally reasonably well defined from measurements. Fluid properties are generally taken from tabular data.

F.2.4.3.10 Flow reduction mechanisms

In assessing flow rate calculations involving liquid flow, account should be taken of the potential for flow reduction mechanisms such as blocking of the flaw by oxide growth or by particle or debris entrapment. For flaws that are very tight, i.e. those with CODs of the same order of magnitude as the particulate size, particulates can lodge in the flaw.

There is currently little guidance on how to assess these effects, though some useful notes on particulate size are given in reference [F.51]. These primarily concern the results of a literature survey, which yielded the values in Table F.4 of particulate diameters and concentrations in nuclear pressurized water reactors (PWRs) and nuclear boiling water reactors (BWRs) in normal operation.

These particles could be large enough to plug a tight flaw in a piping system. The concentrations of particulates in Table F.4 are low enough that particulate plugging occurs only for flaws that have been leaking for days or more at a time, which might happen where visual inspections are infrequent and difficult.

The literature survey was limited to normal operating circumstances. Fault conditions need to be examined on a case-by-case basis.

Table F.4 **Particulates in primary system water**

Water chemistry	**PWR**	**BWR**
Principal particulate composition	Nickel ferrite	Iron oxide magnetite haematite
Primary water particulates		
Size range, μm	0.01 to 100	0.01 to 100
Mass median, μm	0.5 to 5	0.5 to 5
Concentration, ppm	<1.0	<1.0
Make-up water particulates		
Concentration, ppm	<0.5	<0.5

 © The British Standards Institution 2019

F.2.5 Leak detection and flaw stability following breakthrough

F.2.5.1 General

Any LbB procedure aims to show that the leaking flaw remains stable for a sufficient time to allow the leak to be detected. This time for detection should include that necessary to ensure that the signal is not spurious, or to unambiguously identify the source of the leak and to take the subsequent required action. The stability of the leaking flaw should be assessed in terms of the margins to criticality and the potential for further flaw growth. If further time-dependent flaw growth could occur, then margins on length and time to failure should be demonstrated. The assessed time to failure, in conjunction with the estimated flow rate, permits a suitable leak detection system to be selected.

A wide range of leak detection systems is available. Some information and guidance on systems that are available, particularly to the nuclear industry, is given in references [F.56] and [F.57]. Guidance is also given by the US Nuclear Regulatory Commission [F.58].

F.2.5.2 Local leak detection systems

Local leak detection systems monitor specific plant features or segregated regions. Examples include sump pumps, pumps for water systems, humidity detection for steam leaks, gas levels in air for gaseous systems, and radiation monitors for nuclear systems.

F.2.5.3 Global leak detection systems

All global systems detect all leaks (including, for example, valve glands, seals, etc.), and hence any leakage identified by the monitoring equipment should be investigated and the source established. The response times for such systems are relatively long and depend on plant segregation. Leakage through flaws generates acoustic emission that is transmitted through the structure, and, in some circumstances, through the air [F.49]. Wave guide and microphone systems have been developed which offer flexible and sensitive leak detection capabilities for a wide range of fluids. Details of design and deployment are dependent on the application.

F.2.5.4 Assessment of results

The final step in undertaking either of the recommended LbB procedures is to carry out a sensitivity analysis. The sensitivity analysis should take into account the range of likely variations in the main parameters used in the calculations. The sensitivity of the results to variations in materials properties, applied loads and the predicted COA and leak rates is investigated.

A LbB case made in this way is not necessarily conservative, unlike the procedures in Clause **7**, where the use of upper-bound loads and stress intensity factors with lower-bound materials properties and collapse solutions helps to ensure that the assessment is conservative. Although these bounding values provide conservative estimates of limiting flaw length and are therefore recommended for that calculation, they minimize the flaw length at breakthrough and maximize the crack opening displacement, both of which are non-conservative when making a LbB case. Best-estimate values should therefore be used to calculate the flaw length at breakthrough and COA, and then the effect of varying the input parameters examined.

Bibliography for Annex F

Standards publications

There are no standards references in this annex.

Other documents

[F.1] R6 PANEL. *R6: Assessment of the integrity of structures containing defects*. Revision 4, as amended. Gloucester: EDF Energy, 2001.

[F.2] SHARPLES, J.K. and CLAYTON, A.M. A leak-before-break assessment method for pressure vessels and some current unresolved issues. *In: International Journal of Pressure Vessels and Piping*, 1990, 43(1–3), 317–327.

[F.3] US NUCLEAR REGULATORY COMMISSION. *Evaluation of potential for pipe breaks.* NUREG/CR-1061, Report of the US Nuclear Regulatory Commission Piping Review Committee, 1994, 3.

[F.4] WESTERGAARD, H.M. Bearing pressure and cracks. *In: ASME Journal of Applied Mechanics*, June, 1939, 60.

[F.5] TAKAHASHI, Y. Leak-before-break. *In: Comprehensive Structural Integrity*, 2003, 10(7), Paris: Elsevier.

[F.6] WÜTHRICH, C. Crack opening areas in pressure vessels and pipes. *In: Engineering Fracture Mechanics*, 1983, 18(5), 1049–1057.

[F.7] MILLER, A.G. Elastic crack opening displacements and rotations in through-cracks in spheres and cylinders under membrane and bending loading. *In: Engineering Fracture Mechanics*, 1986, 23(4), 631–648.

[F.8] FRANCE, C.C., GREEN, D. and SHARPLES, J.K. *New stress intensity factor and crack opening area solutions for through-wall cracks in pipes and cylinders*, AEA Technology Report AEAT-0643, 1996; Addendum, April, 1999. (See also ASME PVP, 1997, 350, 143–195.)

[F.9] KIM, Y.J., HUH, N.S., PARK, Y.J. and KIM, Y. Elastic-plastic J and COD estimates for axial through-wall cracked pipes. *In: International Journal of Pressure Vessels and Piping,* 2002, 79(6), 451–464.

[F.10] TAKAHASHI, Y. Evaluation of leak-before-break assessment methodology for pipes with a circumferential through-wall crack. Part III: estimation of crack opening area. *In: International Journal of Pressure Vessels and Piping*, 2002, 79(6), 525–536.

[F.11] RAHMAN, S., BRUST, F. W., GHADIALI, N. and WILKOWSKI, G.M. Crack opening area analyses for circumferential through-wall cracks in pipes – Part I: Analytical models. *In: International Journal of Pressure Vessels and Piping*, 1998, 75(5), 357–373.

[F.12] LANGSTON, D.B. *A reference stress approximation for determining crack opening displacements in leak-before-break calculations*. Nuclear Electric Report, 1991, TD/SID/REP/0112.

[F.13] KIM, Y.J., HUH, N.S. and KIM, Y.J. Quantification of pressure-induced hoop stress effect on fracture analysis of circumferential through-wall cracked pipes. *In: Engineering Fracture Mechanics*, 2002, 69(11), 1249–1267.

[F.14] KIM, Y.J., HUH, N.S. and KIM, Y.J. Enhanced reference stress-based J and crack opening displacement estimation method for leak-before-break analysis and comparison with GE/EPRI method. *In: Fatigue and Fracture Engineering Materials and Structures*, 2001, 24(4), 243–254.

 © The British Standards Institution 2019

[F.15] KIM, Y.J., HUH, N.S. and KIM, Y.J. Effect of Lüders strain on engineering crack opening displacement estimations for leak-before-break analysis: Finite element study. *In: Fatigue and Fracture Engineering Materials and Structures*, 2001, 24(9), 617–623.

[F.16] KIM, Y.J., HUH, N.S. and KIM, Y.J. Reference stress based J and COD estimation for leak-before-break analysis of pressurized piping. *In: Proceedings of ECF14*, Krakow, II, 2002, 133–140.

[F.17] KIM, Y.J. and BUDDEN, P.J. A reference stress based COD estimation in LBB analysis. *In: Proceedings of ECF13*, San Sebastian, Elsevier, 2000.

[F.18] KIM, Y.J. and BUDDEN, P.J. Reference stress approximations for J and COD of circumferential through-wall cracked pipes. *In: International Journal of Fracture*, 2002, 116(3), 195–218.

[F.19] FOXEN, J. and RAHMAN, S. Elastic-plastic analysis of small cracks in tubes under internal pressure and bending. *In: Nuclear Engineering Design*, 2000, 197(1–2), 75–87.

[F.20] HUH, N.S., KIM, Y.J., YU, Y.J. and PYO, C.R. Effect of nozzle geometry on leak-before-break analysis of pressurized piping. *In: Engineering Fracture Mechanics*, 2001, 68(16), 1709–1722.

[F.21] RAHMAN, S., GHADIALI, N., WILKOWSKI, G.M., MOBERG, F. and BRICKSTAD, B. Crack opening area analyses for circumferential through-wall cracks in pipes – Part III; Off-center cracks, restraint of bending, thickness transition and weld residual stress. *In: International Journal of Pressure Vessels and Piping,* 1998, 75(5), 397–415.

[F.22] FRANCE, C.C. *Crack opening area and stress intensity factor solutions obtained by finite elements for circumferential through-thickness cracks in cylinders under through wall bending – Effect of modelled cylinder length and end restraints*. AEA Technology Report SPD/D(95)400, 1995.

[F.23] PRICE, R.H. *The effect of nozzle stiffness on the opening of a through wall crack in a spherical pressure vessel*. Nuclear Electric Report TD/SEB/MEM/5015/92, 1992.

[F.24] HUH, N.S., KIM, Y.J. and YU, Y.J. Crack opening analysis of complex cracked pipes. *In: International Journal of Fracture*, 2001, 111(1), 71–86.

[F.25] YU, Y.J., PARK, S.H., SOHN, G.H., KIM, Y.J. and URKO, W. Application of LBB to a nozzle-pipe interface, LBB 95. Specialist meeting on Leak Before Break in Reactor Piping and Vessels; Lyon, France, October 1995. *In: Proceedings of US Nuclear Regulatory Commission,* 1997, NUREG/CP-0155, 81–89.

[F.26] YELLOWLEES, S.F. and TOFT, A. *Elastic crack opening areas in thick-walled cylinders under primary and secondary loading*, Serco Assurance Report. 2002, SA/RD03123200/R01.

[F.27] BEESLEY, M.J. and YELLOWLEES, S.F. *Crack opening areas in plates under combined primary and secondary loading*. AEA Technology Report, 2000, AEAT/RJCB/000073/00.

[F.28] YAHIAOU, K., YELLOWLEES, S.F. and FRANCE, C.C. *Crack opening areas in plates under a self-balancing through thickness residual stress field*. AEA Technology Report, 2000, AEAT-6452.

[F.29] SHARPLES, J.K. and BOUCHARD, P.J. *Assessment of crack opening area for leak rates.* LBB 95; Specialist meeting on Leak Before Break in Reactor Piping and Vessels; Lyon, France, October 1995. *In: Proceedings of US Nuclear Regulatory Commission*, 1997, NUREG/CP-0155, 267–276.

[F.30] RAHMAN S., BRUST, F.W., GHADIALI, N. and WILKOWSKI, G.M. Crack opening area analyses for circumferential through-wall cracks in pipes – Part II; model validations. *In: International Journal of Pressure Vessels and Piping*, 1998, 75(5), 375–396.

[F.31] AHN, S.H., HIDAKA, A. and ANDO, K. Fatigue crack growth and penetration behavior in pipe subject to bending load. *In: Proceedings of the 14th International Conference on Structural Mechanics in Reactor Technology*, Lyon, France, 1997, 4, 113–120.

[F.32] MOULIN, D., CHAPULIOT, S. and DRUBAY, B. *Development of crack shape: LBB methodology for cracked pipes, LBB 95*. Specialist meeting on Leak Before Break in Reactor Piping and Vessels, Lyon, France, October 1995, *In: Proceedings of US Nuclear Regulatory Commission*, 1997, NUREG/CP-0155, 247–255.

[F.33] KIM, Y.J., HUH, N.S. and KIM, Y.J. Reference stress based elastic-plastic fracture analysis for circumferential through-wall cracked pipes under combined tension and bending. *In: Engineering Fracture Mechanics*, 2002, 69(3), 367–388.

[F.34] SHARPLES, J.K. and KEMP, S. *Effect of non-linear geometry on results of finite element calculated crack opening displacements in cylinders*. AEA Report, 1994, AEA/RS/4463.

[F.35] GANTA, B.R. and AYRES, D.J. *Analysis of cracked pipe weldments.* EPRI Report, 1997, NP-5057.

[F.36] DONG, P., RAHMAN, S., WILKOWSKI, G., BRICKSTAD, B. and BERGMAN, M. *Effects of weld residual stresses on crack-opening area analysis of pipes for LBB applications, LBB 95*; Specialist meeting on Leak Before Break in Reactor Piping and Vessels; Lyon, France, October 1995. *In: Proceedings of US Nuclear Regulatory Commission*, 1997, NUREG/CP-0155, 283–298.

[F.37] MAY, K.A., SANDERSON, D.J. and WINTLE, J.B. *Investigation of the effect of plasticity and non-centred bending on crack opening area for leak-before-break of piping systems*. AEA Technology Report, 1994, AEA-RS-4528.

[F.38] HODGSON, A.P. and LEGGATT, R.H. *A review of the behaviour of penetrating fatigue cracks with reference to leak-before-break in the fast reactor*. FRDCC/SIWG/DASG/P(87)156, 1997.

[F.39] CHIVERS, T.C. The influence of surface roughness on fluid flow through cracks. *In: Fatigue and Fracture of Engineering Materials and Structures*, 2002, 25(11), 1095–1102.

[F.40] SHARPLES J.K., MELVIN, G., O'DONNELL, I.J. and BATES, S.K. *Report of wide plate test SSTP13 to investigate leak-before-break of EFR Primary Vessel*. AEA Report AEA/RS/4315, FR/SIWG/FESG/P(93)63, 1993.

[F.41] SHARPLES, J.K., GARDNER, L., SANDERSON, D.J., MELVIN, G.T. and DOBSON, D. *Report of wide plate test SSTP14 to investigate leak-before-break of EFR primary vessel*, AEA Report AEA/RS/4361, FR/SIWG/FESG/P(93)68, 1993.

[F.42] EWING, D.J.F. Simple methods for predicting gas leakage flows through cracks, Paper C376/047. *In: Proceedings of International Conference on Pipework Engineering and Operation*, Institute of Mechanical Engineering, London, 21–22 February, 1989.

[F.43] WILKOWSKI, G., RAHMAN, S., GHADIALI, N. and PAUL, N. *Determination of crack morphology parameters from service failures for leak-rate analyses, LBB 95*; Specialist meeting on Leak Before Break in Reactor Piping and Vessels; Lyon, France, October 1995. *In: Proceedings of US Nuclear Regulatory Commission*, 1997, NUREG/CP-0155, 359–374.

[F.44] WILKINSON, J., SPENCE, G.S.M. and CHANDLER, R.F. *Leakage flow through small cracks – Report of second stage of experimental work* (undertaken in 1990/91), AEA Report, 1991, FMWG/P(91)123D.

[F.45] CHIVERS, T.C. *Assessments of fluid friction factors for use in leak rate calculations*, LBB 95; Specialist meeting on Leak Before Break in Reactor Piping and Vessels; Lyon, France, October 1995. *In: Proceedings of US Nuclear Regulatory Commission*, 1997, NUREG/CP-0155, 349–358.

[F.46] TAGGART, J. *Leak before break – A literature review of leak-rate estimation methods*. Serco Assurance Report, 2002, SA/RJCB/RD03123300/R001.

[F.47] SCHLICHTING, H. *Boundary-layer theory*. New York: McGraw-Hill, 1968.

[F.48] GARDNER, L., WIGHTMAN, A.P. and DOBSON, D. *Stage 5 wide plate test in support of leak-before-break assessment for Chapelcross/Calder Hall reactor pressure vessels*. AEA Technology Report, 1994, AEA/RS/4390.

[F.49] RAWLINGS, P.E.L. *Acoustic monitoring of leak of weld on air release branch 16-12-RO-AR-1B, Reactor 3, Hinkley Point B PS: Part 2, laboratory investigation*. Nuclear Electric Report, 1993, TIGM/MEM/0032/93.

[F.50] SHARPLES, J.K. and CLARKE, P.W. *Background to leakage guidance given for leak-before-break assessments.* AEA Technology Report, 1992, AEA/RS/4227.

[F.51] PAUL, D.D., AHMAD, J., SCOTT, P.M., FLANIGAN, L.F. and WILKOWSKI, G.M. *Evaluation and refinement of leak-rate estimate models: Topical Report*, 1994, NUREG/CR-5128 Rev.1.

[F.52] TAGGART, J. *Leak before break – Developments in leak-rate calculation methods for R6*, 2002, Serco Assurance Report SA/SIS/14606300/R001.

[F.53] HENRY, R.E. and FAUSKE, H.K. The two-phase critical discharge of initially saturated or subcooled liquid. *In: Nuclear Science Engineering*, 1970, Vol. 41, 336–342.

[F.54] BUTTON, B.L., GROGAN, A.F., CHIVERS, T.C. and MANNING, P.T. Gas flow through cracks. *In: ASME Journal of Fluids Engineering*, 1978, 100(4), 453–458.

[F.55] PAUL, D.D., GHADIALI, N., AHMAD, J. and WILKOWSKI, J. *SQUIRT – User's Manual, Version 2.1*, International Piping Integrity Research Group, 1990.

[F.56] MITCHELL, D.H. *Leak detection systems in support of leak before break arguments*, CEGB Report, 1989, RD/B/6205/R89.

[F.57] CHIVERS, T.C. *Aspects of leak detection, LBB 95*; Specialist meeting on leak before break in reactor piping and vessels; Lyon, France, October 1995. *In: Proceedings of US Nuclear Regulatory Commission*, 1997, NUREG/CP-0155, 485–489.

[F.58] US NUCLEAR REGULATORY COMMISSION. *Regulatory Guide I.45, Guide on monitoring and responding to reactor coolant system leakage*, Revision 1. Washington, DC: US NRC, 2008.

This page deliberately left blank

Annex G (informative)

The assessment of locally thinned areas (LTAs)

G.0 Symbols and definitions

For the purposes of this annex, the following symbols, definitions and units apply, unless otherwise indicated at the point of use.

Symbol	Definition	Units
a	Half flaw length for through-thickness flaw, flaw height for surface flaw or half height for embedded flaw	mm
a_i, a_j	Height of flaw i or j to determine flaw interaction	mm
B	Section thickness in plane of flaw	mm
c	Maximum half flaw length in any direction	mm
c_1	Half flaw length in the axial direction	mm
c_2	Half flaw length in the circumferential direction	mm
$c_{1,i}$, $c_{2,i}$, $c_{1,j}$, $c_{2,j}$	Half flaw length used in defining interaction between LTAs	mm
f_c	Factor of safety in analysis of LTA	—
h	Height of elliptical vessel end as illustrated in Figure G.4c)	mm
K_r	Fracture ratio	—
L_r	Ratio of reference stress to yield strength	—
$L_{r,max}$	Permitted limit of L_r	—
M	Folias factor	—
M_i	In-plane bending moment	Nmm
Q	Bulging factor	—
R	Radius of centreline of a bend (see Figure G.3)	mm
r_{eff}	Outside radius for a sphere, spherical vessel end and elliptical vessel end	mm
r_o	Outer radius	mm
s_1, s_2	Distance between potentially interacting flaws	mm
σ	Hoop stress in the sphere or vessel end	N/mm^2
σ_{ref}	Reference stress used for creep and plastic consideration	N/mm^2
σ_{ref1}, σ_{ref2}	Reference stress based on the axial (σ_1) and hoop stress (σ_2) respectively in LTAs assessment in a cylinder	N/mm^2
σ_U	Tensile strength	N/mm^2
σ_Y	Lower yield strength or 0.2% proof strength	N/mm^2
σ_1, σ_2	Axial stress and hoop stress respectively in LTAs assessment in a cylinder	N/mm^2

G.1 Background

The background to this annex is given in references [G.1] and [G.2].

This annex provides guidance on the determination of the acceptability of areas of loss of wall thickness, for example caused by internal or external corrosion, in internally pressurized pipes or pressure vessels. Guidance is given on assessment methods and the data required.

The methods for assessing LTAs given in this annex are based on the methods widely used in the pipeline industry, e.g. ASME B31G and DNVGL-RP-F101 [G.3]. This annex does not preclude the use of other methods.

Simple and conservative rules for assessing interaction between LTAs are given in **G.7**.

G.2 Applicability

G.2.1 General

The methods described in this annex may be used to assess LTAs in pipes and pressure vessels that have been designed to a recognized design code. The methods have been validated for ductile ferritic steels, and for pipes and pressure vessels with a diameter to wall thickness ratio of greater than approximately ten. Additional guidance should be sought before applying these methods to other materials or other geometries.

The guidance is not applicable to every situation that requires a fitness-for-service assessment and further methods could be required (see **G.8**). Alternatively non-linear finite element stress analysis may be used. Such analysis might be required for complex LTA geometries. Guidance on finite element analysis methods is given in **G.9**.

When assessing LTAs, account should be taken of the measurement uncertainty of the flaw dimensions and the structural geometry. The limitations of the measurement techniques (e.g. in-line inspection, ultrasonic testing) should be also be taken into account (see **6.3**).

G.2.2 Applied loads

All of the applied loads should be taken into account when assessing an LTA, e.g. internal pressure and mechanical loads. The methods specified in this annex may be applied to:

a) LTAs in a cylinder subject to a hoop stress, an axial stress or both a hoop stress and an axial stress;

b) LTAs in an elbow subject to a hoop stress, or an axial stress; and

c) LTAs in a sphere or vessel end subject to a hoop stress.

In a pipe or pressure vessel subject to an internal overpressure, the limiting load case is normally the hoop stress. However, if the axial stress is high or if the circumferential extent of the LTA is greater than the longitudinal extent, the axial stress or the combination of the hoop and axial stress might be the limiting load case.

G.2.3 Applicable flaws

The following types of LTA may be assessed using this annex:

a) internal corrosion;

b) external corrosion;

c) corrosion in parent material;

d) corrosion in or adjacent to welds;

e) colonies of interacting corrosion flaws;

f) erosion; and

g) metal-loss (e.g. grinding or burring).

All procedures apply to either internal or external LTAs. They may be applied to LTAs in welds, with the following provisos.

1) There should be no weld flaw present that could interact with the LTA.

2) The weld should not undermatch the parent material in strength.

 © The British Standards Institution 2019

3) Brittle fracture should be unlikely to occur (see **G.2.4**).

G.2.4 Exclusions

This annex does not apply to:

a) external overpressure;

b) cyclic loading;

c) sharp flaws (i.e. cracks);

d) combined LTAs and cracks;

e) LTAs in association with mechanical damage (e.g. dents);

f) metal loss flaws attributable to mechanical damage (e.g. gouges)[G.1)];

g) fabrication flaws in welds;

h) environmentally induced cracking[G.2)];

i) LTAs of depth[G.3)] greater than 80% of the original (i.e. not corroded) wall thickness (i.e. remaining ligament less than 20% of the original wall thickness);

j) LTAs with a remaining ligament less than 1.25 mm for pipes, and 2.5 mm for pressure vessels;

k) LTAs at regions of stress concentration such as nozzles, tees and the knuckle region of vessel heads (but area replacements methods in design codes or finite element analysis might be appropriate; see **G.8** and **G.9**); and

l) LTAs in mechanical joints.

Corrosion-fatigue is discussed in **10.3.3.3**. A fatigue assessment of an LTA based on the assumption that it is a crack-like flaw might be overly conservative. An alternative method is to estimate the stress concentration due to the LTA and then use an appropriate *S-N* curve.

The methods in this annex are applicable only to materials that are operating on the upper shelf. The brittle to ductile transition temperature of the material should be lower than the minimum operating temperature.

The methods are not recommended for applications where brittle fracture is likely to occur. These include:

1) any material with a brittle to ductile transition temperature above the operating temperature;

2) fabricated, forged, formed or cast fittings;

3) bond lines of flash welded (FW) or low frequency electric resistance welded (ERW) butt-welded pipe; and

4) lap welded or furnace butt-welded pipe.

In applications where brittle fracture is likely to occur, the LTAs should be treated as cracks and should be assessed in accordance with Clause **7**.

G.1) Metal loss flaws due to mechanical damage can contain a work hardened layer at their base and can also contain cracking.

G.2) Environmentally induced cracking, such as SCC is not considered here. Guidance on the assessment of crack-like corrosion flaws is given in **10.3.3**.

G.3) "Flaw depth" as used in this annex is equivalent to the dimension "flaw height" as used elsewhere in the standard.

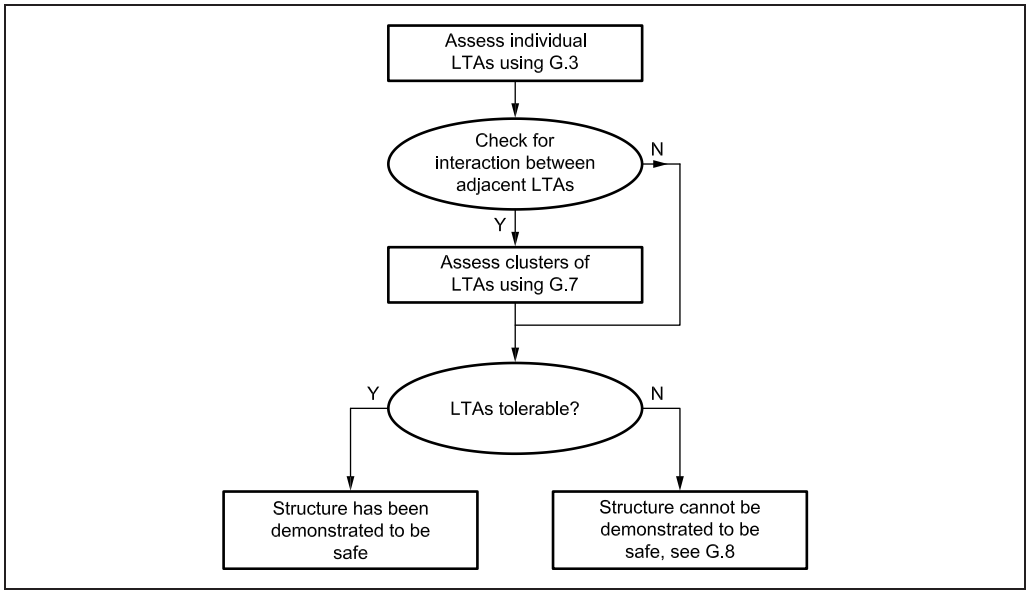
G.2.5 Factors of safety

A factor of safety should be applied in the assessment of an LTA, to ensure that there is a safe margin between the operating loads and the failure load of the LTA and to avoid general yielding. The selection of an appropriate factor of safety is dependent on a number of different factors. The factor of safety should not normally be less than the reciprocal of the design factor of the structure, e.g. for a pipeline with a design factor on the hoop stress of 0.72 the minimum factor of safety is 1.39, and for a pressure vessel with a design factor of 0.67 the minimum factor of safety is 1.5.

G.2.6 Assessment procedure

A flowchart describing the assessment procedure is shown in Figure G.1.

Figure G.1 **Flowchart of assessment procedure**



G.3 The assessment of LTAs

The assessment of LTAs is based on local plastic collapse. $K_r = 0$, i.e. it is not necessary to calculate K_r when assessing an LTA (see exclusions in **G.2.4**). If the assessment point lies below the cut-off ($L_r < L_{r,max}$), the LTA is acceptable; if it lies on or above the cut-off, the LTA is unacceptable.

The cut-off is to prevent local plastic collapse and it is set at the point at which $L_r = L_{r,max}$ where:

$$L_{r,max} = \frac{\sigma_Y + \sigma_U}{2\sigma_Y} \quad \text{(G.1)}$$

For the purposes of defining the cut-off, specified minimum properties should be used.

The load ratio L_r is calculated from the following equation:

$$L_r = \frac{f_c \sigma_{ref}}{\sigma_Y} \quad \text{(G.2)}$$

where:

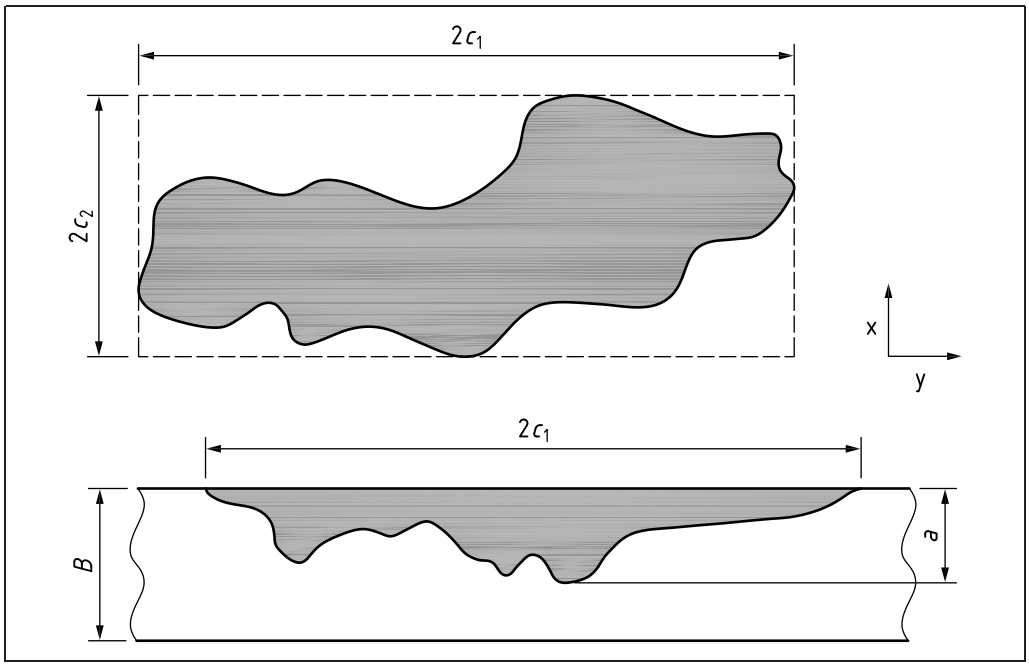
σ_{ref} is obtained from an appropriate reference stress solution (**G.4** to **G.6**);

f_c is a factor of safety (see **G.2.5**).

The reference stress solutions given in **G.4** to **G.6** are applicable only to the assessment of LTAs.

The methods for assessing LTAs are based on the assumption of a rectangular profile, i.e. the dimensions of the LTA are defined by its maximum depth and maximum lengths in the axial and circumferential directions (see Figure G.2). Methods based on a river-bottom profile of an LTA are given in ASME B31G and DNVGL-RP-F101 [G.3].

Figure G.2 **Dimensions of an LTA**



G.4 LTAs in a cylinder

G.4.1 Hoop stress

The reference stress is calculated from the following equation:

$$\sigma_{ref2} = \left[\frac{1 - \left(\frac{a}{B}\right)\frac{1}{Q}}{1 - \left(\frac{a}{B}\right)}\right]\sigma_2 \quad \text{(G.3)}$$

where:

$$Q = \sqrt{1 + 0.62\left(\frac{c_1^2}{r_o B}\right)} \quad \text{(G.4)}$$

G.4.2 Axial stress

The reference stress is calculated from the following equation:

$$\sigma_{ref1} = \left[\frac{\pi\left(1 - \frac{a}{B}\right) + 2\frac{a}{B}\sin\left(\frac{c_2}{r_o}\right)}{\left(1 - \frac{a}{B}\right)\left[\pi - \left(\frac{c_2}{r_o}\right)\left(\frac{a}{B}\right)\right]}\right]\sigma_1 \quad \text{(G.5)}$$

Fully circumferential corrosion can be assessed by setting c_2 equal to πr_o.

G.4.3 Hoop stress and axial stress

The reference stress is calculated from the following equation:

$$\sigma_{ref} = \max(\sigma_{ref1}, \sigma_{ref2}) \text{ for } \sigma_1 \geq 0 \text{ and } \sigma_2 \geq 0 \quad \text{(G.6)}$$

$$\sigma_{ref} = \sigma_{ref2} - \sigma_{ref1} \text{ for } \sigma_1 < 0 \text{ and } \sigma_2 > 0 \quad \text{(G.7)}$$

where:

σ_{ref1} is the reference stress based on the axial stress (**G.4.2**);

σ_{ref2} is the reference stress based on the hoop stress (**G.4.1**).

The assessment of an LTA subject to biaxial loading is based on the Tresca yield criterion. If the net axial stress is tensile, then the method in **G.4.3** reduces to those given in **G.4.1** and **G.4.2**; a separate check is required against both methods.

G.5 LTAs in a bend

G.5.1 Hoop stress

See Figure G.3 for the definition of the geometry. The reference stress is calculated from the following equation:

$$\sigma_{ref2} = 0.85 \left[\frac{1 - \frac{r_o}{2R}}{1 - \frac{r_o}{R}}\right] \left[\frac{1 - \left(\frac{a}{B}\right)\frac{1}{Q}}{1 - \left(\frac{a}{B}\right)}\right] \sigma_2 \quad \text{(G.8)}$$

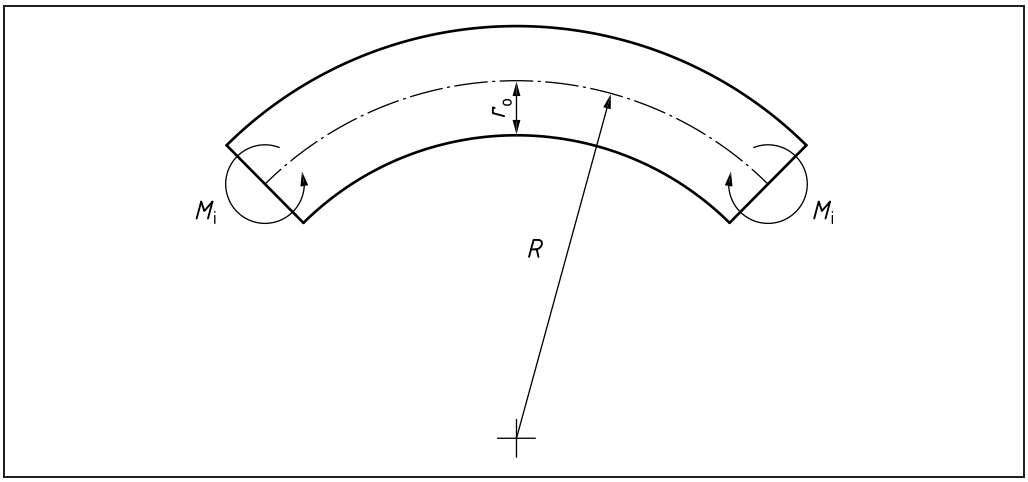
G.5.2 Axial stress

See Figure G.3 for the definition of the geometry. The reference stress is calculated from the following equation:

$$\sigma_{ref1} = \left[\sigma_1 + 0.9\left(\frac{{r_o}^2}{BR}\right)^{2/3} \left\{\frac{4r}{\pi\left[{r_o}^4 - (r_o - B)^4\right]}\right\} M_i\right] \left\{\frac{\pi\left(1 - \frac{a}{B}\right) + 2\frac{a}{B}\sin\left(\frac{c_2}{r_o}\right)}{\left(1 - \frac{a}{B}\right)\left[\pi - \left(\frac{c_2}{r_o}\right)\left(\frac{a}{B}\right)\right]}\right\} \quad \text{(G.9)}$$

Fully circumferential corrosion can be assessed by setting c_2 equal to πr_o.

Figure G.3 **Dimensions of a bend**



G.6 LTAs in a sphere or vessel end

See Figure G.4 for the definition of the geometry. The reference stress is calculated from the following equation:

$$\sigma_{\text{ref}} = \frac{3}{2}\left[\frac{1-\left(\frac{a}{B}\right)\frac{1}{M}}{1-\left(\frac{a}{B}\right)}\right]\sigma \qquad \text{(G.10)}$$

where:

$M = \sqrt{1+1.6\left(\frac{c^2}{r_{\text{eff}}B}\right)}$

r_{eff} is r_o for a sphere and spherical vessel end;

$= \frac{r_o}{3}\left[2+\left(\frac{r_o}{h}\right)^2\right]$ for an elliptical vessel end;

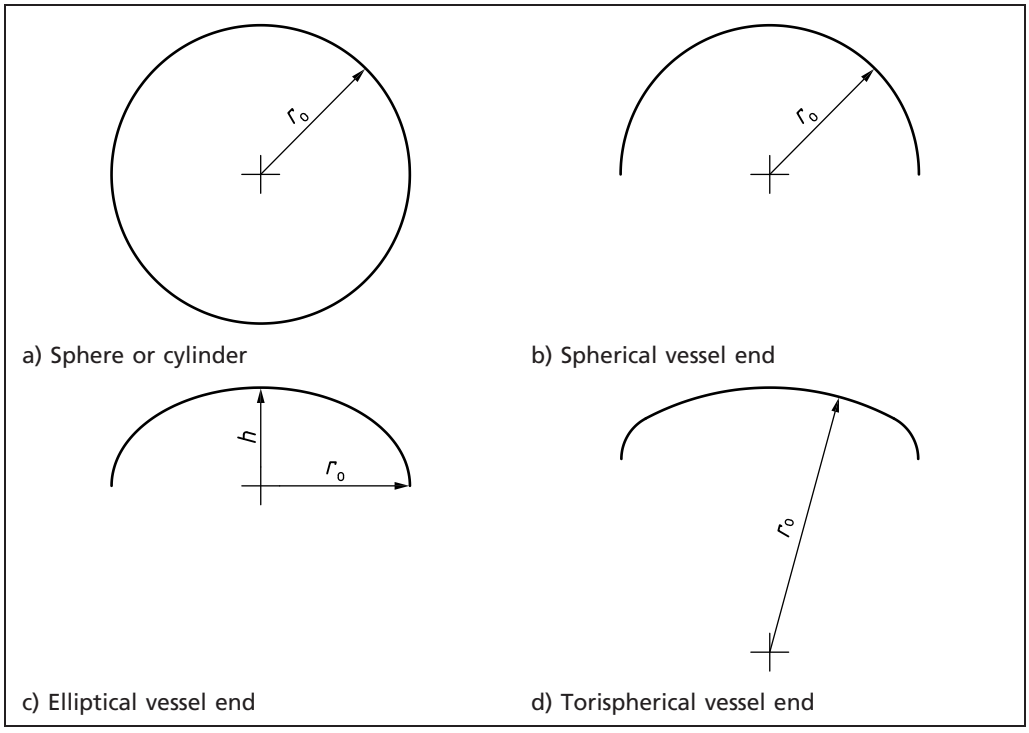
is r_o for a torispherical vessel end, where r_o is the radius of the spherical section of the end;

σ is the hoop stress in the sphere or vessel end.

NOTE 1 The equations are not applicable to shell junctions. The differences in radial stiffnesses between shells of different geometries can produce large bending stresses, and sometimes compressive hoop stress or elevated hoop stresses due to the mismatch.

NOTE 2 The equation for the effective radius for an elliptical vessel end is taken from ASME Boiler and Pressure Vessel Code, Section VIII. Different pressure vessel design codes might give different equations, as described in the relevant design code.

Figure G.4 **Dimensions of a sphere and vessel end**



G.7 Interaction

G.7.1 General

Adjacent LTAs can interact to produce a failure pressure that is lower than that due to either of the isolated LTAs (if they were treated as single flaws). Where interaction occurs, the equations in **G.4** to **G.6** may be used with the overall dimensions of the interacting cluster of adjacent LTAs.

G.7.2 Interaction rules

An LTA is considered to interact with an adjacent LTA if:

a) the axial spacing between the LTAs is less than or equal to the axial or circumferential length of the smaller LTA; or

b) the circumferential spacing between the LTAs is less than or equal to the axial or circumferential length of the smaller LTA; or

c) the spacing is less than 3B (B = wall thickness).

The interaction rule should be applied using the dimensions of individual LTAs, not the dimensions of a cluster of interacting LTAs.

The interaction rules are summarized in Figure G.5.

G.7.3 The size of interacting LTAs

The size of a cluster of interacting LTAs is defined by the overall size of the LTA, i.e. the enveloping rectangle.

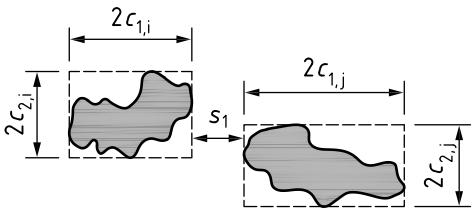
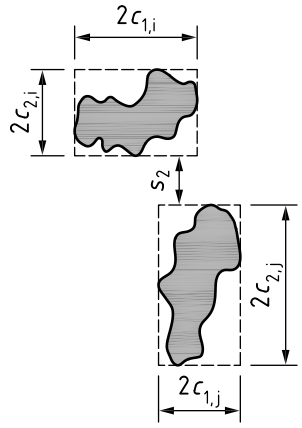
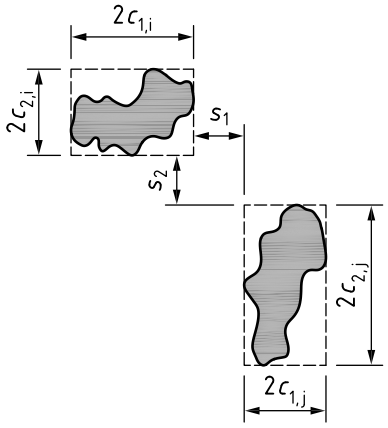
The depth of a cluster of interacting LTAs on a common surface is equal to the depth of the deepest LTA.

The depth of a cluster of interacting LTAs on opposite surfaces is equal to the sum of the depth of the deepest LTAs on the opposite surfaces.

G.8 Further assessment

This annex provides simple and conservative procedures for the assessment of LTAs in pipes or vessels. If the LTAs are found not to be acceptable using the methods given in this annex, alternative courses of action may be taken to assess the remaining strength of the pipe or pressure vessel more accurately. More accurate assessment methods are given in the published literature and in other standards, e.g. ASME B31G, DNVGL-RP-F101 [G.3] and API 579-1/ASME FFS-1. ASME B31G gives a method for assessing a river-bottom profile. DNVGL-RP-F101 gives an alternative method for assessing interaction, a method for assessing a river-bottom profile, and a method for assessing LTAs based on partial safety factors. Other alternatives include detailed finite element analysis and/or full-scale testing. The use of finite element analysis to analyse LTAs is discussed in **G.9**.

Figure G.5 **Interaction between LTAs**

Schematic flaws	Criteria for interaction	Effective dimensions after interaction
	$s_1 \leq 2c_{1,i}$ $(c_{1,i} < c_{1,j})$	$a = \max(a_i, a_j)$ $2c_1 = 2c_{1,i} + 2c_{1,j} + s_1$
	$s_2 \leq 2c_{2,i}$ $(c_{2,i} < c_{2,j})$	$a = \max(a_i, a_j)$ $2c_2 = 2c_{2,i} + 2c_{2,j} + s_2$
	$s_1 \leq 2c_{1,i}$ $(c_{1,i} < c_{1,j})$ and $s_2 \leq 2c_{2,i}$ $(c_{2,i} < c_{2,j})$	$a = \max(a_i, a_j)$ $2c_1 = 2c_{1,i} + 2c_{1,j} + s_1$ $2c_2 = 2c_{2,i} + 2c_{2,j} + s_2$

G.9 Recommendations for conducting non-linear finite element analysis of corrosion flaws in pipelines, pipework and pressure vessels

G.9.1 General

Finite element analysis (FEA) may be used to determine the failure pressure of an internally pressurized ductile pipeline, pipework or a pressure vessel containing LTAs. This approach is particularly suited to assessing LTAs close to or at a major structural discontinuity or if the LTA is subject to external loads, and to assessing LTAs using detailed thickness profile data which can be directly mapped into a three-dimensional finite element model.

The advice given in this subclause provides the necessary details to conduct an FEA with regard to generating a finite element mesh, selection of materials properties, application of loads, post processing of results and the determination of the failure pressure in pipelines, pipework and pressure vessels containing LTAs. The guidance given in this subclause is independent of the finite element code.

G.9.2 Analysis of LTAs in pipelines, pipework and pressure vessels

LTAs in pipelines, pipework or pressure vessels should be assessed using an elastic-plastic FEA. This approach allows the redistribution of stress to be considered directly in the analysis. The plastic collapse load is obtained using an FE model of the structure containing the LTA that incorporates an elastic-plastic material model. The plastic collapse load is predicted by performing an elastic-plastic analysis of the structure subject to specified loading conditions in accordance with a) to f) below.

a) Create a finite element model using the geometry of the structure and the LTAs (including sizing errors as appropriate), the materials properties and the structure constraints and applied loads.

b) Perform a non-linear large-deformation stress analysis of the structure subject to the specified loading conditions.

c) Examine the results of the stress analysis.

d) Determine the failure or critical load based on the variation of local stress or strain states with reference to a validated failure criterion, such as that given in e) and f) below. If the applied loading results in a compressive stress field, then a further FE analysis to determine the critical buckling load should be conducted. All possible buckling mode shapes should be considered in determining the buckling load.

e) For LTAs in pipeline or pipework remote from structural discontinuities, a suitable failure criterion for internal pressure loading is given in **G.9.10**. A factor of safety should be applied to the predicted failure pressure to determine the acceptability of the LTA (see **G.2.5**).

f) For LTAs in pressure vessels, or close to structural discontinuities (such as heads, nozzles or saddles), where the stress field is more complex and there can be significant additional loads, the failure criterion given in **G.9.10** might not be applicable. The acceptability of the LTA should be assessed by considering the predicted load for instability of the LTA (local collapse) and the vessel as a whole (global collapse) and comparing these with the design loads. The local strain state in the LTA should be limited to 2% plastic strain [G.4]. In principle, a strain limit should be related to the uniform elongation of the material rather than being a fixed value. Data on uniform elongation is typically not available. Full-scale testing would be required to validate the use of a strain limit higher than 2% plastic strain.

G.9.3 Modelling

The use of actual pipe or vessel and LTA sizes is preferable but it is not always necessary. The shape of an LTA may be simplified, but its maximum dimensions (axial length, circumferential width and depth) should be retained. Account should also be taken of possible uncertainty in the measurement of the dimensions of the LTA. The minimum value of the wall thickness measured in a local region around the LTA should be used to represent the undamaged component.

The length of pipeline/pipework section simulated should be at least five times the pipe diameter or the axial length of the LTA, whichever is the longer. It might be necessary to include any adjacent features that could cause failure remote from the LTA (i.e. global collapse).

G.9.4 Mesh design

The finite element mesh should be designed to model accurately the structure being analysed. If thickness profile data is available for the LTA, it may be directly mapped into the FE model. In general, regions where high stress

gradients are expected to occur require a fine, uniform mesh compared to regions where stress gradients are less severe. Preliminary sensitivity studies should be undertaken with meshes of increasing refinement. The mesh may be considered adequate once further refinement does not significantly influence the results obtained. The element type should be adequate for the analysis being undertaken. Three-dimensional continuum elements are preferred to shell elements. Second order, 20 noded, reduced integration hexahedral elements should be used. Severe element distortions, especially at the minimum ligament of the LTA, should be avoided. If shell elements are used, they should include variable wall thickness in the formulation and allow the section to be offset to represent internal or external material loss at the LTA. A minimum of 11 material integration points should be used through the thickness.

G.9.5 Boundary conditions

Boundary conditions should be applied to simulate the restraints on the structure and to suppress rigid body movement. The application of appropriate boundary conditions requires an understanding of the general deformation of the structure containing the LTA under its specific operating condition and experience in idealization of structural supporting conditions. For example, for buried or anchored straight pipeline/pipework sections, the boundary conditions used should restrict axial displacement of the pipe. Symmetry boundary conditions can significantly reduce the computer run times and disc space requirements. Symmetry should be used with care for LTAs as they are likely to be asymmetric. If the failure involves buckling, symmetry boundary conditions should not be used as they suppress asymmetric buckling modes.

G.9.6 Applied loading

Forces, external displacements, moments and pressures, etc., should be applied to the FE model to simulate the applied loading. These loads should include service and possible fault or test conditions, taking account of uncertainty in the estimation. If there are multiple loads, the possible combinations of these should be determined to ensure that the worst case is identified.

G.9.7 Materials properties

The required elastic properties in the FE analysis are the elastic modulus and Poisson's ratio. The materials properties used should be adequate for the structure being analysed. Non-linear analysis requires definition of a true stress versus true strain curve of the material over the full range expected in the analysis. This may be constructed from true stresses and strains measured from a tensile test on a round bar specimen. Tensile tests should be conducted at a temperature relevant to the operating condition. Some materials exhibit anisotropic behaviour and hence the test specimen(s) should be taken from both the transverse and longitudinal direction. The true stress versus true strain curve used in the FE analysis should be selected depending on the level of anisotropy exhibited by the material, the mode of loading and the orientation of the LTA.

Alternatively, an approximation to a true stress versus true strain curve may be obtained by converting an engineering stress versus strain curve and linearly extrapolating the curve from the point at its tensile strength in a log-log plot.

Such an approximation generally gives lower bound stress values, particularly at high strain levels. This approach leads to conservative failure predictions.

If actual materials properties are not available then stress versus strain curves may be defined in the following ways:

a) as an elastic-perfectly plastic curve, where a single value of stress which defines the limit of proportionality is required;

b) as a bi-linear curve, where two stress-strain coordinates, of which one defines the limit of proportionality, are required. The second coordinate should be chosen to give a conservative representation of the anticipated material behaviour;

c) as an approximate mathematical relationship such as the Ramberg-Osgood equation, which has been fitted to appropriate materials data. A method for estimating the parameters of the Ramberg-Osgood equation is given in **7.1.3.5**.

G.9.8 Analysis

The finite element stress analysis should be performed using a non-linear analysis procedure that incorporates material plasticity, large strain and large displacement theory. Where significant compressive loads are applied, such as external bending of a pipeline, the analysis procedure should allow for the occurrence of local or global buckling.

The von Mises yield criterion and associated flow rule should be used in the non-linear stress analysis. If the structure is subjected to quasi-static loading, isotropic hardening should be selected. The analysis of significant cyclic loading requires consideration of the cyclic stress-strain behaviour and more complex hardening rules.

Static stress analysis procedures (ignoring dynamic or inertia effects) should generally be used. The sequence of application of loads should be chosen to represent the service condition, as in a non-linear analysis the principle of superposition does not apply. In many cases it is appropriate to apply the pressure load as an initial load and then increment any external loads up to the maximum. The loading increment should be sufficiently small to ensure convergence. Automatic loading incrementation algorithms may be used. However, the termination of an automatic algorithm should not be taken as a structural failure condition, as this can give results which are dependent on the specific FE code or convergence tolerances used.

G.9.9 Assessment of analysis results

Results of von Mises equivalent stress variations and/or equivalent plastic strain variations against loading values should be obtained from the FEA. The stress and/or strain values from one or more positions within the LTA, at which high von Mises equivalent stresses are predicted, should be examined.

In general, the stress variations with increasing load show three distinct stages. The first is a linear response progressing to a point when the limit of proportionality defined by the stress versus strain curve is first reached. At this point a second stage is evident, i.e. a stage where plasticity spreads through the ligament while the maximum von Mises equivalent stress remains approximately constant or increases slowly. This is due to constraint from the surrounding wall. The third stage is dominated by material hardening and begins when the von Mises equivalent stress in the entire ligament exceeds the material's yield strength. Once this stage is reached, the whole ligament deforms plastically but failure does not occur immediately due to strain hardening.

The analysis results should be checked to ensure that failure is not predicted at other parts of the structure remote from the area of metal loss.

G.9.10 Prediction of failure pressure in pipelines and pipework

A method for predicting the failure pressure has been developed and validated against a database of ring expansion and vessel burst test results ([G.5] to [G.13]) where the primary mode of loading was that due to internal pressure. The

range of validity of the tests covers line pipe of strengths up to API 5L grade 690M/X100M, nominal diameter 300 mm to 1 320 mm; nominal wall thickness 4.5 mm to 25.4 mm; and diameter to wall thickness ratio 30 to 100.

The failure pressure may be determined from the von Mises equivalent stress through the minimum ligament of the LTA. The predicted failure pressure is the pressure that causes the averaged von Mises equivalent stress in the ligament to be equal to the material's true tensile strength from a uniaxial tensile test. A factor of safety should be applied to the predicted failure pressure to determine the acceptability of the LTA (see **G.2.5**).

Bibliography for Annex G

Standards publications

For dated references, only the edition cited applies. For undated references, the latest edition of the referenced document (including any amendments) applies.

API 579-1/ASME FFS-1, *Fitness-for-Service*

ASME Boiler and Pressure Vessel Code, Section XI: *Rules for inservice inspection of nuclear power plant components*

ASME B31G, *Manual for determining the remaining strength of corroded pipelines*

Other documents

[G.1] COSHAM, A. and ANDREWS, R.M. The assessment of locally thinned areas: Background to the guidance given in Annex G of BS 7910:2013. *In: International Journal of Pressure Vessels and Pipelines*, January 2019, 169, 177–187. <https://doi.org/10.1016/j.ijpvp.2018.12.008>

[G.2] COSHAM, A. and ANDREWS, R.M. The assessment of locally thinned areas subject to a hoop stress and an axial stress: Background to the guidance given in Annex G of BS 7910:2013. *In: Proceedings of the ASME 2019 38th International Conference on Ocean, Offshore and Arctic Engineering*, OMAE2019, June 9–14, 2019, Glasgow, Scotland, OMAE2019-95532.

[G.3] DNV GL. *Corroded pipelines*. DNVGL-RP-F101. Norway: DNV GL, 2019.

[G.4] SIMS, J.R., HANTZ, B.F. and KUEHN, K.E. A basis for the fitness-for-service evaluation of thin areas in pressure vessels and storage tanks. *In:* BHANDARI, S., MILELLA, P.P. and PENNELL, W.E. eds. *Pressure vessel fracture, fatigue and life management. Proceedings of Pressure vessels and piping conference*, New Orleans, LA, 21–25 June 1992. ASME PVP Vol. 233. New York: ASME, 1992. 51–58. ISBN 0791807746.

[G.5] BATTE, A.D., FU, B., KIRKWOOD, M.G. and VU, D. Advanced methods for integrity assessment of corroded pipelines. *In: Pipes and Pipelines International*, 1997, 42(1), 5–11. ISSN 0032-020X.

[G.6] BATTE, A.D., FU, B., KIRKWOOD, M.G., and VU, D. New methods for determining the remaining strength of corroded pipelines. *In:* C. GUEDES-SOARES et al., eds. *Proceedings of 16th offshore mechanics and arctic engineering conference*, Yokohama, Japan, 13–17 April 1997. New York: ASME, 1997, Vol. 5, 221–228. ISBN 071818039.

[G.7] CHAUHAN, V., SWANKIE, T., ESPINER, R. and WOOD, I. Developments in methods for assessing the remaining strength of corroded pipelines. Paper No. 09115, *In: Proceedings of NACE International Corrosion 2009 Conference and Expo*, Atlanta, Georgia, USA, 22–26 March 2009.

[G.8] CHAUHAN, V., and CROSSLEY, J. *Project #153H Corrosion assessment guidance for high strength steels (Phase 1).* GL Industrial Services Ltd. Report 9017 Issue 4.0, August 2009. <https://primis.phmsa.dot.gov/matrix/FilGet.rdm?fil=4877>

[G.9] LIU, J., MORTIMER, L. and WOOD, A. *Project #153H Corrosion assessment guidance for high strength steels (Phase 2)*. GL Industrial Services Ltd. Report 7930, Issue 3.1, November 2009. <https://primis.phmsa.dot.gov/matrix/FilGet.rdm?fil=5334>

[G.10] CHAUHAN, V. and BRISTER, J. *A review of methods for assessing the remaining strength of corroded pipelines.* GL Industrial Services Ltd. Report 6781. Issue 6.1, November 2009. <http://primis.phmsa.dot.gov/matrix/FilGet.rdm?fil=5278>

[G.11] CHAUHAN, V. and SWANKIE, T. *Project #153M Guidance for Assessing the Remaining Strength of Corroded Pipelines.* GL Noble Denton Report 9492, Issue 3.0, September 2015, US Department of Transportation Pipeline and Hazardous Materials Safety Administration Research and Development website. <https://primis.phmsa.dot.gov/matrix/FilGet.rdm?fil=5684>

[G.12] LIU, J. CHAUHAN, V., NG, P., WHEAT, S and HUGHES, C. *Project #153J Remaining Strength of Corroded Pipe Under Secondary (Biaxial) Loading*. GL Noble Denton Report R9068, Issue 3.0, August 2009, US Department of Transportation Pipeline and Hazardous Materials Safety Administration Research and Development website. <https://primis.phmsa.dot.gov/matrix/FilGet.rdm?fil=4876>

[G.13] MARTIN, M., ANDREWS, R.M. and CHAUHAN, V., *Project #153L The Remaining Strength of Corroded Low Toughness Pipe.* GL Noble Denton Report R9247, Issue 3.0, February 2009, US Department of Transportation Pipeline and Hazardous Materials Safety Administration Research and Development website. <https://primis.phmsa.dot.gov/matrix/FilGet.rdm?fil=12494>

Annex H (informative)

Reporting of assessments

H.0 Symbols and definitions

For the purposes of this annex, the following symbols, definitions and units apply, unless otherwise indicated at the point of use.

Symbol	Definition	Units
A	Constant in fatigue growth relation	see footnote H.1)
C	Material and temperature dependent constant in creep assessment	—
C^*	Creep fracture/crack growth parameter	$MPamh^{-1}$
C_1	Constant in the stress corrosion crack growth equation	see footnote H.2)
E	Elastic modulus	N/mm^2
K	Stress intensity factor (SIF)	$N/mm^{3/2}$
K_{ISCC}	Critical stress intensity factor for stress corrosion cracking	$N/mm^{3/2}$
K_{mat}	Material fracture toughness measured by stress intensity factor	$N/mm^{3/2}$
K_r	Fracture ratio	—
k_m	Stress magnification factor due to misalignment	—
L_r	Ratio of applied load to yield load	—
m	Exponent in fatigue crack growth law (**H.3**)	—
m	Function of yield strength and tensile strength, used in converting K_{mat} to δ_{mat} and vice versa (**H.2**); see Equation (7.16) and Equation (7.17)	—
n	Power-law creep stress exponent	—
$n(scc)$	Exponent in the stress corrosion crack growth relationship	—

H.1) The units and value of A depend on those used to measure da/dN and ΔK, and on the value of the exponent, m. If A is known in one set of units, A_a, the corresponding value for another set of units, A_b is given by:

$$A_b = A_a \frac{f_a}{f_b{}^m}$$

where:

f_a is the conversion factor for da/dN from the first to the second unit system; and

f_b is the conversion factor for ΔK from the first to the second unit system.

H.2) The units and value of C depend on those used to measure da/dt and ΔK, and on the value of the exponent, n. If C is known in one set of units, C_a, the corresponding value for another set of units, C_b, is given by:

$$C_b = C_a \frac{f_a}{f_b{}^n}$$

where:

f_a is the conversion factor for da/dN from the first to the second unit system; and

f_b is the conversion factor for ΔK from the first to the second unit system.

(continued)

Symbol	Definition	Units
P_b	Primary bending stress	N/mm^2
P_m	Primary membrane stress	N/mm^2
Q_b	Secondary bending stress	N/mm^2
Q_m	Secondary membrane stress	N/mm^2
Q	Exponent in creep crack growth equation	—
t_r	Time to rupture determined from creep rupture curve	h
$t_{r,ref}$	Time to creep rupture at reference stress	h
t_i	Crack initiation time, prior to commencement of creep crack growth	h
γ_c	Safety factor for use with creep data	—
ΔP_b	Primary bending stress range	N/mm^2
ΔP_m	Primary membrane stress range	N/mm^2
ΔQ_b	Secondary bending stress range	N/mm^2
ΔQ_m	Secondary membrane stress range	N/mm^2
ε_f	Strain to failure of material, as measured in uniaxial creep test	—
σ_U	Tensile strength	N/mm^2
σ_Y	Lower yield strength or 0.2% proof strength	N/mm^2
σ_{ref}	Reference stress used for creep and plastic collapse consideration	N/mm^2

H.1 General

Reports of assessments carried out in accordance with this British Standard form part of the quality audit. The report should include details of the standards and quality systems used. The information in this annex should be listed as well as comments on uncertainties and reliability.

H.2 Fracture assessments

H.2.1 Analysis details

Analysis details should include:

a) the option of analysis used (1, 2 or 3);

b) whether allowance for mismatch (Annex I) or constraint (Annex N) is included.

H.2.2 Input data

The input data are as follows.

a) *Loading conditions*. Normal operation, fault or transient conditions, 100 year storm, etc.; additional loads and stresses considered (e.g. system stresses, residual stresses); categorization of loads and stresses; stress analysis method (finite element, classical analysis); temperature. Input parameters: P_m, P_b, Q_m, Q_b, SCF.

b) *Materials properties*. Material specification, weld procedure; tensile properties, weld metal and/or parent material yield strength and ultimate strengths at temperature of interest, stress-strain data for Options 2 and 3 assessments; mismatch ratio for Annex I; fracture toughness at temperature

 © The British Standards Institution 2019

of interest; any statistical corrections to fracture toughness in Annex L; whether data are obtained by direct testing or indirect means; source and validity of all data. Input parameters: σ_Y, σ_U, E, stress-strain data, K_{mat}, m.

c) *Definition of flaw*. Flaw type, location, orientation, shape and size; allowance for sizing uncertainties; characterization of multiple flaws, allowance for low toughness high strength situations, whether recharacterization of flaw has been undertaken.

d) *Flaw growth*. Whether any allowance is made for crack extension by sub-critical crack growth mechanism (e.g. ductile tearing, fatigue, creep, stress corrosion); the crack growth laws employed.

e) *Plastic limit load*. Source of limit load and net section stress solutions (e.g. established analysis, non-linear finite element analysis, scale model testing); whether local and/or global collapse are considered.

f) *Stress intensity factor solution*. Source of K solution (e.g. Annex M, published solution, finite element analysis).

H.2.3 Results

The results for each assessment undertaken should include:

- assessment points (L_r, K_r) for the initiation analyses;
- assessment loci (L_r, K_r) for flaw stability analyses;
- assessment points/loci displayed on the appropriate failure assessment diagram;
- reserve factors.

H.2.4 Sensitivity analysis

Input the parameters against which sensitivity studies have been undertaken (e.g. flaw size, materials properties, loading conditions), and the results of each individual study.

Known conservatisms incorporated in the assessment should be listed. In addition, any departures from the recommendations laid down in this British Standard should be reported and justified. A separate statement should be made about the significance of potential failure mechanisms remote from the flawed areas and failures of the flawed area by mechanisms other than fracture (see Clause **8** to Clause **10**).

H.3 Fatigue assessments

H.3.1 Method and criterion of acceptance

General procedure using fracture mechanics (e.g. to show that a flaw is not likely to grow to a critical size in a specified time) or simplified procedure using quality category *S-N* curves (e.g. to show that a flaw has a longer fatigue life than an adjacent standard weld detail). If the quality category method is used, the required quality category should be stated.

H.3.2 Input data

The input data are as follows.

a) *Loading conditions*. Load spectrum; additional loads and stresses considered (e.g. misalignment, residual stresses); categorization of loads and stresses; stress analysis method (e.g. elastic theory, finite element analysis, experimental); cyclic frequency, resolution of variable amplitude loading. Input parameters: ΔP_m, ΔP_b, ΔQ_m, ΔQ_b, k_m.

b) *Operating conditions*. Temperature, environment, etc.

c) *Materials properties*. Material specification, tensile properties, material parameters for the fatigue crack growth law. Input parameters: σ_Y, E, A, m.

d) *Definition of flaw*. Flaw type, location, orientation, shape and size; allowance for sizing errors; whether recategorization of flaw has been undertaken.

e) *Planar flaw growth*. Fatigue crack growth law; fatigue crack growth threshold, choice of quantity category and *S-N* curve.

f) *Limit to crack growth*. Critical flaw size and shape (in which case state the criterion); plate thickness, etc.

g) *Stress intensity factor solution*. Source of K (e.g. Annex M published solution, finite element analysis).

H.3.3 Results

Provide full details of the results, including any relevant graphs (e.g. flaw length versus number of cycles) and conclusions drawn. The results should include details of any other assessment (e.g. fracture assessment) of the flaw being considered.

H.3.4 Sensitivity analysis

Input the parameters against which sensitivity studies have been undertaken (e.g. flaw size, materials properties, loading conditions), and the results of each individual study.

Known conservatisms incorporated in the assessment should be listed. In addition, any departures from the recommendations laid down in this British Standard should be reported and justified.

H.4 Creep assessments

H.4.1 Analysis details

In the analysis, any initiation period, the extent of crack growth and damage accumulation in the ligament ahead of the crack tip are estimated for a cracked component which undergoes creep.

H.4.2 Input data

The input data are as follows.

a) *Loading conditions*. These should include those specified in **H.2.2** and **H.3.2**, and the relevant temperature history.

b) *Materials properties.* Creep deformation, creep rupture and creep crack growth properties of weld metal, HAZ and/or parent material as appropriate; source and validity of all data. Input parameters: C, n, q, t_r, ε_f.

c) *Definition of flaws*. As for **H.2.2.**

d) *Crack initiation and growth*. Crack initiation and growth laws employed, to include all mechanisms of sub-critical crack extension (see **H.2.2** and **H.3.2**).

e) *Creep fracture parameter*, C^*. Source of solution for C^* (e.g. Annex S, published solution, finite element analysis); values of K, σ_{ref}, $t_{r,ref}$ used to estimate C^*.

 © The British Standards Institution 2019

H.4.3 Results

The results for loading and temperature conditions assessed should include:

- initiation period, t_i, at 0.5 mm of crack extension crack size versus time;
- crack growth rates plots versus C^* checks on extent of fatigue and creep crack growth and risk of fracture;
- assessment of margins against failure.

H.4.4 Sensitivity analysis

Input the parameters against which sensitivity studies have been undertaken (e.g. flaw size, loading conditions, materials properties, safety factor γ_c for use with creep data), and the results of each individual study.

Known conservatisms incorporated in the assessment should be listed. In addition, any departures from the recommendations in this British Standard should be recorded and justified.

H.5 Assessments of other modes of failure

H.5.1 Analysis details

Analysis details should include a description of the other modes of failure that are being assessed and, if applicable, details of the environmental effects that are being considered, with reference to **H.2.1** and **H.3.1** as appropriate.

H.5.2 Input data

The input data are as follows.

a) *Loading conditions*. As for **H.2.2** and **H.3.2**, dependent on mode of failure.

b) *Operating conditions*. Temperature, environment, etc.

c) *Materials properties*. Material specification, weld procedure; tensile properties, weld metal and/or parent material yield strength and ultimate strengths at temperature of interest; source and validity of all data. Input parameters: σ_Y, σ_U; also K_{ISCC} and as for **H.2.2** and **H.3.2**, dependent on mode of failure.

d) *Definition of flaw*. As for **H.2.2** and **H.3.2**, dependent on failure mode.

e) *Flaw growth*. Environmental effects, dependent on mode of failure: corrosion and/or erosion; environmentally assisted cracking, C_1, *n(scc)* or corrosion fatigue date; source and validity of all data.

H.5.3 Results

The results should be the same as for **H.2.3** and **H.3.3**.

H.5.4 Sensitivity analysis

Input the parameters against which sensitivity studies have been undertaken (e.g. flaw size, materials properties, loading conditions, environmental effects), and the results of each individual study.

Known conservatisms incorporated in the assessment should be listed. In addition, any departures from the recommendations laid down in this British Standard should be recorded and justified.

Bibliography for Annex H

There are no references in this annex.

 © The British Standards Institution 2019

Annex I (informative)

The significance of strength mismatch on the fracture behaviour of welded joints

I.0 Symbols and definitions

For the purposes of this annex, the following symbols, definitions and units apply, unless otherwise indicated at the point of use.

Symbol	Definition	Units
a	Half flaw length for through-thickness flaw, flaw height for surface flaw or half height for embedded flaw	mm
E	Elastic modulus	N/mm^2
E^{P}	Parent metal elastic modulus	N/mm^2
E^{W}	Weld metal elastic modulus	N/mm^2
F	Scalar characterizing the magnitude of the loads giving rise to primary stresses	N
F_e^{M}	Limit load solution of the mismatch configuration	N
F_e^{P}	Limit load solution for a homogeneous component made of material with yield strength σ_Y^{P}	N
h	Half weld width	mm
K_{mat}	Material fracture toughness	N/mm$^{3/2}$
K_r	Fracture ratio	—
L_r	Ratio of applied load to yield load	—
$L_{r,max}$	Permitted limit of L_r	—
M	Strength mismatch or mismatch ratio, which is the ratio of the yield strength of the weld metal to that of the parent material	—
$M(\varepsilon_{pl})$	Mismatch ratio at a number of plastic strain values, ε_{pl}	—
N	Strain hardening exponent as in Equation (7.27)	—
N^{M}	Strain hardening exponent of a mismatched system	—
N^{P}	Strain hardening exponent of parent metal	—
N^{W}	Strain hardening exponent of weld metal	—
P	Primary stress	N/mm^2
P_m, P_b	Primary membrane and bending stresses	N/mm^2
Q	Secondary stress	N/mm^2
Q_m, Q_b	Secondary membrane and bending stresses	N/mm^2
R_{eH}^{P}	Upper yield strength of the parent metal	N/mm^2
R_{eH}^{W}	Upper yield strength of the weld metal	N/mm^2
$\Delta\varepsilon^{P}$	Change in strain of parent metal used in strength mismatch calculations	—
$\Delta\varepsilon^{W}$	Change in strain of weld metal used in strength mismatch calculations	—
ε_{pl}	Plastic strain	—
λ	Parameter used in constructing Option 1 FAD	—
λ^{M}	Parameter used in mismatch analysis	—
λ^{P}	Parameter of parent metal used in mismatch analysis	—
λ^{W}	Parameter of weld metal used in mismatch analysis	—

(continued)

Symbol	Definition	Units
μ	Parameter used in constructing FAD line, taken as the minimum value of either 0.001(E/σ_Y) or 0.6	—
μ^M	Parameter used in mismatch analysis	—
μ^P, μ^W	Parameter of parent metal and weld metal used in mismatch analysis	—
ν	Poisson's ratio	—
$\sigma^M(2\%)$	Equivalent yield strength at 2% plastic strain for a strength mismatch geometry	N/mm^2
$\sigma^M(9\%)$	Equivalent yield strength at 9% plastic strain for a strength mismatch geometry	N/mm^2
$\sigma^M(\varepsilon_{pl})$	Equivalent stress strain curve for use in constructing an Option 2M FAD	N/mm^2
$\sigma^P(\varepsilon_{pl})$	Uniaxial stress strain curve of parent metal for use in constructing an Option 2M FAD	N/mm^2
$\sigma^P(2\%)$	Parent metal strength at 2% plastic strain	N/mm^2
$\sigma^P(9\%)$	Parent metal strength at 9% plastic strain	N/mm^2
σ_U^P, σ_U^W	Tensile strength of parent and weld metal respectively, used in mismatch solutions	N/mm^2
$\sigma^W(\varepsilon_{pl})$	Uniaxial stress strain curve of weld metal for use in constructing an Option 2M FAD	N/mm^2
$\sigma^W(2\%)$	Weld metal strength at 2% plastic strain	N/mm^2
$\sigma^W(9\%)$	Weld metal strength at 9% plastic strain	N/mm^2
σ_Y	Lower yield strength or 0.2% proof strength	N/mm^2
σ_Y^M	Equivalent yield strength for a strength mismatch geometry	N/mm^2
σ_Y^P	Yield strength of the parent material	N/mm^2
σ_Y^W	Yield strength of the weld material	N/mm^2
ψ	Normalization parameter used in the analysis of welded joints with strength mismatch, defined on a case-by-case basis for each geometry (see Annex P)	—

I.1 General

Unlike homogeneous geometries, welded joints exhibit various patterns of plasticity development, which are due to the presence of material strength mismatch. The occurrence of the various plasticity patterns is dependent on:

a) the strength mismatch factor or the mismatch ratio *M*, which is the ratio of the yield strength of the weld metal to that of the parent; and

b) the geometrical parameters such as the width of the welded structure to be assessed, the crack size, the section thickness and the weld width. These are taken into account in the dimensionless normalization parameter ψ, which is defined on a case-by-case basis for each geometry.

Limit load solutions for welded components given in Annex P are for a flaw at the centre line of the weld material and also at the interface between the weld material and parent material.

For more complex geometries, further development of limit load solutions is required. Pending such solutions, when solutions are not available for the particular geometry of interest, the mismatch effect on the limit load may be

roughly estimated from the existing solutions listed in Annex P or by using finite element (FE) modelling.

This annex on mismatch should not be used in conjunction with Annex N.

I.2 Background and applicability

This annex contains modifications to the procedure outlined in Clause **7** and addresses the significance of strength mismatch in fracture behaviour of welded structure. The effect of strength mismatch is more significant in the post-yield (plastic) regions and the definition of L_r and FAD is therefore modified for higher L_r values, e.g. $L_r > 0.8$.

Assessment procedures usually consider combined primary stresses, P (P_m and P_b), and secondary stresses, Q (Q_m and Q_b). However, research on the subject of strength mismatch is currently focussed mostly on the primary stresses, and caution should therefore be exercised in using increased load margins in cases where secondary stresses dominate. Results of analyses considering primary loadings suggest that margins are little affected for small primary loads, specifically for $L_r < 0.8$.

This annex is therefore more applicable to components loaded predominantly by mechanical loads, than, for example, to as-welded components containing high residual stresses.

The presence of mismatch in a welded joint changes the pattern of yielding and associated crack tip constraint. Treatment of constraint for homogenous materials is provided in Annex N. However, Annex I should not be used in combination with Annex N.

The procedures in this annex may be applied to multi-material combinations provided that relevant input data, particularly mismatch limit load solutions, are available. Currently, only two-material limit load solutions are available (see Annex P) and this annex is therefore limited to two-material models only. It might, however, be possible to use available solutions for a multi-material configuration by simplifying it to combinations of two-material configurations, and use the procedure detailed in **I.3**.

The method used is not suitable for two materials with very different values of E and ν, and is intended for assessment of crack initiation only.

The procedures outlined in this annex are underpinned by the reference stress J prediction method using an equivalent stress-strain relationship for a flawed body with strength and strain hardening mismatch (see [I.1] and [I.2]). The general method given in **I.3.8** Option 2M is described in [I.3] to [I.5] and the method given in **I.3.8** Option 1M is described in [I.6].

I.3 Strength mismatch assessment procedure

I.3.1 General

The procedure described in **I.3** is similar to that in **7.2**, with some modifications in order to include the effect of strength mismatch. The main change involves the determination of a mismatch limit load using the solutions provided in Annex P based on the equivalent stress-strain relationship of an equivalent material in Step 2 and subsequently used to construct the FAD and to define L_r in Step 6.

For the mismatch procedure the following steps should be completed.

a) Step 1: ensure that the information associated with **7.2.4**, **7.2.5** and **7.2.7** is available.

b) Step 2: determine tensile properties for the constituent materials in the vicinity of the crack (**I.3.2**), including the definition of the tensile properties

for an "equivalent" material (**I.3.2**) if Option 1M (**I.3.7**) or Option 2M (**I.3.8**) FAD is selected respectively.

c) Step 3: select and define the FAD (**I.3.6**).

d) Step 4: determine the fracture toughness of the material of interest (**I.3.3**).

e) Step 5: calculate K_r (**I.3.4**).

f) Step 6: calculate L_r from the mismatch limit load solution (**I.3.5** and Annex P).

I.3.2 Material tensile properties

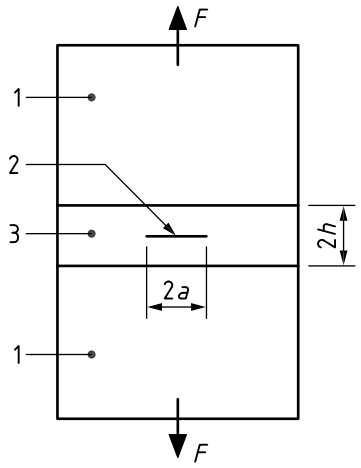
The tensile properties of the constituent materials in the vicinity of a crack should be defined. For the assessment of welded joints, it is conservative to use the tensile properties of the weaker material as suggested in **7.2**. Following the procedures in **7.1.3**, the relevant yield, ultimate tensile and flow strengths enable the Option 1 FAD of **7.3.3** to be defined. Where the Option 2 FAD in **7.3.4** is to be determined, it is also necessary to determine the uniaxial tensile stress-strain curve for the weaker material.

To reduce the conservatism, the tensile properties of both weld and parent materials should be taken into account. An equivalent material should be defined to represent the entire welded joint using limit load solutions provided in Annex P, and the procedure as detailed below should be followed.

Define the mismatch ratio, M, for the geometry of interest. For the idealized two-material geometry shown in Figure I.1 the mismatch ratio is defined by Equation (I.1):

$$M = \frac{\sigma_Y^W}{\sigma_Y^P} \tag{I.1}$$

Figure I.1 **Idealized weld geometry – the parent and weld metals have yield strengths of σ_Y^W and σ_Y^P respectively**



Key

1 Parent material

2 Crack [A)]

3 Weld [B)]

[A)] 2*a* denotes the crack length.

[B)] 2*h* denotes the weld width.

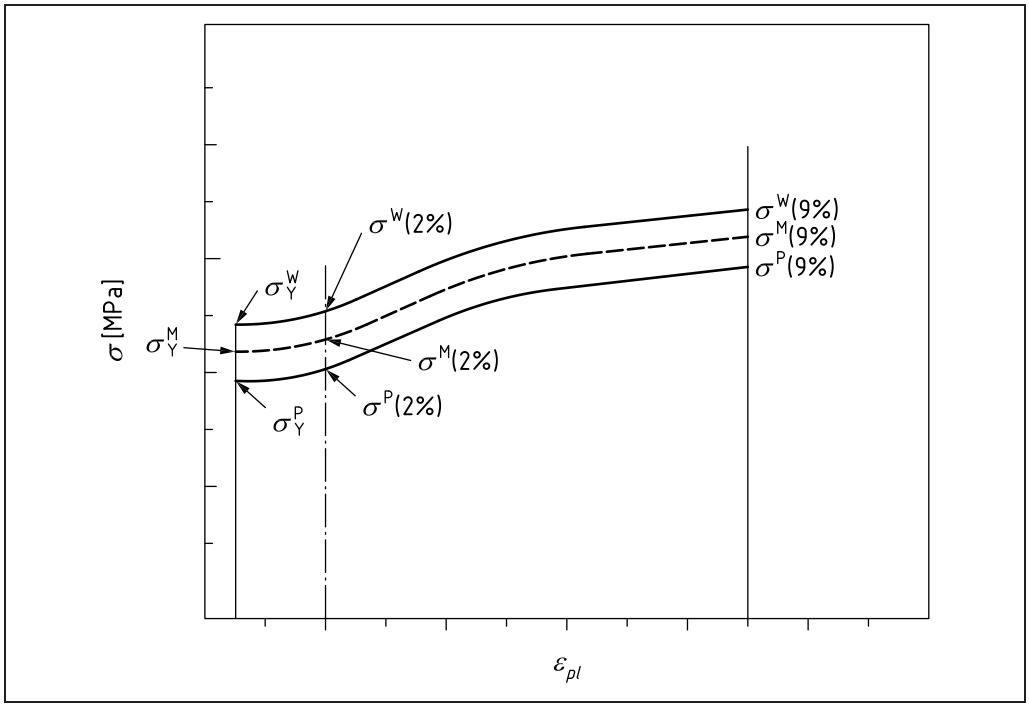
Where uniaxial stress-strain curves of weld (denoted by W) and parent metal (denoted by P) are available, the mismatch ratio is defined at a number of plastic strain values, ε_{pl}, as illustrated in Figure I.2 and Equation (I.2):

$$M(\varepsilon_{pl}) = \frac{\sigma_Y^W(\varepsilon_{pl})}{\sigma_Y^P(\varepsilon_{pl})} \quad \text{(I.2)}$$

where the shapes of the stress-strain curves are similar, M is a weak function of plastic strain and a single value of M might be adequate.

For each value of M defined by Equation (I.2), a mismatch limit load (see Annex P) and F_e^M/F_e^P ratio (where F_e^P is the limit load for a homogeneous component made of material with yield strength σ_Y^P and F_e^M is the limit load solution of the mismatch configuration) should be evaluated.

Figure I.2 **Idealized definition of mismatch ratio, *M*, and construction of the equivalent stress-strain curve (weighted average of the other two curves)**



Define an equivalent yield strength, σ_Y^M, for the strength mismatched geometry using Equation (I.3):

$$\sigma_Y^M = \left(\frac{F_e^M}{F_e^P}\right)\sigma_Y^P \quad \text{(I.3)}$$

where:

$\frac{F_e^M}{F_e^P}$ is defined for $M = M(0.2\%)$.

Where uniaxial stress-strain curves are available for the weld and parent materials, an equivalent stress versus plastic strain curve, for use in constructing an Option 2M FAD, is defined as:

$$\sigma^M(\varepsilon_{pl}) = \frac{\left(\frac{F_e^M}{F_e^P} - 1\right)\sigma^W(\varepsilon_{pl}) + \left(M - \frac{F_e^M}{F_e^P}\right)\sigma^P(\varepsilon_{pl})}{(M-1)} \quad \text{(I.4)}$$

where:

$\frac{F_e^M}{F_e^P}$ is defined for $M = M(0.2\%)$.

Total strain is obtained by adding the elastic strain, σ_Y^M/E, to the plastic strain, ε_{pl}.

I.3.3 Determination of fracture toughness

The fracture toughness of the material in the vicinity of the crack tip should be used in assessments. The initial notch and the subsequent fatigue crack can be introduced at different locations such as at the weld centreline and/or at the HAZ/fusion line. Fracture toughness is established using the testing standards indicated in Annex L.

I.3.4 Calculation of K_r

The value of K_r should be evaluated in accordance with **7.3.6** [see Equation (7.38) and Equation (7.39)] for both primary and secondary stresses. The value of K_{mat} to be used in the calculations should be determined in accordance with **7.1.4**.

I.3.5 Calculation of L_r

For a mismatched configuration, L_r in **7.3.7** should be replaced by the following equation:

$$L_r = \frac{F}{F_e^M} \tag{I.5}$$

The mismatch limit load is defined as the value of load at plastic collapse assuming that the materials in the component are elastic-perfectly plastic with yield strengths σ_Y^P and σ_Y^W for a two-material combination (parent and weld materials).

A compendium of the currently available mismatch limit load solutions is provided in Annex P.

I.3.6 Construction of failure assessment diagrams (FADs)

The FAD may be constructed in accordance with Option 1 and Option 2 FADS in **7.3**, depending on the information available and the accuracy required of the analyses. The modifications to Option 1 (**7.3.3**) and Option 2 (**7.3.4**) failure assessment curves for strength mismatch and the change to the L_r cut-off ($L_{r,max}$) should also be included.

The approach is very similar to that in **7.3**. However, an equivalent yield strength [Equation (I.3)], or an equivalent stress-strain curve [Equation (I.4)], should be used to construct the FAD. As the latter is a weighted average of those for the constituent materials (Figure I.2), the resulting FAD is expected to be similar in shape to those for the constituent materials.

I.3.7 Option 1M

I.3.7.1 General

Three combinations of stress strain behaviour may be considered in this option:

a) both parent and weld metal exhibit continuous yielding behaviour;

b) both parent and weld metal exhibit discontinuous yielding (Lüder's plateau);

c) one of the materials exhibits discontinuous yielding (Lüder's plateau) and the other has a continuous yielding behaviour.

Option 1M FADs are constructed using values of L_r and $f(L_r)$ for an equivalent material with tensile properties defined in Equation (I.3). In general, for all combinations of yield behaviour, this requires:

1) calculation of the strength mismatch ratio, M [Equation (I.1)];

2) determination of the strength mismatch limit load, F_e^M (Annex P);

3) calculation of N^M(hardening exponent of an equivalent material) using Equation (I.6):

$$N^M = \frac{(M-1)}{\frac{(F_e^M/F_e^P - 1)}{N^W} + \frac{(M - F_e^M/F_e^P)}{N^P}} \quad \text{(I.6)}$$

where:

$$N^W = 0.3\left(1 - \frac{\sigma_Y^W}{\sigma_U^W}\right)$$

$$N^P = 0.3\left(1 - \frac{\sigma_Y^P}{\sigma_U^P}\right)$$

4) calculation of $L_{r,max}$ under strength mismatch conditions using Equation (I.7), which differs from that defined in Equation (7.25) in **7.3.2**:

$$L_{r,max} = \frac{1}{2}\left(1 + \frac{0.3}{0.3 - N^M}\right) \quad \text{(I.7)}$$

5) calculation of $f(L_r)$ using the guidance given in **I.3.7.2** to **I.3.7.4**.

I.3.7.2 Both parent and weld metal exhibit continuous yielding behaviour

In this case the equations for $f(L_r)$ are those given in **7.3.3** [Equation (7.26) to Equation (7.28)] but with the values modified to address equivalent mismatch materials properties defined by Equation (I.3).

Values of μ and N in Equation (7.26) to Equation (7.28) are replaced by μ^M and N^M, defined in terms of an equivalent mismatch material:

$$\mu^M = \min\left[\frac{(M-1)}{\frac{(F_e^M/F_e^P - 1)}{\mu^W} + \frac{(M - F_e^M/F_e^P)}{\mu^P}}; 0.6\right] \quad \text{(I.8)}$$

where:

$$\mu^W = \min\left(\frac{0.001E^W}{\sigma_Y^W}; 0.6\right);$$

$$\mu^P = \min\left(\frac{0.001E^P}{\sigma_Y^P}; 0.6\right).$$

I.3.7.3 Both parent and weld metal exhibit discontinuous yielding

Where both parent and weld metal exhibit discontinuous yielding, the equations for $f(L_r)$ are those given in **7.3.3** [Equation (7.29) to Equation (7.32)], with the values of λ, N modified to address an equivalent mismatch material, as described below:

$$\lambda^M = \frac{(F_e^M/F_e^P - 1)\lambda^W + (M - F_e^M/F_e^P)\lambda^P}{(M-1)} \quad \text{(I.9)}$$

where:

$$\lambda^W = 1 + \frac{E^W \Delta\varepsilon^W}{R_{eH}^W}$$

$$\Delta\varepsilon^{W} = 0.0375\left(1 - \frac{\sigma_Y^W}{1\ 000}\right)$$

$$\lambda^{P} = 1 + \frac{E^{P}\Delta\varepsilon^{P}}{R_{eH}^{P}})$$

$$\Delta\varepsilon^{P} = 0.0375\left(1 - \frac{\sigma_Y^P}{1\ 000}\right)$$

I.3.7.4 Discontinuous yielding expected for only one material

In cases where only one material exhibits, or is expected to exhibit, discontinuous yielding, the failure assessment curve, $f(L_r)$ is a combination of those described in **I.3.7.2** and **I.3.7.3** and is discontinuous at $L_r = 1$.

I.3.7.5 Only the weld metal exhibits discontinuous yielding

In this case, $f(L_r)$ is based on Equation (7.26) and Equation (7.30) to Equation (7.32) in **7.3.3**, with some necessary modifications explained below.

For $0 \leq L_r < 1$, $f(L_r)$ is defined by Equation (I.10):

$$f(L_r) = (1 + 0.5L_r)^{-0.5}\left[0.3 + 0.7\exp\left(-\mu^{M}L_r^6\right)\right] \quad \text{(I.10)}$$

where:

μ^{M} is defined by Equation (I.11):

$$\mu^{M} = \min\left[\frac{(M-1)}{\frac{(M - F_e^M/F_e^P)}{\mu^P}}; 0.6\right] \quad \text{(I.11)}$$

$$\mu^{P} = \min\left(\frac{0.001E^{P}}{\sigma_Y^P}; 0.6\right)$$

At $L_r = 1$, $f(L_r)$ is defined as:

$$f(L_r) = \min\left[\left(\lambda^{M} + \frac{1}{2\lambda^{M}}\right)^{-0.5}; \left\{0.816\ 5\left[0.3 + 0.7\exp\left(-\mu^{M}\right)\right]\right\}\right] \quad \text{(I.12)}$$

with λ replaced by λ^{M} defined in Equation (I.13):

$$\lambda^{M} = \frac{\left(F_e^M/F_e^P - 1\right)\lambda^{W}}{(M-1)} \quad \text{(I.13)}$$

NOTE λ^{W} *is defined in* ***I.3.7.3****.*

For $1 < L_r < L_{r,max}$, $f(L_r)$ is defined as in Equation (I.14):

$$f(L_r) = f(L_r = 1)L_r^{\left(\frac{N^M - 1}{2N^M}\right)} \quad \text{(I.14)}$$

where N^{M} is defined in Equation (I.6) and $L_{r,max}$ is defined by Equation (I.7):

For $L_r \geq L_{r,max}$:

$$f(L_r) = 0 \quad \text{(I.15)}$$

I.3.7.6 Only the parent metal exhibits discontinuous yielding

In this case, $f(L_r)$ is based upon Equation (7.26) and Equation (7.30) to Equation (7.32) in **7.3.3**, with some necessary modifications explained below.

 © The British Standards Institution 2019

For $0 \leq L_r < 1$, $f(L_r)$ is as follows:

$$f(L_r) = (1 + 0.5L_r)^{-0.5}\left[0.3 + 0.7\exp\left(-\mu^M L_r^6\right)\right] \quad \text{(I.16)}$$

where μ^M is defined by Equation (I.17):

$$\mu^M = \min\left[\frac{(M-1)}{\left(F_e^M/F_e^P - 1\right)/\mu^W}; 0.6\right] \quad \text{(I.17)}$$

$$\mu^W = \min\left(0.001E^W/\sigma_Y^W; 0.6\right)$$

At $L_r = 1$, $f(L_r)$ is defined as:

$$f(L_r) = \min\left[\left(\lambda^M + \frac{1}{2\lambda^M}\right)^{-0.5}; \left\{0.816\ 5\left[0.3 + 0.7\exp\left(-\mu^M\right)\right]\right\}\right] \quad \text{(I.18)}$$

with λ replaced by λ^M defined in Equation (I.19):

$$\lambda^M = \frac{\left(M - F_e^M/F_e^P\right)\lambda^P}{(M-1)} \quad \text{(I.19)}$$

NOTE λ^P *is defined in* ***I.3.7.3****.*

For $1 < L_r < L_{r,max}$, $f(L_r)$ is defined as in Equation (I.20):

$$f(L_r) = f(1)L_r^{\left(\frac{N^M-1}{2N^M}\right)} \quad \text{(I.20)}$$

where N^M is defined in Equation (I.6) and $L_{r,max}$ is defined by Equation (I.7).

For $L_r \geq L_{r,max}$

$$f(L_r) = 0 \quad \text{(I.21)}$$

I.3.8 Option 2M

This option of analysis can be used where the full stress strain curves of parent material and weld material are known. In this case the mismatch ratio is defined as a function of plastic strain ε_{pl} [as in Equation (I.2)]. An equivalent stress-plastic strain curve, σ^M (ε_{pl}), for the mismatch material is obtained from Equation (I.4) and used in construction of the FAD.

Values of $f(L_r)$ should be calculated and plotted over small enough strain intervals by means of Equation (7.34) in **7.3.4** to give a good representation of the material's behaviour. In general, this requires calculations at L_r values of 0.7, 0.9, 0.98, 1.00, 1.02, 1.10, 1.20, etc. up to $L_r = L_{r,max}$. L_r for the loading on the structure should be calculated using the yield limit load for the mismatch conditions, F_e^M (Annex P).

Bibliography for Annex I

Standards publications

There are no standards references in this annex.

Other documents

[I.1] LEI, Y. and AINSWORTH, R.A. A J integral estimation method for cracks in welds with mismatched mechanical properties. *In: International Journal of Pressure Vessels and Piping,* 1997, 70(3), 237–246.

[I.2] LEI, Y. and AINSWORTH, R.A. The estimation of J in three-point-bend specimens with crack in a mismatched weld. *In: International Journal of Pressure Vessels and Piping*, 1997, 70(3), 247–257.

[I.3] LEI, Y. and AINSWORTH, R.A. Failure assessment diagrams for cracks in welds with mismatched mechanical properties. *In: Proceedings of the 1996 ASME PVP Conference, July 21–26 1996, Montreal, Canada*, Fatigue and Fracture, ASME PVP V324 Number 2, 65–73.

[I.4] LEI, Y. and AINSWORTH, R.A. *A Modified R6 Procedure for Cracks in Welds with Mismatched Mechanical Properties, Part 1: Description of the Method*. Nuclear Electric Report ED/GEN/REP/0173/95, 1996.

[I.5] LEI, Y. and AINSWORTH, R.A. *A Modified R6 Procedure for Cracks in Welds with Mismatched Mechanical Properties, Part 2: Validation of the procedure by finite element results*. Nuclear Electric Report ED/GEN/REP/0007/99, 1996.

[I.6] YUN-JAE, K. *Draft procedure for mis-match*, SINTAP milestone report: Task 1.5, GKSS Report SINTAP/GKSS/16, 1998. <http://www.eurofitnet.org/sintap_GKSS-16.pdf>

Annex J (informative)

Use of Charpy V-notch impact tests to estimate fracture toughness

J.0 Symbols and definitions

For the purposes of this annex, the following symbols, definitions and units apply, unless otherwise indicated at the point of use.

Symbol	Definition	Units
B	Section thickness in plane of flaw	mm
B_{ss}	Sub-sized Charpy specimen thickness	mm
C	Function of material yield strength and upper shelf energy (C_v^{us})	—
C_v	Charpy V-notch impact energy	J
C_{vi}	Charpy energy associated with the i-th specimen examined	J
C_v^{us}	Average upper shelf energy	J
E	Elastic modulus	N/mm^2
$K_{J0.2}$	Fracture toughness at initiation of stable ductile tearing	$MPa\sqrt{m}$
K_{mat}	Material fracture toughness measured by stress intensity factor	$MPa\sqrt{m}$
$K_{mat0.2}$	Fracture toughness for initiation of ductile tearing at ductile crack extension of 0.2 mm	$MPa\sqrt{m}$
n	Number of Charpy data available	—
P_f	Probability of exceedance	—
SFA_i	Shear fracture appearance of the i-th specimen examined	%
T	Temperature at which K_{mat} is to be determined	°C
T_{Cv}	Lowest temperature at which the Charpy test data are available	°C
T_K	Temperature term describing the scatter in Charpy versus fracture toughness correlation	°C
T_0	Temperature for a median toughness of 100 $MPa\sqrt{m}$ in 25 mm thick specimens	°C
T_{27J}	Temperature for an average energy of 27 J measured in a standard 10 mm × 10 mm Charpy V specimen	°C
T_{40J}	Temperature for an average energy of 40 J measured in a standard 10 mm × 10 mm Charpy V specimen	°C
T_{us}	Lowest test temperature at which upper shelf behaviour is observed	°C
ΔT_{ss}	Difference in temperature between a full-sized and sub-sized Charpy specimen for a normalized energy of $34J/cm^2$	°C
ν	Poisson's ratio	—
σ_Y	Yield strength	N/mm^2

NOTE The units for K_{mat} in this annex are $MPa\sqrt{m}$; in order to convert this into $N/mm^{3/2}$ units, multiply by 31.63.

J.1 General

The background to this annex is given in references [J.1] and [J.2].

Direct determination of fracture toughness by testing is always preferable, but where this is not possible an estimate of K_{mat} may be obtained from correlations with Charpy V-notch impact test data taken from material of the same general microstructural type (e.g. weld metal, HAZ, parent material) in which the flaw is situated. The orientation of the Charpy V-notch specimens should be such as to reproduce the fracture path that would result from the flaw under consideration.

Three correlations are described in **J.2**; each one is appropriate for ferritic steels and provides estimates of K_{mat} under quasi-static loading conditions. The three correlations are as follows.

a) A lower bound relation for near lower shelf behaviour, where Charpy energy has been obtained at a single temperature (see **J.2.1**).

b) A relation for lower transitional behaviour based upon the Master Curve approach (see reference [J.3]), where the Charpy temperature for an energy of 27 J or 40 J (T_{27J} or T_{40J}) has been established (see **J.2.2**). Guidance is provided to establish T_{27J} for an incomplete Charpy transition curve, including data obtained at a single temperature (see reference [J.2]).

c) A relation that limits K_{mat} (estimated in accordance with **J.2.1** and **J.2.2**) to ensure that materials with low upper shelf Charpy energy are not assumed to have high fracture toughness (see **J.2.5**). An alternative equation is provided for modern low carbon, low sulfur steels.

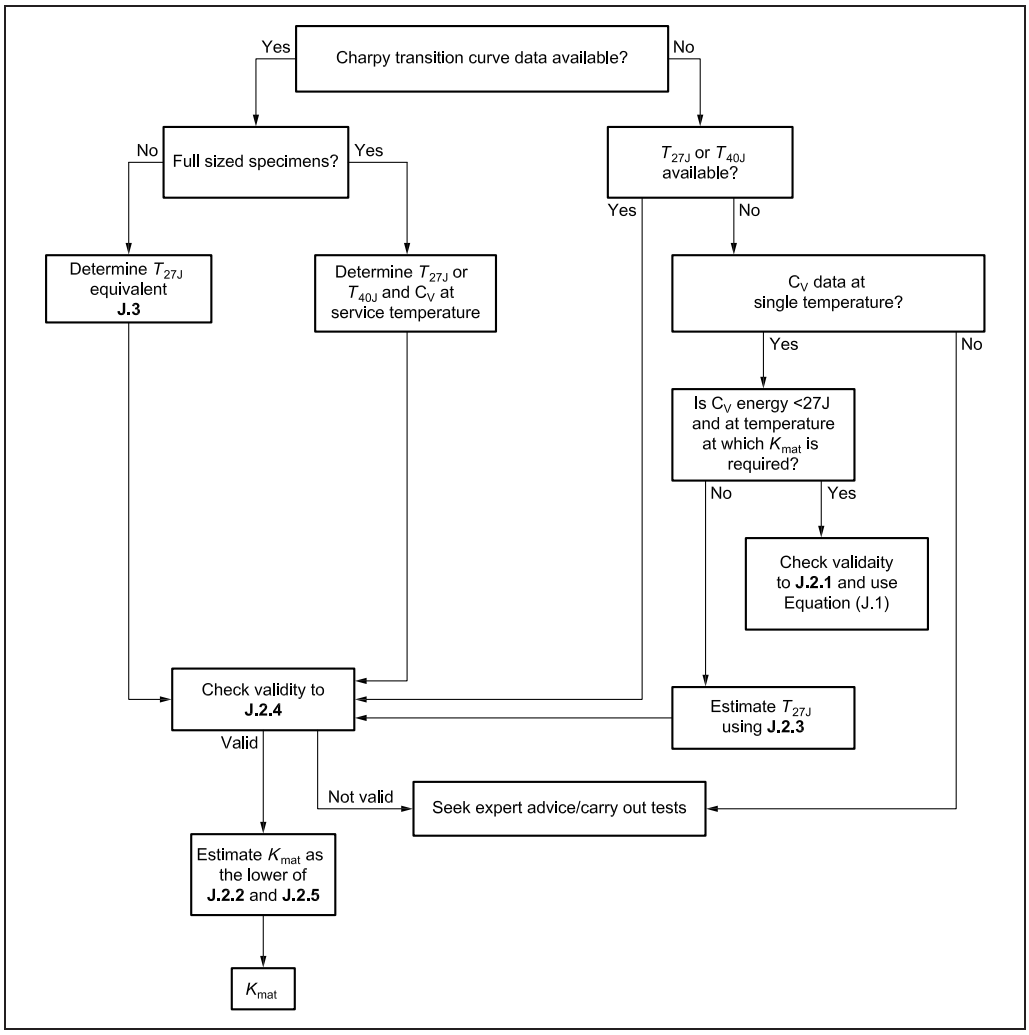
To ensure conservative estimates of fracture toughness, especially in steels with potentially low upper shelf fracture toughness, fracture toughness estimates should be the lower of a) and c), or b) and c), as appropriate, at the service temperature.

Figure J.1 shows a flowchart for the selection of an appropriate correlation based on available data. All correlations described are between Charpy impact energy (measured on standard 10 mm × 10 mm, 2 mm deep V-notched specimens) and fracture toughness values in terms of K_{mat}. Where impact energy is from sub-sized Charpy specimens, the procedures described in **J.3** should be used.

NOTE The estimates of K_{mat} provided by these correlations are intended to replicate the fracture toughness that would be determined had a specimen of thickness "B" been tested. Equation (J.1) and Equation (J.2) are derived from the Master Curve, which is based on a weak link model of fracture. Consequently, the dimension "B" should actually be based on the effective crack front length present in the component being assessed. However, custom and use has shown that the application of these correlations provides an acceptable estimate of K_{mat} when the component thickness is used.

 © The British Standards Institution 2019

Figure J.1 **Flowchart for selecting an appropriate correlation for estimating fracture toughness from Charpy data**



J.2 Charpy/fracture toughness correlations

J.2.1 Near lower shelf behaviour

Where Charpy results are available at the temperature at which K_{mat} is required and the energy is 27 J or less, Equation (J.1) (see [J.4]) may be used to estimate fracture toughness.

$$K_{mat} = \left[\left(12\sqrt{C_v} - 20\right)\left(\frac{25}{B}\right)^{0.25}\right] + 20 \qquad \text{(J.1)}$$

In this case, C_v is the minimum Charpy V-notch impact energy at the service temperature (in J) for energies 27J or less (but greater than 3 J), and 80% or more crystallinity.

*NOTE Equation (J.1) is conservative with respect to Equation (J.5) for temperatures below T_{27J} but is not always conservative (at P_f = 0.05) at higher temperatures. The range of temperatures over which this is the case is minimized by the limit imposed by **J.2.5**.*

J.2.2 Transitional behaviour based on the Master Curve

For ferritic steels, a correlation between the 27 J and 40 J Charpy transition temperatures (T_{27J} and T_{40J}) and the 100 MPa$\sqrt{}$m fracture toughness transition temperature (T_0) in 25 mm thick specimens is described by Equation (J.2) and

Equation (J.3) (see ASTM E1921). T_{27J} and T_{40J} are defined as the temperatures for which the average from three tests is 27 J or 40 J, respectively, provided that the minimum is not less than 19 J or 28 J, respectively.

$$T_0 = T_{27J} - 18\,^{\circ}\mathrm{C}\,(\text{standard deviation} = 15\,^{\circ}\mathrm{C}) \quad \text{(J.2)}$$

$$T_0 = T_{40J} - 24\,^{\circ}\mathrm{C}\,(\text{standard deviation} = 15\,^{\circ}\mathrm{C}) \quad \text{(J.3)}$$

An alternative and less conservative equation for determining T_0 from T_{27J} can be used in place of Equation (J.2) if the room temperature yield strength and upper shelf energy of the steel is known:

$$T_0 = T_{27J} - 87 + \frac{\sigma_Y}{12} + \frac{1\,000}{C_V^{us}}\ (\text{standard deviation} = 18\,^{\circ}\mathrm{C}) \quad \text{(J.4)}$$

The Master Curve approach allows for the following factors:

a) thickness effect;

b) fracture toughness distribution;

c) shape of fracture toughness transition curve for ferritic steels and welds; and

d) required probability of achieving a particular value of K_{mat}.

The fracture toughness transition curve is described by the Master Curve as follows:

$$K_{mat} = 20 + \{11 + 77\exp[0.019(T - T_0 - T_K)]\}\left(\frac{25}{B}\right)^{0.25}\left[\ln\left(\frac{1}{1 - P_f}\right)\right]^{0.25} \quad \text{(J.5)}$$

Equation (J.2) and Equation (J.3) are associated with a standard deviation of 15 °C and Equation (J.4) with a standard deviation of 18 °C. For a 90% confidence in the determination of T_0, the T_K term in Equation (J.5) is 25 °C when using Equation (J.2) and Equation (J.3), and 30 °C when using Equation (J.4). Lower values for T_K may be used if supported by experimental data for the material of interest. The use of P_f = 0.05 (5%) is recommended unless experimental evidence supports the use of a higher probability for a given steel.

NOTE 1 Equation (J.2) to Equation (J.5) are not applicable to ductile behaviour. Consequently, the Charpy specimen fracture appearance at T_{27J} or T_{40J} needs to show a high crystallinity (~70%).

NOTE 2 T_{27J} and T_{40J} are derived from the Charpy energy versus temperature transition curve. If the minimum energy requirement is not achieved then this is an indication of excessive scatter in Charpy toughness (e.g. as can be observed when testing welds and HAZs) and either three additional tests are carried out and the average of the six tests is used to estimate T_{27J} or T_{40J}, provided that all three additional tests exceed the minimum energy requirement, or T_{27J} or T_{40J} are derived from a lower bound to the transition curve. If T_{27J} or T_{40J} are derived from a material specification requirement then these values can be used directly in Equation (J.2) and Equation (J.3) without any further correction.

NOTE 3 Where bi-modal Charpy transition data are obtained, T_{27J} should be estimated from the lower transition curve or, if this is not possible, fracture toughness can be estimated from Equation (J.1) at the appropriate temperature.

NOTE 4 Reference Charpy energies of 27 J and 40 J have been chosen as they correspond to typical requirements in steel specifications. The original correlations were based on reference energies of 28 J and 41 J, but the difference is considered to have an insignificant impact on the estimation of toughness according to the procedures described here. Equation (J.3) provides a more conservative (>10 °C) estimate of T_0 than does Equation (J.2) when T_{40J} exceeds T_{27J} by >15 °C.

NOTE 5 Equation (J.4) was derived from fracture toughness tests conducted on single edge notch bend tests which meet the requirements of ASTM E1921.

NOTE 6 Equation (J.3) was derived from nuclear pressure vessel steels in irradiated and unirradiated condition (see reference [J.5]).

J.2.3 Transitional behaviour with incomplete Charpy transition curve

For the cases when there is an incomplete Charpy transition curve or when only single temperature Charpy data are available in the ductile to brittle transition, the T_{27J} may be estimated using the following relations (see [J.4]):

$$T_{27J} = T_{Cv} - \frac{C}{4}\ln\frac{C_v\left(C_v^{us} - 27\right)}{27\left(C_v^{us} - C_v\right)} \quad \text{(J.6)}$$

In this case, C_v is the average Charpy impact value (J) in the data set at test temperature T_{Cv}.

The parameter C is calculated as:

$$C = 34\,^{\circ}\text{C} + \frac{\sigma_Y}{35.1} - \frac{C_v^{us}}{14.3} \quad \text{(J.7)}$$

If the upper shelf energy (C_v^{us}) is unknown, it should be taken as the highest value of Charpy energy recorded in the set of data.

If both impact energy and shear fracture appearance data are available, the upper shelf energy can be estimated more accurately from:

$$C_v^{us} \approx 100\frac{\sum_{i=1}^{n}\frac{C_{vi}}{SFA_i}}{n} \quad \text{(J.8)}$$

If only upper shelf energy data are available, then the lowest test temperature for the corresponding upper shelf energy is used for the transition temperature determination. In this case, the transition temperature is estimated from the following function, with the parameter C as defined in Equation (J.7):

$$T_{27J} = T_{us} - \left\{C\ \ln\left[\frac{19\left(C_v^{us} - 27\right)}{27}\right]\right\}/4 \quad \text{(J.9)}$$

NOTE If data are available at more than one temperature, the estimate of T_{27J} using Equation (J.6) is conducted on data obtained at the lowest test temperature.

In order to minimize non-conservatisms in estimating T_{27J} in Equation (J.6) due to scatter in inhomogeneous materials, weld metals and HAZs, C_v^{us} should be based on the average of at least three tests, and the maximum value should be not more than 120% of the average.

J.2.4 Validity limits

The validity of the correlation based upon the Master Curve approach for pressure vessel-type steels and structural steels is well established. Further examples of its application have been demonstrated [J.6] with data sets from parent plates, sections, linepipe, weld metals and HAZs.

A number of situations have been identified which could result in non-conservative predictions. These include:

a) cases where Charpy specimens exhibit unusual fracture behaviour, such as fracture path deviation (where the fracture propagates out of the region being tested). This has been observed in narrow welds such as those made by laser and electron beam welding;

b) presence of splits on the fracture surface;

c) through-thickness variation of microstructure and properties such that the Charpy specimen does not test the region of lowest toughness. This is more likely to be a problem in inhomogeneous materials such as weld metals and HAZs. This can be minimized by ensuring that the Charpy specimens test regions of suspected low toughness. Expert advice might be necessary to select such regions; and

d) severely cold worked material.

In these instances, Equation (J.5) might be inappropriate and expert advice should be sought.

J.2.5 Upper limit for K_{mat}

To avoid overestimating fracture toughness at the service temperature in materials with potentially low upper shelf Charpy energy, K_{mat} (estimated in accordance with **J.2.1** and **J.2.2**) should not exceed the value given by Equation (J.10).

$$K_{mat} = 0.54\ C_v + 55 \quad \text{(J.10)}$$

In this case, C_v is the average Charpy V-notch impact energy (J) at the service temperature for which K_{mat} is required.

NOTE 1 Equation (J.10) is derived from PD 6493:1991, Appendix B[J.1)]. This restricts the use of Equation (J.10) to ferritic steels with yield strengths <480 N/mm^2.

NOTE 2 An example of the use of Equation (J.5) and Equation (J.10) is as follows. A 60 mm thick, high sulfur ferritic steel with a yield strength of less than 480 N/mm^2 has a T_{27J} of –50 °C and a Charpy energy of 60 J at the service temperature of 0 °C. From Equation (J.2), T_0 is estimated as –68 °C. From Equation (J.5), T_K is 25 °C and K_{mat} is estimated as 90.8 MPa$\sqrt{m}$ at 0 °C for P_f = 0.05. Equation (J.10) provides an estimate of 87.4 MPa$\sqrt{m}$ at 0 °C. Therefore the best estimate for K_{mat} in accordance with this annex is 87.4 MPa$\sqrt{m}$ at 0 °C.

Equation (J.10) is intended to be applied to old, high sulfur steels that have potentially poor tearing resistance. It can be very restrictive when applied to modern, low carbon, low sulfur (≤0.01% S) steels. An alternative that has been found to be useful for modern steels [J.7] uses upper shelf Charpy energy to estimate the fracture toughness for the initiation of ductile tearing, defined as ductile crack extension of 0.2 mm, $K_{mat0.2}$. Fracture toughness is derived from the upper shelf Charpy energy defined as the energy at which there is 100% shear (0% cleavage fracture) in the Charpy specimen. Fracture toughness is given by:

$$K_{mat0.2} = K_{J0.2} = \sqrt{\frac{E\left[0.53\left(C_v^{us}\right)^{1.28}\right]\left[0.2^{0.133\left(C_v^{us}\right)^{0.256}}\right]}{1000\left(1-\nu^2\right)}} \quad \text{(J.11)}$$

NOTE 3 Equation (J.10) and Equation (J.11) can also be used to estimate upper shelf fracture toughness provided that 100% shear fracture appearance is achieved in the Charpy test at the assessment temperature. In this instance it is recommended that C_v^{us} is obtained from test data and that Equation (J.8) is not used.

NOTE 4 The temperature at the start of the upper shelf on the Charpy transition curve (where 100% shear fracture appearance occurs) does not necessarily correspond to the start of the upper shelf on the fracture toughness (K_{mat}) transition curve (where cleavage does not occur). Non-conservative estimates of upper shelf fracture toughness will be made if the temperature at the start of the upper shelf Charpy transition curve is less than the temperature at the start of the fracture toughness upper shelf transition curve. Generally, safe estimates of upper shelf fracture toughness will be made if the start of the upper shelf fracture Charpy transition curve is higher than the start of the fracture transition curve. It is not possible to provide general advice on the difference between the temperatures at the start of the Charpy and fracture toughness transition curves, since this depends on material, tensile properties and thickness. Expert advice should be sought if the upper shelf equations are used and brittle (cleavage) fracture cannot be excluded.

J.1) This is withdrawn.

J.3 Treatment of sub-sized Charpy data

When Charpy data has been obtained from sub-sized specimens (i.e. specimens that are identical to standard 10 mm × 10 mm specimens except in terms of thickness) because either:

a) the material being tested is less than 10 mm thick; or

b) the product shape does not permit full-sized specimens to be extracted;

then the procedure in 1) to 4) should be used to determine T_{27J} in Equation (J.2).

1) Sub-sized specimens have a lower transition temperature and lower impact energy capacity than full-sized Charpy specimens.

2) The energy of 27 J in the full-sized specimen corresponds to a normalized energy in the net section of 34 J/cm^2.

3) The corresponding energy in the sub-sized specimen is obtained by assuming that the normalized energy in the net section is 34 J/cm^2.

4) The temperature at which this energy is measured is shifted upwards by ΔT_{ss} to correspond to a full-sized specimen.

$$\Delta T_{ss} = -51.4 \ln\left[2(B_{ss}/10)^{0.25} - 1\right] \quad \text{(J.12)}$$

NOTE An example of the use of this procedure is as follows. A 5 mm thick sub-sized Charpy specimen is removed from a 7 mm thick component. In the sub-sized specimen, the equivalent to 27 J in a full-sized specimen is 14 J. The temperature at which this energy is measured in the sub sized Charpy specimen is shifted upwards by 20 °C to give the equivalent T_{27J} in a full sized specimen i.e. $T_{27J} = T_{14J} + \Delta T_{ss}$.

Equation (J.2) and Equation (J.5) are then used to estimate K_{mat}. The dimension B in Equation (J.5) is 7 mm.

Bibliography for Annex J

Standards publications

For dated references, only the edition cited applies. For undated references, the latest edition of the referenced document (including any amendments) applies.

ASTM E1921, *Standard test method for determination of reference temperature, T_o, for ferritic steels in the transition range*

PD 6493:1991, *Guidance on methods for assessing the acceptability of flaws in fusion welded structures*

Other documents

[J.1] HADLEY, I. and PISARSKI, H.G. Materials properties for Engineering Critical Assessment: Background to the advice given in BS 7910:2013. *In: International Journal of Pressure Vessels and Piping*, 168, December 2018, 191–199. <https://doi.org/10.1016/j.ijpvp.2018.10.016>

[J.2] PISARSKI, H.G. and BEZENSEK, B. Estimating fracture toughness from Charpy data, OMAE2019-95787. *In: Proceedings of the ASME 2019 38th International Conference on Ocean, Offshore and Arctic Engineering (OMAE 2019)*, June 9–14, 2019, Glasgow, Scotland.

[J.3] WALLIN, K. Simple theoretical Charpy V-K_{Ic} correlation for irradiation embrittlement. *In:* D.L. MARRIOTT, T.R. MAYER and W.H. BARNFORD, eds. *Innovative Approaches to Irradiation Damage and Fracture Analysis*. New York: ASME. 1989, PVP-170. 93.100. ISBN 0791803260.

[J.4] WALLIN, K. *Fracture toughness of engineering materials – Estimation and application*. FESI/EMAS Publishing, 2011. ISBN 978 0 9552994 6 9.

[J.5] SOKOLOV, M. and NANSTAD, R. Comparison of Irradiation-Induced Shifts of K_{Jc} and Charpy Impact Toughness for Reactor Pressure Vessel Steels. *In: Effects of Radiation on Materials: 18th International Symposium*, ed. R. Nanstad, M. Hamilton, F. Garner, and A. Kumar (West Conshohocken, PA: ASTM International, 1999), 167–90. <https://doi.org/10.1520/STP13863S>

[J.6] BANNISTER, A.C. *Determination of fracture toughness from Charpy impact energy: procedure and validation*. British Steel Report No. SINTAP/BS/17. Swinden Technology Centre, 1998. <http://www.eurofitnet.org/sintap_BRITISH_STEEL_BS-17.pdf>

[J.7] LUCON, E., WALLIN, K., LANGENBERG, P. and PISARSKI, H. The use of Charpy/fracture toughness correlations in the FITNET procedure. OMAE 2005-67569. *In: Proceedings of OMAE 2005*, 24th International Conference on offshore mechanics and arctic engineering. June 12–17, 2005, Halkidiki, Greece.

Annex K (informative)

Probabilistic assessment

K.0 Symbols and definitions

For the purposes of this annex, the following symbols, definitions and units apply, unless otherwise indicated at the point of use.

Symbol	Definition	Units
A	Constant in fatigue growth relation	see footnote K.1)
A_{av}	Average creep parameter	—
a_{av}	Average value of crack extension based on probabilistic analysis	mm
a_f	Final flaw size	mm
C^*	Creep fracture/crack growth parameter	$MPamh^{-1}$
D_c	Total accumulated creep damage	—
da/dN	Crack growth rate with cycles	mm/cycle
da/dt	Crack growth rate with time	mm/h
F_{char}	Characteristic values of loads	N
F_{design}	Design load to be considered for stress calculation	N
$f(K_I)$	Probability density function for fracture toughness	—
$f_x(X)$	A known joint probability density function of the random vector X	—
$g(X)$	Limit state function of the random vector X	—
$g_{FAD}(X)$, $g_{L_r}(X)$	Limit state function of FAD and L_r for a continuous yielding FAD in a Level II reliability analysis	—
K	Stress intensity factor (SIF)	$N/mm^{3/2}$
K_I	Applied tensile (mode I) stress intensity factor	$N/mm^{3/2}$
K_{Ic}	Plane strain fracture toughness	$N/mm^{3/2}$
K_{mat}	Characteristic material fracture toughness determined in terms of stress intensity factor	$N/mm^{3/2}$
K_{max}	Maximum stress intensity factor	$N/mm^{3/2}$
K_{min}	Minimum stress intensity factor	$N/mm^{3/2}$
K_r	Fracture ratio	—
k	Shape parameter of the Weibull distribution	—
L	Probability density functions of the load or resistance effects	—
M_k	Stress intensity magnification factor	—
m	Exponent in fatigue crack growth law	—

K.1) The units and value of A depend on those used to measure da/dN and ΔK, and on the value of the exponent, m. If A is known in one set of units, A_a, the corresponding value for another set of units, A_b is given by:

$$A_b = A_a \frac{f_a}{f_b{}^m}$$

where:

f_a is the conversion factor for da/dN from the first to the second unit system; and

f_b is the conversion factor for ΔK from the first to the second unit system.

(continued)

Symbol	Definition	Units
N	Number of cycles	—
P(a)	Probability occurrence of an event "a"	—
$P[K]$	Probability of fracture toughness exceeding the value given	—
P_F	Probability of failure	—
q	Exponent in creep crack growth equation	—
R	Ratio of minimum to stress intensity factor, K_{min}, to maximum stress intensity factor, K_{max}, in fatigue analysis	—
R_T	Specified minimum target reliability	—
R_{char}	Characteristic resistance	—
T	Temperature at which K_{mat} is to be determined	°C
T_i	Test temperature for a specimen i	°C
T_0	Temperature for a median toughness of 100 MPa$\sqrt{m}$ in 25 mm thick specimens	°C
t	Time	hours, days, weeks, months or years as appropriate
t_{ri}	Exponential function of μ_c	—
X	Vector of basic random variables	—
Z	Parameter defined by Equation (K.22):	—
Z_A	Relationship used in probabilistic creep crack growth calculation	—
β	Reliability	—
β_R, β_T	Reliability index used in calculating P_F	—
$\Gamma(z)$	Gamma function	—
γ_F, γ_R	Partial safety factors	—
ΔK	Stress intensity factor range	N/mm$^{3/2}$
ΔK_0	Stress range threshold below which crack growth does not occur	N/mm$^{3/2}$
Δt_i	Time during which the structure is subjected to stress, σ_i, and temperature, T_i	hours, days, weeks, months or years as appropriate
δ_A	Standard deviation of the logarithm of A	—
δ_C	Standard deviation of the logarithm of the rupture time	h
θ	Weibull distribution scale parameter	—
μ_A	Mean value of the logarithm of A	—
μ_{Klc}	Mean value of K_{Ic}	N/mm$^{3/2}$
μ_{Kmat}	Mean value of the normal probability density function of fracture toughness	N/mm$^{3/2}$
μ_{LogNor}	Lognormal distribution parameter	—
μ_c	Mean value of the logarithm of the rupture time ln(τ)	—

 © The British Standards Institution 2019

(continued)

Symbol	Definition	Units
$\sigma_{K\text{Ic}}$	Standard deviation of K_{Ic}	—
$\sigma_{K\text{mat}}$	Standard deviation of the normal probability density function of fracture toughness	$N/mm^{3/2}$
σ_{LogNor}	Lognormal distribution parameter	—
τ	Rupture time expressed as a random variable	h
Φ	Cumulative distribution function of a normalized Gaussian distribution	—
Ω	Normalized Gaussian random variable N(0;1)	—

K.1 General

The background to this annex is given in references [K.1] and [K.2].

The application of deterministic fracture mechanics assessment procedures to the prediction of fitness-for-service requires the use of data that are often subject to considerable uncertainty. The use of extreme bounding values for the relevant parameters can lead, in some circumstances, to unacceptably over-conservative predictions of structural integrity. An alternative approach is to use reliability assessment methods, also known as probabilistic assessment methods. Reliability/probabilistic assessment methods have been the subject of considerable interest in recent years with the adoption of risk-based approaches to the safety management of engineering structures in various industrial sectors. They allow for parameter uncertainties and enable the estimation of the probability of failure of structures containing flaws. These methods have been applied in practice, in the context of risk-based decision making, design, during fabrication and for the scheduling of in-service inspection.

In this annex, methods of probabilistic defect assessment are described which enable the probability of failure [K.2)] to be calculated for a given set of parameters and their corresponding statistical distribution.

K.2 Context of probabilistic assessment

There is a variety of contexts in which a probabilistic assessment or reliability analysis might be useful.

Decisions can be informed through the application of risk assessment principles. Here risk is understood as being the product of the probability of an event (e.g. a structural failure) and the consequences were that event to occur (e.g. life safety or economic loss).

The subject of this annex is the probability of a failure. The term "reliability" is a measure of the reciprocal of probability of failure, thus a component with low reliability has a high probability of failure.

Applications where a probabilistic approach might be applicable include support to safety cases which can require demonstration of suitable management of life-safety risk; input to quantitative risk assessments; or planning of inspections for fatigue assessment.

[K.2)] In this context, "failure" means an assessment point outside the failure assessment diagram. This does not necessarily mean failure of the component or structure.

K.3 Sources of uncertainty

The prerequisite for structural reliability analysis is the uncertainty modelling of the problem under analysis. The uncertainty can arise from natural variability (aleatoric uncertainty) or from lack of knowledge (epistemic uncertainty). Uncertainty associated with lack of knowledge can, in principle, be reduced by collecting more or better information. Uncertainty arising from natural variability cannot be reduced.

Sources of uncertainty can include ([K.3], [K.4]):

- physical uncertainty;
- measurement uncertainty;
- statistical uncertainty;
- model uncertainty;
- human factor uncertainty.

K.4 Target reliability

Target reliability values may be employed to ensure an appropriate probability of achieving a relevant performance level. The target reliability measures depend on the failure consequence as well as the cost and effort to reduce the probability of failure.

A structural system is required to achieve one or more defined performance requirements as per its designed function (see, for example, ISO 2394:2015). Performance levels are associated with limit states, e.g. serviceability limit states or ultimate limit states.

The performance levels can be associated with:

- direct and indirect economic losses;
- societal consequences resulting from fatalities and injuries;
- environmental impact.

The target reliability should generally correspond to a reference period, e.g. the annual failure probability or failure probability over a different period such as the service life. A commonly used measure is the return period which is defined as the mean time between failures. For large return periods, the annual failure probability is the reciprocal of the return period.

If the relevant consequence is the risk to human life, annual failure probabilities are preferred.

Target reliability levels can be established considering a variety of criteria.

a) Calibration against established codified design practice. This method acknowledges that design codes can encapsulate considerable historical experience. It also acknowledges the often notional nature of the reliability analysis.

b) The target level for risk assessment based on experience of failures. This method is particularly useful when the functional reliability of the system is more important than the reliability of its individual components. In the automotive industry or electronic components manufacturing, component reliability is determined by the failure rate data of real components. The failure rate data is then used in system reliability calculations.

c) Economic value analysis (cost-benefit analysis). Target reliabilities are specified to maximize the expected value of benefits over the life cycle of the structure.

d) The application of risk management criteria based on the principle that risk should be as low as reasonably practicable (ALARP). Here risk is required, as a minimum, to be below a tolerable threshold. In addition it should be demonstrated that reasonably practicable measures have been taken to further mitigate the risks. For a measure not to be adopted, the costs of the mitigation measures should be shown to outweigh the benefits.

e) ISO 2394:2015 suggests that life-safety targets be developed using the "marginal lifesaving cost principle (MLSC)". This is analogous to the ALARP principle in UK practice, i.e. subject to being below a tolerable maximum probability level, the failure probability is set at a point where marginal costs to improve life safety start to exceed the marginal benefits. The benefits of life safety are assessed using a "life quality index" (LQI).

The target reliability pertains to the ability of a structural system to achieve its performance requirement. The system or components thereof might be degrading (e.g. by fatigue) and subject to permanent or time-dependent loading processes which might result in overload (e.g. fracture or system collapse). Appropriate component reliability targets which are demonstrated to achieve the system target should be derived.

A number of standards and codes of practice recommend a reasonable value for target reliability which takes due account of considerations of life-safety, environmental and economic risks.

Comparison of calculated probability against target reliability derived from frequentist failure rates should be treated with care. This is due to mutual dependency between analysis uncertainties and target reliability values.

The uncertainties built into a structural reliability analysis differ from real life reliabilities due to the deviation of calculated reliabilities from gross errors which occurs in real life. In addition to real life uncertainties, i.e. the physical uncertainty, the reliability assessment comprises model uncertainty and statistical uncertainty.

The probability of failure from a reliability analysis is, to a large extent, a nominal value. This is because it is highly reliant on the modelling of the random variables and the structural limit state and performance models. It should be the aim to develop the models and distributions from data and to account for epistemic (statistical uncertainties, modelling uncertainties, etc.) as objectively as possible. In spite of these efforts, the calculated reliability will largely remain a notional value, instead of an actuarial reliability value. As a result, the calculated reliabilities should ideally be compared with target reliability values derived using similar assumptions and models to those on which the reliability analysis is based. This drawback means that target reliability quantities can only be used for particular applications.

Table K.1 gives some examples of target reliabilities specified by certain codes and standards.

Table K.1 **Examples of target reliabilities specified by codes and standards**

Environment	Scope	Limit state function	Minimum reliability index	Maximum probability of failure
Eurocode. Basis of structural design (BS EN 1990)	Buildings and civil engineering works	Ultimate limit states	3.3 to 4.3 for 50 years reference period and 4.2 to 5.2 for annual	4.8×10^{-4} to 8.5×10^{-6} for 50 years reference period and 1.3×10^{-5} to 1.0×10^{-7} for annual
	Residential and office buildings, public buildings where consequences of failure are medium (e.g. an office building)	Fatigue limit state	1.5 to 3.8 for 50 years reference period	6.7×10^{-2} to 7.2×10^{-5} for 50 years reference period
Ship structural committee [K.5]	Ship hull structures	Ultimate limit state	3 to 5.5 Ship service life	1.4×10^{-3} to 1.9×10^{-8}
		Fatigue limit state	2 to 3.5 Ship service life	2.3×10^{-2} to 2.3×10^{-4}
ISO 2394:2015	General principles on reliability for structures	Life quality index	3.1 to 4.2 annual	10^{-3} to 10^{-5} annual
		Economic	3.1 to 4.7 annual	10^{-3} to 10^{-6} annual
DNV Classification Note 30.6 [K.6]	Marine and offshore structures		3.09 to 4.75 annual	10^{-3} to 10^{-6} annual
DNV RP C210 [K.7]	Marine and offshore structures		Fatigue	9.1×10^{-5} cumulative (Design fatigue factor = 10)
NORSOK N001 rev 8 2012 [K.8]	Marine structures		General	Probability of personnel being on the facility simultaneous with environmental actions damaging main safety functions is less than 10^{-4} per annum
UK HSE Technical policy relating to extreme weather hazards [K.9]	Offshore structures			10 000 year return period storm

 © The British Standards Institution 2019

K.5 Reliability analysis methods

K.5.1 General

The reliability analysis aims to calculate the probability of failure to achieve a particular limit state for a given model of the loading and resistance processes.

Denote the vector of basic random variables as **X**. A general limit state function is defined such that the region defined by:

$$G(\mathbf{X}) \leq 0 \tag{K.1}$$

denotes failure to achieve the limit state.

Where the random variables are independent of time, the probability of failure to achieve the limit state is given by the integral of the joint probability density function of **x** over the failure region:

$$P_F = \int_{G(x)\leq 0} f_X(\mathbf{x})dx \tag{K.2}$$

where $f_X(\mathbf{x})$ is the multivariate probability density function of random variables, **X**.

The reliability index, β_R, is often quoted. This is related to the probability of failure, P_F, by:

$$P_F = 1 - \Phi(\beta_R) = \Phi(-\beta_R) \tag{K.3}$$

where Φ denotes the cumulative distribution function of a normalized Gaussian distribution.

Alternatively, the probability of failure can be set to reflect a specified minimum target reliability, R_T, for the structural component. The corresponding reliability index, β_T, is from Equation (K.4):

$$\beta_T = \Phi^{-1}(1 - P_F) = \Phi^{-1}(R_T) \tag{K.4}$$

from which critical values of parameters can be determined.

In general, situations where one or more of the random variables is a time-dependent random process, e.g. environmental loading or a degradation process such as fatigue, the time dependency needs to be accounted for.

There is a large variety of methods available for approximating the probability of failure or failure rate for a particular limit state function and random model. These include ISO 2394:2015 and reference [K.4]:

- direct integration within the failure surface (e.g. R6 Level III [K.10]);
- first order/second order reliability method (FORM/SORM);
- Monte Carlo Simulation.

The methods are often categorized on the basis of their accuracy in calculating the failure probability. Level III methods are the most accurate and can include direct integration of the probability density function over the failure region using numerical integration or Monte Carlo simulation. Level II methods are more approximate and include the first and second order reliability methods. Level I methods often refer to simplified approximations used to estimate failure probability using pre-calibrated partial safety factors.

Failure predictions can be very sensitive to the input data and hence the successful application of probabilistic procedures requires that appropriate probability distributions are available. In practice, adequate data might not be available for all the critical variables and extreme care should therefore be exercised before assumptions and approximations are made. In such situations, conservative estimates should be made, based on expert advice, and a sensitivity analysis performed. The successful application of probabilistic procedures

requires a high level of expertise and experience, and probabilistic assessments should be undertaken only by appropriate specialists.

Where approximate methods are used, their accuracy should be verified for some typical cases against more exact methods.

Different levels of reliability analysis are possible depending on the level of details applied in the uncertainty modelling.

K.5.2 Partial safety factor format

The partial safety factor format, also referred to as Level I method, is based on the application of partial safety factors (PSFs) to the nominal or characteristics values of the variables in the deterministic formulation of the limit state function.

Partial safety factors are applied to the individual input variables in a design equation to give the required target reliability without the need for a full probabilistic assessment.

The values of the partial safety factors require calibration using more advanced reliability analysis.

The loads to be considered for the stress calculation are characteristic values of loads:

$$F_{\text{design}} = \gamma_F F_{\text{char}} \tag{K.5}$$

The design resistance is defined as the characteristic resistance divided by the resistance partial safety factor:

$$F_{\text{design}} = R_{\text{char}}/\gamma_R \tag{K.6}$$

The design equation to be satisfied to ensure that the target level of reliability is achieved is:

$$\gamma_F F_{\text{char}} < R_{\text{char}}/\gamma_R \tag{K.7}$$

Partial safety factors are not unique, and different combinations of partial safety factors can be derived from the calibration process for any particular target reliability. Partial safety factors depend not just on the target reliability required but also on the scatter or uncertainty of the main input data.

Editions of BS 7910 prior to 2019 included tables of generic PSFs intended for use with fracture assessment. A re-appraisal of the method [K.1] has confirmed that the use of these PSFs has a tendency to overestimate probability of failure, sometimes by several orders of magnitude, especially for the case of materials with high fracture toughness. In terms of overall risk (in which both the probability and consequences of failure need to be considered) the use of PSFs could therefore mislead the user, and so the PSF tables have been removed from the 2019 revision.

Note that, whilst the limitations of the PSF approach (including the so-called "modelling error") were understood and described at the time of publication [K.11], its computational simplicity was intended to compensate for these limitations. The availability of probabilistic software tools now makes Level II/Level III methods more feasible. Another option is to derive tailored (i.e. model-specific) PSFs.

K.6 Fatigue crack growth assessment

K.6.1 General

The basic elements of a Level II fatigue crack growth and fracture reliability assessment are as follows (fracture reliability assessment methods are given in **K.7**):

a) specification of the probability distributions and parameters for the relevant parameters, i.e. the initial flaw size, the final flaw size, the fatigue crack growth rate parameters (including the threshold stress intensity factor range), the stress intensity factor and the stress ranges. The distribution for the final flaw size in situations where fracture is the failure mode is determined by the fracture procedure. In such situations the distributions for thef racture assessment parameters are also required. For the Option 1 fracture procedure, distributions are therefore required for the material toughness, the mechanical properties, the residual stress distribution and the applied stress;

b) specification of the fatigue crack growth law. Suitable alternatives to the Paris Law can be used;

c) specification of the method to be used to calculate the stress intensity factor and the failure criterion;

d) definition of the requirement, e.g. determination of the probability of failure or the inspection interval, and establishment of the corresponding limit state function;

e) selection of an appropriate reliability analysis computer program and performance of the analysis;

f) performance of a sensitivity analysis of the results to the input parameters.

It is evident that probabilistic fatigue crack growth and fracture assessment are dependent on the availability of a significant amount of information on parameter distributions and are therefore subject to significant uncertainties. These are discussed further in **K.6.2**. A particularly large source of uncertainty in fracture mechanics assessment, which is relevant to both the fatigue crack growth and fracture aspects of the assessment, is the information about the flaw size and distribution.

K.6.2 Random variable modelling

K.6.2.1 General

For fatigue analysis using the Paris Law, there are three main sources of uncertainty [K.12]:

- representation of the log(da/dN) versus log(ΔK) plot by several line segments;
- modelling of crack growth in complex joints;
- calculation of the fatigue loading.

Additionally, for fatigue in inhomogeneous material found in welded joints [i.e. weld metal, heat affected zone (HAZ) and base metal], with cracks typically initiating at the weld toe from welding defects and propagating through the HAZ, weld metal and into the base metal, the crack growth model should be representative of fatigue in these different regions [K.13].

The model uncertainty is dependent on the complexity of the model used. Sometimes there is a trade-off between analytical sophistication and model uncertainty. However, a complex model does not necessarily lead to improved accuracy as demonstrated by a benchmark study from NEA [K.14].

K.6.2.2 Uncertainty models for stress intensity factors

Uncertainties can arise from:

- the application of standard K_I stress intensity factor solutions (e.g. [K.15] and [K.16]) in conjunction with suitable magnification (M_k) factors;
- parametric equations being approximations from regression analysis.

There is limited information on uncertainty factors for stress intensity factors. An uncertainty factor with unit bias and a COV of 0.2 for stress intensity factor is given in reference [K.17].

Parametric curves from a study on M_k factors for T-butt welds [K.18] are adopted in this British Standard. The uncertainties from these curves are very small with COV < 0.015.

K.6.2.3 Flaw size

K.6.2.3.1 General

Flaw size is a primary source of uncertainty in flaw assessment (Annex T gives further information on flaw detectability and sizing errors). A wide-ranging review of NDT research is described in reference [K.19]. A detailed review of probabilistic NDT data is addressed specifically in reference [K.20].

For any probabilistic failure analysis to be credible it is necessary to have a good estimate of the flaw size and distribution. It is also necessary that any function used to describe the flaw size distribution should be as accurate as practicable at the tail of the distribution. The goodness of fit is not critical for small flaw sizes, as such flaws are not important in determining the probability of failure and they are likely to be more subject to measurement errors (i.e. reliability of the NDT method) than are large flaws.

Uncertainty modelling of flaw size may be described for three distinct categories of flaw:

a) flaw size given by NDT;

b) flaws not detected by NDT;

c) single flaw dimension given by NDT.

Guidance on how the flaw size distribution should be defined in each situation is given in **K.6.2.3.2** to **K.6.2.3.4**. In some situations (where one or more flaws have been detected), it might be appropriate to combine the failure probabilities arising due to more than one of a), b) or c).

K.6.2.3.2 Flaw size given by NDT

In the situation given in **K.6.2.3.1**a), the assessment is concerned with a known flaw, reported by NDT. The analogous deterministic assessment is covered in **T.4**, where the reported size is adjusted by a fixed tolerance to allow for possible sizing errors. By contrast, a probabilistic assessment adjusts the reported size by a statistical distribution, which effectively seeks to encapsulate all possible sizing errors. In many cases, the fixed sizing tolerances cited in **T.7** correspond to specific confidence limits, e.g. a two-sided 80% confidence interval. These confidence limits may be converted to distribution parameters (e.g. mean and standard deviation) by reference to standard probability tables; see **T.5** for the case of two-sided 80% confidence intervals for normally distributed sizing errors.

Errors in the sizing of flaws by NDT can be modelled by either normal or log-normal distributions [K.19]. However, unless there is evidence to the contrary, a normal distribution should be assumed ([K.20], [K.21]). In general, sizing errors are functions of flaw type, materials properties, environment, human factors,

surface condition and the inspection technique. Ultrasonic sizing errors can also vary with flaw size (see also Annex T).

When more than one flaw has been reported by NDT, a probabilistic assessment usually focuses on, at least initially, the most severe flaw detected (typically the largest one). But, in principle, the procedure can be repeated for more than one flaw. In this case, the sizing errors for two different flaws can often be treated as independent random variables. However, this assumption might not be appropriate if the primary sizing errors [K.20] have a common mode component, e.g. if the flaws are sized using the same ultrasonic probe without recalibrating between the two sizing measurements.

K.6.2.3.3 Flaws not detected by NDT

In the situation given in **K.6.2.3.1**b), the assessment is concerned with unknown flaws that might not have been reported by NDT. The analogous deterministic assessment is covered in **T.3**, where the ECA is based on a fixed size, which is judged to correspond to adequate inspection reliability. By contrast, a probabilistic assessment describes the flaw size by a statistical distribution, which effectively seeks to encapsulate all possible flaws that might have escaped detection by NDT.

Reference [K.19] gives a review of initial flaw size distributions. Initial flaw size distributions are typically modelled using exponential, Weibull, log-normal or extreme value distributions. A distribution should be selected based on empirical data for a comparable situation. The initial size distribution may be adjusted (multiplied) by the probability of non-detection if an estimate of this is available (e.g. from inspection trials).

Reference [K.22] gives guidance on probabilistic (Bayesian) updating of flaw distributions based on observed field data. Reference [K.23] gives specific information on cracking mechanisms arising in nuclear environments.

By definition, probability density functions are normalized so that the area under the curve is equal to unity. When calculating a failure probability, the overall frequency of occurrence of flaws should be estimated as well. Different definitions of defect rates can be used so any probabilistic assessment should include a clear statement of the definition being used [K.19].

NOTE If, for instance, the defect rate is expressed as the number of flaws per metre of weld, then the derived failure probability is the likelihood of failure of a given metre of weld; but if the flaw rate is expressed as the number of flaws per vessel, then the derived failure probability is the likelihood of failure of a given vessel.

K.6.2.3.4 Single flaw dimension given by NDT

In the situation given in **K.6.2.3.1**c), just one flaw dimension is reported by NDT. This can, for instance, arise when the only practicable inspection method is a surface technique (such as MPI or penetrant testing), in which case the flaw length is reported by NDT but the through-wall extent is unknown. In this case, the reported dimension (typically the length) can be treated as in **K.6.2.3.2**. However, the aspect ratio of the flaw should then be treated essentially as described in **K.6.2.3.3**. Reference [K.19] gives a review of literature pertaining to the initial aspect ratio distributions of defects.

K.6.2.4 Paris parameters *A* and *m*

Two main methods are available to model the crack growth variability through the use of random variables *A* and *m*:

a) *A* and *m* are correlated variables ([K.24], [K.25]);

b) *m* is deterministic and *A* is a variable ([K.26], [K.27]).

The following least squares regression curves relating A and m are available:

1) from test data in reference [K.24] and [K.28], and derived in reference [K.29]:

$$\ln(A) = -14.289 - 3.829\,m \quad \text{(K.6a)}$$

(units in MPa$\sqrt{}$m and da/dN in m/cycle) with the 95% confidence interval for the slope m as (4, 3.66) and the 95% confidence interval for the intercept as (–14.83, –13.75)

2) from reference [K.25]:

$$\ln(A) = -15.59 - 3.47\,m \quad \text{(K.6b)}$$

In most reliability calculations, only A is modelled as a variable.

If specific evidence concerning crack growth uncertainty parameters is lacking, the values in Table K.2 or Table K.3 may be used. The values in Table K.2 from references [K.30] and [K.31] were originally based on data from references [K.24] and [K.32] respectively.

Table K.2 **Paris Law parameters including uncertainty in *A* for a one-stage model (*N*, mm)**

Environment	Source	*m*	ln(*A*)		
			Distribution	Mean	Standard deviation
Weld in air	DNV [K.31]	3.1	Normal	–29.84	0.55
Weld in air	Snijder *et al* [K.32]	3.07	Normal	–29.16	0.31
Parent metal in air	Snijder *et al* [K.32]	2.8	Normal	–27.76	0.23
Weld in seawater	DNV ([K.31], [K.34])	3.5	Normal	–31.01	0.77
		3.1 (with CP)	Normal	–29.84	0.55

The corresponding data for the two stage fatigue crack growth model are shown in Table K.3 (based on Table 8.3, Table 8.4 and reference [K.34]).

NOTE Values here are derived directly from Table 8.3 and Table 8.4 but are presented here in terms of mean and standard deviation of the natural logarithm of A.

Table K.3 **Paris Law parameters including uncertainty in *A* for a two-stage model (*N*, mm)**

	R	*m*		ln(*A*)		
				Distribution	**Mean**	**Standard deviation**
In air						
Stage A	<0.5	8.16		Normal	–59.68	0.64
	≥0.5	5.10		Normal	–39.88	0.74
Stage B	<0.5	2.88		Normal	–28.55	0.27
	≥0.5	2.88		Normal	–28.17	0.39
Freely corroding marine environment						
Stage A	<0.5	3.42		Normal	–31.14	0.52
	≥0.5	3.42		Normal	–30.56	0.58
Stage B	<0.5	1.30		Normal	–15.88	0.21
	≥0.5	1.11		Normal	–14.38	0.14
Marine environment with cathodic protection at –850 mV (Ag/AgCl)						
Stage A	<0.5	8.16		Normal	–59.68	0.64
	≥0.5	5.10		Normal	–39.88	0.74
Stage B	<0.5	2.67		Normal	–25.99	0.47
	≥0.5	2.67		Normal	–25.84	0.61
Marine environment with cathodic protection at –1 100 mV (Ag/AgCl)						
Stage A	<0.5	8.16		Normal	–59.68	0.64
	≥0.5	5.10		Normal	–39.88	0.74
Stage B	<0.5	1.40		Normal	–16.71	0.26
	≥0.5	1.40		Normal	–16.76	0.33

K.6.2.5 Fatigue crack growth threshold ΔK_0

Provided that a standard load-shedding procedure is used with reasonable care, a reproducible threshold value should be obtained with a scatter of no more than 10% (i.e. +5% from the mean value) [K.35]. For values from different batches of material, a further 10% may be assumed. The main sources of uncertainty in the threshold parameter are the *R*-ratio and microstructural properties.

K.7 Fracture assessment: Level II analysis

K.7.1 General

The probabilistic procedure described in this subclause enables the calculation of the probability of failure for two situations:

- flaw size given by NDT;
- flaw not detected by NDT.

The procedure uses two different limit state functions, $g(X)$:

$$g_{FAD}(X) = g_{FAD}(K_{mat},\sigma_Y,a) = f_{FAD} - K_r \quad (K.7)$$

$$g_{L_r}(\sigma_Y,\sigma_U,a) = L_{r,max} - L_r \quad (K.8)$$

These limit state functions are based on the continuous yielding FAD only (Option 1). Then, to calculate the probability of failure, a multidimensional integral has to be evaluated:

$$P_F = P_r[g(\mathbf{x}) < 0] = \int_{g(\mathbf{x})<0} f_X(\mathbf{x})dx \quad \text{(K.8)}$$

K.7.2 Random parameters

The key random parameters are:

a) fracture toughness;

b) yield strength;

c) ultimate tensile strength;

d) flaw size;

   1) flaw size given by NDT;

   2) flaw not detected by NDT;

e) frequency of occurrence of flaws;

f) residual stress distribution;

g) stress intensity factor;

h) FAD modelling uncertainty.

These random parameters are treated as not being correlated with each other. The parameters can follow a normal, lognormal, Weibull or some special distributions (for the flaw size).

Yield and ultimate tensile strengths can be dealt with separately from the fracture uncertainty models except when the correlation is of concern.

K.7.3 Fracture toughness

Fracture toughness is one of the most uncertain parameters in flaw assessment with toughness data for welded joints being very variable, especially for ferritic steels in the transition region (see Annex L and Clause **7**).

The fracture toughness can follow a normal, lognormal or Weibull distribution. Parameter estimation of chosen fracture toughness distribution may be made using an appropriate statistical method. Maximum likelihood estimate (MLE or MML), least square method (LSM), good linear unbiased estimation (GLUE) and method of moments (MOM) are commonly used methods, among which maximum likelihood estimate is found to be the optimum method, particularly when a Weibull distribution is assumed. For a more detailed discussion of the subject of estimation of distribution parameters, see references [K.35] and [K.36]. The normal probability density function has the following form:

$$f(K_I) = \frac{1}{\sigma_{K\text{mat}}\sqrt{2\pi}} \exp\left[-\frac{1}{2}\left(\frac{K_I - \mu_{K\text{mat}}}{\sigma_{K\text{mat}}}\right)^2\right] \quad \text{(K.9)}$$

where:

$\mu_{K\text{mat}}$ is the mean value;

$\sigma_{K\text{mat}}$ is the standard deviation.

The lognormal probability density function has the following form:

$$f(K_I) = \frac{1}{K_I \sigma_{LogNor}\sqrt{2\pi}} \exp\left[-\frac{1}{2}\left(\frac{\ln(K_I) - \mu_{LogNor}}{\sigma_{LogNor}}\right)^2\right], K_I > 0 \quad \text{(K.10)}$$

μ_{LogNor} and σ_{LogNor} are related to the mean, μ_{Kmat}, and standard deviation, σ_{Kmat}, of the fracture toughness respectively as follows:

$$\mu_{LogNor} = \ln(\mu_{Kmat}) - \frac{1}{2}(\sigma_{LogNor})^2 \quad \text{(K.11)}$$

$$\sigma_{LogNor} = \sqrt{\ln\left[1 + \left(\frac{\sigma_{Kmat}}{\mu_{Kmat}}\right)^2\right]} \quad \text{(K.12)}$$

The Weibull probability density function has the following form:

$$f(K_I) = \frac{k}{\theta}\left(\frac{K_I}{\theta}\right)^{k-1} \exp\left[-\left(\frac{K_I}{\theta}\right)^k\right], K_I > 0 \quad \text{(K.13)}$$

The mean and standard deviation of the fracture toughness, μ_{KIc} and σ_{KIc}, are related to the Weibull distribution parameters as follows:

$$\mu_{KIc} = \frac{\theta}{k}\Gamma\left(\frac{1}{k}\right) \quad \text{(K.14)}$$

$$\sigma_{KIc} = \sqrt{\frac{\theta^2}{k}\left\{2\Gamma\left(\frac{2}{k}\right) - \frac{1}{k}\left[\Gamma\left(\frac{1}{k}\right)\right]^2\right\}} \quad \text{(K.15)}$$

where:

$\Gamma(z)$ is the gamma function defined by the integral.

$$\Gamma(z) = \int_0^\infty t^{z-1} e^{-t} dt \quad \text{(K.16)}$$

The Master Curve approach (see also Annex J and Annex L) has been developed by Wallin and co-workers ([K.36] to [K.41]) to define the expected toughness of ferritic steels in the ductile-to-brittle transition using Charpy data from one energy level only. This concept is also included in the SINTAP and FITNET projects ([K.42], [K.43]). This is a significant advance in the probabilistic modelling of fracture toughness as the method has built the physical variability into its mathematical form, which is described by a Weibull distribution.

At $P[K] = 0.5$, the fracture toughness can be described by the Master Curve thus:

$$K_{mat,median} = 30 + 70\exp[0.019(T - T_0)] \quad \text{(K.17)}$$

Based on the Master Curve analysis, Osage, Wirsching and Mansour [K.44] modelled the fracture toughness uncertainty as a two-parameter Weibull distribution with a COV of 0.25 as a reasonable approximation to the three-parameter Weibull distribution.

Sokolov [K.45] applied the Master Curve to the ASME K_{Ic} database and showed that the Master Curve modelled the scatter of K_{Ic} from different materials very well. The reference temperature was determined for the eleven materials in the database. Material could be characterized on the same level of fracture toughness.

In parallel to the Master Curve development, the probability distribution of fracture toughness has been investigated for the Local Approach [K.46]. The physical argument is almost identical to the Master Curve approach. Indeed, the Local Approach allows for the effects of size, scatter and constraints. The challenge is to establish a satisfactory procedure to define the statistical parameters.

K.7.4 Yield strength and ultimate tensile strength

The yield strength and ultimate tensile strength are often described by a normal, lognormal or Weibull distribution. The yield and ultimate strengths are correlated. Some guidance is provided in the Joint Committee on Structural Safety (JCSS) probabilistic model code [K.47].

K.7.5 Flaw size

For information on uncertainty modelling for flaw size, see **K.6.2.3**.

K.7.6 Residual stresses

The assessment of residual stresses is a source of significant uncertainty due to the limited information on distributions in different weld geometries and the inherent variability associated with residual stresses (see Annex Q for further information).

K.7.7 Stress intensity factor

For information on uncertainty modelling for stress intensity factors, see **K.6.2.2**.

K.7.8 Failure Assessment Line

Modelling uncertainty associated with the failure assessment line is discussed in reference [K.48].

K.8 Creep crack growth

K.8.1 Determination of creep rupture life

The main input data required for assessing structures prone to creep damage are the rupture time, defined as a function of the temperature, T, and stress, σ. Experiments indicate that the rupture time shows significant scatter and hence it should be considered as a random variable.

A lognormal distribution can be selected to describe the randomness of the rupture time as follows:

$$\ln \tau = \mu_c + \delta_c \Omega \qquad \text{(K.18)}$$

The total accumulated creep damage, D_c, can be obtained using the life fraction rule. Assuming that the operation of the structure investigated is broken into a series of blocks $[\sigma_i; T_i]$ during which the load/stress, σ_i, and the temperature, T_i, are sensibly constant, the total accumulated damage is then given by the following equation:

$$D_c = \sum_{i=1}^{n} \frac{\Delta t_i}{\tau_i(\sigma_i; T_i)} \qquad \text{(K.19)}$$

Values of t_i are given by Equation (K.18). Substituting Equation (K.18) into Equation (K.19) and introducing the relation $t_{ri} = \exp[\mu_c(\sigma_i; T_i)]$ leads to:

$$D_c = \exp(-\delta_c \Omega) \sum_{i=1}^{n} \frac{\Delta t_i}{t_{ri}} \tag{K.20}$$

The total creep damage accumulation, D_c, should be less than unity ($D_c < 1$) for rupture not to occur within the structure. The probability that D_c is less than 1 can be expressed as follows:

$$P(D_c < 1) = P(\ln D_c < 0) = P\left(-\delta_c \Omega + \ln \sum_{i=1}^{n} \frac{\Delta t_i}{t_{ri}} < 0\right) = P\left(\Omega > \frac{1}{\delta_c} \ln \sum_{i=1}^{n} \frac{\Delta t_i}{t_{ri}}\right) = 1 - \Phi(Z) \tag{K.21}$$

where:

$$Z = \frac{1}{\delta_c} \ln \sum_{i=1}^{n} \frac{\Delta t_i}{t_{ri}} \tag{K.22}$$

As the creep damage cannot exceed a value of 1, the probability $P(D_c \geq 1)$ reduces to the probability $P(D_c = 1)$, and hence using Equation (K.21), the probability of rupture is given by:

$$P(D_c = 1) = \Phi(Z) \tag{K.23}$$

K.8.2 Stochastic creep crack growth

In the case of a cracked structure operating in the creep regime, the creep crack growth rate can be correlated satisfactorily in terms of the creep fracture parameter C^* using the following relation:

$$\frac{da}{dt} = A(C^*)^q \tag{K.24}$$

Material parameters A and q can both be considered as random variables. However, experimental results show that the parameter q does not exhibit significant scatter and hence it is generally considered as a constant. The scatter in the random variable A is usually described by a log-normal distribution as follows:

$$\ln A = \mu_A + \delta_A \Omega \tag{K.25}$$

When several of the inputs to the creep crack growth assessment are considered as random variables (e.g. initial flaw size, creep rupture time, creep crack growth constant A), the determination of the distribution function of the flaw size becomes a complex mathematical expression that is hard to evaluate using numerical integration. In this case, the use of suitable numerical methods, such as Monte Carlo techniques, is required. However, if a sensitivity analysis of the key inputs to the creep crack growth assessment shows that the scatter in the creep crack growth constant A has a dominant effect, then the other input data can be assumed constant and a simplified procedure can be employed. In this case, Equation (K.24) can be integrated numerically and the crack size $a(t_1)$ at time t_1 can be derived as follows:

$$a(t_1) = \int_0^{t_1} A(C^*)^q dt = \exp(\delta_A \Omega) \int_0^{t_1} A_{av}(C^*)^q dt = \exp(\delta_A \Omega) a_{av}(t_1) \tag{K.26}$$

where:

$$\begin{aligned} A_{av} &= \exp(\mu_A) \\ a_{av}(t_1) &= 0 \int^{t_1} A_{av}(C^*)^q dt \end{aligned} \tag{K.27}$$

The probability of the crack size $a(t_1)$ being less than a given crack size a_f is given by:

$$P(a \leq a_f) = P(\ln a \leq \ln a_f) = P\left\{\Omega \leq \frac{\ln a_f - \ln[a_{av}(t_1)]}{\delta_A}\right\} = \Phi(Z_A) \quad \text{(K.28)}$$

where Z_A is defined by the following relation:

$$Z_A = \frac{\ln a_f - \ln[a_{av}(t_1)]}{\delta_A} \quad \text{(K.29)}$$

Equation (K.28) defines the distribution function of the crack size at time t_1. If the calculation is performed for different values of time t_1 then the distribution function of crack size becomes a function of time. Furthermore, the probability of exceeding the crack size, a_f, is $P(a > a_f) = 1 - \Phi(Z_A)$. If a_f is selected as the critical crack size, the probability of fracture is given by the value $1 - \Phi(Z_A)$.

Bibliography for Annex K

Standards publications

For dated references, only the edition cited applies. For undated references, the latest edition of the referenced document (including any amendments) applies.

BS EN 1990, *Basis of structural design*

ISO 2394:2015, *General principles on reliability for structures*

Other documents

[K.1] HADLEY, I. and WU, G. Treatment of reliability in fracture assessments using BS 7910 Annex K, *In: International Journal of Pressure Vessels and Piping*, 168, December 2018, 310–322. <https://doi.org/10.1016/j.ijpvp.2018.11.006>

[K.2] AMIRAFSHARI, A. and STACEY, A., Review of available probabilistic models of the crack growth parameters in Paris equation. *In: Proceedings of the ASME 2019 38th International Conference on Ocean, Offshore and Arctic Engineering (OMAE 2019)*, June 9–14, 2019, Glasgow, Scotland, OMAE2019-961.

[K.3] THOFT-CHRISTENSEN, P. and BAKER, M.J. *Structural reliability theory and its applications*. New York: Springer-Verlag, 1982.

[K.4] MELCHERS, R.E. *Structural reliability – Analysis and prediction*. New York: Ellis Horwood Ltd/John Wiley, 1987.

[K.5] MANSOUR, A., WIRSCHING, P., WHITE, G. and AYYUB, B. *Probability based ship design: implementation of design guidelines*. SSC-392, Ship Structural Committee, 1996.

[K.6] DNV. *Structural reliability analysis of marine structures*, DNV Classification Note 30.6, 1992. <https://rules.dnvgl.com/docs/pdf/DNV/cn/1992-07/Cn30-6.pdf>

[K.7] DNV GL-RP-C210. *Probabilistic methods for planning of inspection for fatigue cracks in offshore structures*, 2015. <https://rules.dnvgl.com/docs/pdf/DNVGL/RP/2015-11/DNVGL-RP-C210.pdf>

[K.8] NORSOK Standard N001, *Integrity of offshore platforms*, Edition 8, 2012. <http://www.standard.no/pagefiles/17477/n-001r7.pdf>

[K.9] HEALTH AND SAFETY EXECUTIVE. *Technical policy for extreme weather hazards*. HSE, 2005. <http://www.hse.gov.uk/offshore/extremeweather.htm>

[K.10] R6 PANEL. *R6: Assessment of the integrity of structures containing defects*. Revision 4, as amended. Gloucester: EDF Energy, 2001.

[K.11] AEA Technology Plc. *Partial safety factors for SINTAP procedure*. HSE Offshore Technology Report 2000/020, prepared by AEA Technology Plc for the Health and Safety Executive, London: The Stationery Office, 2002. <http://www.hse.gov.uk/research/otopdf/2000/oto00020.pdf>

[K.12] MOAN, T., VÅRDAL, O.T. and JOHANNESEN, J. Application of Probabilistic Fracture Mechanics Analysis for Reassessment of Fatigue Life of a Floating Production Unit: Theory and Validation. *In: OMAE 2000, 19th International Conference of Offshore Mechanics and Arctic Engineering*, February 14–17, New Orleans, Louisiana, USA. New York: ASME, 2000.

[K.13] KIRKEMO, F. Applications of probabilistic fracture mechanics to offshore structures. *In: Applied Mechanics Review*, 1988, (41)2, 61–84.

[K.14] NEA COMMITTEE ON THE SAFETY OF NUCLEAR INSTALLATION. *Report on the benchmark on fatigue propagation of a semielliptical crack in a plate subjected to constant cyclic bending*. NEA/CSNI/R(97)8. OECD, 1998. <http://www.oecd-nea.org/nsd/docs/1997/csni-r97-8.pdf>

[K.15] NEWMAN, J.C. and RAJU, I.S. An empirical stress intensity factor eqn. for the surface crack. *In: Engineering Fracture Mechanics*, 1981, 1–2(15), 185–192.

[K.16] RAJU, I.S. and NEWMAN, J.C. Stress intensity factors for a wide range of semi-elliptical surface cracks in finite thickness plates. *In: Engineering Fracture Mechanics*. 1979, 11(4), 817–829. ISSN 0013-7944.

[K.17] JOHANNESEN, J.M., MOAN, T. and VÅRDAL, O.T. Probabilistic inspection planning of fixed offshore structures. ICASP8. Rotterdam: Balkena, 2000. Applications of Statistics and Probability: Civil Engineering and Risk Analysis. *In: Proceedings of the ICASP-8 Conference*, Sydney, NSW, Australia, 12–15 December 1999.

[K.18] BOWNESS, D. and LEE, M.M.K. *Fracture mechanics assessment of fatigue cracks in offshore tubular structures*. HSE Offshore Technology Report 2000/077 for HSE, EPSRC, and Chevron Oil. London: The Stationery Office, 2002.

[K.19] CRUTZEN, S., FRANK, F., FABBRI, L., LEMAITRE, P., SCHNEIDER, C. and VISSER, W. *Compilation of NDE effectiveness data. SINTAP Task 3.4 (Safety factors and risk) final report*. JRC, European Commission, Petten, March 1999. <http://www.eurofitnet.org/sintap_JRC_final_report.pdf>

[K.20] ZHAO, W. and STACEY, A. Review of defect distributions for probabilistic structural integrity assessment. OMAE 2002-28616. *In: Proceedings of the 21st International Conference on Offshore Mechanics and Arctic Engineering, June 23–28, 2002, Oslo*, Norway. ASME CD-ROM (Non-Audio).

[K.21] HEALTH AND SAFETY EXECUTIVE. *Best practice for the procurement and conduct of non-destructive testing. Part 4: Ultrasonic sizing errors and their implication for defect assessment*. HSE Gas and Process Safety Technology Division, April 2008. <http://www.hse.gov.uk/comah/sragtech/ndt4.pdf>

[K.22] BURDEKIN, F.M. and TOWNEND, P.H. Reliability aspects of fracture on stress concentration regions in offshore structures. *In: 2nd International Symposium on Integrity of Offshore Structures*. London: Applied Science, 1981.

[K.23] TANG, W.H. Probabilistic updating of flaw information. *In: Journal of Testing and Evaluation*, 1973, 1(6). ISSN 1945-7553.

[K.24] WÅLE, J. *Crack characterisation for in-service inspection planning – An update. SKI report*, 2006, 24. <https://www.stralsakerhetsmyndigheten.se/contentassets/5453777d9daa4471b5c3b68b554e56f3/200624-crack-characterisation-for-in-service-inspection-planning-an-update>

[K.25] GURNEY, T.R. *Fatigue of welded structures*. 2nd ed. Cambridge, UK: Cambridge University Press, 1979. ISBN 0-521-22558-2.

[K.26] TANAKA, K. and MATSUOKA, S. A tentative explanation for two parameters, C and m, in Paris equation of fatigue crack growth. *In: International Journal of Fracture*, October 1977, 13(5), 563–583.

[K.27] LIDIARD, A.B. Probabilistic fracture mechanics. *In: Proceedings of Fracture mechanics – Current status, future prospects*. Oxford: Pergamon Press, 1979.

[K.28] SLATCHER, S. The probability of failure due to fatigue crack growth from a weld toe. *In: Proceedings of the International Conference on Fatigue of welded constructions*, Brighton, UK, April 1987.

[K.29] CLARK, W.G., Jr. and HUDAK, S.J., Jr. The analysis of fatigue crack growth rate data. *In: J. J. Burke and V. Weiss (eds). Application of Fracture Mechanics to Design*. 1979, 22, New York: Plenum Press, 67–81.

[K.30] CORTIE, M.B. and GARRETT, G.G. On the correlation between the C and m in the Paris equation for fatigue crack propagation. *In: Engineering Fracture Mechanics*, 1988, (30)1, 49–58.

[K.31] DNV. *Fatigue strength analysis for mobile offshore units. Classification Notes,* No. 30-2. DNV, August 1984.

[K.32] SNIJDER, H.H., GIJBERS. F.B.J., DIJKSTRA. O.D. and TER AVEST. F.J. Probabilistic fracture mechanics approach of fatigue and brittle fracture in tubular joints. *In: Noordhoek and J de Back, eds. Steel in Marine Structures*. Amsterdam: Elsevier, 1987, 927–939.

[K.33] MADDOX, S.J. *An analysis of fatigue cracks in fillet welded joints. Welding Institute Report E/49/72*, January 1973.[K.3)]

[K.34] HSE report OTH 511, *A review of fatigue crack growth rates in air and seawater*, 1998. <http://www.hse.gov.uk/research/othpdf/500-599/oth511.pdf>

[K.35] TAYLOR, D.A. *Fatigue thresholds*. London: Butterworths, 1989. ISBN 0408039213.

[K.36] WALLIN, K. *Optimized estimation of the Weibull distribution parameters*. Technical Research Centre of Finland, Metallilaboratorio, 1989.

[K.37] WALLIN, K. *Fracture toughness of engineering materials: Estimation and application*. EMAS publishing, 2011.

[K.38] WALLIN, K. and RINTAMAA, R. *Statistical reevaluation of the ASME K_{IC} and K_{IR} fracture toughness reference curves*. 23rd MPA Seminar, Stuttgart, October 1997.

[K.39] WALLIN, K. *Effect of strain rate on the fracture toughness reference temperature T_0 for ferritic steels*. Recent Advances in Fracture – A Symposium Dedicated to Professor Emeritus Frank A. McClintock, 1997.

[K.40] PISARSKI, H.G. and WALLIN, K. The SINTAP fracture toughness estimation procedure. *In: Engineering Fracture Mechanics*, 2000, 67(6), 613–624.

[K.3)] This reference is available on request from TWI.

[K.41] MERKLE, J.G., WALLIN, K. and McCABE, D.E. *Technical basis for an ASTM standard on determining the reference temperature, T_o, for ferritic steels in the transition range*. U.S. NRC NUREG Report/CR5504, Oak Ridge National Laboratory, 1998.

[K.42] KOÇAK, M., WEBSTER, S., JANOSCH, J.J., AINSWORTH, R.A. and KOERS, R. *FITNET Fitness-for-Service (FFS) – Procedure (Volume 1)*. Geesthacht: GKSS Research Centre, 2008. ISBN 978-3-940923-00-4.

NOTE 1 This procedure is out of print and was effectively superseded by BS 7910:2013.

[K.43] KOÇAK, M., HADLEY, I., SZAVAI, S., TKACH, Y and TAYLOR, N. *FITNET Fitness-for-Service (FFS) – Annex (Volume 2)*. Geesthacht, Germany: GKSS Research Centre, 2008. ISBN 978-3-9409-2301-1.

NOTE 2 This procedure is out of print and was effectively superseded by BS 7910:2013.

[K.44] OSAGE, D., WIRSCHING, P.H. and MANSOUR, A.E. *Application of partial safety factors for pressure containing rquipment*. ASME PVP Conference, Seattle, WA, July 2000.

[K.45] SOKOLOV, M.A. Statistical Analysis of the ASME K_{Ic} data base. *In: Journal of Pressure Vessel Technology*, Feb. 1998, 120(1), 24–28.

[K.46] PINEAU, A. Development of the Local Approach to fracture over the past 25 years: theory and applications. *In: Anales de la Mecánica de Fractura*, 2007, 1, 9–24.

[K.47] Joint Committee on Structural Safety Probabilistic Model Code, ISBN 978-3-909386-79-6. <https://www.jcss.byg.dtu.dk/Publications/Probabilistic_Model_Code>

[K.48] MUHAMMED, A., PISARSKI, H.G. and STACEY, A., *Using wide plate test results to improve predictions from probabilistic fracture mechanics*, Paper presented at ECF 13, San Sebastian, Spain, 6–9 September 2000.

This page deliberately left blank

Annex L (informative)

Fracture toughness determination for welds

L.0 Symbols and definitions

For the purposes of this annex, the following symbols, definitions and units apply, unless otherwise indicated at the point of use.

NOTE In applying the Master Curve method, care needs to be taken over the choice of units. In this annex, the units employed, unless otherwise stated, are those used in the original formulation of the method and published papers. Thus, lengths are in metres (m), yield strength and modulus of elasticity in MPa (N/mm^2) and fracture toughness in MPa$\sqrt{m}$.

Symbol	Definition	Units
a_0	Initial flaw length	m
B	Section thickness in plane of flaw	m
b_0	Size of the uncracked ligament, equal to ($W - a_0$)	m
c	Half flaw length for surface or embedded flaw	m
E	Elastic modulus	MPa (N/mm^2)
J	Line or surface integral that encloses the crack front from one crack surface to the other, used to characterize the local stress-strain field around the crack tip	N/mm
$\dot{K}$	Rate of increase in SIF (stress intensity factor)	MPa$\sqrt{}$ms^{-1}
K_B	Toughness determined from specimens with thickness B	MPa$\sqrt{}$m
$K_{B(limit)}$	Limiting value of K_B	MPa$\sqrt{}$m
K_{CENS}, $K_{CENS}(T_0)$	Estimate of K when using Master Curve method	MPa$\sqrt{}$m
K_i	Individual fracture toughness value	MPa$\sqrt{}$m
$K_{0.025}$	Adjusted value of fracture toughness, equivalent to that for a specimen size of 0.025 m	MPa$\sqrt{}$m
$K_{i(min)}$	Minimum value of individual fracture toughness K_i	MPa$\sqrt{}$m
K_{mat}	Material fracture toughness measured by stress intensity factor	MPa$\sqrt{}$m
$K_{mat(l)}$	Value of K_{mat} adjusted for length of crack front, l, in m, for $l < 2B$	MPa$\sqrt{}$m
$K_{mat(0.025)}$	Characteristic fracture toughness for a reference thickness of 0.025 m	MPa$\sqrt{}$m
K_0, $K_{0(min)}$, $K_{0(stage2)}$, $K_{0(stage3)}$,	Estimates of K when using Master Curve method	MPa$\sqrt{}$m
l	Length of the crack front in the Master Curve method	m
P_f	Fractile representing the cumulative failure probability for fracture toughness distribution derived from experiment data	—
r	Number of specimens which failed by brittle fracture	—
T	Temperature at which K_{mat} is to be determined	°C

(continued)

Symbol	Definition	Units
T_i	Test temperature of a specimen of fracture toughness K_i, adjusted to a 0.025 m specimen size using Equation (L.3)	°C
T_0	Temperature for a median fracture toughness of 100 MPa$\sqrt{}$m in 0.025 m thick specimens	°C
$T_{0,st}$	Temperature term used in MML method	K
$T_{0(max)}$, $T_{0(stage2)}$, $T_{0(stage3)}$	Temperature terms used in MML method	°C
W	Specimen/structural width	m
z	Total number of data set in the set, including those censored, for Master Curve Maximum Likelihood (MML) method; or, total number of valid tests (specimens) in data set	—
Γ	Parameter used in Equation (L.16)	—
Δa_0	Initial crack length	m
ΔT_0	Shift in the Master Curve reference temperature, T_0	°C
δ_i	Kronecker's delta	—
ν	Poisson's ratio	—
σ_Y	Lower yield strength or 0.2% proof strength	MPa

L.1 General

The background to this annex is given in reference [L.1].

Weldment fracture toughness data are required for the fracture assessment of flaws in welds (weld metal and associated HAZ). The assessment of flaws such as HAZ hydrogen cracking, lack of side wall fusion flaws and in-service fatigue cracks which can propagate through the HAZ require HAZ fracture toughness data, while weld metal fracture toughness data are necessary for assessing weld metal hydrogen cracks, solidification cracks, lack of root fusion flaws, etc. This annex gives guidance on the formulation of test procedures suitable for the assessment of flaws in welds in steel. The fracture toughness test procedures should normally be in accordance with BS EN ISO 15653, BS 7448 or ISO 12135 as appropriate.

NOTE 1 Yield strength and elastic modulus are also required at the fracture toughness test temperature.

*NOTE 2 The Master Curve method has been developed for analysing fracture toughness data derived from deeply notched high constraint specimens such as SENB (Single Edge-Notched Bend) and CT (Compact Tension) specimens. There is less experience in applying these methods for low constraint specimens such as SENT (Single Edge-Notched Tension) specimens, e.g. as described in BS 8571, or shallow notch SENB. However, in principle they are applicable, provided that all the qualification requirements in **L.9.2** are achieved.*

Although the procedures described here are focussed on welds and HAZs, they are also applicable to parent material, especially if it is inhomogeneous, such as can occur in thick section plate, forgings and castings.

The determination of HAZ toughness presents particular problems owing to the small size and heterogeneous nature of the HAZ. The test should sample the potentially lowest toughness HAZ microstructure at the crack tip. Expert advice might be necessary to identify this microstructure. Furthermore, fracture

toughness tests on HAZ material generally show a higher degree of scatter than tests on parent metal or weld metal. This is due to the inherent variability of the HAZ microstructures, the different proportions of each microstructure sampled in each test and the formation of low toughness microstructures, often termed local brittle zones (LBZs), in some welds. These effects are generally more apparent in joints tested in the as-welded condition in comparison with joints tested in the fully heat treated condition. Apart from the practical consideration that several specimens with different crack tip locations might be required to sample the HAZ microstructure of interest, the higher degree of scatter might necessitate carrying out a greater number of tests and employing statistical methods in order to characterize HAZ toughness effectively.

There are also problems associated with determining weld metal fracture toughness because weld metals are also heterogeneous, especially those tested in the as-welded condition. Depending on the welding process employed, these can be wide or narrow. The latter can present similar problems as HAZs with respect to testing and scatter. Weld metal can also show variations in fracture toughness over larger distances than HAZ. In particular, weld root toughness can differ markedly from that remote from the root.

L.2 Test philosophy

Fracture toughness tests may be carried out to provide data for general purpose assessments of unspecified flaws or to provide data for the assessment of specified flaws.

Fracture toughness tests on welding procedure qualification plates are normally used to characterize weldment toughness. Such data may be used for assessments where the dimensions and location of the flaws in the structure are not known (e.g. assessments of post-weld heat treatment or inspection requirements). For major construction projects involving large numbers of welding procedures, it could be preferable to plan a programme of testing covering specific material variables and welding parameters (**L.4.1**, **L.4.2**) rather than test individual welding procedures.

Fracture toughness tests may also be conducted on samples taken from the structural component being assessed. This tends to minimize potential problems of ensuring that materials and microstructures being tested are representative. However, the possibility of variations in material and welding procedures used in construction should be recognized when selecting suitable samples for testing.

Results already obtained from earlier test programmes may be used instead of generating new data provided that they are relevant to the structural component being assessed. The results of test programmes might be amenable to statistical analysis and might give a higher degree of confidence for critical applications where the consequences of failure are severe.

Shallow crack fracture toughness tests, such as described in BS EN ISO 15653, may also be used to provide data for a specific assessment, where the dimensions and location of the flaw are known, or where such a test geometry enables the target microstructure to be tested. When shallow crack test data are used, the results should be representative of the crack tip constraint in the component. Further guidance is provided in Annex N.

L.3 Microstructures in steel weldments

L.3.1 Heat affected zones (HAZs)

The base metal adjacent to the weld fusion line is subject to complex thermo-mechanical cycles during welding, which vary with the distance from the fusion line and the sequence in which individual weld beads are deposited. The base material is transformed into a range of different HAZ microstructures, which

change with increasing distance from the fusion line and through the thickness of the joint. The type of microstructure generated is principally dependent on the cooling rate, material composition and subsequent heat treatment. In the as-welded condition, immediately adjacent to the fusion line, the HAZ microstructure consists of a grain coarsened region (GCHAZ) which can be partially transformed by subsequent welding passes into grain refined (GRHAZ), intercritically reheated grain coarsened (ICGCHAZ), or sub-critically reheated grain coarsened (SCGCHAZ) regions. Further from the fusion boundary, the HAZ microstructure changes to GRHAZ, intercritical (ICHAZ), and sub-critical (SCHAZ) regions, each of which is modified by subsequent welding passes.

For structural steels with specified minimum yield strengths up to approximately 460 N/mm^2, the lowest toughness regions of the HAZ are believed to be the GCHAZ adjacent to the fusion line and the boundary of the ICHAZ and the SCHAZ.

NOTE BS EN 10225:2009, which is concerned with steels with specified minimum yield strengths in the range 355 N/mm^2 to 460 N/mm^2, requires specimens to be notched into the GCHAZ and the SCHAZ/ICHAZ boundary.

In steels that are sensitive to strain ageing, the lowest toughness regions are located in the SCHAZ. Both in these materials and in other steels, selection of the HAZ microstructure(s) to be tested should take account of available fracture toughness data and other relevant information.

L.3.2 Weld metals

There are similar variations in microstructures in weld metals as HAZs. After the first run of a multi-pass weld has been deposited, each subsequent run creates HAZs in the runs that precede it. However, unless the weld is particularly narrow, the testing problems are generally less severe compared to HAZs, because it is generally easier to ensure that the various regions have been sampled by the fatigue crack tip. An important feature is that the roots of multi-pass welds are subjected to straining and ageing (see **L.4.2**) and, for this reason, the root tends to be the region of lowest toughness, especially in the as-welded condition. In order to assess this, tests on non-standard shallow crack fracture toughness specimens might be necessary to characterize weld root regions in welds made from one side only, e.g. V welds.

If the weld is narrow and significantly stronger than the adjacent material, a phenomenon called crack path deviation can occur in the specimen at certain temperatures. Fracture initiates in a microstructure other than that in which the crack tip is located so that appropriate fracture toughness cannot be obtained. There is no simple solution to this problem, and expert advice should be sought to devise a suitable testing procedure and to interpret the results.

NOTE A possible solution is to employ the fracture toughness value obtained at the highest temperature at which crack path deviation does not occur. However, this could be very conservative if the assessment temperature is significantly higher.

L.4 Test requirements

L.4.1 Materials

The chemical composition, manufacturing route and heat treatment of the parent material can affect HAZ and weld metal fracture toughness. Fracture toughness data are only applicable to a particular assessment if the test material is representative of that of the structure. As a general rule, the chemical composition of the steel used to make the test specimen should lie within the actual composition range for the particular grade and material thickness used in the structure or the target composition range proposed by the steel maker. For some applications, more stringent requirements might be necessary and, in particular circumstances, it might be appropriate to test material from the same

heat or plate as that in which the flaw is located. When weld metal fracture toughness is to be determined, the consumables used and welding procedures employed should be the same as those used for the structure to be assessed.

L.4.2 Welding

Where possible, the test panel should be welded with the same welding procedure as that used in the structure. However, minor differences in procedure might be acceptable. Procedural variables that affect HAZ and weld metal fracture toughness are as follows:

a) welding heat input;

b) bead overlap (bead size, weave technique, bevel angle);

c) welding consumable (for the weld metal);

d) weld metal strength (for the HAZ);

e) welding process;

f) joint preparation;

g) back-gouging/grinding to weld root;

h) degree of restraint (for the weld metal); and

i) post-weld heat treatment (PWHT).

The relative importance of these variables can vary considerably, and more precise information can often be obtained by examining trends in available fracture toughness data.

In some circumstances, it is necessary for test welds to differ from structural welds in order to facilitate testing, in particular, for full thickness tests on HAZs, a square weld bevel (K- or half-K). This helps to ensure that the crack plane is parallel to the plane of the HAZ, thereby maximizing the amount of HAZ microstructure sampled by the crack tip (see BS EN ISO 15653).

Special specimen preparation and testing requirements might be necessary to determine the fracture toughness of SCHAZs in older, coarse grained as-rolled steels, and also old and modern weld metals that are susceptible to strain ageing. Further information is given by Dolby and Saunders [L.2] and Dawes [L.3].

L.4.3 Specimen geometry

Specimens for fracture tests should normally conform to the requirements of the testing standard (BS 7448, ISO 12135, BS EN ISO 15653).

Tests may also be carried out using square section ($B \times B$) SENB specimens that model the actual orientation and height of the flaw. Guidance is given in BS EN ISO 15653 which enables testing shallow cracks in weld metals (such as the weld root region in single V welds) or in the HAZs of attachment welds or capping passes.

L.5 Test procedure

Fracture toughness tests on standard specimens should be conducted at quasi-static loading rates in accordance with BS EN ISO 15653, BS 7448-1, BS 7448-4, ISO 12135, ASTM E1820 or ASTM E1921 as appropriate. Strength mismatch between the parent material and weld can influence the fracture toughness of the weld metal and HAZ, so the qualification limits for CTOD (Crack Tip Opening Displacement) and J determination given in BS EN ISO 15653 should be employed. Where strength mismatch is outside the limits of that standard, an appropriate analysis procedure should be used to determine fracture toughness.

L.6 Metallographic validation

Where they are required, metallographic examinations should be undertaken in accordance with BS EN ISO 15653. For weld positional testing, a detailed microstructural examination is generally not required. However, for microstructure-specific tests it is necessary to show that the crack tip has sampled the type and proportion of the specified microstructure. Experimental evidence indicates that the exact location of the crack tip, and the amount of the relevant microstructure at the crack tip, affect toughness values [L.4]. This is especially important when testing very narrow welds (e.g. made by laser or electron beam welding) where microstructures and mechanical properties change rapidly over small distances. Toyoda and Thaulow ([L.5], [L.6]) and Francois and Burdekin [L.7] suggest that lower bound toughness values are obtained if metallographic examination shows that regions of the specified microstructure are located within 0.5 mm from the appropriate microstructural boundary in the central 75% of the specimen thickness.

NOTE This is a specification requirement for offshore structural steels given in BS EN 10225:2009, Annex E.

For ferritic steels, experimental evidence indicates that within the HAZ close to the fusion boundary, the lowest resistance to cleavage initiation is associated with the GCHAZ and the ICGCHAZ. Consequently, the specified microstructure for the test includes these microstructures when they are present in the weld.

L.7 Number of tests required

The number of valid test results (i.e. results from specimens where the fatigue crack samples the type and proportion of specified microstructure) required to characterize the HAZ/weld fracture toughness is dependent on the degree of scatter in the results (see **L.6**). If the HAZ/weld exhibits upper shelf behaviour and scatter is limited, then three valid test results might be sufficient (see **7.1.6**).

NOTE BS EN 10225:2009, Annex E requires full thickness specimens and three valid tests for each specified notch location.

If the HAZ/weld is operating in the ductile/brittle transition region or excessive scatter is anticipated, a larger number of test results might be required to characterize HAZ/weld toughness. The number is dependent on the type of statistical analysis required (see **L.8**).

Additional tests might be required to fulfil the metallographic validation criteria given in **L.6** and sufficient material should be provided for re-tests.

L.8 Analysis of test results

The validated results should be subjected to data analysis procedures in accordance with **7.1.4.6** or **7.1.5**, as appropriate. Where only CTOD fracture toughness data are available, **7.1.4.6** may be used to transform the results in equivalent K fracture toughness values. The statistical treatment of fracture toughness data based on the Master Curve is described in **L.9**.

L.9 Statistical treatment of fracture toughness data based on the Master Curve

L.9.1 General

The Master Curve method is designed for the statistical analysis of steels which fracture by cleavage. Consequently, it is applicable where fracture occurs on the lower shelf and transition region of the brittle to ductile transition curve. Furthermore, it is based on the weakest link statistics and is applicable where fracture is initiation-controlled, i.e. the specimen fracture surface shows an initiation site. The method is not strictly applicable when fracture is

propagation-controlled, i.e. where fracture occurs uniformly along the crack front and there is no unique initiation site. This can occur on the lower shelf when very low fracture values are recorded or where initiation is by intergranular fracture rather than cleavage. However, for practical engineering applications these effects can be ignored, and the methods described here are applicable. Further information on the Master Curve method and its limitations can be found in references [L.1] and [L.8].

For homogeneous steels such as parent material and welds in the fully post-weld heat treated condition, statistical analysis of the data may be based on the method described in ASTM E1921. For inhomogeneous material, which can include parent material such as thick section material, forgings and castings, weld metal and HAZs in the as-welded or partially heat treated condition, the Master Curve method may be used. This procedure, which is based on maximum likelihood, is known as the MML method and involves three stages in the analysis of fracture toughness data. The first stage (Stage 1) is identical to that described in ASTM E1921. The second stage (Stage 2) helps to identify whether the data set is scattered by providing a lower tail MML estimation. If the estimates of fracture toughness from the two stages are the same, then the data may be assumed to be homogeneous and after applying a size adjustment the appropriate K_{mat} is calculated. If they are different, then the result from either Stage 2, which is normally lower than Stage 1 or, depending on the number of tests, Stage 3 is used. Stage 3 performs a minimum value estimation to check and makes allowance for outliers, possibly due to gross inhomogeneities in the material. It incorporates an additional safety factor when the number of tests is small.

All three stages should be employed when the number of tests to be analysed is between three and nine. With an increasing number of tests, the influence of the penalty (i.e. the additional safety factor) for small data sets is gradually reduced. For ten and more tests, only Stage 1 and Stage 2 should be used. However, Stage 3 may still be employed for indicative purposes, especially where there is evidence of gross inhomogeneity in the material (e.g. for weld or HAZ material). In such cases, it may be judged that the characteristic value is based upon the stage 3 result, or alternatively, such a result may be used as guidance in a sensitivity analysis or used to indicate the need for more experimental data, when appropriate.

Two procedures are described: the first is applicable when fracture toughness data have been obtained over a range of temperatures (**L.9.4**) and the second when data are obtained at a single temperature (**L.9.5**). However, before these can be used, fracture toughness data need to be qualified in accordance with **L.9.2** and **L.9.3**.

L.9.2 Qualification

Fracture toughness data should meet the the qualification requirements of the chosen testing standard (see **L.5**) and the following:

a) K_B (fracture toughness determined from the test) < $K_{B(limit)}$:

$$K_{B(limit)} = \left[\frac{Eb_0\sigma_Y}{(1-\nu^2)30}\right]^{0.5} \quad \text{(L.1)}$$

b) The test terminates in cleavage after less than $0.05(W - a_0)$ or 0.001 m, whichever is the smaller, of slow-stable crack growth. If these criteria are not met, the test is invalid and should be treated as a censored datum. The censored datum should be assigned a dummy value as follows:

- if the fracture takes place above the $K_{B(limit)}$ (i.e. $K_B > K_{B(limit)}$) use the $K_{B(limit)}$ value;

- if no fracture takes place and the $K_{B(limit)}$ was exceeded, use the $K_{B(limit)}$ value;
- if the slow-stable crack growth limit is exceeded, use the highest K_B from the valid data.

L.9.3 Specimen size adjustment

Adjust all results from specimens whose thickness is not 0.025 m in accordance with Equation (L.2):

$$K_i = K_{0.025} = 20 + (K_B - 20)\left(\frac{B}{0.025}\right)^{0.25} \quad \text{(L.2)}$$

where:

This subclause is applicable to both thicker and thinner specimens.

L.9.4 Master Curve Maximum Likelihood (MML) method for data obtained over a range of temperatures

L.9.4.1 MML Stage 1

Stage 1 is the standard Master Curve determination of the transition temperature T_0. This corresponds to the temperature where the median fracture toughness for a 0.025 m thick specimen has the value 100 MPa$\sqrt{}$m. The procedure described in ASTM E1921 may be used to determine T_0. A summary of that procedure, for test data that have met the qualification requirements, is given in this subclause. This is applicable only where experimental data employed in these analyses lie within the temperature range (T_0 ±50) °C.

T_0 is estimated from K_i using the maximum likelihood expression [Equation (L.3)]:

$$\sum_{i=1}^{z} \frac{\delta_i \exp[0.019(T_i - T_0)]}{11 + 77\exp[0.019(T_i - T_0)]} - \sum_{i=1}^{z} \frac{(K_i - 20)^4 \exp[0.019(T_i - T_0)]}{\{11 + 77\exp[0.019(T_i - T_0)]\}^5} = 0 \quad \text{(L.3)}$$

where:

T_i is the test temperature of specimen *i* with a fracture toughness K_i adjusted to a 0.025 m thickness using Equation (L.2).

δ_i is a censoring parameter (Kronecker's delta) and is 1 if the datum is valid [i.e. meets the requirements of **L.9.2**a) and **L.9.2**b)] or 0 if the datum is a dummy substitute value [i.e.does not meet the requirements of **L.9.2**a) and **L.9.2**b)].

Equation (L.3) is optimized by repeatedly calculating T_0 using an iterative process,to obtain a final estimate of T_0. The summations are performed over values of *i* from 1 to *z*, where *z* is the total number of data in the set, including those censored.

L.9.4.2 MML Stage 2: Lower tail MML estimation.

Stage 2 performs a lower tail MML estimation, which involves further censoring the K_i data used in Stage 1 and is conducted in accordance with steps a) to c) below.

a) Censor all data for which the toughness K_i exceeds the K_{CENS} value given by Equation (L.4) to be equal to the K_{CENS}, setting censoring parameter, δ_i, equal to 0 for the censored data and to 1 for all remaining data:

$$K_{CENS}(T_0) = 30 + 70\exp[0.019(T_i - T_0)] \quad \text{(L.4)}$$

b) The censored data now represents the upper tail of the data set, whilst the un-censored data the lower tail. A new estimate of T_0 is obtained by

 © The British Standards Institution 2019

performing the MML analysis in accordance with Stage 1 using Equation (L.3).

c) Compare the two values of T_0. If the new T_0 is higher than the previous T_0, repeat the upper-tail censoring according to Equation (L.4), using the new value as a benchmark. Continue the iteration until a constant value of T_0 is obtained. This value is designated $T_{0(\text{stage2})}$.

L.9.4.3 MML Stage 3: Minimum value estimation

If the number of specimens in the data set is less than 10, perform Stage 3 (minimum value estimation) in accordance with steps a) to c) below. The minimum value estimation here refers to the highest estimation for T_0.

a) Calculate the maximum value of T_0 (based on a single data point) in accordance with Equation (L.5) using all non-censored data, i.e. where $\delta_i = 1$. This value is designated $T_{0(\text{max})}$.

$$T_{0(\text{max})} = \max \left| T_i - \frac{\ln\left\{ \frac{\left[K_i - 20\left(\frac{z}{\ln 2}\right)^{0.25} - 11 \right]}{77} \right\}}{0.019} \right. \quad \text{(L.5)}$$

where:

z is the total number of valid tests (specimens) in the data set, $\delta_i = 1$.

b) Compare $T_{0(\text{max})}$ and T_0 obtained from Stage 2, i.e. $T_{0(\text{stage2})}$. If $T_{0(\text{max})} - 8\ ^\circ\text{C} > T_{0(\text{stage2})}$, it is an indication that the data is inhomogeneous, and $T_{0(\text{max})}$ should be taken as the representative value of T_0. Otherwise, $T_{0(\text{stage2})}$ may be taken as the representative value.

c) Determine the final value of $T_{0(\text{max})}$ using Equation (L.6), which is a small data set safety correction. This value is designated $T_{0(\text{stage3})}$.

$$T_{0(\text{stage3})} = T_{0(\text{max})} + \frac{14}{\sqrt{r}} \quad \text{(L.6)}$$

where:

$T_{0(\text{max})}$ is the value of T_0 from MML Stage 3 analysis;

$T_{0(\text{stage3})}$ is the final $T_{0(\text{max})}$ value corrected for a small data set.

L.9.4.4 For fracture toughness data obtained at different temperatures using the MML method, an estimate of K_{mat} for the reference thickness of 0.025 m needs to be made from T_0. From the appropriate value of T_0 obtained from Stage 1 to Stage 3, determine the characteristic fracture toughness value $K_{\text{mat}(0.025)}$ for a reference thickness of 0.025 m.

$$K_{\text{mat}(0.025)} = 20 + \{11 + 77\exp[0.019(T - T_0)]\}[-\ln(1 - P_f)]^{0.25} \quad \text{(L.7)}$$

The choice of P_f depends on the level of safety required in the assessment. Typical values selected for P_f are 0.05 when failure of the component being assessed results in loss of life, and 0.2 when failure would result in loss of function of the component and no direct loss of life. A value $P_f = 0.2$ is considered to be consistent with the principles of **7.1.7.3** and **7.1.7.4**.

Next, $K_{\text{mat}(0.025)}$ should be corrected for the size of interest in accordance with **L.9.6**.

L.9.5 Master Curve method for fracture toughness data obtained at the same temperature

L.9.5.1 General

When fracture toughness data are obtained at the same temperature, the results are analysed in three stages to obtain an estimate for K_0; this represents the 63rd percentile of the Weibull distribution. After size correction, fracture toughness, K_{mat} is then estimated from K_0. The procedure for Stage 1 is similar to that described in ASTM E1921 and a summary is provided in references [L.9] and [L.10].

L.9.5.2 MML Stage 1: Determination of MML median value

Experimental data are first evaluated with respect to their validity and censored according to **L.9.2**. Next, the specimen size adjustment is made according to **L.9.3** to obtain K_i. K_0 is then calculated from Equation (L.8):

$$K_0 = 20 + \left[\frac{\sum_{i=1}^{z} (K_i - 20)^4}{\sum_{i=1}^{z} \delta_i} \right]^{0.25} \quad \text{(L.8)}$$

where K_i and δ_i have the same meanings as in Equation (L.3).

L.9.5.3 MML Stage 2: Lower tail MML estimation

Stage 2 performs a lower tail MML estimation following steps a) to c) below by censoring the values above the 50th percentile (median value for the Weibull distribution).

a) Censor all data whose fracture toughness K_i exceeds a K_{CENS} value given by Equation (L.9) below to be equal to K_{CENS}, setting δ_i for the censored data to 0 and to 1 for the remaining valid data.

$$K_{CENS}(K_0) = 20 + \left[(K_0 - 20)(\ln 2)^{0.25} \right] \quad \text{(L.9)}$$

b) Using the censored and remaining data, obtain a new estimate of K_0 using Equation (L.8).

c) Compare the two values of K_0. If the new K_0 is smaller than the previous K_0, repeat the upper-tail censoring according to Equation (L.9), using the new value as a benchmark. Continue the iteration until a constant value of K_0 is obtained. This value is designated $K_{0(stage2)}$. If the iteration converges to multiple roots, then the lowest root is designated $K_{0(stage2)}$.

L.9.5.4 MML Stage 3: Minimum value estimation

If the number of specimens in the data set is less than 10, perform Stage 3 (minimum value estimation) in accordance with steps a) to c) below. This is the lowest estimate for K_0 from the data set.

a) Calculate the minimum value of K_0, $K_{0(min)}$, from the lowest measured $K_{i(min)}$ using all non-censored data, i.e. where δ_i = 1:

$$K_{0(min)} = 20 + \left[(K_{i(min)} - 20) \left(\frac{z}{\ln 2} \right) \right]^{0.25} \quad \text{(L.10)}$$

b) Compare $K_{0(min)}$ and $K_{0(stage2)}$. If $K_{0(min)} < 0.9K_{0(stage2)}$, this is an indication that the data is inhomogeneous, and $K_{0(min)}$ should be taken as the representative value of K_0. Otherwise, $K_{0(stage2)}$ may be taken as the representative value.

 © The British Standards Institution 2019

c) Determine the final value of K_0, which is a small data set safety correction, using Equation (L.11). This value is designated $K_{0(stage3)}$:

$$K_{0(stage3)} = 20 + \frac{K_{0(min)} - 20}{1 + (0.25/\sqrt{r})} \quad \text{(L.11)}$$

where:

$K_{0(min)}$ is the value of K_0 from MML Stage 3 analysis;

$K_{0(stage3)}$ is the final $K_{0(min)}$ value including small data set correction and r is the number of specimens which failed by brittle fracture.

NOTE 1 Stage 3 is normally used when the data set is small (<10 results) and is intended to identify inhomogeneity and enables the fracture toughness distribution to be adjusted in a conservative manner. This is considered necessary because with few data it might not be possible to identify whether the low result is actually part of the lower tail distribution (Stage 2) or an outlier. A response to this situation could be to call for more tests to confirm whether or not the result is indeed an outlier, or for further investigation into the causes of the low result.

For fracture toughness data obtained at the same temperature using the MML method, an estimate of K_{mat} for a reference thickness of 0.025 m is made. From the appropriate value of K_0 obtained from Stages 1 to 3, $K_{0(min)}$, determine the characteristic fracture toughness value $K_{mat(0.025)}$ for a reference thickness of 0.025 m:

$$K_{mat(0.025)} = 20 + \left[K_{0(min)} - 20\right]\left[-\ln(1 - P_f)\right]^{0.25} \quad \text{(L.12)}$$

The choice of P_f depends on the level of safety required in the assessment, i.e. the target probability of failure and the consequences of failure. Suggested values for P_f are given in **L.9.4.3**.

Next, $K_{mat(0.025)}$ is corrected to the notional crack front length (l) of interest in accordance with **L.9.6**.

NOTE 2 K_0 is related to T_0 using the following equation:

$$K_0 = 31 + 77\exp[0.019(T - T_0)] \quad \text{(L.13)}$$

Care should be exercised if the equation is used outside the temperature range (T_0 ±50) °C, or if K_0 is used to estimate T_0 and the experimental data are obtained at a significantly higher temperature than T_0 (i.e. more than 15 °C higher).

L.9.6 Value of K_{mat} for use in integrity assessment

Since the Master Curve method is based on the weakest link statistics, the estimated value of fracture toughness for a reference thickness of 0.025 m depends on the crack front length present in the structural component. Equation (L.14) is used to make that adjustment:

$$K_{mat} = K_{mat(l)} = 20 + \left[K_{mat(0.025)} - 20\right](0.025/l)^{0.25} \quad \text{(L.14)}$$

NOTE 1 When the flaw size is unknown (e.g. when a limiting flaw size is being estimated), an iterative method needs to be used to adjust l and K_{mat} until a constant value is achieved.

NOTE 2 K_{mat} may be used directly in integrity assessments or after corrections have been applied to allow for differences in crack-tip constraint between the specimen and structure in accordance with Annex N.

NOTE 3 The length l is defined as the length of the crack front over which the stress intensity factor, K is constant. This is difficult to define without detailed analysis of the crack shape. For practical purposes the following approach is recommended: for surface breaking cracks l = 2c, for embedded cracks, l = 4c, for through wall thickness cracks l = 2B.

*NOTE 4 Some experts restrict Equation (L.14) to $l \geq 0.025$ m. However, the basis for this view is uncertain, especially as the Master Curve method is often applied to the analysis of fracture toughness data obtained from 0.010 m thick specimens. For this reason, no lower limit to l is defined in **L.9.6**. Nevertheless, caution needs to be exercised when applying Equation (L.14) to crack lengths less than 0.025 m when fracture toughness data have been generated using specimen thicknesses greater than 0.025 m (i.e. $l > 0.025$ m).*

NOTE 5 The correction to fracture toughness for crack length given by Equation (L.14) is inconsistent with the procedure described in the rest of the standard, where fracture toughness is determined on a specimen representing the full thickness of the component. However, since the Master Curve method is based on weakest link statistics the crack length correction is considered to be necessary.

L.9.7 Correction for loading rate within the ductile-to-brittle transition region

Fracture toughness tests are normally carried out at quasi-static loading rates defined by the testing standard. Where these results need to be applied to structural components made from ferritic/bainitic steels which are subjected to dynamic loading, a reduction in fracture toughness within the ductile-to-brittle transition region is expected. This is manifest as a shift of the transition curve to a higher temperature. This shift may be derived from the shift in the Master Curve reference temperature, T_0, using the following equations:

$$\Delta T_0 = \frac{T_{0,st} \ln(\dot{K})}{\Gamma - \ln(\dot{K})} \quad \text{(L.15)}$$

where:

$$\Gamma = 9.9 \exp\left[\left(\frac{T_{0,st}}{190}\right)^{1.66} + \left(\frac{\sigma_Y}{722}\right)^{1.09}\right] \quad \text{(L.16)}$$

where:

$T_{0,st}$ is T_0 (in Kelvin, i.e.°C + 273) determined from quasi-static tests (see **L.9.4** and **L.9.4.2**);

σ_Y is the quasi-statically determined yield strength (see **7.1.3.1**) at temperature $T_{0,st}$.

The ΔT_0 value established from Equation (L.15) is added to T_0 described in **L.9.4**. This sum ($\Delta T_0 + T_0$) is then used to determine loading rate corrected $K_{mat(0.025)}$ from Equation (L.7) and K_{mat} for the integrity assessment in accordance with **L.9.6** using Equation (L.14).

Bibliography for Annex L

Standards publications

For dated references, only the edition cited applies. For undated references, the latest edition of the referenced document (including any amendments) applies.

ASTM E1820, *Standard test method for measurement of fracture toughness*

ASTM E1921, *Standard test method for determination of reference temperature, T_o, for ferritic steels in the transition range*

BS 7448 (all parts), *Fracture mechanics toughness tests*

BS 8571, *Method of test for determination of fracture toughness in metallic materials using single edge notched tension (SENT) specimens*

BS EN 10225:2009, *Weldable structural steels for fixed offshore structures – Technical delivery conditions*

BS EN ISO 15653, *Metallic materials – Method of test for the determination of quasistatic fracture toughness of welds*

ISO 12135, *Metallic materials – Unified method of test for the determination of quasistatic fracture toughness*

Other documents

[L.1] HADLEY, I. and PISARSKI H.G. Materials properties for engineering critical assessment: Background to the advice given in BS 7910:2013. *In: International Journal of Pressure Vessels and Piping*, December 2018, 168, 191–199. <https://doi.org/10.1016/j.ijpvp.2018.10.016>

[L.2] DOLBY, R.E. and SAUNDERS, G.G. Sub-critical HAZ fracture toughness of C-Mn steels. *In: Metal Construction and British Welding Journal*, 1972, 4(5), 185–190. ISSN 0307-7896.

[L.3] DAWES, M.G. Significance of locally intensified strain ageing to the fracture toughness of welded structures. *In:* W.G. REUTER et al., eds. *Proceedings of 26th Conference on Fracture Mechanics*. STP 1256. Philadelphia: ASTM, 1995. ISBN 0803119968.

[L.4] PISARSKI, H.G. and HARRISON, P.L. Welding procedures for heat affected zone fracture toughness assessment. *In: Recent Trends in Welding Science and Technology*. JWR 89. Gatlinburg, Tennn. USA, May 14–18 1989. ASM International, 833–840.

[L.5] THAULOW, C., HAUGE, M., PAAUW, A.J., TOYODA, M. and MINAMI, F. Effect of notch tip location in CTOD testing of the heat affected zone of steel weldments. *In: ECF 10 – Structural integrity: Experiments, Models and Applications*, Berlin, 1994. <http://www.gruppofrattura.it/ocs/index.php/esis/ECF10/paper/viewFile/5660/2806>

[L.6] THAULOW, C. and TOYODA, M. *Strength mis-match effect on fracture behaviour of HAZ. Mis-Matching of interfaces and welds*, Edited by K.-H. Schwalbe and M. Koçak, 1997, GKSS Research Center Publications, Geesthacht, FRG, 75–98.

[L.7] FRANÇOIS, D. and BURDEKIN, F.M. State of the art résumé on significance of local brittle zones. *In: Welding in the World 41*, 1998, 138–143, Pergamon, 26/01/2015.

[L.8] WALLIN, K. 2011. *Fracture toughness of engineering materials – Estimation and application*. FESI/EMAS Publishing. ISBN 978 0 9552994 6 9.

[L.9] MERKLE, J.G., WALLIN, K. and McCABE, D.E. *Technical Basis for an ASTM Standard on Determining the Reference Temperature, T_0, for Ferritic Steels in the Transition Range*. U.S. NRC NUREG Report/CR5504, Oak Ridge National Laboratory, 1998.

[L.10] PISARSKI, H.G. and WALLIN, K. The SINTAP fracture toughness estimation procedure. *In: Engineering Fracture Mechanics*, 67(2000), 613–624.

This page deliberately left blank

Annex M (informative)

Stress intensity factor solutions

M.0 Symbols and definitions

For the purposes of this annex, the following symbols, definitions and units apply, unless otherwise indicated at the point of use.

Symbol	Definition	Units
A	Parameter used in defining stress intensity solutions	—
A_1	Area of rectangle which demarcates flaw	mm^2
A_2	Full load bearing area containing flaw	mm^2
a	Half flaw length for through-thickness flaw, flaw height for surface flaw or half height for embedded flaw	mm
B	Section thickness in plane of flaw	mm
B'	Effective section thickness ($2a + 2p$)	mm
c	Half flaw length for surface or embedded flaw	mm
$2c_c$	Flaw length (surface or embedded flaw)	mm
d	Subscript to define deepest point	—
f_w	Finite width correction factor	—
f_{wb}	Modified finite width correction factor for bending component	—
f_{wm}	Modified finite width correction factor for membrane component	—
f_θ, f_i, f_i^d, f_i^s, f_1, f_2, f_3	Parameters used in calculating stress intensity factor solutions	—
G_p	Influence coefficient used in calculating stress intensity factor solutions due to internal pressure (see **M.8**)	—
G_1	Influence coefficient used in calculating stress intensity factor solutions due to uniform loading (see **M.8**)	—
G_2	Influence coefficient used in calculating stress intensity factor solutions due to linear loading (see **M.8**)	—
G_1, G_2, G_{11}, G_{12}, G_{13}, G_{21}, G_{22}, G_{23}	Parameters used in calculating stress intensity factor solutions (see **M.4** and **M.5**)	—
g, g_1, g_2..., etc.	Parameters in calculating stress intensity factor solutions	—
H, H_1, H_2	Parameter used in calculating stress intensity factor solutions	—
h	Weld leg length	mm
K_b	Stress intensity factor for the bending component of stress	$N/mm^{3/2}$
K_I	Applied tensile (mode I) stress intensity factor	$N/mm^{3/2}$
$K_I^{bending}$	Contributions to K_I of through-wall bending	$N/mm^{3/2}$
$K_I^{membrane}$	Contribution of through-wall bending (tensile on outside surface, compressive on inside surface) stresses to K_I	$N/mm^{3/2}$

(continued)

Symbol	Definition	Units
$K_{\text{single crack}}$	Stress intensity factor for a single corner crack at a hole	N/mm$^{3/2}$
$K_{\text{symmetric crack}}$	Stress intensity factor for a symmetric crack	N/mm$^{3/2}$
k_m	Stress concentration factor due to misalignment	—
k_{tb}	Bending stress concentration factor	—
k_{tm}	Membrane stress concentration factor	—
L	Attachment length	mm
M	Bulging correction factor	—
M_S, M_T	Stress magnification factors	—
M_{global}	Global moment	Nmm
M_k	Stress intensity correction factor	—
M_m, M_b, M_{km}, M_{kb}	Stress intensity magnification factors	—
$M_m(d)$, $M_m(s)$, $M_b(d)$, $M_b(s)$	Stress intensity magnification factors of membrane and bending components at surface (s) and deepest point (d) of a crack	—
M_m*, M_b*	Factors used in calculating M_m and M_b	—
M_1, M_2, M_3, M_4	Parameters used in calculating stress intensity factor solutions	—
n	Factor used in calculating stress intensity factor solutions for corner flaws at hole; n = 1 for a single flaw; n = 2 for two symmetric flaws	—
P_b	Primary bending stress	N/mm^2
P_m	Primary membrane stress	N/mm^2
$P_{m,b}$	Primary membrane stress due to global bending moments	N/mm^2
p	Shortest distance from material surface to embedded flaw	mm
p	Internal pressure	N/mm^2
Q_b	Secondary bending stress	N/mm^2
Q_m	Secondary membrane stress	N/mm^2
q	Parameter used in calculating stress intensity factor solutions	—
r	Radius of hole, round bar or bolt as appropriate	mm
r_i	Internal radius	mm
r_m	Mean radius	mm
r_o	External radius	mm
s	Subscript to define free surface point	—
t_w	Weld throat thickness	mm
v	Factor used in calculating M_k at weld toe	—
W	Specimen or structural width	mm
w	Factor used in calculating M_k at weld toe	—
Y	Stress intensity correction factor	—
$(Y\sigma)_p$	Contribution to K_I due to primary stress	N/mm^2
$(Y\sigma)_s$	Contribution to K_I due to secondary stress	N/mm^2
$(Y\Delta\sigma)_p$	Contribution to ΔK_I due to primary stress	N/mm^2

 © The British Standards Institution 2019

(continued)

Symbol	Definition	Units
Z	Measure of position through the thickness	mm
ΔK_I	Range of stress intensity factor in fatigue	$N/mm^{3/2}$
ΔP_b	Range of bending stress in fatigue	N/mm^2
ΔP_m	Range of membrane stress in fatigue	N/mm^2
$\Delta\sigma$	Stress range in fatigue	N/mm^2
Θ	Parametric angle to identify position along an elliptical flaw front	Radians
λ, λ_0, λ_1, λ_2..., etc.	Parameters used in calculating stress intensity factors	—
μ, μ_0, μ_1	Parameters used in calculating stress intensity factors	—
ν	Poisson's ratio	—
σ	Stress	N/mm^2
σ_i	Component of polynomial description of stress distribution	N/mm^2
σ_{ref}	Reference stress	N/mm^2
Φ	Complete elliptical integral of the second kind	—

M.1 General

The background to this annex is given in reference [M.1].

This annex contains stress intensity factor, K_I, solutions for a range of flaw types that are likely to arise in welded joints. Additional stress intensity factor solutions have been published in the form of handbooks ([M.2] to [M.6]) for a wide range of geometry and loading configurations. Alternatively, numerical analysis methods (e.g. finite elements) or weight function techniques [M.7] may be used to derive stress intensity factors, but the basis of the method and the results should be fully documented.

The validity of the solutions given in this annex is limited strictly to the ranges stated; no extrapolation outside these limits should be carried out. For assessing plastic collapse, matching sets of reference stress (σ_{ref}) and limit load solutions are provided in Annex P.

The general form of the stress intensity factor solution given in this annex is:

$$K_I = (Y\sigma)\sqrt{\pi a} \quad \text{(M.1)}$$

For fatigue assessments the corresponding stress intensity factor range is:

$$\Delta K_I = Y(\Delta\sigma)\sqrt{\pi a} \quad \text{(M.2)}$$

For fracture assessments the following equation applies:

$$Y\sigma = (Y\sigma)_p + (Y\sigma)_s \quad \text{(M.3)}$$

These are calculated as follows:

$$(Y\sigma)_p = Mf_w\{k_{tm}M_{km}M_mP_m + k_{tb}M_{kb}M_b[P_b + (k_m - 1)P_m]\} \quad \text{(M.4)}$$

$$(Y\sigma)_s = M_mQ_m + M_bQ_b \quad \text{(M.5)}$$

For fatigue assessments the following equation applies:

$$(Y\Delta\sigma)_p = Mf_w\{k_{tm}M_{km}M_m\Delta P_m + k_{tb}M_{kb}M_b[\Delta P_b + (k_m - 1)\Delta\sigma_m]\} \quad \text{(M.6)}$$

In Equation (M.1) to Equation (M.6), expressions for M, f_w, M_m and M_b are given in **M.2** to **M.10** for different types of flaws in different configurations. M_{km} and M_{kb} apply when the flaw is in a region of local stress concentration and are given in **M.1**. Guidance on k_{tm}, k_{tb} and k_m is given in **6.4.4** and Annex D.

All solutions exclude the possible effects of crack face pressure for pressurized components. While the effect is likely to be small, there might be circumstances where it needs to be taken into account. In such cases, the effect of crack face pressure may be determined directly using suitable FEA. Alternatively, the compendium of stress intensity factor solutions in API 579-1/ASME FFS-1:2016, Annex 9B may be used, where solutions are provided for cylinders and spheres subject to internal pressure for different crack types and orientations.

M.2 Net area, misalignment and stress concentration effects

The estimation methods for stress intensity factor K_I do not always allow for situations:

- where the flaw area is significant compared to the load bearing cross-section area;
- where misalignment or angular distortion occurs; or
- for long flaws in curved shells subject to internal pressure where bulging effects can occur.

Where the actual flaw area is greater than 10% of the load bearing cross-section area (generally BW), K_I should be multiplied by the f_w factor. Formulae for f_w are given in this annex for different geometries; where there is no formula specified for the geometry under consideration, Equation (M.7) should be used:

$$f_w = [\sec(\pi A_1/2A_2)]^{0.5} \quad \text{(M.7)}$$

where:

$A_2 = BW$

$A_1 = 2ac$ for surface flaws

$A_1 = 4ac$ for embedded flaws

$A_1 = 2aB$ for through-thickness flaws

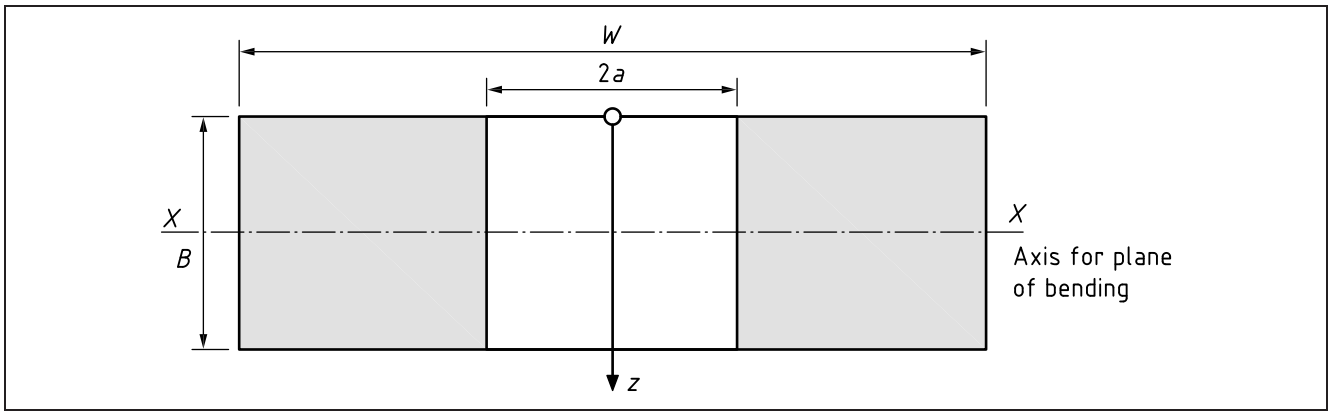
M.3 Stress intensity factors for plates

M.3.1 Through-thickness flaws in plates

See Figure M.1 for the definition of the geometry. The stress intensity factor, taken from Rooke and Cartwright [M.4] and the R6 procedure [M.8], is given by Equation (M.1) to Equation (M.6), where:

$$M = M_m = 1$$
$$f_w = [\sec(\pi a/W)]^{0.5} \quad \text{(M.8)}$$
$$M_b = 1 - \frac{2z}{B}$$

Figure M.1 **Through-thickness flaw geometry**



M.3.2 Edge flaws in plates

This solution is from Rooke and Cartwright [M.4]. See Figure M.2 for the definition of the geometry.

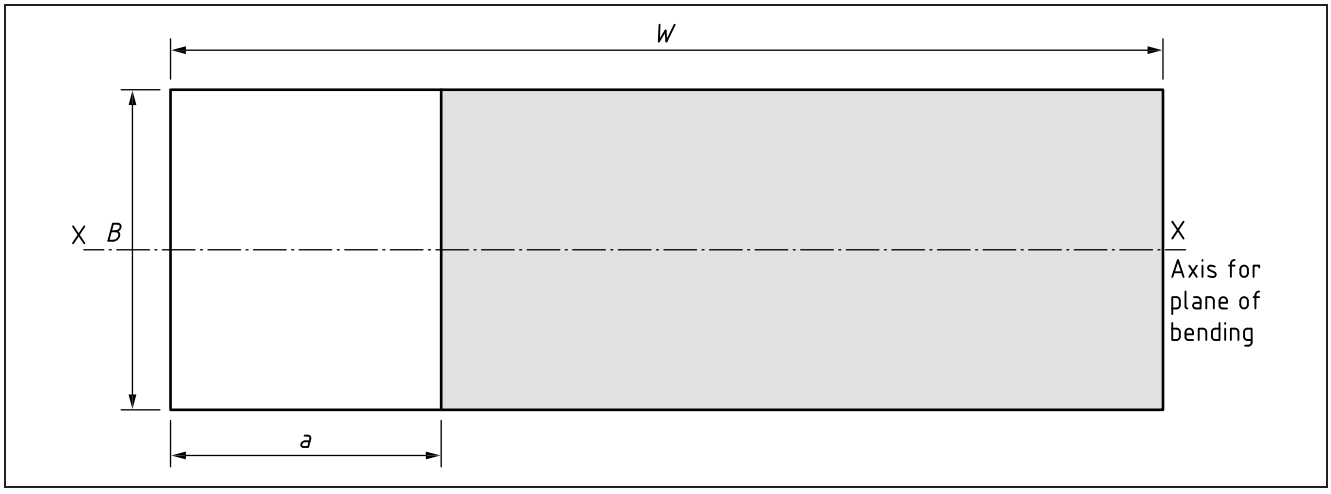
The stress intensity factor is given by Equation (M.1) to Equation (M.6), where, for $a/W \leq 0.6$:

$$M = 1$$

$$M_m = M_b = 1.12 - 0.23\left(\frac{a}{W}\right) + 10.6\left(\frac{a}{W}\right)^2 - 21.7\left(\frac{a}{W}\right)^3 + 30.4\left(\frac{a}{W}\right)^4 \quad \text{(M.9)}$$

*NOTE This solution has the same form as that for extended surface flaws (**M.4.3**), Equation (M.15), although the plate membrane and bending stresses have been superimposed. Equation (M.9) does not account for in-plane bending (e.g. SENB specimen). In such cases, a modified form of the extended surface flaw solution may be used.*

Figure M.2 **Edge flaw geometry**



M.4 Stress intensity factor solutions for plates containing surface and embedded flaws

M.4.1 Surface flaws in plates; solution for uniform tension and/or through-wall bending

M.4.1.1 General

This solution is taken from Newman and Raju [M.9] and is suitable for cases in which the stress distribution across the uncracked body can be expressed in terms of uniform membrane stress, bending stress, or a combination of the two. Where the stress distribution is described by a polynomial, the solution given in **M.4.2.2** offers higher accuracy.

See Figure M.3 for the definition of the geometry. The stress intensity factor solution presented in this subclause should be applied to both normal restraint and pin-jointed boundary conditions (see **P.6.1**). The stress intensity factor is given by Equation (M.1) to Equation (M.6), where:

$$M = 1$$

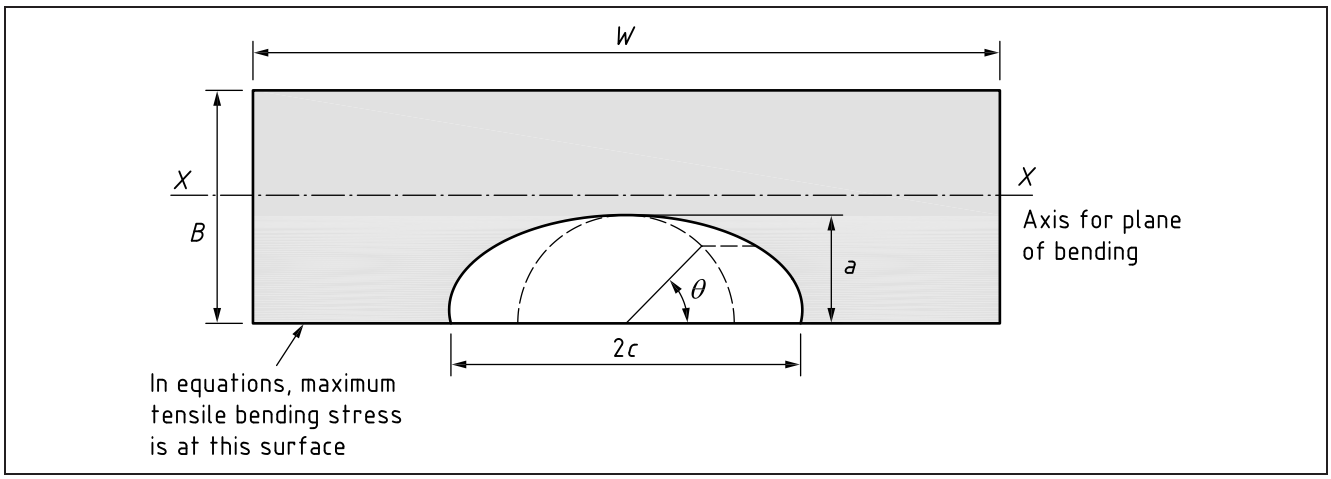
$$f_w = \left\{ \sec\left[\left(\frac{\pi c}{W}\right) \left(\frac{a}{B}\right)^{0.5} \right] \right\}^{0.5} \qquad \text{which equals 1.0 if } a/2c = 0$$

NOTE This equation for f_w is applicable up to $2c/W = 0.8$.

M_m is as defined in **M.4.1.2**;

M_b is as defined in **M.4.1.3**.

Figure M.3 **Surface flaw**



M.4.1.2 Membrane loading

M.4.1.2.1 Conditions

The following conditions apply:

$$0 < \left(\frac{a}{2c}\right) \leq 1.0$$

$$0 \leq \theta \leq \pi$$

and:

$$\left(\frac{a}{B}\right) < 1.25\left[\left(\frac{a}{c}\right) + 0.6\right] \qquad \text{for } 0 < a/2c \leq 0.1$$

$$\left(\frac{a}{B}\right) < 1.0 \qquad \text{for } 0.1 < a/2c \leq 1.0$$

 © The British Standards Institution 2019

M.4.1.2.2 Solution

The solution is as follows.

$$M_m = \left[M_1 + M_2\left(\frac{a}{B}\right)^2 + M_3\left(\frac{a}{B}\right)^4\right]\frac{gf_\theta}{\Phi} \quad \text{(M.10)}$$

where:

$M_1 = 1.13 - 0.09\left(\frac{a}{c}\right)$ for $0 < a/2c \leq 0.5$

$M_1 = \left(\frac{c}{a}\right)^{0.5}\left[1 + 0.04\left(\frac{c}{a}\right)\right]$ for $0.5 < a/2c \leq 1.0$

$M_2 = \left[\frac{0.89}{0.2 + (a/c)}\right] - 0.54$ for $0 < a/2c \leq 0.5$

$M_2 = 0.2\left(\frac{c}{a}\right)^4$ for $0.5 < a/2c \leq 1.0$

$M_3 = 0.5 - \frac{1}{0.65 + \left(\frac{a}{c}\right)} + 14\left(1 - \frac{a}{c}\right)^{24}$ for $0 < a/2c \leq 0.5$

$M_3 = -0.11\left(\frac{c}{a}\right)^4$ for $0.5 < a/2c \leq 1.0$

$g = 1 + \left[0.1 + 0.35\left(\frac{a}{B}\right)^2\right](1 - \sin\theta)^2$ for $0 < a/2c \leq 0.5$

$g = 1 + \left[0.1 + 0.35\left(\frac{c}{a}\right)\left(\frac{a}{B}\right)^2\right](1 - \sin\theta)^2$ for $0.5 < a/2c \leq 1.0$

$f_\theta = \left[\left(\frac{a}{c}\right)^2\cos^2\theta + \sin^2\theta\right]^{0.25}$ for $0 < a/2c \leq 0.5$

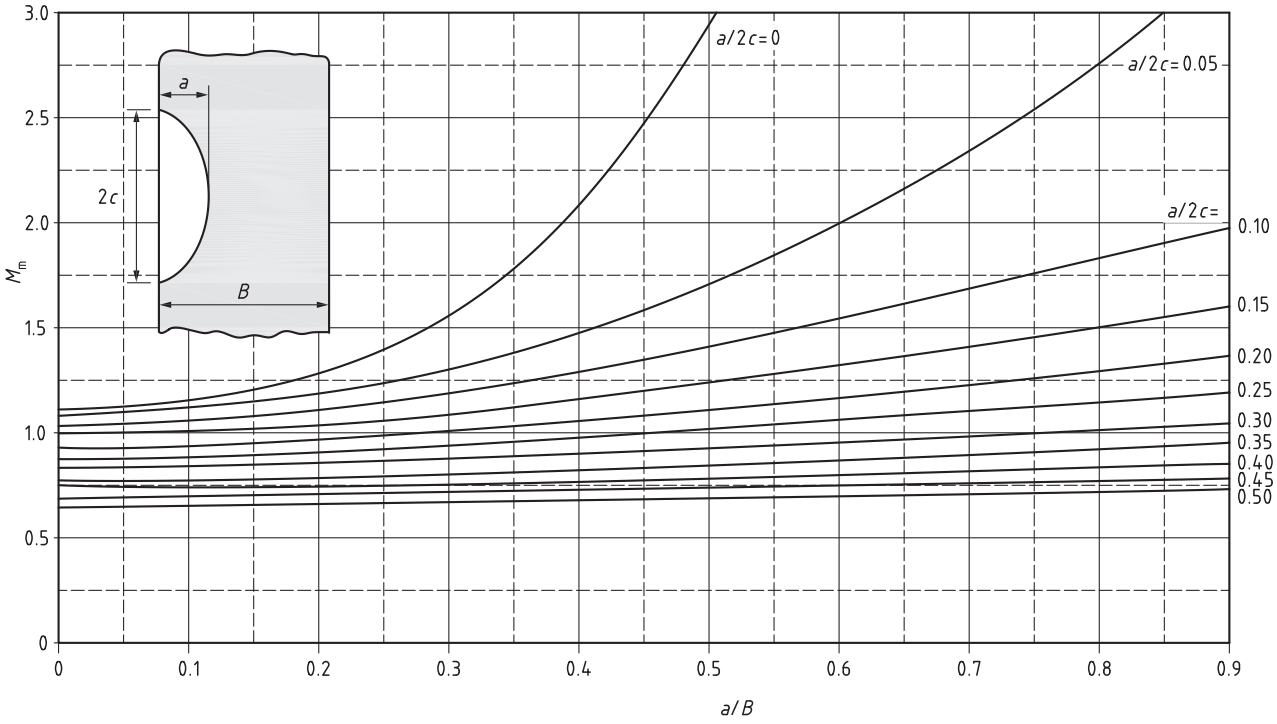
$f_\theta = \left[\left(\frac{c}{a}\right)^2\sin^2\theta + \cos^2\theta\right]^{0.25}$ for $0.5 < a/2c \leq 1.0$

Φ, the complete elliptic integral of the second kind, may be determined from standard tables or from the following solution, which is sufficiently accurate:

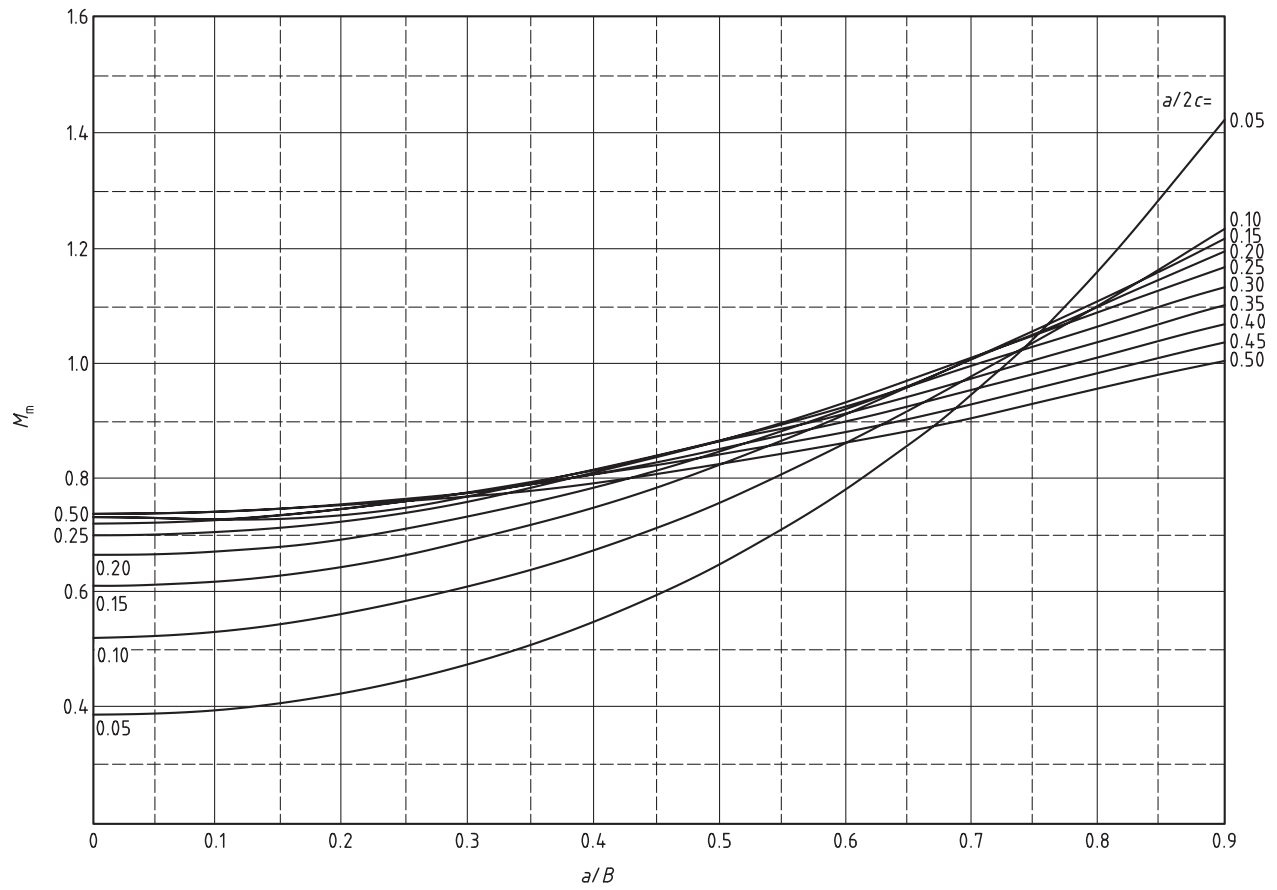
$$\Phi = \left[1 + 1.464\left(\frac{a}{c}\right)^{1.65}\right]^{0.5} \quad \text{for } 0 < a/2c \leq 0.5$$
$$\Phi = \left[1 + 1.464\left(\frac{c}{a}\right)^{1.65}\right]^{0.5} \quad \text{for } 0.5 < a/2c \leq 1.0 \quad \text{(M.11)}$$

Graphical solutions for M_m are given in Figure M.4a) and Figure M.4b).

Figure M.4 **Stress intensity magnification factor M_m for surface flaws in tension**



a) At deepest point along flaw front, i.e. $\theta = \pi/2$ rad



b) At flaw tip on material surface, i.e. $\theta = 0$ rad

M.4.1.2.3 Simplifications

The following simplifications may be used as indicated.

a) At the deepest point on the crack front:

$g = 1$

$f_\theta = 1$ for $0 < a/2c \leq 0.5$

$f_\theta = \left(\frac{c}{a}\right)^{0.5}$ for $0.5 < a/2c \leq 1$

b) At the ends of the crack, $\theta = 0$, so that:

$g = 1.1 + 0.35\left(\frac{a}{B}\right)^2$ for $0 < a/2c \leq 0.5$

$g = 1.1 + 0.35\left(\frac{c}{a}\right)\left(\frac{a}{B}\right)^2$ for $0.5 < a/2c \leq 1.0$

$f_\theta = \left(\frac{a}{c}\right)^{0.5}$ for $0 < a/2c \leq 0.5$

$f_\theta = 1.0$ for $0.5 < a/2c \leq 1.0$

c) If $a/2c > 1.0$, use the solution for $a/2c = 1.0$.

M.4.1.3 Bending loading

M.4.1.3.1 Conditions

The conditions should be in accordance with **M.4.1.2.1**.

M.4.1.3.2 Solutions

The solutions are as follows.

$$M_b = HM_m \quad \text{(M.12)}$$

where:

$H = H_1 + (H_2 - H_1)\sin^q\theta$

M_m is calculated from Equation (M.10).

where:

$q = 0.2 + \left(\frac{a}{c}\right) + 0.6\left(\frac{a}{B}\right)$ for $0 < a/2c \leq 0.5$

$q = 0.2 + \left(\frac{c}{a}\right) + 0.6\left(\frac{a}{B}\right)$ for $0.5 < a/2c \leq 1.0$

$H_1 = 1 - 0.34\left(\frac{a}{B}\right) - 0.11\left(\frac{a}{c}\right)\left(\frac{a}{B}\right)$ for $0 < a/2c \leq 0.5$

$H_1 = 1 - \left[0.04 + 0.41\left(\frac{c}{a}\right)\right]\left(\frac{a}{B}\right) + \left[0.55 - 1.93\left(\frac{c}{a}\right)^{0.75} + 1.38\left(\frac{c}{a}\right)^{1.5}\right]\left(\frac{a}{B}\right)^2$ for $0.5 < a/2c \leq 1.0$

$H_2 = 1 + G_1\left(\frac{a}{B}\right) + G_2\left(\frac{a}{B}\right)^2$

where:

$G_1 = -1.22 - 0.12\left(\frac{a}{c}\right)$ for $0 < a/2c \leq 0.5$

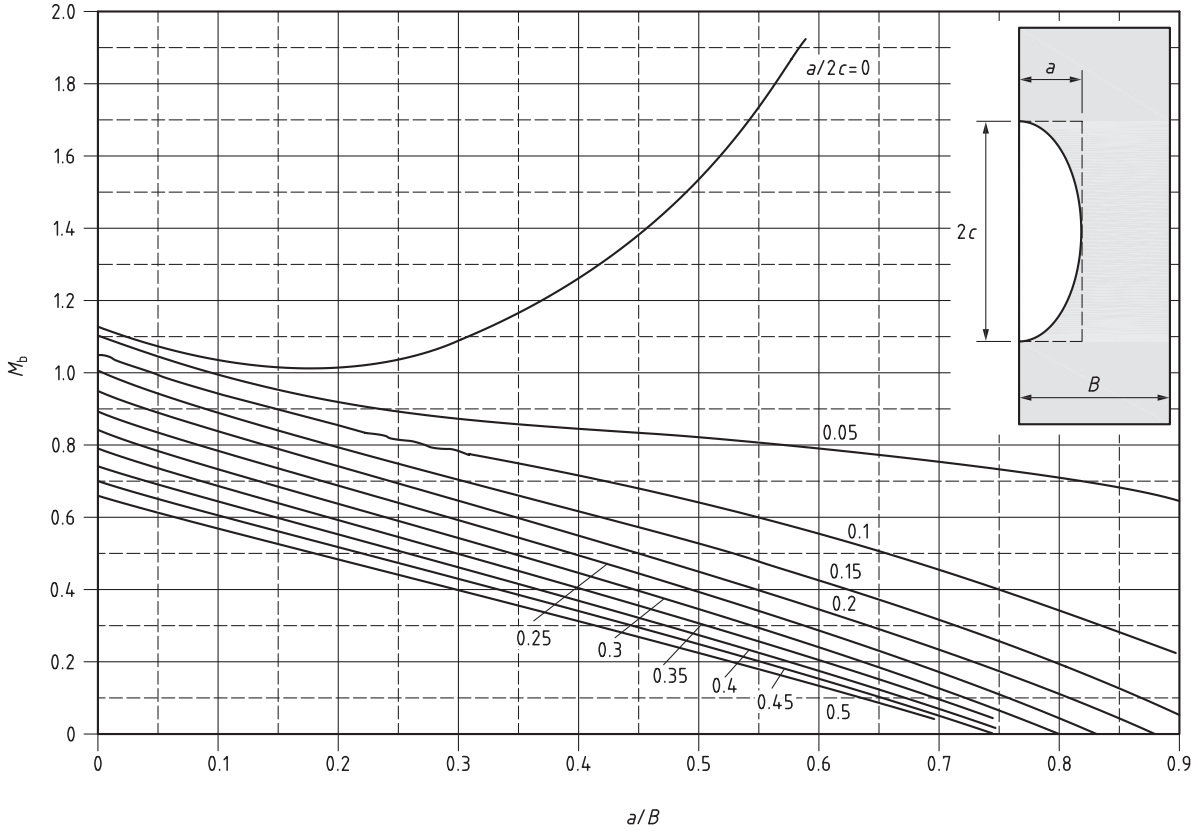
$G_1 = -2.11 + 0.77\left(\frac{c}{a}\right)$ for $0.5 < a/2c \leq 1.0$

$G_2 = 0.55 - 1.05\left(\frac{a}{c}\right)^{0.75} + 0.47\left(\frac{a}{c}\right)^{1.5}$ for $0 < a/2c \leq 0.5$

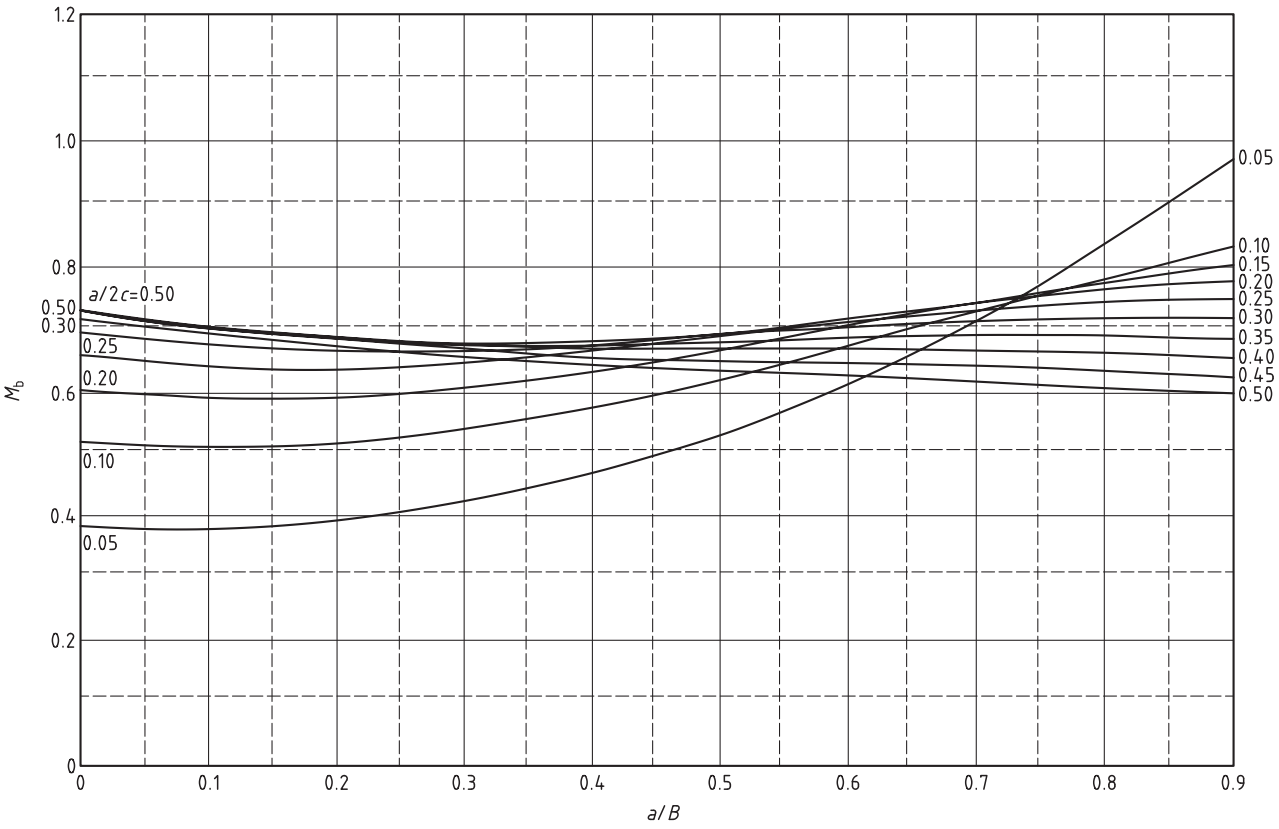
$G_2 = 0.55 - 0.72\left(\frac{c}{a}\right)^{0.75} + 0.14\left(\frac{c}{a}\right)^{1.5}$ for $0.5 < a/2c \leq 1.0$

Graphical solutions for M_b are given in Figure M.5a) and Figure M.5b).

Figure M.5 **Stress intensity magnification factor M_b for surface flaws in bending**



a) At the deepest point along front flaw, i.e. $\theta = \pi/2$ rad



b) At flaw tip on material surface, i.e. $\theta = 0$ rad

M.4.1.3.3 Simplifications

The following simplifications may be used as indicated.

a) At the deepest point on the crack front, $\theta = \pi/2$ so that $H = H_2$ and:

$f_\theta = 1$ for $0 < a/2c \leq 0.5$

$f_\theta = \left(\frac{c}{a}\right)^{0.5}$ for $0.5 < a/2c \leq 1$

b) At the ends of the crack, $\theta = 0$, so that:

$f_\theta = \left(\frac{a}{c}\right)^{0.5}$ for $0 < a/2c \leq 0.5$

$f_\theta = 1.0$ for $0.5 < a/2c \leq 1$

$H = H_1$

c) If $a/2c > 1.0$, use the solution for $a/2c = 1.0$.

M.4.2 Surface flaws in plates; solution for polynomial stress distribution

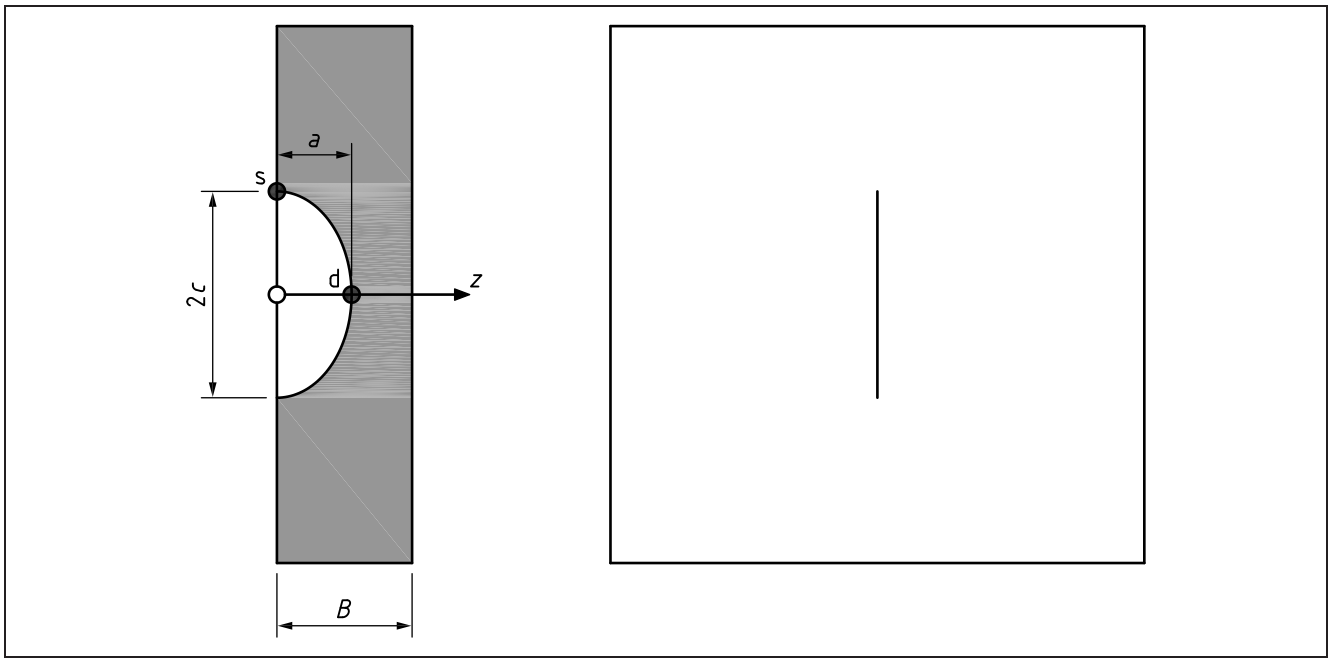
M.4.2.1 General

In cases for which the stress distribution across the unflawed plate can be described in the form of a polynomial equation, the solutions given here might give more accurate results than those given in **M.4.1**.

M.4.2.2 Finite surface flaw in an infinite width plate

This solution, adapted from R6 [M.8], originates from Fett and Munz [M.10] and from Fett et al [M.11], and is particularly suitable for situations in which the stress distribution across the uncracked section is expressed in the form of a polynomial. The format of this solution (and the solution given in **M.4.4**) is slightly different from that used elsewhere in this annex, but retains the convention that the stress distribution is defined across the section thickness (in contrast with R6, which uses the stress distribution across the flaw).
See Figure M.6 for the definition of the geometry.

Figure M.6 **Finite surface flaw in an infinite width plate**



The stress intensity factor, K_I, is given by:

$$K_I = \sqrt{\pi a} \sum_{i=0}^{5} \sigma_i \left(\frac{a}{B}\right)^i f_i\left(\frac{a}{B}, \frac{2c}{a}\right) \quad \text{(M.13)}$$

σ_i (i = 0 to 5) are stress components which define the stress distribution σ with:

$$\sigma = \sigma(z) = \sum_{i=0}^{5} \sigma_i \left(\frac{z}{B}\right)^i \text{ for } 0 \leq z \leq B \quad \text{(M.14)}$$

where:

σ is taken normal to the prospective flaw plane in an unflawed plate;

z is the distance from the plate surface as shown in Figure M.6;

f_i (i = 0 to 5) are geometry functions which are given in Table M.1 and Table M.2, for the deepest point of the flaw, f_i^d, and at the intersection of the flaw with the free surface, f_i^s, respectively.

The parameters used in Table M.1 and Table M.2 are defined in Figure M.6.

Table M.1 **Geometry functions for a finite surface flaw in an infinite width plate – deepest point of flaw**

2*c*/*a* = 2						
a*/*B	f_0^d	f_1^d	f_2^d	f_3^d	f_4^d	f_5^d
0	0.659	0.471	0.387	0.337	0.299	0.266
0.2	0.663	0.473	0.388	0.337	0.299	0.269
0.4	0.678	0.479	0.390	0.339	0.300	0.271
0.6	0.692	0.486	0.396	0.342	0.304	0.274
0.8	0.697	0.497	0.405	0.349	0.309	0.278
2*c*/*a* = 5/2						
a*/*B	f_0^d	f_1^d	f_2^d	f_3^d	f_4^d	f_5^d
0	0.741	0.510	0.411	0.346	0.300	0.266
0.2	0.746	0.512	0.413	0.352	0.306	0.270
0.4	0.771	0.519	0.416	0.356	0.309	0.278
0.6	0.800	0.531	0.422	0.362	0.317	0.284
0.8	0.820	0.548	0.436	0.375	0.326	0.295
2*c*/*a* = 10/3						
a*/*B	f_0^d	f_1^d	f_2^d	f_3^d	f_4^d	f_5^d
0	0.833	0.549	0.425	0.351	0.301	0.267
0.2	0.841	0.554	0.430	0.359	0.309	0.271
0.4	0.885	0.568	0.442	0.371	0.320	0.285
0.6	0.930	0.587	0.454	0.381	0.331	0.295
0.8	0.960	0.605	0.476	0.399	0.346	0.310
2*c*/*a* = 5						
a*/*B	f_0^d	f_1^d	f_2^d	f_3^d	f_4^d	f_5^d
0	0.939	0.580	0.434	0.353	0.302	0.268
0.2	0.957	0.595	0.446	0.363	0.310	0.273
0.4	1.057	0.631	0.475	0.389	0.332	0.292
0.6	1.146	0.668	0.495	0.407	0.350	0.309
0.8	1.190	0.698	0.521	0.428	0.367	0.324
2*c*/*a* = 10						
a*/*B	f_0^d	f_1^d	f_2^d	f_3^d	f_4^d	f_5^d
0	1.053	0.606	0.443	0.357	0.302	0.269
0.2	1.106	0.640	0.467	0.374	0.314	0.277
0.4	1.306	0.724	0.525	0.420	0.348	0.304
0.6	1.572	0.815	0.571	0.448	0.377	0.327
0.8	1.701	0.880	0.614	0.481	0.399	0.343
2*c*/*a* $\rightarrow \infty$						
a*/*B	f_0^d	f_1^d	f_2^d	f_3^d	f_4^d	f_5^d
0	1.123	0.682	0.524	0.440	0.386	0.344
0.2	1.380	0.784	0.582	0.478	0.414	0.369
0.4	2.106	1.059	0.735	0.578	0.485	0.423
0.6	4.025	1.750	1.105	0.814	0.651	0.548
0.8	11.92	4.437	2.484	1.655	1.235	0.977

Table M.2 **Geometry functions for a finite surface flaw in an infinite width plate – intersection of flaw with free surface**

2*c*/*a* = 2						
a*/*B	f_0^s	f_1^s	f_2^s	f_3^s	f_4^s	f_5^s
0	0.716	0.118	0.041	0.022	0.014	0.010
0.2	0.729	0.123	0.045	0.023	0.014	0.010
0.4	0.777	0.133	0.050	0.026	0.015	0.011
0.6	0.839	0.148	0.058	0.029	0.018	0.012
0.8	0.917	0.167	0.066	0.035	0.022	0.015
2*c*/*a* = 5/2						
a*/*B	f_0^s	f_1^s	f_2^s	f_3^s	f_4^s	f_5^s
0	0.730	0.124	0.041	0.021	0.013	0.010
0.2	0.749	0.126	0.046	0.023	0.014	0.010
0.4	0.795	0.144	0.054	0.028	0.017	0.012
0.6	0.901	0.167	0.066	0.033	0.021	0.015
0.8	0.995	0.193	0.076	0.042	0.026	0.017
2*c*/*a* = 10/3						
a*/*B	f_0^s	f_1^s	f_2^s	f_3^s	f_4^s	f_5^s
0	0.723	0.118	0.039	0.019	0.011	0.008
0.2	0.747	0.125	0.044	0.022	0.014	0.010
0.4	0.803	0.145	0.056	0.029	0.018	0.012
0.6	0.934	0.180	0.072	0.037	0.023	0.016
0.8	1.070	0.218	0.087	0.047	0.029	0.020
2*c*/*a* = 5						
a*/*B	f_0^s	f_1^s	f_2^s	f_3^s	f_4^s	f_5^s
0	0.673	0.104	0.032	0.015	0.009	0.006
0.2	0.704	0.114	0.038	0.018	0.011	0.007
0.4	0.792	0.139	0.053	0.027	0.016	0.011
0.6	0.921	0.183	0.074	0.038	0.024	0.017
0.8	1.147	0.244	0.097	0.052	0.032	0.021
2*c*/*a* = 10						
a*/*B	f_0^s	f_1^s	f_2^s	f_3^s	f_4^s	f_5^s
0	0.516	0.069	0.017	0.009	0.005	0.004
0.2	0.554	0.076	0.022	0.011	0.007	0.005
0.4	0.655	0.099	0.039	0.019	0.012	0.008
0.6	0.840	0.157	0.063	0.032	0.020	0.013
0.8	1.143	0.243	0.099	0.055	0.034	0.023
2*c*/*a* $\rightarrow \infty$						
a*/*B	f_0^s	f_1^s	f_2^s	f_3^s	f_4^s	f_5^s
0	0.000	0.000	0.000	0.000	0.000	0.000
0.2	0.000	0.000	0.000	0.000	0.000	0.000
0.4	0.000	0.000	0.000	0.000	0.000	0.000
0.6	0.000	0.000	0.000	0.000	0.000	0.000
0.8	0.000	0.000	0.000	0.000	0.000	0.000

 © The British Standards Institution 2019

M.4.3 Extended surface flaws in plates; solution for uniform tension and/or through-wall bending

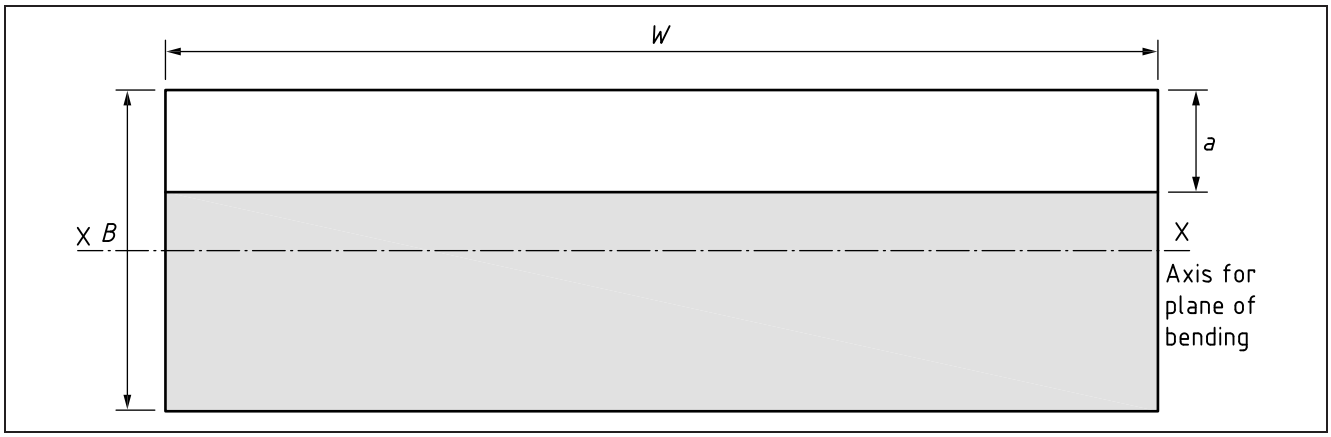
This solution is from Tada et al [M.2] and is suitable for cases in which the stress distribution across the uncracked body can be expressed in terms of uniform membrane stress, bending stress, or a combination of the two. Where the stress distribution is described by a polynomial, the solution given in **M.4.4** offers higher accuracy.

See Figure M.7 for the definition of the geometry. The stress intensity factor is given by Equation (M.1) to Equation (M.6), where $f_w = 1$, and M_m and M_b are given by Equation (M.15) and Equation (M.16) for $a/B \leq 0.6$:

$$M_m = 1.12 - 0.23\left(\frac{a}{B}\right) + 10.6\left(\frac{a}{B}\right)^2 - 21.7\left(\frac{a}{B}\right)^3 + 30.4\left(\frac{a}{B}\right)^4 \quad \text{(M.15)}$$

$$M_b = 1.12 - 1.39\left(\frac{a}{B}\right) + 7.32\left(\frac{a}{B}\right)^2 - 13.1\left(\frac{a}{B}\right)^3 + 14\left(\frac{a}{B}\right)^4 \quad \text{(M.16)}$$

Figure M.7 **Extended flaw geometry**

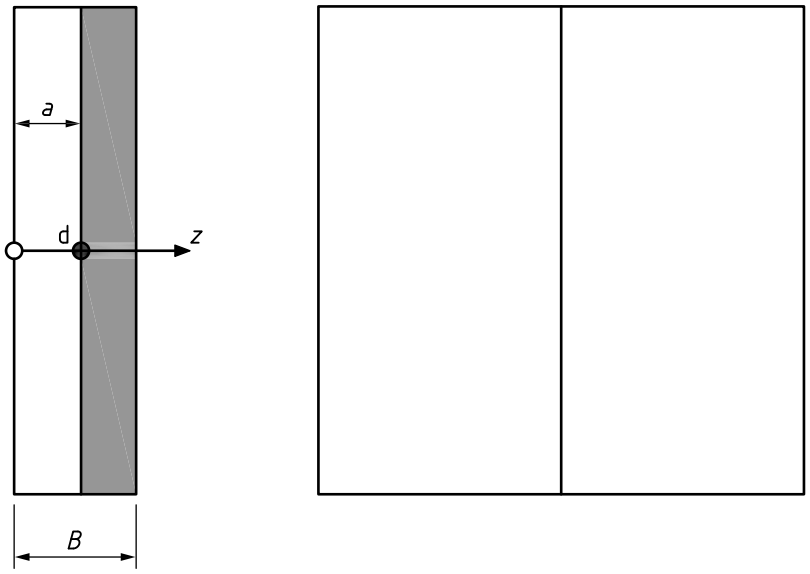


M.4.4 Extended surface flaw in an infinite width plate; solution for the case where the unflawed stress profile through the section is represented as a polynomial equation

This solution, adapted from R6 [M.8], originates from Wu and Carlsson [M.12] and is particularly suitable for situations in which the stress distribution across the uncracked section is expressed in the form of a polynomial. The format of this solution (and the solution given in **M.4.2.2**) therefore differs from that used elsewhere in this annex.

See Figure M.8 for the definition of the geometry.

Figure M.8 **Extended surface flaw in an infinite width plate**



The stress intensity factor K_I is given by:

$$K_I = \frac{1}{\sqrt{2\pi a}} \int_0^a \sigma(z) \sum_{i=1}^{i=5} f_i \left(\frac{a}{B}\right) \left(1 - \frac{z}{a}\right)^{i-(3/2)} dz \qquad \text{(M.17)}$$

The stress state $\sigma = \sigma(z)$ is to be taken normal to the prospective flaw plane in an unflawed plate. The coordinate z is defined in Figure M.8.

The geometry functions f_i (i = 1 to 5) are given in Table M.3. Parameters used in the table are defined in Figure M.8.

Table M.3 **Geometry functions for an extended surface flaw in an infinite width plate**

a/B	f_1^d	f_2^d	f_3^d	f_4^d	f_5^d
0	2.000	0.977	1.142	-0.350	-0.091
0.1	2.000	1.419	1.138	-0.355	-0.076
0.2	2.000	2.537	1.238	-0.347	-0.056
0.3	2.000	4.238	1.680	-0.410	-0.019
0.4	2.000	6.636	2.805	-0.611	0.039
0.5	2.000	10.02	5.500	-1.340	0.218
0.6	2.000	15.04	11.88	-3.607	0.786
0.7	2.000	23.18	28.03	-10.50	2.587
0.8	2.000	38.81	78.75	-36.60	9.871
0.9	2.000	82.70	351.0	-207.1	60.86

 © The British Standards Institution 2019

M.4.5 Embedded flaws in plates

M.4.5.1 General

This solution is taken from Newman and Raju [M.9]. See Figure M.9 for the definition of the geometry. The stress intensity factor is given by Equation (M.1) to Equation (M.6), where:

$$M = 1$$

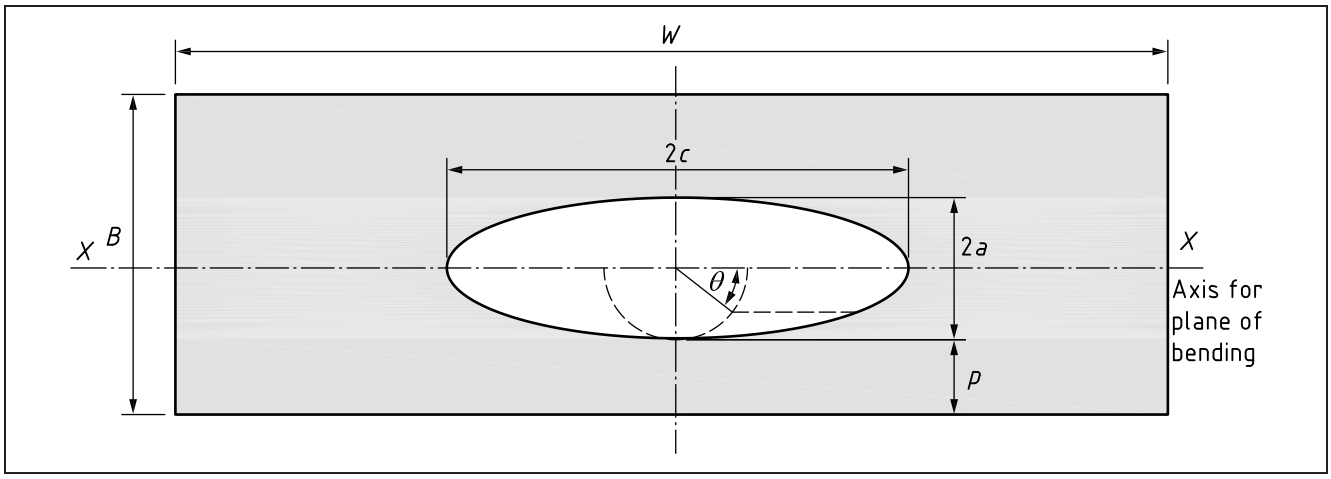
$$f_W = \left\{ \sec\left[\left(\frac{\pi c}{W}\right) \left(\frac{2a}{B'}\right)^{0.5} \right] \right\}^{0.5}$$

NOTE This is applicable up to 2c/W = 0.8

M_m is as defined in **M.4.5.2** where B' is the effective thickness, equal to $2a + 2p$;

M_b is as defined in **M.4.5.3** where B' is the effective thickness, equal to $2a + 2p$.

Figure M.9 **Embedded flaw**



M.4.5.2 Membrane loading

M.4.5.2.1 Conditions

The conditions for membrane loading are:

$$\left(\frac{a}{B'}\right) < 0.625\left(\frac{a}{c} + 0.6\right) \qquad \text{for } 0 < a/2c \leq 0.1$$

$$0 < \left(\frac{a}{2c}\right) \leq 1.0$$

$$\left(\frac{2c}{W}\right) < 0.5$$

$$-\pi \leq \theta \leq \pi$$

where:

B' is the effective thickness, equal to $2a + 2p$.

M.4.5.2.2 Solution

The solution is as follows.

$$M_m = \left[M_1 + M_2\left(\frac{2a}{B'}\right)^2 + M_3\left(\frac{2a}{B'}\right)^4\right]\frac{gf\theta}{\Phi} \quad \text{(M.18)}$$

where:

Φ is defined in Equation (M.11)

$M_1 = 1$ for $0 < a/2c \leq 0.5$

$M_1 = \left(\frac{c}{a}\right)^{0.5}$ for $0.5 < a/2c \leq 1.0$

$$M_2 = \frac{0.05}{0.11 + (a/c)^{1.5}}$$

$$M_3 = \frac{0.29}{0.23 + (a/c)^{1.5}}$$

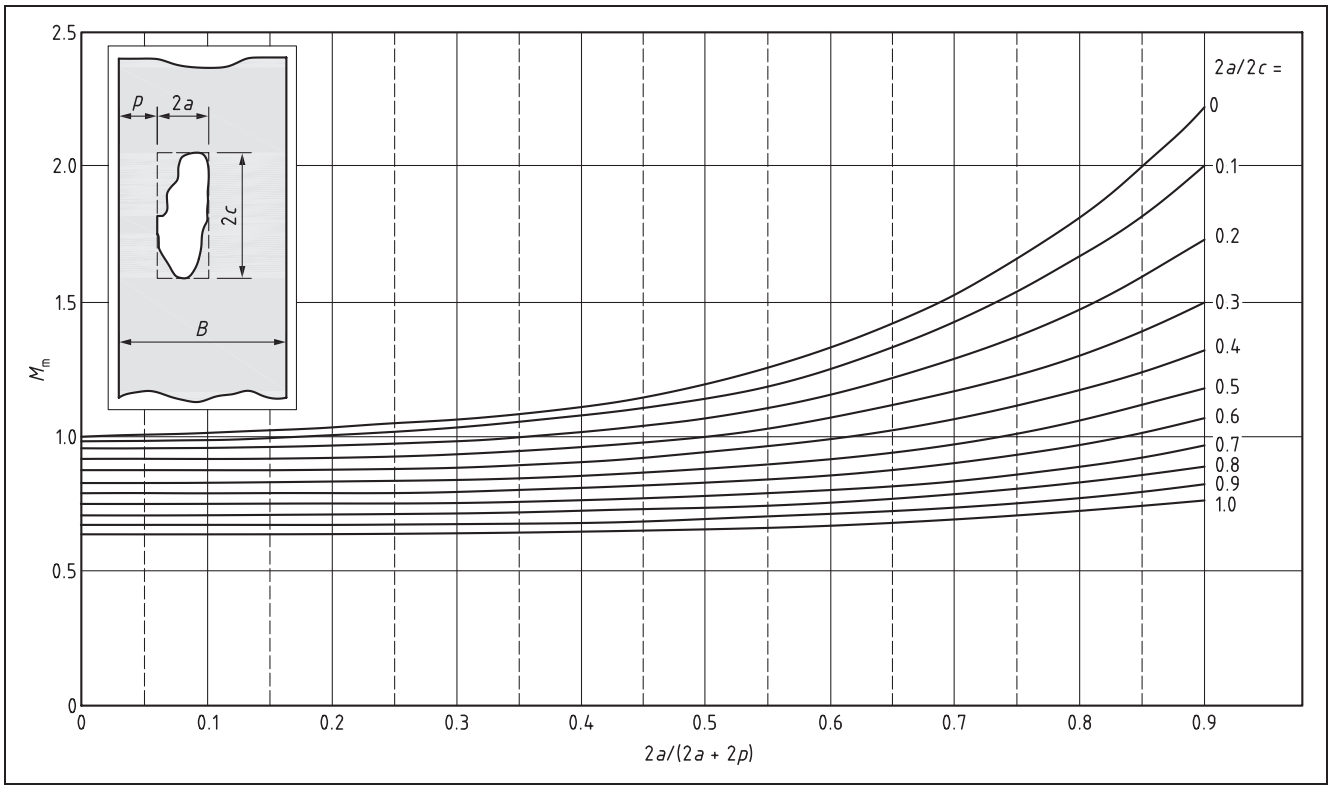
$$g = 1 - \left\{\frac{(2a/B')^4\left[2.6 - (4a/B')^{0.5}\right]}{1 + 4(a/c)}\right\}|\cos\theta|$$

$f_\theta = \left[\left(\frac{a}{c}\right)^2\cos^2\theta + sin^2\theta\right]^{0.25}$ for $0 < a/2c \leq 0.5$

$f_\theta = \left[\left(\frac{c}{a}\right)^2\sin^2\theta + cos^2\theta\right]^{0.25}$ for $0.5 < a/2c \leq 1.0$

A graphical solution for M_m is given in Figure M.10.

Figure M.10 **Stress intensity magnification factor M_m for embedded flaws in tension (at point nearest material surface)**



M.4.5.2.3 Simplifications

The following simplifications may be used as indicated.

a) At the point on the crack front closest to the material surface, $\theta = \pi/2$, so that:

$$g = 1$$

$$f_\theta = 1 \qquad \text{for } 0 < a/2c \leq 0.5$$

$$f_\theta = \left(\frac{c}{a}\right)^{0.5} \qquad \text{for } 0.5 < a/2c \leq 1.0$$

b) At the ends of the crack, $\theta = 0$, so that:

$$g = 1 - \left\{\frac{(2a/B')^4[2.6 - (4a/B')]^{0.5}}{1 + 4(a/c)}\right\}$$

and:

$$f_\theta = \left(\frac{a}{c}\right)^{0.5} \qquad \text{for } 0 < a/2c \leq 0.5$$

$$f_\theta = 1 \qquad \text{for } 0.5 < a/2c \leq 1.0$$

c) When $a/2c > 1.0$, use the solution for $a/2c = 1.0$.

M.4.5.3 Bending loading

M.4.5.3.1 Conditions

The conditions for bending loading are:

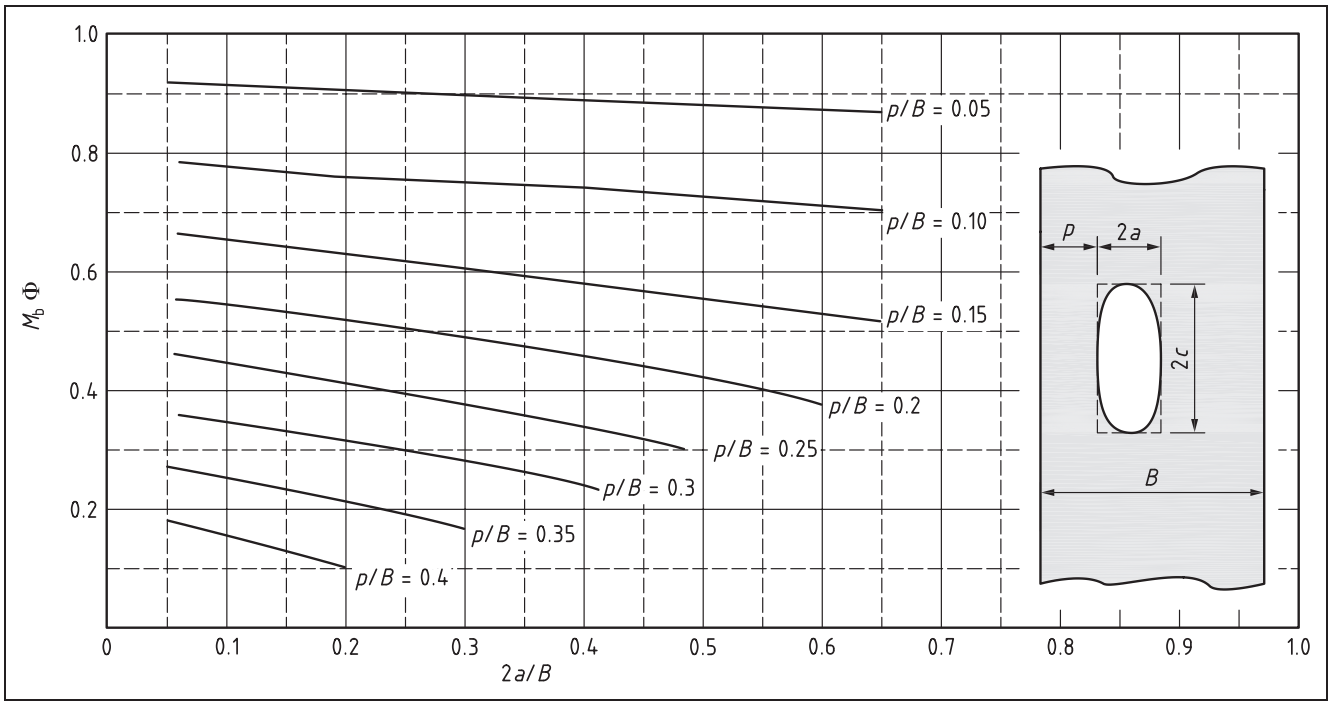
$0 < a/2c \leq 0.5$

$\theta = \pi/2$ (i.e. solution only refers to the ends of the minor axis of the elliptical crack).

A graphical solution for M_b, derived from Shah and Kobayashi [M.13], is given in Figure M.11.

NOTE The solution for M_b given in Figure M.11 dates back to the 1980 edition of PD 6493, but its exact origins are uncertain, since Newman and Raju [M.9] did not produce solutions for embedded flaws under bending. A comparison between the BS 7910 solution and those given in other procedures is given in reference [M.13].

Figure M.11 **Stress intensity magnification factor M_b for embedded flaws in bending**



M.4.5.3.2 Solution

The solution is as follows.

$$M_b = \frac{\left[\lambda_1 + \lambda_2\left(\frac{p}{B}\right) + \lambda_3\left(\frac{a}{B}\right) + \lambda_4\left(\frac{pa}{B^2}\right)\right]}{\Phi} \qquad \text{(M.19)}$$

where:

$\lambda_1 = 1.044$	for $p/B \leq 0.184\ 1$
$\lambda_2 = -2.44$	for $p/B \leq 0.184\ 1$
$\lambda_3 = 0$	for $p/B \leq 0.184\ 1$
$\lambda_4 = -3.166$	for $p/B \leq 0.184\ 1$
$\lambda_1 = 0.94$	for $p/B > 0.184\ 1$ and $a/B \leq 0.125$
$\lambda_2 = -1.875$	for $p/B > 0.184\ 1$ and $a/B \leq 0.125$
$\lambda_3 = -0.114\ 6$	for $p/B > 0.184\ 1$ and $a/B \leq 0.125$
$\lambda_4 = -1.844$	for $p/B > 0.184\ 1$ and $a/B \leq 0.125$
$\lambda_1 = 1.06$	for $p/B > 0.184\ 1$ and $a/B > 0.125$
$\lambda_2 = -2.20$	for $p/B > 0.184\ 1$ and $a/B > 0.125$
$\lambda_3 = \lambda_4 = -0.666\ 6$	for $p/B > 0.184\ 1$ and $a/B > 0.125$

 © The British Standards Institution 2019

M.5 Stress intensity factor solutions for plates containing corner flaws

M.5.1 Corner flaws in plates

M.5.1.1 General

This solution is taken from Newman and Raju [M.9]. See Figure M.12 for the definition of the geometry. The stress intensity factor is given by Equation (M.1) to Equation (M.6), where:

$M = 1$

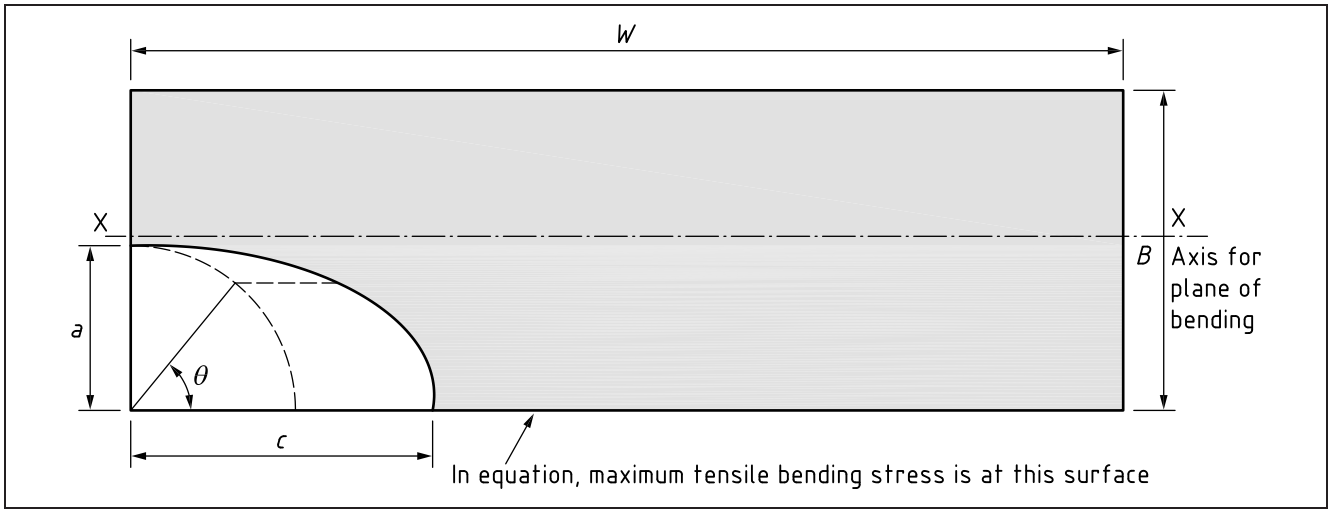
$f_W = 1 - 0.2\lambda + 9.4\lambda^2 - 19.4\lambda^3 + 27.1\lambda^4$ for $c/W \leq 0.5$

where:

$$\lambda = \left(\frac{c}{W}\right)\sqrt{(a/B)}$$

Solutions for M_m and M_b are given in **M.5.1.2** and **M.5.1.3** respectively.

Figure M.12 **Corner flaw geometry**



M.5.1.2 Membrane loading

M.5.1.2.1 Conditions

The conditions for membrane loading are:

$0.2 \leq a/c \leq 2$

$a/B < 1$

$0 \leq \theta \leq \pi/2$

$c/W < 0.5$

M.5.1.2.2 Solution

The solution is as follows.

$$M_m = \left[M_1 + M_2\left(\frac{a}{B}\right)^2 + M_3\left(\frac{a}{B}\right)^4\right]\frac{g_1 g_2 f_\theta}{\Phi} \quad \text{(M.20)}$$

where:

Φ is defined in Equation (M.11)

$M_1 = 1.08 - 0.03(a/c)$ for $0.2 \leq a/c \leq 1$

$M_1 = \left[1.08 - 0.03\left(\frac{c}{a}\right)\right]\left(\frac{c}{a}\right)^{0.5}$ for $1 < a/c \leq 2$

$$M_2 = \left\{\frac{1.06}{[0.3 + (a/c)]}\right\} - 0.44 \qquad \text{for } 0.2 \le a/c \le 1$$

$$M_2 = 0.375\left(\frac{c}{a}\right)^2 \qquad \text{for } 1 < a/c \le 2$$

$$M_3 = -0.5 + 0.25\left(\frac{a}{c}\right) + 14.8\left[1 - \left(\frac{a}{c}\right)\right]^{15} \qquad \text{for } 0.2 \le a/c \le 1$$

$$M_3 = -0.25\left(\frac{c}{a}\right)^2 \qquad \text{for } 1 < a/c \le 2$$

$$g_1 = 1 + \left[0.08 + 0.4\left(\frac{a}{B}\right)^2\right](1 - \sin\theta)^3 \qquad \text{for } 0.2 \le a/c \le 1$$

$$g_1 = 1 + \left[0.08 + 0.4\left(\frac{c}{B}\right)^2\right](1 - \sin\theta)^3 \qquad \text{for } 1 < a/c \le 2$$

$$g_2 = 1 + \left[0.08 + 0.15\left(\frac{a}{B}\right)^2\right](1 - \cos\theta)^3 \qquad \text{for } 0.2 \le a/c \le 1$$

$$g_2 = 1 + \left[0.08 + 0.15\left(\frac{c}{B}\right)^2\right](1 - \cos\theta)^3 \qquad \text{for } 1 < a/c \le 2$$

$$f_\theta = \left[\left(\frac{a}{c}\right)^2 \cos^2\theta + \sin^2\theta\right]^{0.25} \qquad \text{for } 0.2 \le a/c \le 1$$

$$f_\theta = \left[\left(\frac{c}{a}\right)^2 \sin^2\theta + \cos^2\theta\right]^{0.25} \qquad \text{for } 1 < a/c \le 2$$

M.5.1.3 Bending loading

M.5.1.3.1 Conditions

The conditions for bending loading should be in accordance with **M.5.1.2.1**.

M.5.1.3.2 Solution

The solution is as follows.

$$M_b = HM_m \qquad \text{(M.21)}$$

where:

M_m is given by Equation (M.20)

$$H = H_1 + (H_2 - H_1)\sin^q\theta$$

$$q = 0.2 + \left(\frac{a}{c}\right) + 0.6\left(\frac{a}{B}\right) \qquad \text{for } 0.2 \le a/c \le 1$$

$$q = 0.2 + \left(\frac{c}{a}\right) + 0.6\left(\frac{a}{B}\right) \qquad \text{for } 1 < a/c \le 2$$

$$H_1 = 1 - 0.34\left(\frac{a}{B}\right) - 0.11\left(\frac{a}{c}\right)\left(\frac{a}{B}\right) \qquad \text{for } 0.2 \le a/c \le 1$$

$$H_1 = 1 - \left[0.04 + 0.41\left(\frac{c}{a}\right)\right]\left(\frac{a}{B}\right) + \left[0.55 - 1.93\left(\frac{c}{a}\right)^{0.75} + 1.38\left(\frac{c}{a}\right)^{1.5}\right]\left(\frac{a}{B}\right)^2 \qquad \text{for } 1 < a/c \le 2$$

$$H_2 = 1 + G_1\left(\frac{a}{B}\right) + G_2\left(\frac{a}{B}\right)^2$$

where:

$$G_1 = -1.22 - 0.12\left(\frac{a}{c}\right) \qquad \text{for } 0.2 \le a/c \le 1$$

$$G_1 = -2.11 + 0.77\left(\frac{c}{a}\right) \qquad \text{for } 1 < a/c \le 2$$

$$G_2 = 0.64 - 1.05\left(\frac{a}{c}\right)^{0.75} + 0.47\left(\frac{a}{c}\right)^{1.5} \qquad \text{for } 0.2 \le a/c \le 1$$

$$G_2 = 0.64 - 0.72\left(\frac{c}{a}\right)^{0.75} + 0.14\left(\frac{c}{a}\right)^{1.5} \qquad \text{for } 1 < a/c \le 2$$

M.5.2 Corner flaws at hole

M.5.2.1 General

This solution is taken from Newman and Raju [M.9]. See Figure M.13 for the definition of the geometry. Equation (M.1) to Equation (M.6) give the stress intensity factor, where:

$M = 1$

$$f_w = \left\{ \sec\left(\frac{\pi r}{W}\right) \sec\left[\frac{\pi(2r + nc)}{4(W/2 - c) + 2nc} \sqrt{(a/B)} \right] \right\}^{0.5}$$

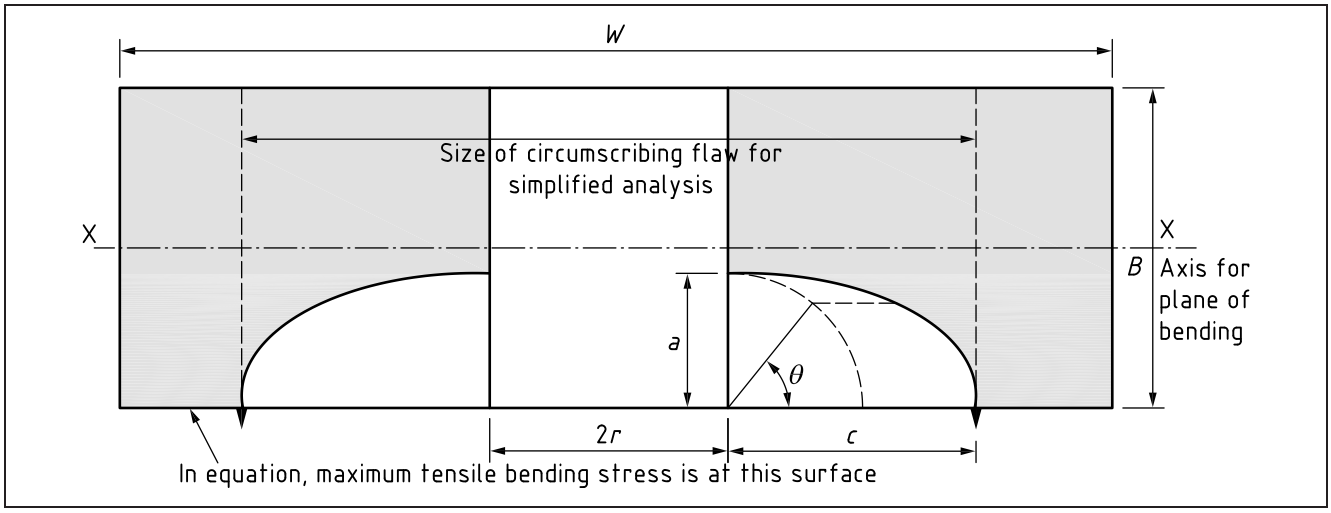
where:

$n = 1$ for a single flaw

$n = 2$ for two symmetric flaws

The formula for calculating f_w takes into account finite width effects and the stress concentrating effect of the hole. Solutions for M_m and M_b are given in **M.5.2.2** and **M.5.2.3** respectively.

Figure M.13 **Corner flaw at hole geometry**



M.5.2.2 Membrane loading

M.5.2.2.1 Conditions

The conditions for membrane loading are:

$0.2 \leq a/c \leq 2$

$a/B < 1$

$0.5 \leq r/B \leq 2$

$2(r + c)/W \leq 0.5$

$0 \leq \theta \leq \pi/2$

M.5.2.2.2 Solution

The solution is as follows.

$$M_m = \left[M_1 + M_2\left(\frac{a}{B}\right)^2 + M_3\left(\frac{a}{B}\right)^4\right]\frac{g_1 g_2 g_3 g_4 f_\theta}{\Phi} \quad \text{(M.22)}$$

where:

Φ is defined in Equation (M.20)

$M_1 = 1.13 - 0.09\left(\frac{a}{c}\right)$ for $0.2 \le a/c \le 1$

$M_1 = \left[1 + 0.04\left(\frac{c}{a}\right)\right]\sqrt{(c/a)}$ for $1 < a/c \le 2$

$M_2 = -0.54 + \frac{0.89}{[0.2 + (a/c)]}$ for $0.2 \le a/c \le 1$

$M_2 = 0.2\left(\frac{c}{a}\right)^4$ for $1 < a/c \le 2$

$M_3 = 0.5 - \left\{\frac{1}{[0.65 + (a/c)]}\right\} + 14[1 - (a/c)]^{24}$ for $0.2 \le a/c \le 1$

$M_3 = -0.11\left(\frac{c}{a}\right)^4$ for $1 < a/c \le 2$

$g_1 = 1 + \left[0.1 + 0.35\left(\frac{a}{B}\right)^2\right](1 - \sin\theta)^2$ for $0.2 \le a/c \le 1$

$g_1 = 1 + \left[0.1 + 0.35\left(\frac{c}{a}\right)\left(\frac{a}{B}\right)^2\right](1 - \sin\theta)^2$ for $1 < a/c \le 2$

$$g_2 = \frac{1 + 0.358\lambda + 1.425\lambda^2 - 1.578\lambda^3 + 2.156\lambda^4}{1 + 0.13\lambda^2}$$

where:

$$\lambda = \frac{1}{[1 + (c/r)\cos(\mu\theta)]}$$

$\mu = 0.85$

$g_3 = \left[1 + 0.04\left(\frac{a}{c}\right)\right]\left[1 + 0.1(1 - \cos\theta)^2\right]\left[0.85 + 0.15\left(\frac{a}{B}\right)^{0.25}\right]$ for $0.2 \le a/c \le 1$

$g_3 = \left[1.13 + 0.09\left(\frac{c}{a}\right)\right]\left[1 + 0.1(1 - \cos\theta)^2\right]\left[0.85 + 0.15\left(\frac{a}{B}\right)^{0.25}\right]$ for $1 < a/c \le 2$

$g_4 = 1 - 0.7\left(1 - \frac{a}{B}\right)\left(\frac{a}{c} - 0.2\right)\left(1 - \frac{a}{c}\right)$ for $0.2 \le a/c \le 1$

$g_4 = 1$ for $1 < a/c \le 2$

$f_\theta = \left[\left(\frac{a}{c}\right)^2 \cos^2\theta + \sin^2\theta\right]^{0.25}$ for $0.2 \le a/c \le 1$.

$f_\theta = \left[\left(\frac{c}{a}\right)^2 sin^2\theta + \cos^2\theta\right]^{0.25}$ for $1 < a/c \le 2$

M.5.2.3 Bending loading

M.5.2.3.1 Conditions

The conditions for bending loading are as described in **M.5.2.2.1**.

M.5.2.3.2 Solution

The solution is as follows.

$$M_b = HM_m \quad \text{(M.23)}$$

where:

M_m is given by Equation (M.22)

$$\mu = 0.85 - 0.25\left(\frac{a}{B}\right)^{0.25} \quad \text{for bending}$$

$$H = H_1 + (H_2 - H_1)\sin^q\theta$$

$$q = 0.1 + 1.3\left(\frac{a}{B}\right) + 1.1\left(\frac{a}{c}\right) - 0.7\left(\frac{a}{c}\right)\left(\frac{a}{B}\right) \quad \text{for } 0.2 \le a/c \le 1$$

$$q = 0.2 + \left(\frac{c}{a}\right) + 0.6\left(\frac{a}{B}\right) \quad \text{for } 1 < a/c \le 2$$

$$H_1 = 1 + G_{11}\left(\frac{a}{B}\right) + G_{12}\left(\frac{a}{B}\right)^2 + G_{13}\left(\frac{a}{B}\right)^3$$

$$H_2 = 1 + G_{21}\left(\frac{a}{B}\right) + G_{22}\left(\frac{a}{B}\right)^2 + G_{23}\left(\frac{a}{B}\right)^3$$

where:

$$G_{11} = -0.43 - 0.74\left(\frac{a}{c}\right) - 0.84\left(\frac{a}{c}\right)^2 \quad \text{for } 0.2 \le a/c \le 1$$

$$G_{11} = -2.07 + 0.06\left(\frac{c}{a}\right) \quad \text{for } 1 < a/c \le 2$$

$$G_{12} = 1.25 - 1.19\left(\frac{a}{c}\right) + 4.39\left(\frac{a}{c}\right)^2 \quad \text{for } 0.2 \le a/c \le 1$$

$$G_{12} = 4.35 + 0.16\left(\frac{c}{a}\right) \quad \text{for } 1 < a/c \le 2$$

$$G_{13} = -1.94 + 4.22\left(\frac{a}{c}\right) - 5.51\left(\frac{a}{c}\right)^2 \quad \text{for } 0.2 \le a/c \le 1$$

$$G_{13} = -2.93 - 0.3\left(\frac{c}{a}\right) \quad \text{for } 1 < a/c \le 2$$

$$G_{21} = -1.5 - 0.04\left(\frac{a}{c}\right) - 1.73\left(\frac{a}{c}\right)^2 \quad \text{for } 0.2 \le a/c \le 1$$

$$G_{21} = -3.64 + 0.37\left(\frac{c}{a}\right) \quad \text{for } 1 < a/c \le 2$$

$$G_{22} = 1.71 - 3.17\left(\frac{a}{c}\right) + 6.84\left(\frac{a}{c}\right)^2 \quad \text{for } 0.2 \le a/c \le 1$$

$$G_{22} = 5.87 - 0.49\left(\frac{c}{a}\right) \quad \text{for } 1 < a/c \le 2$$

$$G_{23} = -1.28 + 2.71\left(\frac{a}{c}\right) - 5.22\left(\frac{a}{c}\right)^2 \quad \text{for } 0.2 \le a/c \le 1$$

$$G_{23} = -4.32 + 0.53\left(\frac{c}{a}\right) \quad \text{for } 1 < a/c \le 2$$

M.5.3 Single corner flaw at hole

The stress intensity factor for a single corner crack at a hole ($K_{\text{single crack}}$) may be estimated from $K_{\text{symmetric crack}}$ using the following equation:

$$K_{\text{single crack}} = K_{\text{symmetric crack}}\left[\frac{(4/\pi) + (ac/2\text{Br})}{(4/\pi) + (ac/\text{Br})}\right]^{0.5} \quad \text{(M.24)}$$

$K_{\text{symmetric crack}}$ is evaluated from Equation (M.1) to Equation (M.6) with M_m and M_b from Equation (M.22) and Equation (M.23) and the modified finite width correction factor, f_w, defined in **M.5.2.1**.

M.5.4 Flaws in nozzles

The flat plate solution in **M.5.2** may be applied to radial internal corner flaws in nozzles, with appropriate stress concentration factors.

M.6 Stress intensity factor solutions for curved shells (cylinders and spheres) under internal pressure

M.6.1 General

The finite width correction factor, f_w, is given in **M.2**.

Unless justified otherwise, for curved shells under internal pressure the bulging correction factor, M, is calculated from the following expressions.

a) For through-thickness flaws in spheres, and for axial through-thickness flaws in pipes and cylinders:

$$M = \left[1 + 1.6\left(\frac{a^2}{r_i B}\right)\right]^{0.5} \quad \text{(M.25)}$$

b) For surface flaws in spheres, and for axial surface flaws in cylinders:

$$M = \frac{1 - [a/(BM_T)]}{1 - (a/B)} \quad \text{(M.26)}$$

where:

$$M_T = \left[1 + 1.6\left(\frac{c^2}{r_i B}\right)\right]^{0.5}$$

See Kiefner et al [M.14] and Willoughby and Davey [M.15].

c) For other cases, e.g. embedded flaws, circumferential flaws in cylinders or for flaws at nozzles in pressure vessels, the bulging correction factor M = 1.

M.6.2 Surface flaws

Solutions for M_m are given in **M.4.1.2** and for M_b in **M.4.1.3**.

M.6.3 Embedded flaws

Solutions for M_m are given in **M.4.5.2** and for M_b in **M.4.5.3**.

M.6.4 Extended or fully circumferential flaws

Solutions for M_m and M_b are given in **M.4.3**.

M.7 Stress intensity factor solutions for cylinders under internal pressure and mechanical loads

M.7.1 General

The finite width correction, f_w, is as given in **M.2**.

Table M.4a) to Table M.11 may be used to determine the applied stress intensity factor for combined internal pressure and mechanical loads, within the specified range of application. Interpolation is permitted for values falling between those quoted. When M_m and M_b are calculated from Table M.4a) to Table M.11, these include any bulging effect and the general bulging factor M from **M.2** should be taken as 1.

M.7.2 Cylinders containing axial flaws

M.7.2.1 Through-thickness flaws oriented axially

This solution is taken from France et al [M.16]. See Figure M.14 for the definition of the geometry. The stress intensity factor solution is calculated from Equation (M.1) to Equation (M.6), where:

$K_I = K_I^{membrane} + K_I^{bending}$

$M = 1$

$M_m = M_1 + M_2$ at the outside surface

$M_m = M_1 - M_2$ at the inside surface

$M_b = M_3 + M_4$ at the outside surface

$M_b = M_3 - M_4$ at the inside surface

where:

$K_I^{membrane}$ is the contribution of membrane stresses to K_I, calculated from Equation (M.1) to Equation (M.6);

$K_I^{bending}$ is the contribution of through-wall bending (tensile on outside surface, compressive on inside surface) stresses to K_I, calculated from Equation (M.1) to Equation (M.6).

NOTE 1 Bulging is taken into account by the parameter λ: see Equation (M.27).

For membrane and through-wall bending loading, M_1 to M_4 are given in Table M.4a) to Table M.4d) in terms of λ.

$$\lambda = \left[12\left(1-\nu^2\right)\right]^{0.25} \frac{a}{\sqrt{r_m B}} \quad \text{(M.27)}$$

NOTE 2 These solutions are valid for long cylinders or pressure vessels with closed ends.

Range of application:

$0 \leq \lambda \leq 12.211$

$5 \leq r_m/B \leq 100$

Figure M.14 **Through-thickness flaw in cylinder oriented axially**

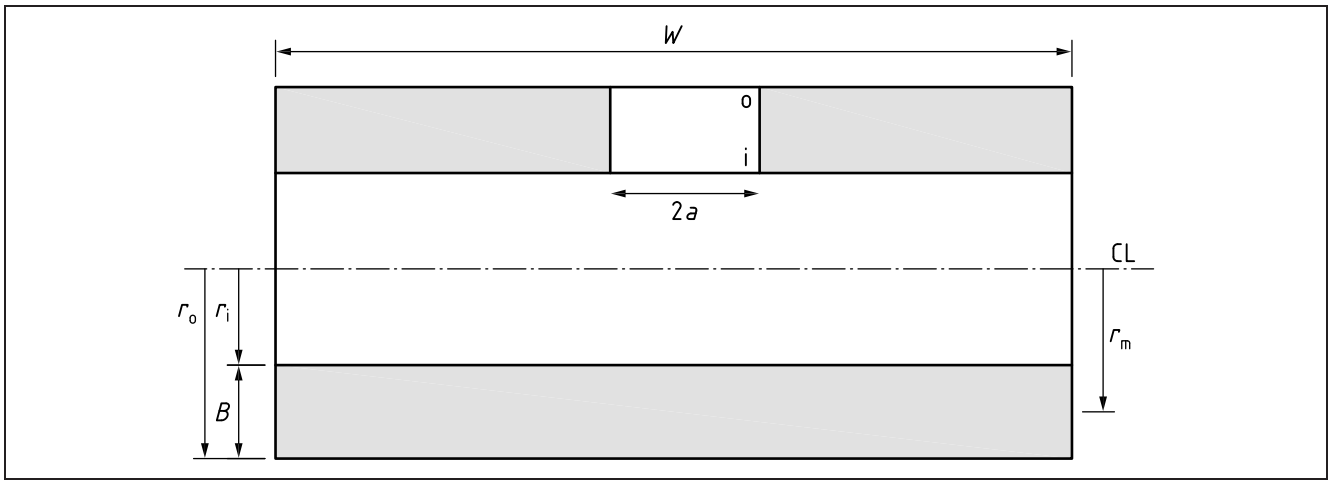


Table M.4a) **M_1 for axial through-thickness in cylinders: membrane loading**

Parameter, λ	r_m/B = 5	r_m/B = 10	r_m/B = 20	r_m/B = 50	r_m/B = 100
0.000	1.000	1.000	1.000	1.000	1.000
0.862	—	1.158	—	—	—
0.910	—	—	—	—	1.264
1.016	1.433	—	1.249	—	—
1.285	—	—	—	1.383	—
1.818	—	—	—	—	1.609
1.928	—	—	—	1.663	—
2.012	—	1.636	—	—	—
2.032	1.912	—	1.691	—	—
3.636	—	—	—	—	2.543
3.856	—	—	—	2.642	—
4.024	—	2.604	—	—	—
4.065	3.133	—	2.709	—	—
5.784	—	—	—	3.613	—
6.036	—	3.527	—	—	—
6.097	4.116	—	3.650	—	—
6.362	—	—	—	—	3.927
7.712	—	—	—	4.534	—
7.926	4.980	—	—	—	—
8.048	—	4.377	—	—	—
8.130	—	—	4.605	—	—
8.186	—	—	—	—	4.799
9.959	5.873	—	—	—	—
9.998	—	—	—	—	5.628
10.162	—	—	5.463	—	—
10.283	—	—	—	5.688	—
11.816	—	—	—	—	6.416
11.991	6.687	—	—	—	—
12.072	—	5.874	—	—	—
12.194	—	—	6.257	—	—
12.211	—	—	—	6.503	—

 © The British Standards Institution 2019

Table M.4b) **M_2 for axial through-thickness in cylinders: membrane loading**

Parameter, λ	r_m/B = 5	r_m/B = 10	r_m/B = 20	r_m/B = 50	r_m/B = 100
0.000	0.000	0.000	0.000	0.000	0.000
0.862	—	0.093	—	—	—
0.910	—	—	—	—	0.143
1.016	0.098	—	0.125	—	—
1.285	—	—	—	0.165	—
1.818	—	—	—	—	0.229
1.928	—	—	—	0.205	—
2.012	—	0.156	—	—	—
2.032	0.143	—	0.182	—	—
3.636	—	—	—	—	0.218
3.856	—	—	—	0.161	—
4.024	—	0.041	—	—	—
4.065	–0.030	—	0.089	—	—
5.784	—	—	—	–0.077	—
6.036	—	–0.264	—	—	—
6.097	–0.419	—	–0.200	—	—
6.362	—	—	—	—	–0.126
7.712	—	—	—	–0.436	—
7.926	–0.851	—	—	—	—
8.048	—	–0.684	—	—	—
8.130	—	—	–0.622	—	—
8.186	—	—	—	—	–0.475
9.959	–1.358	—	—	—	—
9.998	—	—	—	—	–0.884
10.162	—	—	–1.122	—	—
10.283	—	—	—	–1.034	—
11.816	—	—	—	—	–1.339
11.991	–1.829	—	—	—	—
12.072	—	–1.718	—	—	—
12.194	—	—	–1.700	—	—
12.211	—	—	—	–1.543	—

Table M.4c) **M_3 for axial through-thickness in cylinders: bending loading**

Parameter, λ	r_m/B = 5	r_m/B = 10	r_m/B = 20	r_m/B = 50	r_m/B = 100
0.000	0.000	0.000	0.000	0.000	0.000
0.862	—	0.040	—	—	—
0.910	—	—	—	—	0.025
1.016	0.053	—	0.040	—	—
1.285	—	—	—	0.042	—
1.818	—	—	—	—	0.055
1.928	—	—	—	0.060	—
2.012	—	0.075	—	—	—
2.032	0.083	—	0.068	—	—
3.636	—	—	—	—	0.095
3.856	—	—	—	0.097	—
4.024	—	0.109	—	—	—
4.065	0.121	—	0.103	—	—
5.784	—	—	—	0.119	—
6.036	—	0.128	—	—	—
6.097	0.139	—	0.123	—	—
6.362	—	—	—	—	0.127
7.712	—	—	—	0.134	—
7.926	0.150	—	—	—	—
8.048	—	0.138	—	—	—
8.130	—	—	0.135	—	—
8.186	—	—	—	—	0.139
9.959	0.161	—	—	—	—
9.998	—	—	—	—	0.147
10.162	—	—	0.143	—	—
10.283	—	—	—	0.145	—
11.816	—	—	—	—	0.151
11.991	0.171	—	—	—	—
12.072	—	0.150	—	—	—
12.194	—	—	0.146	—	—
12.211	—	—	—	0.150	—

Table M.4d) **M_4 for axial through-thickness in cylinders: membrane loading**

Parameter, λ	r_m/B = 5	r_m/B = 10	r_m/B = 20	r_m/B = 50	r_m/B = 100
0.000	1.000	1.000	1.000	1.000	1.000
0.862	—	0.694	—	—	—
0.910	—	—	—	—	0.637
1.016	0.701	—	0.659	—	—
1.285	—	—	—	0.629	—
1.818	—	—	—	—	0.598
1.928	—	—	—	0.600	—
2.012	—	0.608	—	—	—
2.032	0.604	—	0.602	—	—
3.636	—	—	—	—	0.527
3.856	—	—	—	0.529	—
4.024	—	0.517	—	—	—
4.065	0.493	—	0.524	—	—
5.784	—	—	—	0.474	—
6.036	—	0.453	—	—	—
6.097	0.417	—	0.467	—	—
6.362	—	—	—	—	0.448
7.712	—	—	—	0.430	—
7.926	0.364	—	—	—	—
8.048	—	0.403	—	—	—
8.130	—	—	0.421	—	—
8.186	—	—	—	—	0.407
9.959	0.314	—	—	—	—
9.998	—	—	—	—	0.374
10.162	—	—	0.382	—	—
10.283	—	—	—	0.381	—
11.816	—	—	—	—	0.348
11.991	0.276	—	—	—	—
12.072	—	0.328	—	—	—
12.194	—	—	0.355	—	—
12.211	—	—	—	0.353	—

M.7.2.2 Internal surface flaws oriented axially

This solution is taken from Newman and Raju ([M.17], [M.18], [M.19]).
See Figure M.15 for the definition of the geometry. The stress intensity factor solution is calculated from Equation (M.1) to Equation (M.6), where:

$M = f_w = 1$

M_m and M_b for the deepest point in the flaw (d) and for the points where the flaw intersects the free surface (s) are given in Table M.5.

The range of application is:

$0 \leq a/B \leq 0.8$

$0.05 \leq a/c \leq 1$

$0.1 \leq B/r_i \leq 0.25$

$2c/W \leq 0.15$

Figure M.15 **Internal surface flaw in cylinder oriented axially**

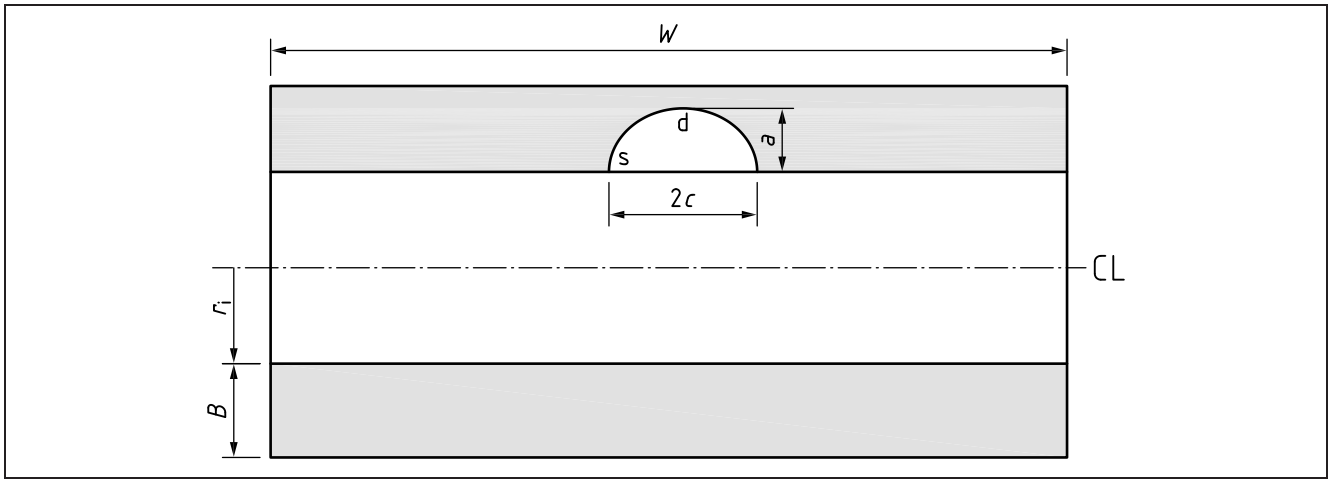


Table M.5 M_m and M_b for axial internal surface flaw in cylinder

a/B	M_m(d)	M_b(d)	M_m(s)	M_b(s)	a/B	M_m(d)	M_b(d)	M_m(s)	M_b(s)
a/c = 1.0, B/r_i = 0.1					**a/c = 1.0, B/r_i = 0.25**				
0.0	0.663	0.663	0.729	0.729	0.0	0.663	0.663	0.729	0.729
0.2	0.647	0.464	0.726	0.676	0.2	0.643	0.461	0.719	0.669
0.4	0.661	0.291	0.760	0.649	0.4	0.656	0.288	0.745	0.638
0.6	0.677	0.110	0.804	0.623	0.6	0.677	0.107	0.785	0.610
0.8	0.694	–0.080	0.859	0.599	0.8	0.704	–0.079	0.838	0.585
a/c = 0.4, B/r_i = 0.1					**a/c = 0.4, B/r_i = 0.25**				
0.0	0.951	0.951	0.662	0.662	0.0	0.951	0.951	0.662	0.662
0.2	0.932	0.698	0.676	0.632	0.2	0.919	0.688	0.669	0.627
0.4	1.016	0.519	0.768	0.651	0.4	0.998	0.506	0.759	0.644
0.6	1.109	0.316	0.896	0.674	0.6	1.110	0.311	0.889	0.666
0.8	1.211	0.090	1.060	0.700	0.8	1.255	0.103	1.060	0.694
a/c = 0.2, B/r_i = 0.1					**a/c = 0.2, B B/r_i = 0.25**				
0.0	1.059	1.059	0.521	0.521	0.0	1.059	1.059	0.521	0.521
0.2	1.062	0.806	0.578	0.548	0.2	1.045	0.791	0.577	0.547
0.4	1.260	0.677	0.695	0.597	0.4	1.240	0.663	0.698	0.599
0.6	1.500	0.515	0.876	0.660	0.6	1.514	0.515	0.887	0.665
0.8	1.783	0.320	1.123	0.737	0.8	1.865	0.348	1.144	0.745
a/c = 0.1, B/r_i = 0.1					**a/c = 0.1, B/r_i = 0.25**				
0.0	1.103	1.103	0.384	0.384	0.0	1.103	1.103	0.384	0.384
0.2	1.172	0.897	0.451	0.429	0.2	1.153	0.881	0.451	0.428
0.4	1.494	0.834	0.582	0.503	0.4	1.470	0.816	0.585	0.504
0.6	1.985	0.765	0.820	0.623	0.6	2.003	0.765	0.830	0.627
0.8	2.737	0.689	1.219	0.810	0.8	2.864	0.749	1.242	0.819
a/c = 0.05, B/r_i = 0.1					**a/c = 0.05, B B/r_i = 0.25**				
0.0	1.120	1.120	0.275	0.275	0.0	1.120	1.120	0.275	0.275
0.2	1.231	0.946	0.335	0.318	0.2	1.211	0.929	0.334	0.318
0.4	1.701	0.971	0.469	0.406	0.4	1.674	0.950	0.471	0.407
0.6	2.619	1.080	0.765	0.584	0.6	2.285	1.079	0.774	0.587
0.8	4.364	1.301	1.374	0.919	0.8	3.163	1.081	1.400	0.928

M.7.2.3 Extended internal surface flaws oriented axially

This solution is taken from Newman and Raju ([M.17], [M.18], [M.19]). See Figure M.16 for the definition of the geometry. The stress intensity factor solution is calculated from Equation (M.1) to Equation (M.6), where:

$M = f_w = 1$

M_m is given in Table M.6 for the deepest point in the flaw;

M_b is given in Table M.6 for the deepest point in the flaw;

The range of application is:

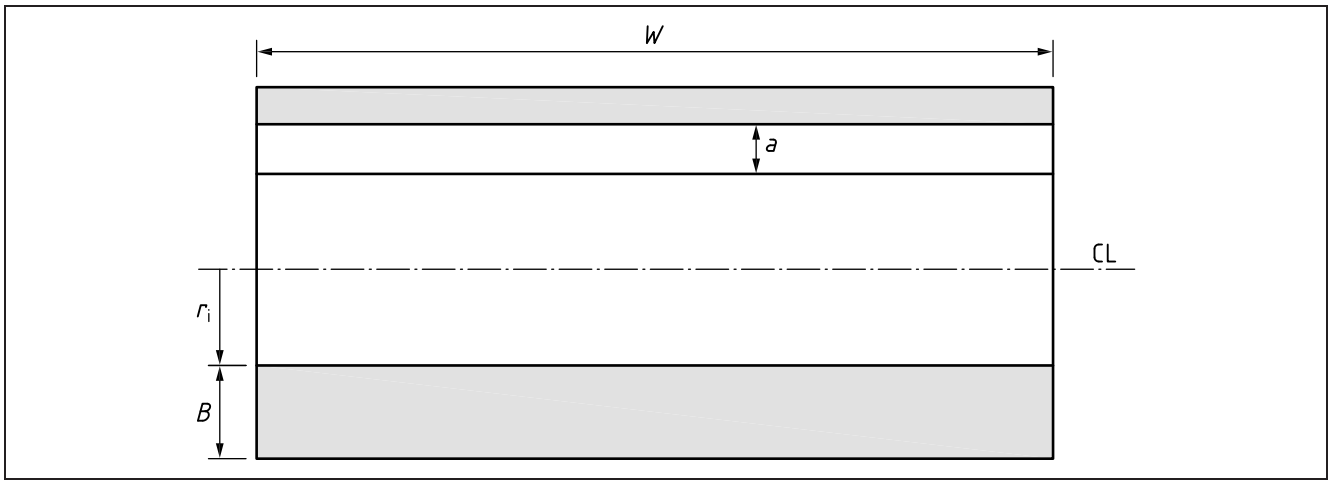
$0 \leq a/B \leq 0.8$

$0.1 \leq B/r_i \leq 0.25$

Table M.6 **M_m and M_b for extended axial internal surface flaw in cylinder**

B/r_i = 0.1			B/r_i = 0.25		
a/B	M_m	M_b	a/B	M_m	M_b
0.0	1.122	1.122	0.0	1.122	1.122
0.2	1.380	1.018	0.2	1.304	1.002
0.4	1.930	1.143	0.4	1.784	1.033
0.6	2.960	1.484	0.6	2.566	1.094
0.8	4.820	1.990	0.8	3.461	0.949

Figure M.16 **Extended internal surface flaw in cylinder orientated axially**



M.7.2.4 External surface flaws in cylinders oriented axially

This solution is taken from Newman and Raju ([M.17], [M.18], [M.19]).
See Figure M.17 for the definition of the geometry. The stress intensity factor solution is calculated from Equation (M.1) to Equation (M.6), where:

$$M = f_w = 1$$

M_m and M_b are given in Table M.7 for the deepest point in the flaw (d) and for the points where the flaw intersects the free surface (s).

The range of application is:

$0 \leq a/B \leq 0.8$

$0.05 \leq a/c \leq 1$

$0.1 \leq B/r_i \leq 0.25$

$2c/W \leq 0.15$

 © The British Standards Institution 2019

Figure M.17 **External surface flaw in cylinder oriented axially**

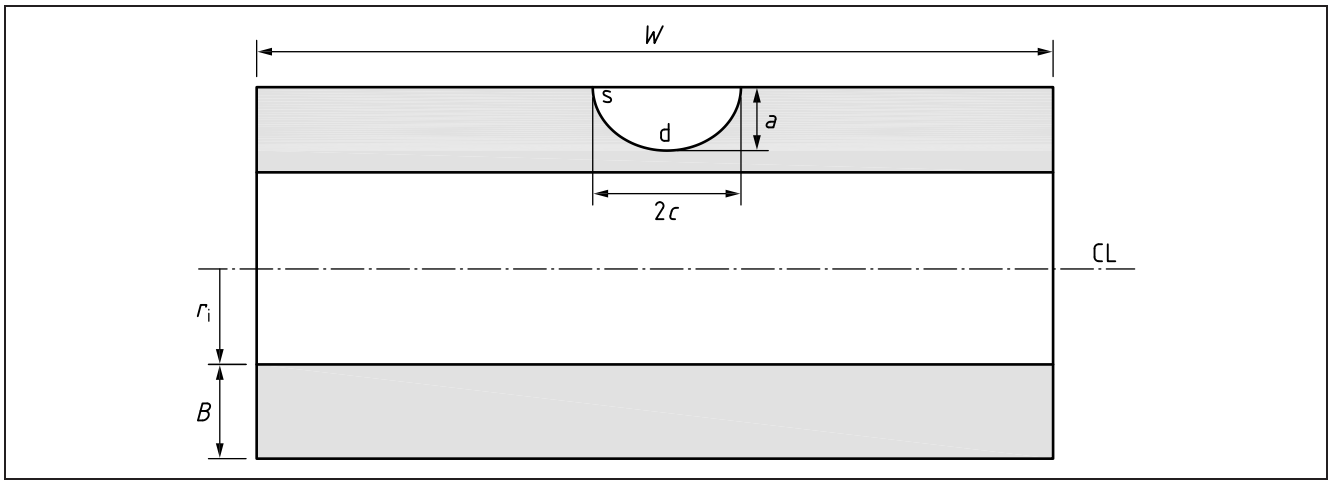


Table M.7 M_m and M_b for axial external surface flaw in cylinder

a/B	M_m(d)	M_b(d)	M_m(s)	M_b(s)	a/B	M_m(d)	M_b(d)	M_m(s)	M_b(s)
a/c = 1.0, B/r_i = 0.1					**a/c = 1.0, B/r_i = 0.25**				
0.0	0.663	0.663	0.729	0.729	0.0	0.663	0.663	0.729	0.729
0.2	0.653	0.470	0.736	0.685	0.2	0.656	0.473	0.741	0.689
0.4	0.675	0.301	0.783	0.666	0.4	0.683	0.307	0.793	0.673
0.6	0.695	0.122	0.846	0.649	0.6	0.710	0.131	0.864	0.659
0.8	0.712	–0.068	0.926	0.634	0.8	0.736	–0.055	0.954	0.647
a/c = 0.4, B/r_i = 0.1					**a/c = 0.4, B/r_i = 0.25**				
0.0	0.951	0.951	0.662	0.662	0.0	0.951	0.951	0.662	0.662
0.2	0.953	0.716	0.685	0.641	0.2	0.964	0.726	0.689	0.644
0.4	1.077	0.561	0.799	0.673	0.4	1.110	0.582	0.806	0.678
0.6	1.213	0.377	0.970	0.715	0.6	1.289	0.417	0.982	0.721
0.8	1.361	0.167	1.198	0.769	0.8	1.502	0.230	1.217	0.775
a/c = 0.2, B/r_i = 0.1					**a/c = 0.2, B/r_i = 0.25**				
0.0	1.059	1.059	0.521	0.521	0.0	1.059	1.059	0.521	0.521
0.2	1.092	0.831	0.583	0.552	0.2	1.106	0.844	0.583	0.552
0.4	1.370	0.750	0.706	0.606	0.4	1.410	0.776	0.693	0.598
0.6	1.735	0.644	0.912	0.681	0.6	1.838	0.693	0.867	0.659
0.8	2.188	0.514	1.202	0.780	0.8	2.390	0.595	1.105	0.736
a/c = 0.1, B/r_i = 0.1					**a/c = 0.1, B/r_i = 0.25**				
0.0	1.103	1.103	0.384	0.384	0.0	1.103	1.103	0.384	0.384
0.2	1.206	0.926	0.455	0.432	0.2	1.222	0.939	0.455	0.432
0.4	1.624	0.923	0.592	0.510	0.4	1.672	0.955	0.581	0.504
0.6	2.295	0.957	0.853	0.643	0.6	2.432	1.029	0.811	0.622
0.8	3.360	1.108	1.305	0.857	0.8	3.670	1.128	1.199	0.809
a/c = 0.05, B/r_i = 0.1					**a/c = 0.05, B/r_i = 0.25**				
0.0	1.120	1.120	0.275	0.275	0.0	1.120	1.120	0.275	0.275
0.2	1.266	0.976	0.338	0.321	0.2	1.282	0.991	0.338	0.321
0.4	1.849	1.075	0.477	0.412	0.4	1.753	1.011	0.468	0.407
0.6	2.628	1.349	0.796	0.602	0.6	2.581	1.107	0.757	0.583
0.8	4.090	1.549	1.471	0.972	0.8	3.839	1.153	1.352	0.918

M.7.2.5 Extended external surface flaws in cylinders oriented axially

This solution is taken from Anderson et al [M.20]. See Figure M.18 for the definition of the geometry. The stress intensity factor solution is calculated from Equation (M.1) to Equation (M.6), where:

$$M = f_w = 1$$

M_m and M_b are given in Table M.8.

The range of application is:

$$0 \leq a/B \leq 0.8$$

$$0.001\ B/r_i \leq 0.333\ 333$$

Figure M.18 **Extended axial external surface flaw in cylinder**

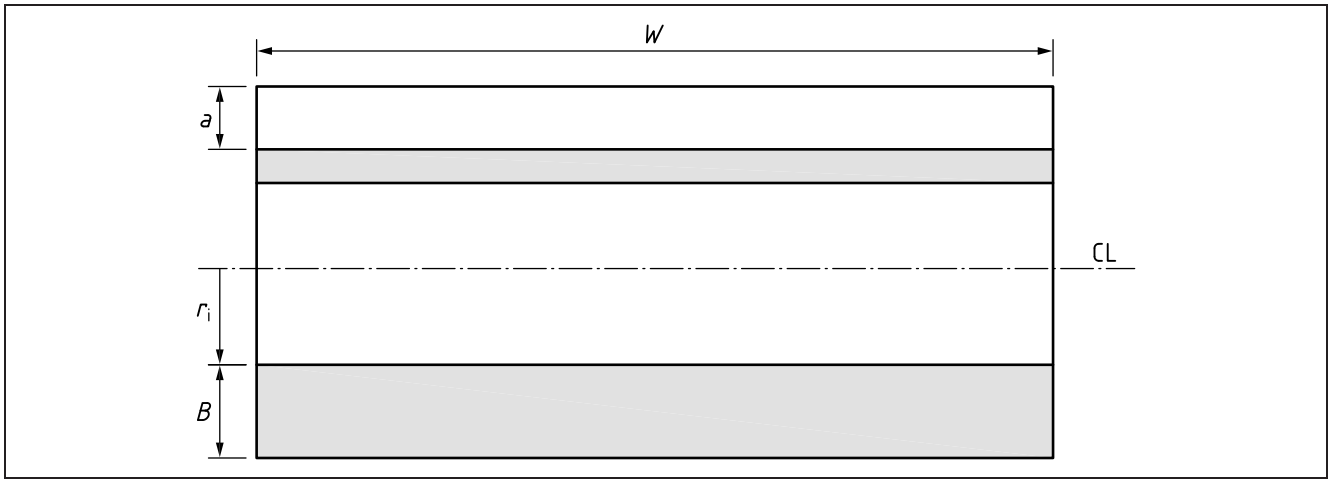


Table M.8 **M_m and M_b for extended axial external surface flaw in cylinder**

B/r_i	a/B	M_m	M_b
0.001	0.0	1.120 000	1.120 000
	0.2	1.362 492	1.052 320
	0.4	2.106 159	1.258 945
	0.6	4.023 909	1.912 231
	0.8	11.90 9190	4.657 704
0.00333	0.0	1.120 000	1.120 000
	0.2	1.357 654	1.048 520
	0.4	2.098 131	1.253 795
	0.6	3.988 986	1.893 041
	0.8	11.418 040	4.448 136
0.01	0.0	1.120 000	1.120 000
	0.2	1.355 914	1.047 032
	0.4	2.086 534	1.245 785
	0.6	3.923 337	1.856 235
	0.8	10.534 910	4.060 550
0.01667	0.0	1.120 000	1.120 000
	0.2	1.354 559	1.045 929
	0.4	2.075 495	1.238 148
	0.6	3.858 610	1.820 100
	0.8	9.814 990	3.742 856

Table M.8 M_m and M_b for extended axial external surface flaw in cylinder *(continued)*

B/r_i	a/B	M_m	M_b
0.025	0.0	1.120 000	1.120 000
	0.2	1.352 815	1.044 438
	0.4	2.058 880	1.227 570
	0.6	3.783 314	1.777 812
	0.8	9.072 502	3.416 980
0.05	0.0	1.120 000	1.120 000
	0.2	1.348 153	1.040 533
	0.4	2.028 188	1.205 201
	0.6	3.584 289	1.665 773
	0.8	7.522 466	2.733 754
0.1	0.0	1.120 000	1.120 000
	0.2	1.338 976	1.032 891
	0.4	1.964 321	1.160 635
	0.6	3.270 363	1.543 946
	0.8	5.839 919	1.993 885
0.2	0.0	1.120 000	1.120 000
	0.2	1.324 199	1.020 313
	0.4	1.861 734	1.089 804
	0.6	2.864 663	1.261 675
	0.8	4.412 961	1.367 035
0.333 333	0.0	1.120 000	1.120 000
	0.2	1.310 620	1.008 616
	0.4	1.768 778	1.024 620
	0.6	2.576 840	1.098 873
	0.8	3.652 018	1.033 655

M.7.2.6 Embedded flaws

The flat plate solution in **M.4.5** may be applied to embedded flaws in shells.

M.7.3 Curved shells containing circumferential flaws

M.7.3.1 Through-thickness flaws oriented circumferentially

This solution is from France et al [M.16]. See Figure M.19 for the definition of the geometry. The stress intensity factor solution is calculated from Equation (M.1) to Equation (M.6), where:

$K_I = K_I^{membrane} + K_I^{bending}$

$M = 1$

$M_m = M_1 + M_2$ at the outside surface

$M_m = M_1 - M_2$ at the inside surface

$M_b = M_3 + M_4$ at the outside surface

$M_b = M_3 - M_4$ at the inside surface

$K_I^{membrane}$ is the contribution of membrane stresses to K_I, calculated from Equation (M.1) to Equation (M.6)

$K_I^{bending}$ is the contribution of through-wall bending (tensile on outside surface, compressive on inside surface) stresses to K_I, calculated from Equation (M.1) to Equation (M.6)

For membrane and through-wall bending loading, M_1 to M_4 are given in Table M.9a) to Table M.9d) in terms of the parameter λ, referred to in Equation (M.27). For membrane loading, P_m should be multiplied by a factor of β, where:

$$\beta = \left[\frac{2r_m}{a}\tan\left(\frac{a}{2r_m}\right)\right]^{0.5} \quad \text{(M.28)}$$

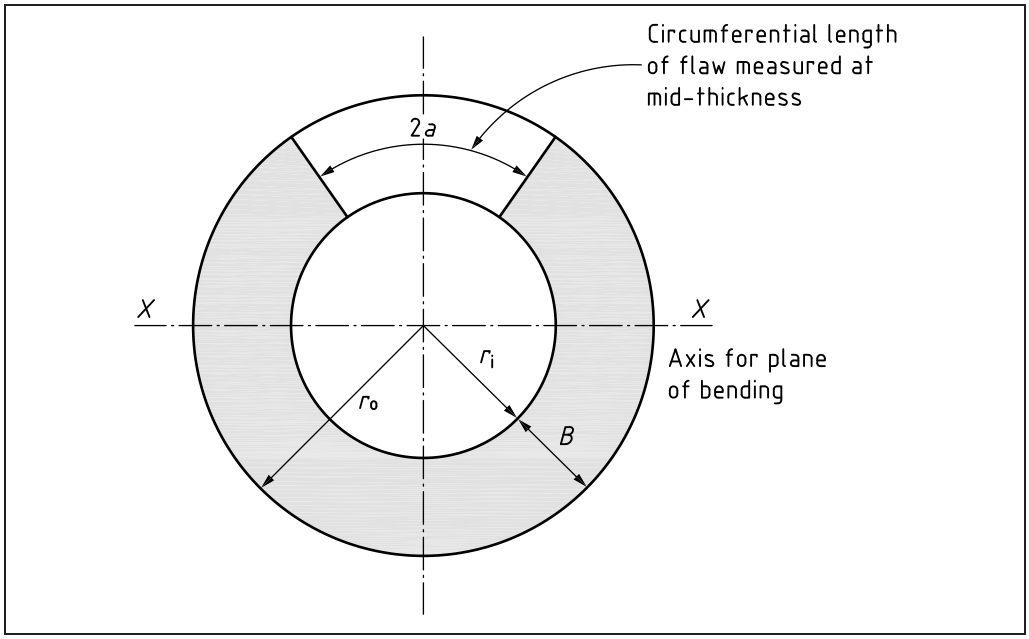
NOTE These solutions are valid for long cylinders or pressure vessels with closed ends.

The range of application is:

$0 \leq \lambda \leq 15.143$

$5 \leq r_m/B \leq 100$

Figure M.19 **Through-thickness flaw in cylinder oriented circumferentially**



 © The British Standards Institution 2019

Table M.9a) **M_1 for circumferential through-thickness in cylinders: membrane loading**

Parameter, λ	r_m/B = 5	r_m/B = 10	r_m/B = 20	r_m/B = 50	r_m/B = 100
0.000	1.000	1.000	1.000	1.000	1.000
0.177	1.248	—	—	—	—
0.251	—	1.032	—	—	—
0.355	1.290	—	1.050	—	—
0.502	—	1.066	—	—	—
0.561	—	—	—	1.061	—
0.709	—	—	1.085	—	—
0.793	—	—	—	—	1.088
1.064	1.406	—	—	—	—
1.122	—	—	—	1.096	—
1.505	—	1.192	—	—	—
1.586	—	—	—	—	1.139
1.596	1.522	—	—	—	—
2.128	—	—	1.276	—	—
2.257	—	1.324	—	—	—
2.306	1.723	—	—	—	—
3.193	2.044	—	1.469	—	—
3.261	—	1.545	—	—	—
3.365	—	—	—	1.378	—
3.902	2.367	—	—	—	—
4.515	—	1.864	—	—	—
4.612	—	—	1.752	—	—
4.759	—	—	—	—	1.425
4.789	2.883	—	—	—	—
5.498	3.414	—	—	—	—
5.518	—	2.164	—	—	—
6.385	4.301	—	2.140	—	—
6.772	—	2.641	—	—	—
7.139	—	—	—	—	1.732
7.776	—	3.117	—	—	—
7.804	—	—	2.495	—	—
9.032	—	3.917	—	—	—
9.578	—	—	3.040	—	—
10.096	—	—	—	2.588	—
10.997	—	—	3.580	—	—
12.770	—	—	4.502	—	—
15.143	—	—	—	3.623	—

Table M.9b) **M_2 for circumferential through-thickness flaws in cylinders: membrane loading**

Parameter, λ	r_m/B = 5	r_m/B = 10	r_m/B = 20	r_m/B = 50	r_m/B = 100
0.000	0.000	0.000	0.000	0.000	0.000
0.177	0.069	—	—	—	—
0.251	—	0.035	—	—	—
0.355	0.077	—	0.034	—	—
0.502	—	0.057	—	—	—
0.561	—	—	—	0.045	—
0.709	—	—	0.069	—	—
0.793	—	—	—	—	0.063
1.064	0.140	—	—	—	—
1.122	—	—	—	0.087	—
1.505	—	0.121	—	—	—
1.586	—	—	—	—	0.102
1.596	0.153	—	—	—	—
2.128	—	—	0.116	—	—
2.257	—	0.108	—	—	—
2.306	0.112	—	—	—	—
3.193	–0.014	—	0.041	—	—
3.261	—	0.019	—	—	—
3.365	—	—	—	0.043	—
3.902	–0.158	—	—	—	—
4.515	—	–0.153	—	—	—
4.612	—	—	–0.119	—	—
4.759	—	—	—	—	–0.082
4.789	–0.385	—	—	—	—
5.498	–0.622	—	—	—	—
5.518	—	–0.328	—	—	—
6.385	–1.015	—	–0.318	—	—
6.772	—	–0.528	—	—	—
7.139	—	—	—	—	–0.277
7.776	—	–0.747	—	—	—
7.804	—	—	–0.485	—	—
9.032	—	–1.071	—	—	—
9.578	—	—	–0.762	—	—
10.096	—	—	—	–0.585	—
10.997	—	—	–0.944	—	—
12.770	—	—	–1.281	—	—
15.143	—	—	—	–1.126	—

Table M.9c) **M_3 for circumferential through-thickness flaws in cylinders: bending loading**

Parameter, λ	r_m/B = 5	r_m/B = 10	r_m/B = 20	r_m/B = 50	r_m/B = 100
0.000	0.000	0.000	0.000	0.000	0.000
0.177	0.023	—	—	—	—
0.251	—	0.021	—	—	—
0.355	0.037	—	0.015	—	—
0.502	—	0.028	—	—	—
0.561	—	—	—	0.013	—
0.709	—	—	0.025	—	—
0.793	—	—	—	—	0.012
1.064	0.064	—	—	—	—
1.122	—	—	—	0.026	—
1.505	—	0.054	—	—	—
1.586	—	—	—	—	0.025
1.596	0.079	—	—	—	—
2.128	—	—	0.048	—	—
2.257	—	0.063	—	—	—
2.306	0.092	—	—	—	—
3.193	0.106	—	0.052	—	—
3.261	—	0.069	—	—	—
3.365	—	—	—	0.043	—
3.902	0.117	—	—	—	—
4.515	—	0.074	—	—	—
4.612	—	—	0.052	—	—
4.759	—	—	—	—	0.032
4.789	0.135	—	—	—	—
5.498	0.156	—	—	—	—
5.518	—	0.079	—	—	—
6.385	0.191	—	0.054	—	—
6.772	—	0.088	—	—	—
7.139	—	—	—	—	0.033
7.776	—	0.100	—	—	—
7.804	—	—	0.059	—	—
9.032	—	0.119	—	—	—
9.578	—	—	0.065	—	—
10.096	—	—	—	0.046	—
10.997	—	—	0.068	—	—
12.770	—	—	0.078	—	—
15.143	—	—	—	0.029	—

Table M.9d) **M_4 for circumferential through-thickness flaws in cylinders: bending loading**

Parameter, λ	r_m/B = 5	r_m/B = 10	r_m/B = 20	r_m/B = 50	r_m/B = 100
0.000	1.000	1.000	1.000	1.000	1.000
0.177	0.918	—	—	—	—
0.251	—	0.828	—	—	—
0.355	0.816	—	0.750	—	—
0.502	—	0.733	—	—	—
0.561	—	—	—	0.673	—
0.709	—	—	0.666	—	—
0.793	—	—	—	—	0.633
1.064	0.624	—	—	—	—
1.122	—	—	—	0.587	—
1.505	—	0.544	—	—	—
1.586	—	—	—	—	0.544
1.596	0.533	—	—	—	—
2.128	—	—	0.465	—	—
2.257	—	0.450	—	—	—
2.306	0.441	—	—	—	—
3.193	0.361	—	0.373	—	—
3.261	—	0.364	—	—	—
3.365	—	—	—	0.364	—
3.902	0.315	—	—	—	—
4.515	—	0.299	—	—	—
4.612	—	—	0.301	—	—
4.759	—	—	—	—	0.293
4.789	0.270	—	—	—	—
5.498	0.239	—	—	—	—
5.518	—	0.264	—	—	—
6.385	0.203	—	0.249	—	—
6.772	—	0.230	—	—	—
7.139	—	—	—	—	0.228
7.776	—	0.205	—	—	—
7.804	—	—	0.218	—	—
9.032	—	0.179	—	—	—
9.578	—	—	0.187	—	—
10.096	—	—	—	0.184	—
10.997	—	—	0.182	—	—
12.770	—	—	0.161	—	—
15.143	—	—	—	0.205	—

 © The British Standards Institution 2019

M.7.3.2 Internal surface flaws oriented circumferentially

This solution derives from several sources: Newman and Raju ([M.17], [M.18]), Dedhia and Harris [M.21], and Bergman and Brickstad [M.22].

See Figure M.20 for the definition of the geometry. The stress intensity factor solution is calculated from Equation (M.1) to Equation (M.6), where:

$$M = f_w = 1$$

M_m and M_b are given in Table M.10 for the deepest point in the flaw (d) and for the points where the flaw intersects the free surface (s).

A global bending moment on the cylinder can be included by adding $P_{m,b}$ to P_m, where:

$$P_{m,b} = \frac{4M_{global}(r_i + a)}{\pi\left[(r_i + B)^4 - r_i^4\right]} \quad \text{(M.29)}$$

The range of application is:

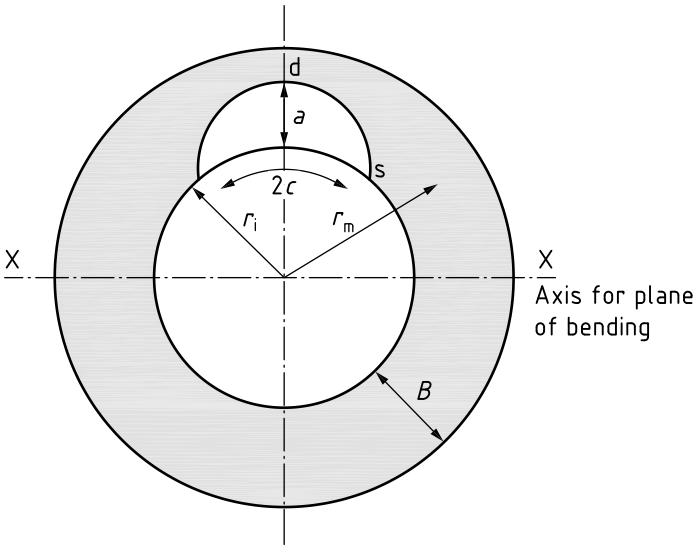
$0 \leq a/B \leq 0.8$

$0.1 \leq a/c \leq 1$

$0.1 \leq B/r_i \leq 0.2$

For values of $B/r_i < 0.1$, the use of flat plate solutions (**M.4.1**) is recommended.

Figure M.20 **Internal surface flaw in cylinder oriented circumferentially**



Key

d Deepest point

s Surface point

Table M.10 M_m and M_b for circumferential internal surface flaw in cylinder

a/B	M_m(d)	M_b(d)	M_m(s)	M_b(s)	a/B	M_m(d)	M_b(d)	M_m(s)	M_b(s)
a/c = 1.0, B/r_i = 0.1					**a/c = 1.0, B/r_i = 0.2**				
0.0	0.663	0.663	0.729	0.729	0.0	0.663	0.663	0.729	0.729
0.2	0.667	0.574	0.681	0.623	0.2	0.667	0.582	0.681	0.623
0.4	0.670	0.327	0.706	0.528	0.4	0.670	0.334	0.706	0.528
0.6	0.686	0.140	0.733	0.431	0.6	0.686	0.117	0.733	0.431
0.8	0.702	–0.105	0.764	0.332	0.8	0.702	–0.099	0.764	0.332
a/c = 0.5,B/r_i = 0.1					**a/c = 0.5, B/r_i = 0.2**				
0.0	0.896	0.896	0.697	0.697	0.0	0.896	0.896	0.697	0.697
0.2	0.999	0.731	0.731	0.628	0.2	1.004	0.735	0.731	0.628
0.4	1.031	0.504	0.801	0.563	0.4	1.030	0.503	0.801	0.563
0.6	1.121	0.306	0.889	0.502	0.6	1.124	0.305	0.889	0.502
0.8	1.148	0.014	0.993	0.445	0.8	1.192	0.027	0.993	0.445
a/c = 0.2, B/r_i = 0.1					**a/c = 0.2, B/r_i = 0.2**				
0.0	1.059	1.059	0.521	0.521	0.0	1.059	1.059	0.521	0.521
0.2	1.168	0.870	0.617	0.623	0.2	1.144	0.851	0.617	0.623
0.4	1.375	0.736	0.835	0.591	0.4	1.318	0.698	0.835	0.591
0.6	1.599	0.561	1.048	0.556	0.6	1.517	0.515	1.048	0.556
0.8	1.803	0.269	1.255	0.519	0.8	1.782	0.253	1.255	0.519
a/c = 0.1, B/r_i = 0.1					**a/c = 0.1, B/r_i = 0.2**				
0.0	1.103	1.103	0.384	0.384	0.0	1.103	1.103	0.384	0.384
0.2	1.219	0.921	0.482	0.487	0.2	1.214	0.903	0.482	0.487
0.4	1.529	0.829	0.700	0.498	0.4	1.382	0.776	0.700	0.498
0.6	1.939	0.677	0.981	0.525	0.6	1.661	0.624	0.981	0.525
0.8	2.411	0.479	1.363	0.570	0.8	2.031	0.386	1.363	0.570

M.7.3.3 Extended internal flaws

This solution derives from several sources: Dedhia and Harris [M.21], Joseph and Erdogan [M.23], and Andrasic and Parker [M.24].

See Figure M.21 for the definition of the geometry. The stress intensity factor solution is calculated from Equation (M.1) to Equation (M.6), where:

$$M = f_w = 1$$

M_m and M_b are given in Table M.11.

Loading, in terms of a global moment, M_{global}, can be accounted for by adding the term in Equation (M.29) to the primary stress, P_m.

The range of application is:

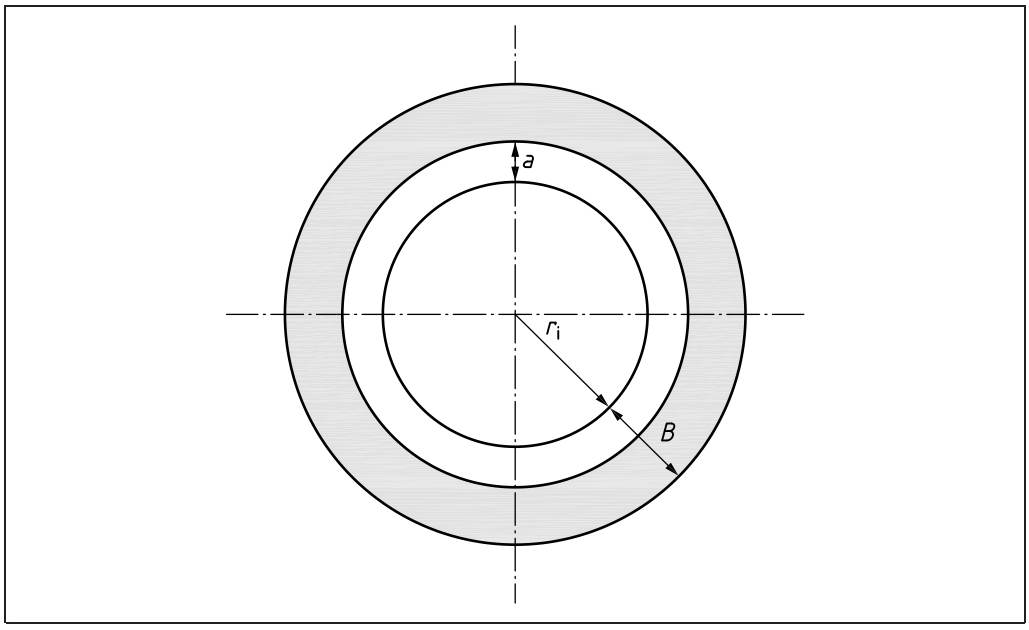
$$0 \leq a/B \leq 0.8$$

$$0.1 \leq B/r_i \leq 0.2$$

Table M.11 **M_m and M_b for extended circumferential internal surface flaw in cylindrical shell**

B/r_i = 0.1			B/r_i = 0.2		
a/B	M_m	M_b	a/B	M_m	M_b
0.0	1.122	1.122	0.0	1.122	1.122
0.2	1.261	0.954	0.2	1.215	0.933
0.4	1.582	0.909	0.4	1.446	0.810
0.6	2.091	0.810	0.6	1.804	0.650
0.8	2.599	0.600	0.8	2.280	0.411

Figure M.21 **Extended internal surface flaw in cylinder**



M.7.3.4 External surface flaws oriented circumferentially

The flat plate solution in **M.4.1** may be applied to circumferential external surface flaws in cylinders.

M.7.3.5 Extended external surface flaws

This solution comes from Rooke and Cartwright [M.4]. See Figure M.22 for the definition of the geometry.

NOTE This solution is appropriate for membrane loading only; bending stresses P_b and Q_b need to be added to P_m and Q_m for assessment purposes.

The stress intensity factor solution is calculated from Equation (M.1) to Equation (M.6), where:

$$M = f_w = 1$$

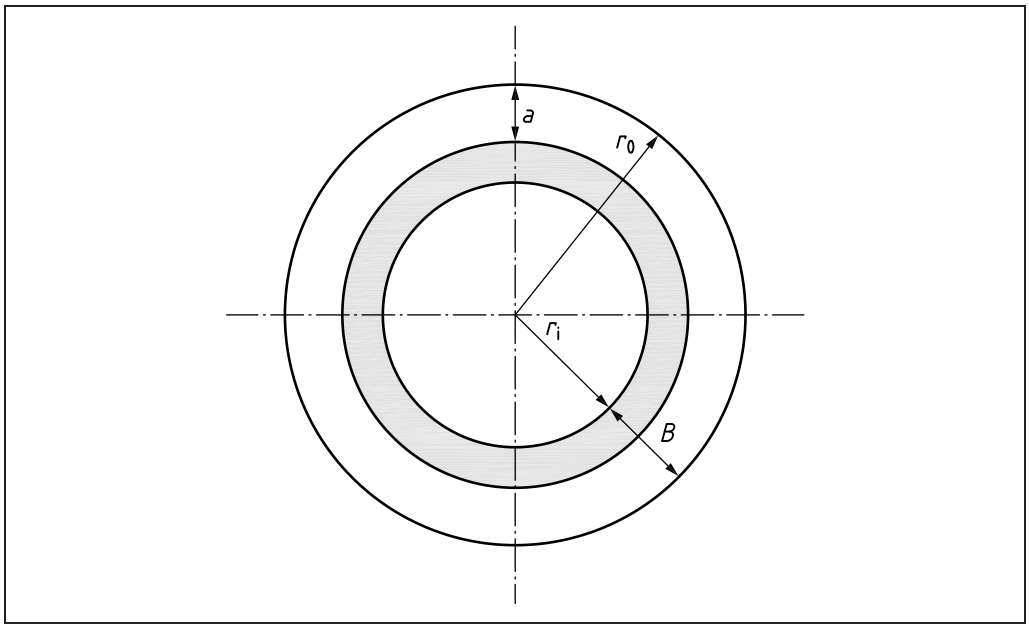
$$M_b = M_m = \frac{1-\lambda^2}{\left\{[1-(1-\lambda)\mu]^2 - \lambda^2\right\}}\left\{0.8 + \frac{(1-\lambda)\mu}{1-(1-\lambda)\mu}\left[4 + \frac{1.08\lambda}{(1-\lambda)(1-\mu)}\right]\right\}^{-0.5} \quad \text{(M.30)}$$

where:

$$\lambda = \left(\frac{r_i}{r_o}\right)$$

$$\mu = \left(\frac{a}{B}\right)$$

Figure M.22 **Extended external surface flaw in cylinder**



M.7.3.6 Embedded flaws

The flat plate solution in **M.4.5** may be applied to embedded flaws in shells.

M.8 Stress intensity factor solutions for spheres containing through thickness flaws

This solution comes from Anderson [M.25]. For an equatorial through-thickness flaw in a sphere, as illustrated in Figure M.23, with a stress distribution consisting of a uniform membrane stress, P_m, and a through-wall bending stress, P_b, the stress intensity factor is given by:

$$K_I = [P_m G_1 + P_b(G_1 - 2G_2)]\sqrt{\pi a} \quad \text{(M.31)}$$

The influence coefficients G_1 and G_2 are listed in Table M.12 as a function of r_i/B and λ, where:

$$\lambda = \frac{1.818a}{\sqrt{r_i B}}$$

Two sets of values of G_1 and G_2 are provided for the determination of the stress intensity factor at either the inside surface or the outside surface.

The range of application is:

$$3 \leq r_i/B \leq 100$$

The recommended solution is considered applicable only for flaws that extend less than 50% of the circumference, i.e. $2a < \pi\ (r_i + B)$. It has been reported in reference [M.25] that the recommended solution can give rise to anomalous results in the case of longer flaws (approximately $\lambda > 6.5$) subject to membrane loading; the solution should be used with caution in such cases.

In the case of internal pressure, the stress intensity factor can be written in terms of the nominal (average) hoop stress:

$$K_I = \frac{pr_o^2}{r_o^2 - r_i^2} G_p \sqrt{\pi a} \quad \text{(M.32)}$$

where p is internal pressure and discrete values of G_p are given in Table M.12.

Table M.12 **Influence coefficients at points A and B for an equatorial through-thickness flaw in a sphere**

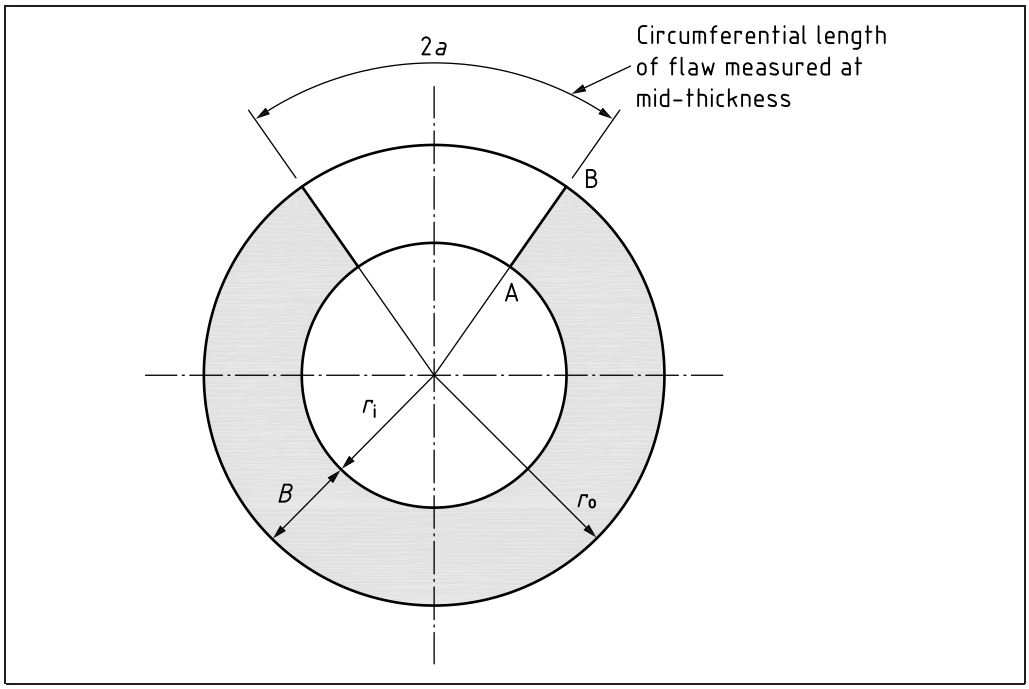
r_i/B	λ	Uniform loading (G_1)		Linear loading (G_2)		Internal pressure (G_p)	
		Inside surface	Outside surface	Inside surface	Outside surface	Inside surface	Outside surface
3	0	0.866	1	0	1	0.983 06	0.916 39
	0.131 9	0.831 1	0.966 8	0.028 9	0.991 7	0.958 31	1.039 26
	0.263 8	0.828 6	1.025 2	0.055 2	1.007 3	0.942 23	1.080 93
	0.659 5	0.865 8	1.210 3	0.142 6	1.041	0.935 51	1.172 72
	1.319	1.065 1	1.494 7	0.320 8	1.131 6	1.099 52	1.389 24
	2.638	1.964 3	2.014 7	0.885	1.335 1	1.943 42	1.789 42
	3.957	3.471 9	2.361 2	1.724 9	1.459 7	3.379 71	1.959 79
	5.276	5.609 2	2.381 7	2.892 2	1.443 1	5.446 91	1.774 37
	6.595	7.350 5	2.114	3.820 1	1.268 9	7.120 42	1.344 31
	7.914	12.484	1.025 8	6.539 1	0.668 7	12.102 3	–0.077 4
	9.233	18.011	–0.726	—	—	17.517 8	–1.567 2
5	0	0.912 9	1	0	1	0.993 12	0.935 13
	0.153 3	0.879	0.986	0.049 4	1.001	0.987 79	1.068 97
	0.459 8	8.890 2	1.142 3	0.123 6	1.014 1	0.955 15	1.132 74
	0.919 5	0.982 7	1.358 9	0.234	1.070 2	1.017 95	1.291 42
	1.532 5	1.266 8	1.667 6	0.426	1.172 5	1.261 81	1.536 78
	3.065 1	2.564 5	2.286 6	1.197 9	1.431 2	2.507 48	2.020 03
	4.597 6	4.735 7	2.649 6	2.362 4	1.563 6	4.578 25	2.140 5
	6.130 1	7.523 7	2.550 7	3.836 2	1.486 3	7.262 28	1.769 39
	7.662 7	10.797	2.045 2	5.538	1.195 1	10.401 6	0.966 37
	8.943 4	16.504	0.706	8.500 3	0.487 1	15.921 9	–0.657 4
	10.728	25.473	–2.021	13.144	–0.97	24.731 4	–1.642 2
10	0	0.953 5	1	0	1	0.998 11	0.960 05
	0.198 7	0.9207	1.0278	—	—	1.005 69	1.081 45
	0.397 3	0.931 1	1.135 5	—	—	0.980 35	1.122 15
	0.993 4	1.059 7	1.430 9	0.277 4	1.079 1	1.077 33	1.359 89
	1.986 7	1.642 6	1.954 2	0.643 8	1.274	1.610 13	1. 797 64
	3.973 4	3.928 4	2.742 1	1.898 3	1.606 7	3.804 29	2.354 62
	5.960 2	7.683 3	2.974 3	3.842 6	1.675 9	7.386 88	2.190 11
	7.946 9	13.05	2.406 8	6.594 5	1.362 6	12.534 8	1.129 03
	9.933 6	20.604	0.794 9	10.439	0.514 8	19.800 5	–0.883 4
	11.92	30.445	–1.844	15.45	–0.861	29.356 4	–2.352 2
	13.907	43.35	–4.735	22.019	–2.383	42.509 5	5.383 81

Table M.12 **Influence coefficients at points A and B for an equatorial through-thickness flaw in a sphere** *(continued)*

r_i/B	λ	Uniform loading (G_1)		Linear loading (G_2)		Internal pressure (G_p)	
		Inside surface	Outside surface	Inside surface	Outside surface	Inside surface	Outside surface
20	0	0.975 9	1	0	1	0.999 5	0.977 7
	0.134 1	0.948	1.006 6	—	—	1.031 77	1.073 29
	0.268 2	0.953 7	1.088 2	0.128 2	0.977	0.999 69	1.088 04
	0.402 3	0.959 9	1.154	0.155 9	0.981 8	0.990 28	1.128 65
	0.804 6	1.030 4	1.358 6	0.240 2	1.040 6	1.042 11	1.302 44
	1.341	1.250 5	1.652 6	0.399	1.149 7	1.246 03	1.566 47
	2.681 9	2.323	2.361 4	1.016 8	1.434 5	2.254 23	2.149 82
	5.363 9	6.482	3.194	3.190 8	1.785 5	6.236 42	2.562 76
	8.045 8	13.238	2.870 1	6.613 1	1.578 8	12.683 1	1.571 64
	10.728	23.215	1.122 5	11.648	0.675 6	22.242 5	–0.841 7
60	0	0.991 8	1	0	1	0.999 94	0.991 98
	0.158 3	0.977 5	1.054 2	0.128	0.958 6	1.006 21	1.073 75
	0.224 9	0.977	1.087 2	0.144 2	0.951 6	0.993 31	1.083 46
	0.469 4	0.99	1.206 6	0.183 7	0.971 1	0.988 3	1.182 72
	1.349 3	1.279 2	1.702 1	0.403 9	1.152 2	1.260 89	1.633 01
	2.248 9	1.930 7	2.216 2	0.786 9	1.363 5	1.884 94	2.079 98
	4.497 8	4.820 3	3.179 6	2.301 9	1.772 2	4.635 72	2.738 26
	8.995 6	15.929	3.027 2	7.878	1.631 9	15.241 7	1.512 56
	13.493	34.004	–0.32	16.863	–0.069	32.543 5	–2.532 1
100	0	0.995	1	0	1	0.999 98	0.995 11
	0.173 1	0.982 3	1.070 3	0.142 3	0.943 4	0.991 37	1.062 81
	0.576 9	1.009 2	1.267 4	0.204 6	0.981 4	0.996 38	1.225 49
	1.730 6	1.522 9	1.945 7	0.543 2	1.239 7	1.487	1.859 16
	2.884 3	2.585 5	2.582 2	1.127 5	1.505 3	2.509 7	2.391 73
	5.768 5	7.202 5	3.493 1	3.479 4	1.892 2	6.909 38	2.816 21
	11.537	24.958	1.793 6	12.283	0.989 3	23.856 7	–0.374 2
	17.306	53.643	–4.219	26.45	–2.03	51.649 5	–2.467 7

 © The British Standards Institution 2019

Figure M.23 **Through-thickness flaw in spherical shell**



M.9 Stress intensity factor solutions for tubular joints

See Annex B for guidance on the determination of appropriate stress intensity factors.

M.10 Stress intensity factor solutions for round bars and bolts

M.10.1 Straight-fronted flaws in round bars

This solution comes from James and Mills [M.26]. See Figure M.24 for the definition of the geometry. The stress intensity factor is calculated from Equation (M.1) to Equation (M.6), where:

$$M = M_{km} = M_{kb} = f_w = 1$$

where:

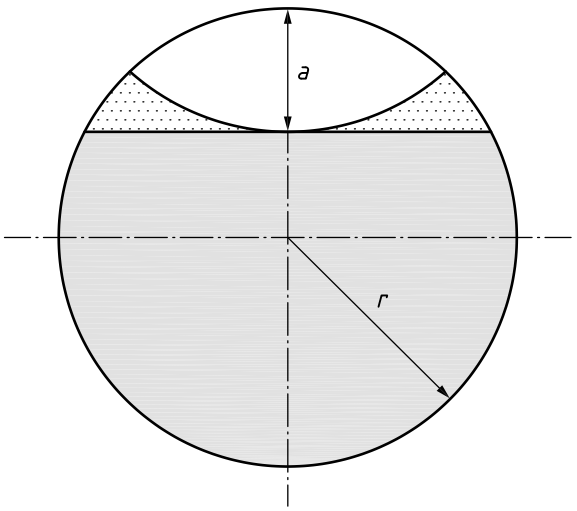
$$M_m = 0.926 - 1.771\left(\frac{a}{2r}\right) + 26.421\left(\frac{a}{2r}\right)^2 - 78.481\left(\frac{a}{2r}\right)^3 + 87.911\left(\frac{a}{2r}\right)^4 \quad \text{(M.33)}$$

$$M_b = 1.04 - 3.64\left(\frac{a}{2r}\right) + 16.86\left(\frac{a}{2r}\right)^2 - 32.59\left(\frac{a}{2r}\right)^3 + 28.41\left(\frac{a}{2r}\right)^4 \quad \text{(M.34)}$$

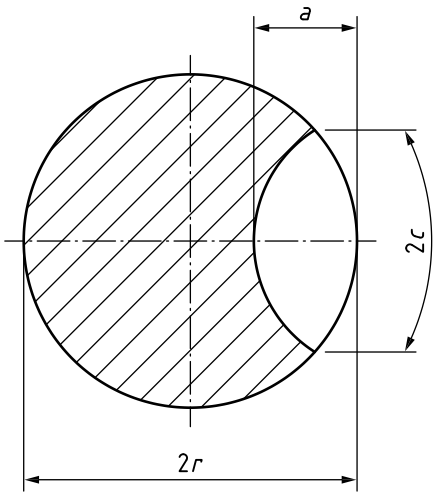
The range of application is:

$$0.0625 < a/2r < 0.625$$

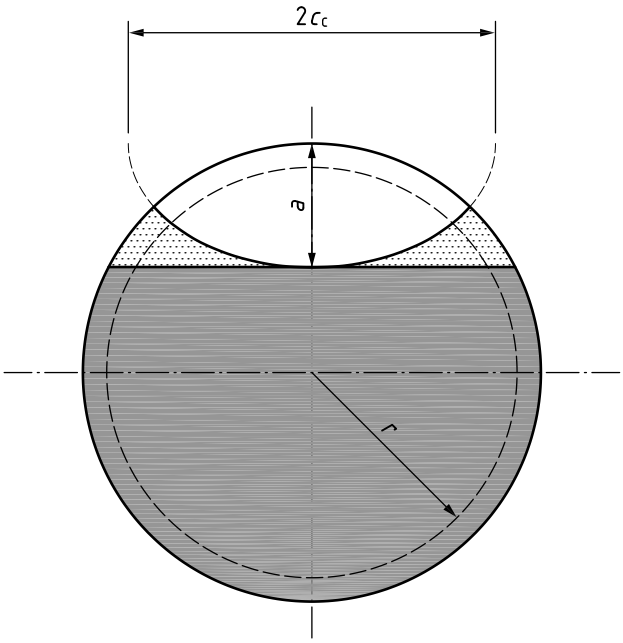
Figure M.24 **Flaws in bars and bolts**



a) Straight-fronted and semicircular flaws in round bars



b) Semi-elliptical flaw in round bars



c) Semi-elliptical surface flaw in bolts

M.10.2 Semicircular surface flaws in round bars

This solution comes from James and Mills [M.26]. See Figure M.24 for the definition of the geometry. The stress intensity factor solution is calculated from Equation (M.1) to Equation (M.6), where:

$$M = M_{km} = M_{kb} = f_w = 1$$

where:

$$M_m = g\left\{0.752 + 2.02\left(\frac{a}{2r}\right) + 0.37\left[1 - \sin\left(\frac{\pi a}{4r}\right)\right]^3\right\} \quad \text{(M.35)}$$

$$M_b = g\left\{0.923 + 0.199\left[1 - \sin\left(\frac{\pi a}{4r}\right)\right]^4\right\} \quad \text{(M.36)}$$

where:

$$g = \frac{\frac{1.84}{\pi}\left[\frac{\tan(\pi a/4r)}{\pi a/4r}\right]^{0.5}}{\cos(\pi a/4r)} \quad \text{(M.37)}$$

The range of application is:

$a/2r < 0.6$

*NOTE K solutions for straight-fronted flaws in round bars (**M.10.1**) are generally conservative compared with semicircular surface flaws.*

M.10.3 Semi-elliptical surface flaws in round bars

This solution comes from Raju and Newman [M.27]. See Figure M.24 for the definition of the geometry. The stress intensity factor solution is calculated from Equation (M.1) to Equation (M.6), where:

$M = M_{km} = M_{kb} = f_w = 1$

M_m and M_b at the deepest and surface points of the semi-elliptical flaw are given in Table M.13 and Table M.14 respectively.

Table M.13 **M_m for semi-elliptical flaw in a round bar under tension loading**

M_m at deepest point				M_m at surface			
a/r	*a/c*			*a/r*	*a/c*		
	0.6	**0.8**	**1.0**		**0.6**	**0.8**	**1.0**
0.10	0.867	0.744	0.645	0.10	0.731	0.743	0.736
0.25	0.921	0.763	0.647	0.25	0.782	0.776	0.757
0.40	1.031	0.797	0.661	0.40	0.884	0.846	0.803
0.55	1.226	0.865	0.692	0.55	1.041	0.941	0.864
0.70	1.437	0.978	0.749	0.70	1.187	1.064	0.940

Table M.14 **M_b for semi-elliptical flaw in a round bar under bending loading**

M_b at deepest point				M_b at surface			
a/r	*a/c*			*a/r*	*a/c*		
	0.6	**0.8**	**1.0**		**0.6**	**0.8**	**1.0**
0.10	0.811	0.694	0.598	0.10	0.710	0.725	0.719
0.25	0.773	0.635	0.533	0.25	0.707	0.718	0.710
0.40	0.771	0.585	0.477	0.40	0.712	0.725	0.708
0.55	0.815	0.560	0.435	0.55	0.724	0.733	0.706
0.70	0.827	0.551	0.401	0.70	0.686	0.732	0.705

M.10.4 Semi-elliptical surface flaws in bolts

M.10.4.1 Solution 1

This solution comes from Toribio [M.28]. See Figure M.24 for the definition of the geometry. This solution has been developed for the ISO M8 × 1.0 bolt geometry. An alternative solution for threaded bolts (UNF) is given in **M.10.4.2**. The stress intensity factor is calculated from Equation (M.1) to Equation (M.6), where:

$$M = M_{km} = M_{kb} = f_w = 1$$

where:

$$M_m = M_b = \lambda_0 + \lambda_1\left(\frac{a}{2r}\right) + \lambda_2\left(\frac{a}{2r}\right)^2 \quad \text{(M.38)}$$

where the following apply for the conditions indicated in a) and b).

a) Tension loading, M_m, at the deepest point in the flaw:

$$\lambda_0 = 1.015\,5 - 0.2375\left(\frac{a}{c}\right)$$

$$\lambda_1 = -0.584 + 0.015\left(\frac{a}{c}\right)$$

$$\lambda_2 = 6.45575 - 3.34875\left(\frac{a}{c}\right)$$

Intersection of the flaw with the free surface:

$$\lambda_0 = 0.4695 + 0.8225\left(\frac{a}{c}\right)$$

$$\lambda_1 = 0.377\,75 - 1.47875\left(\frac{a}{c}\right)$$

$$\lambda_2 = -0.160\,25 + 2.94625\left(\frac{a}{c}\right)$$

b) Bending loading, M_b, at the deepest point in the flaw:

$$\lambda_0 = 0.89375 - 0.36375\left(\frac{a}{c}\right)$$

$$\lambda_1 = -0.55925 + 0.36625\left(\frac{a}{c}\right)$$

$$\lambda_2 = 2.379 - 1.88\left(\frac{a}{c}\right)$$

Intersection of the flaw with the free surface:

$$\lambda_0 = 0.6535 - 0.0925\left(\frac{a}{c}\right)$$

$$\lambda_1 = 1.14875 + 1.55875\left(\frac{a}{c}\right)$$

$$\lambda_2 = 3.028 - 1.855\left(\frac{a}{c}\right)$$

The range of application is:

$0.2 \leq a/c \leq 1$;

$0.14 \leq a/2r \leq 0.5$.

 © The British Standards Institution 2019

M.10.4.2 Solution 2

An alternative solution for semicircular surface flaws in threaded bolts (UNF) in tension is given by James and Mills [M.26] and is calculated from Equation (M.1) to Equation (M.6), where:

$$M = M_{km} = M_{kb} = f_w = 1$$

where:

$$M_m = 2.043 \exp\left[-31.332\left(\tfrac{a}{2r}\right)\right] + 0.650\,7 + 0.536\,7\left(\tfrac{a}{2r}\right) + 3.046\,9\left(\tfrac{a}{2r}\right)^2 - 19.504\left(\tfrac{a}{2r}\right)^3 + 45.647\left(\tfrac{a}{2r}\right)^4 \quad \text{(M.39)}$$

*NOTE This solution is based on a combination of solutions for semicircular surface flaws (**M.10.2**) and straight-fronted flaws in round bars for a/2r > 0.4 (**M.10.1**), together with thread effects for a/2r < 0.1.*

The range of application is:

$$0.004 \leq a/2r \leq 0.65$$

Equation (M.39) can be used for flaws in smooth bars if the exponential term is set to zero. Equation (M.40) is a similar expression given for bending loading; this solution does not include thread effects.

$$M_b = 0.630\,1 + 0.03488\left(\frac{a}{2r}\right)^2 - 3.3365 + 13.406\left(\frac{a}{2r}\right)^3 - 6.002\,1\left(\frac{a}{2r}\right)^4 \quad \text{(M.40)}$$

M.10.5 Fully circumferential flaws in round bars

This solution comes from Tada et al [M.2]. See Figure M.25 for the definition of the geometry. The stress intensity factor solution is calculated from Equation (M.1) to Equation (M.6), where:

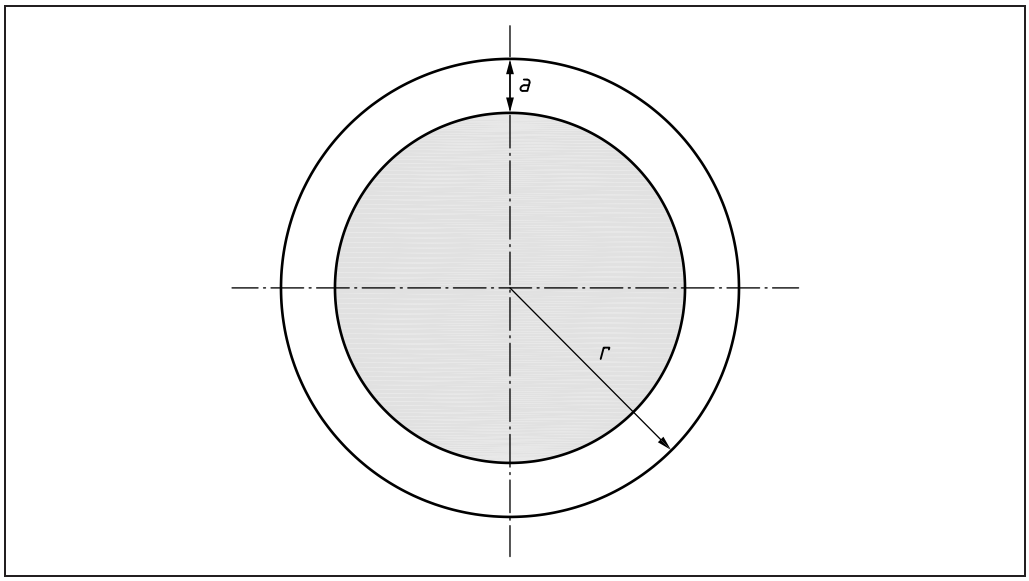
$$M = M_{km} = M_{kb} = f_w = 1$$

where:

$$M_m = \frac{r^{1.5}}{2(r-a)^{1.5}}\left[1 + 0.5\left(\frac{r-a}{r}\right) + 0.375\left(\frac{r-a}{r}\right)^2 - 0.363\left(\frac{r-a}{r}\right)^3 + 0.731\left(\frac{r-a}{r}\right)^4\right] \quad \text{(M.41)}$$

$$M_b = \frac{0.375r^{2.5}}{(r-a)^{2.5}}\left\{1 + 0.5\left(\frac{r-a}{r}\right) + 0.375\left(\frac{r-a}{r}\right)^2 + 0.313\left(\frac{r-a}{r}\right)^3 + 0.273\left(\frac{r-a}{r}\right)^4 + 0.537\left(\frac{r-a}{r}\right)^5\right\} \quad \text{(M.42)}$$

Figure M.25 **Fully circumferential flaw in a round bar**



M.11 Welded joints

M.11.1 Surface cracks at weld toes

M.11.1.1 General

When a flaw or crack is situated in a region of local stress concentration, such as the weld toe, the effect of the field of stress concentration should be included when calculating K_I [M.1)]. Unless the K_I solution being used already incorporates the influence of the stress concentration, the correction factor, M_k, should be introduced, which is a function of crack size, geometry and loading. In general, the correction factor, M_k, is the ratio of the K for a crack in material with stress concentration to the K for the same crack in material without stress concentration. Thus, M_k normally decreases with increases in through-thickness distance z from the weld toe to unity at crack heights of typically 30% of material thickness. For butt welds, T-butt welds, full penetration cruciform joints and members with fillet or butt-welded attachments, M_k has been found to be a function of z, L and L/B [M.2)]. Here z is the height, measured from the weld toe, and L is the overall length of the attachment measured from weld toe to weld toe [M.29], as illustrated in Figure M.26. The M_{km} and M_{kb} stress intensity factor magnification factors, for membrane and bending loading, are required for the general stress intensity factor solutions in Equation (M.1) to Equation (M.6). The resulting relationships are given in **M.11.1.2** and **M.11.1.3**.

M_k has been calculated by 2D finite element analysis for profiles representing sections of the welded joint geometry. Thus, M_k is directly applicable to the case of a straight-fronted weld toe surface crack (i.e. $a/2c = 0$). However, it can also be applied to semi-elliptical cracks ($0 < a/2c \leq 0.5$) and other planar surface-breaking flaws. The nature of the finite element model used to calculate M_k is such that the solutions produced are not applicable for $z = 0$, and near-surface

M.1) This approach contrasts with that used in the application of the fatigue design rules (e.g. BS 7608). In applying such rules, the design data, obtained from fatigue tests on welded specimens, already incorporate the influence of the weld stress concentration factor and are therefore used in conjunction with the nominal stress range near the weld.

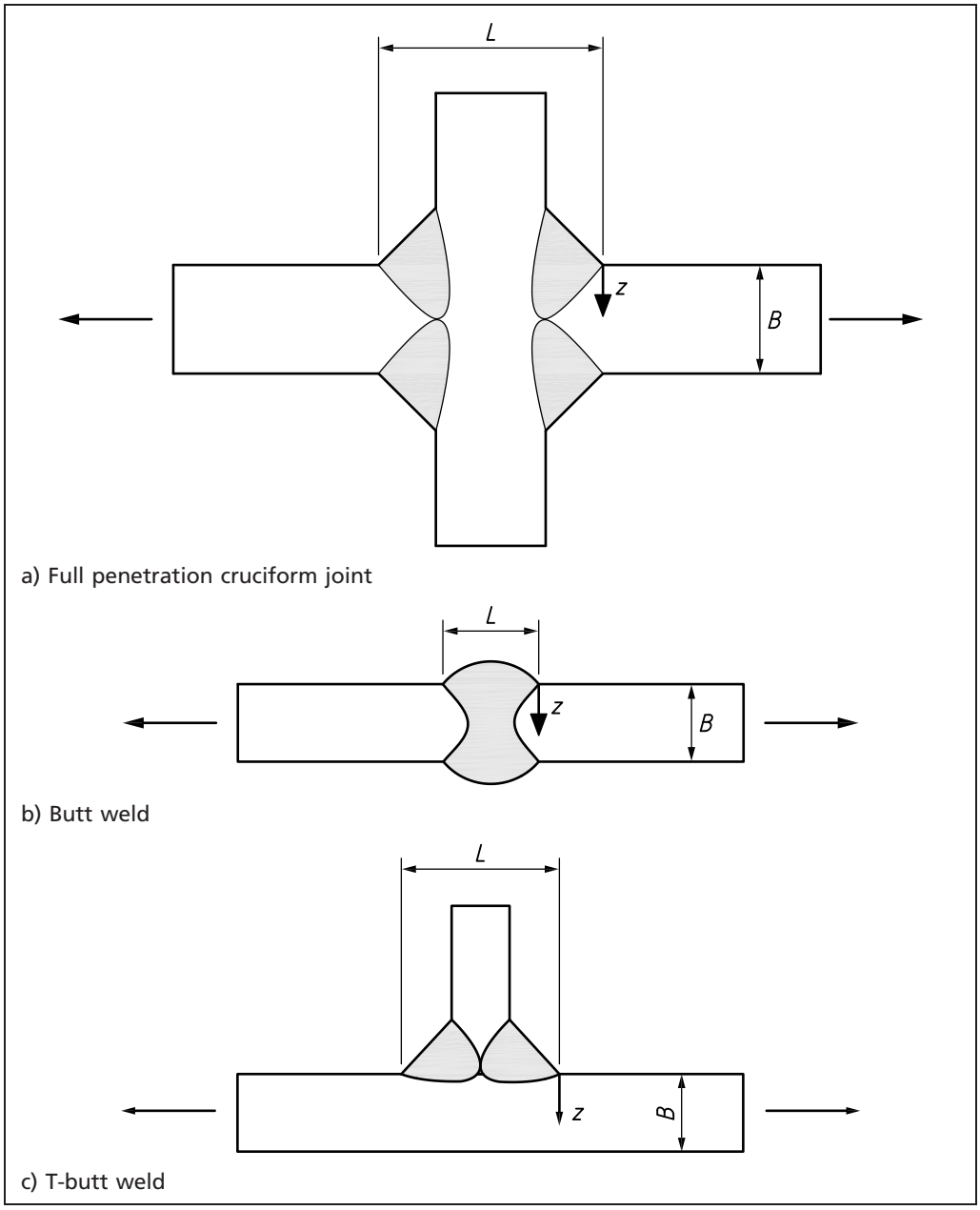
M.2) If the assessment is based on the use of the hot-spot stress range determined according to BS 7608, the influence of L/B is reduced such that M_k values for $L/B = 0.5$ may be used.

M_k values should be used (z = 0.15 mm) for the intersection of surface flaws with the weld toe and through-thickness flaws at weld toes.

The solutions presented apply for 45° weld profiles: M_k is slightly lower for lower angles and vice versa [M.30]. More accurate solutions based on 3D-stress analysis of semi-elliptical cracks at weld toes are available ([M.31], [M.32], [M.33], [M.34]). One such solution [M.31] is presented in **M.11.1.3**.

For fillet or partial penetration welded load-carrying T-joints or cruciform joints (Figure M.27), L/B is not relevant, but the weld throat thickness, t_w, is [M.30]. The resulting M_k solutions are given in **M.11.1.2**.

Figure M.26 **Welded joint geometries**



M.11.1.2 Solution based on 2D finite element analysis

This solution comes from Maddox and Andrews [M.29]. The following solutions apply:

$$M_k = v(z/B)^w \quad \text{down to } M_k = 1 \tag{M.43}$$

where:

- v has the value given in Table M.15 for flaws at the toes of full penetration or attachment welds;
- w has the value given in Table M.15 for flaws at the toes of full penetration or attachment welds;

For flaws at the toes of load-carrying fillet or partial penetration welds (see Figure M.27), the values of v and w are those corresponding to $L/B > 2$ for axial loading or $L/B \geq 1$ for bending, and the resulting value of v is multiplied by $(B/t_w)^{0.5}$.

Figure M.27 **Transverse load-carrying cruciform joint**

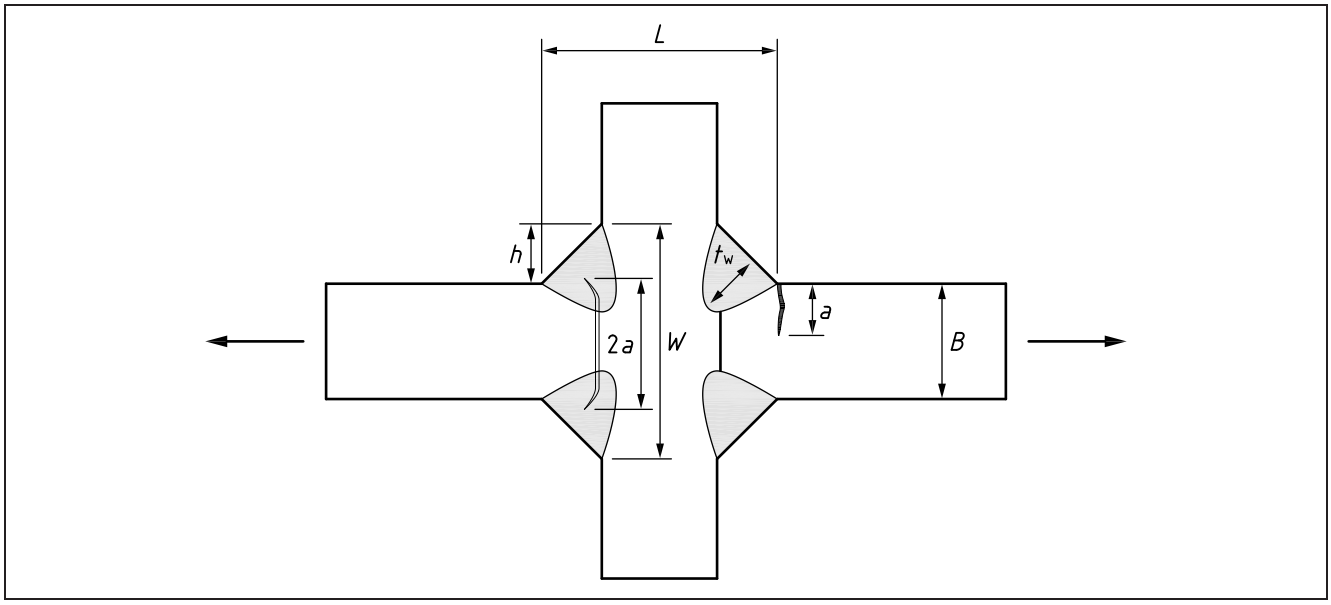


Table M.15 **Values of *v* and *w* for axial and bending loading**

Loading mode	*L*/*B*	*z*/*B*	*v*	*w*
Axial	≤2	$\leq 0.05(L/B)^{0.55}$	$0.51(L/B)^{0.27}$	–0.31
		$>0.05(L/B)^{0.55}$	0.83	$-0.15(L/B)^{0.46}$
	>2	≤0.073	0.615	–0.31
		>0.073	0.83	–0.20
Bending	≤1	$\leq 0.03(L/B)^{0.55}$	$0.45(L/B)^{0.21}$	–0.31
		$>0.03(L/B)^{0.55}$	0.68	$-0.19(L/B)^{0.21}$
	>1	≤0.03	0.45	–0.31
		>0.03	0.68	–0.19

M.11.1.3 Solution based on 3D finite element modelling

M.11.1.3.1 General

Alternative stress intensity magnification factor solutions, M_k, for the deepest points and surface points of a semi-elliptical weld-toe flaw (see Figure M.26) are given in **M.11.1.3.2** and **M.11.1.3.3**, based on the work of Bowness and Lee [M.31]. The solutions were obtained by curve fitting to individual finite element analyses. Verification and limited validation of this solution has been carried out for fatigue crack growth rate in pipeline girth welds [M.34]. Bowness and Lee include the weld profile angle as variables, but the following simplified solutions are valid for 45° weld profiles with sharp radii (less than 0.1B) and for the following parametric ranges:

$0.005 < a/B < 0.9$

$0.1 \leq a/c \leq 1.0$

$0.5 \leq L/B \leq 2.75$ (for $L/B > 2.75$, use the value for $L/B = 2.75$)

M.11.1.3.2 Deepest point

For the deepest point of the flaw, the solutions are given in Equation (M.44) and Equation (M.45).

a) Membrane

$$M_{km} = f_1\left(\frac{a}{B}, \frac{a}{c}\right) + f_2\left(\frac{a}{B}\right) + f_3\left(\frac{a}{B}, \frac{L}{B}\right) \quad \text{(M.44)}$$

where:

$$f_1\left(\frac{a}{B}, \frac{a}{c}\right) = 0.43358\left(\frac{a}{B}\right)^{\left\{g_1 + \left[g_2\left(\frac{a}{B}\right)\right]^{g_3}\right\}} + 0.931\ 63\exp\left[\left(\frac{a}{B}\right)^{-0.050966}\right] + g_4$$

$$f_2\left(\frac{a}{B}\right) = -0.215\ 21\left[1 - \left(\frac{a}{B}\right)\right]^{176.419\ 9} + 2.814\ 1\left(\frac{a}{B}\right)^{-0.107\ 40\left(\frac{a}{B}\right)}$$

$$f_3\left(\frac{a}{B}, \frac{L}{B}\right) = 0.339\ 94\left(\frac{a}{B}\right)^{g_5} + 1.949\ 3\left(\frac{a}{B}\right)^{0.230\ 03} + \left[g_6\left(\frac{a}{B}\right)^2 + g_7\left(\frac{a}{B}\right) + g_8\right]$$

where:

$$g_1 = -1.034\ 3\left(\frac{a}{c}\right)^2 - 0.1565\ 7\left(\frac{a}{c}\right) + 1.340\ 9$$

$$g_2 = 1.321\ 8\left(\frac{a}{c}\right)^{-0.611\ 53}$$

$$g_3 = -0.872\ 38\left(\frac{a}{c}\right) + 1.278\ 8$$

$$g_4 = -0.461\ 90\left(\frac{a}{c}\right)^3 + 0.670\ 90\left(\frac{a}{c}\right)^2 - 0.375\ 71\left(\frac{a}{c}\right) + 4.651\ 1$$

$$g_5 = -0.015\ 647\left(\frac{L}{B}\right)^3 + 0.090\ 889\left(\frac{L}{B}\right)^2 - 0.171\ 80\left(\frac{L}{B}\right) - 0.245\ 87$$

$$g_6 = -0.201\ 36\left(\frac{L}{B}\right)^2 + 0.933\ 11\left(\frac{L}{B}\right) - 0.414\ 96$$

$$g_7 = 0.201\ 88\left(\frac{L}{B}\right)^2 - 0.978\ 57\left(\frac{L}{B}\right) + 0.068\ 225$$

$$g_8 = -0.027\ 338\left(\frac{L}{B}\right)^2 + 0.125\ 51\left(\frac{L}{B}\right) - 11.218$$

If Equation (M.44) gives a value of $M_k < 1.0$, assume that $M_k = 1.0$.

b) Bending

If $0.005 \leq a/B \leq 0.5$, then the following expression applies:

$$M_{kb} = f_1\left(\frac{a}{B}, \frac{a}{c}\right) + f_2\left(\frac{a}{B}\right) + f_3\left(\frac{a}{B}, \frac{L}{B}\right) \quad \text{(M.45)}$$

where:

$$f_1\left(\frac{a}{B}, \frac{a}{c}\right) = 0.065\,916\left(\frac{a}{B}\right)^{\left\{g_1 + \left[g_2\left(\frac{a}{B}\right)\right]^{g_3}\right\}} + 0.520\,86\exp\left[\left(\frac{a}{B}\right)^{-0.103\,64}\right] + g_4$$

$$f_2\left(\frac{a}{B}\right) = -0.021\,95\left[1 - \left(\frac{a}{B}\right)\right]^{2.808\,6} + 0.021\,403\left(\frac{a}{B}\right)^{g_5}$$

$$f_3\left(\frac{a}{B}, \frac{L}{B}\right) = 0.233\,44\left(\frac{a}{B}\right)^{g_6} + 0.148\,27\left(\frac{a}{B}\right)^{-0.200\,77} + \left[g_7\left(\frac{a}{B}\right)^2 + g_8\left(\frac{a}{B}\right) + g_9\right]$$

where:

$$g_1 = -0.014\,992\left(\frac{a}{c}\right)^2 - 0.021\,401\left(\frac{a}{c}\right) - 0.238\,51$$

$$g_2 = 0.617\,75\left(\frac{a}{c}\right)^{-1.027\,8}$$

$$g_3 = 0.000\,132\,42\left(\frac{a}{c}\right) - 1.474\,4$$

$$g_4 = -0.287\,83\left(\frac{a}{c}\right)^3 + 0.587\,06\left(\frac{a}{c}\right)^2 - 0.371\,98\left(\frac{a}{c}\right) - 0.898\,87$$

$$g_5 = -17.195\left(\frac{a}{B}\right)^2 + 12.468\left(\frac{a}{B}\right) - 0.516\,62$$

$$g_6 = -0.059\,798\left(\frac{L}{B}\right)^3 + 0.380\,91\left(\frac{L}{B}\right)^2 - 0.802\,203\,7\left(\frac{L}{B}\right) + 0.319\,06$$

$$g_7 = -0.358\,48\left(\frac{L}{B}\right)^2 + 1.397\,5\left(\frac{L}{B}\right) - 1.753\,5$$

$$g_8 = 0.312\,88\left(\frac{L}{B}\right)^2 - 1.359\,9\left(\frac{L}{B}\right) + 1.6611$$

$$g_9 = -0.001\,470\,1\left(\frac{L}{B}\right)^2 - 0.002\,507\,4\left(\frac{L}{B}\right) - 0.008\,984\,6$$

If Equation (M.45) gives a value of $M_k < 1.0$, assume that $M_k = 1.0$.

If $0.5 < a/B \leq 0.9$, $M_{kb} = 1.0$

M.11.1.3.3 Surface point

For the surface point of the flaw, the solutions are given in Equation (M.46) and Equation (M.47).

a) Membrane

$$M_{km} = f_1\left(\frac{a}{B}, \frac{c}{a}, \frac{L}{B}\right) \times f_2\left(\frac{a}{B}, \frac{a}{c}\right) \times f_3\left(\frac{a}{B}, \frac{a}{c}, \frac{L}{B}\right) \quad \text{(M.46)}$$

where:

$$f_1\left(\frac{a}{B}, \frac{c}{a}, \frac{L}{B}\right) = g_1\left(\frac{a}{B}\right)^{\left[g_2(c/a)^2 + g_3(c/a) + g_4\right]} + g_5\left[1 - \left(\frac{a}{B}\right)\right]^{\left[g_6(c/a)^2 + g_7(c/a) + g_8\right]}$$

$$f_2\left(\frac{a}{B}, \frac{a}{c}\right) = \left[-0.286\,39\left(\frac{a}{c}\right)^2 + 0.354\,11\left(\frac{a}{c}\right) + 1.643\,0\right]\left(\frac{a}{B}\right)^{g_9} + 0.274\,49\left[1 - \left(\frac{a}{B}\right)\right]^{g_{10}}$$

$$f_3\left(\frac{a}{B}, \frac{a}{c}, \frac{L}{B}\right) = g_{11}\left(\frac{a}{B}\right)^{0.754\,29} + g_{12}\exp\left[\left(\frac{a}{B}\right)^{g_{13}}\right]$$

where:

$$g_1 = 0.007\ 815\ 7\left(\frac{c}{a}\right)^2 - 0.070\ 664\left(\frac{c}{a}\right) + 1.850\ 8$$

$$g_2 = -0.000\ 054\ 546\left(\frac{L}{B}\right)^2 + 0.000\ 136\ 51\left(\frac{L}{B}\right) - 0.000\ 478\ 44$$

$$g_3 = 0.000\ 491\ 92\left(\frac{L}{B}\right)^2 - 0.001\ 359\ 5\left(\frac{L}{B}\right) + 0.011\ 400$$

$$g_4 = 0.007\ 165\ 4\left(\frac{L}{B}\right)^2 - 0.033\ 399\left(\frac{L}{B}\right) - 0.250\ 64$$

$$g_5 = -0.018\ 640\left(\frac{c}{a}\right)^2 + 0.243\ 11\left(\frac{c}{a}\right) - 1.764\ 4$$

$$g_6 = -0.001\ 671\ 3\left(\frac{L}{B}\right)^2 + 0.009\ 062\ 0\left(\frac{L}{B}\right) - 0.016\ 479$$

$$g_7 = -0.003\ 161\ 5\left(\frac{L}{B}\right)^2 - 0.010\ 944\left(\frac{L}{B}\right) + 0.139\ 67$$

$$g_8 = -0.045\ 206\left(\frac{L}{B}\right)^3 + 0.323\ 80\left(\frac{L}{B}\right)^2 - 0.689\ 35\left(\frac{L}{B}\right) + 1.495\ 4$$

$$g_9 = -0.254\ 73\left(\frac{a}{c}\right)^2 + 0.409\ 28\left(\frac{a}{c}\right) + 0.002\ 189\ 2$$

$$g_{10} = 37.423\left(\frac{a}{c}\right)^2 - 15.741\left(\frac{a}{c}\right) + 64.903$$

$$g_{11} = -0.105\ 53\left(\frac{L}{B}\right)^3 + 0.598\ 94\left(\frac{L}{B}\right)^2 - 1.094\ 2\left(\frac{L}{B}\right) - 1.265\ 0$$

$$g_{12} = 0.043\ 891\left(\frac{L}{B}\right)^3 - 0.248\ 98\left(\frac{L}{B}\right)^2 + 0.447\ 32\left(\frac{L}{B}\right) + 0.601\ 36$$

$$g_{13} = -0.011\ 411\left(\frac{a}{c}\right)^2 + 0.004\ 369\ 5\left(\frac{a}{c}\right) + 0.517\ 32$$

If Equation (M.46) gives a value of $M_k < 1.0$, assume that $M_k = 1.0$.

b) Bending

$$M_{kb} = f_1\left(\frac{a}{B}, \frac{c}{a}, \frac{L}{B}\right) \times f_2\left(\frac{a}{B}, \frac{a}{c}\right) \times f_3\left(\frac{a}{B}, \frac{a}{c}, \frac{L}{B}\right) \quad \text{(M.47)}$$

where:

$$f_1\left(\frac{a}{B}, \frac{c}{a}, \frac{L}{B}\right) = g_1\left(\frac{a}{B}\right)^{\left[g_2(c/a)^2 + g_3(c/a) + g_4\right]} + g_5\left[1 - \left(\frac{a}{B}\right)\right]^{\left[g_6(c/a)^2 + g_7(c/a) + g_8\right]} + g_9$$

$$f_2\left(\frac{a}{B}, \frac{a}{c}\right) = \left[-0.350\ 06\left(\frac{a}{c}\right)^2 + 0.407\ 68\left(\frac{a}{c}\right) + 1.705\ 3\right]\left(\frac{a}{B}\right)^{g_{10}} + 0.249\ 88\left[1 - \left(\frac{a}{B}\right)\right]^{g_{11}}$$

$$f_3\left(\frac{a}{B}, \frac{a}{c}, \frac{L}{B}\right) = g_{12}\left(\frac{a}{B}\right)^{0.947\ 61} + g_{13}\exp\left[\left(\frac{a}{B}\right)^{g_{14}}\right]$$

where:

$$g_1 = 0.002\ 323\ 2\left(\frac{c}{a}\right)^2 - 0.000\ 371\ 56\left(\frac{c}{a}\right) + 4.598\ 5$$

$$g_2 = -0.000\ 044\ 010\left(\frac{L}{B}\right)^2 + 0.000\ 144\ 25\left(\frac{L}{B}\right) - 0.000\ 867\ 06$$

$$g_3 = 0.000\ 399\ 51\left(\frac{L}{B}\right)^2 - 0.001\ 371\ 5\left(\frac{L}{B}\right) + 0.014\ 251$$

$$g_4 = 0.004\ 616\ 9\left(\frac{L}{B}\right)^2 - 0.017\ 917\left(\frac{L}{B}\right) - 0.163\ 35$$

$$g_5 = -0.018\ 524\left(\frac{c}{a}\right)^2 + 0.278\ 10\left(\frac{c}{a}\right) - 5.425\ 3$$

$$g_6 = -0.000\ 379\ 81\left(\frac{L}{B}\right)^2 + 0.002\ 507\ 8\left(\frac{L}{B}\right) + 0.000\ 146\ 93$$

$$g_7 = -0.003\ 850\ 8\left(\frac{L}{B}\right)^2 + 0.002\ 321\ 2\left(\frac{L}{B}\right) - 0.026\ 862$$

$$g_8 = -0.011\ 911\left(\frac{L}{B}\right)^3 + 0.082\ 625\left(\frac{L}{B}\right)^2 - 0.160\ 86\left(\frac{L}{B}\right) + 1.230\ 2$$

$$g_9 = 0.277\ 98\left(\frac{a}{B}\right)^3 - 1.214\ 4\left(\frac{a}{B}\right)^2 - 2.468\ 0\left(\frac{a}{B}\right) + 0.099\ 981$$

$$g_{10} = -0.259\ 22\left(\frac{a}{c}\right)^2 + 0.395\ 66\left(\frac{a}{c}\right) + 0.011\ 759$$

$$g_{11} = 6.597\ 4\left(\frac{a}{c}\right)^2 + 55.787\left(\frac{a}{c}\right) + 37.053$$

$$g_{12} = -0.148\ 95\left(\frac{L}{B}\right)^3 + 0.815\ 26\left(\frac{L}{B}\right)^2 - 1.479\ 5\left(\frac{L}{B}\right) - 0.898\ 08$$

$$g_{13} = 0.055\ 459\left(\frac{L}{B}\right)^3 - 0.301\ 80\left(\frac{L}{B}\right)^2 + 0.541\ 54\left(\frac{L}{B}\right) + 0.534\ 33$$

$$g_{14} = -0.013\ 43\left(\frac{a}{c}\right)^2 + 0.006\ 670\ 2\left(\frac{a}{c}\right) + 0.759\ 39$$

If Equation (M.47) gives a value of $M_k < 1.0$, assume that $M_k = 1.0$.

M.11.1.4 Surface crack at the root of a weld toe

The solutions given for M_k in **M.11.1.2** and **M.11.1.3** were developed for fatigue assessment of flaws at the toes of fillet and butt welds. They might not be suitable for assessing flaws at girth weld root toes, where the weld width is relatively small, misalignment ("hi-lo") might be present, and there might be thickness differences either side of the weld. A 2D solution for this geometry is given in references [M.35] and [M.36].

M.11.2 Weld root flaws in cruciform joints

M.11.2.1 General

This solution comes from Noblett and Andrews [M.37]. See Figure M.27 for the definition of the geometry.

NOTE This refers only to straight fronted cracks (a/2c = 0).

The stress intensity factor solution is calculated from Equation (M.1) to Equation (M.6), where:

$M = M_m = M_b = 1$

σ is the stress in the loaded member.

The influence of joint geometry on stress intensity factors for root flaws in fillet and partial penetration welds is accounted for by the application of modified finite width correction and stress intensity factor magnification factors, f_{wm}, f_{wb}, M_{km} and M_{kb}, for membrane and bending loading.

M.11.2.2 Membrane loading

The solution is given by:

$$f_{wm} = \left\{ \sec\left[\frac{\pi}{2} \left(\frac{2a}{W} \right) \right] \right\}^{0.5} \quad \text{(M.48)}$$

$$M_{km} = \lambda_0 + \lambda_1 \left(\frac{2a}{W} \right) + \lambda_2 \left(\frac{2a}{W} \right)^2 \quad \text{(M.49)}$$

where:

$\lambda_0 = 0.956 - 0.343(h/B)$

$\lambda_1 = -1.219 + 6.210(h/B) - 12.220(h/B)^2 + 9.704(h/B)^3 - 2.741(h/B)^4$

$\lambda_2 = 1.954 - 7.938(h/B) + 13.299(h/B)^2 - 9.541(h/B)^3 + 2.513(h/B)^4$

The range of application is:

$0.1 \leq 2a/W \leq 0.7$

$0.2 \leq h/B \leq 1.2$

M.11.2.3 Bending loading

The solution is given by:

$$f_{wb} = \frac{\alpha}{2} \frac{(1-\alpha)^{0.5}}{1-\alpha^3} \left(1 + \frac{1}{2}\alpha + \frac{3}{8}\alpha^2 - \frac{11}{16}\alpha^3 + 0.464\alpha^4 \right) \quad \text{(M.50)}$$

where:

$$\alpha = \frac{2a}{W}$$

$$M_{kb} = \exp(\lambda_0) \left(\frac{2a}{W} \right)^{\lambda_1} \left(\frac{2a}{W} \right)^{\lambda_2 \ln(2a/W)} \quad \text{for } 0.2 \leq h/B \leq 0.7$$

$$M_{kb} = exp(\mu_0) \left(\frac{2a}{W} \right)^{\mu_1} \quad \text{for } 0.7 < h/B \leq 1.2$$

where:

$$\lambda_0 = 0.792 - 3.560\left(\frac{h}{B} \right) + 1.276\left(\frac{h}{B} \right)^2$$

$$\lambda_1 = 1.064 - 4.898\left(\frac{h}{B} \right) + 3.670\left(\frac{h}{B} \right)^2$$

$$\lambda_2 = 0.496 - 1.328\left(\frac{h}{B} \right) + 1.012\left(\frac{h}{B} \right)^2$$

$$\mu_0 = 0.285\left(\frac{h}{B} \right)^2 - 1.866\left(\frac{h}{B} \right)$$

$$\mu_1 = 0.028\left(\frac{h}{B} \right) - 0.761$$

The range of application is:

$0.1 \leq 2a/W \leq 0.7$

Bibliography for Annex M

Standards publications

API 579-1/ASME FFS-1:2016, *Fitness-for-service*

BS 7608, *Guide to fatigue design and assessment of steel products*

PD 6493:1980 (withdrawn), *Guidance on some methods for the derivation of acceptance levels for defects in fusion welded joints*

Other documents

[M.1] HADLEY, I. and LEI, Y. Outline of the fracture clauses of BS 7910:2013. *In: International Journal of Pressure Vessels and Piping*, 168, December 2018, 289–300. <https://doi.org/10.1016/j.ijpvp.2018.11.004>

[M.2] TADA, H., PARIS, P. and IRWIN, G. *The stress analysis of cracks handbook.* Third edition. Hellertown, MA: Del Research Corporation, 2000.

[M.3] MURAKAMI, Y. *Stress intensity factor handbook*. Vols. 1 and 2. Oxford: Pergamon Press, 1987. Vol. 3. Kyoto, Japan: Society of Materials Science, 1992.

[M.4] ROOKE, D.P. and CARTWRIGHT, D.J. *Compendium of stress-intensity factors*. London: The Stationery Office, 1976. ISBN 0117713368.

[M.5] SIH, G.C. *Handbook of stress intensity factors*. Bethlehem, PA: Lehigh University, Institute of Fracture and Solid Mechanics, 1973.

[M.6] GRAY, T.G.F. *Handbook of crack opening data* (includes disk). Abington, Cambs: Abington Publishing, 1992. ISBN 1855730979.

[M.7] OORE, M. and BURNS, D.J. Estimation of stress intensity factors for irregular cracks subjected to arbitrary normal stress fields. *In: Proceedings of 4th International Conference on Pressure Vessel Technology, Vol. 1: Materials, fracture and fatigue*, London, 19–23 May 1980. London: Institution of Mechanical Engineers, 1980. Paper C25/80: 139–147. ISBN 0852984596.

[M.8] R6 PANEL. *R6: Assessment of the integrity of structures containing defects. Revision 4, as amended*. Gloucester: EDF Energy, 2001.

[M.9] NEWMAN, J.C. and RAJU, I.S. Stress intensity factor equation for cracks in three-dimensional finite bodies. *In: Fracture Mechanics: Proceedings of 14th Symposium*. Vol. I: Theory and Analysis. STP 791. Philadelphia: ASTM, 1983, 238–265.

[M.10] FETT, T. and MUNZ, D. *Stress Intensity factors and weight functions*. Southampton: Computational Mechanics Publications, 1997.

[M.11] FETT, T., MUNZ, D. and NEUMANN, J. Local stress intensity factors for surface cracks in plates under power-shaped stress distributions. *In: Engineering Fracture Mechanics*, 1990, 36, 647–651.

[M.12] WU, X.R. and CARLSSON, A.J. *Weight functions and stress intensity factor solutions*. Oxford: Pergamon Press, 1991.

[M.13] SHAH, R. C. and KOBAYASHI, A.S. Stress Intensity Factor for an Elliptical Crack under Arbitrary Normal Loading. *In: Engineering Fracture Mechanics*. 1971, 3, 71–96.

[M.14] KIEFNER, J.F., MAXEY W.A., EIBER, R.J. and DUFFY, A.R. Failure stress levels of flaws in pressurized cylinders. *In: Proceedings of Progress in Flaw Growth and Toughness Testing, Philadelphia, 28–30 August*. ASTM STP 536, 1973, 461–481.

[M.15] WILLOUGHBY, A.A. and DAVEY, T.G. Plastic collapse at part wall flaws in plates. *In:* R.P. WEI, ed. *Fracture mechanics: Perspectives and directions. Proceedings of the 20th national symposium*. STP 1020. Bethlehem, PA, June 23–25, 1987. Philadelphia: ASTM, 1989, 390–409. ISBN 0803112505.

[M.16] FRANCE, C.C, GREEN, D. and SHARPLES, J.K. *New stress intensity factor and crack opening area solutions for through-wall cracks in pipes and cylinders*. AEA Technology Report AEAT-0643, 1996; Addendum, April, 1999. (See also ASME PVP, 1997, 350, 143–195.)

[M.17] NEWMAN, J.C. Jr and RAJU, I.S. Stress-intensity factor equations for cracks in three-dimensional finite bodies, *In: Fracture Mechanics: fourteenth symposium – Volume I; Theory and Analysis, ASTM STP 791, JC Lewis and G Sines Eds.*, American Society for Testing and Materials, 1983, I-238-I-265.

[M.18] NEWMAN, J.C. and RAJU, I.S. An empirical stress intensity factor equation for the surface crack. *In: Engineering Fracture Mechanics*, 1981, 1-2(15), 185–192. ISSN 0013-7944.

[M.19] RAJU, I.S. and NEWMAN, J.C. Stress intensity factor influence coefficients for internal and external surface cracks in cylindrical vessels. *In:* S.S. PALUSAMY and S.G. SAMPATH, eds. *Aspects of fracture mechanics in pressure vessels and piping. Presented at pressure vessels and piping conference*, Orlando, FL, June 27–July 2 1982. New York: ASME. ASME PVP Volume 58, 37–48.

[M.20] ANDERSON, T.L., THORWALD, G., REVELLE, R.J., OSAGE, D.A., JANELLE, J.L. and FUHRY, M.E. Development of stress intensity factor solutions for surface and embedded cracks in API579. *In: WRC Bulletin 471*. New York, NY: Welding Research Council Inc., May 2003.

[M.21] DEDHIA, D.D. and HARRIS, D.O. Improved influence functions for part-circumferential cracks in pipes. *In:* G.M. WILKOWSKI, ed. *Circumferential cracks in pressure vessels and piping*. Presented at the 4th national congress on pressure vessel and piping technology, Portland, Oregon, June 19–24 1983. Volume 2. New York: ASME. PVP Volume 95, 35–48.

[M.22] BERGMAN, M. and BRICKSTAD, B. Stress intensity factors for circumferential cracks in pipes analyzed by FEM using line spring elements. *In: International Journal of Fracture*, 47(1), r17-r19, 1991. <https://doi.org/10.1007/bf00037044>

[M.23] JOSEPH, P.F. and ERDOGAN, F. Surface crack problem in plates. *In: International Journal of Fracture*, 1989, 41(2), 105–131. ISSN 0376-9429.

[M.24] ANDRASIC, C.P. and PARKER, A.P. Dimensionless stress intensity factors for cracked thick cylinders under polynomial crack face loadings. *In: Engineering Fracture Mechanics*, 1984, 19(1), 187–193. ISSN 0013-7944.

[M.25] ANDERSON, T.L. Stress intensity and crack growth opening area solutions for through-wall cracks in cylinders and spheres. *In: WRC Bulletin 478*. New York, NY: Welding Research Council Inc., January 2003. ISSN 0043-2326.

[M.26] JAMES, L.A. and MILLS, W.J. Review and synthesis of stress intensity factor solutions applicable to cracks in bolts. *In: Engineering Fracture Mechanics*, 1988, 30(5), 641–653. ISSN 0013-7944.

[M.27] RAJU, I.S. and NEWMAN, J.C. Stress-intensity factors for circumferential surface cracks in pipe and rods under tension and bending loads. *In: Fracture Mechanics*: Seventeenth Volume, ASTM STP 905, JH Underwood, R Chait, CW Smith, DP Wilhem, WA Andrews and JC Newman, Eds, American Society for Testing and Materials, Philadelphia, 1986, 789–805.

[M.28] TORIBIO, J. Effect of crack shape and loading conditions on the stress intensity factor for a cracked bolt. *In: S.T. BARBAS et al., eds. Proc. 11th international conference on offshore mechanics and arctic engineering (OMAE '92)*. Vol. III-B Materials Engineering. Calgary, Canada, June 7–12 1992. New York: ASME: 363–370. ISBN 0791809129.

[M.29] MADDOX, S.J. and ANDREWS, R.M. Stress intensity factors for weld toe cracks. *In: M.H. ALIABADI, C.A. BREBBIA and D.J. CARTWRIGHT, eds. Localized damage computer-aided assessment and control. Proceedings of the 1st international conference on computer-aided assessment and control of localized damage. Portsmouth, UK, June 26–28 1990. Volume 2*. Southampton: Computational Mechanics Pubs, 1990, 329–342. ISBN 1853120685.

[M.30] HOBBACHER, A. Stress intensity factors of welded joints. *In: Engineering Fracture Mechanics*. 1993, 46(2), 173–182 and 49(2), 323. ISSN 0013-7944.

[M.31] BOWNESS, D. and LEE, M.M.K. *Fracture mechanics assessment of fatigue cracks in offshore tubular structures*. HSE Offshore Technology Report 2000/077 for HSE, EPSRC, and Chevron Oil. London: The Stationery Office, 2002. <http://www.hse.gov.uk/research/otopdf/2000/oto00077.pdf>[M.3)]

[M.32] THURLBECK, S.D. *A fracture mechanics based methodology for the assessment of weld toe cracks in tubular offshore joints*. PhD Thesis, Department of Civil and Structural Engineering, University of Manchester Institute of Science & Technology, UK. 1991.

[M.33] CHEAITANI, M.J., THURLBECK, S.D. and BURDEKIN, F.M. Fatigue, fracture and plastic collapse of offshore tubular joints using BSI PD 6493:1991. *In: M.M. SALAMA et al. eds. Proceedings of the 14th International conference on offshore mechanics and arctic engineering (OMAE 1995). Copenhagen, Denmark, June 18-22 1995*. New York: ASME, 1995. Volume 3, 41–54. ISBN 0791813096.

[M.34] ZHANG, Y.H., MADDOX, S.J. and RAZMJOO, G.R. *Experimental study and prediction of fatigue crack growth in girth welded pipe*s. OMAE 2002-28595, presented at OMAE Offshore Mechanics and Arctic Engineering Conference, 23–28 June 2002, Oslo, Norway.

[M.35] ZHANG, Y-H., LONDON, T. and DE BONO, D. *M_k solutions for fatigue assessment of flaws at weld root toes in girth welds*. TWI Industrial Member Report 1084/2017.

[M.36] ZHANG, Y-H., LONDON, T. and DE BONO, D. Developing M_k solutions for fatigue crack growth assessment of flaws at weld root toes in girth welds. *In: OMAE2018 77067, 37th International Conference on Ocean, Offshore and Arctic Engineering,* Madrid, Spain, June 17–22, 2018.

[M.37] NOBLETT, J.E. and ANDREWS, R.M. *A stress intensity factor solution for root defects in fillet and partial penetration welds*. TWI Research Report 575/1996. Abington, Cambs: TWI, 1996.

[M.3)] Note that earlier revisions of BS 7910 included a reference to a paper by Bowness and Lee, published in the International Journal of Fracture. Some errors in the equations there were subsequently found; reference [M.31], which is the original source of the equations, is recommended instead.

Annex N (informative)

Allowance for constraint effects

N.0 Symbols and definitions

For the purposes of this annex, the following symbols, definitions and units apply, unless otherwise indicated at the point of use.

Symbol	Definition	Units
a	Half flaw length for through-thickness flaw, flaw height for surface flaw or half height for embedded flaw	mm
a_j	Flaw length after ductile tearing	mm
a_0	Initial flaw size	mm
B	Section thickness in plane of flaw	mm
B^*	Biaxiality parameter of Leevers and Radon	—
c	Half flaw length for surface or embedded flaw	mm
E	Elastic modulus	N/mm^2
F^L	Reserve factor on load	—
g_{ij}	Angular function of θ in the T-stress definition of β	—
$2H$	Distance between the (outermost) points at which loading is applied	mm
J	J-integral	N/mm
$J_{0.2BL}$	Size insensitive fracture resistance, J, at 0.2 mm stable crack extension offset from the construction (blunting) line	N/mm
K^c_{mat}	Constraint-corrected fracture toughness	N/mm$^{3/2}$
$K^c_{mat}(\Delta a_j)$	Constraint-corrected fracture toughness after a given amount, (Δa_j), of ductile tearing	N/mm$^{3/2}$
K_I	Applied tensile (mode I) stress intensity factor (SIF)	N/mm$^{3/2}$
K^p_I	Stress intensity factor due to primary stresses	N/mm$^{3/2}$
K^s_I	Stress intensity factor due to secondary stress	N/mm$^{3/2}$
K_{mat}	Material fracture toughness	N/mm$^{3/2}$
$K_{mat}(\Delta a_j)$	Fracture toughness after a given amount, (Δa_j), of ductile tearing	N/mm$^{3/2}$
K_r	Fracture ratio	—
K^p_r	Contribution to K_r from primary stresses	—
K^s_r	Contribution to K_r from secondary stresses	—
$K_{0.2BL}$	Value of initiation toughness, calculated from $J_{0.2BL}$	N/mm$^{3/2}$
k	Material- and temperature-dependent constraint constant	—
L_r	Ratio of reference stress to yield stress	—
$L_{r,max}$	Maximum permitted limit of L_r	—
m	Weibull model exponent	—
n	Strain-hardening exponent, e.g. see Equation (7.6)	—

(continued)

Symbol	Definition	Units
$O(r^{1/2})$	Higher-order terms in Williams' expanded crack tip stress field	N/mm^2
P_b	Primary bending stress	N/mm^2
P_f	Fractile representing the cumulative failure probability for fracture toughness distribution derived from experiment data	—
P_m	Primary membrane stress	N/mm^2
Q	Elastic-plastic constraint parameter	—
Q^p	Value of Q under primary stress alone	—
Q^s	Value of Q under secondary stress alone	—
r	Distance ahead of crack tip	mm
r_i	Internal radius	mm
T	Temperature at which K_{mat} is to be determined	°C
T	T-stress	N/mm^2 (MPa)
T^p	T-stress for the primary stress	N/mm^2 (MPa)
T^s	T-stress for the secondary stress	N/mm^2 (MPa)
T_0	Temperature for a median toughness of 100 MPa$\sqrt{}$m in 0.025 m thick specimens (see also **L.9.3.1**)	°C
$T_{0,deep}$	Master Curve transition temperature obtained from high constraint specimens in accordance with ASTM E1921	°C
V	Plasticity correction factor	—
W	Structure width (or half-width) in plane of flaw	mm
X_0, X_1, X_2... X_6	Polynomial coefficients	—
α	Material and temperature dependent constraint constant	—
α''	Function of a, c, B and W used in calculation of collapse stresses	—
β	Normalized constraint parameter	—
β_Q, β_T	Normalized constraint parameter for Q parameter and T-stress	—
Δa	Increment in a due to ductile tearing	mm
Δa_j	Intermediate value of tearing flaw extension	mm
δ_{ij}, δ_{1i}, δ_{1j}	Knonecker's delta	—
θ	Parametric angle to identify position along an elliptical flaw front	Radians
ρ	Plasticity interaction factor	—
ρ_c	Plasticity interaction factor corrected for constraint	—
ρ_l	Parameter used in replacing ρ	—
σ_{ij}	Stress field close to a crack tip	N/mm^2
σ_{ij}^{ssy}	Stress field close to a crack tip under small-scale yielding in plane strain, for the same value of J as that used to evaluate σ_{ij}, and for a remote stress field corresponding to the T = 0 field	N/mm^2
σ^p	Stress arising from primary loads	N/mm^2

 © The British Standards Institution 2019

(continued)

Symbol	Definition	Units
σ_{ref}	Reference stress used for creep and plastic consideration, sometimes calculated from plane strain von Mises limit load	N/mm^2
σ^s	Stress arising from secondary loads	N/mm^2
σ_Y	Lower yield strength or 0.2% proof strength	N/mm^2

N.1 General

The background to this annex is described in reference [N.1].

The basic procedures of Clause **7** enable an assessment to be made of the resistance to fracture and plastic collapse of a flawed component. Associated with an assessment are reserve factors which indicate the proximity to the limiting conditions. However, these limiting conditions incorporate an element of conservatism that leads to reserve factors in general being underestimated.

A particular conservatism implicit in the procedure is that the value of fracture toughness K_{mat}, used to define K_r, is normally derived from deeply cracked bend specimens using recommended testing standards and validity criteria, e.g. BS 7448-1 and BS EN ISO 15653. These are designed to ensure plane strain conditions and high hydrostatic stresses near the crack tip to provide a materials property independent of specimen size and geometry. However, there is considerable evidence that the material resistance to fracture is increased when specimens with shallow flaws, or specimens loaded in tension, are tested as described in references [N.1] to [N.6]. These conditions lead to lower hydrostatic stresses at the crack tip, and less restrained plastic flow fields referred to as lower constraint.

There has been considerable research into quantifying the geometry dependence of the material resistance to fracture using the so-called constraint parameters as described in references [N.7] to [N.9]. This has led to proposals for incorporating constraint in fracture assessments as described in references [N.10] to [N.14]. This annex uses these proposals to set out procedures for including constraint in the overall procedure of Clause **7**. These procedures do not replace those of Clause **7**. They may be used in conjunction with that approach to estimate any increase in reserve factors likely to arise under conditions of low constraint.

This annex describes the procedures to be followed. Subclause **N.2** provides guidance on when and how to perform the additional calculations and how to obtain the additional materials data required to follow the procedures. Subclause **N.3** provides input for a constraint analysis and summarizes available solutions for common geometries.

The procedures of this annex are applicable only to Mode I loading. Combinations of primary and secondary stresses are also included in the procedures.

This annex addresses the loss of constraint under plane strain conditions. Use of a specimen thickness, where practicable, equal to the component thickness is recommended.

There is considerable debate about the most appropriate parameter to describe constraint effects. This annex is limited in scope to the *T*-stress and *Q* parameter. However, a similar approach could be developed for other constraint parameters provided that their load dependence could be quantified ([N.15]).

This annex gives guidance on the inclusion of constraint-dependent toughness in a FAD-based assessment using two inputs: the magnitude of load-dependent constraint defined by the *T*-stress or *Q* parameter, and the constraint sensitivity

of the material toughness defined by the parameters α and k. An alternative method for constraint correction of cleavage fracture toughness data only, without characterizing the effect on the FAD, is available in BS ISO 27306, for four geometries. A discussion of the differences between BS ISO 27306 and the procedures in this annex can be found in reference [N.1].

Unlike K_I, the *T*-stress and *Q* parameter are affected by stresses acting parallel to the crack plane. Biaxial loading therefore needs to be included where appropriate by using a value of *T*-stress or *Q* parameter that accounts for the presence of biaxial loading, e.g. **N.3.2.2.2** or **N.3.2.3.2.**

This annex on constraint should not be used in conjunction with Annex I.

N.2 Procedures

N.2.1 General

Two alternative procedures set out in **N.2.2** and **N.2.3** may be used. The first involves a modification to the FAD but retains the definition of K_r. The second retains the FAD but modifies the definition of K_r. Here the procedures are presented with K_r defined using the parameter ρ for the secondary stress, but the principles also apply to definition of K_r using the parameter *V* for the secondary stress. Each procedure follows the steps in **7.2** apart from **7.2.6** and **7.2.3**, which are replaced by **N.2.2** and **N.2.3** respectively. Guidance on how to perform these steps is contained in **N.2.4** along with guidance on assessing the significance of the results. This latter guidance, in **N.2.4.6**, might be useful in deciding which of the two procedures to follow.

N.2.2 Procedure I: modification to the FAD

N.2.2.1 Evaluate a normalized constraint parameter, β (**N.2.4.2**), for the structure.

N.2.2.2 Define the influence of constraint on material resistance to fracture, relative to the data determined in **7.2.3**, in terms of β and the material parameters, α and k (**N.2.4.3**).

N.2.2.3 Modify the failure assessment diagram of **7.2.6**, using the parameters β, α and k (**N.2.4.4**).

N.2.2.4 Calculate K_r. K_r^p is calculated as in **7.2.9**, with K_{mat} or $K_{mat}(\Delta a_j)$ as defined with respect to the fracture toughness relevant to conditions of high constraint. K_r^s is also defined with respect to K_{mat} or $K_{mat}(\Delta a_j)$ but the parameter ρ is replaced by a related parameter ρ_l.

For an initiation analysis:

$$K_r^s = \frac{K_I^S(a_0)}{K_{mat}} + \rho_l(a_0) \quad \text{(N.1)}$$

For a ductile tearing analysis:

$$K_r^s = \frac{K_I^S(a_j)}{K_{mat}(\Delta a_j)} + \rho_l(a_j) \quad \text{(N.2)}$$

for flaw sizes $a_j = a_0 + \Delta a_j$.

Advice on calculation of the parameter ρ_l is given in **N.2.4.5**.

N.2.3 Procedure II: modification to K_r

N.2.3.1 Evaluate a normalized constraint parameter, β (**N.2.4.2**).

N.2.3.2 Evaluate βL_r, a measure of structural constraint.

N.2.3.3 Evaluate the material toughness, K_{mat}^c, appropriate to the level of constraint, βL_r (**N.2.4.3**).

N.2.3.4 Calculate K_r. The procedures in **7.2.9** are not followed. Instead, the definition of K_r is as follows.

For an initiation analysis:

$$K_r^p = \frac{K_I^p(a_0)}{K_{mat}^c} \quad \text{(N.3)}$$

$$K_r^s = \frac{K_I^s(a_0)}{K_{mat}^c} + \rho(a_0) \quad \text{(N.4)}$$

For a ductile tearing analysis:

$$K_r^p = \frac{K_I^p(a_j)}{K_{mat}^c(\Delta a_j)} \quad \text{(N.5)}$$

$$K_r^s = \frac{K_I^s(a_j)}{K_{mat}^c(\Delta a_j)} + \rho(a_j) \quad \text{(N.6)}$$

for flaw sizes $a_j = a_0 + \Delta a_j$.

$K_{mat}^c(\Delta a_j)$ is the fracture toughness after the given amount, (Δa_j), of ductile tearing, allowing for the influence of constraint (**N.2.4.3**). ρ is evaluated in accordance with Annex R and the modifications in **N.2.4.5** are not required.

N.2.3.5 Plot points (L_r, K_r) on the FAD, **7.2.10**, and assess in the conventional way.

N.2.4 Background notes and guidance on using the procedure

N.2.4.1 Definition of loads

Subclause **7.2** requires loads to be categorized and defined. These should be conservatively represented in the following respects.

a) Bending effects should be properly included. Constraint levels are higher under bending than tension and, therefore, a representation of a stress distribution which overestimates the tension component but underestimates the bending component could provide a conservative estimate of L_r but underestimate the level of constraint (i.e. overestimate the toughness). In cases of uncertainty, sensitivity studies should be carried out.

b) Biaxial loading should be included. Stresses parallel to the crack plane do not affect K_I but they do affect constraint. It is therefore important to use a value of constraint that accounts for biaxial loads where appropriate, e.g. **N.3.2.2.2** or **N.3.2.3.2**.

N.2.4.2 Evaluation of structural constraint, β

Advice is given on the calculation of β for constraint described by both the elastic *T*-stress and the hydrostatic *Q* parameter. Whichever parameter is adopted, materials data are required (**N.2.4.3**) as a function of that parameter. As the *T*-stress requires only elastic calculation, this approach should be adopted for initial calculations. The *Q* parameter is expected to provide more accurate assessments, particularly when plasticity becomes widespread (higher L_r), and should be used when more refined estimates of load margins are required or as part of sensitivity studies.

As a broad guidance, the *T*-stress is recommended for use for $L_r \leq 1$ and the *Q* parameter is recommended for $L_r > 1$. The *T*-stress and *Q* parameter give very similar results for $L_r \leq 1$.

a) **The *T*-stress definition of *β*.** The stresses σ_{ij} close to a crack tip, calculated elastically, may be written as:

$$\sigma_{ij} = \frac{K_I}{(2\pi r)^{0.5}} g_{ij}(\theta) + T\delta_{1i}\delta_{1j} + O\left(r^{0.5}\right) \quad \text{(N.7)}$$

for polar coordinates (r,θ) centred at the crack tip.

T-stress is the second order term that can be regarded as the stress parallel to the crack flanks.

The value of *T*-stress is influenced by remote stresses as well as geometry, flaw size and loading.

The value of *T*-stress may be calculated from elastic finite-element analysis using a number of different methods which are described in reference [N.16]. This reference also contains normalized *T*-stress solutions for a range of two and three dimensional geometries. The value of β_T is then defined by:

$$\beta_T = \frac{T^p}{L_r \sigma_Y} + \frac{T^s}{L_r \sigma_Y} \quad \text{(N.8)}$$

The contributions to the *T*-stress from primary and secondary stresses are additive such that:

$$T = T^p + T^s \quad \text{(N.9)}$$

L_r is inversely proportional to yield strength (see **7.3.7**) and T^p is proportional to L_r such that β_T is independent of both the load magnitude and the value of yield strength for σ^p stresses acting alone: it is a function of geometry, flaw size and the type of loading only.

For combined primary and secondary stresses, β_T reduces with increasing σ^p loads (increasing L_r) for constant σ^s loading. In the limit $L_r \rightarrow 0$, $\beta_T \rightarrow \infty$ but the product $\beta_T L_r$ remains finite and equal to T^s/σ_Y. It is this product $\beta_T L_r$ which is recommended in **N.2.4.3**, **N.2.4.4** and **N.2.4.5**.

In the literature, values of T^p are often presented, normalized by the stress intensity factor and flaw size in the form of the biaxiality parameter B^* of Leevers and Radon [N.17]:

$$B^* = T^p \sqrt{\pi a} \,/\, K_I^p \quad \text{(N.10)}$$

or in terms of some nominal applied stress. As values of K_I^p and L_r are required to perform an assessment, it is straightforward to convert these solutions into values of β_T [N.18].

A compendium of β_T solutions is given in **N.3.2**.

b) **The *Q* parameter definition of *β*.** For elastic-plastic materials, the stresses close to a crack tip may be written approximately as:

$$\sigma_{ij} = \sigma_{ij}^{ssy} + Q\sigma_Y\delta_{ij} \quad \text{(N.11)}$$

where *Q* is a stress-scaling parameter that varies slightly with distance from the crack tip and has been defined in references [N.10] and [N.19] at the normalized distance $r/(J/\sigma_Y) = 2$ directly ahead of the crack.

 © The British Standards Institution 2019

The value of the Q parameter may be calculated from elastic-plastic finite-element analysis using methods described in reference [N.10]. The value of β_Q is then defined by:

$$\beta_Q = \frac{Q}{L_r} \tag{N.12}$$

In general, the value of the Q parameter is a function of geometry, flaw size, type of loading, the material stress-strain curve and the magnitude of the loading. Therefore, available solutions in the literature such as references [N.10], [N.11], [N.15], and [N.18] to [N.23] are of more restricted application than the corresponding solutions for the T-stress.

For $L_r \leq 0.5$, the value of Q^p may be estimated [N.11] from:

$$Q^p = \frac{T^p}{\sigma_Y} \qquad \text{for } -0.5 < \frac{T^p}{\sigma_Y} \leq 0 \tag{N.13}$$

$$Q^p = \frac{0.5T^p}{\sigma_Y} \qquad \text{for } 0 < \frac{T^p}{\sigma_Y} < 0.5 \tag{N.14}$$

Where more detailed information about the material strain hardening characteristics is known, these estimates may be improved by using small-scale yielding approximations in reference [N.10]. Ainsworth and O'Dowd [N.11] have shown that defining Q^p from T^p also provides a conservative estimate of constraint for a number of cases at $L_r > 0.5$. However, they also showed that for a centre-cracked tension geometry under biaxial loading the constraint level was higher when defined in terms of Q^p than T^p at higher loads ($L_r > 0.5$). Therefore, solutions in the literature should be consulted to assess whether the use of T^p is likely to lead to conservative over estimates of Q^p at high loads.

In the absence of a detailed inelastic analysis of the body containing a flaw under σ^s stresses, an estimate of Q^s may be obtained from TS, the value of T-stress from an elastic analysis of the secondary stresses:

$$Q^s = \frac{T^s}{\sigma_Y} \tag{N.15}$$

NOTE Weight function methods may be used to evaluate T^s for non-linear distributions of secondary stress; see reference [N.24].

For combined primary and secondary stresses, a value of Q is required for the particular combination being examined. In the absence of a detailed evaluation of Q, it may be estimated for $Q^p < 0$ from:

$$Q = Q^p + Q^s \qquad \text{for } Q^s > 0 \tag{N.16}$$

and, for $Q^s < 0$, as:

$$Q = Q^p + Q^s(1 - L_r) \qquad \text{for } Q^s \text{ and } L_r \leq 1 \tag{N.17}$$

$$Q = Q^p \qquad \text{for } Q^s < 0 \text{ and } L_r > 1 \tag{N.18}$$

N.2.4.3 Influence of constraint on material resistance to fracture

N.2.4.3.1 General

To use the procedure of **N.2**, it is necessary to define the material fracture resistance at the level of constraint evaluated using the methods of **N.2.4.2**. This constraint dependent toughness is denoted K^{c}_{mat} and is dependent on βL_r.

At high values of constraint ($\beta L_r > 0$), K^{c}_{mat} may be simply taken as equal to K_{mat}. For negative levels of constraint ($\beta L_r < 0$), the influence of constraint can be broadly summarized as follows:

- in the cleavage region, K^{c}_{mat} increases as βL_r becomes more negative;
- in the ductile region, there appears to be little influence of constraint on the fracture toughness, $K_{0.2BL}$, relating to initiation of ductile tearing, but the fracture toughness after crack growth, Δa, increases as βL_r becomes more negative;
- for ferritic steels, there is a shift in the brittle to ductile transition region to lower temperatures as βL_r becomes more negative [N.24].

N.2.4.3.2 K^{c}_{mat} defined using material constraint parameters α and k

Ainsworth and O'Dowd [N.11] have shown that the increase in fracture toughness in both the brittle and ductile regimes may be represented by an expression of the form:

$$K^{c}_{mat} = K_{mat} \quad \text{when } \beta L_r > 0 \tag{N.19}$$

$$K^{c}_{mat} = K_{mat}\left[1 + \alpha(-\beta L_r)^{k}\right] \quad \text{when } \beta L_r \leq 0 \tag{N.20}$$

In the ductile region, α and k are, additionally, functions of ductile crack growth. Other forms of Equation (N.19) and Equation (N.20) have been used in the literature, for example in references [N.12] and [N.20], and the principles of this annex are not restricted to any particular relationship between K^{c}_{mat} and K_{mat}.

Values of α, k in Equation (N.20) may be obtained by any of the following four approaches.

a) Specimens may be tested with several different levels of constraint to obtain data in the range of βL_r of interest; see for example reference [N.25] and curve-fitting to obtain α and k as shown in Figure N.1.

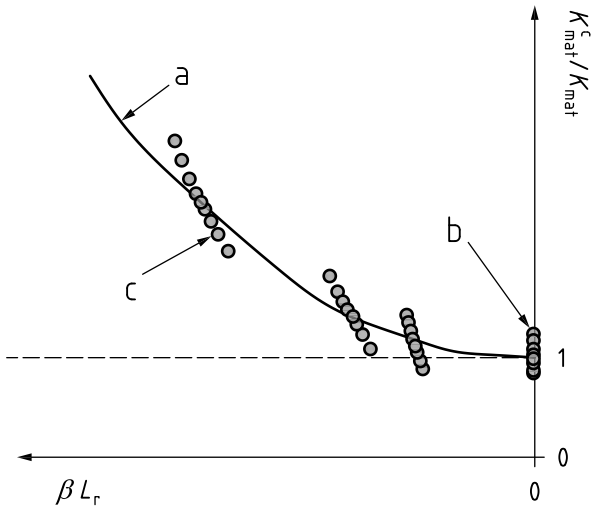
b) The lookup tables in **N.3.3.2** (taken from reference [N.26]) may be used. For cleavage fracture behaviour, this enables the parameters α and k to be readily established based on a knowledge of the yield and work hardening behaviour of the material at the temperature of interest and the Beremin fracture model parameter m. Gao et al [N.26] provides a suitable method for calibrating the value of m using finite element analysis and fracture toughness data from two different levels of constraint.

c) When the Beremin parameter m is unknown, a combination of limited material testing may be used in conjunction with the look-up tables. These provide a number of possible α, k pairs for a given work hardening behaviour. Testing specimens of one low-constraint geometry or crack size identifies which of the possible α, k pairs fit the limited test data.

d) Mechanistic modelling may be used; see for example references [N.8], [N.9] and [N.27].

 © The British Standards Institution 2019

Figure N.1 **Schematic showing curve fitting of low constraint test data to obtain α and k**



Key

a Equation (N.20) defined by α and k
b High constraint data
c Lower constraint data

Reference [N.28] indicates that α and k are independent of the failure probability at which K_{mat} is defined. Figure N.1 depicts the use of P_f = 50% but other probabilities may also be used. In the event that different P_f values lead to differences in the curve fit, the α and k values resulting in the lowest curve for the lowest constraint levels of interest should be selected in order to be conservative.

N.2.4.3.3 K^c_{mat} defined using Master Curve transition temperature

The Master Curve transition temperature for cleavage fracture is defined in **L.9.3.1**. The following equation was suggested in reference [N.24] to estimate the shift in the transition temperature T_0 as a function of T-stress:

$$T_0 \approx T_{0,deep} + \frac{T}{10\ \text{MPa}/^\circ\text{C}} \quad \text{(N.21)}$$

This shift leads to the following expression:

$$K^c_{mat} = 20\text{MPa}\sqrt{\text{m}} + (K_{mat} - 20)\exp\left[0.019\left(-\frac{T}{10\text{MPa}}\right)\right] \quad \text{for } T\text{-stress} < 0 \text{ (N.22)}$$

N.2.4.3.4 K^c_{mat} determined using low constraint testing

K^c_{mat} corresponding to one specific level of β can be determined directly using testing. However, using this approach the values of K^c_{mat} at levels of constraint other than that of the test specimen are unknown and Procedure I in **N.2.2** cannot therefore be used (see reference [N.29]. Care should be taken to ensure that the constraint level in the test specimen is not less than that generated by the flaw in the component to be assessed.

Testing at several different levels of constraint enables the approach in **N.2.4.3.2** to be applied.

Test specimens that have been used to generate fracture toughness data at low constraint levels include single edge notch tension (SENT) specimens (e.g. BS 8571), three point bend specimens with shallow cracks (e.g. BS EN ISO 15653, ASTM E1820), centre cracked plates under tension and plates under tension with semi-elliptical surface flaws.

N.2.4.4 Construction of modified FAD

The FAD should initially be constructed according to one of the options in **7.3**. If this is denoted:

$$\begin{aligned} K_r &= f(L_r) && \text{when } L_r \le L_{r,max} \\ K_r &= 0 && \text{when } L_r > L_{r,max} \end{aligned} \qquad \text{(N.23)}$$

where $f(L_r)$ takes one of the forms summarized in **7.3**, the modified FAD is:

$$\begin{aligned} Kr &= f(Lr)\left(\frac{K^c_{mat}}{K_{mat}}\right) && \text{when } L_r \le L_{r,max} \\ K_r &= 0 && \text{when } L_r > L_{r,max} \end{aligned} \qquad \text{(N.24)}$$

Where K^c_{mat} is defined by Equation (N.20) for $\beta < 0$, this becomes:

$$K_r = f(L_r)\left[1 + \alpha(-\beta L_r)^k\right] \qquad \text{when } L_r \le L_{r,max} \qquad \text{(N.25)}$$

Some modified FADs using the Option 1 curve and α, k, β taken as constants are shown in Figure N.1, taken from [N.25]. For $\alpha = 0$ or $\beta = 0$ the curves reduce to the Option 1 curve. The cut-off $L_{r,max}$ is not depicted but this is independent of constraint.

The following are properties of modified FADs.

a) Whereas the Option 1 curve is independent of geometry and material, the Option 1 curve modified by Equation (N.24) or Equation (N.25) is dependent on geometry (through β), on material toughness properties (through α, k) and also on material tensile properties if β is defined in terms of the Q parameter.

b) Whereas the Option 2 curve is independent of geometry and dependent only on material tensile properties, the modified Option 2 curve is dependent on geometry and material toughness properties.

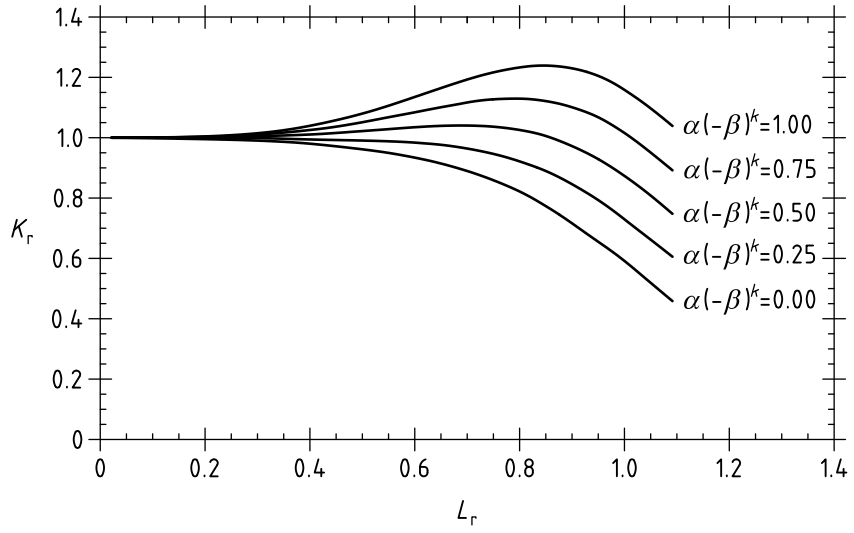
c) Whereas the Option 3 curve is dependent only on geometry and material tensile properties, the modified Option 3 curve is also dependent on material toughness properties.

d) In view of a) to c), when performing a ductile tearing analysis, the failure assessment line is a function of ductile crack growth through its influence on geometry (β depends on crack size) and material (α, k, or $K^c_{mat} = K_{mat}$ can depend on Δa). Some care is then needed in defining the tangency condition (**7.3.8**) (see references [N.30] to [N.32]) and this is discussed in **N.2.4.6**.

e) For combined loading where β increases with reducing L_r, the value of βL_r is finite at $L_r \rightarrow 0$ ([N.13], [N.14]). Consequently, the failure assessment curves intersect the axis at values of K_r greater than unity in contrast to the curves shown in Figure N.2 for constant β.

 © The British Standards Institution 2019

Figure N.2 **Modifications to the Option 1 failure assessment curve (continuous yielding) for various values of the material parameter, α, and constraint levels, β (< 0)**



NOTE Equation (N.24) with k = 3 assumed.

N.2.4.5 Calculation of parameter ρ_c

The value of ρ_c is:

$$\rho_c = \rho\left(\frac{K^c_{mat}}{K_{mat}}\right) \quad \text{(N.26)}$$

where ρ is as defined in Annex R.

When K^c_{mat} is defined by Equation (N.20) for $\beta < 0$, ρ becomes:

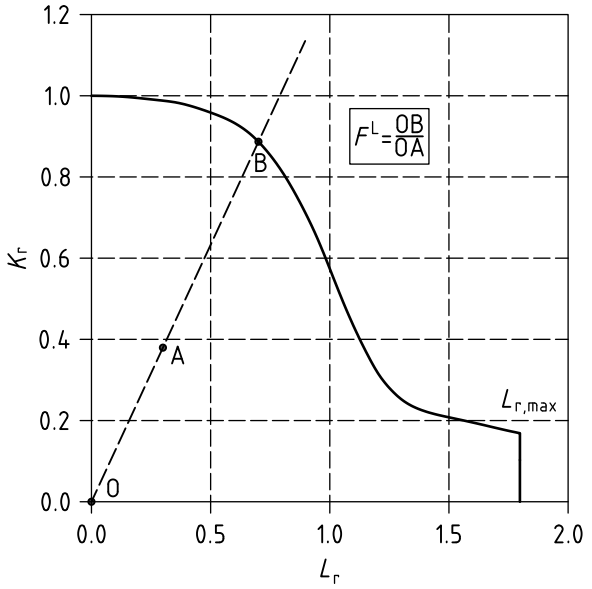
$$\rho_l = \rho\left[1 + \alpha(-\beta L_r)^k\right] \quad \text{(N.27)}$$

N.2.4.6 Assessment of the significance of results

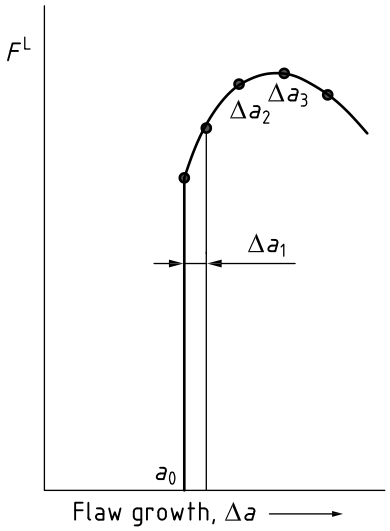
The significance of results should be assessed in accordance with this subclause, with reserve factors defined in terms of the assessed conditions and those which produce a limiting condition.

When an initiation analysis is performed for a single primary load, the graphical construction of Figure N.3 may be used to define the load factor, F^L, when following Procedure I of **N.2.2**. When following Procedure II of **N.2.3** this construction should not be used, as K_r is no longer directly proportional to load because of the dependence of K^c_{mat} on βL_r. The limiting condition, and hence the reserve factor, is obtained by finding the intersection with the failure assessment curve of the locus of assessment points (L_r, K_r) for different values of load.

Figure N.3 **FAD analysis for (a) fracture initiation and (b) ductile tearing**



a) FAD analysis: fracture initiation



b) FAD analysis: tearing resistance

When performing a tearing analysis, the reserve factor on load, F^L, should be calculated as a function of postulated flaw growth. Following Procedure I (**N.2.2**), the load factor might change as a result of changes in L_r, K_r and the failure assessment curve. Following Procedure II (**N.2.3**), the failure assessment curve does not change unless an Option 3 curve is constructed at each crack extension. The limiting condition is obtained by plotting F^L as a function of postulated growth as depicted in Figure N.3. When extensive crack growth data are available, a maximum in this plot is obtained. This corresponds to the tangency condition cited in **7.3.8**, but with the failure assessment curve changing with crack extension (see for example references [N.23] to [N.32]).

Sensitivity studies following the principles of **N.2.4.6** should be carried out to establish confidence in any increased reserve factors obtained by following the procedures in this annex.

Parameters of interest which may be explored are as follows:

a) the constraint parameter β: its sensitivity to any assumptions about the nature of the loading (tension, bending), its definition in terms of the *T*-stress or *Q* parameter and any estimate used for combined primary and secondary stresses;

b) the materials property K^c_{mat}: the extent to which lower bound properties have been used, uncertainties in modelling predictions, and uncertainties in fitting equations such as Equation (N.20) to data by assessing the sensitivity to values of α and k.

N.3 Inputs for constraint analysis

N.3.1 General

A constraint analysis of **N.2.4.3.2** requires two inputs in addition to the conventional approach of Clause **7**. Firstly, the level of constraint is characterized using a normalized parameter β (**N.3.2**), defined in terms of the constraint parameters *T*-stress or *Q* parameter. Secondly, the sensitivity of the material toughness to the level of constraint is characterized using the material constraint parameters α and k. These may be obtained using several methods as described in **N.2.4.3.2**. One method (applicable only when the constraint is expressed in terms of the *T*-stress parameter) is to use the tables presented in **N.3.3.2**.

N.3.2 Compendium of β_T solutions

N.3.2.1 General

In **N.2**, the level of constraint is taken into account through the normalized constraint parameter, β. This normalized constraint parameter is defined in terms of the *T*-stress or *Q* parameter, such that $\beta_T = T/(L_r\sigma_Y)$, and $\beta_Q = Q/L_r$, where $L_r = \sigma_{ref}/\sigma_Y$. *T* is the elastic *T*-stress and *Q* is the elastic-plastic constraint parameter.

Within **N.3.2**, a compendium of β_T solutions is presented for various geometries.

NOTE Only β_T solutions are included.

For each solution there is a figure of the geometry, the polynomial coefficients defining β_T in terms of *a*/*W* or *a*/*B*, the reference stress solution used and the source references. The values of *T*-stress used as input to β_T have been derived from finite element analyses for a range of *a*/*W* or *a*/*B*, with the value at $a/W \rightarrow 0$ or $a/B \rightarrow 0$ fitted to an analytical solution.

The value of β_T depends on the reference stress solution used to evaluate L_r. The β_T solutions listed here assume plane strain conditions, consistent with the scope of the procedures of **N.2** and the von Mises yield criterion. The particular value of β_T required for application of **N.2** should use the same limit load as that used in the determination of L_r. Where necessary, the appropriate β_T may be derived from the solutions given here using simple scaling by the ratio of the respective limit loads.

Using this compendium, it is possible to determine a value of β_T, for a particular geometry with a particular crack size, and hence, in conjunction with the materials constraint-dependent toughness variation, apply the procedures of **N.2**. Conditions of high constraint can lead to values of $\beta \geq 0$. In such cases, the procedures of **N.2** are not applicable as they lead to an increase in reserve factors, and Option 1 to Option 3 given in Clause **7** should be followed.

The geometries which are considered in **N.3.2** are described in detail in the following subclauses. For each of the geometries a solution for β_T is given for a range of normalized crack lengths.

N.3.2.2 Flaws in plates

N.3.2.2.1 Centre-cracked plate (CCP) in uniaxial tension

See Figure M.1 for the definition of the geometry. The distance between the points at which loading is applied is defined as 2*H*. See Table N.1 for polynomial coefficients defining β_T, from references [N.33] to [N.35].

Table N.1 **Polynomial coefficients defining β_T for CCP**

Geometry	2*H*/*W*	X_0	X_1	X_2	X_3	X_4
CCP	1	–1.1547	1.1476	–2.4091	4.059	–1.9907
CCP	>1.5	–1.1547	1.1511	–0.7826	0.4751	–0.1761

$$\beta_T = X_0 + X_1\left(\frac{2a}{W}\right) + X_2\left(\frac{2a}{W}\right)^2 + X_3\left(\frac{2a}{W}\right)^3 + X_4\left(\frac{2a}{W}\right)^4 \quad \text{for } 0 \leq 2a/W \leq 0.6 \tag{N.28}$$

Reference stress solution used:

$$\sigma_{ref} = \frac{\sqrt{3}P_m}{2(1-2a/W)} \quad \text{(N.29)}$$

where σ_{ref} is obtained using the plane strain von Mises limit load (see reference [N.36]).

N.3.2.2.2 Centre-cracked plate: equibiaxial tension (CCPB)

See Figure M.1 for the definition of the geometry. The distance between the points at which loading is applied is defined as 2*H*. See Table N.2 for polynomial coefficients defining β_T, from references [N.33] to [N.35].

Table N.2 **Polynomial coefficients defining β_T for CCPB**

Geometry	2*H*/*W*	X_0	X_1	X_2	X_3	X_4
CCPB	1	0	–0.3642	2.423	–16.156	18.606
CCPB	> 1.5	0	–0.2777	2.6472	–12.499	12.122

$$\beta_T = X_0 + X_1\left(\frac{2a}{W}\right) + X_2\left(\frac{2a}{W}\right)^2 + X_3\left(\frac{2a}{W}\right)^3 + X_4\left(\frac{2a}{W}\right)^4 \quad \text{for } 0 \le 2a/W \le 0.6 \quad \text{(N.30)}$$

Reference stress solution used:

$$\sigma_{ref} = \frac{\sqrt{3}P_m}{2} \quad \text{for } 2a/W < 0.5 \quad \text{(N.31)}$$

$$\sigma_{ref} = \left(\frac{\sqrt{3}P_m}{2}\right)\left[\frac{2a/W}{(1-2a/W)}\right] \quad \text{for } 2a/W \ge 0.5 \quad \text{(N.32)}$$

where σ_{ref} is obtained using the plane strain von Mises limit load (see reference [N.18]).

N.3.2.2.3 Double edge-notched plate: uniaxial tension (DENT)

See Figure P.1 for the definition of the geometry: the double edge-notched plate contains two edge flaws directly opposite each other. The distance between the points at which loading is applied is defined as 2*H*. See Table N.3 for polynomial coefficients defining β_T, taken from references [N.16], [N.33] and [N.35].

Table N.3 **Polynomial coefficients defining β_T for DENT**

Geometry	2*H*/*W*	X_0	X_1	X_2	X_3	X_4
DENT	2	–0.5889	–0.0097	1.1103	–1.3852	0.6573

$$\beta_T = X_0 + X_1\left(\frac{2a}{W}\right) + X_2\left(\frac{2a}{W}\right)^2 + X_3\left(\frac{2a}{W}\right)^3 + X_4\left(\frac{2a}{W}\right)^4 \quad \text{for } 0 \le 2a/W \le 0.6 \quad \text{(N.33)}$$

Reference stress solution used:

$$\sigma_{ref} = \frac{\sqrt{3}P_m}{2}\frac{1}{\left[1+\ln\left(\frac{W-a}{(W-2a)}\right)\right]\left(1-\frac{2a}{W}\right)} \quad \text{for } 0 \le 2a/W \le 0.884 \quad \text{(N.34)}$$

where σ_{ref} is obtained using the plane strain von Mises limit load (see reference [N.36]).

N.3.2.2.4 Single edge-notched plate: uniaxial tension (SENT)

See Figure M.2 for the definition of the geometry. The distance between the points at which loading is applied is defined as 2*H*. See Table N.4 for polynomial coefficients defining β_T, taken from references [N.16], [N.33] and [N.35].

Table N.4 **Polynomial coefficients defining β_T for SENT**

Geometry	*H/W*	X_0	X_1	X_2	X_3	X_4
SENT Pin Loading	6	–0.5889	–0.0128	0.5512	4.651	–4.6703
SENT Fixed Grip	6	–0.5889	0.0930	0.9194	–0.4032	0.5566
SENT Fixed Grip	2.5	–0.5889	0.1022	1.5888	–2.7591	1.4230

$$\beta_T = X_0 + X_1\left(\frac{a}{W}\right) + X_2\left(\frac{a}{W}\right)^2 + X_3\left(\frac{a}{W}\right)^3 + X_4\left(\frac{a}{W}\right)^4 \quad \text{for } 0 \le a/W \le 0.8 \quad \text{(N.35)}$$

Reference stress solution used for pin loading:

$$\sigma_{ref} = \frac{\sqrt{3}P_m}{2}\frac{1}{\left[1 - \left(\frac{a}{w}\right) - 1.232\left(\frac{a}{w}\right)^2 + \left(\frac{a}{w}\right)^3 + 22\left(\frac{a}{w}\right)^3\left(0.545 - \frac{a}{w}\right)^2\right]} \quad \text{(N.36)}$$

for $a/w \le 0.545$

$$\sigma_{ref} = \frac{\sqrt{3}P_m}{2}\frac{1}{1.702\left\{\left[\left(\frac{a}{w} - 0.206\right)^2 + 0.5876\left(1 - \frac{a}{w}\right)^2\right]^{0.5} - \left(\frac{a}{w} - 0.206\right)\right\}} \quad \text{(N.37)}$$

for $a/w > 0.545$

Reference stress solution used for fixed grip loading:

$$\sigma_{ref} = \frac{\sqrt{3}P_m}{2}\frac{1}{1 - (a/W)} \quad \text{(N.38)}$$

where σ_{ref} is obtained using the plane strain von Mises limit load (see reference [N.36]).

N.3.2.2.5 Single edge-notched plate: pure bending (SEB)

See Figure M.2 for the definition of the geometry. The distance between the points at which loading is applied is defined as 2*H*. See Table N.5 for polynomial coefficients defining β_T, taken from references [N.16], [N.33] and [N.35].

Table N.5 **Polynomial coefficients defining β_T for SEB**

Geometry	*H/W*	X_0	X_1	X_2	X_3	X_4
SEB	6	–0.8833	2.8825	0.5863	–5.7069	3.5896

$$\beta_T = X_0 + X_1\left(\frac{a}{W}\right) + X_2\left(\frac{a}{W}\right)^2 + X_3\left(\frac{a}{W}\right)^3 + X_4\left(\frac{a}{W}\right)^4 \text{ for } 0 \le= a/W \le 0.8 \quad \text{(N.39)}$$

Reference stress solution used:

$$\sigma_{ref} = \frac{P_b}{\sqrt{3}}\frac{1}{\left[1 + 1.686\left(\frac{a}{w}\right)^2\right]\left(1 - \frac{a}{w}\right)^2} \qquad \text{for } a/W \le 0.295 \quad \text{(N.40)}$$

$$\sigma_{ref} = \frac{P_b}{\sqrt{3}} \frac{1}{1.2606[1-(a/w)]^2} \quad \text{for } a/W > 0.295 \tag{N.41}$$

where σ_{ref} is obtained using the plane strain von Mises limit load (see reference [N.36]).

N.3.2.2.6 Single edge-notched plate: 3 point bend (SENB)

See Figure M.2 for the definition of the geometry. The distance between the two outermost bend points is defined as $2H$. See Table N.6 for polynomial coefficients defining β_T, taken from references [N.16], [N.33] and [N.35].

Table N.6 **Polynomial coefficients defining β_T for SENB**

Geometry	*H/W*	X_0	X_1	X_2	X_3	X_4	X_5	X_6
SENB	2	–0.7887	–0.1795	32.9014	–153.45	316.11	–308.47	115.18

$$\beta_T = X_0 + X_1\left(\frac{a}{W}\right) + X_2\left(\frac{a}{W}\right)^2 + X_3\left(\frac{a}{W}\right)^3 + X_4\left(\frac{a}{W}\right)^4 + X_5\left(\frac{a}{W}\right)^5 + X_6\left(\frac{a}{W}\right)^6 \quad \text{for } 0 \le a/W \le 0.8 \tag{N.42}$$

Reference stress solution used:

$$\sigma_{ref} = \frac{P_b}{\sqrt{3}} \frac{1}{\left[1.12 + 1.13\left(\frac{a}{W}\right) - 3.194\left(\frac{a}{W}\right)^2\right]\left(1-\frac{a}{W}\right)^2} \quad \text{for } 0 < a/W \le 0.18 \tag{N.43}$$

$$\sigma_{ref} = \frac{P_b}{\sqrt{3}} \frac{1}{1.22[1-(a/W)]^2} \quad \text{for } 0.18 < a/W \le 1 \tag{N.44}$$

where σ_{ref} is obtained using the plane strain von Mises limit load from reference [N.36].

N.3.2.2.7 Compact tension specimen (CT)

A graphical solution for the CT specimen is given in reference [N.37], which shows positive values for β_T across the range $0.22 < a/W < 0.8$; an approximate fit is given in Table N.7 (see reference [N.37]).

Table N.7 **Polynomial coefficients defining β_T for CT**

Geometry	X_0	X_1	X_2	X_3	X_4	X_5	X_6
CT	–4.640	40.302	–117.45	150.84	–52.043	–61.08	45.391

 © The British Standards Institution 2019

N.3.2.2.8 Surface-cracked plate (SCP): uniaxial tension

See Figure M.3 for the definition of the geometry and Table N.8 for polynomial coefficients defining β_T for a square plate geometry (full height/full width = 1) (see reference [N.38]).

Table N.8 **Polynomial coefficients defining β_T for SCP: uniaxial tension**

Geometry	X_0	X_1	X_2	X_3
SCP	–0.581176	0.795958	–4.70569	6.16031
(deepest point of flaw, θ = 90°)	+0.429125 (a/c)	–6.53119 (a/c)	+28.4706 (a/c)	–40.1692 (a/c)
	–0.670213 $(a/c)^2$	+12.1073 $(a/c)^2$	–51.1588 $(a/c)^2$	+68.7053 $(a/c)^2$
	+0.290259 $(a/c)^3$	–6.47294 $(a/c)^3$	+27.3436 $(a/c)^3$	–35.4684 $(a/c)^3$
SCP	0.062026	0.59687	–0.020640	–7.82399
(surface of flaw, θ = 5°)	–1.49614 (a/c)	–4.2027 (a/c)	+13.1854 (a/c)	+19.532 (a/c)
	+0.94377 $(a/c)^2$	+6.94022 $a/c)^2$	–30.022 $(a/c)^2$	–14.4551 $(a/c)^2$
	–0.15367 $(a/c)^3$	–3.29765 $(a/c)^3$	+16.3561 $(a/c)^3$	+3.36514 $(a/c)^3$
SCP	–0.541934	0.824373	–7.40441	16.495
(middle point of flaw, θ = 45°)	+0.235102 (a/c)	–4.75413 (a/c)	+42.3294 (a/c)	–85.4066 (a/c)
	–0.147745 $(a/c)^2$	+7.94842 $(a/c)^2$	–68.7977 $(a/c)^2$	+133.613 $(a/c)^2$
	–0.0892144 $(a/c)^3$	–4.04742 $(a/c)^3$	+34.1067 $(a/c)^3$	–65.1123 $(a/c)^3$

$$\beta_T = (1-\alpha'')\left[X_0 + X_1\left(\frac{a}{B}\right)^2 + X_2\left(\frac{a}{B}\right)^4 + X_3\left(\frac{a}{B}\right)^6\right] \quad \text{for } 0 \le a/B \le 0.8 \text{ and } 0.2 \le a/c \le 0.8 \tag{N.45}$$

where:

$$\alpha'' = \frac{a/B}{1+(B/c)} \qquad \text{for } W \ge 2(c+B)$$

$$\alpha'' = \frac{2a/B}{c/W} \qquad \text{for } W < 2(c+B)$$

Reference stress solution used:

$$\sigma_{ref} = \frac{P_m}{(1-\alpha'')} \tag{N.46}$$

where σ_{ref} is derived from Equation P.15, which assumes normal restraint.

N.3.2.2.9 Surface-cracked plate: bending (SCPB)

See Figure M.3 for the definition of the geometry and Table N.9 for polynomial coefficients defining β_T for a square plate geometry (full height/full width = 1) (see reference [N.37]).

Table N.9 **Polynomial coefficients defining β_T for SCPB**

Geometry	X_0	X_1	X_2	X_3
SCPB	–0.37758	4.61176	–9.85178	10.8584
(deepest point of flaw, θ = 90°)	+0.346823(a/c)	–5.35305(a/c)	+20.786(a/c)	–30.3672(a/c)
	–0.539154(a/c)^2	+9.4601(a/c)^2	–36.8869(a/c)^2	+49.8859(a/c)^2
	+0.221408(a/c)^3	–5.03237(a/c)^3	+19.806(a/c)^3	–25.7138(a/c)^3
SCPB	0.0433442	0.787135	–1.66573	–2.80697
(surface of flaw, θ = 5°)	–1.4636(a/c)	–5.06806(a/c)	+16.8231(a/c)	+1.64157(a/c)
	+0.97000(a/c)^2	+8.63486(a/c)^2	–31.5732(a/c)^2	+6.29347(a/c)^2
	–0.182882(a/c)^3	–4.13922(a/c)^3	+15.831(a/c)^3	–4.54519(a/c)^3
SCPB	–0.38791	3.03526	–7.24926	10.5771
(middle point of flaw, θ = 45°)	+0.129756(a/c)	–2.16281(a/c)	+19.3245614(a/c)	–40.7667(a/c)
	–0.0248056(a/c)^2	2.87454(a/c)^2	–30.9815(a/c)^2	+64.1264(a/c)^2
	–0.134278(a/c)^3	–1.22346(a/c)^3	+15.1343(a/c)^3	–31.2725(a/c)^3

$$\beta_T = \frac{3(1-\alpha'')^2}{2}\left[X_0 + X_1\left(\frac{a}{B}\right)^2 + X_2\left(\frac{a}{B}\right)^4 + X_3\left(\frac{a}{B}\right)^6\right] \quad \begin{array}{l}\text{for } 0 \le a/B \le 0.8 \text{ and} \\ 0.2 \le a/c \le 0.8\end{array} \tag{N.47}$$

where:

$$\alpha'' = \frac{a/B}{1+(B/c)} \qquad \text{for } W \ge 2(c+B)$$

$$\alpha'' = \frac{2a/B}{c/W} \qquad \text{for } W < 2(c+B)$$

Reference stress solution used:

$$\sigma_{ref} = \frac{2P_b}{3(1-\alpha'')^2} \tag{N.48}$$

where σ_{ref} is derived from Equation P.15 and Equation P.16 from references [N.17] and [N.39].

 © The British Standards Institution 2019

N.3.2.3 Flaws in cylinders

N.3.2.3.1 Extended internal circumferential surface flaw in a cylinder

See Figure M.21 for the definition of the geometry and Table N.10 for polynomial coefficients defining β_T. The distance between the points at which load is applied is defined as $2H$. See Table N.10 for polynomial coefficients defining β_T (H/B = 10), taken from references [N.33] and [N.40].

Table N.10 **Polynomial coefficients defining β_T for extended internal circumferential surface flaw in a cylinder**

Geometry	r_i/B	X_0	X_1	X_2	X_3	X_4	X_5	X_6
Extended internal circumferential surface flaw in cylinder	2.5	–0.51	–0.5247	5.2871	–19.103	36.294	–35.242	13.536
	5	–0.51	–0.4074	4.0608	–13.768	27.014	–28.024	11.33
	10	–0.51	–0.349	3.3111	–11.111	24.588	–27.936	11.687
	20	–0.51	–0.3175	2.7925	–9.3521	23.048	–26.86	10.808

$$\beta_T = X_0 + X_1\left(\frac{a}{B}\right) + X_2\left(\frac{a}{B}\right)^2 + X_3\left(\frac{a}{B}\right)^3 + X_4\left(\frac{a}{B}\right)^4 + X_5\left(\frac{a}{B}\right)^5 + X_6\left(\frac{a}{B}\right)^6 \quad \text{for } 0 \le a/B \le 0.8 \tag{N.49}$$

Reference stress solution used:

$$\sigma_{ref} = \frac{P_m}{\left(1-\frac{a}{B}\right)\left\{\left[\frac{a}{2(B-a)}\right] + \left[1-\frac{3}{4}\left(\frac{a}{B-a}\right)^2\right]^{0.5}\right\}} \quad \text{for } a/B \le \frac{1}{1+\sqrt{3}} \tag{N.50}$$

$$\sigma_{ref} = \frac{\sqrt{3}P_m}{2}\frac{1}{[1 - (a/B)]} \quad \text{for } a/B \ge \frac{1}{1+\sqrt{3}} \tag{N.51}$$

where σ_{ref} is derived from Annex P, using the von Mises yield criterion, from references [N.33] and [N.40].

N.3.2.3.2 Internal circumferential surface flaw in a cylinder (biaxial tension)

The loading considered corresponds to an internally pressurized cylinder closed at both ends where the axial (longitudinal) stress is half the hoop (circumferential) stress, resulting in a biaxial stress state. See Figure M.20 for the definition of the geometry and Table N.11 for polynomial coefficients defining β_T, taken from reference [N.41].

Table N.11 **Polynomial coefficients defining β_T for internal circumferential surface flaw in a cylinder (biaxial tension)**

r_m/B	Geometry	X_0	X_1	X_2	X_3
5	(deepest point of flaw, θ = 90°)	–0.6256	+0.6805	–0.5174	–0.2293
		+0.4631($c/\pi r_i$)	–7.7886($c/\pi r_i$)	+25.26($c/\pi r_i$)	–28.143($c/\pi r_i$)
		–0.5289($c/\pi r_i$)^2	+8.8378($c/\pi r_i$)^2	–27.407($c/\pi r_i$)^2	+28.289($c/\pi r_i$)^2
	(surface of flaw, θ = 5°)	–3.7555	+47.752	–98.191	+60.477
		+22.18($c/\pi r_i$)	–338.46($c/\pi r_i$)	+755.96($c/\pi r_i$)	–481.17($c/\pi r_i$)
		–36.009($c/\pi r_i$)^2	+548.73($c/\pi r_i$)^2	–1273.2($c/\pi r_i$)^2	+823.96($c/\pi r_i$)^2
	(middle point of flaw, θ = 45°)	–0.5407	–0.3765	+3.3936	–2.0885
		–0.2046($c/\pi r_i$)	+1.0107($c/\pi r_i$)	–11.457($c/\pi r_i$)	+1.542($c/\pi r_i$)
		+0.3711($c/\pi r_i$)^2	–2.6533($c/\pi r_i$)^2	+21.696($c/\pi r_i$)^2	–9.6($c/\pi r_i$)^2
10	(deepest point of flaw, θ = 90°)	–0.5436	–0.1774	+1.2429	–1.7033
		+0.367($c/\pi r_i$)	–6.0894($c/\pi r_i$)	+20.036($c/\pi r_i$)	–21.6($c/\pi r_i$)
		–0.4333($c/\pi r_i$)^2	+7.3222($c/\pi r_i$)^2	–23.644($c/\pi r_i$)^2	+24.116($c/\pi r_i$)^2
	(surface of flaw, θ = 5°)	+0.0094	–9.2828	+49.594	–42.144
		–3.7789($c/\pi r_i$)	+60.578($c/\pi r_i$)	–322.37($c/\pi r_i$)	+278.43($c/\pi r_i$)
		+6.1244($c/\pi r_i$)^2	–96.689($c/\pi r_i$)^2	+505.06($c/\pi r_i$)^2	–440.18($c/\pi r_i$)^2
	(middle point of flaw, θ = 45°)	–0.5232	–0.4236	+1.6787	–0.8994
		–0.0603($c/\pi r_i$)	–0.1652($c/\pi r_i$)	–0.3228($c/\pi r_i$)	–6.2293($c/\pi r_i$)
		+0.1533($c/\pi r_i$)^2	–0.5756($c/\pi r_i$)^2	+3.0289($c/\pi r_i$)^2	+6.2($c/\pi r_i$)^2
20	(deepest point of flaw, θ = 90°)	–0.4455	–1.0276	+2.9256	–2.6487
		+0.1711($c/\pi r_i$)	–2.7389($c/\pi r_i$)	+8.4631($c/\pi r_i$)	–9.5893($c/\pi r_i$)
		–0.2089($c/\pi r_i$)^2	+3.4978($c/\pi r_i$)^2	–11.076($c/\pi r_i$)^2	+12.307($c/\pi r_i$)^2
	(surface of flaw, θ = 5°)	–0.6458	+1.3191	–1.8561	+4.7443
		+1.2764($c/\pi r_i$)	–13.854($c/\pi r_i$)	+24.505($c/\pi r_i$)	–41.147($c/\pi r_i$)
		–2.0222($c/\pi r_i$)^2	+21.607($c/\pi r_i$)^2	–37.829($c/\pi r_i$)^2	+63.018($c/\pi r_i$)^2
	(middle point of flaw, θ = 45°)	–0.4642	–0.8022	+2.1267	–1.7442
		–0.0059($c/\pi r_i$)	–0.2777($c/\pi r_i$)	–0.2888($c/\pi r_i$)	–1.0832($c/\pi r_i$)
		+0.0378($c/\pi r_i$)^2	+0.2333($c/\pi r_i$)^2	+0.6022($c/\pi r_i$)^2	+1.4911($c/\pi r_i$)^2

$$\beta_T = \frac{\left(1-\frac{a}{B}\right)\left[\pi - \left(\frac{c}{r}\right)\left(\frac{a}{B}\right)\right]}{\left[\pi\left(1-\frac{a}{B}\right) + 2\left(\frac{a}{B}\right)\sin\left(\frac{c}{r}\right)\right]}\left[X_0 + X_1\left(\frac{a}{B}\right) + X_2\left(\frac{a}{B}\right)^2 + X_3\left(\frac{a}{B}\right)^3\right] \quad \text{(N.52)}$$

for $0.1 \leq (c/\pi ri) \leq 0.4$ and $0.1 \leq a/B \leq 0.75$

The reference stress solution used is **P.28**.

 © The British Standards Institution 2019

N.3.2.3.3 Internal circumferential surface flaw in a cylinder (uniaxial tension)

This loading scenario can occur during global pipe bending when the flaw being assessed is located on the outer bend radius where the pipe wall is effectively in uniaxial tension. See Figure M.20 for the definition of the geometry and Table N.12 for polynomial coefficients defining β_T, taken from reference [N.41].

Table N.12 **Polynomial coefficients defining β_T for internal circumferential surface flaw in a cylinder (uniaxial tension)**

r_m/B	Geometry	X_0	X_1	X_2	X_3
5	(deepest point of flaw, θ = 90°)	–0.453	+0.171	–0.008	–0.3738
		$+0.2768(c/\pi r_i)$	$-5.4093(c/\pi r_i)$	$+18.622(c/\pi r_i)$	$-21.926(c/\pi r_i)$
		$-0.2689(c/\pi r_i)^2$	$+6.0267(c/\pi r_i)^2$	$-20.418(c/\pi r_i)^2$	$+23.304(c/\pi r_i)^2$
	(surface of flaw, θ = 5°)	–0.7463	+5.0092	–13.45	+8.8807
		$+2.1449(c/\pi r_i)$	$-36.411(c/\pi r_i)$	$+99.929(c/\pi r_i)$	$-67.729(c/\pi r_i)$
		$-1.6978(c/\pi r_i)^2$	$+58.76(c/\pi r_i)^2$	$-164.88(c/\pi r_i)^2$	$+113.45(c/\pi r_i)^2$
	(middle point of flaw, θ = 45°)	–0.4068	–0.6836	+1.5928	–1.0261
		$-0.075(c/\pi r_i)$	$+0.1942(c/\pi r_i)$	$-1.5692(c/\pi r_i)$	$-3.0854(c/\pi r_i)$
		$+0.6733(c/\pi r_i)^2$	$-0.4578(c/\pi r_i)^2$	$+4.0378(c/\pi r_i)^2$	$+1.3756(c/\pi r_i)^2$
10	(deepest point of flaw, θ = 90°)	–0.4072	–0.8667	+2.0793	–2.2023
		$+0.2759(c/\pi r_i)$	$-5.0517(c/\pi r_i)$	$+17.042(c/\pi r_i)$	$-18.782(c/\pi r_i)$
		$-0.3444(c/\pi r_i)^2$	$+6.4067(c/\pi r_i)^2$	$-20.973(c/\pi r_i)^2$	$+22.071(c/\pi r_i)^2$
	(surface of flaw, θ = 5°)	–0.797	+2.7292	–5.273	+3.598
		$+2.3552(c/\pi r_i)$	$-19.74(c/\pi r_i)$	$+35.297(c/\pi r_i)$	$-23.214(c/\pi r_i)$
		$-1.8778(c/\pi r_i)^2$	$+30.793(c/\pi r_i)^2$	$-52.247(c/\pi r_i)^2$	$+32.431(c/\pi r_i)^2$
	(middle point of flaw, θ = 45°)	–0.4134	–0.8077	+1.667	–0.9758
		$+0.0251(c/\pi r_i)$	$-0.8649(c/\pi r_i)$	$+3.1677(c/\pi r_i)$	$-7.6692(c/\pi r_i)$
		$+0.4578(c/\pi r_i)^2$	$+2.1378(c/\pi r_i)^2$	$-6.2467(c/\pi r_i)^2$	$+12.184(c/\pi r_i)^2$
20	(deepest point of flaw, θ = 90°)	–0.2845	–1.901	+4.352	–3.6827
		$+0.2367(c/\pi r_i)$	$-3.7962(c/\pi r_i)$	$+12.444(c/\pi r_i)$	$-13.874(c/\pi r_i)$
		$-0.4133(c/\pi r_i)^2$	$+5.6711(c/\pi r_i)^2$	$-17.371(c/\pi r_i)^2$	$+18.378(c/\pi r_i)^2$
	(surface of flaw, θ = 5°)	–0.6017	+1.0482	–3.398	+3.4298
		$+1.5417(c/\pi r_i)$	$-14.111(c/\pi r_i)$	$+41.297(c/\pi r_i)$	$-40.825(c/\pi r_i)$
		$-1.1(c/\pi r_i)^2$	$+27.027(c/\pi r_i)^2$	$-76.949(c/\pi r_i)^2$	$+75.007(c/\pi r_i)^2$
	(middle point of flaw, θ = 45°)	–0.3715	–1.2804	+2.9216	–2.5041
		$-0.0799(c/\pi r_i)$	$-0.3994(c/\pi r_i)$	$-0.3857(c/\pi r_i)$	$-2.0547(c/\pi r_i)$
		$+0.6111(c/\pi r_i)^2$	$+0.4644(c/\pi r_i)^2$	$-1.8067(c/\pi r_i)^2$	$+5.4(c/\pi r_i)^2$

$$\beta_T = \frac{\left(1-\frac{a}{B}\right)\left[\pi - \left(\frac{c}{r}\right)\left(\frac{a}{B}\right)\right]}{\left[\pi\left(1-\frac{a}{B}\right) + 2\left(\frac{a}{B}\right)\sin\left(\frac{c}{r}\right)\right]}\left[X_0 + X_1\left(\frac{a}{B}\right) + X_2\left(\frac{a}{B}\right)^2 + X_3\left(\frac{a}{B}\right)^3\right] \quad \text{(N.53)}$$

for $0.1 \leq (c/\pi ri) \leq 0.4$ and $0.1 \leq a/B \leq 0.75$

The reference stress solution used is **P.28**.

N.3.3 Look-up tables for constraint corrected FAD

N.3.3.1 General

This subclause provides a set of look-up tables that define the material parameters α and k used in **N.2**, Equation (N.20), to define the constraint sensitivity of material toughness for cleavage fracture behaviour. The look-up tables were developed by Sherry et al in reference [N.28] within the framework of VOCALIST (see references [N.42] and [N.43]).

The material parameters α and k are given as a function of tensile properties (E/σ_Y) and (n) and the Weibull model exponent (m), with constraint quantified in terms of T/σ_Y (**N.3.3.2**). Once identified, these parameters may be applied to Equation (N.20) to define the ratio K^c_{mat}/K_{mat} for the material and at the temperature of interest. This ratio is largely independent of cleavage fracture probability and hence may be used to assess the influence of constraint on lower bound, mean and/or upper bound toughness properties as appropriate.

To use the look-up tables, values of the elastic modulus (E), yield strength (σ_Y), strain hardening exponent (n) and the Weibull model exponent (m) are required for the material and at the temperature of interest.

NOTE 1 Calibration of the Weibull exponent m is a subject of ongoing debate. Early guidance on calibration advocated the use of notched specimen data [N.44]. However, it is now recommended that, where possible, the parameter m is calibrated against pre-cracked specimen data [N.26]. Current best practice is to use data derived from both high and low constraint fracture toughness specimens, such as deep and shallow-cracked bend specimens. This enables the calibrated model to be applied to interpolate between constraints states used for calibration, rather than to extrapolate outside the range of applicability. A suitable method for calibrating m is given in reference [N.26]. A review of the calibration methods available is provided in references [N.45] and [N.46].

NOTE 2 Alternative look-up tables for obtaining α and k values that do not require knowledge of m have recently been developed for both cleavage fracture and ductile tearing, e.g. reference [N.47].

N.3.3.2 Look-up tables for α and k defined with respect to T/σ_Y

Look-up tables for α and k defined with respect to T/σ_Y are given as Table N.13 to Table N.28.

 © The British Standards Institution 2019

Table N.13 α and k defined with respect to T/σ_Y for $n = 5$

$n = 5$	$m = 5$		$m = 7.5$		$m = 10$		$m = 12.5$		$m = 15$		$m = 17.5$		$m = 20$	
E/σ_Y	α	k	α	k	α	k	α	k	α	k	α	k	α	k
450	0.708	2.13	1.013	1.67	1.087	1.41	1.017	1.30	0.889	1.28	0.789	1.30	0.806	1.29
475	0.761	2.15	1.036	1.68	1.091	1.41	1.010	1.30	0.878	1.28	0.778	1.30	0.793	1.30
500	0.797	2.14	1.053	1.67	1.097	1.41	1.009	1.30	0.873	1.28	0.772	1.30	0.786	1.30
525	0.826	2.11	1.069	1.66	1.103	1.41	1.010	1.30	0.871	1.28	0.768	1.30	0.783	1.31
550	0.851	2.08	1.083	1.65	1.110	1.41	1.012	1.30	0.870	1.29	0.766	1.31	0.781	1.31
575	0.874	2.04	1.097	1.64	1.117	1.41	1.014	1.31	0.870	1.29	0.765	1.31	0.780	1.32
600	0.894	2.00	1.110	1.62	1.125	1.41	1.018	1.31	0.870	1.29	0.764	1.31	0.780	1.33
625	0.913	1.95	1.123	1.61	1.132	1.41	1.021	1.32	0.872	1.30	0.764	1.31	0.781	1.33
650	0.930	1.90	1.135	1.59	1.140	1.41	1.025	1.32	0.873	1.30	0.765	1.32	0.782	1.34
675	0.946	1.85	1.147	1.58	1.148	1.41	1.030	1.33	0.875	1.30	0.765	1.32	0.783	1.35
700	0.962	1.80	1.159	1.56	1.156	1.41	1.034	1.33	0.877	1.31	0.767	1.32	0.785	1.36
725	0.976	1.74	1.171	1.54	1.164	1.41	1.039	1.34	0.880	1.31	0.768	1.32	0.787	1.36
750	0.990	1.69	1.182	1.52	1.172	1.41	1.044	1.34	0.882	1.31	0.769	1.33	0.790	1.37

© The British Standards Institution 2019

Table N.14 α and k defined with respect to T/σ_Y for $n = 6$

$n = 6$	$m = 5$		$m = 7.5$		$m = 10$		$m = 12.5$		$m = 15$		$m = 17.5$		$m = 20$	
E/σ_Y	α	k	α	k	α	k	α	k	α	k	α	k	α	k
425	0.704	2.13	1.177	1.76	1.397	1.54	1.453	1.43	1.433	1.39	1.425	1.38	1.517	1.37
450	0.760	2.18	1.202	1.78	1.403	1.54	1.453	1.43	1.442	1.39	1.461	1.39	1.600	1.38
475	0.799	2.18	1.224	1.78	1.409	1.54	1.449	1.42	1.435	1.39	1.460	1.39	1.615	1.39
500	0.832	2.17	1.243	1.77	1.415	1.54	1.444	1.42	1.421	1.39	1.441	1.39	1.598	1.39
525	0.859	2.15	1.260	1.77	1.421	1.54	1.437	1.42	1.402	1.38	1.412	1.38	1.562	1.38
550	0.884	2.12	1.277	1.76	1.427	1.53	1.429	1.42	1.380	1.38	1.376	1.38	1.513	1.38
575	0.907	2.09	1.294	1.74	1.433	1.53	1.421	1.42	1.356	1.37	1.335	1.37	1.455	1.37
600	0.927	2.05	1.309	1.73	1.439	1.53	1.413	1.41	1.331	1.37	1.290	1.36	1.389	1.37
625	0.947	2.01	1.325	1.72	1.444	1.53	1.404	1.41	1.303	1.36	1.241	1.35	1.318	1.36
650	0.965	1.96	1.340	1.70	1.450	1.52	1.395	1.41	1.275	1.35	1.190	1.34	1.241	1.35
675	0.982	1.91	1.355	1.69	1.455	1.52	1.385	1.41	1.245	1.35	1.136	1.32	1.160	1.34

Table N.15 α and k defined with respect to T/σ_Y for $n = 7$

$n = 7$	$m = 5$		$m = 7.5$		$m = 10$		$m = 12.5$		$m = 15$		$m = 17.5$		$m = 20$	
E/σ_Y	α	k	α	k	α	k	α	k	α	k	α	k	α	k
425	0.756	2.24	1.409	1.90	1.765	1.69	1.916	1.56	1.954	1.50	1.972	1.47	2.062	1.43
450	0.801	2.27	1.434	1.91	1.775	1.69	1.916	1.56	1.951	1.50	1.973	1.47	2.076	1.43
475	0.838	2.28	1.457	1.91	1.784	1.69	1.914	1.55	1.940	1.49	1.958	1.46	2.062	1.43
500	0.870	2.26	1.479	1.91	1.794	1.68	1.911	1.55	1.926	1.48	1.934	1.45	2.031	1.43
525	0.898	2.24	1.499	1.90	1.803	1.68	1.907	1.55	1.909	1.48	1.904	1.44	1.990	1.42
550	0.924	2.22	1.519	1.89	1.812	1.68	1.903	1.55	1.889	1.47	1.869	1.43	1.941	1.41
575	0.948	2.18	1.538	1.88	1.821	1.68	1.899	1.54	1.869	1.46	1.831	1.42	1.886	1.40
600	0.971	2.14	1.556	1.87	1.830	1.67	1.894	1.54	1.847	1.46	1.791	1.41	1.826	1.39
625	0.992	2.10	1.575	1.86	1.839	1.67	1.889	1.54	1.824	1.45	1.748	1.40	1.763	1.38
650	1.013	2.06	1.593	1.84	1.848	1.67	1.883	1.53	1.800	1.44	1.703	1.38	1.695	1.37
675	1.032	2.01	1.610	1.83	1.857	1.67	1.877	1.53	1.776	1.43	1.657	1.37	1.625	1.36

© The British Standards Institution 2019

Table N.16 α and k defined with respect to T/σ_Y for n = 8

n = 8	m = 5		m = 7.5		m = 10		m = 12.5		m = 15		m = 17.5		m = 20	
E/σ_Y	α	k	α	k	α	k	α	k	α	k	α	k	α	k
400	0.733	2.28	1.584	2.02	2.109	1.83	2.385	1.71	2.491	1.63	2.504	1.58	2.503	1.52
425	0.785	2.34	1.614	2.03	2.123	1.83	2.384	1.70	2.472	1.62	2.460	1.56	2.421	1.50
450	0.825	2.36	1.640	2.04	2.139	1.83	2.392	1.70	2.472	1.62	2.448	1.56	2.393	1.49
475	0.861	2.36	1.665	2.04	2.156	1.83	2.404	1.70	2.480	1.61	2.452	1.55	2.391	1.49
500	0.893	2.35	1.687	2.04	2.173	1.83	2.418	1.70	2.493	1.61	2.465	1.55	2.403	1.49
525	0.924	2.33	1.710	2.03	2.190	1.83	2.434	1.70	2.510	1.61	2.484	1.55	2.426	1.49
550	0.953	2.30	1.731	2.02	2.208	1.83	2.452	1.70	2.529	1.61	2.508	1.55	2.456	1.49
575	0.980	2.27	1.752	2.02	2.226	1.83	2.470	1.70	2.551	1.62	2.536	1.55	2.493	1.50
600	1.007	2.24	1.773	2.01	2.244	1.83	2.489	1.71	2.575	1.62	2.567	1.55	2.535	1.50
625	1.032	2.20	1.793	1.99	2.263	1.83	2.509	1.71	2.599	1.62	2.601	1.56	2.580	1.51
650	1.057	2.16	1.813	1.98	2.281	1.84	2.530	1.72	2.626	1.62	2.637	1.56	2.630	1.52
675	1.082	2.11	1.833	1.97	2.300	1.84	2.550	1.72	2.653	1.63	2.674	1.56	2.682	1.53

Table N.17 α and k defined with respect to T/σ_Y for $n = 9$

$n = 9$	$m = 5$		$m = 7.5$		$m = 10$		$m = 12.5$		$m = 15$		$m = 17.5$		$m = 20$	
E/σ_Y	α	k	α	k	α	k	α	k	α	k	α	k	α	k
400	0.756	2.33	1.701	2.09	2.372	1.94	2.813	1.84	3.068	1.77	3.184	1.70	3.203	1.62
425	0.798	2.36	1.728	2.10	2.389	1.94	2.822	1.83	3.068	1.76	3.168	1.70	3.162	1.61
450	0.835	2.37	1.752	2.11	2.408	1.94	2.841	1.83	3.087	1.76	3.184	1.69	3.171	1.61
475	0.870	2.37	1.776	2.11	2.429	1.94	2.864	1.83	3.116	1.76	3.220	1.70	3.210	1.61
500	0.903	2.36	1.799	2.11	2.451	1.94	2.892	1.84	3.153	1.77	3.268	1.70	3.268	1.62
525	0.936	2.35	1.822	2.10	2.474	1.94	2.922	1.84	3.195	1.77	3.325	1.71	3.341	1.63
550	0.967	2.33	1.844	2.10	2.496	1.95	2.953	1.85	3.242	1.78	3.390	1.72	3.425	1.65
575	0.998	2.30	1.865	2.09	2.520	1.95	2.987	1.85	3.292	1.79	3.461	1.73	3.518	1.66
600	1.028	2.27	1.887	2.08	2.544	1.95	3.022	1.86	3.345	1.80	3.536	1.74	3.618	1.68
625	1.058	2.24	1.908	2.08	2.568	1.96	3.058	1.87	3.400	1.81	3.615	1.75	3.725	1.70
650	1.087	2.21	1.929	2.07	2.592	1.96	3.095	1.88	3.457	1.82	3.698	1.77	3.837	1.71
675	1.116	2.17	1.950	2.06	2.616	1.96	3.133	1.89	3.516	1.83	3.784	1.78	3.954	1.73

© The British Standards Institution 2019

Table N.18 α and k defined with respect to T/σ_Y for n = 10

n = 10	m = 5		m = 7.5		m = 10		m = 12.5		m = 15		m = 17.5		m = 20	
E/σ_Y	α	k	α	k	α	k	α	k	α	k	α	k	α	k
350	0.681	2.17	1.722	2.10	2.565	2.03	3.225	1.98	3.720	1.93	4.064	1.87	4.276	1.79
375	0.727	2.27	1.750	2.12	2.575	2.03	3.214	1.96	3.682	1.91	3.992	1.85	4.160	1.76
400	0.768	2.32	1.776	2.14	2.591	2.03	3.225	1.96	3.689	1.90	3.993	1.85	4.147	1.76
425	0.806	2.35	1.800	2.15	2.611	2.03	3.247	1.95	3.715	1.90	4.022	1.85	4.177	1.76
450	0.843	2.36	1.824	2.15	2.633	2.03	3.275	1.96	3.752	1.91	4.070	1.85	4.231	1.76
475	0.879	2.36	1.847	2.15	2.656	2.03	3.306	1.96	3.797	1.91	4.129	1.86	4.303	1.77
500	0.914	2.36	1.870	2.15	2.680	2.03	3.340	1.97	3.847	1.92	4.197	1.87	4.387	1.79
525	0.948	2.35	1.893	2.15	2.705	2.04	3.377	1.97	3.902	1.93	4.272	1.88	4.481	1.80
550	0.982	2.33	1.915	2.15	2.730	2.04	3.415	1.98	3.960	1.94	4.353	1.90	4.582	1.82
575	1.016	2.32	1.937	2.14	2.755	2.04	3.455	1.99	4.021	1.95	4.438	1.91	4.690	1.84
600	1.049	2.30	1.959	2.14	2.781	2.05	3.496	2.00	4.084	1.96	4.527	1.92	4.804	1.86
625	1.083	2.28	1.981	2.13	2.808	2.05	3.538	2.01	4.150	1.98	4.619	1.94	4.922	1.88
650	1.115	2.25	2.003	2.13	2.834	2.06	3.581	2.02	4.217	1.99	4.714	1.96	5.045	1.90

Table N.19 α and k defined with respect to T/σ_Y for n = 11

n = 11	m = 5		m = 7.5		m = 10		m = 12.5		m = 15		m = 17.5		m = 20	
E/σ_Y	α	k	α	k	α	k	α	k	α	k	α	k	α	k
325	0.656	2.11	1.761	2.12	2.747	2.11	3.599	2.09	4.300	2.06	4.837	2.00	5.193	1.92
350	0.699	2.21	1.785	2.15	2.756	2.11	3.597	2.08	4.292	2.05	4.824	1.99	5.177	1.91
375	0.739	2.27	1.808	2.16	2.772	2.11	3.613	2.07	4.312	2.05	4.850	2.00	5.209	1.91
400	0.778	2.31	1.831	2.18	2.792	2.11	3.637	2.07	4.345	2.05	4.894	2.00	5.262	1.91
425	0.816	2.33	1.855	2.18	2.813	2.11	3.666	2.07	4.387	2.05	4.949	2.01	5.328	1.92
450	0.854	2.34	1.878	2.19	2.836	2.11	3.698	2.08	4.434	2.06	5.012	2.02	5.402	1.93
475	0.892	2.35	1.901	2.19	2.860	2.11	3.733	2.08	4.485	2.07	5.080	2.03	5.484	1.94
500	0.929	2.36	1.924	2.19	2.884	2.12	3.769	2.09	4.539	2.07	5.153	2.04	5.571	1.96
525	0.966	2.35	1.947	2.19	2.910	2.12	3.807	2.09	4.596	2.08	5.229	2.05	5.661	1.97
550	1.003	2.35	1.970	2.19	2.935	2.12	3.847	2.10	4.654	2.09	5.308	2.07	5.756	1.99
575	1.039	2.34	1.994	2.19	2.962	2.13	3.887	2.11	4.715	2.10	5.389	2.08	5.853	2.00
600	1.076	2.33	2.017	2.19	2.988	2.13	3.929	2.12	4.777	2.11	5.473	2.09	5.953	2.02

© The British Standards Institution 2019

Table N.20 α and k defined with respect to T/σ_Y for n = 12

n = 12	m = 5		m = 7.5		m = 10		m = 12.5		m = 15		m = 17.5		m = 20	
E/σ_Y	α	k	α	k	α	k	α	k	α	k	α	k	α	k
300	0.630	2.05	1.792	2.14	2.916	2.19	3.958	2.20	4.872	2.18	5.616	2.13	6.143	2.05
325	0.670	2.15	1.810	2.17	2.925	2.18	3.968	2.19	4.895	2.18	5.660	2.14	6.220	2.05
350	0.710	2.22	1.831	2.19	2.940	2.18	3.988	2.19	4.929	2.18	5.713	2.14	6.294	2.06
375	0.750	2.26	1.853	2.20	2.959	2.18	4.014	2.19	4.968	2.19	5.770	2.15	6.367	2.06
400	0.790	2.30	1.876	2.21	2.979	2.18	4.043	2.19	5.012	2.19	5.829	2.16	6.440	2.07
425	0.830	2.33	1.899	2.22	3.001	2.18	4.074	2.19	5.057	2.20	5.890	2.17	6.511	2.08
450	0.870	2.35	1.923	2.23	3.024	2.19	4.106	2.19	5.105	2.20	5.952	2.18	6.583	2.09
475	0.909	2.36	1.946	2.23	3.047	2.19	4.140	2.19	5.154	2.21	6.016	2.19	6.654	2.10
500	0.949	2.37	1.970	2.24	3.071	2.19	4.175	2.20	5.204	2.22	6.080	2.20	6.724	2.11
525	0.989	2.38	1.994	2.24	3.096	2.19	4.211	2.20	5.255	2.22	6.145	2.21	6.795	2.12
550	1.028	2.39	2.018	2.24	3.122	2.20	4.248	2.21	5.308	2.23	6.210	2.22	6.865	2.13
575	1.068	2.39	2.043	2.24	3.147	2.20	4.285	2.21	5.360	2.24	6.276	2.23	6.935	2.15

Table N.21 α and k defined with respect to T/σ_Y for n = 13

n = 13	m = 5		m = 7.5		m = 10		m = 12.5		m = 15		m = 17.5		m = 20	
E/σ_Y	α	k	α	k	α	k	α	k	α	k	α	k	α	k
275	0.603	1.98	1.816	2.15	3.074	2.26	4.306	2.31	5.438	2.30	6.398	2.26	7.112	2.18
300	0.642	2.09	1.830	2.18	3.083	2.25	4.328	2.30	5.488	2.31	6.491	2.28	7.261	2.19
325	0.683	2.17	1.849	2.20	3.098	2.25	4.352	2.30	5.534	2.31	6.567	2.29	7.371	2.20
350	0.724	2.22	1.869	2.22	3.115	2.25	4.379	2.29	5.579	2.32	6.633	2.30	7.460	2.21
375	0.765	2.27	1.891	2.23	3.134	2.25	4.407	2.29	5.622	2.32	6.694	2.31	7.535	2.22
400	0.807	2.31	1.914	2.25	3.154	2.25	4.435	2.29	5.665	2.33	6.750	2.32	7.600	2.22
425	0.848	2.34	1.938	2.26	3.176	2.25	4.464	2.29	5.706	2.33	6.803	2.33	7.658	2.23
450	0.890	2.37	1.962	2.26	3.198	2.26	4.494	2.30	5.747	2.34	6.854	2.33	7.710	2.24
475	0.933	2.39	1.987	2.27	3.220	2.26	4.524	2.30	5.788	2.34	6.903	2.34	7.758	2.24
500	0.975	2.41	2.012	2.28	3.244	2.26	4.555	2.30	5.829	2.35	6.949	2.35	7.801	2.25
525	1.017	2.43	2.037	2.29	3.268	2.26	4.586	2.30	5.869	2.35	6.994	2.35	7.840	2.25
550	1.059	2.44	2.063	2.29	3.292	2.26	4.617	2.30	5.909	2.35	7.038	2.36	7.877	2.26

© The British Standards Institution 2019

Table N.22 α and k defined with respect to T/σ_Y for n = 14

n = 14	m = 5		m = 7.5		m = 10		m = 12.5		m = 15		m = 17.5		m = 20	
E/σ_Y	α	k	α	k	α	k	α	k	α	k	α	k	α	k
250	0.576	1.92	1.835	2.17	3.225	2.32	4.644	2.41	5.993	2.42	7.169	2.39	8.072	2.30
275	0.615	2.03	1.845	2.20	3.234	2.32	4.676	2.40	6.066	2.43	7.301	2.41	8.276	2.32
300	0.655	2.11	1.861	2.22	3.247	2.32	4.704	2.40	6.124	2.44	7.397	2.43	8.414	2.34
325	0.697	2.18	1.880	2.24	3.263	2.32	4.731	2.40	6.172	2.45	7.472	2.44	8.516	2.34
350	0.740	2.24	1.901	2.25	3.280	2.32	4.758	2.40	6.215	2.45	7.533	2.45	8.593	2.35
375	0.783	2.29	1.924	2.27	3.299	2.32	4.783	2.39	6.253	2.45	7.584	2.45	8.652	2.36
400	0.827	2.33	1.948	2.28	3.318	2.32	4.808	2.39	6.288	2.46	7.627	2.46	8.697	2.36
425	0.871	2.37	1.973	2.29	3.338	2.32	4.833	2.39	6.320	2.46	7.665	2.46	8.731	2.36
450	0.916	2.41	1.998	2.31	3.359	2.32	4.857	2.39	6.350	2.46	7.697	2.47	8.756	2.36
475	0.960	2.44	2.025	2.32	3.380	2.32	4.881	2.39	6.378	2.46	7.725	2.47	8.774	2.36
500	1.005	2.47	2.051	2.33	3.402	2.32	4.904	2.39	6.404	2.46	7.749	2.47	8.785	2.36
525	1.050	2.50	2.079	2.34	3.424	2.32	4.928	2.38	6.429	2.46	7.770	2.47	8.790	2.36

Table N.23 α and k defined with respect to T/σ_Y for n = 15

n = 15	m = 5		m = 7.5		m = 10		m = 12.5		m = 15		m = 17.5		m = 20	
E/σ_Y	α	k	α	k	α	k	α	k	α	k	α	k	α	k
200	0.519	1.69	1.865	2.13	3.369	2.39	4.909	2.50	6.364	2.51	7.612	2.45	8.531	2.37
225	0.549	1.86	1.851	2.18	3.368	2.39	4.970	2.50	6.526	2.54	7.907	2.51	8.984	2.42
250	0.587	1.97	1.856	2.21	3.376	2.38	5.011	2.50	6.622	2.55	8.075	2.54	9.233	2.44
275	0.628	2.06	1.869	2.23	3.388	2.38	5.043	2.50	6.692	2.56	8.191	2.55	9.398	2.46
300	0.671	2.14	1.886	2.25	3.402	2.38	5.071	2.50	6.745	2.57	8.275	2.57	9.513	2.47
325	0.715	2.20	1.906	2.27	3.418	2.38	5.096	2.49	6.787	2.57	8.338	2.58	9.595	2.47
350	0.759	2.26	1.929	2.29	3.434	2.38	5.118	2.49	6.821	2.57	8.385	2.58	9.652	2.48
375	0.805	2.32	1.953	2.31	3.452	2.38	5.138	2.48	6.849	2.57	8.421	2.59	9.690	2.48
400	0.851	2.37	1.978	2.32	3.470	2.38	5.157	2.48	6.872	2.57	8.447	2.59	9.712	2.48
425	0.898	2.42	2.005	2.34	3.489	2.38	5.175	2.48	6.891	2.57	8.465	2.59	9.722	2.47
450	0.945	2.47	2.033	2.35	3.508	2.38	5.192	2.47	6.907	2.56	8.476	2.59	9.721	2.47
475	0.992	2.51	2.061	2.36	3.527	2.38	5.207	2.47	6.919	2.56	8.481	2.59	9.710	2.47
500	1.039	2.55	2.091	2.38	3.547	2.37	5.222	2.46	6.929	2.56	8.481	2.58	9.692	2.46

© The British Standards Institution 2019

Table N.24 α and k defined with respect to T/σ_Y for n = 16

n = 16	m = 5		m = 7.5		m = 10		m = 12.5		m = 15		m = 17.5		m = 20	
E/σ_Y	α	k	α	k	α	k	α	k	α	k	α	k	α	k
175	0.496	1.64	1.889	2.15	3.502	2.45	5.194	2.58	6.818	2.61	8.232	2.55	9.292	2.47
200	0.523	1.79	1.865	2.18	3.503	2.45	5.277	2.59	7.025	2.64	8.587	2.61	9.803	2.52
225	0.560	1.90	1.864	2.21	3.511	2.44	5.329	2.59	7.147	2.66	8.793	2.65	10.10	2.55
250	0.600	2.00	1.873	2.24	3.521	2.44	5.367	2.59	7.230	2.67	8.931	2.67	10.29	2.57
275	0.643	2.08	1.887	2.26	3.534	2.44	5.397	2.59	7.291	2.68	9.029	2.68	10.43	2.58
300	0.688	2.16	1.906	2.29	3.548	2.44	5.421	2.58	7.335	2.68	9.099	2.69	10.52	2.58
325	0.734	2.23	1.928	2.31	3.562	2.44	5.440	2.58	7.368	2.68	9.149	2.70	10.59	2.58
350	0.781	2.30	1.953	2.33	3.577	2.44	5.457	2.57	7.391	2.68	9.182	2.70	10.63	2.58
375	0.829	2.36	1.979	2.34	3.593	2.43	5.470	2.57	7.407	2.68	9.202	2.70	10.65	2.58
400	0.878	2.43	2.007	2.36	3.610	2.43	5.482	2.56	7.417	2.67	9.211	2.70	10.66	2.58
425	0.927	2.49	2.036	2.38	3.627	2.43	5.491	2.55	7.422	2.67	9.211	2.70	10.65	2.57
450	0.976	2.54	2.066	2.40	3.644	2.43	5.499	2.54	7.422	2.66	9.204	2.69	10.64	2.56

Table N.25 α and k defined with respect to T/σ_Y for n = 17

n = 17	m = 5		m = 7.5		m = 10		m = 12.5		m = 15		m = 17.5		m = 20	
E/σ_Y	α	k	α	k	α	k	α	k	α	k	α	k	α	k
150	0.476	1.58	1.917	2.16	3.628	2.50	5.444	2.66	7.201	2.69	8.736	2.63	9.884	2.55
175	0.498	1.72	1.879	2.19	3.630	2.50	5.557	2.67	7.467	2.73	9.167	2.70	10.46	2.60
200	0.532	1.83	1.869	2.22	3.637	2.50	5.625	2.68	7.623	2.76	9.422	2.74	10.81	2.63
225	0.572	1.93	1.872	2.24	3.646	2.50	5.671	2.68	7.728	2.77	9.594	2.77	11.05	2.65
250	0.614	2.02	1.884	2.27	3.657	2.50	5.706	2.68	7.801	2.78	9.716	2.79	11.22	2.66
275	0.659	2.11	1.901	2.29	3.669	2.49	5.731	2.67	7.853	2.79	9.803	2.80	11.35	2.67
300	0.706	2.19	1.922	2.32	3.682	2.49	5.750	2.66	7.889	2.79	9.864	2.81	11.44	2.67
325	0.754	2.27	1.946	2.34	3.695	2.49	5.763	2.66	7.913	2.78	9.906	2.81	11.50	2.67
350	0.804	2.34	1.973	2.36	3.709	2.48	5.773	2.65	7.926	2.78	9.930	2.81	11.55	2.67
375	0.854	2.42	2.002	2.38	3.723	2.48	5.779	2.64	7.931	2.77	9.941	2.81	11.57	2.67
400	0.905	2.49	2.033	2.41	3.737	2.48	5.782	2.63	7.929	2.76	9.941	2.81	11.58	2.66
425	0.956	2.56	2.065	2.43	3.752	2.48	5.782	2.62	7.920	2.76	9.931	2.80	11.58	2.66

© The British Standards Institution 2019

Table N.26 α and k defined with respect to T/σ_Y for n = 18

n = 18	m = 5		m = 7.5		m = 10		m = 12.5		m = 15		m = 17.5		m = 20	
E/σ_Y	α	k	α	k	α	k	α	k	α	k	α	k	α	k
125	0.464	1.53	1.963	2.17	3.741	2.54	5.625	2.71	7.441	2.74	9.016	2.67	10.18	2.58
150	0.476	1.64	1.898	2.19	3.744	2.55	5.789	2.74	7.806	2.80	9.571	2.76	10.86	2.64
175	0.505	1.74	1.874	2.21	3.751	2.55	5.883	2.75	8.017	2.84	9.900	2.81	11.28	2.68
200	0.541	1.84	1.869	2.24	3.760	2.55	5.946	2.76	8.158	2.86	10.13	2.84	11.58	2.70
225	0.582	1.94	1.874	2.26	3.770	2.54	5.990	2.75	8.258	2.87	10.29	2.87	11.82	2.72
250	0.627	2.03	1.888	2.29	3.781	2.54	6.022	2.75	8.328	2.88	10.42	2.88	12.00	2.73
275	0.673	2.12	1.907	2.31	3.792	2.54	6.044	2.74	8.378	2.88	10.51	2.89	12.15	2.74
300	0.722	2.21	1.930	2.34	3.803	2.54	6.058	2.74	8.410	2.88	10.58	2.90	12.27	2.75
325	0.772	2.30	1.957	2.37	3.815	2.53	6.066	2.73	8.430	2.88	10.62	2.91	12.37	2.75
350	0.823	2.39	1.987	2.39	3.828	2.53	6.070	2.72	8.437	2.87	10.66	2.91	12.45	2.75
375	0.876	2.47	2.020	2.42	3.840	2.53	6.069	2.70	8.436	2.86	10.67	2.91	12.51	2.75
400	0.929	2.56	2.054	2.44	3.853	2.52	6.064	2.69	8.426	2.85	10.68	2.91	12.56	2.75

Table N.27 α and k defined with respect to T/σ_Y for n = 19

n = 19	m = 5		m = 7.5		m = 10		m = 12.5		m = 15		m = 17.5		m = 20	
E/σ_Y	α	k	α	k	α	k	α	k	α	k	α	k	α	k
100	0.521	1.62	2.149	2.23	3.881	2.57	5.591	2.70	7.150	2.68	8.431	2.59	9.307	2.49
125	0.485	1.55	1.974	2.19	3.898	2.58	5.961	2.77	7.865	2.80	9.313	2.69	10.01	2.49
150	0.488	1.57	1.894	2.18	3.913	2.59	6.170	2.81	8.286	2.86	9.886	2.76	10.59	2.52
175	0.509	1.62	1.853	2.19	3.927	2.60	6.312	2.84	8.586	2.91	10.33	2.82	11.13	2.55
200	0.539	1.69	1.836	2.21	3.941	2.60	6.414	2.85	8.815	2.95	10.70	2.87	11.63	2.60
225	0.576	1.77	1.834	2.23	3.954	2.60	6.491	2.86	8.995	2.98	11.02	2.91	12.12	2.64
250	0.618	1.87	1.843	2.25	3.967	2.60	6.548	2.87	9.140	3.00	11.30	2.96	12.59	2.69
275	0.664	1.97	1.861	2.28	3.980	2.60	6.589	2.87	9.258	3.02	11.56	3.00	13.05	2.74
300	0.712	2.08	1.887	2.32	3.993	2.60	6.618	2.87	9.353	3.03	11.78	3.03	13.50	2.80
325	0.764	2.19	1.918	2.35	4.005	2.60	6.638	2.86	9.430	3.05	11.99	3.07	13.95	2.85
350	0.817	2.31	1.955	2.39	4.018	2.60	6.648	2.86	9.491	3.06	12.19	3.11	14.39	2.91
375	0.872	2.43	1.996	2.43	4.030	2.60	6.652	2.85	9.539	3.06	12.37	3.14	14.82	2.97

© The British Standards Institution 2019

Table N.28 α and k defined with respect to T/σ_Y for n = 20

n = 20	m = 5		m = 7.5		m = 10		m = 12.5		m = 15		m = 17.5		m = 20	
E/σ_Y	α	k	α	k	α	k	α	k	α	k	α	k	α	k
125	0.463	1.56	1.941	2.19	3.840	2.58	5.913	2.78	7.918	2.82	9.608	2.76	10.74	2.62
150	0.480	1.64	1.888	2.20	3.848	2.58	6.063	2.80	8.237	2.88	10.07	2.82	11.28	2.66
175	0.509	1.72	1.865	2.22	3.857	2.58	6.161	2.81	8.451	2.91	10.40	2.87	11.69	2.69
200	0.546	1.81	1.860	2.24	3.868	2.58	6.229	2.82	8.604	2.93	10.65	2.90	12.03	2.71
225	0.587	1.90	1.865	2.27	3.878	2.58	6.278	2.82	8.717	2.95	10.85	2.93	12.33	2.74
250	0.632	2.00	1.880	2.29	3.889	2.58	6.312	2.82	8.801	2.96	11.01	2.95	12.59	2.76
275	0.680	2.10	1.900	2.32	3.899	2.58	6.335	2.81	8.862	2.96	11.14	2.97	12.82	2.78
300	0.730	2.20	1.926	2.35	3.911	2.57	6.349	2.80	8.905	2.96	11.24	2.99	13.03	2.80
325	0.781	2.30	1.956	2.38	3.922	2.57	6.355	2.79	8.933	2.96	11.33	3.00	13.23	2.82
350	0.834	2.40	1.990	2.41	3.933	2.57	6.356	2.78	8.948	2.96	11.40	3.01	13.41	2.83
375	0.889	2.51	2.026	2.44	3.944	2.56	6.351	2.77	8.953	2.95	11.46	3.02	13.57	2.85
400	0.944	2.61	2.066	2.47	3.956	2.56	6.341	2.76	8.948	2.95	11.50	3.02	13.73	2.87

Bibliography for Annex N

Standards publications

For dated references, only the edition cited applies. For undated references, the latest edition of the referenced document (including any amendments) applies.

BS 7448-1, *Fracture mechanics toughness tests – Method for determination of KIc, critical CTOD and critical J values of metallic materials*

BS ISO 27306, *Metallic materials – Method of constraint loss correction of CTOD fracture toughness for fracture assessment of steel components*

BS 8571, *Method of test for determination of fracture toughness in metallic materials using single edge notched tension (SENT) specimens*

BS EN ISO 15653, *Metallic materials – Method of test for the determination of quasistatic fracture toughness of welds*

ASTM E1820, *Standard test method for measurement of fracture toughness*

ASTM E1921, *Standard test method for determination of reference temperature, T_o, for ferritic steels in the transition range*

Other documents

[N.1] HADLEY, I. and HORN, A. Treatment of constraint in BS 7910:2013, ISO 27306 and DNVGL-RP-F108, *In: International Journal of Pressure Vessels and Piping*, 169, January 2019, 77–93. <https://doi.org/10.1016/j.ijpvp.2018.11.015>

[N.2] SOREM, W.A., DODDS, R.H. and ROLFE, S.T. Effects of crack depth on elastic plastic fracture toughness. *In: International Journal of Fracture*, 1991, 47(2), 105–126.

[N.3] LANDES, J.D., McCABE, D.E. and ERNST, H.A. *Geometry effects on the R-curve. In:* J.D. LANDES, A. SAXENA and J.G. MERKLE, eds. *non-linear fracture mechanics: Volume 2 – Elastic Plastic Fracture*, 1989, ASTM STP 905, 123–143.

[N.4] SUMPTER, J.D.G. and HANCOCK, J.W. Status review of the *J* plus *T* stress fracture analysis method. *In:* K-H. SCHWALBE and C. BERGERS, eds. *Proceedings of the 10th European Conference on Fracture.* Vol I, 617–626. Warley, UK: EMAS, 1994.

[N.5] SCHWALBE, K.H. and HEERENS, J. R-curve testing and relevance to structural assessment. *In: Fatigue and Fracture Engineering Materials and Structures*, 1998, 21(10), 1259-1271.

[N.6] LIDBURY, D.P.G., BIRKETT, R.P. and BEARDSMORE, D.W. *Validation of transition temperature behaviour in fullsize components*. AEA Technology Report 0802. 1997.

[N.7] HANCOCK, J.W., REUTER, W.G. and PARKS, D.M. Constraint and toughness parameterized by *T*. *In:* E.M. HACKETT, K-H. SCHWALBE and R.H. DODDS, eds. *Constraint Effects in Fracture.* ASTM STP, 2003, 1171, 21–40.

[N.8] BURSTOW, M.C. and HOWARD, I.C. Predicting the effects of crack tip constraint on material resistance curves using ductile damage theory. *In: Fatigue and Fracture Engineering Materials and Structures*, 1996, 19(4), 461–474.

[N.9] SHERRY, A.H., SANDERSON, D.J., LIDBURY, D.P.G., AINSWORTH, R.A. and KIKUCHI, K. The application of local approach to assess the influence of in-plane constraint on cleavage fracture. ASME Pressure Vessels and Piping Conference. *In: ASME PVP*, 1995, 304, 495–501.

[N.10] O'DOWD, N.P. and SHIH, C.F. Family of crack tip fields characterised by a triaxiality parameter: Part II – Fracture applications. *In: Journal of the Mechanics and Physics of Solids*, 1992, 40(5), 939–963.

[N.11] AINSWORTH, R.A. and O'DOWD, N.P. Constraint in the failure assessment diagram approach for fracture assessment. *In: ASME Journal of Pressure Vessel Technology*, 1995, 117(3), 260–267.

[N.12] MacLENNAN, I. and HANCOCK, J.W. Constraint based failure assessment diagrams. *In: Proceedings of the Royal Society London*, 1995, A451, 757–777.

[N.13] AINSWORTH, R.A. *Constraint effects in R6 for combined primary and secondary stresses*. Nuclear Electric Report EPD/GEN/REP/0013/96. 199.

[N.14] AINSWORTH, R. A., SANDERSON, D.J., HOOTON, D.G. and SHERRY, A.H. Constraint effects in R6 for combined primary and secondary stresses. ASME Pressure Vessels and Piping Conference, Montreal, *In: ASME Pressure Vessels and Piping Conference*, 1996, Volume 324.

[N.15] SATTARI-FAR, I. *Solutions of constraint parameters Q, Q_m and H in SEN(B) and SEN(T) Specimens*, SAQ Report SINTAP/SAQ/01. 1996.

[N.16] SHERRY, A.H., FRANCE, C.C. and GOLDTHORPE, M.R. Compendium of *T*-stress solutions for two and three dimensional cracked geometries. *In: Fatigue and Fracture Engineering Materials and Structures*, 1995, 18(1), 141–155.

[N.17] LEEVERS P.S. and RADON, J.C. Inherent stress biaxiality in various fracture specimen geometries. *In: International Journal of Fracture (IJF)*, 1982, 19, 311–325.

[N.18] SANDERSON, D.J., SHERRY, A.H. and O'DOWD, N.P. *Compendium of β solutions for use with the R6 modified framework*. AEA Report AEA-TSD-0981. 1996.

[N.19] O'DOWD, N.P. and SHIH, C.F. Family of crack tip fields characterised by a triaxiality parameter: Part I – Structure of fields. *In: Journal of the Mechanics and Physics of Solids*, 1991, 39(8), 989–1015.

[N.20] O'DOWD, N.P. and SHIH, C.F. Two-parameter fracture mechanics: theory and applications. *In: Proceedings of ASTM 24th National Symposium on Fracture Mechanics*, Gatlinburg, Tennessee, USA. 1992.

[N.21] SATTARI-FAR, I. *Solutions of constraint parameters Q, Q_m and H in surface cracked plates under uniaxial and biaxial loading*. SAQ Report SINTAP/SAQ/04. 1997.

[N.22] SATTARI-FAR, I. *Solutions of constraint parameters Q, Q_m and H for surface cracks in cylinders under internal pressure and combined internal pressure and thermal load*. SAQ Report SINTAP/SAQ/07. 1998.

[N.23] SATTARI-FAR, I. *Solutions of constraint parameters Q, Q_m and H in different cracked geometries*. SAQ Report SINTAP/SAQ/08. 1998.

[N.24] WALLIN, K. Quantifying T_{stress} controlled constraint by the Master Curve Transition Temperature T_0. *In: Engineering Fracture Mechanics*, 2001, 68(3), 303–328.

[N.25] SHERRY, A.H. *Constraint effects on fracture assessment within an R6 framework*. AEA Report AEA RS 4544. 1994.

[N.26] GAO, X., RUGGIERI, C. and DODDS, R.H. Calibration of Weibull stress parameters using fracture toughness data. *In: International Journal of Fracture*, 1998, 92(2), 175–200.

[N.27] GOLDTHORPE, M.R. and WIESNER, C.S. *Microchemical predictions of fracture toughness for pressure vessel steel using a coupled model*. ASTM STP 1332. 1998.

[N.28] SHERRY, A.H., WILKES, M.A., BEARDSMORE, D.W. and LIDBURY, D.P.G. Material Constraint Parameters for the Assessment of Shallow Defects in Structural Components – Part I: Parameter Solutions. *In: Engineering Fracture Mechanics*, 2005, 72(15), 2396–2415.

[N.29] ZHANG, Z., XU, J., NYHUS, B. and ØSTBY, E. SENT (single edge notch tension) methodology for pipeline applications. *In: European Conference on Fracture*, ECF18, Aug 29 – Sep 03, 2010, Dresden, Germany.

[N.30] BILBY, B.A., HOWARD, I.C. and LI, Z.H. Failure assessment diagrams I: the tangency condition for ductile tearing instability. *In: Proceedings of the Royal Society London*, 1994, A444, 461–482.

[N.31] BILBY, B.A., HOWARD, I.C. and LI, Z.H. Failure assessment diagrams IV: the inclusion of constraint parameters. *In: Proceedings of the Royal Society London*, 1995, A448, 281–291.

[N.32] BILBY, B.A., HOWARD, I.C. and LI, Z.H. The use of constraint-modified failure assessment lines in failure assessment diagrams. *In: International Journal of Fracture*, 1996, 75(4), 323–334.

[N.33] HARLIN, G. and WILLIS, J.R. The influence of crack size on the ductile-brittle transition. *In: Proceedings of the Royal Society London*, 1988, A415, 197–226.

[N.34] FETT, T. *T*-Stresses in rectangular plates and circular disks. *In: Engineering Fracture Mechanics*, 1998, 60(5–6), 631–652.

[N.35] PATEL, R.D. *Determination of β_T solutions for various geometries using elastic finite element analyses*. British Energy Report E/REP/ATEC/0040/GEN/02. 2002.

[N.36] MILLER, A. G. Review of Limit Loads of Structures Containing Defects. *In: International Journal of Pressure Vessel and Piping*, 1988, 32(1–4), 197–327.

[N.37] AINSWORTH, R.A. A constraint-based failure assessment diagram for fracture assessment. *In: International Journal of Pressure Vessels and Piping*, 1995, 64, 277–285.

[N.38] WANG, X. Elastic *T*-stress solutions for semi-elliptical surface cracks in finite thickness plates. *In: Engineering Fracture Mechanics*, 2003, 70(6), 731–756.

[N.39] R5 PANEL. *R5 Assessment Procedure for the High Temperature Response of Structures (as amended)*. Report R5, Issue 3, UK: EDF Energy, 2014.

[N.40] PATEL, R.D. *Determination of β_T solutions for various geometries using elastic finite element analyses – Part II*. British Energy Report E/REP/BDBB/0019/GEN/03. 2003.

[N.41] HUH, N.S. Elastic *T* stress estimates for circumferential surface-cracked cylinders. *In: Fatigue and Fracture Engineering Materials and Structures*, 2006, 29(1), 57–69.

[N.42] LIDBURY, D.P.G. Validation of constraint based methodology in structural integrity – Project overview and update. *In: Proceedings of ASME Pressure Vessels and Piping Conference*, 2005, San Diego, USA.

[N.43] LIDBURY, D.P.G., SHERRY, A.H., BASS, B.R., GILLES, P., CONNORS, D., EISELE, U., KEIM, E., KEINANEN, H., WALLIN, K., LAUEROVA, D., MARIE, S., NAGEL, G., NILSSON, K., SIEGELE, D. and WADIER, Y. Validation of constraint-based methodology in structural integrity of ferritic steels for nuclear reactor pressure vessels. *In: Fatigue and Fracture of Engineering Materials and Structures*, 2006, 29(9–10), 829–849.

[N.44] BEREMIN, F.M. A local criterion for cleavage fracture of a nuclear pressure vessel steel. *In: Metallurgical Transactions*, 1983, Volume 14A, 2277–2287.

[N.45] RUGGIERI, C., GAO, X. and DODDS, R.H. Transferability of elastic-plastic fracture toughness using the Weibull stress approach: significance of parameter calibration. *In: Engineering Fracture Mechanics*, 2000, 67(2), 101–117.

[N.46] WASILUK, B., PETTI, J.P. and DODDS, R.H. Temperature dependence of Weibull stress parameters: Studies using the Euro-material. *In: Engineering Fracture Mechanics*, 2006, 73(8), 1046–1069.

[N.37] SEAL, C.K. and SHERRY, A.H. Predicting the effect of constraint on cleavage and ductile fracture toughness using area contour toughness scaling. *In: Engineering Fracture Mechanics*, 2017, 186, 347–367.

Annex O (informative)

Consideration of proof testing and warm prestressing

O.0 Symbols and definitions

For the purposes of this annex, the following symbols, definitions and units apply, unless otherwise indicated at the point of use.

Symbol	Definition	Units
a_{proof}	Maximum flaw size which would have survived proof test	mm
E'	Elastic modulus corrected for constraint conditions, $E' = E$ for plane stress, $E' = E/(1 - \nu^2)$ for plane strain	N/mm^2
J	Line or surface integral that encloses the crack front from one crack surface to the other, used to characterize the local stress-strain field around the crack tip	N/mm
K_f	Stress intensity factor at failure	N/mm$^{3/2}$
K_I	Applied tensile (mode I) stress intensity factor (SIF)	N/mm$^{3/2}$
K_J	fracture toughness derived from J-integral	N/mm$^{3/2}$
K_{mat}	Material fracture toughness measured by stress intensity factor	N/mm$^{3/2}$
K_r	Fracture ratio of applied elastic K value to K_{mat}	—
K_1	Stress intensity factor following preload	N/mm$^{3/2}$
K_2	Stress intensity factor following unload	N/mm$^{3/2}$
L	Load	—
L_r	Ratio of applied load to yield load	—
T_1	Temperature at preload	°C
T_2	Temperature at reload	°C
β	Plasticity correction factor, $\beta = 1$ for plane stress, $\beta = 3$ for plane strain	—
ΔK_R	Additional stress intensity factor at failure due to reload	N/mm$^{3/2}$
ΔK_u	SIF decrement (equal to $K_f - K_2$) due to unloading during warm prestressing; additional SIF at failure due to reload	N/mm$^{3/2}$
σ_a	Applied stress	N/mm^2
σ'_f	Appropriate value of flow strength at the assessment temperature	N/mm^2
σ_{ref}	Reference stress used for creep and plastic consideration; it is sometimes calculated from plane strain von Mises limit load as in Annex N	N/mm^2
σ_Y	Lower yield strength or 0.2% proof strength	N/mm^2
σ'_Y	Yield strength of the material in the vicinity of the flaw, as defined in **7.2.4**	N/mm^2
σ_{Y1}	Yield strength at preload conditions	N/mm^2

O.1 General

This annex, based predominantly on Chapter III.10 of R6 [O.1], describes how the loading history due to a) proof or overload tests or b) warm prestressing of a structure containing flaws can be taken into account when performing an integrity assessment using the procedures in Clause **7**. The effect of loading history is quantified with regard to mechanical relaxation of residual stresses and enhancement of lower shelf fracture resistance. The latter is only applicable when the preload constitutes a warm prestress.

The procedures set out in this annex enable these effects to be quantified. In practice, the different phenomena can interact and it might not be possible to separate the different effects simply.

Extended flaws and conventional high-constraint fracture toughness data derived using the methods of **7.1.4** are generally assumed in the procedures of this annex. Changes in the shape of the flaw as it extends are not considered. The effects of low constraint, for example short flaws under predominantly tension loading, or weld mismatch may, in principle, be taken into account when assessing the effects of a proof test using the methods in Annex N and Annex I, respectively. Similarly, the effects of flaw shape changes may also be considered. However, in these cases consideration needs to be given at each stage of the procedure so as to elucidate the effects, and sensitivity studies should be conducted to assess the overall conservatism of the assessment.

O.2 Proof or overload testing

A "proof test" is taken to mean any overload test on a component which is performed to provide assurance of integrity during subsequent operation at a lower load ([O.2] to [O.4]). The main potential benefits of a proof test either at start-of-life or following a period of service can be summarized as:

a) some confirmation that the intent of the quality assurance programme used in construction has been realized;

b) some assurance of future safe operation;

c) mechanical stress relief of residual stresses;

d) formation of residual compressive zones at stress raisers; and

e) the exclusion of certain flaw size and materials property combinations.

These potential benefits can be eroded in service by material degradation as a consequence of the operating environment or by the presence of stresses dissimilar to those in the proof test, as discussed in this subclause. A repeated proof test following a period of operation may be used to mitigate in-service degradation. The benefits of periodic proof tests increase when performed in conjunction with inspection.

For practical reasons, the proof test is often carried out at a temperature different from the service temperature. Hence, the descriptions "cold" proof test and "hot" proof test are used to describe the cases where the proof test temperature is lower or greater than, respectively, the subsequent service condition. The effects of different materials properties at these two temperatures should be taken into account in a proof test argument. Any change in materials properties between the time of the proof test and the subsequent assessment, that could occur due to irradiation, ageing, warm prestressing (see **O.4**) or other mechanisms, should be taken into account. However, any apparent enhancement of fracture toughness due to the effects of a warm prestress is only relevant in cases where the proof test is performed at temperatures above the ductile-to-brittle transition temperature and subsequent assessments correspond to brittle fracture. The effect of sub-critical crack growth due to fatigue, creep, ductile tearing or environmentally assisted cracking

mechanisms subsequent to the proof test should be taken into account when carrying out any in-service assessment using this annex. Significant damage or crack growth during a proof test can also undermine its potential benefits, and should be taken into account when performing an assessment [O.5]. The particular case of mechanical relief of welding residual stresses due to a proof test is discussed in **O.3**.

Proof test arguments are of greatest value when the loading in service is of a similar nature to that of the proof test. When the service stresses are due to other forms of loading, primary or secondary, the benefits of the proof test are less. For example, proof tests performed under mode II shear loading can lead to an apparent decrease in subsequent mode I toughness [O.6]. Thus, pressure vessels proof loaded under pressure or crane structures tested under dead weight are examples where a benefit from proof testing could be realized.

A use of a proof test argument is illustrated schematically in Figure O.1. Sensitivity studies comprise an important part of a proof test argument. Differing bounding assumptions are conservative in the various steps of the argument. The use of consistently conservative data is therefore likely to be unrealistic and overly conservative. Probabilistic methods are particularly attractive in treating this aspect. In particular, the following information can be derived from the proof test:

1) the size of flaw which could remain in the component and not have caused failure at the time of the proof test;

2) the amount of overload required to assure a given service life; and

3) an estimate of the original flaw size which would be limiting under subsequent assessment conditions; this is particularly useful in regions of plant where in-service inspection is impracticable.

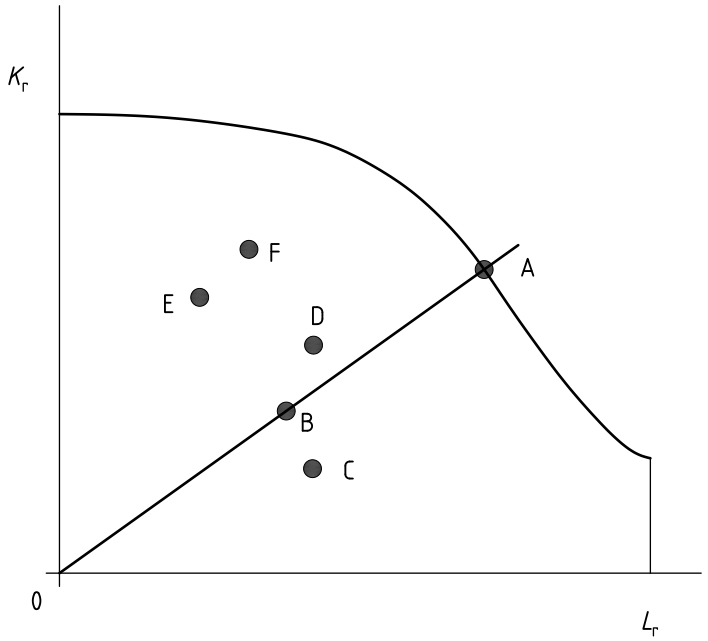
An alternative approach to take benefit from survival of a proof test may be used to quantify the assured service life assuming a flaw of the smallest detectable size at the time of the test. Growth of the flaw of this size in service may be considered.

The benefits of a proof test, in the case of steel nuclear reactor pressure vessels, tend to be less for newer vessels, due to a combination of modern high toughness materials, improved design and inspection and the range of possible fault conditions. The value of deterministic and probabilistic assessments of proof tests for older reactors constructed of lower toughness materials less susceptible to ductile crack growth at the proof test temperature has, however, been demonstrated.

The procedures in this annex are based on deterministic methods. Probabilistic approaches provide valuable additional support to deterministic analyses in quantifying proof test benefits. In particular they enable the effects of materials property assumptions at different steps of the procedures to be rationally treated, but estimates of the statistical distributions of the variable quantities are required.

The case of a single proof or overload test is considered here. Evidence suggests that multiple-cycle proof tests do not confer any additional benefit compared with a single load cycle within a deterministic analysis ([O.4], [O.7], [O.8]). However, multiple-cycle proof tests might be beneficial within a probabilistic framework in increasing the overall reliability [O.8] of a population. In particular, flaws initially slightly smaller than the maximum size of flaw which would have survived the proof test might then be detected.

Figure O.1 **Schematic illustration of a proof test argument**



Key

Point A	Assessment point at proof test conditions. This defines a_{proof}, the maximum size of flaw which would have survived the proof test
Point B	Assessment point for flaw of size a_{proof} and proof test materials properties at the normal operating load. A load margin is then 0A/0B
Point C	Assessment point for flaw of size a_{proof} and load and materials properties appropriate to normal operating conditions
Point D	Effect on Point C of including secondary loads
Point E	Effect on Point D of in-service property changes leading to reduction in K_{mat} and increase in σ_Y
Point F	Effect on Point E of in-service sub-critical crack growth. If point F is within the failure assessment curve, a proof test argument may be made

O.3 Relaxation of residual stress

In the assessment of a flawed component that has been proof tested, the residual stress level assumed in the fracture analysis should be taken [O.4] as a uniform stress equal to the lower of the following factors.

$$\sigma'_Y \text{ or } \left(1.4 - \frac{\sigma_{ref}}{\sigma'_f}\right)\sigma'_Y \qquad \text{(O.1)}$$

where:

σ_{ref} is the maximum reference stress under the proof load conditions (see **7.2.8**, **7.3.7** and Annex P);

σ'_Y is the appropriate material yield strength at the proof test temperature;

σ'_f is the flow strength (assumed to be the average of the yield and tensile strengths) at the proof test temperature.

The upper limit for σ_{ref} should be σ'_f and the lower limit should be 0.4 σ'_f.

The assumed residual stress level should always be greater than or equal to zero.

Where a flaw in a proof loaded structure is believed to have initiated during service, after the proof loading, the residual stress level in fracture analysis should be taken as a uniform stress equal to the lower of:

$$\sigma'_Y \text{ or } (1.1\sigma'_Y - 0.8\sigma_a) \quad \text{(O.2)}$$

where:

σ_a is the applied stress due to proof loads at the location of interest [O.7].

NOTE The equations above were derived from uniaxial loading and the extent of residual stress relief might be lower in biaxially loaded structures.

The upper limit for σ_a should be σ'_Y and the lower limit should be 0.3 σ'_Y.

The applied stress, σ_a, is a stress normal to the plane of the flaw and should be taken as the lower of the membrane stress in the section containing the location of interest, or the total stress at the location of interest including membrane, bending and stress concentration effects. The total stress can be lower than the membrane stress if the bending stress is negative or if there is a stress de-concentration effect, such as the convex side of a welded joint with angular misalignment.

O.4 Warm prestressing

O.4.1 General

This subclause is only applicable when used in conjunction with the fracture procedures in Clause **7**.

A warm prestress (WPS) is an initial preload applied to a ferritic structure containing a pre-existing flaw which is carried out at a temperature above the ductile-brittle transition temperature, and at a higher temperature or in a less-embrittled state than that corresponding to the subsequent service assessment. A WPS argument differs from a proof test argument in conferring added resistance to fracture under the assessment conditions; that is, it is considered to elevate the stress intensity factor at fracture, K_f, above the corresponding fracture toughness, K_{mat}, in the absence of the WPS ([O.4], [O.9] to [O.18]).

In service assessments using the procedure given in Clause **7**, the fracture toughness used in evaluating K_r is then taken as K_f.

There are three types of cycle which are conventionally used to demonstrate the WPS effect (Figure O.2). The temperatures at which the preload and reload to failure occur are denoted by T_1 and T_2, respectively, in each case. Similarly, the stress intensity factors due to the preload and following the unload are denoted K_1 and K_2 respectively.

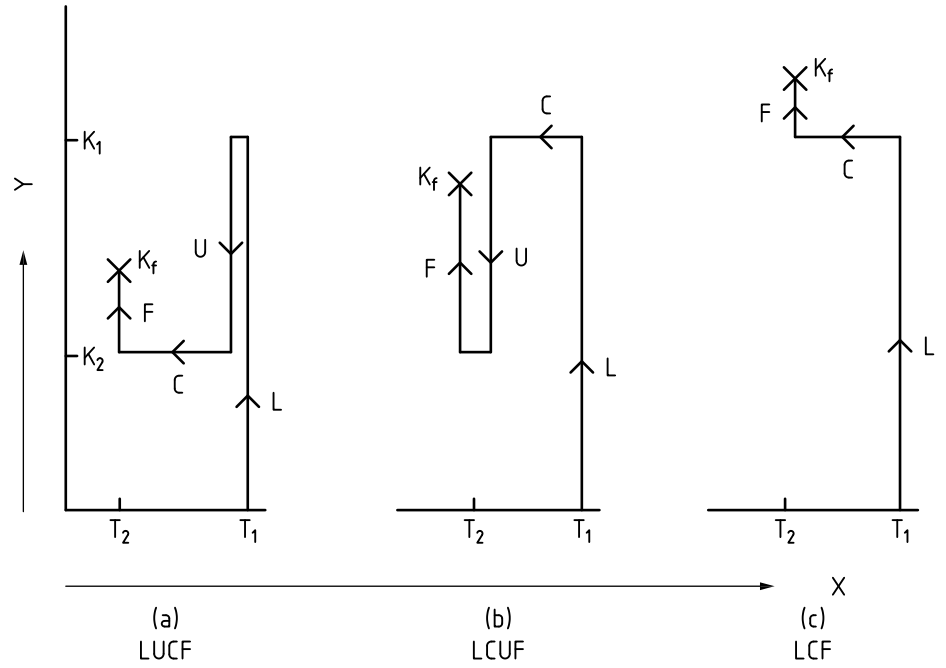
a) Load-Unload-Cool-Fracture (LUCF), where the structure is preloaded at temperature T_1 to stress intensity factor K_1, unloaded to stress intensity factor K_2, cooled to temperature T_2 and reloaded to fracture. The case where $T_2 = T_1$ is permissible if hardening mechanisms have occurred prior to the reload to fracture.

b) Load-Cool-Unload-Fracture (LCUF), where cooling to T_2 takes place prior to unloading and reloading to fracture.

c) Load-Cool-Fracture (LCF). This is similar to the LCUF cycle except that no unloading occurs prior to the imposition of extra load to fracture.

The greatest benefit in terms of maximizing K_f is given by the LCF cycle, the least by the LUCF cycle with full unloading. Intermediate forms of cycle, where partial unloading occurs prior to reloading to failure, and where the temperature and loading are simultaneously reduced, give benefits lying between these two limits.

Figure O.2 **Typical warm prestress cycles**



Key

L	Load	X	Temperature
U	Unload	Y	Stress intensity factor
C	Cool		
F	Fracture		

This subclause gives advice on quantifying the benefit of a WPS. Two levels of argument are set out:

1) a simplified, conservative approach; and

2) a more detailed calculational route which might be of value when the simplified route is insufficient.

For a WPS argument to be made according to the procedure given in this subclause, the following conditions should be met.

i) The failure mechanism at the service condition should be transgranular cleavage or intergranular brittle fracture ([O.4], [O.16]).

ii) The flow properties of the material should increase between the WPS and the service failure condition; this might be due to a decrease in temperature or due to in-service hardening.

iii) There should be no significant sub-critical crack growth between the WPS and the service failure condition. The amount of any such crack growth should be much less than the extent of the residual plastic zone following unloading ([O.7], [O.18]). Approximate formulae for estimating this plastic zone size are given in [O.9] to [O.11].

iv) The stress intensity factor, K_1, due to the WPS loading exceeds the fracture toughness, K_{mat}, at the reload condition.

v) Small-scale yielding conditions hold, i.e. $(K_I/\sigma_{Y1})^2/2\beta\pi$ is much less than the size of the uncracked ligament and any relevant structural dimensions. Here σ_{Y1} is the yield strength at the preload and β = 1 or 3 in-plane stress or plane strain, respectively. There is evidence ([O.3], [O.7], [O.11]) that, for increasing preloads, the benefits on the apparent reload fracture toughness lessen. Indeed, in the limit of extensive plasticity, the toughness might

actually be reduced compared to its value in the absence of the WPS. References [O.3], [O.11] give further advice in cases of large preloads.

vi) The preload and reload should be in the same direction; that is, both tensile or both compressive at the crack tip. A compressive preload followed by a tensile reload can reduce the apparent fracture toughness.

O.4.2 Simplified WPS argument

Failure is avoided if the stress intensity factor during cooling is constant or monotonically falling to a value K_2. This is often referred to as the "conservative warm prestressing principle". A benefit is obtained if K_2 exceeds the fracture toughness in the absence of a WPS, K_{mat}, and is consistent with maximum benefit from an LCF cycle. Margins against failure are not given by this simplified argument. In order to quantify margins it is necessary to use the detailed approach in **O.4.3**.

A particular example of this simplified WPS argument is in the assessment of thermal down-shocks, such as a pressurized thermal shock (PTS) transient in a steel nuclear reactor pressure vessel, where brittle fracture might otherwise be conceded ([O.4], [O.17]). The loading history during the thermal shock event is regarded as a WPS. It is argued that failure does not occur when the instantaneous stress intensity factor K_I exceeds the corresponding K_{mat} if K_I reduces with temperature. The maximum size of flaw which satisfies this criterion may then be compared with the size of the largest flaw which might have escaped detection to derive a margin on crack size. Any sub-critical growth of the latter flaw between inspection and the service assessment time should be allowed for.

Some experimental validation of the simplified WPS argument applied to pressurized thermal shock events is presented in [O.4] and [O.17].

O.4.3 Full WPS procedure

O.4.3.1 The procedure is based on the equations in [O.15]. It includes an interpolation between the bounding cases of LUCF with full unloading and the LCF cycle. The fracture toughness used in service assessments using the procedure of the main text is then K_f. The procedures in **O.4.3.2** to **O.4.3.5** should be carried out in quantifying the effect of the WPS on K_f for a given structural geometry and flaw dimensions.

O.4.3.2 Determine the temperature and loading corresponding to the WPS.

O.4.3.3 Determine the stress intensity factor decrement due to the unload, $\Delta K_u = K_1 - K_2$. It follows that ΔK_u is independent of the magnitude of any system or residual stresses incorporated in the total stress intensity factors K_1 and K_2 at the preload and unload phases, and depends on the contribution due to the varying load only.

O.4.3.4 Evaluate the fracture toughness, K_{mat}, of the material at the assessment time, but neglecting the effects of the WPS. The effects of any degrading mechanism, such as strain ageing or irradiation embrittlement which might have occurred between the time of the WPS and the subsequent assessment, should be taken into account. A lower bound value of K_{mat} should be adopted both for consistency with the procedures of Clause **7** and to conservatively predict the elevation in K_f [see Equation (O.3)].

O.4.3.5 Evaluate the stress intensity factor at failure from:

$$K_f = K_2 + \sqrt{K_{mat}\,\Delta K_u} + 0.15\,K_{mat} \qquad \text{(O.3)}$$

when $K_{mat} < \Delta K_u$.

If $K_{mat} \geq \Delta K_u$ the conditions $K_2 = K_1$ and $\Delta K_u = 0$ are imposed in Equation (O.3).

If the calculated $K_f \leq K_{mat}$ then no WPS benefit is estimated and $K_f = K_{mat}$. The value $\Delta K_R = K_f - K_2$ is the additional stress intensity factor at failure due to the reload.

No additional benefit should be claimed from repeated applications of a WPS as experimental data suggest no significant further effect ([O.7], [O.13]). Similarly, benefit should not be claimed from both residual stress reduction due to a WPS (**O.3**) and an apparent enhancement in K_f using this subclause ([O.7], [O.13]).

O.4.4 The WPS effect

The benefits of a WPS in thick-section components have been attributed [O.4] mainly to the establishment of a compressive residual stress zone ahead of the crack tip. However, the effects of crack-tip blunting and strain hardening have also been claimed as significant by a number of authors. Experimental demonstration of the WPS effect has been reported in many references ([O.4], [O.15], [O.17]) using both small specimen and feature tests. A number of alternative quantitative models of WPS benefits have been developed. These include both global models based on crack driving force ([O.3], [O.9] to [O.11]) and energetic [O.19] considerations, and local models ([O.4],[O.19],[O.20]) which use micro-mechanistic local approach methods. Validation of the model predictions against both specimen and large-scale test data is summarized in, for example, [O.4] and [O.17].

Issues of this annex prior to 2019 restricted the application of WPS to cleavage fracture, consistent with the conclusions of R6 [O.1]. However, it has been argued [O.4] that this restriction is unnecessary and that a WPS benefit both exists in the case of failure by stress-controlled intergranular brittle fracture mechanisms and can also be quantified using existing WPS models. There is experimental evidence for this assertion [O.16]. Hence the restriction on fracture mode has been relaxed at this issue.

Some applications of the simplified WPS argument in **O.4.2** have used the crack driving force $K_J = \sqrt{E'J}$ based on the elastic-plastic crack driving force J, rather than the elastic stress intensity factor, K_I. K_J was compared with the fracture toughness curve during the entire pressurized thermal shock event, enabling tearing under rising load to be excluded prior to WPS benefit on unloading. This usage is consistent with **O.4.2** as, for practical pressurized thermal shock histories, K_J decreases when K_I decreases on cooling.

Equation (O.3) was shown [O.15] to predict similar results to the detailed models in [O.9] to [O.11]. These detailed models include a dependence on yield stress. Approximate estimates of K_f may also be calculated using a simpler model [O.9] which does not contain an explicit dependence on yield stress. Similar simple and more complex expressions are also given in [O.3] and [O.12]. The simple models were recommended in the 2005 edition of BS 7910 and were based on consideration of the bounding LUCF cycle. Equation (O.3) allows for the range of cycles between LUCF and LCF to be considered. It was shown [O.15] to give a lower bound to a large body of test data when used with lower bound estimates of K_{mat}, and a good fit to the overall test data when using median toughness data.

The restriction to limit sub-critical crack growth between the WPS and loading to failure is based on modelling [O.18] and experimental observation ([O.4], [O.14]); under this condition no deleterious effect was found. When significant fatigue crack growth occurred by cycling to a lower load following unload to K_2, [O.15] showed that good agreement between Equation (O.3) and the experimental failure loads could be achieved for two particular test data by substituting K_2 for K_1. Use of the unmodified K_1 was non-conservative.

 © The British Standards Institution 2019

Bibliography for Annex O

Standards publications

There are no standards references in this annex.

Other documents

[O.1] R6 PANEL. *R6: Assessment of the integrity of structures containing defects*. Revision 4, as amended. Gloucester: EDF Energy, 2001.

[O.2] FORMBY, C.L. Use of the overpressure test to indicate fitness for purpose of a ferritic pressure vessel. *In: International Journal of Pressure Vessels and Piping*, 1985, 19, 47–68.

[O.3] SMITH, D.J. and GARWOOD, S.J. The significance of prior overload on fracture resistance:a critical review. *In: International Journal of Pressure Vessels and Piping*, 1990, 41, 255–296.

[O.4] LEGGATT, R.H. 1988. Investigations of proposed procedures for the inclusion of residual stresses in the revised fracture sections of PD 6493. *In: Proceedings of International Conference on Residual Stresses (ICRS2)*, Nancy, France, 23–25 November 1988.

[O.5] HALFORD, G.R. Over pressure proof factors for fatigue loaded pressure vessels. *In: ASME Pressure Vessels and Piping conference*, 1994, 290, 49–56.

[O.6] SWANKIE, T.D. and SMITH, D.J. Low temperature mixed mode fracture of a pressure vessel steel subject to prior loading. *In: Engineering Fracture Mechanics*, 1998, 61(3–4), 387–405.

[O.7] MUHAMMED, A. *The effect of prior overload and its application in structural integrity assessments*. TWI Report SINTAP/TWI/014. Cambridge: TWI, 1998.

[O.8] McCLUNG, R.C., CHELL, G.G., MILLWATER, H.R., RUSSELL, D.A. and ORIENT, G.E. *A comparison of single-cycle versus multiple-cycle proof testing strategies*. NASA Report NASA/CR1999209426. Springfield, Va.: National Technical Information Service, 1999.

[O.9] CHELL, G.G. and HAIGH, J.R. The effect of warm prestressing on proof tested pressure vessels. *In: International Journal of Pressure Vessels and Piping*, 1986, 23, 121–132.

[O.10] CHELL, G.G. Some fracture mechanics applications of warm prestressing to pressure vessels. *In: Proceedings of the 4th International Conference on Pressure Vessel Technology*, 1980, 1, 117–124.

[O.11] CHELL, G.G. and CURRY, D.A. Mechanics and mechanisms of cleavage fracture, Section 8 'Generalised loading'. *In: G.G. Chell, ed. Developments in fracture mechanics – 2*. 161177. London: Applied Science, 1981.

[O.12] SMITH, D.J. and GARWOOD, S.J. Application of theoretical methods to predict overload effects on fracture toughness of A533B. *In: International Journal of Pressure Vessels and Piping*, 1990, 41, 333–357.

[O.13] BURDEKIN, F.M. and LIDBURY, D.P.G. Views of TAGSI on the current position with regard to benefits of warm prestressing. *In: International Journal of Pressure Vessels and Piping*, 1999, 76, 885–890.

[O.14] FOWLER, H.J. *The influence of warm prestressing and proof loading on the cleavage fracture toughness of ferritic steels*. PhD Thesis, University of Bristol, 1998.

[O.15] WALLIN, K. Master Curve implementation of the warm prestress effect. *In: Engineering Fracture Mechanics*, 2003, 70, 2587–2602.

[O.16] CHENG, J. and NOBLE, F.W. The warm prestressing effect in steels undergoing intergranular fracture. *In: Fatigue and Fracture of Engineering Materials and Structures*, 1997, 20, 1399–1411.

[O.17] LIDBURY, D.P.G., SHERRY, A.H., PUGH, C.E. and BASS, B.R. The performance of largescale structures and validation of assessment procedures. *In: I. Milne, R Ritchie, B. L. Karihaloo, Comprehensive Structural Integrity*. Volume 7, Chapter 14, 529–566. Amsterdam: Elsevier, 2003.

[O.18] CHELL, G.G. The effects of subcritical crack growth on the fracture behaviour of cracked ferritic steels after warm prestressing. *In: Fatigue and Fracture Engineering Materials and Structures*, 1986, 9, 259–274.

[O.19] WADIER, Y. and BONNAMY, M. The energy approach of elasticplastic fracture mechanics applied to the analysis of the warm prestress effect. *In: ASME Pressure Vessels and Piping conference*, 2003, Volume 461, 89–96.

[O.20] PINEAU, A. Practical application of local approach methods. *In: I. Milne, R. Ritchie, B. L. Karihaloo, Comprehensive Structural Integrity*. Volume 7, Chapter 5, 177–225. Amsterdam: Elsevier, 2003.

 © The British Standards Institution 2019

Annex P (informative)

Compendium of reference stress and limit load solutions for homogeneous and strength mismatched structures

P.0 Symbols and definitions

For the purposes of this annex, the following symbols, definitions and units apply, unless otherwise indicated at the point of use.

Symbol	Definition	Units
A, B	Parameters used in calculating reference stress and/or limit load solutions (**P.13.3**)	—
A_b	Parameter used in calculating bending stresses as functions of moments	—
a	Half flaw length for through-thickness flaw, flaw height for surface flaw or half height for embedded flaw	mm
B	Section thickness in plane of flaw	mm
B_b	Parameter used in calculating bending stresses as functions of moments	—
b	Ratio of thickness b_1/b_2 used in calculating limit load solutions for cladded materials	—
b_1, b_2	Thickness of materials in a clad plate	mm
c	Half flaw length for surface or embedded flaw	mm
c_3	Parameter used in calculating reference stress solutions	—
d_1, d_2	Parameters used in calculating reference stress and/or limit load solutions	—
F	Tension or tensile force	N
F_e^M, $F_e^{M(1)}$, $F_e^{M(2)}$, $F_e^{M(3)}$ ...	Limit load solution of the mismatch configuration	N
F_e^N	Limit load	N
F_e^P	Limit load solution for a homogeneous component made of material with yield strength σ_Y^P	N
F_e^{clad}	Tensile limit load of the whole clad system	N
$F_e^{(h)}$	Tensile limit load of the homogeneous plate containing a through-thickness flaw made of the softer material (here material 2) with yield strength $\sigma_Y^{Material\ 2}$ and thickness of $B = b_1 + b_2$	N
$F_e(\lambda)$	Limit load as a function of load ratio	N
F_e^1, F_e^2	Limit load of material 1, material 2	N
f_a, f_b, f_c ... f_e	Parameters used in calculating reference stress and/or limit load solutions	—
f_{ps}	Parameter used in limit load calculation for cylinder under internal pressure	—
f_1, f_2, f_3, f_θ	Parameters used in calculating stress intensity factor solutions	—
$2H$	Distance between the (outermost) points at which loading is applied	mm

(continued)

Symbol	Definition	Units
h	Half weld width	mm
h_1, h_2	Parameter used in calculating reference stresses and/or limit load solutions	—
k	Normalized crack offset equal to $[(B/2) - p - a]/B$	—
k_2	Shear yield strength of material 2	N/mm^2
L_r	Ratio of applied load to yield load, or reference stress to yield strength	—
L_r^b	Normalized limit moment	—
L_r^N	Normalized limit force	—
M	Global bending moment	Nmm
M	Strength mismatch ratio; the ratio of the yield strength of the weld metal to that of the parent material	—
M_S, M_T,M_t	Stress magnification factors	—
M^b	Bending moment	Nmm
M_e^M, $M_e^{M(1)}$, $M_e^{M(2)}$, $M_e^{M(3)}$ ...	Limit moment of the mismatched system	Nmm
M_e^P	Limit moment for plate made wholly of parent material	Nmm
M_e^b	Limit bending moment	Nmm
M_{ex}	Parameter used in calculating limit load	Nmm
$M_e(\lambda)$	Limit moment as a function of load ratio	Nmm
M_i	In-plane moment	Nmm
M_{in}	Parameter used in calculating limit load	Nmm
M_o	Out-of-plane moment	Nmm
m	Applied axisymmetric through-wall bending moment per unit angle of cross-section	Nmm
$(m)_L$	Limit axisymmetric through wall bending moment per unit angle of cross-section	Nmm
P	Applied load	N
P_L	Limit load	N/mm
P_b	Primary bending stress	N/mm^2
$P_{b,l}$	Primary bending stress due to locally applied bending loads	N/mm^2
P_m	Primary membrane stress	N/mm^2
$P_{m,a}$	Primary membrane stress due to global axial loads	N/mm^2
$P_{m,b}$	Primary membrane stress due to global bending moments	N/mm^2
$P_{m,p}$	Primary membrane stress due to pressure loading	N/mm^2
p	Shortest distance from material surface to embedded flaw	mm
p'	Internal pressure	N/mm^2
p_L	Limit pressure	N/mm^2
r	Radius of round bar or bolt	mm
r_i	Internal radius	mm
r_m	Mean radius	mm

 © The British Standards Institution 2019

(continued)

Symbol	Definition	Units
r_o	External radius	mm
W	Structural width in plane of flaw	mm
w	Half width in plane of flaw	mm
α	Parameter used in defining limit load solutions for thick-walled pipes/cylinders containing circumferential flaws under combined tension and global bending	—
α_0, α_2	Parameter used in calculating reference stress/limit load solutions	—
α''	Function of a, c, B and W used in calculation of collapse stresses	—
β	Parameter used in calculating reference stress/limit load solutions	—
β_∞	Parameter used in calculating reference stress/limit load solutions for flaw at interface of a bi-material joint under plane strain conditions	—
θ	Term used for limit load calculation	—
λ	Load ratio (ratio of bending to membrane stress, P_b/P_m)	—
λ_s	Factor used in collapse analysis of cylinders	—
σ_b	Bending stress	N/mm^2
$\sigma_{n,b}$	Bending component of collapse stress	N/mm^2
$\sigma_{n,m}$	Membrane component of collapse stress	N/mm^2
σ_{ref}	Reference stress used for creep and plastic collapse consideration; sometimes calculated from plane strain von Mises limit load as in Annex N	N/mm^2
$\sigma_{ref\ corner\ crack.\ no\ hole}$	Reference stress of a corner crack in a plate when no hole is present	N/mm^2
$\sigma_{ref,b}$	Reference stress used for pure bending	N/mm^2
$\sigma_{ref,hole}$	Reference stress for corner flaws at hole under combined tension and bending	N/mm^2
$\sigma_{ref,m}$	Reference stress used for pure membrane	N/mm^2
$\sigma_{ref,no\ hole}$	Reference stress of a corner crack when no hole is present	N/mm^2
σ_Y	Lower yield strength or 0.2% proof strength	N/mm^2
$\sigma_Y^{Material\ 1}$, $\sigma_Y^{Material\ 2}$	Yield strength of materials 1 and 2 in a clad plate	—
σ_Y^P	Yield strength of the parent material	N/mm^2
σ_Y^W	Yield strength of the weld material	N/mm^2
σ_2	Tresca yield criterion	N/mm^2
χ	Factor used in collapse analysis of bolts	—
ψ	Normalization parameter used in the analysis of welded joints with strength mismatch, defined on a case-by-case basis as shown	—
ψ, ψ_1, ψ_2, ψ_3, ψ_4	Parameters used in calculating reference stress and/or limit load solutions	—

P.1 General

The background to this annex is given in reference [P.1].

During a fracture assessment of a flawed component (Clause **7**), the limit load or reference stress is used to evaluate the load ratio parameter, L_r (**7.3.7**), which is a measure of how close a structure is to plastic collapse. This annex provides reference stress or limit load solutions for several of the most commonly used basic geometries, i.e. plates, pipes/cylinders, spheres, round bars and bolts. Limit load solutions for strength mismatched structures (e.g. welded structures in which the weld metal and parent metal have significantly different tensile properties) are also provided for the most commonly used basic geometries. The solutions given in this annex are mostly from published literature and some industry reports. Solutions for homogeneous structures are taken from references [P.2] to [P.13], and those for mismatched structures, including some clad structures, are taken from references [P.14] to [P.20].

For a flawed structure, the limit load solution and the reference stress solution for a given loading system are equivalent in terms of defining L_r. All the reference stress solutions in this annex were derived from available limit load solutions. For some geometries subjected to combined loading, the solutions are presented in terms of limit load solutions rather than reference stress, in the interests of simplicity.

The limit load solutions provided in this annex or used to derive the reference stress solutions in this annex are all based on elastic-perfectly plastic material behaviour without considering the effect of strain hardening of the material.

Some additional reference stress solutions, needed in order to calculate constraint parameters, are given in Annex N.

P.2 Defining L_r using the solutions of this annex

The fracture assessment of this British Standard uses the *J*-integral based failure assessment diagram (FAD) method (see Clause **7**) which is underpinned by the reference stress *J* scheme [P.21]. The loading parameter, L_r, used in the fracture assessment is a very important parameter in the reference stress *J* prediction method. Therefore, selecting proper reference stress/limit load solutions used to define L_r should primarily consider obtaining more accurate but conservative *J* predictions via the reference stress method.

In the context of fracture assessment of a flawed structure, parameter L_r can be defined using reference stresses, σ_{ref}, as indicated in Equation (P.1a), by dividing it by the yield strength, σ_Y, of the material. Alternatively, it can be defined by the limit load of the flawed structure as a ratio of the total applied load giving rise to the primary stresses to the corresponding limit load of the flawed structure:

$$L_r = \frac{\sigma_{ref}}{\sigma_Y} = \frac{P}{P_L}\left(= \frac{\text{applied load}}{\text{limit load}}\right) \tag{P.1a}$$

where applied load, P, can be due to force, F, bending moment, M^b, axisymmetric through-wall bending moment per unit angle of cross-section, m, or internal pressure, p'. For these loading cases, L_r is calculated using Equation (P.1b) to Equation (P.1e):

$$L_r = \frac{F}{F_e^N} \tag{P.1b}$$

$$L_r = \frac{M^b}{M_e^b} \tag{P.1c}$$

$$L_r = \frac{m}{(m)_L} \tag{P.1d}$$

$$L_r = \frac{p'}{p_L} \quad \text{(P.1e)}$$

Most of the reference stress solutions given in this annex are based on the membrane stress, P_m, and bending stress, P_b, calculated across an equivalent unflawed section of a component. In pure tension, P_m is the average force, F, divided by the cross-sectional area. In other more complex situations, P_m should be calculated as the mean stress through the section thickness. For convenience, the conversion formulae between bending stress, P_b, and bending moment, M_b, or applied axisymmetric through-wall bending moment per unit angle of cross-section, m, are given in Table P.1

For combined loading, the evaluation of L_r can be complex. In this case, the individual limit loads are evaluated for the load ratio relevant to the assessment point, e.g. for proportional loading conditions, and L_r may be defined by any individual load component and the corresponding limit load. For example, for a component under combined tensile force, F, and global bending, M, L_r may be obtained from:

$$L_r = \frac{F}{F_e(\lambda)} = \frac{M}{M_e(\lambda)} \quad \text{(P.2)}$$

where:

$F_e(\lambda)$ is the limit force for a given λ value;

$M_e(\lambda)$ is the limit moment for a given λ value.

Table P.1 **Calculation of bending stresses as functions of moments**

Structure type	Bending stress, P_b	Location
Plate	$\left(\frac{6}{WB^2}\right)M^b$	Tensile stress at wall surface (W is plate width)
Pipe with internal circumferential defect (axisymmetric bend)	$\left(\frac{6}{r_m B^2 A_b}\right)m$ $A_b = \frac{12-(B/r_m)^2}{2(6+B/r_m)}$	Tensile stress at inner wall surface
Pipe with external circumferential defect (axisymmetric bend)	$\left(\frac{6}{r_m B^2 B_b}\right)m$ $B_b = \frac{12-(B/r_m)^2}{2(6-B/r_m)}$	Tensile stress at outer wall surface
Pipe with internal or external circumferential defect (cantilever bend)	$\left\{\frac{2(2+B/r_m)}{\pi r_m^2 B\left[4+(B/r_m)^2\right]}\right\}M^b$	Peak tensile stress at outer wall surface
Solid round bar with centrally embedded circular defect (axisymmetric bend)	$\left(\frac{24}{r^3}\right)m$	Tensile stress at centre of bar (r is bar radius)
Solid round bar with external circumferential defect (axisymmetric bend)	$\left(\frac{12}{r^3}\right)m$	Tensile stress at surface of bar (r is bar radius)
Solid round bar (cantilever bend)	$\left(\frac{4}{\pi r^3}\right)M^b$	Peak tensile stress at surface of bar (r is bar radius)

P.3 Collapse modes

It is important to recognize how L_r (proximity to plastic collapse) and K_r (proximity to brittle or ductile fracture) are linked through the FAD (see Clause **7**). In general terms, an increased proximity to plastic collapse also means lower capacity to resist failure due to crack brittle/ductile fracture, and vice versa. For components with small flaws made of materials with high fracture toughness, failure might be controlled by plastic collapse.

Three potential plastic collapse modes can be identified:

a) local collapse;

b) net section (global) collapse; and

c) gross section collapse.

Net section (global) collapse load denotes the collapse of the structural section containing the flaw.

Local collapse denotes the collapse of the remaining ligament adjacent to the flaw being assessed. A local collapse solution usually gives a higher value of L_r than does a global collapse solution.

Gross section collapse denotes the collapse of the structure by gross straining that occurs when collapse takes place away from the flawed section or is unaffected by the presence of the flaw. This mode is outside the scope of this annex.

In elastic-plastic structures, the plastic strains at the ligament can become large before the global limit is reached, and hence the "local collapse load" at which gross plasticity occurs in the ligament is sometimes more relevant to ligament fracture.

Each reference stress/limit load solution in this annex is marked with "global solution" or "local solution", indicating that the solution was derived on an assumption of net section collapse or local ligament/area yielding, respectively.

P.4 Reference stress and/or limit load solutions for flawed plates

P.4.1 Through-thickness flaws in plates under combined tension and through-thickness bending (global solution)

See Figure M.1 for the definition of the geometry. The reference stress is calculated (see reference [P.5]) from the following equation:

$$\sigma_{\text{ref}} = \frac{P_{\text{b}} + \left(P_{\text{b}}^2 + 9P_{\text{m}}^2\right)^{0.5}}{3[1 - (2a/W)]} \quad \text{(P.3)}$$

*NOTE See **M.3.1** for the stress intensity factor solution for this geometry.*

P.4.2 Single edge cracked plate under combined tension and through-thickness bending (global solution)

See Figure M.2 for the definition of the geometry. The reference stress is calculated (see reference [P.5]) from the following equation:

$$\sigma_{\text{ref}} = \frac{P_{\text{b}} + \left(P_{\text{b}}^2 + 9P_{\text{m}}^2\right)^{0.5}}{3(1 - \alpha'')} \quad \text{(P.4)}$$

where:

$$\alpha'' = \frac{a}{W}$$

*NOTE 1 See **M.3.2** for the stress intensity factor solution for this geometry.*

NOTE 2 This solution ignores the in-plane bending moment due to tension.

 © The British Standards Institution 2019

P.4.3 Double edge cracked plate under tension (global solution)

See Figure P.1 for the definition of the geometry. The plastic collapse, L_r, is given by Equation (P.1b), where the limit load, F_e^N, is calculated (see reference [P.2]) from:

$$F_e^N = \beta 2B(w-a)\sigma_Y \qquad \text{for plane stress} \tag{P.5}$$

where:

$$\beta = 1 + 0.54\frac{a}{w} \qquad \text{for } 0 \le \frac{a}{w} \le 0.286 \tag{P.6a}$$

$$\beta = \frac{2}{\sqrt{3}} \qquad \text{for } 0.286 < \frac{a}{w} < 1 \tag{P.6b}$$

or:

$$F_e^N = \beta\frac{4}{\sqrt{3}}B(w-a)\sigma_Y \qquad \text{for plane strain} \tag{P.7}$$

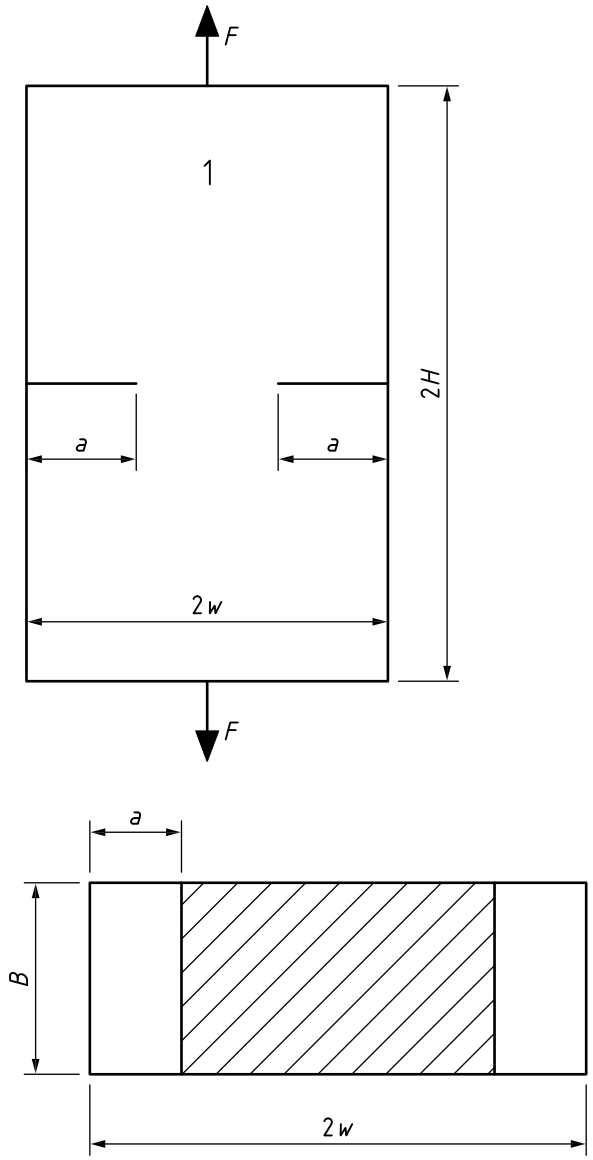
$$\beta = 1 + \ln\left(\frac{2w-a}{2w-2a}\right) \qquad \text{for } 0 \le \frac{a}{w} \le 0.884 \tag{P.8a}$$

$$\beta = 1 + \frac{\pi}{2} \qquad \text{for } 0.884 < \frac{a}{w} < 1 \tag{P.8b}$$

NOTE 1 There is currently no stress intensity factor solution defined for this geometry in Annex M.

NOTE 2 This is a von Mises solution.

Figure P.1 **Double edge cracked plate under tension**



Key
1 Parent material

P.5 Reference stress solutions for flat plates containing surface and embedded flaws

P.5.1 Surface flaws in plates under combined tension and through-thickness bending (local/global solution)

See Figure M.3 for the definition of the geometry. The reference stress is calculated (see reference [P.4]) from Equation (P.9) or Equation (P.10).

a) Normal bending restraint (e.g. fixed-grip tension plus bending):

$$\sigma_{\text{ref}} = \frac{P_{\text{b}} + \left[P_{\text{b}}^2 + 9P_{\text{m}}^2(1-\alpha'')^2\right]^{0.5}}{3(1-\alpha'')^2} \qquad \text{(P.9)}$$

b) Negligible bending restraint (e.g. pin jointed):

$$\sigma_{\text{ref}} = \frac{P_{\text{b}} + 3P_{\text{m}}\alpha'' + \left[(P_{\text{b}} + 3P_{\text{m}}\alpha'')^2 + 9P_{\text{m}}^2(1-\alpha'')^2\right]^{0.5}}{3(1-\alpha'')^2} \quad \text{(P.10)}$$

where:

$\alpha'' = \dfrac{a/B}{1+(B/c)}$ for $W \geq 2(c + B)$ (local solution)

$\alpha'' = \left(\dfrac{a}{B}\right)\left(\dfrac{2c}{W}\right)$ for $W < 2(c + B)$ (global solution)

*NOTE 1 See **M.4.1** for the stress intensity factor solution for this geometry.*

NOTE 2 This solution is based on an equivalent extended surface flaw in a plate and is not suitable for very deep flaws. For through-wall flaws (a/B = 1), this solution does not reproduce Equation (P.3).

NOTE 3 For exact global solutions, refer to R6 [P.22].

P.5.2 Extended surface flaws in plates under combined tension and through-thickness bending (global solution)

See Figure M.7 for the definition of the geometry. The reference stress is calculated (see reference [P.4]) from Equation (P.9) and Equation (P.10) where α" = a/B.

*NOTE See **M.4.2** for the stress intensity factor solution for this geometry.*

P.5.3 Embedded flaws in plates under combined tension and through-thickness bending (local/global solution)

See Figure M.8 for the definition of the geometry. The reference stress solution is calculated (see reference [P.4]) from Equation (P.11):

$$\sigma_{\text{ref}} = \frac{P_{\text{b}} + 3P_{\text{m}}\alpha'' + \left\{(P_{\text{b}} + 3P_{\text{m}}\alpha'')^2 + 9P_{\text{m}}^2\left[(1-\alpha'')^2 + 4(p\alpha''/B)\right]\right\}^{0.5}}{3\left[(1-\alpha'')^2 + 4(p\alpha''/B)\right]} \quad \text{(P.11)}$$

where:

$\alpha'' = \dfrac{2a/\text{B}}{1+(B/\text{c})}$ for $W \geq 2(c + B)$ (local solution)

$\alpha'' = \left(\dfrac{2a}{B}\right)\left(\dfrac{2c}{W}\right)$ for $W < 2(c + B)$ (global solution)

where:

$a/B \leq 0.5 - p/B$

*NOTE 1 See **M.4.3** for the stress intensity factor solution for this geometry.*

NOTE 2 This solution is based on an equivalent extended embedded flaw in a plate and is not suitable for very deep flaws. For through-wall flaws (2a/B = 1, p = 0), this solution does not reproduce Equation (P.3).

P.5.4 Extended embedded flaws in plates under combined tension and through-thickness bending (global solution)

See Figure P.2 for the definition of the geometry. The reference stress solution is calculated (see references [P.4], [P.5]) from Equation (P.12).

$$\sigma_{\text{ref}} = \frac{2(\lambda+\alpha)+\sqrt{4(\lambda+\alpha)^2+c_3}}{c_3}P_{\text{m}} \qquad \text{for } \alpha \le \alpha_2 \qquad \text{(P.12)}$$

where:

$$\lambda = \frac{1}{6}\frac{P_{\text{b}}}{P_{\text{m}}}$$

$$\alpha = \frac{a}{B}$$

$$\alpha_2 = \frac{1}{2}\left[\frac{(B/2)-p-a}{B}\right]$$

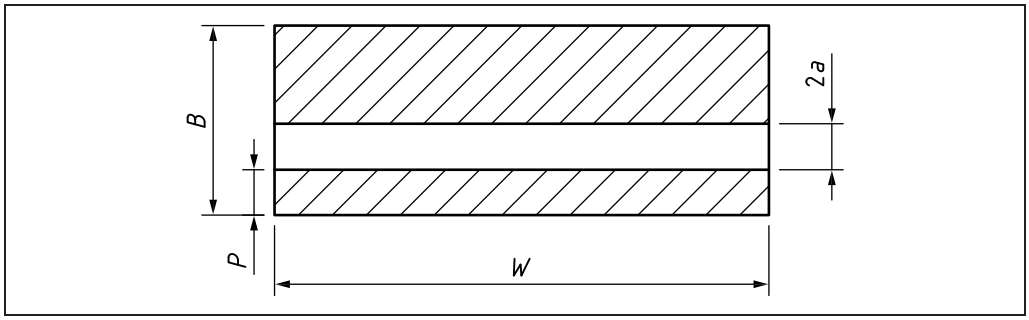
$$c_3 = 1 - 8\alpha k - 4\alpha^2$$

NOTE 1 This solution is equivalent to Equation (P.11) when α" = 2a/B is used in the equation.

NOTE 2 There is currently no stress intensity factor solution defined for this geometry in Annex M.

NOTE 3 This solution may also be applied to embedded flaws in shells.

Figure P.2 **Extended embedded flaw in a plate**



P.6 Reference stress solutions for flat plates containing corner flaws

P.6.1 Corner flaws in plates under combined tension and through-thickness bending (local/global solution)

See Figure M.12 for the definition of the geometry. The reference stress can be estimated from Equation (P.9) and Equation (P.10) where:

$$\alpha'' = \frac{a/B}{1+(2B/c)} \qquad \text{for } W \ge c + 2B \qquad \text{(local solution)}$$

$$\alpha'' = \left(\frac{a}{B}\right)\left(\frac{c}{W}\right) \qquad \text{for } W < c + 2B \qquad \text{(global solution)}$$

NOTE 1 Equation (P.9) and Equation (P.10) are valid where local collapse would occur in the ligament, B – a, and c << W.

Local collapse of the ligament (*W* – *c*) is not described by Equation (P.9) and Equation (P.10). Where this is considered to be a possible failure mechanism, the flaw should be recharacterized as an edge flaw circumscribing the corner flaw.

*NOTE 2 See **M.5.1** for the stress intensity factor solution for this geometry.*

P.6.2 Corner flaws at hole under combined tension and through-thickness bending (local/global solution)

See Figure M.13 for the definition of the geometry. A conservative estimate of σ_{ref} can be made by recharacterizing the flaw as a through-thickness flaw circumscribing the corner flaws and applying Equation (P.3).

Alternatively, the reference stress can be estimated by using Equation (P.9) and Equation (P.10), adapting the values of α" and net section stress to account for the loss of section area due to the hole. This is expressed by Equation (P.13):

$$\sigma_{ref,hole} = \left(\frac{W}{W-2r}\right)\sigma_{ref,\ no\ hole} \qquad (P.13)$$

The values of α" are as follows:

$$\alpha'' = \frac{a/B}{1+(B/c)} \qquad \text{for } W - 2r \geq 2\,(c + B) \qquad \text{(local solution)}$$

$$\alpha'' = \left(\frac{a}{B}\right)\left(\frac{2c}{W-2r}\right) \qquad \text{for } W - 2r < 2\,(c + B) \qquad \text{(global solution)}$$

The equations in this subclause are valid only where local collapse occurs in the ligament ($B - a$).

*NOTE See **M.5.2** for the stress intensity factor solution for this geometry.*

P.6.3 Single corner flaw at hole under combined tension and through-thickness bending (local/global solution)

A conservative estimate of the net section stress may be made by recharacterizing the flaw as a through-thickness flaw circumscribing the corner flaw.

Alternatively, the reference stress may be estimated by using Equation (P.9) and Equation (P.10) and adapting the values of α" and net section stress to account for the loss of section area due to the hole. This is expressed by Equation (P.14):

$$\sigma_{ref,hole} = \left(\frac{W}{W-2r}\right)\sigma_{ref\ corner\ crack.\ no\ hole} \qquad (P.14)$$

The values of α" are as follows:

$$\alpha'' = \frac{a/\mathrm{B}}{1+(2B/\mathrm{c})} \qquad \text{for } W - 2r \geq 2(c + B) \qquad \text{(local solution)}$$

$$\alpha'' = \left(\frac{a}{B}\right)\left(\frac{c}{W-2r}\right) \qquad \text{for } W - 2r < 2(c + B) \qquad \text{(global solution)}$$

The equations in this subclause are valid only where local collapse occurs in the ligament ($B - a$) and $c << W/2 - r$.

*NOTE See **M.5.3** for the stress intensity factor solution for this geometry.*

P.7 Other geometries

For most other geometries, the local collapse and net section collapse stress formulae for plates are conservative, sometimes excessively so. This includes embedded flaws in pipes/cylinders, flaws at nozzles in pressure vessels, surface flaws and short ($2c < 0.2\pi r$) surface flaws, circumferentially orientated, in nozzles or pipes under tension or bending.

In cases where the plastic collapse solution for a particular flaw geometry is unknown, a conservative estimate of the reference stress can be made by assuming that the flaw is equivalent to a simplified rectangular cross-section flaw circumscribing the existing flaw.

In cases where the plastic collapse loads are known for tension and bending applied separately, σ_{ref} under combined tension and bending can be conservatively estimated from the following expression:

$$\sigma_{ref} \leq \left|\sigma_{ref,b}\right| + \sigma_{ref,m} \quad \text{(P.15)}$$

In cases where plastic collapse is likely to evolve from volumetric flaws, these flaws may be treated as embedded flaws using the expression for σ_{ref} in Equation (P.11).

NOTE The method described in this subclause is an approximate one. In the event of doubt, finite element assessment is recommended.

P.8 Reference stress and/or limit load solutions for pipes/cylinders with axial flaws

P.8.1 Through-thickness flaws in thin-walled pipe/cylinder under membrane stress and through-thickness bending (global solution)

See Figure M.13 for the definition of the geometry. The reference stress is calculated (see references [P.5] and [P.7]) from Equation (P.16):

$$\sigma_{ref} = M_T P_m + \frac{2P_b}{3(1-2a/W)} \quad \text{(P.16)}$$

where:

$$M_T = \left[1 + 1.6\left(\frac{a^2}{r_i B}\right)\right]^{0.5}$$

*NOTE See **M.7.2.1** for the stress intensity factor solution for this geometry.*

P.8.2 Internal surface flaw in thin-walled pipe/cylinder under membrane stress and through-thickness bending (local solution)

See Figure M.14 for the definition of the geometry. The reference stress is calculated (see references [P.4] and [P.9]) from the Equation (P.17):

$$\sigma_{ref} = M_s P_m + \frac{2P_b}{3(1-\alpha'')^2} \quad \text{(P.17)}$$

where:

$$M_S = \frac{1-[a/(BM_t)]}{1-(a/B)}$$

$$M_t = \sqrt{1 + 1.6\left(\frac{c^2}{r_i B}\right)}$$

$$\alpha'' = \frac{a/B}{1+B/c} \qquad \text{for } W \geq 2\ (c+B)$$

$$\alpha'' = \left(\frac{a}{B}\right)\left(\frac{2c}{W}\right) \qquad \text{for } W < 2\ (c+B)$$

NOTE 1 Equation (P.17) is based on the original Folias solution for thin-walled cylinders [P.7].

*NOTE 2 See **M.7.2.2** for the stress intensity factor solution for this geometry.*

P.8.3 Extended internal surface flaw in thin-walled pipe/cylinder under membrane stress and through-thickness bending (global solution)

See Figure M.15 for the definition of the geometry. The reference stress is calculated from Equation (P.17), where:

$$\alpha'' = \frac{a}{B}$$

$$c = \frac{W}{2}$$

$$M_s = \frac{1}{1-(a/B)}$$

*NOTE See **M.7.2.3** for the stress intensity factor solution for this geometry.*

P.8.4 External surface flaw in thin-walled pipe/cylinder under membrane stress and through-thickness bending (local solution)

See Figure M.16 for the definition of the geometry. The reference stress is calculated (see references [P.4] and [P.9]) from Equation (P.17) by substituting the outer radius for the inner radius in equations.

*NOTE See **M.7.2.4** for the stress intensity factor solution for this geometry.*

P.8.5 Extended external surface flaw in thin-walled pipe/cylinder under membrane stress and through-thickness bending (global solution)

See Figure M.17 for the definition of the geometry. The reference stress is calculated from Equation (P.17), where:

$$M_s = \frac{1}{1-(a/B)}$$

$$\alpha'' = \frac{a}{B}$$

$$c = \frac{W}{2}$$

*NOTE See **M.7.2.5** for the stress intensity factor solution for this geometry.*

P.8.6 Internal surface flaw in thick-walled pipe/cylinder under internal pressure (local solution)

See Figure M.14 for the definition of the geometry. The local limit load solution, taking into account defect-face pressure (see reference [P.10]), is:

$$\frac{p_L}{\sigma_Y} = \frac{1}{h_1/c+1}\left[\frac{h_1}{c}\ln(1+\eta_i) + f_{ps}(1+\alpha\eta_i)\ln\left(\frac{1+\eta_i}{1+\alpha\eta_i}\right)\right] \quad \text{(P.18)}$$

where:

$$\frac{h_1}{c} = \frac{(1-\alpha)f_{ps}\left[\ln(1+\alpha\eta_i) - \alpha\eta_i\ln\left(\frac{1+\eta_i}{1+\alpha\eta_i}\right)\right]}{M_{in}\left[\ln(1+\eta_i) - f_{ps}\left\{\frac{1}{M_{in}}\ln(1+\alpha\eta_i) + \left[1+\alpha\eta_i\left(1-\frac{1}{M_{in}}\right)\right]\ln\left(\frac{1+\eta_i}{1+\alpha\eta_i}\right)\right\}\right]}$$

$$f_{ps} = \frac{1}{1+1/2\alpha\eta_i} \text{ for } \Phi \le 1$$

$$f_{ps} = \frac{\Phi}{\Phi+\frac{1}{2}\alpha\eta_i} \quad \text{for } \Phi > 1$$

where:

$$M_{in} = \left[1 + 1.4\frac{\alpha\eta_i}{\Phi^2(1+\alpha\eta_i)}\right]^{0.5}$$

$$\alpha = \frac{a}{B}$$

$$\eta_i = \frac{B}{r_i}$$

$$\Phi = \frac{a}{c}$$

To obtain the global limit load solution for an extended axial internal surface crack in a thick-walled cylinder under internal pressure, set Φ = 0 and $1/M_{in}$ = 0.

*NOTE See **M.7.2.2** for the stress intensity factor solution for this geometry.*

P.8.7 External surface flaw in thick-walled pipe/cylinder under internal pressure (local solution)

See Figure M.16 for the definition of the geometry. The local limit load solution (see reference [P.10]) is:

$$\frac{p_L}{\sigma_Y} = \frac{1}{h_2/c + 1}\left[\frac{h_2}{c}\ln(1+\eta_i) + \ln(1+\eta_i - \alpha\eta_i)\right] \quad \text{(P.19)}$$

where:

$$\frac{h_2}{c} = \frac{1-\alpha}{M_{ex} - 1}$$

$$M_{ex} = \left[1 + 1.4\frac{\alpha\eta_i}{(1+\eta_i)\Phi^2}\right]^{0.5}$$

$$\alpha = \frac{a}{B}$$

$$\eta_i = \frac{B}{r_i}$$

$$\Phi = \frac{a}{c}$$

To obtain the limit load solution for an extended axial external surface crack in a thick-walled cylinder under internal pressure, set Φ = 0 and $1/M_{ex}$ = 0.

*NOTE See **M.7.2.4** for the stress intensity factor solution for this geometry.*

P.8.8 External surface flaw in thick-walled pipe/cylinder under membrane stress and through-thickness bending (local solution)

See Figure M.16 for the definition of the geometry. The limit membrane stress, $\sigma_{n,m}$, and/or limit bending stress, $\sigma_{n,b}$, based on the local yield criterion is calculated (see references [P.11] and [P.12]) using the normalized limit force, L_r^N, and/or moment, L_r^b:

$$L_r^N = \frac{\sigma_{n,m}}{\sigma_Y} \quad \text{(P.20)}$$

$$L_r^b = \frac{2}{3}\frac{\sigma_{n,b}}{\sigma_Y} \quad \text{(P.21)}$$

where:

$$L_r^N = \begin{Bmatrix} \dfrac{d_1}{2\lambda + \dfrac{a\psi}{1+\psi} + \sqrt{\left(2\lambda + \dfrac{a\psi}{1+\psi}\right)^2 + d_1}} \\ \dfrac{d_2}{2\lambda + \psi(1-a) + \sqrt{[2\lambda + \psi(1-a)]^2 + (1+\psi)d_2}} \end{Bmatrix} \quad \begin{matrix} \text{for } a \le a_0 \\ \text{for } a > a_0 \end{matrix}$$

$$L_r^b = \begin{Bmatrix} \dfrac{4\lambda d_1}{2\lambda + \dfrac{a\psi}{1+\psi} + \sqrt{\left(2\lambda + \dfrac{a\psi}{1+\psi}\right)^2 + d_1}} \\ \dfrac{4\lambda d_2}{2\lambda + \psi(1-a) + \sqrt{[2\lambda + \psi(1-a)]^2 + (1+\psi)d_2}} \end{Bmatrix} \quad \begin{matrix} \text{for } a \le a_0 \\ \text{for } a > a_0 \end{matrix}$$

and where:

$$d_1 = \left(1 - \frac{a\psi}{1+\psi}\right)^2 + \frac{2a^2\psi}{(1+\psi)^2}$$

$$d_2 = \left(1 - \frac{a\psi}{1+\psi}\right)[1 - \psi(1-a)] + \frac{2a(1-a)\psi}{1+\psi}$$

$$a_0 = -\left(\lambda - \frac{1}{2}\right) + \sqrt{\left(\lambda - \frac{1}{2}\right)^2 + \frac{2(1+\psi)\lambda}{2+\psi}}$$

$$\lambda = \frac{1}{6}\frac{P_b}{P_m}$$

$$a = \frac{a}{B}$$

$$\psi = \frac{c}{B}$$

$$\beta = \frac{2c}{W}$$

For pure tension (λ = 0) and pure bending ($\lambda \to \infty$):

a_0 = 1 for λ = 0

$a_0 = \dfrac{\psi + 1}{\psi + 2}$ for $\lambda \to \infty$

The validity range of this solution is:

$$\beta \le \frac{\psi}{1+\psi}$$

NOTE 1 This solution is based on the local solution for a surface crack in a plate under combined tension and bending in [P.11] and [P.12]. Therefore, this solution can be used for both thin and thick cylinders.

*NOTE 2 For pure pressure, this solution might be inconsistent with **P.8.7**.*

*NOTE 3 See **M.7.2.4** for the stress intensity factor solution for this geometry.*

P.9 Reference stress and/or limit load solutions for thin-walled pipes/cylinders with circumferential flaws

P.9.1 Through-thickness flaw in thin-walled pipe/cylinder under combined tension, bending and internal pressure

See Figure M.18 for the definition of the geometry. The reference stress (see references [P.3], [P.5] and [P.8]) is calculated from:

$$\sigma_{\text{ref}} = \frac{\pi\left(P_{\text{m,a}} + P_{\text{m,p}}\right)}{\pi - \dfrac{a}{r_{\text{m}}} - 2\arcsin\left[\dfrac{1}{2}\sin(a/r_{\text{m}})\right]} + \frac{\pi P_{\text{m,b}}}{\pi - (a/r_{\text{m}}) - 2\dfrac{\sin^2(a/r_{\text{m}})}{\pi - (a/r_{\text{m}})} - \dfrac{\sin(2a/r_{\text{m}})}{2}} + \frac{2P_{\text{b,l}}}{3[1 - (a/\pi r_{\text{m}})]} \tag{P.22}$$

The range of application is:

$0 \leq 2a/(\pi r_{\text{m}}) \leq 0.5$

$0 < B/r_{\text{m}} \leq 0.2$

Where the cylinder under consideration is part of a pin-jointed structure and where the flaw length is greater than 1/8 of the circumference, Equation (P.22) might be non-conservative and secondary bending should be taken into account by calculating the true position of the neutral axis.

NOTE 1 For pressure and/or tension, Equation (P.22) is a global solution. The solution might be non-conservative for pure pressure when $a/(\pi r_{\text{i}}) \leq 0.5$.

*NOTE 2 See **M.7.3.1** for the stress intensity factor solution for this geometry.*

P.9.2 Internal circumferential surface flaw in thin-walled pipe/cylinder under combined tension, bending and pressure (local/global solution)

See Figure M.19 for the definition of the geometry. The reference stress (see references [P.4] and [P.8]) is calculated from Equation (P.23):

$$\sigma_{\text{ref}} = \frac{P_{\text{m}}[\pi(1 - a/B) + 2(a/B)\sin(c/r_{\text{i}})]}{(1 - a/B)[\pi - (c/r_{\text{i}})(a/B)]} + \frac{2P_{\text{b}}}{3(1 - \alpha'')^2} \tag{P.23}$$

where:

$\alpha'' = \dfrac{a/\text{B}}{[1 + (B/\text{c})]}$ for $\pi r_{\text{i}} \geq c + B$

α" = $(a/B)(c/\pi r_{\text{i}})$ for $\pi r_{\text{i}} < c + B$

P_{m} is the total membrane stress due to external bending, axial loads and pressure;

P_{b} is the total through-thickness bending stress due to external bending and/or local misalignment.

The range of application is:

$c/(\pi r_{\text{i}}) \leq 1$

NOTE 1 For pressure and/or tension, Equation (P.23) is an approximate global solution for small surface flaws. For shallow and short flaws under pressure, the solution might be non-conservative. For pure global bending, the solution might be very conservative.

*NOTE 2 See **M.7.3.2** for the stress intensity factor solution for this geometry.*

P.9.3 Extended circumferential internal surface flaw in thin-walled pipe/cylinder under combined tension, bending and pressure

See Figure M.20 for the definition of the geometry. The reference stress (see references [P.4] and [P.8]) is calculated from Equation (P.23) where:

$$\alpha'' = \frac{a}{B}$$

$$c = \pi r_i$$

NOTE 1 For pressure and/or tension, Equation (P.23) is an approximate global solution for small surface flaws. For shallow and short flaws under pressure, the solution might be non-conservative. For pure global bending, the solution might be very conservative.

*NOTE 2 See **M.7.3.3** for the stress intensity factor solution for this geometry.*

P.9.4 External circumferential surface flaw in thin-walled pipe/cylinder under combined tension, bending and pressure (local/global solution)

Equation (P.23) may be applied in order to calculate the reference stress relating to circumferential flaws in cylinders by substituting the outer radius for the inner radius in the equations.

NOTE 1 For pressure and/or tension, Equation (P.23) is an approximate global solution for small surface flaws. For shallow and short flaws under pressure, the solution might be non-conservative. For pure global bending, the solution might be very conservative.

*NOTE 2 See **M.7.3.4** for the stress intensity factor solution for this geometry.*

P.9.5 Extended circumferential external surface flaw in thin-walled pipe/cylinder under combined tension, bending and pressure

See Figure M.21 for the definition of the geometry. The reference stress (see references [P.4] and [P.8]) is calculated from Equation (P.23), where:

$$\alpha'' = \frac{a}{B}$$

$$c = \pi r_o$$

NOTE 1 For pressure and/or tension, Equation (P.23) is an approximate global solutionfor small surface flaws. For shallow and short flaws under pressure, the solution might be non-conservative. For pure global bending, the solution might be very conservative.

*NOTE 2 See **M.7.3.5** for the stress intensity factor solution for this geometry.*

P.9.6 Embedded flaws in thin-walled pipe/cylinder

The flat plate solution in Equation (P.11) may be applied to embedded flaws in pipes/cylinders.

NOTE 1 Equation (P.11) is a plate solution that does not consider stresses parallel to the flaw. Therefore, it might underestimate the reference stress for cylinders with small circumferential flaws under pressure dominated loading.

*NOTE 2 See **M.7.3.6** for the stress intensity factor solution for this geometry.*

P.10 Limit load solutions for thick-walled pipes/cylinders containing circumferential flaws under combined tension and global bending (global solution)

See Figure P.3 for the definition of the geometry. The limit load in terms of force, F_e^N, or in terms of bending moment, M_e^b, can be calculated (see reference [P.13]) as follows:

$$L_r^N = \frac{F_e^N}{2\pi r_m B \sigma_Y} \tag{P.24}$$

$$L_r^b = \frac{M_e^b}{4 r_m^2 B \sigma_Y} \tag{P.25}$$

where r_m is the mean radius of the pipe and equal to r_i + (B/2).

Normalized limit load, L_r^N, and normalized limit moment, L_r^b, are to be obtained from the solution of the following equation systems.

- For $\theta + \beta \leq \pi$, where the whole crack is inside the tensile stress zone:

$$\frac{\beta}{\pi} = \frac{1}{2}\left(1 - f_a \alpha \frac{\theta}{\pi} - L_r^N\right) \tag{P.26a}$$

$$L_r^b = f_b \sin\beta - \frac{1}{2}\alpha f_c \sin\theta \tag{P.26b}$$

- For $\theta + \beta > \pi$, where part of the crack is inside the compression zone:

$$\frac{\beta}{\pi} = 1 - \frac{1 + L_r^N - (1 - f_e)\theta/\pi}{2 f_e} \tag{P.27a}$$

$$L_r^b = f_b\left[f_d \sin\beta + \frac{1}{2}(1 - f_d)\sin\theta\right] \tag{P.27b}$$

where:

$$f_a = 1 - \frac{1}{2}\eta + \frac{1}{2}\alpha\eta \quad \text{for an internal flaw}$$

$$f_a = 1 + \frac{1}{2}\eta - \frac{1}{2}\alpha\eta \quad \text{for an external flaw}$$

$$f_b = 1 + \frac{1}{12}\eta^2$$

$$f_c = 1 - \eta + \frac{1}{4}\eta^2 + \alpha\eta - \frac{1}{2}\alpha\eta^2 + \frac{1}{3}\alpha^2\eta^2 \quad \text{for an internal flaw}$$

$$f_c = 1 + \eta + \frac{1}{4}\eta^2 - \alpha\eta - \frac{1}{2}\alpha\eta^2 + \frac{1}{3}\alpha^2\eta^2 \quad \text{for an external flaw}$$

$$f_d = \frac{(1-\alpha)\left[1 + \alpha\eta - \frac{1}{6}\alpha\eta^2 + \frac{1}{3}\alpha^2\eta^2 + \frac{1}{12}\eta^2\right]}{f_b} \quad \text{for an internal flaw}$$

$$f_d = \frac{(1-\alpha)\left[1 - \alpha\eta - \frac{1}{6}\alpha\eta^2 + \frac{1}{3}\alpha^2\eta^2 + \frac{1}{12}\eta^2\right]}{f_b} \quad \text{for an external flaw}$$

$$f_e = 1 - \alpha + \frac{1}{2}\alpha\eta - \frac{1}{2}\alpha^2\eta \quad \text{for an internal flaw}$$

$$f_e = 1 - \alpha - \frac{1}{2}\alpha\eta + \frac{1}{2}\alpha^2\eta \quad \text{for an external flaw}$$

and where:

$$\alpha = \frac{a}{B}$$

$$\eta = \frac{B}{r_m}$$

$$\lambda = \frac{M^b}{r_m F^N} = \frac{L_r^b}{(\pi/2)L_r^N}$$

For through-thickness flaws, α should be set to 1.

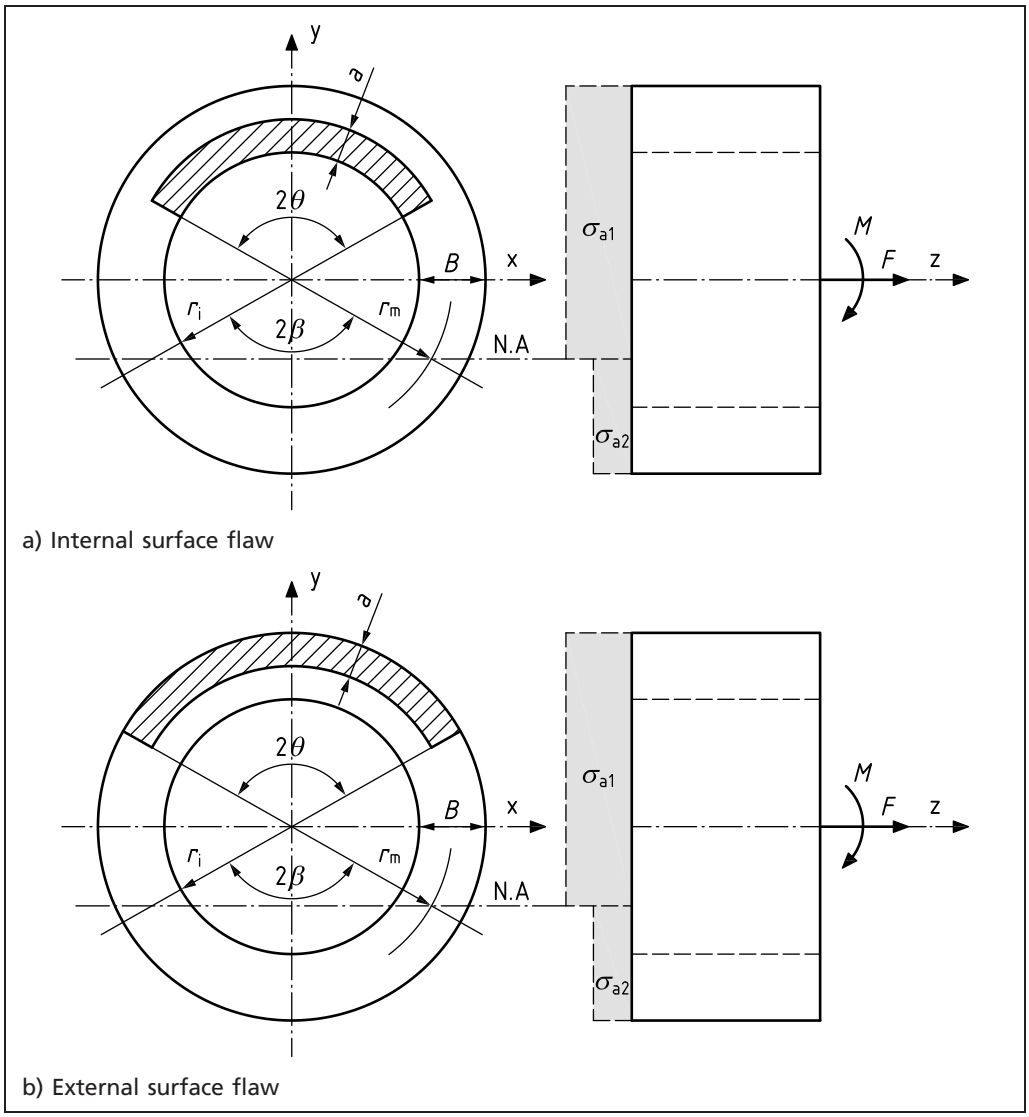
For fully circumferential flaws, θ should be set to π.

For the case of pure tension, λ and L_r^b should be set to 0; for the case of pure bending, $\lambda \rightarrow \infty$ and L_r^N should be set to 0.

NOTE 1 This is a net section collapse solution. When $\theta + \beta > \pi$, crack closure is ignored.

*NOTE 2 See **M.7.3.1** to **M.7.3.5** for the stress intensity factor solutions for this geometry.*

Figure P.3 **Circumferential internal and external surface flaws in thick-walled cylinders under combined tension and bending**



P.11 Reference stress solution for thin-walled spheres with through-thickness flaw (global solution)

See Figure M.22 for the definition of the geometry. The reference stress (see references [P.4] and [P.6]) is calculated from Equation (P.28):

$$\sigma_{ref} = \frac{P_m\left(1+\sqrt{1+\frac{8\lambda_s^2}{\cos^2\Phi_s}}\right)}{2} + \frac{2P_b}{3[1\ -\ (a/\pi r_i)]} \quad \text{(P.28)}$$

where:

$$\lambda_s = \frac{a}{\sqrt{B(r_i + B/2)}}$$

$$\Phi_s \frac{a}{r_i + B/2}$$

The range of application is:

$0 \leq B/r_i \leq 0.1$

$0 < 2a/\pi(r_i + B/2) < 1$

*NOTE See **M.8** for the stress intensity factor solution for this geometry.*

P.12 Reference stress and limit load solutions for round bars and bolts

P.12.1 Straight-fronted, semicircular and semi-elliptical surface flaws in round bars and semi-elliptical surface flaws in bolts

See Figure M.23 for the definition of the geometry. The reference stress (see reference [P.2]) for a semi-elliptical flaw in a bolt or a bar can be conservatively estimated by assuming that the flaw is equivalent to a chordal surface flaw in a bolt or bar where the chordal flaw encompasses the semi-elliptical flaw. The reference stress may be calculated from the following equation:

$$\sigma_{ref} = \sigma_{n,m} + |\sigma_{n,b}| \quad \text{(P.29)}$$

where:

$$\sigma_{n,m} = \frac{\pi P_m}{\frac{\pi}{2} + \beta + \frac{1}{2}\sin 2\beta}$$

NOTE 1 $\sigma_{n,m}$ is conservative for a/2r = 0.4.

$$\beta = \arcsin\left(\frac{r-a}{r}\right)$$

$$\sigma_{n,b} = \frac{3\pi}{16\chi} P_b$$

χ has the values given in Table P.2.

 © The British Standards Institution 2019

Table P.2 **Values of χ for bending loading**

a/2*r*	χ, lower bound
0	1
0.05	0.958
0.1	0.889
0.15	0.810
0.2	0.725
0.25	0.640
0.3	0.556
0.35	0.475
0.4	0.400
0.45	0.329
0.5	0.265
0.55	0.208
0.6	0.158
0.65	0.116
0.7	0.080 0
0.75	0.051 6
0.8	0.030 0
0.85	0.014 8
0.9	0.005 5
0.95	0.001 0
1.0	0

*NOTE 2 See **M.10.1** for the stress intensity factor solution for the straight-fronted flaws in round bars, **M.10.2** for the stress intensity factor solution for the semi-circular surface flaws in round bars, **M.10.3** for the stress intensity factor solution for the semi-elliptical surface flaws in round bars and **M.10.4** for the stress intensity factor solution for the semi-elliptical surface flaws in bolts.*

P.12.2 Circumferential flaw in round bars

See Figure M.24 for the definition of the geometry. The reference stress can be conservatively estimated from Equation (P.30):

$$\sigma_{\text{ref}} = \frac{P_{\text{m}}}{(1 - a/r)^2} + \frac{3\pi P_{\text{b}}}{16(1 - a/r)^3} \quad \text{(P.30)}$$

*NOTE See **M.10.5** for the stress intensity factor solution for this geometry.*

P.13 Limit load solutions for strength mismatch

P.13.1 General

Unlike homogeneous plates, welded plates exhibit various patterns of plasticity development, which are due to the presence of material mismatch. The occurrence of various plasticity patterns depends on the following (see reference [P.23]):

a) the strength mismatch factor or the mismatch ratio, *M*, which is the ratio of the yield strength of the weld metal to that of the parent material; and

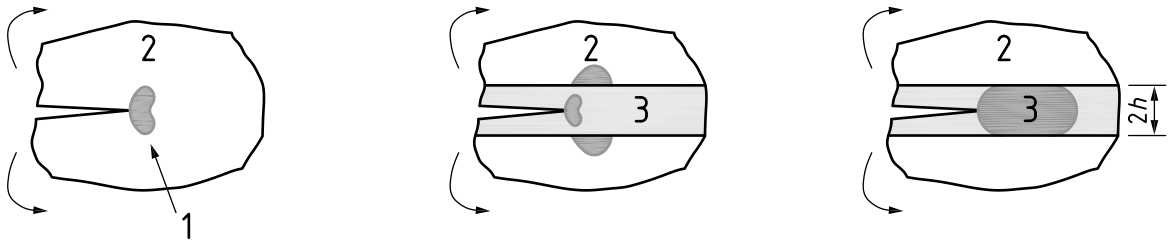
b) the geometrical parameters such as plate width, flaw size, weld width and slenderness ratio, ψ, which are defined on a case-by-case basis in this annex.

Such plasticity development patterns play an important role in determining the mismatch limit load. Figure P.4 depicts possible patterns of plasticity development for the mismatched plate with a crack in the centre line of the weld metal.

For undermatching, plastic deformations can either be confined to the weld metal (see Figure P.4 and reference [P.23]) or penetrate to the parent material plate. Solutions should be derived for both cases and the lower of the two should be adopted as the limit load. For overmatching, plastic deformations can either spread to the parent material plate (see Figure P.4), or be confined to the parent material plate. Again, solutions should be derived for both cases and the lower of the two should be adopted as the limit load.

Subclauses P.13 and P.14 should be used in conjunction with Annex I.

Figure P.4 **Classification of plasticity deformation patterns for mismatched structures**



a) Homogeneous structure

$\sigma_Y^{\text{Parent material}} < \sigma_Y^{\text{Weld material}}$

Remote plasticity at the parent metal

b) Strength overmatched welded structure

$\sigma_Y^{\text{Parent material}} > \sigma_Y^{\text{Weld material}}$

Confined plasticity within weld zone

c) Strength undermatched welded structure

Key

1 Plastic zone
2 Parent metal
3 Weld metal

The methods used for deriving the mismatch limit load solutions are mainly plastic limit analysis and finite element analysis. These solutions are expressed in the form of parametric equations for ease of application. All solutions presented in this annex are taken from references [P.14], [P.15], [P.16], [P.17] and [P.18].

P.13.2 Through-thickness flaws in plates under tension (global solution)

P.13.2.1 General

See Figure P.5 for the definition of the geometry. The limit load for the plate made wholly of parent material, F_e^P, is calculated (see references [P.14], [P.15] [P.16] and [P.17]) as follows:

a) for the plane stress condition:

$$F_e^P = 2B(w-a)\sigma_Y^P \quad \text{(P.32)}$$

b) for the plane strain condition:

$$F_e^P = \frac{4}{\sqrt{3}}B(w-a)\sigma_Y^P \quad \text{(P.33)}$$

The normalized ligament size to be used in the subsequent calculations is calculated from:

$$\psi = \frac{w-a}{h} \quad \text{(P.34)}$$

P.13.2.2 Flaw at the centre line of the weld material

P.13.2.2.1 Plane stress

For undermatching ($M < 1$), the limit load of the mismatched system, F_e^M, is calculated from:

$$\frac{F_e^M}{F_e^P} = M \qquad \text{for } 0 \le \psi \le 1.43 \qquad \text{(P.35a)}$$

$$\frac{F_e^M}{F_e^P} = \min\left[\frac{F_e^{M(1)}}{F_e^P}, \frac{F_e^{M(2)}}{F_e^P}\right] \qquad \text{for } \psi > 1.43 \qquad \text{(P.35b)}$$

where:

$$\frac{F_e^{M(1)}}{F_e^P} = M\left[\frac{2}{\sqrt{3}} - \left(\frac{2-\sqrt{3}}{\sqrt{3}}\right)\frac{1.43}{\psi}\right]$$

$$\frac{F_e^{M(2)}}{F_e^P} = 1 - (1-M)\frac{1.43}{\psi}$$

For overmatching ($M > 1$), the limit load of the mismatched system, F_e^M, is calculated from:

$$\frac{F_e^M}{F_e^P} = \min\left(\frac{F_e^{M(3)}}{F_e^P}, \frac{1}{1-a/w}\right) \qquad \text{(P.36)}$$

where:

$$\frac{F_e^{M(3)}}{F_e^P} = M \qquad \text{for } \psi \le \psi_1$$

$$\frac{F_e^{M(3)}}{F_e^P} = \left[\frac{24(M-1)}{25}\frac{\psi_1}{\psi} + \frac{M+24}{25}\right] \qquad \text{for } \psi > \psi_1.$$

where:

$$\psi_1 = \{1 + 0.43\exp[-5(M-1)]\}\exp[-(M-1)/5]$$

P.13.2.2.2 Plane strain

For undermatching ($M < 1$), the limit load of the mismatched system, F_e^M, is calculated from:

$$\frac{F_e^M}{F_e^P} = M \qquad \text{for } 0 \le \psi \le 1 \qquad \text{(P.37a)}$$

$$\frac{F_e^M}{F_e^P} = \min\left(\frac{F_e^{M(4)}}{F_e^P}, \frac{F_e^{M(5)}}{F_e^P}\right) \qquad \text{for } \psi > 1 \qquad \text{(P.37b)}$$

where:

$$\frac{F_e^{M(4)}}{F_e^P} = 1 - (1-M)\frac{1}{\psi}$$

$$\frac{F_e^{M(5)}}{F_e^P} = M\left[1.0 + 0.462\frac{(\psi-1)^2}{\psi} - 0.044\frac{(\psi-1)^3}{\psi}\right] \qquad \text{for } 1 \le \psi \le 3.6$$

$$\frac{F_e^{M(5)}}{F_e^P} = M\left[2.571 - \frac{3.254}{\psi}\right] \qquad \text{for } 3.6 < \psi \le 5.0$$

$$\frac{F_e^{M(5)}}{F_e^P} = M\left[1.291 + 0.125\psi + \frac{0.019}{\psi}\right] \qquad \text{for } \psi > 5.0$$

For overmatching ($M > 1$), the limit load of the mismatched system, F_e^M, is calculated from:

$$\frac{F_e^M}{F_e^P} = \min\left(\frac{F_e^{M(6)}}{F_e^P}, \frac{1}{1-a/w}\right) \quad \text{(P.38)}$$

where:

$$\frac{F_e^{M(6)}}{F_e^P} = M \quad \text{for } 0 < \psi \le \psi_2$$

$$\frac{F_e^{M(6)}}{F_e^P} = \left[\frac{24(M-1)}{25}\frac{\psi_2}{\psi} + \frac{M+24}{25}\right] \quad \text{for } \psi > \psi_2$$

where:

$\psi_2 = \exp[-(M-1)/5]$

P.13.2.3 Flaw at the interface between weld material and parent material

P.13.2.3.1 Plane stress

For undermatching ($M < 1$), the limit load of the mismatched system, F_e^M, is calculated (see reference [P.17]) from:

$$\frac{F_e^M}{F_e^P} = M\left\{1.095 - 0.095\exp\left[-\frac{(1-M)}{0.108M}\right]\right\} \quad \text{for all } \psi \quad \text{(P.39)}$$

For overmatching ($M > 1$), the limit load of the mismatched system, F_e^M, is calculated from:

$$\frac{F_e^M}{F_e^P} = 1 \quad \text{for all } \psi \quad \text{(P.40)}$$

P.13.2.3.2 Plane strain

For undermatching ($M < 1$), the limit load of the mismatched system, F_e^M, is calculated from:

$$\frac{F_e^M}{F_e^P} = \min\left\{\frac{F_e^{M(8)}}{F_e^P}, \frac{F_e^{M(9)}}{F_e^P}\right\} \quad \text{(P.41)}$$

where:

$$\frac{F_e^{M(8)}}{F_e^P} = f_1 \quad \text{for } 0 \le \psi \le \psi_3 = 2\left[1 - \left(2-\sqrt{2}\right)(1-M)\right]$$

$$\frac{F_e^{M(8)}}{F_e^P} = 1 - (1-f_1)\psi_3/\psi \quad \text{for } \psi_3 = 2\left[1 - \left(2-\sqrt{2}\right)(1-M)\right] < \psi$$

$f_1 = 1.3M$ for $M \le 0.5$

$$f_1 = M\left[1 + 0.52\left(\frac{1-M}{M}\right) - 0.22\left(\frac{1-M}{M}\right)^2\right] \quad \text{for } 0.5 < M \le 1.0$$

$$\frac{F_e^{M(9)}}{F_e^P} = 1.3M \quad \text{for } 0 \le \psi \le \sqrt{2}$$

$$\frac{F_e^{M(9)}}{F_e^P} = M\left[1.3 + 0.394\frac{\left(\psi-\sqrt{2}\right)^2}{\psi} - 0.027\frac{\left(\psi-\sqrt{2}\right)^3}{\psi}\right] \quad \text{for } \sqrt{2} < \psi \le 4.2$$

$$\frac{F_e^{M(9)}}{F_e^P} = M\left(2.881 - \frac{4.123}{\psi}\right) \quad \text{for } 4.2 < \psi \le 6.2$$

$$\frac{F_e^{M(9)}}{F_e^P} = M\left(1.294 + 0.125\psi - \frac{0.909}{\psi}\right) \qquad \text{for } \psi > 6.2$$

NOTE An error in the original source has been corrected here (see [P.17]).

For overmatching ($M > 1$), the limit load of the mismatched system, F_e^M, is calculated from:

$$\frac{F_e^M}{F_e^P} = \min\left[\frac{F_e^{M(10)}}{F_e^P}, \frac{1}{1 - a/w}\right] \tag{P.42}$$

where:

$$\frac{F_e^{M(10)}}{F_e^P} = f_2 \qquad \text{for } 0 \le \psi \le \sqrt{2}$$

$$\frac{F_e^{M(10)}}{F_e^P} = \left[f_2 - \frac{(M+24)}{25}\right] \exp\left[-\frac{\left(\psi - \sqrt{2}\right)}{4M-1}\right] + \frac{M+24}{25} \quad \text{for } \psi > \sqrt{2}$$

where:

$f_2 = 1 + 0.52(M - 1) - 0.22(M - 1)^2$ for $1 \le M < 2$

$f_2 = 1.30$ for $M \ge 2$

P.13.2.4 Flaw at the interface of a bi-material joint

P.13.2.4.1 Plane stress

The limit load of the mismatched system, F_e^M, is calculated from:

$$\frac{F_e^M}{F_e^P} = \min\left[\frac{F_e^{M(11)}}{F_e^P}, \frac{1}{1 - a/w}\right] \tag{P.43}$$

where:

$$\frac{F_e^{M(11)}}{F_e^P} = 1.095 - 0.095 \exp\left[\frac{(1-M)}{0.108}\right]$$

P.13.2.4.2 Plane strain

The limit load of the mismatched system, F_e^M, is calculated from:

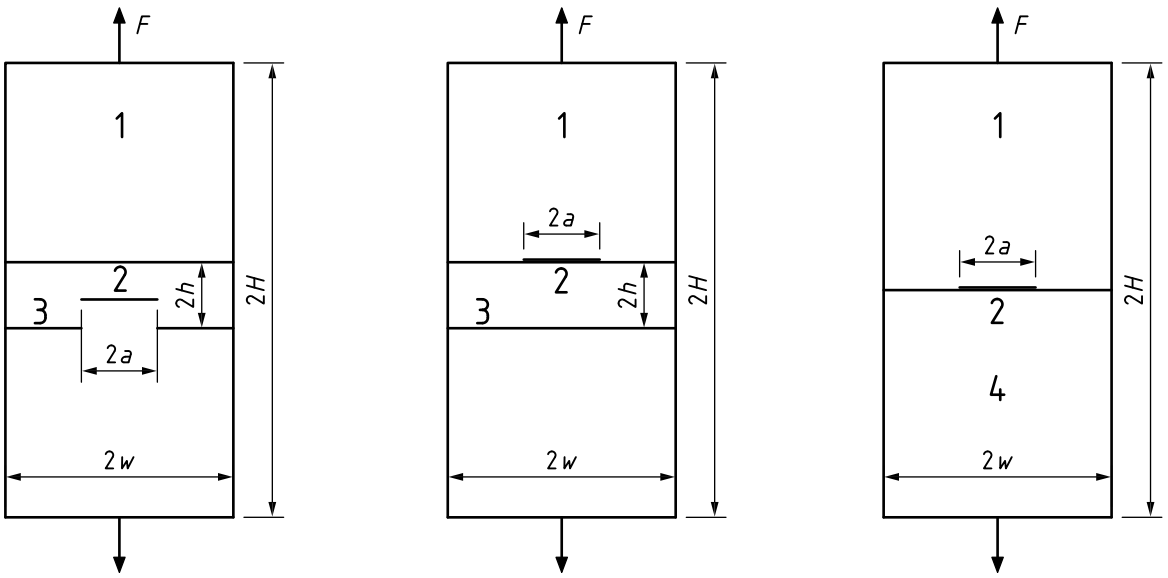
$$\frac{F_e^M}{F_e^P} = \min\left(\frac{F_e^{M(12)}}{F_e^P}, \frac{1}{1 - a/w}\right) \tag{P.44}$$

where:

$$\frac{F_e^{M(12)}}{F_e^P} = 1 + 0.52(M-1) - 0.22(M-1)^2 \qquad \text{for } 1 \le M \le 2$$

$$\frac{F_e^{M(12)}}{F_e^P} = 1.30 \qquad \text{for } M > 2$$

Figure P.5 **Centre cracked plate under tension [$\psi = (w - a)/h$]**



a) Flaw at the centre of the weld

b) Flaw at the interface between weld and parent material

c) Flaw at the interface of a bi-material joint

Key

1 Parent material 1
2 Flaw
3 Weld
4 Parent material 2

P.13.3 Double edge cracked plate under tension (global solution)

P.13.3.1 General

See Figure P.6 for the definition of the geometry. The limit load for the plate made wholly of parent material, F_e^P, is calculated (see references [P.14] and [P.18]) from Equation (P.5) for plane stress conditions and from Equation (P.7) for plane strain conditions by substituting σ_{YP} for σ_Y in the equations. The normalized ligament size, ψ, is calculated from Equation (P.34).

P.13.3.2 Flaw at the centre line of the weld material

P.13.3.2.1 Plane stress

For undermatching ($M < 1$), the limit load of the mismatched system, F_e^M, is calculated from:

$$\frac{F_e^M}{F_e^P} = M \qquad \text{for all } \psi \tag{P.45}$$

For overmatching ($M > 1$), the limit load of the mismatched system, F_e^M, is calculated from:

$$\frac{F_e^M}{F_e^P} = \min\left[\frac{F_e^{M(1)}}{F_e^P}, \frac{F_e^{M(2)}}{F_e^P}\right] \tag{P.46}$$

where:

$$\frac{F_e^{M(1)}}{F_e^P} = \frac{1}{\beta}\frac{1}{(1 - a/w)}$$

 © The British Standards Institution 2019

$$\frac{F_e^{M(2)}}{F_e^P} = M \qquad \text{for } 0 \le \psi \le \psi_1$$

$$\frac{F_e^{M(2)}}{F_e^P} = \frac{M+24}{25} + (M-1)\left[1.06\frac{\psi_1}{\psi} - 0.1\left(\frac{\psi_1}{\psi}\right)^M\right] \qquad \text{for } \psi \ge \psi_1$$

where:

$\psi_1 = \exp[-2(M-1)/5]$

β is calculated from Equation (P.6a) and Equation (P.6b).

P.13.3.2.2 Plane strain

For undermatching ($M < 1$), the limit load of the mismatched system, F_e^M, is calculated from:

$$\frac{F_e^M}{F_e^P} = M \qquad \text{for } 0 \le \psi \le 0.5 \qquad \text{(P.47a)}$$

$$\frac{F_e^M}{F_e^P} = \min\left(\frac{F_e^{M(2)}}{F_e^P}, \frac{F_e^{M(3)}}{F_e^P}\right) \qquad \text{for } \psi > 0.5 \qquad \text{(P.47b)}$$

where:

$$\frac{F_e^{M(2)}}{F_e^P} = 1 - (1-M)\frac{0.5}{\psi}$$

$$\frac{F_e^{M(3)}}{F_e^P} = \frac{M\left[\beta + A(\psi - 0.5) + B(\psi - 0.5)^2\right]}{\beta} \qquad \text{for } 0.5 \le \psi \le \psi_2$$

$$\frac{F_e^{M(3)}}{F_e^P} = \frac{M(0.25\psi + 2.2172)}{\beta} \qquad \text{for } \psi > \psi_2$$

where:

β is calculated from Equation (P.8a) and Equation (P.8b)

$$A = 0.25 - \frac{\beta - 2.3422}{\psi_2 - 0.5} \qquad \text{for } 0 \le \frac{a}{w} \le 0.35$$

$$A = 0.25 - \frac{2(\beta - 2.3422)}{\psi_2 - 0.5} \qquad \text{for } \frac{a}{w} > 0.35$$

$$B = 0 \qquad \text{for } 0 \le \frac{a}{w} \le 0.35$$

$$B = \frac{\beta - 2.3422}{(\psi_2 - 0.5)^2} \qquad \text{for } \frac{a}{w} > 0.35$$

$\psi_2 = 16.3 - 35.2(a/w) + 19.9(a/w)^2$

For overmatching ($M > 1$), the limit load of the mismatched system, F_e^M, is calculated from:

$$\frac{F_e^M}{F_e^P} = \min\left[\frac{F_e^{M(4)}}{F_e^P}, \frac{F_e^{M(5)}}{F_e^P}\right] \qquad \text{(P.48)}$$

where:

$$\frac{F_e^{M(4)}}{F_e^P} = M \qquad \text{for } \psi \le \psi_3$$

$$\frac{F_e^{M(4)}}{F_e^P} = \frac{49(M-1)}{50}\frac{\psi_1}{\psi} + \frac{M+49}{50} \qquad \text{for } \psi > \psi_3$$

$$\frac{F_e^{M(5)}}{F_e^P} = \frac{1}{\beta}\frac{1}{[1-(a/w)]}$$

where:

$$\psi_3 = 0.3\exp\left[\frac{-(M-1)}{0.5}\right] + 0.2$$

P.13.3.3 Flaw at the interface between weld material and parent material

P.13.3.3.1 Plane stress

For undermatching ($M < 1$), the limit load of the mismatched system, F_e^M, is calculated from:

$$\frac{F_e^M}{F_e^P} = M \qquad \text{for all } \psi \qquad \text{(P.49)}$$

For overmatching ($M > 1$), the limit load of the mismatched system, F_e^M, is calculated from:

$$\frac{F_e^M}{F_e^P} = 1 \qquad \text{for all } \psi \qquad \text{(P.50)}$$

P.13.3.3.2 Plane strain

For undermatching ($M < 1$), the limit load of the mismatched system, F_e^M, is calculated from:

$$\frac{F_e^M}{F_e^P} = M \qquad \text{for } 0 \le \psi \le 1 \qquad \text{(P.51a)}$$

$$\frac{F_e^M}{F_e^P} = \min\left[\frac{F_e^{M(5)}}{F_e^P}, \frac{F_e^{M(6)}}{F_e^P}\right] \qquad \text{for } 1 < \psi \qquad \text{(P.51b)}$$

where:

$$\frac{F_e^{M(5)}}{F_e^P} = 1 - (1-M)\frac{1}{\psi}$$

$$\frac{F_e^{M(6)}}{F_e^P} = \frac{M\left[\beta + A(\psi-1) + B(\psi-1)^2\right]}{\beta} \qquad \text{for } 1 \le \psi \le \psi_4$$

$$\frac{F_e^{M(6)}}{F_e^P} \frac{M(0.125\psi + 2.2172)}{\beta} \qquad \text{for } \psi > \psi_4$$

where:

β is calculated from Equation (P.8a) and Equation (P.8b)

$$A = 0.125 - \frac{\beta - 2.3422}{\psi_4 - 1} \qquad \text{for } 0 < \frac{a}{w} \le 0.35$$

$$A = 0.125 - \frac{2(\beta - 2.3422)}{\psi_4 - 1} \qquad \text{for } 0.35 < \frac{a}{w}$$

$$B = 0 \qquad \text{for } 0 < \frac{a}{w} \le 0.35$$

$$B = \frac{\beta - 2.3422}{(\psi_4 - 1)^2} \qquad \text{for } 0.35 < \frac{a}{w}$$

$$\Psi_4 = 32.6 - 70.4\left(\frac{a}{w}\right) + 39.8\left(\frac{a}{w}\right)^2$$

For overmatching ($M > 1$), the limit load of the mismatched system, F_e^M, is calculated from:

$$\frac{F_e^M}{F_e^P} = 1 \qquad \text{for all } \psi \qquad \text{(P.52)}$$

P.13.3.4 Flaw at the interface of a bi-material joint

P.13.3.4.1 Plane stress

Under plane stress, the solution is given by Equation (P.53).

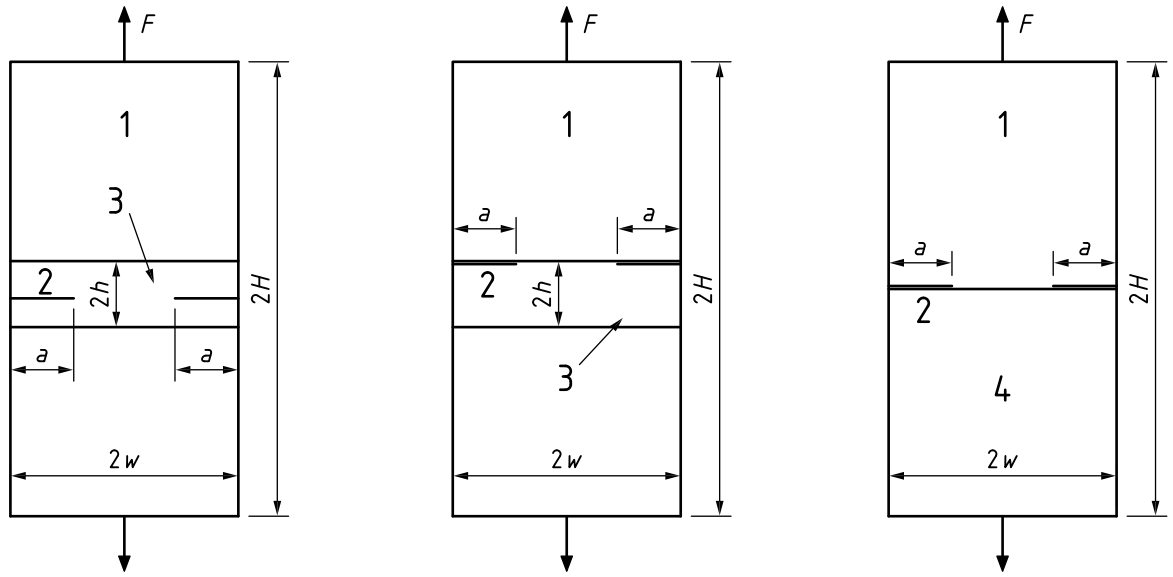
$$\frac{F_e^M}{F_e^P} = 1 \tag{P.53}$$

P.13.3.4.2 Plane strain

Under plane strain, the solution is given by Equation (P.54).

$$\frac{F_e^M}{F_e^P} = 1 \tag{P.54}$$

Figure P.6 **Double edge cracked plate under tension [$\psi = (w - a)/h$]**



a) Flaw at the centre line of the weld

b) Flaw at the interface between weld and parent material

c) Flaw at the interface of a bi-material joint

Key

1 Parent material 1
2 Flaw
3 Weld
4 Parent material 2

P.13.4 Single edge cracked plate under in-plane bending (global solution)

P.13.4.1 General

See Figure P.7 for the definition of the geometry.

The limit moment for the plate made wholly of parent material, M_e^P, is calculated (see references [P.14], [P.15], [P.16] and [P.17]) from:

$$M_e^P = 0.4641 \frac{\sigma_Y^P}{\sqrt{3}} B(W - a)^2 \tag{P.55}$$

for plane stress and:

$$M_e^P = \beta \frac{\sigma_Y^P}{\sqrt{3}} B(W - a)^2 \tag{P.56}$$

for plane strain where:

$$\beta = 0.500 + 0.808\left(\frac{a}{W}\right) - 1.245\left(\frac{a}{W}\right)^2 \qquad \text{for } 0 \le \frac{a}{W} \le 0.3 \qquad \text{(P.57a)}$$

$$\beta = 0.631 \qquad \text{for } 0.3 < \frac{a}{W} < 1 \qquad \text{(P.57b)}$$

$$\psi = (W - a)/h \qquad \text{(P.57c)}$$

P.13.4.2 Flaw at the centre line of the weld material

P.13.4.2.1 Plane stress

For undermatching ($M < 1$), the limit moment of the mismatched system, M_e^M, is calculated from:

$$\frac{M_e^M}{M_e^P} = M \qquad \text{for all } \psi \qquad \text{(P.58)}$$

For overmatching ($M > 1$), the limit moment of the mismatched system, M_e^M, is calculated from:

$$\frac{M_e^M}{M_e^P} = \min\left[\frac{M_e^{M(1)}}{M_e^P}, \frac{1}{(1 - a/W)^2}\right] \qquad \text{(P.59)}$$

where:

$$\frac{M_e^M}{M_e^P} = M \qquad \text{for } 0 \le \psi \le \psi_1$$

$$\frac{M_e^{M(1)}}{M_e^P} = \frac{M+49}{50} + \left[\frac{49(M-1)}{50} + 1 - \sqrt{M-1}\right]\frac{\psi_1}{\psi} + \left(-1 + \sqrt{M-1}\right)\left(\frac{\psi_1}{\psi}\right)^M \qquad \text{for } \psi > \psi_1$$

where:

$$\Psi_1 = \{2.0 + 0.7\exp[-(M-1)]\}\exp[-(M-1)/8]$$

P.13.4.2.2 Plane strain

For undermatching ($M < 1$), the limit moment of the mismatched system, M_e^M, is calculated from:

$$\frac{M_e^M}{M_e^P} = M \qquad \text{for } 0 \le \psi \le 2.0 \qquad \text{(P.60a)}$$

$$\frac{M_e^M}{M_e^P} = \min\left[\frac{M_e^{M(2)}}{M_e^P}, \frac{M_e^{M(3)}}{M_e^P}\right] \qquad \text{for } \psi > 2.0 \qquad \text{(P.60b)}$$

where:

$$\frac{M_e^{M(2)}}{M_e^P} = \left[\frac{9(M-1)}{10}\right]\exp\left[-\frac{(\psi-2)}{20(1-M)}\right] + \frac{M+9}{10}$$

and where for $0 < a/W \le 0.3$:

$$\frac{M_e^{M(3)}}{M_e^P} = M\left[1 + 1.0342\left(\frac{\psi-2}{10}\right)^2 - 0.422\left(\frac{\psi-2}{10}\right)^3\right] \text{ for } 2 < \psi \le 15$$

$$\frac{M_e^{M(3)}}{M_e^P} = M\left[0.9982 + 0.5480\left(\frac{\psi}{10}\right)\right] \qquad \text{for } \psi > 15$$

and where for $a/W > 0.3$:

$$\frac{M_e^{M(3)}}{M_e^P} = M\left[1.094 - 1.017\left(\frac{\psi}{10}\right) + 3.129\left(\frac{\psi}{10}\right)^2 - 1.952\left(\frac{\psi}{10}\right)^3\right] \qquad \text{for } 2.0 \le \psi \le 7.0$$

$$\frac{M_e^{M(3)}}{M_e^P} = M\left[0.900 + 0.494\left(\frac{(\Psi)}{10}\right)\right] \quad \text{for } \psi > 7.0$$

For overmatching ($M > 1$), the limit moment of the mismatched system, M_e^M, is calculated from:

$$\frac{M_e^M}{M_e^P} = \min\left[\frac{M_e^{M(4)}}{M_e^P}, \frac{1}{\beta}\frac{1}{(1-a/W)^2}\right] \quad \text{(P.61)}$$

where:

$$\frac{M_e^{M(4)}}{M_e^P} = M \quad \text{for } 0 \le \psi \le \psi_2$$

$$\frac{M_e^{M(4)}}{M_e^P} = \frac{M+49}{50} + (M-1)\left[\left(0.98 - 0.3\sqrt{M-1}\right)\frac{\psi_2}{\psi} + 0.3\sqrt{M-1}\left(\frac{\psi_2}{\psi}\right)^M\right] \quad \text{for } \psi > \psi_2$$

$$\psi_2 = 2\exp\left(-\frac{M-1}{10a/W}\right) \quad \text{for } 0 < a/W \le 0.3$$

$$\psi_2 = 2\exp\left(-\frac{M-1}{8}\right) \quad \text{for } 0.3 < a/W < 1$$

P.13.4.3 Flaw at the interface between weld material and parent material

P.13.4.3.1 Plane stress

For undermatching ($M < 1$), the limit moment of the mismatched system, M_e^M, is calculated (see references [P.17] and [P.18]) from:

$$\frac{M_e^M}{M_e^P} = M\{1.04 - 0.04\exp[-(1-M)/0.13M]\} \quad \text{for all } \psi \quad \text{(P.62)}$$

For overmatching ($M > 1$), the limit moment of the mismatched system, M_e^M, is calculated from:

$$\frac{M_e^M}{M_e^P} = 1 \quad \text{for all } \psi \quad \text{(P.63)}$$

P.13.4.3.2 Plane strain

For undermatching ($M < 1$), the limit moment of the mismatched system, M_e^M, is calculated (see references [P.17] and [P.18]) from:

$$\frac{M_e^M}{M_e^P} = M \quad \text{for } 0 \le \psi \le 4 \quad \text{(P.64a)}$$

$$\frac{M_e^M}{M_e^P} = \min\left[\frac{M_e^{M(5)}}{M_e^P}, \frac{M_e^{M(6)}}{M_e^P}\right] \quad \text{for } \psi > 4 \quad \text{(P.64b)}$$

where:

$$\frac{M_e^{M(5)}}{M_e^P} = \left(M - \frac{M+9}{10}\right)\left(1 + \frac{\psi-4}{8.5\sqrt{1-M}}\right)\exp\left(-\frac{\psi-4}{8.5\sqrt{1-M}}\right) + \frac{M+9}{10} \quad \text{for } \psi > 4$$

and where for $0 < a/W \le 0.3$:

$$\frac{M_e^{M(6)}}{M_e^P} = M\left[1 + \frac{5.377 - 3\beta}{\beta}\left(\frac{\Psi-4}{10}\right)^2 + \frac{2\beta - 3.377}{\beta}\left(\frac{\Psi-4}{10}\right)^3\right] \quad \text{for } 4 < \psi \le 14$$

$$\frac{M_e^{M(6)}}{M_e^P} = \frac{M}{\beta}\left(1.377 + 0.623\frac{\Psi-4}{10}\right) \quad \text{for } \psi > 14$$

and β is calculated from Equation (P.57a), for 0.3 > a/W:

$$\frac{M_e^{M(6)}}{M_e^P} = M\left[1.06 + 0.522\left(\frac{\Psi - 4}{10}\right)^2 - 0.133\left(\frac{\Psi - 4}{10}\right)^3\right] \qquad \text{for } 4 < \psi \leq 14$$

$$\frac{M_e^{M(6)}}{M_e^P} = M\left(0.955 + 0.494\frac{\Psi - 4}{10}\right) \qquad \text{for } 14 < \psi$$

For overmatching (M > 1), the limit moment of the mismatched system, M_e^M, is calculated from:

$$\frac{M_e^M}{M_e^P} = 1 \qquad \text{for all } \psi \qquad \text{(P.65)}$$

P.13.4.4 Flaw at the interface of a bi-material joint

P.13.4.4.1 Plane stress

The limit moment of the mismatched system, M_e^M, is calculated from:

$$\frac{M_e^M}{M_e^P} = 1.04 - 0.04\exp\left(-\frac{M-1}{0.13}\right) \qquad \text{(P.66)}$$

P.13.4.4.2 Plane strain

The limit moment of the mismatched system, M_e^M, is calculated from:

$$\frac{M_e^M}{M_e^P} = (\beta - \beta_\infty)\exp\left(-\frac{M-1}{a/W}\right) + \beta_\infty \qquad \text{for } 0 < a/W \leq 0.3 \qquad \text{(P.67a)}$$

$$\frac{M_e^M}{M_e^P} = (\beta - \beta_\infty)\exp\left(-\frac{M-1}{0.3}\right) + \beta_\infty \qquad \text{for } 0.3 < a/W \leq 1 \qquad \text{(P.67b)}$$

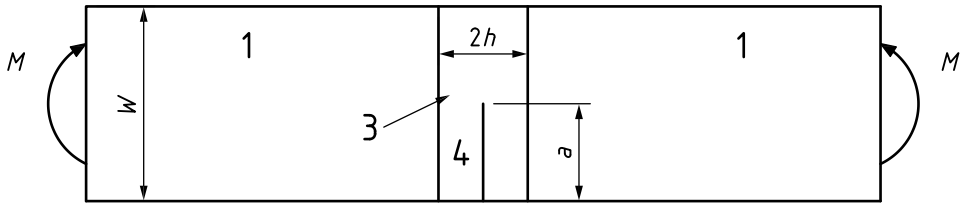
where:

β is calculated from Equation (P.57a)

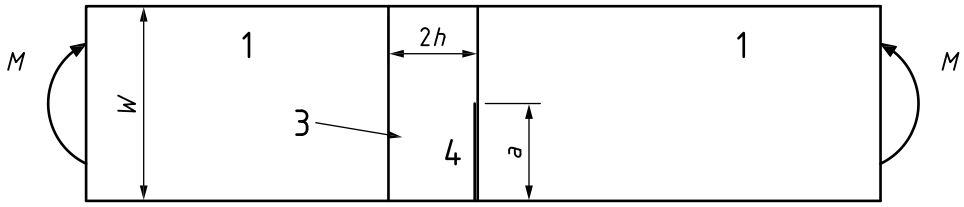
$\beta_\infty = 0.5 + 0.89\left(\frac{a}{W}\right) - 1.165\left(\frac{a}{W}\right)^2$ for $0 < a/W \leq 0.4$

β_∞ = 0.67 for $0.4 < a/W \leq 1$

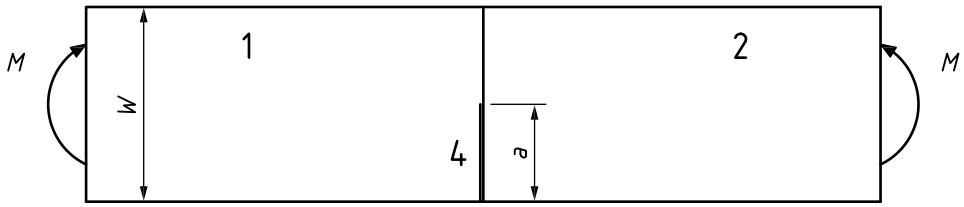
Figure P.7 **Single edge cracked plate under in-plane bending**



a) Flaw at the centre of the weld



b) Flaw at the interface between the weld and parent material



c) Flaw at the interface of a bi-material joint

Key

1 Parent material 1
2 Parent material 2
3 Weld
4 Flaw

P.13.5 Thin-walled pipes/cylinders under tension (global solution)

P.13.5.1 General

The definition of ψ for this solution is as follows:

$$\psi = (B - a)/h$$

See Figure P.8 for the definition of the geometry. The limit load for the pipe made wholly of parent material (see reference [P.14]) is:

$$F_e^P = 2\frac{\sigma_Y^P}{\sqrt{3}}\pi\left[r_o^2 - (r_i + a)^2\right] \quad \text{(P.68a)}$$

or, alternatively [P.24]:

$$F_e^P = 2\pi r_m(B-a)\sigma_Y^P\left\{\left(\frac{a}{2(B-a)}\right) + \left[1 - \frac{3}{4}\left(\frac{a}{B-a}\right)^2\right]^{0.5}\right\} \quad \text{for } a \le \frac{B}{1+\sqrt{3}} \quad \text{(P.68b)}$$

$$F_e^P = \frac{2}{\sqrt{3}}\sigma_Y^P[2\pi r_m(B-a)] \quad \text{for } a > \frac{B}{1+\sqrt{3}} \quad \text{(P.68c)}$$

where:

$$r_m = r_i + \frac{B}{2}$$

P.13.5.2 Flaw at the centre line of the weld material

For undermatching ($M < 1$), the limit load of the mismatched system, F_e^M, is calculated from:

$$\frac{F_e^M}{F_e^P} = M \qquad \text{for } 0 \le \psi \le 1 \qquad \text{(P.69a)}$$

$$\frac{F_e^M}{F_e^P} = \min\left[\frac{F_e^{M(1)}}{F_e^P}, \frac{F_e^{M(2)}}{F_e^P}\right] \qquad \text{for } 1 < \psi \qquad \text{(P.69b)}$$

where:

$$\frac{F_e^{M(1)}}{F_e^P} = M\left(1 + \frac{\psi - 1}{3\sqrt{3}}\right)$$

$$\frac{F_e^{M(2)}}{F_e^P} = 1 - (1 - M)\frac{1}{\psi}$$

For overmatching ($M > 1$), the limit load of the mismatched system, F_e^M, is calculated from:

$$\frac{F_e^M}{F_e^P} = \min\left[\frac{F_e^{M(3)}}{F_e^P}, \frac{1}{1 - a/B}\right] \qquad \text{(P.70)}$$

$$\frac{F_e^M}{F_e^P} = M \qquad \text{for } \psi \le \psi_1 = \exp[-2(M - 1)/5]$$

$$\frac{F_e^{M(3)}}{F_e^P} = \frac{24(M - 1)}{25}\frac{\psi_1}{\psi} + \frac{M + 24}{25} \qquad \text{for } \psi \ge \psi_1 = \exp[-2(M - 1)/5]$$

P.13.5.3 Flaw at the interface between weld material and parent material

For undermatching ($M < 1$), the limit load of the mismatched system, F_e^M, is calculated from:

$$\frac{F_e^M}{F_e^P} = M \qquad \text{for } 0 \le \psi \le 2 \qquad \text{(P.71a)}$$

$$\frac{F_e^M}{F_e^P} = \min\left[\frac{F_e^{M(4)}}{F_e^P}, \frac{F_e^{M(5)}}{F_e^P}\right] \qquad \text{for } \psi > 2 \qquad \text{(P.71b)}$$

where:

$$\frac{F_e^{M(4)}}{F_e^P} = M\left(1 + \frac{\psi - 2}{6\sqrt{3}}\right)$$

$$\frac{F_e^{M(5)}}{F_e^P} = 1 - (1 - M)\frac{2}{\psi}$$

For overmatching ($M > 1$), the limit load of the mismatched system, F_e^M, is calculated from:

$$\frac{F_e^M}{F_e^P} = 1 \quad \text{for all } \psi \qquad \text{(P.72)}$$

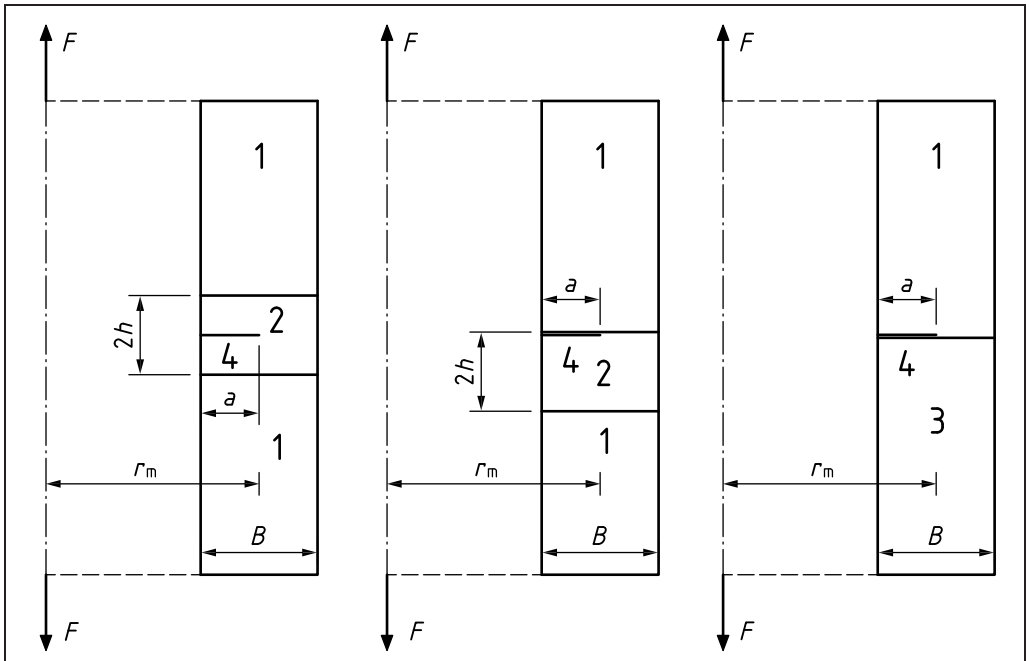
 © The British Standards Institution 2019

P.13.5.4 Flaw at the interface of a bi-material joint

For both plane strain and plane stress conditions, the following equation should be used:

$$\frac{F_e^M}{F_e^P} = 1 \qquad \text{(P.73)}$$

Figure P.8 **Fully circumferential internal flaw in thin-walled pipe/cylinder under tension**



a) Flaw at the centre line of the weld

b) Flaw at the interface between weld and parent plate

c) Flaw at the interface of a bi-material joint

Key

1	Parent material 1
2	Weld
3	Parent material 2
4	Flaw

P.14 Through-thickness flaws in clad plates under tension (global solution)

See Figure P.9 for the definition of the geometry. For a centre cracked clad plate, a closed-form expression for the tensile limit load under plane stress condition is proposed in reference [P.19] as:

$$\frac{F_e^{clad}}{F_e^{(h)}} = \frac{1}{4} b_2 B^{-1} (1 + Mb) \left(2 + \frac{\sigma_Y^{\text{Material 2}}}{k_2} \right) \qquad \text{(P.74)}$$

where:

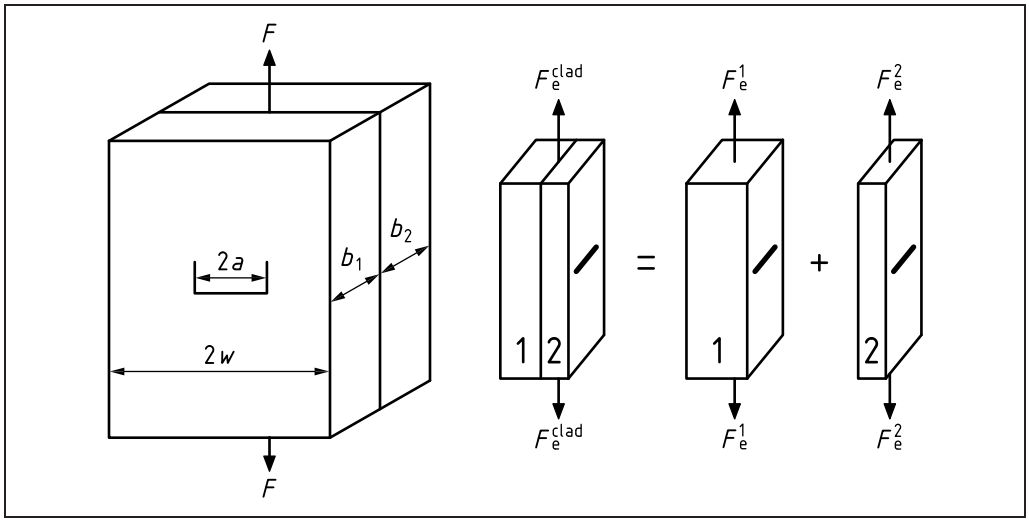
$F_e^{(h)} = 2B\sigma_Y^{\text{Material 2}}(W - a)$ is the tensile limit load of the homogeneous plate containing a through-thickness flaw made of the softer material (here material 2) with yield strength $\sigma_Y^{\text{Material 2}}$ and thickness of $B = b_1 + b_2$;

$b = b_1/b_2$

$M = \dfrac{\sigma_Y^{\text{Material 1}}}{\sigma_Y^{\text{Material 2}}}$ is the strength mismatch ratio with $\sigma_Y^{\text{Material 1}}$, the yield strength of the higher yield strength material (here material 1)

Alternatively, the limit load of the clad plate can be derived using the rule of mixtures as proposed and validated in [P.19] and [P.20].

Figure P.9 **Centre through-thickness crack in a clad plate under tension**



By substituting the corresponding values of b, M, k_2, $F_e^{(h)}$ and B into Equation (P.74), and after some simplifications, based on the Tresca yield criterion ($\sigma_Y^{\text{Material 2}} = 2k_2$), a simple tensile limit load solution can be found for the clad plate as:

$$\frac{F_e^{\text{clad}}}{F_e^{(h)}} = \frac{b_2}{b_1 + b_2}\left(1 + \frac{F_e^1}{F_e^2}\right) \tag{P.75}$$

and after simplification:

$$F_e^{\text{clad}} = \sum_{i=1}^{n} F_e^i \tag{P.76}$$

in which F_e^{clad} is as defined in Equation (P.74) and $F_e^i (i = 1, 2)$ is the tensile limit load for the plate containing the through-thickness flaw, where each constituent of the clad system is designated as F_e^1 and F_e^2.

Bibliography for Annex P

Standards publications

There are no standards references in this annex.

Other documents

[P.1] HADLEY, I. and LEI, Y. Outline of the fracture clauses of BS 7910:2013. *In: International Journal of Pressure Vessels and Piping*, 168, December 2018, 289–300. <https://doi.org/10.1016/j.ijpvp.2018.11.004>

[P.2] MILLER, A.G. Review of limit loads of structures containing defects. *In: International Journal of Pressure Vessel and Piping*, 1988, 32(1–4), 197–327.

[P.3] KANNINEN, M.F. et al. *Mechanical fracture predictions for sensitized stainless steel piping with circumferential cracks*. EPRI NP-192, 1976.

[P.4] WILLOUGHBY, A.A. and DAVEY, T.G. 1989. Plastic collapse at part wall flaws in plates. *In:* R.P. WEI, ed. *Fracture mechanics: perspectives and directions. Proceedings of the 20th National Symposium*. STP 1020. Bethlehem, PA, June 23–25 1987. Philadelphia: ASTM: 390–409. ISBN 0803112505.

[P.5] LEI, Y. and BUDDEN, P. Limit load solutions for plates with embedded cracks under combined tension and bending. *In: International Journal of Pressure Vessels and Piping*, 2004, 81, 589–597.

[P.6] BURDEKIN, F.M. and TAYLOR, T.E. Fracture in spherical pressure vessels. *In: Journal of Mechanical Engineering Science*, 1969, 11, 468–497.

[P.7] FOLIAS, E.S. An axial crack in a pressurized cylindrical shell. *In*: *International Journal of Fracture*, 1984, 26(4), 251–260. ISSN: 03769429.

[P.8] KASTNER, W., ROHRICH, E., SCHMITT, W. and STEINBUCH, R. Critical crack sizes in ductile piping. *In*: *International Journal of Pressure Vessels and Piping*, 1981, 9(3), 197–219. ISSN: 03080161.

[P.9] KIEFNER, J.F., MAXEY W.A., EIBER, R.J. and DUFFY, A.R. Failure stress levels of flaws in pressurized cylinders. *In: Proceedings of Progress in Flaw Growth and Toughness Testing, Philadelphia*, 28–30 August. ASTM STP 536, 1973. 461–481.

[P.10] LEI, Y. A review of limit load solutions for cylinders with axial cracks and development of new solutions. *In*: *International Journal of Pressure Vessels and Piping*, 2008, 85, 825–850.

[P.11] LEI, Y. J-Integral and limit load analysis of semi-elliptical surface cracks in plates under combined tension and bending. *In*: *International Journal of Pressure Vessels and Piping*, 2004, 81, 43–56.

[P.12] LEI, Y. *Local limit load solutions for plates with surface cracks under combined tension and bending*. British Energy Generation Ltd. Engineering Advice Note E/EAN/BBGB/0014/GEN/08. 2008.

[P.13] JONES, M.R. and ESHELBY, J.M. *Limit solutions for circumferentially cracked cylinders under internal pressure and combined tension and bending*. Nuclear Electric Report TD/SID/REP/0032. 1990.

[P.14] SCHWALBE, K.H., KIM, Y.J., HAO, S., CORNEC, A. and KOÇAK, M. *EFAM ETMMM, The ETM method for assessing the significance of cracklike defects in joints with mechanical heterogeneity (strength mismatch)*. GKSS Report GKSS/97/G/9. Geesthacht, Germany: GKSS, 1997.

[P.15] KIM, Y.J. and SCHWALBE, K.H. Mismatch effect on plastic yield loads in idealized weldments: I - Weld centre cracks. *In*: *Engineering Fracture Mechanics*, 2001, 68, 163–182.

[P.16] KIM, Y.J. and SCHWALBE, K.H. Mismatch effect on plastic yield loads in idealized weldments: II – Heat affected zone cracks. *In*: *Engineering Fracture Mechanics*, 2001, 68, 183–199.

[P.17] LEI, Y. *A review of R6 Section IV.2 Limit load solutions for strength mismatch*, British Energy Report E/REP/BBGB/0003/GEN/06, 2006.

[P.18] KIM, Y.J. and SCHWALBE, K.H. Compendium of yield load solutions for strength mis-matched DE(T), SE(B) and C(T) specimens. *In*: *Engineering Fracture Mechanics*, 2001, 68(9), 1137–1151.

[P.19] ALEXANDROV, S. and KOÇAK, M. Limit load solutions for bilayer plates with a through crack subject to tension. *In*: *Engineering Fracture Mechanics*, 1999, 64, 507–511.

[P.20] MOTARJEMI, A.K. and KOÇAK, M. Tensile yield load solutions for centre cracked bilayer (clad) plates with and without repair welds. *In*: *Science and Technology of Welding and Joining*, 2002, 7, No 5, 299–305.

[P.21] AINSWORTH, R.A. The assessment of defects in structures of strain hardening material. *In: Engineering Fracture Mechanics*, 1984, 19, 633–642.

[P.22] R6. *Assessment of the integrity of structures containing defects*. Revision 4, Amendment 11, 2015, EDF Energy Nuclear Generation Ltd., Gloucester, UK.

[P.23] KOÇAK, M. Structural integrity of welded structures: process – property – performance (3P) relationship. *In: Proceedings of the 63rd Annual Assembly & International Conference of the International Institute of Welding*. Houdremont Lecture, July 11–17 2010, Istanbul, Turkey.

[P.24] AINSWORTH, R.A. *Plastic collapse load of a thin-walled cylinder under axial load with a fully circumferential crack*. Nuclear Electric Engineering Advice Note EPD/GEN/EAN/0085/98. Barnwood, Gloucester: British Energy Generation Ltd., 1998.

Annex Q (informative)

Residual stress distributions in as-welded joints

Q.0 Symbols and definitions

For the purposes of this annex, the following symbols, definitions and units apply, unless otherwise indicated at the point of use.

Symbol	Definition	Units
A_b	Parameter used in calculating longitudinal residual stresses	—
B	Section thickness in plane of flaw	mm
E_1	Electrical energy per unit length of weld	J/mm
K_b	Stress intensity factor for the bending component of stress	$N/mm^{3/2}$
K_m	Stress intensity factor for the membrane component of stress	$N/mm^{3/2}$
K_{rs}	SIF for residual stress profile	$N/mm^{3/2}$
K_{sb}	SIF for self-balancing component of residual stress profile	$N/mm^{3/2}$
K_{sb}^{max}	Maximum SIF for self-balancing component	$N/mm^{3/2}$
r	Pipe radius	mm
W	Weld width	mm
z	Measure of position through the thickness	mm
σ_b	Bending stress	N/mm^2
σ_m	Membrane stress	N/mm^2
σ_R	Residual stress	N/mm^2
σ_R^L	Longitudinal residual stress	N/mm^2
$\sigma_R^{L,B}$	Longitudinal residual stress at bore	N/mm^2
$\sigma_R^{L,O}$	Longitudinal residual stress at the outer surface	N/mm^2
σ_R^T	Transverse residual stress	N/mm^2
σ_{sb}	Self-balancing stress component	N/mm^2
σ_Y	Lower yield strength or 0.2% proof strength	N/mm^2
$\boldsymbol{\sigma}_Y^P$	Yield strength of parent metal	N/mm^2
$\boldsymbol{\sigma}_Y^W$	Yield strength of weld metal	N/mm^2

Q.1 General

The general background to this annex is given in reference [Q.1], and information specific to pipeline girth welds is given in reference [Q.2].

This annex provides guidance on residual stress profiles for assessing flaws in as-welded joints, i.e. welds that have not been subjected to post-weld heat treatment (PWHT). These profiles may be used when a simple membrane stress assumption (**7.1.8**) does not provide adequate margins in the assessment results. Alternatively, for more accurate assessments the residual stress distribution may be determined from mock-up weldments and/or FEA modelling of the welding procedure ([Q.3], [Q.4]).

The information provided generally refers to ferritic steels and austenitic stainless steels, and is based on upper bound fits to experimental residual stress data [Q.1].

The data used to determine the residual stress profiles have been obtained predominantly from arc welds.

Guidance on residual stresses for welds that have been subjected to PWHT is provided in **7.1.8**.

The following weldments are considered:

a) plate butt and pipe seam welds;

b) pipe butt welds (note that the guidance does not currently address narrow gap welds);

c) T-butt welds (plate to plate);

d) T-butt welds (tubular/pipe); and

NOTE 1 This includes offshore tubular T-joints.

e) repair welds.

For each of these, the recommended as-welded residual stress profile is presented along with its decomposition into membrane (σ_m), bending (σ_b) and self-balancing stress components (σ_{sb}). In terms of the bending stress component, the linearization has been taken over the whole section, such that it is valid for any flaw height. The separation into the three components has been done using two integrals for the membrane and bending. The sum of these has then been subtracted from the total stress to give the self-balancing component [Q.5].

The recommended residual stress distributions are valid for a range of thicknesses, yield strengths and electrical heat input given in Table Q.1 and Table Q.2.

Table Q.1 **Assessment ranges for as-welded residual stress distributions in ferritic steels**

Geometry	**Thickness** (mm)	**Yield strength (0.2% proof strength)** (MPa)	**Electrical heat input per unit length** (kJ/mm)
Plate butt welds	24 to 300	310 to 740	1.6 to 4.9
Pipe circumferential butt welds	9 to 84	225 to 780	0.35 to 1.9
Pipe seam welds	50 to 85	345 to 780	Not known
T-butt welds	25 to 100	375 to 420	1.4
Tubular and pipe to plate welds	22 to 50	360 to 490	0.6 to 2.0
Repair welds	75 to 152	500 to 590	1.2 to 1.6

Table Q.2 **Assessment ranges for as-welded residual stress distributions in austenitic stainless steels (pipe butt welds only)**

Geometry	**Thickness** (mm)	**Yield strength** (MPa)	**Electrical heat input per unit length** (kJ/mm)
Pipe circumferential butt welds	16 to 110	272 to 338	1.0 to 2.4

The user should confirm that the residual stress distributions are representative of the welded joint being assessed.

The stress intensity factor solutions for the membrane (σ_m) and bending (σ_b) components can be obtained from Annex M. These solutions are generally those for load controlled situations, whereas residual stresses are more aligned to displacement controlled situations. Load controlled stress intensity factor solutions generally provide conservatively higher values than those of displacement controlled solutions.

The stress intensity factor, K_{rs}, for the residual stress profile should be evaluated as:

$$K_{rs} = K_m + K_b + K_{sb} \quad \text{(Q.1)}$$

where:

K_m is obtained in accordance with Annex M;

K_b is obtained in accordance with Annex M;

K_{sb} for surface breaking flaws is conservatively evaluated from a pre-determined peak value (as provided in Table Q.3 to Table Q.12) multiplied by $\sigma_Y\sqrt{B}$, or more accurately determined from the solutions provided in Annex M using the self-balancing component of the residual stress profile;

K_{sb} for through-wall flaws is evaluated from the maximum value of the stress for the self-balancing component of residual stress profile multiplied by $0.43\sqrt{(\pi B)}$.

σ_Y is the yield strength of the parent, σ_Y^P, or weld, σ_Y^W, material. For longitudinal residual stresses, $\sigma_Y = \max(\sigma_Y^P, \sigma_Y^W)$ and for transverse residual stresses, $\sigma_Y = \min(\sigma_Y^P, \sigma_Y^W)$. σ_Y should be taken as mean 0.2% proof strength for ferritic materials and mean 1% proof strength for austenitic materials.

*NOTE 1 If the approach given in Equation (Q.1) gives a higher value of K_{rs} than the simple approach given in **7.1.10.2**, then the use of **7.1.10.2** is recommended instead.*

*NOTE 2 The solutions in **M.4.2** and **M.4.4** may be used to evaluate the stress intensity factor (for surface breaking flaws) for the full residual stress profile where it is given as a polynomial equation.*

In this annex, the recommended residual stress profiles are illustrated graphically with the σ_m, σ_b and σ_{sb} components. In addition, tabular information is given on the σ_m and σ_b values, the σ_{sb} equation and the predetermined normalized peak K_{sb} (i.e. K_{sb}^{max}), the value of which should be multiplied by $\sigma_Y\sqrt{B}$ in order to obtain K_{sb}.

The distributions are expressed in terms of the normalized depth through the wall thickness (z/B) and the normalized residual stress in the longitudinal or transverse directions (σ_R^L/σ_Y or σ_R^T/σ_Y). The normalized depth, z/B, is measured from the surface on which the last weld bead is deposited, except where specified otherwise.

For cylindrical components, the residual stress profiles are presented in terms of z/B, where $z = 0$ at the bore surface, and B is the thickness. For surface flaws emanating from the outer surface, the profiles may be recharacterized by replacing z/B by $1 - z/B$ in the polynomial equations, and taking z from the outer surface.

For other geometries, $z = 0$ represents the surface on which the last weld bead is deposited.

In relation to the profiles given in **Q.3.2**, when there is uncertainty on heat input levels, it might be necessary to consider a worst case scenario by selecting the profile which results in the most conservative assessment result.

The profiles given are appropriate for assessing flaws that lie within a distance of W from the weld toes, where W is the weld width. Flaws situated outside of this range should be assessed on a case-by-case basis.

Q.2 Plate butt welds and pipe axial seam welds

Q.2.1 Longitudinal residual stresses (i.e. parallel to the weld length)

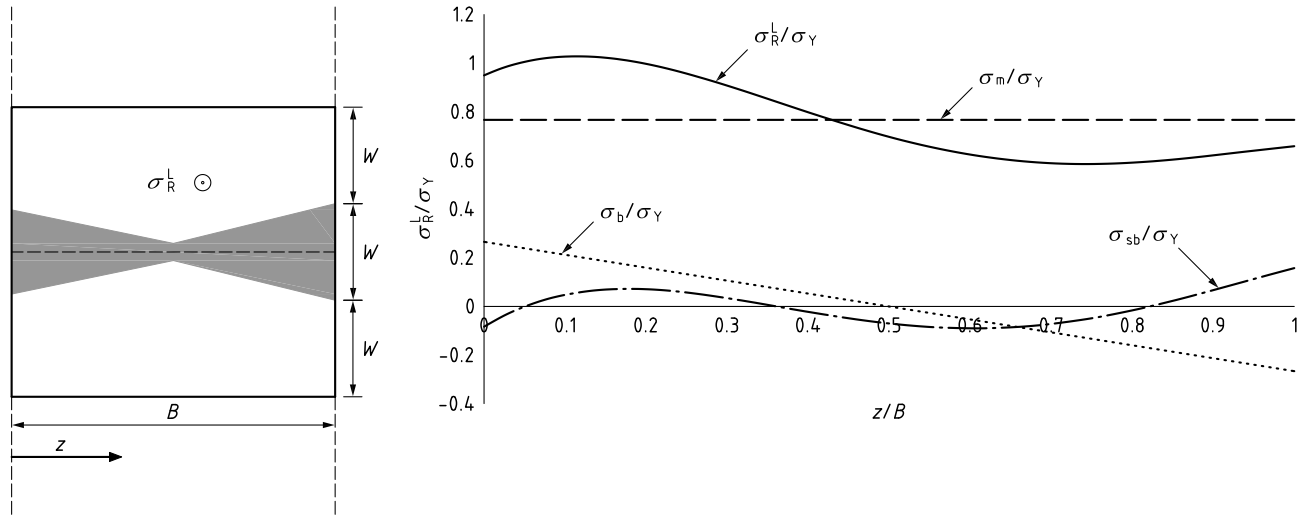
For austenitic steel, the following equation applies (see also Figure Q.1):

$$\frac{\sigma_R^L}{\sigma_Y} = \left[0.95 + 1.505\left(\frac{z}{B}\right) - 8.287\left(\frac{z}{B}\right)^2 + 10.571\left(\frac{z}{B}\right)^3 - 4.08\left(\frac{z}{B}\right)^4\right] \quad \text{(Q.2)}$$

For ferritic steels, the following equation applies:

$$\frac{\sigma_R^L}{\sigma_Y} = 1 \quad \text{(Q.3)}$$

Figure Q.1 **Components of longitudinal residual stress distribution for plate butt welds and pipe axial seam welds (austenitic steel)**



a) Weld schematic b) Stress component

See Table Q.3 for the components of longitudinal residual stresses.

Table Q.3 **Components of longitudinal stress and K_{sb}^{max} for plate butt welds and pipe axial seam welds (austenitic steel)**

$\frac{\sigma_m}{\sigma_Y}$	$\frac{\sigma_b}{\sigma_Y}$	$\frac{\sigma_{sb}}{\sigma_Y}$	$\frac{K_{sb}^{max}}{(\sigma_Y\sqrt{B})}$
0.767	0.266 Full profile: $0.266 - 0.532\left(\frac{z}{B}\right)$	$-0.0829 + 2.037\left(\frac{z}{B}\right) - 8.287\left(\frac{z}{B}\right)^2 + 10.571\left(\frac{z}{B}\right)^3 - 4.08\left(\frac{z}{B}\right)^4$	0.063

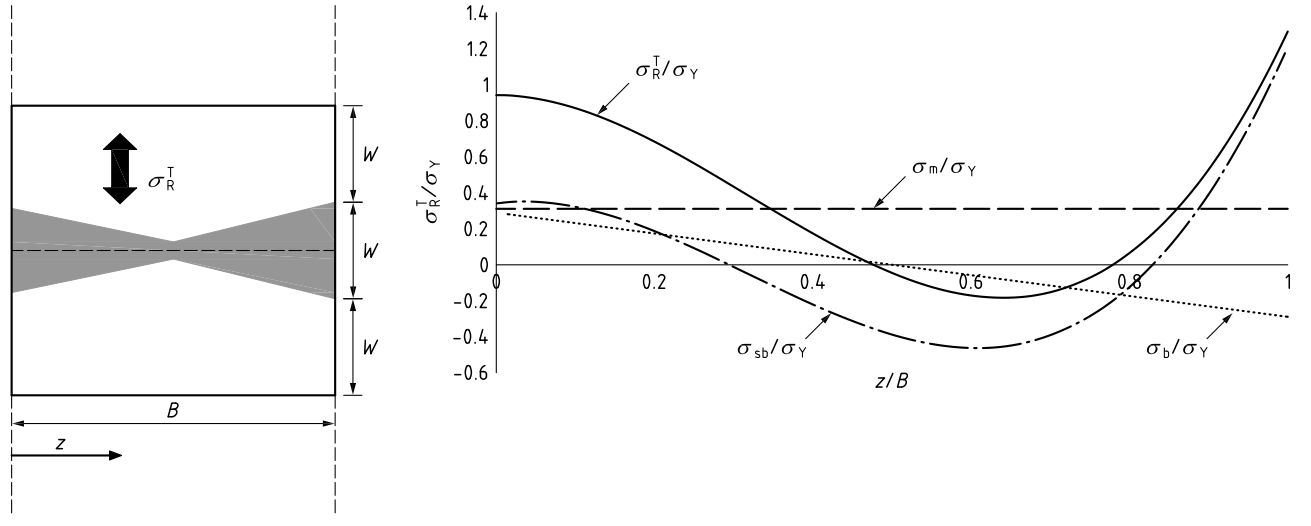
NOTE When used for axial seam welds, this stress profile is applicable only where the ratio of pipe radius to wall thickness exceeds 10, i.e. r/B > 10.

Q.2.2 Transverse residual stresses (i.e. perpendicular to the weld length)

Transverse residual stresses are highly variable. The upper bound transverse residual stress distribution for ferritic and austenitic steels, under minimum restraint, should be calculated from the following equation (see also Figure Q.2):

$$\frac{\sigma_R^T}{\sigma_Y} = \left[0.9415 - 0.0319\left(\frac{z}{B}\right) - 8.3394\left(\frac{z}{B}\right)^2 + 8.660\left(\frac{z}{B}\right)^3\right] \quad \text{(Q.4)}$$

Figure Q.2 **Components of transverse stress distribution for plate butt welds and axial seam welds (austenitic and ferritic steels)**



a) Weld schematic b) Stress components

See Table Q.4 for the components of transverse residual stresses.

Table Q.4 **Components of transverse stress and K_{sb}^{max} for plate butt welds and axial seam welds (austenitic and ferritic steel)**

$\frac{\sigma_m}{\sigma_Y}$	$\frac{\sigma_b}{\sigma_Y}$	$\frac{\sigma_{sb}}{\sigma_Y}$	$\frac{K_{sb}^{max}}{(\sigma_Y\sqrt{B})}$
0.311	0.289 Full profile: $0.289 - 0.578\left(\frac{z}{B}\right)$	$0.341\,5 + 0.546\,1\left(\frac{z}{B}\right) - 8.339\,4\left(\frac{z}{B}\right)^2 + 8.66\left(\frac{z}{B}\right)^3$	0.347

NOTE When used for axial seam welds, this stress profile is applicable only where the pipe r/B ratio > 10.

Q.3 Pipe butt welds

Q.3.1 Longitudinal residual stresses (i.e. parallel to the weld length and circumferential to the pipe)

The longitudinal residual stress distribution for ferritic and austenitic steel pipe butt welds is represented conservatively by a linear profile defined by a stress equal to σ_Y at the outer surface and $\sigma_R^{L,B}$ at the bore, and is calculated from the following equations (see also Figure Q.3):

$$\sigma_R^{L,O} = \sigma_Y \quad \text{(Q.5)}$$

$$\sigma_R^{L,B} = A_b\sigma_Y \quad \text{(Q.6)}$$

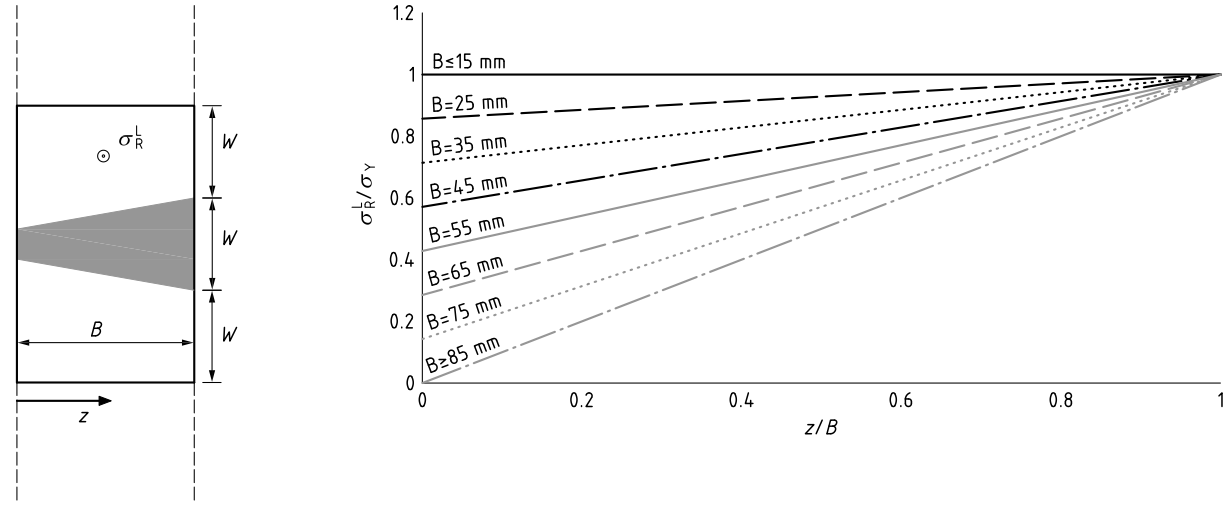
where:

$A_b = 1$ for $B \leq 15$ mm

$A_b = 1 - 0.0143(B - 15)$ for $15 < B \leq 85$ mm

$A_b = 0$ for $B > 85$ mm

Figure Q.3 **Components of longitudinal stress distribution for pipe butt welds (ferritic and austenitic steels)**



a) Weld schematic b) Stress components

See Table Q.5 for the stress components of longitudinal stress distribution for pipe butt welds (ferritic and austenitic steels).

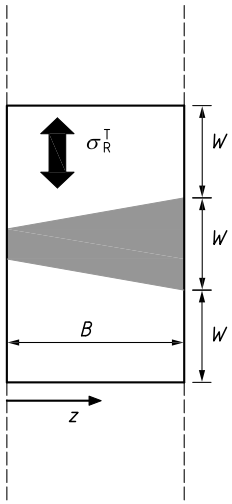
Table Q.5 **Components of longitudinal stress and K_{sb}^{max} for pipe butt welds (ferritic and austenitic steels)**

Wall thickness	$\frac{\sigma_m}{\sigma_Y}$	$\frac{\sigma_b}{\sigma_Y}$	$\frac{\sigma_{sb}}{\sigma_Y}$	$\frac{K_{sb}^{max}}{(\sigma_Y\sqrt{B})}$
B ≤15 mm	1	0	0	0
15 < B ≤ 85 mm	$\frac{2-0.0143(B-15)}{2}$	$\frac{0.0143(B-15)}{2}$ Full profile: $0.0143(B-15)\left(\frac{z}{B}-0.5\right)$	0	0
B > 85 mm	0.5	0.5 Full profile: $0.5+\left(\frac{Z}{B}-1\right)$	0	0

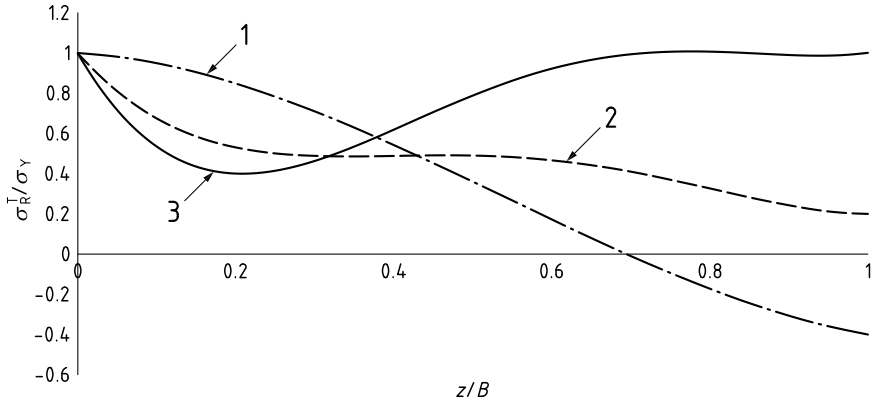
Q.3.2 Transverse residual stresses (i.e. perpendicular to the weld length and parallel to the axis of the pipe)

The transverse residual stress profile for pipe butt-welded joints is influenced by the electrical energy per unit length of weld, E_1, and the wall thickness. Distributions are given below and in Figure Q.4 as a function of z/B and E_1/B, where z is measured from the bore and E_1 is the electrical energy per unit length of the largest weld run in J/mm which is equal to (welding current) × (welding voltage) / (welding travel speed).

Figure Q.4 **Components of transverse stress distribution for pipe butt welds (ferritic steels)**

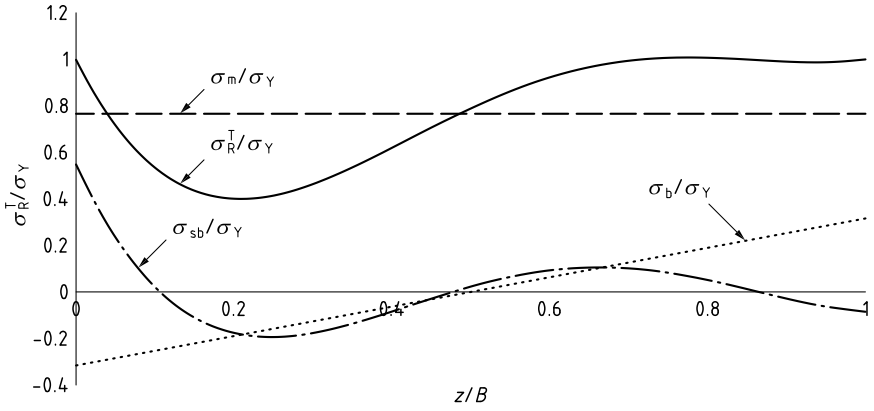


a) Weld schematic



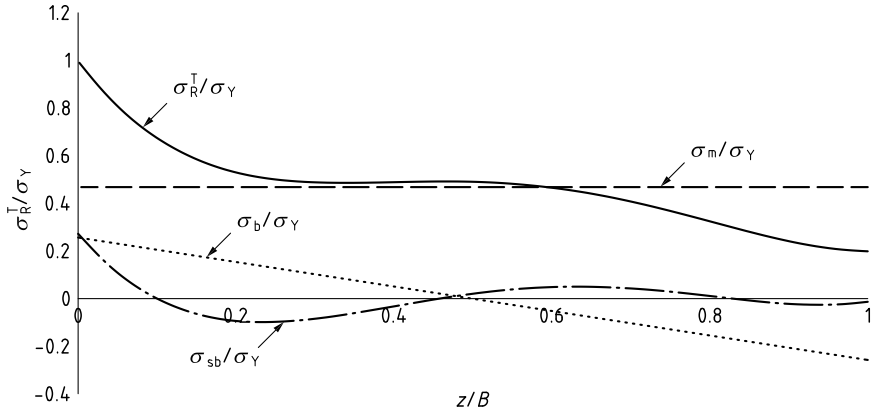
Key
1 Low heat input
2 Medium heat input
3 High heat input

b) Transverse residual stress profiles for low, medium and high heat input



c) Plot of decomposed components of transverse stresses in ferritic pipe butt welds made with a low heat input $E_1/B \leq 50$ J/mm^2

$$\frac{\sigma_R^T}{\sigma_Y} = 1 - 6.80\left(\frac{z}{B}\right) + 24.30\left(\frac{z}{B}\right)^2 - 28.68\left(\frac{z}{B}\right)^3 + 11.18\left(\frac{z}{B}\right)^4$$

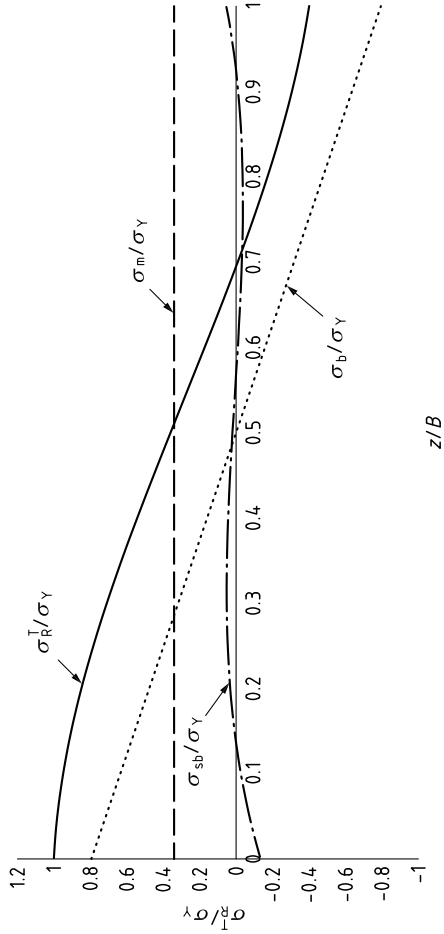


d) Plot of decomposed components of transverse stresses in ferritic pipe butt welds made with a medium heat input, $50 < E_1/B \leq 120$ J/mm^2

$$\frac{\sigma_R^T}{\sigma_Y} = 1 - 4.43\left(\frac{z}{B}\right) + 13.53\left(\frac{z}{B}\right)^2 - 16.93\left(\frac{z}{B}\right)^3 + 7.03\left(\frac{z}{B}\right)^4$$

© The British Standards Institution 2019

Figure Q.4 **Components of transverse stress distribution for pipe butt welds (ferritic steels)** *(continued)*



e) Plot of decomposed components of transverse stresses in ferritic pipe butt welds made with a high heat input, $E_1/B \geq 120$ J/mm^2

$$\frac{\sigma_R^T}{\sigma_Y} = 1 - 0.22\left(\frac{Z}{B}\right) - 3.06\left(\frac{Z}{B}\right)^2 + 1.88\left(\frac{Z}{B}\right)^3$$

See Table Q.6 for the stress components of each type of weld.

Table Q.6 **Components of transverse stress and K_{sb}^{max} for pipe butt welds (ferritic steel)**

Heat input	$\frac{\sigma_m}{\sigma_Y}$	$\frac{\sigma_b}{\sigma_Y}$	$\frac{\sigma_{sb}}{\sigma_Y}$	$\frac{K_{sb}^{max}}{(\sigma_Y\sqrt{B})}$
Low heat input	0.766	–0.316 Full profile: $-\left[0.316-0.632\left(\frac{z}{B}\right)\right]$	$0.55-7.432\left(\frac{z}{B}\right)+24.30\left(\frac{z}{B}\right)^2-28.68\left(\frac{z}{B}\right)^3+11.18\left(\frac{z}{B}\right)^4$	0.16
Medium heat input	0.469	0.257 Full profile: $0.257-0.514\left(\frac{z}{B}\right)$	$0.274-3.916\left(\frac{z}{B}\right)+13.53\left(\frac{z}{B}\right)^2-16.93\left(\frac{z}{B}\right)^3+7.03\left(\frac{z}{B}\right)^4$	0.08
High heat input	0.340	0.794 Full profile: $0.794-1.588\left(\frac{z}{B}\right)$	$-0.134+1.368\left(\frac{z}{B}\right)-3.06\left(\frac{z}{B}\right)^2+1.88\left(\frac{z}{B}\right)^3$	0.013

For austenitic steels, the same distribution equation as ferritic steels should be used for high input welds. For medium/low heat input welds where $E_1/B \leq 120$ J/mm^2, the low heat input ferritic equation should be used.

See Table Q.7 for the transverse stress components for austenitic steels.

Table Q.7 **Components of transverse stress and K_{sb}^{max} for pipe butt welds (austenitic steel)**

Heat input	$\frac{\sigma_m}{\sigma_Y}$	$\frac{\sigma_b}{\sigma_Y}$	$\frac{\sigma_{sb}}{\sigma_Y}$	$\frac{K_{sb}^{max}}{(\sigma_Y\sqrt{B})}$
Low/ medium heat input	0.766	–0.316 Full profile: $-\left[0.316-0.632\left(\frac{z}{B}\right)\right]$	$0.55-7.432\left(\frac{z}{B}\right)+24.30\left(\frac{z}{B}\right)^2-28.68\left(\frac{z}{B}\right)^3+11.18\left(\frac{z}{B}\right)^4$	0.16
High heat input	0.340	0.794 Full profile: $0.794-1.588\left(\frac{z}{B}\right)$	$-0.134+1.368\left(\frac{z}{B}\right)-3.06\left(\frac{z}{B}\right)^2+1.88\left(\frac{z}{B}\right)^3$	0.013

Q.4 T-butt welds (plate to plate)

Q.4.1 Longitudinal residual stresses

For longitudinal stresses (ferritic steels), the following equation applies (see also Figure Q.5):

$$\frac{\sigma_R^L}{\sigma_Y}=\left[0.75+4.766\left(\frac{z}{B}\right)-26.696\left(\frac{z}{B}\right)^2+38.11\left(\frac{z}{B}\right)^3-16.82\left(\frac{z}{B}\right)^4\right] \quad \text{(Q.7)}$$

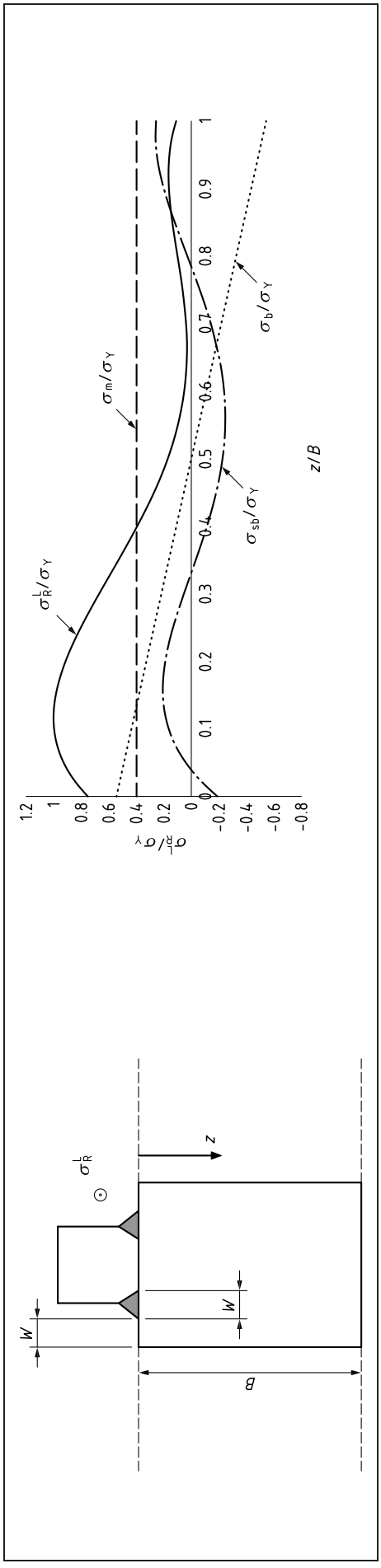


Figure Q.5 **Components of longitudinal stress distribution for plate to plate T-butt welds (ferritic steels)**

See Table Q.8 for the stress components of longitudinal residual stress for plate to plate T-butt welds (ferritic steel).

Table Q.8 **Components of longitudinal stress and K_{sb}^{max} for plate to plate T-butt welds (ferritic steels)**

$\frac{\sigma_m}{\sigma_Y}$	$\frac{\sigma_b}{\sigma_Y}$	$\frac{\sigma_{sb}}{\sigma_Y}$	$\frac{K_{sb}^{max}}{(\sigma_Y\sqrt{B})}$
0.398	0.543 Full profile: $0.543 - 1.086\left(\frac{z}{B}\right)$	$-0.1915 + 5.853\left(\frac{z}{B}\right) - 26.696\left(\frac{z}{B}\right)^2 + 38.11\left(\frac{z}{B}\right)^3 - 16.82\left(\frac{z}{B}\right)^4$	0.17

For longitudinal stresses (austenitic steels), the following equation applies.

$$\frac{\sigma_R^L}{\sigma_Y} = 1 - \left(\frac{z}{B}\right) \quad \text{(Q.8)}$$

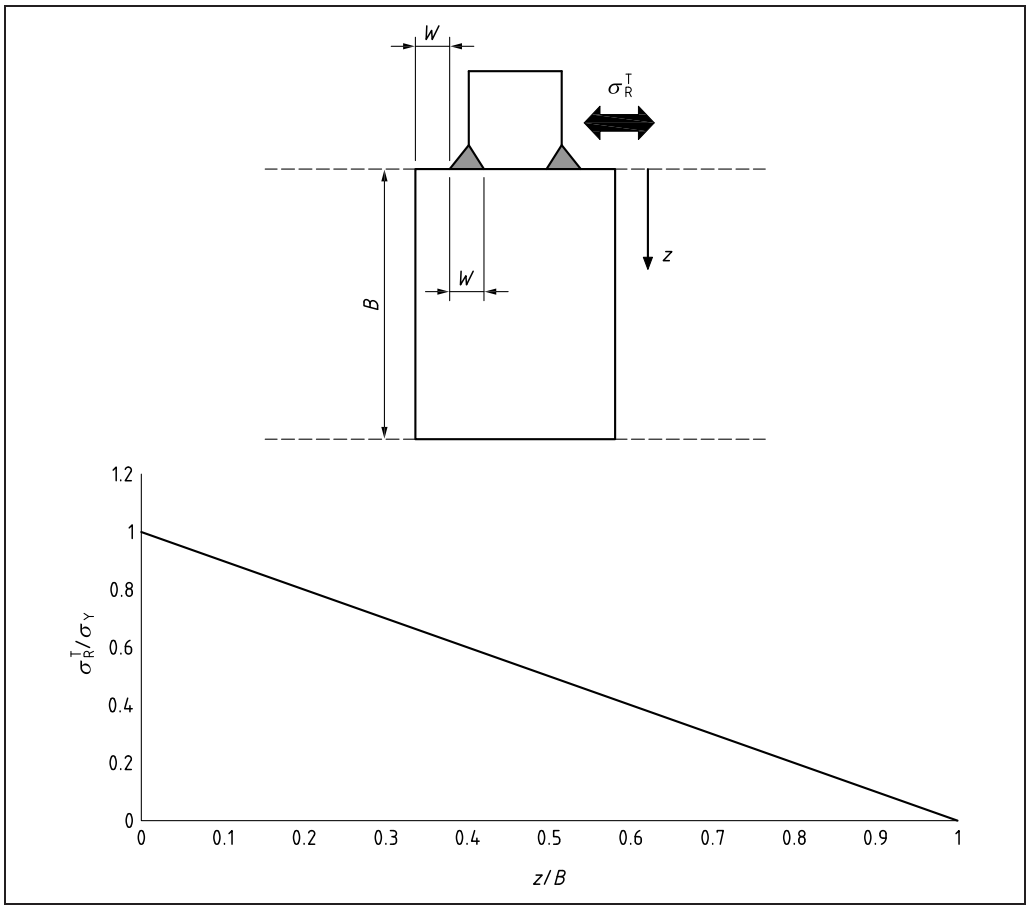
See Table Q.9 for the stress components of longitudinal residual stress for plate to plate T-butt welds (austenitic steels) [and for stress components of transverse residual stress for plate to plate T-butt welds (ferritic and austenitic steels)].

Q.4.2 Transverse residual stresses

For transverse stresses (austenitic and ferritic steels), the following equation applies (see also Figure Q.6):

$$\frac{\sigma_R^T}{\sigma_Y} = 1 - \left(\frac{z}{B}\right) \quad \text{(Q.9)}$$

Figure Q.6 **Components of transverse stress distribution for plate to plate T-butt welds (austenitic and ferritic steels)**



See Table Q.9 for the stress components of transverse residual stress for plate to plate T-butt welds (ferritic and austenitic steels) [and for stress components of longitudinal residual stress for plate to plate T-butt welds (austenitic steels)].

Table Q.9 **Components of transverse stress and K_{sb}^{max} for plate to plate T-butt welds (ferritic and austenitic steels) and longitudinal stress and K_{sb}^{max} for plate to plate T-butt welds (austenitic steels)**

$\frac{\sigma_m}{\sigma_Y}$	$\frac{\sigma_b}{\sigma_Y}$	$\frac{\sigma_{sb}}{\sigma_Y}$	$\frac{K_{sb}^{max}}{(\sigma_Y\sqrt{B})}$
0.5	0.5 Full profile: $0.5 - \left(\frac{z}{B}\right)$	0	0

Q.5 Tubular T-butt welds

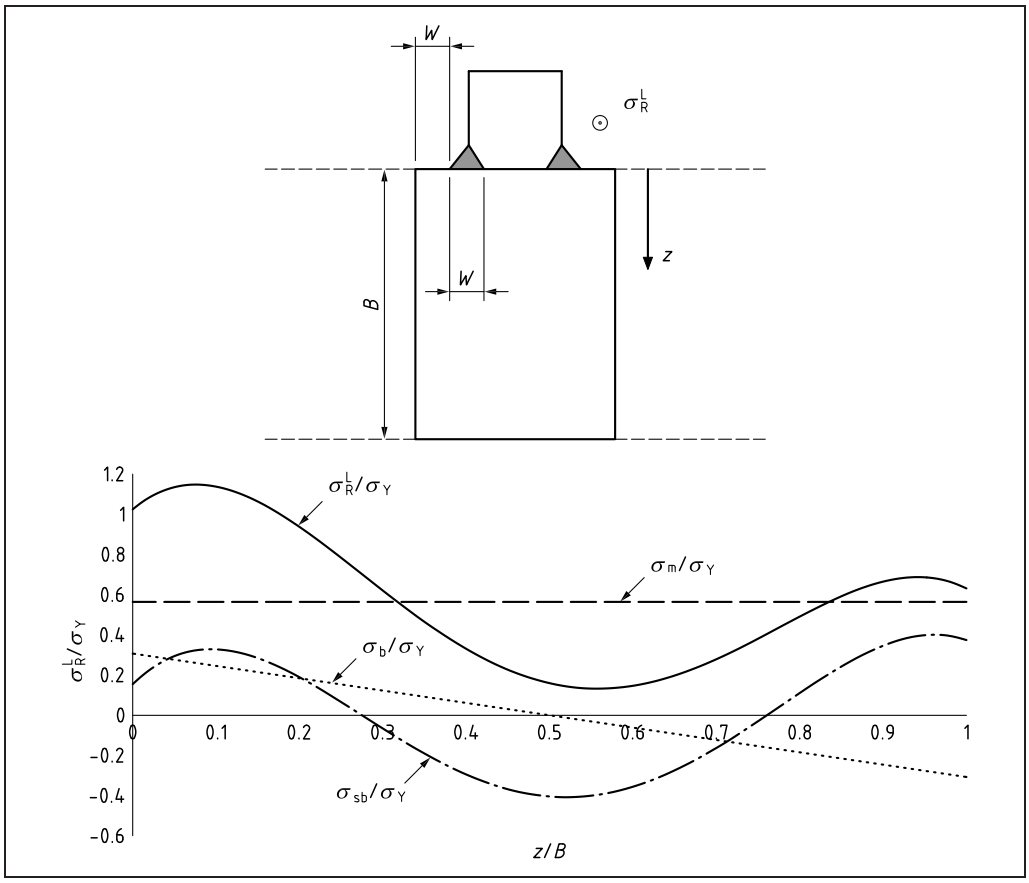
Q.5.1 Longitudinal residual stresses

For longitudinal stresses (ferritic steels), the following equation applies (see also Figure Q.7):

$$\frac{\sigma_R^L}{\sigma_Y} = \left[1.025 + 3.478\left(\frac{z}{B}\right) - 27.861\left(\frac{z}{B}\right)^2 + 45.788\left(\frac{z}{B}\right)^3 - 21.799\left(\frac{z}{B}\right)^4\right] \qquad \text{(Q.10)}$$

 © The British Standards Institution 2019

Figure Q.7 **Components of longitudinal stress distribution for tubular T-butt welds (ferritic steels)**



See Table Q.10 for the stress components of T-butt and fillet welds.

Table Q.10 **Components of longitudinal stress and K_{sb}^{max} for tubular T-butt welds (ferritic steels)**

$\frac{\sigma_m}{\sigma_Y}$	$\frac{\sigma_b}{\sigma_Y}$	$\frac{\sigma_{sb}}{\sigma_Y}$	$\frac{K_{sb}^{max}}{(\sigma_Y\sqrt{B})}$
0.564	0.307 Full profile: $0.307 - 0.614\left(\frac{z}{B}\right)$	$0.1541 + 4.0918\left(\frac{z}{B}\right) - 27.861\left(\frac{z}{B}\right)^2 + 45.788\left(\frac{z}{B}\right)^3 - 21.799\left(\frac{z}{B}\right)^4$	0.3

For longitudinal stresses (austenitic steels), the following equation applies.

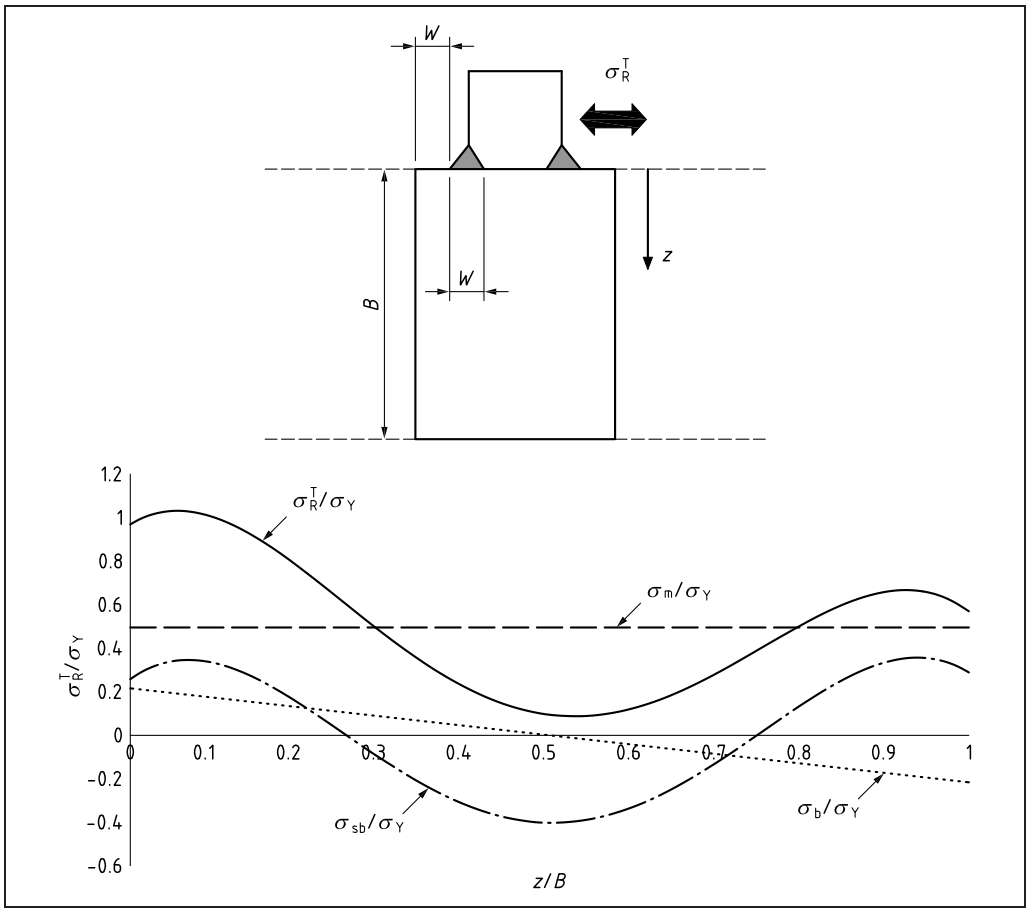
$$\frac{\sigma_R^L}{\sigma_Y} = 1 \qquad \text{(Q.11)}$$

Q.5.2 Transverse residual stresses

For transverse stresses (ferritic steels), the following equation applies (see also Figure Q.8):

$$\frac{\sigma_R^T}{\sigma_Y} = \left[0.97 + 2.3267\left(\frac{z}{B}\right) - 24.125\left(\frac{z}{B}\right)^2 + 42.485\left(\frac{z}{B}\right)^3 - 21.087\left(\frac{z}{B}\right)^4\right] \qquad \text{(Q.12)}$$

Figure Q.8 **Components of transverse stress distribution for tubular T-butt welds (ferritic steels)**



See Table Q.11 for the stress components of transverse residual stress.

Table Q.11 **Components of transverse stress and K_{sb}^{max} for tubular T-butt welds (ferritic steels)**

$\frac{\sigma_m}{\sigma_Y}$	$\frac{\sigma_b}{\sigma_Y}$	$\frac{\sigma_{sb}}{\sigma_Y}$	$\frac{K_{sb}^{max}}{(\sigma_Y\sqrt{B})}$
0.496	0.216 Full profile: $0.216 - 0.432\left(\frac{z}{B}\right)$	$0.258 + 2.758\left(\frac{z}{B}\right) - 24.125\left(\frac{z}{B}\right)^2 + 42.485\left(\frac{z}{B}\right)^3 - 21.087\left(\frac{z}{B}\right)^4$	0.21

For transverse stresses (austenitic steels), the following equation applies.

$$\frac{\sigma_R^T}{\sigma_Y} = 1 \qquad \text{(Q.13)}$$

Q.6 Repair welds

The recommended transverse and longitudinal through-thickness residual stress profiles, which are identical to each other, are shown in Figure Q.9 and Table Q.12 and may be used for all lengths of repair.

For cracks starting from $z/B = 0$, the repair residual stress profile shown in Figure Q.9 should be used. For cracks starting from $z/B = 1$, the residual stress distribution for the original weld should be used.

$$\frac{\sigma_R^L}{\sigma_Y} = \frac{\sigma_R^T}{\sigma_Y} = 1 \qquad \text{for } \frac{z}{B} \le z_r \tag{Q.14}$$

$$\frac{\sigma_R^L}{\sigma_Y} = \frac{\sigma_R^T}{\sigma_Y} = \frac{1}{(1 - z_r)} - \frac{1}{(1 - z_r)}\left(\frac{z}{B}\right) \qquad \text{for } z_r < \frac{z}{B} < 1 \tag{Q.15}$$

$$\frac{\sigma_R^L}{\sigma_Y} = \frac{\sigma_R^T}{\sigma_Y} = 0 \qquad \text{for } \frac{z}{B} = 1 \tag{Q.16}$$

Figure Q.9 **Residual stress profile for repair welds (transverse and longitudinal)**

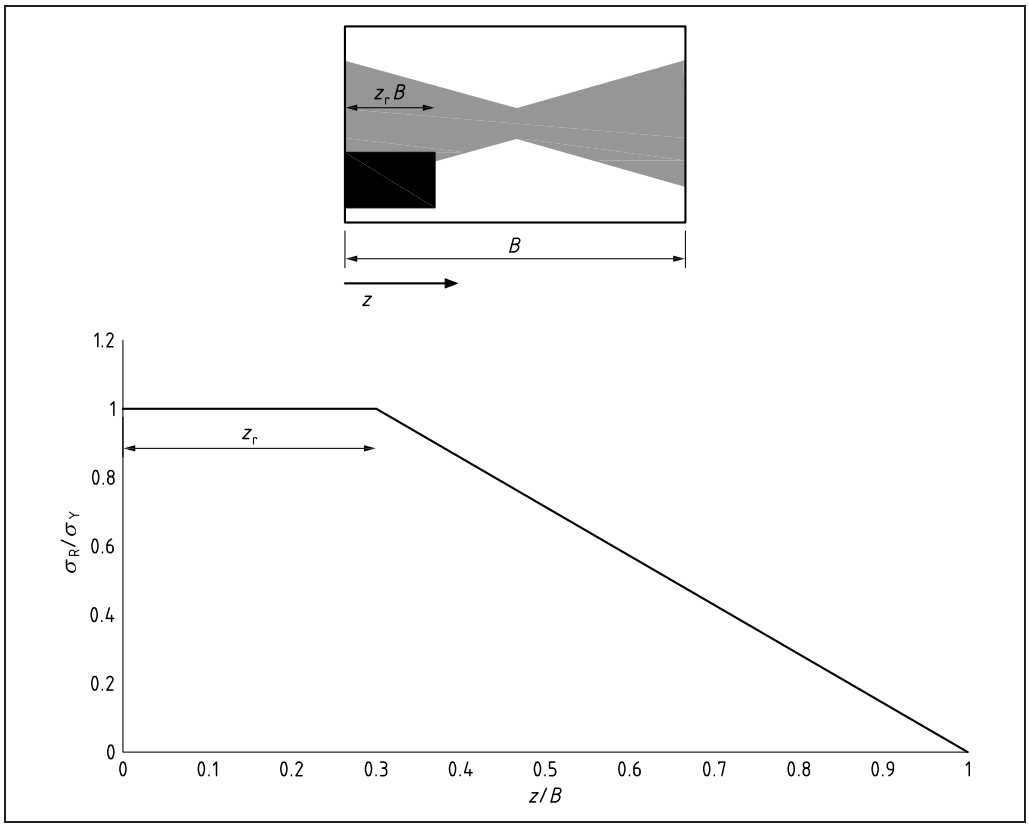


Table Q.12 **Components of transverse and longitudinal stress distribution for repair welds (ferritic and austenitic steels)**

Depth of repair	$\frac{\sigma_m}{\sigma_Y}$	$\frac{\sigma_b}{\sigma_Y}$	$\frac{\sigma_{sb}}{\sigma_Y}$	$\frac{K_{sb}^{max}}{(\sigma_Y\sqrt{B})}$
$\frac{z}{B} \le z_r$	1	0	0	0
$z_r < \frac{z}{B} < 1$ [A)]	$\frac{0.5}{(1 - z_r)}$	$\frac{0.5}{(1 - z_r)}$ $\frac{0.5}{(1 - z_r)} - \frac{1}{(1 - z_r)}\left(\frac{z}{B}\right)$	0	0
$\frac{z}{B} = 1$	0	0	0	0

[A)] Where z_r is the normalized depth of the repair in respect of B.

Bibliography for Annex Q

Standards publications

There are no standards references in this annex.

Other documents

[Q.1] SHARPLES, J. and HADLEY, I. Treatment of residual stress in fracture assessment: background to the advice given in BS 7910:2013. *In: International Journal of Pressure Vessels and Piping*, 168, December 2018, 323–334. <https://doi.org/10.1016/j.ijpvp.2018.11.005>

[Q.2] WU, G. and SISAN, A.M. Residual stress in pipeline girth welds – A review of recent data and modelling in the context of BS 7910. *In: International Journal of Pressure Vessels and Piping*, 169(2019), 142–152. <https://doi.org/10.1016/j.ijpvp.2018.12.004>

[Q.3] R6 PANEL. *R6: Assessment of the integrity of structures containing defects*. Revision 4, as amended. Gloucester: EDF Energy, 2001.

[Q.4] BATE, S. and SMITH, M. Determination of residual stresses in welded components by finite element analysis. *In: Materials Science and Technology*, 32(14), 1505–1516, 2016.

[Q.5] SHARPLES, J., GILL, P., WEI, L. and BATE, S. Revised guidance on residual stresses in BS 7910, PVP2011-57071. *In: Proceedings of the ASME 2011 Pressure Vessels & Piping Division Conference*, July 17–21 2011. Baltimore, Maryland, USA. New York: ASME, 2011.

 © The British Standards Institution 2019

Annex R (informative)

Determination of plasticity interaction effects with combined primary and secondary loading

R.0 Symbols and definitions

For the purposes of this annex, the following symbols, definitions and units apply, unless otherwise indicated at the point of use.

Symbol	Definition	Units
K_I^p	Stress intensity factor due to primary stress	N/mm$^{3/2}$
K_I^s	Stress intensity factor due to secondary stress	N/mm$^{3/2}$
$K_I^{s,res}$	Elastic stress intensity factor due to residual stresses	N/mm$^{3/2}$
$K_I^{s,sec}$	Stress intensity factor due to other secondary stresses (e.g. thermal stresses)	N/mm$^{3/2}$
K_J^s	Elastic plastic stress intensity factor	N/mm$^{3/2}$
K_{mat}	Material fracture toughness measured by stress intensity factor	N/mm$^{3/2}$
K_r	Fracture ratio	—
K_r^p	Contribution to K_r from primary stresses	—
K_r^s	Contribution to K_r from secondary stresses	—
K_{rs}	SIF for residual stress profile	N/mm$^{3/2}$
L_r	Ratio of applied load to yield load	—
V	Plasticity correction factor	—
ρ	Plasticity interaction factor	—
ρ_1	Parameter used in determining ρ	—

R.1 General

When structures are loaded by a combination of primary and secondary stresses, plasticity effects occur which cannot be evaluated by a simple linear addition of the effects resulting from the two independent stress systems.

Subclause **R.2** provides two alternative approaches used in the definition of K_r^s (the secondary stress component of the K_r parameter) to cover interaction between these two stress systems. These are simplified approaches based on elastic calculations for the evaluation of ρ or V. This is most appropriate for cases when secondary loads are small.

The first approach is based on the additive term ρ [R.1]. The second approach uses a multiplying factor V applied to K_I^s [R.2]. This annex gives methods for the determination of both ρ and V.

The equations in **R.2** are not applicable when there are secondary stresses only, as the geometric parameter K_I^p/L_r, and hence $K_I^s/(K_I^p/L_r)$, is undefined. In the case of secondary stress acting alone, consistent with R6 [R.3], K_r^p and ρ are set to zero, or V to unity, and the assessment then uses K_J^s as determined in II.6.5 of R6 [R.3] and hence $K_r^s = K_J^s/K_{mat}$ in Clause **7**. Similarly, the guidance in II.6.6.3 of R6 [R.3] should be followed when elastic follow-up is significant in the flawed section. Alternatively, the relevant stresses may be conservatively classified as primary in accordance with Clause **7**.

Subclause **R.3** refers to methods available in R6 [R.3] for evaluation of V for situations in which the simplified route provided in **R.2** is not applicable or when it leads to over-conservative assessments.

Combined residual and other secondary stresses are addressed in **R.4**.

R.2 Simplified procedure for the evaluation of ρ or V

R.2.1 General

Plasticity corrections for secondary stresses are not important when the secondary load is small. The value of ρ is restricted to ≥ 0 and reduces to 0 beyond the limit load of the structure. The values of ρ and V are dependent on L_r and on the ratio $K_I^s/(K_I^p/L_r)$. This approach is most appropriate when this ratio is ≤ 4.

For large secondary stresses [$K_I^s/(K_I^p/L_r) > 4$], plastic redistribution of stress is likely to be important and the values of ρ or V given in **R.2.2** could possibly be over-conservative.

R.2.2 Procedure for determining ρ or V

Evaluate K_I^s, the linear elastic stress intensity factor for the flaw size of interest, using the elastically-calculated secondary stresses. K_I^s is positive when it tends to open the crack.

If $K_I^s < 0$, then K_I^s is set to zero and ρ is also set to zero. Similarly, V is set to unity. The problem then reduces to one of primary stresses alone and the remainder of this subclause is not applicable; see Clause **7** for the procedure that is used to assess the primary loads alone.

Evaluate the ratio K_I^p/L_r where L_r and K_I^p are as defined in Clause **7**.

Evaluate $K_I^s/(K_I^p/L_r)$.

To evaluate ρ, evaluate ρ_1 from Equation (R.1):

$$\begin{aligned} &\rho_1 = 0.1\left[K_I^s\left(\frac{L_r}{K_I^p}\right)\right]^{0.714} - \\ &0.007\left[K_I^s\left(\frac{L_r}{K_I^p}\right)\right]^2 + 0.00003\left[K_I^s\left(\frac{L_r}{K_I^p}\right)\right]^5 && \text{for } K_I^s\left(\frac{L_r}{K_I^p}\right) < 5.2 \\ &\rho_1 = 0.25 && \text{for } K_I^s\left(\frac{L_r}{K_I^p}\right) \geq 5.2 \end{aligned} \qquad \text{(R.1)}$$

Then if $0 < \rho_1 \leq 0.25$, evaluate ρ from:

$$\begin{aligned} &\rho = \rho_1 && \text{for } L_r \leq 0.8 \\ &\rho = 4\rho_1\,(1.05 - L_r) && \text{for } 0.8 < L_r < 1.05 \\ &\rho = 0 && \text{for } L_r \geq 1.05 \end{aligned} \qquad \text{(R.2)}$$

NOTE 1 $0 \leq \rho \leq \rho_1$ and ρ increases with increasing $K_I^s/(K_I^p/L_r)$ or with reducing L_r.

To evaluate V:

$$\begin{aligned} &V = \min\left[1 + 0.2L_r + 0.02K_I^s\left(\frac{L_r}{K_I^p}\right)(1 + 2L_r); (3.1 - 2L_r)\right] && \text{for } L_r \leq 1.05 \\ &V = 0.4 && \text{for } L_r > 1.05 \end{aligned} \qquad \text{(R.3)}$$

If Equation (7.24b) has been invoked to determine the level of residual stress, then all values of V evaluated by Equation (R.3) that are less than 1.0 should be reset to 1.0.

 © The British Standards Institution 2019

NOTE 2 ρ was included in previous versions of BS 7910 and R6 [R.3] and has been retained here for consistency with other sections and annexes. Although the detailed derivations of ρ and V (not given in this annex) produce equivalent results, there might be slight differences in assessment results obtained from these simplified procedures. However, both methods remain conservative.

NOTE 3 The use of $V \geq 1$ [if Equation (7.24b) has been invoked] and $V = 0.4$ otherwise is intended to provide continuity with both earlier revisions of BS 7910 and the current revision of R6.

R.3 Alternative procedures

This subclause is most appropriate when the ratio $K_I^s/(K_I^p/L_r)$ evaluated in **R.2** > 4. It should also be applied when primary stresses are low and the conservatism given by the method of **R.2** is excessive.

For the above situations (excluding those where there are significant stresses in the directions parallel to the flaw), and/or when there are secondary stresses acting alone and where there are only moderate amounts of elastic follow-up in the flawed section, the detailed procedure provided in Section II.6 of R6 [R.3] can be used for evaluating *V*. This detailed route requires an estimate of the inelastic response of the structure and includes methods based on analysing the uncracked body under secondary loadings alone.

An alternative approach for the evaluation of *V* is available in II.6.6.4 of R6 [R.3] for sensitivity studies, which might provide a less conservative assessment when there are significant stresses in the directions parallel to the flaw.

R.4 Combined residual stresses and other secondary stresses

The effect of combined residual stresses and other secondary stresses (e.g. thermal stresses) below yield may be treated using the methods of **R.2** based on elastic calculations. Full account of the residual stresses is taken. That is to say that in the procedure set out in **R.2**:

$$K_I^s = K_I^{s,sec} + K_I^{s,res} \quad \text{(R.4)}$$

For combined residual and secondary stresses greater than yield, a less conservative method is available in II.6.8 of R6 [R.3].

Annex Q contains residual stress profiles for various weldments in the as-welded condition. A route is provided in Annex Q for evaluating stress intensity factor (K_{rs}) values for the residual stress profiles for flaws situated in the welded region.

Bibliography for Annex R

Standards publications

There are no standards references in this annex.

Other documents

[R.1] AINSWORTH, R.A. The treatment of thermal and residual stresses in fracture assessments. *In: Engineering Fracture Mechanics*, 1986, 24:65–76.

[R.2] AINSWORTH, R.A., SMITH, S.D. and WIESNER, C.S. *Treatment of thermal and residual stresses in the SINTAP defect assessment procedure*. British Energy Generation Report EDP/GEN/REP/0423/99 and SINTAP/NE/018. 1999. <http://www.eurofitnet.org/sintap_index.html>

[R.3] R6 PANEL. *R6: Assessment of the integrity of structures containing defects*. Revision 4, as amended. Gloucester: EDF Energy, 2001.

 © The British Standards Institution 2019 *This page deliberately left blank*

Annex S (informative)

Information for making high temperature crack growth assessments

S.0 Symbols and definitions

For the purposes of this annex, the following symbols, definitions and units apply, unless otherwise indicated at the point of use.

Symbol	Definition	Units
A	Temperature-dependent constant in creep strain rate equation	$MPa^{-n}h^{-1}$
A_A	Constant associated with the average creep rate for a given temperature	$MPa^{-n}h^{-1}$
A_s	Secondary creep constant	$MPa^{-n}h^{-1}$
a	Half flaw length for through-thickness flaw, flaw height for surface flaw or half height for embedded flaw	mm
$\dot{a}_c$	Rate of crack propagation in height direction due to creep	$mm{\cdot}h^{-1}$
$C(t)$	Transient crack tip parameter	$MPamh^{-1}$
C^*	Creep fracture/crack growth parameter	$MPamh^{-1}$
D_c	Total accumulated creep damage	—
I_n	Dimensionless function of strain hardening exponent in Hutchinson-Rice-Rosengren stress field distribution	—
K	Stress intensity factor (SIF)	$MPa\sqrt{m}$
K_{mat}	Characteristic fracture toughness	$MPa\sqrt{m}$
K^p	Elastically calculated stress intensity factor due to primary load	$MPa\sqrt{m}$
k	Reference stress correction factor for welds	—
n	Power-law creep stress exponent [Equation (S.2)]	—
n_A	Constant associated with the average creep rate for a given temperature	—
n_s	Exponent associated with the secondary creep rate for a given temperature	—
q	Exponent in creep crack growth equation	—
r_c	Size of creep damage zone	μm
t	Time	h
t_{CD}	Time to failure of plant by bulk creep rupture, measured from initial start-up (Clause **9** and Annex S)	h
t_i	Crack initiation time, prior to commencement of creep crack growth	h
t_r	Time to rupture	h
t_{red}	Redistribution time	h
$t_{r,ref}$	Time to creep rupture at reference stress	h
Δa_i	Crack extension at initiation period	mm
ΔK	Stress intensity factor range	$MPa\sqrt{m}$
$\dot{\varepsilon}_c^A$	Average creep rate	/h
$\dot{\varepsilon}_c^s$	Secondary creep rate	/h
ε_c	Accumulated creep strain	—

(continued)

Symbol	Definition	Units
ε_f	Strain to failure of material, as measured in uniaxial creep tests	—
ε_f^*	Multiaxial stress dependent creep failure strain of material	—
$\dot{\varepsilon}_{ref}$	Creep strain at reference stress	/h
σ_{ref}	Reference stress used for creep and plastic consideration	N/mm^2
$\sigma_{ref,hom}$	Homogenous cracked-body reference stress, obtained from Equation (9.5)	N/mm^2

S.1 Materials data

S.1.1 General

The background to this annex is described in reference [S.1].

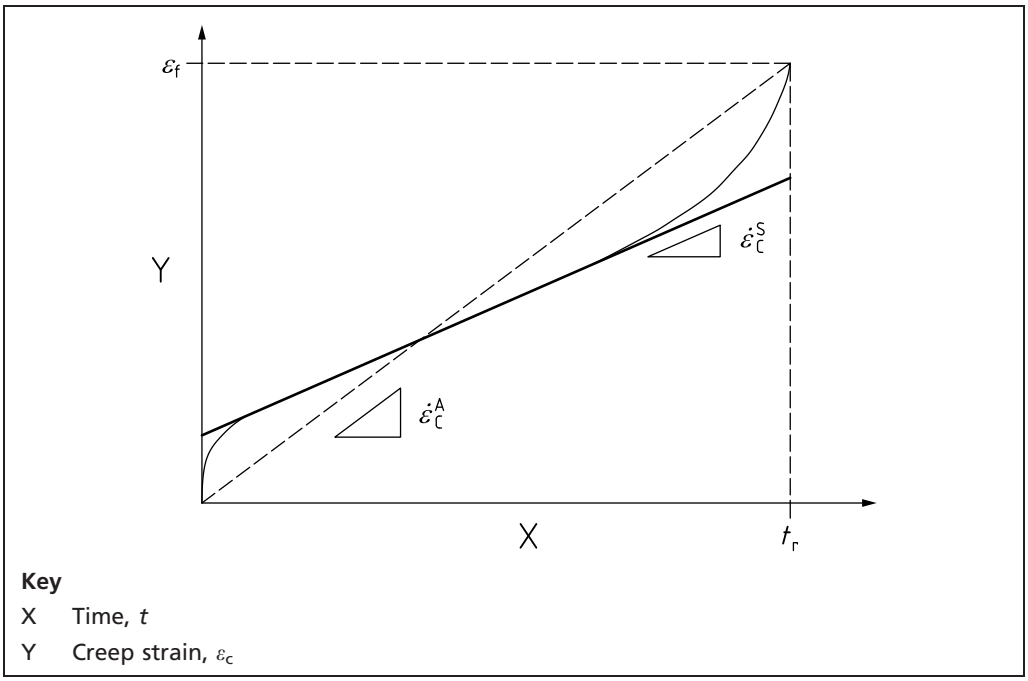
S.1.2 Tensile properties

Stress-strain data for some materials, including yield strength and ultimate tensile strength, can be obtained from PD 6525-1 and references [S.2], [S.3] and [S.4].

S.1.3 Creep strain versus time curves

Strain versus time curves, as schematically illustrated in Figure S.1, can be obtained from published information for some materials. For a number of austenitic and alloy ferritic steels, creep strain versus time data are available directly in tabular form in Appendix A3 of sub-section A, of RCC-MR [S.2]. Where strain versus time data are not available explicitly, they can be derived from ISO-strain curves, such as those shown in Figure S.2a), by cross-plotting as shown in Figure S.2b).

Figure S.1 **General form of a creep curve defining the average and secondary creep strain rates**

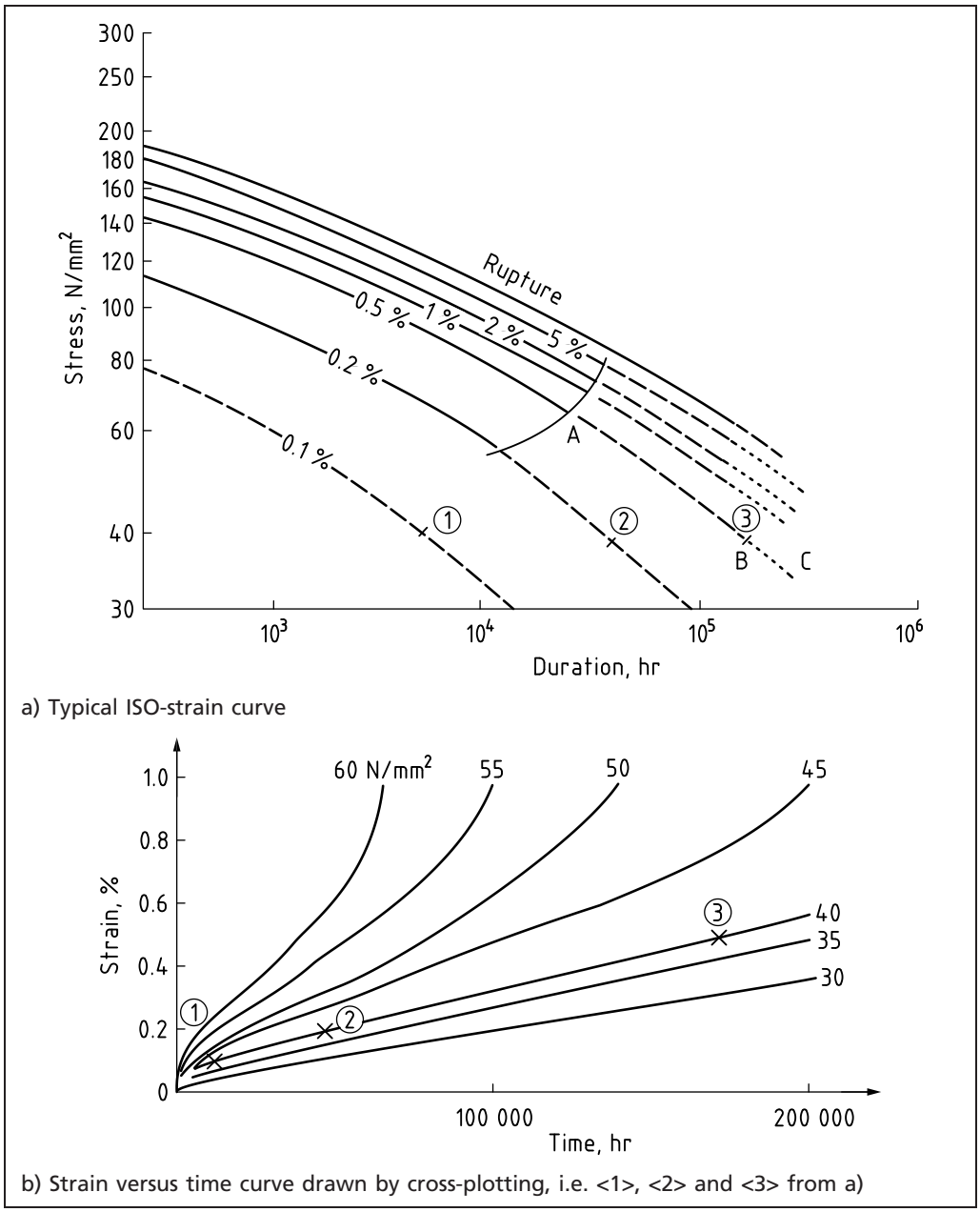


Key

X Time, t

Y Creep strain, ε_c

Figure S.2 **General form of a creep curve defining the average and secondary creep strain rates**



ISO-strain curves are presented in reference [S.4] for the following materials over the temperature range given:

- carbon-manganese steel: 400 °C to 500 °C;
- ½Cr½MoV steel: 475 °C to 600 °C;
- 1Cr½Mo steel: 475 °C to 600 °C;
- 2¼Cr1Mo steel: 475 °C to 600 °C;
- 9Cr1Mo steel (P91): 475 °C to 625 °C;
- 12Cr1MoV(W) steel (P92): 500 °C to 625 °C;
- alloy 800: 600 °C to 1 000 °C.

Wrought ferritic steels in the normalized and tempered or annealed conditions (as specified in the relevant standard), having the following alloy compositions, may be considered to be creep ductile (this excludes weld metals or HAZ):

a) carbon-manganese steels:
   1) ½CrMoV;
   2) 1Cr½Mo;
   3) 2¼ Cr1Mo;
   4) 9Cr1Mo;
   5) 12Cr1MoV(W);
b) solution treated austenitic steels of the 300-series:
   1) types 304, 304H and 304L;
   2) types 316, 316H, 316L and 316L(N);
   3) types 321 and 312H;
   4) Alloy 800 and 800H.

The creep strain rate behaviour of some materials is often represented by a power-law relation (see Clause **9**, Equation 9.2) and the secondary creep strain rate used to describe the material's creep behaviour. The secondary creep strain rate is given as:

$$\dot{\varepsilon}_c^s = A_s \sigma^{n_s} \quad \text{(S.1)}$$

However, in order to account for the three regions of the creep curve, the average creep strain rate may be employed, which, for a given stress, is defined by the ratio of the creep ductility to time to rupture. The stress dependency of the average creep rate may also be described by a power law relationship:

$$\dot{\varepsilon}_c^A = \frac{\varepsilon_f}{t_r} = A_A \sigma^{n_A} \quad \text{(S.2)}$$

For most engineering alloys $\dot{\varepsilon}_c^A$ is approximately between two and three times $\dot{\varepsilon}_c^s$. Making use of average creep rates is more conservative for the assessment.

The average creep strain rate may be employed to estimate the material's behaviour when only creep rupture data are available.

Where ISO-strain curves are not available, it is sometimes possible to derive the strain versus time curves from a cross-plot of isochronous curves. These are given, for certain materials, in references [S.2], [S.4], the ASME Boiler and Pressure Vessel Code, Section III, or ASME Case N-47 [S.5].

S.1.4 Uniaxial creep properties

Detailed analyses require creep tests to be performed in order to obtain data specific to the material. If material specific data are not available, then refer to National Institute for Materials Science (NIMS) database, for example [S.6] (see Table S.1). The material can embrittle with ageing; the creep ductility of short-term tests can therefore be higher than long-term tests. Therefore, the operating lifetime should be taken into account when performing an assessment and data obtained from tests of an appropriate duration.

 © The British Standards Institution 2019

Table S.1 **Mean uniaxial creep properties for different steels for short (<10 000 h) and long-term tests**

Material	Temperature °C	Long-term		Short-term	
		$Log_{10}(A_A)$	n_A	$Log_{10}(A_A)$	n_A
Carbon steel	400	–11.2	3.6	–21.5	8.0
	450	–10.9	4.0	–12.5	4.9
	500	–11.6	4.7	—	—
1Cr-1Mo-V	450	–19.8	6.5	–57.0	20.8
	500	–28.4	10.4	–42.3	15.9
	550	–17.1	6.1	–30.2	11.8
	600	–7.1	2.1	–20.9	8.6
	650	–4.5	1.4	–9.4	4.0
1.25Cr-0.5Mo	500	–10.9	3.5	—	—
	550	–13.3	5.4	–12.6	5.9
	600	–7.8	3.1	—	—
	650	–8.4	4.3	—	—
2.25Cr-1Mo	450	–24.6	8.8	—	—
	475	–14.5	5.1	—	—
	500	–17.5	6.6	—	—
	550	–15.1	6.1	—	—
	600	–11.6	5.2	—	—
	650	–6.5	2.9	—	—
12Cr1MoV(W) (P92)	550	—	—	–52.1	21.1
	600	–35.6	15.1	—	—
	650	–25.0	11.4	—	—
	700	–17.0	8.5	—	—
	750	—	—	–9.8	5.5
AISI 304	500	–28.1	10.5	—	—
	550	–28.0	11.1	—	—
	600	–21.3	8.5	—	—
	650	–11.9	4.5	–22.0	9.7
	700	–6.0	1.6	–20.6	9.7
	750	–9.1	3.8	–21.0	10.6
	800	—	—	–9.7	4.6
AISI 316	550	–30.1	11.2	–48.9	18.6
	600	–18.0	7.0	–23.2	9.2
	650	–13.6	5.3	–18.6	7.9
	700	–9.0	3.4	–16.4	7.5
	750	–6.5	2.5	–13.8	6.8
	800	–9.3	4.8	—	—
Alloy 800	600	–12.2	4.0	–25.6	9.9
	650	–21.2	9.0	—	—
	700	–16.0	7.1	–19.9	9.0
	750	—	—	–24.7	11.8
	800	–9.8	4.3	–14.5	7.4
	900	–10.4	6.1	—	—
	1000	–7.0	5.0	—	—

Table S.1 **Mean uniaxial creep properties for different steels for short (<10 000 h) and long-term tests** *(continued)*

Material	Temperature °C	Long-term		Short-term	
		$Log_{10}(A_A)$	n_A	$Log_{10}(A_A)$	n_A
9Cr1M0 (P91) (Average creep rate)	450	–32.3	11.4	–101.6	38.4
	500	–36.4	13.8	—	—
	550	–17.5	6.4	–30.4	12.2
	600	–4.5	0.7	–24.1	10.4
	650	–8.1	2.9	–16.4	7.6
	700	–9.4	4.7	—	—
9Cr1Mo (P91) Cross-weld (Average creep rate)	550	—	—	–28.2	11.7
	600	—	—	–22.6	10.1
	650	—	—	–15.1	7.5
9Cr1Mo (P91) (Minimum creep rate)	500	–38.4	13.5	—	—
	550	–40.0	15.0	—	—
	600	–13.8	3.8	–31.3	12.3
	650	–13.6	4.4	–16.8	6.3

NOTE The units of A_A are for stress in MPa and time in hours.

S.1.5 Fatigue crack propagation rate

In the absence of plasticity, the fatigue crack propagation rate at high temperatures is defined by Equation (9.12).

Further data can be found in references [S.7], [S.8], [S.9] and [S.10].

Where cracks are propagated by fatigue through material heavily damaged by prior creep (i.e. with a D_c > approximately 0.8), propagation rates are likely to be increased. In these circumstances, a factor should be applied to the data, depending on the amount of prior creep damage. This factor should be experimentally determined.

S.1.6 Creep crack propagation rate

Where crack propagation data are not available for the material used in the component, estimates can be obtained from the following equations, using the data given in Table S.2. Depending upon the material, further information might be available in the published literature (see for example references [S.11], [S.12], [S.13] and [S.14]).

$$\dot{a}c = A(C^*)^q \tag{S.3}$$

The constants in Table S.2 lead to growth rates in mm/h if C^* is in units of $MPamh^{-1}$.

Both mean and upper bound data are presented; use of the upper bound data results in lower estimates of remaining life. For thicker components with increased triaxiality, plane strain conditions prevail and crack propagation rates might be higher; specialist advice should be sought regarding the appropriate values to be used.

For materials not covered by Table S.2, two methods are available to estimate crack propagation rates, although the results might not be upper bound.

 © The British Standards Institution 2019

Table S.2 **Mean uniaxial creep properties for different steels for short (<10 000 h) and long-term tests**

Material	Temperature range of data, °C	Upper bound		Mean	
		A	*q*	*A*	*q*
Carbon steel	482 to 538	15.0	1.00	6.0	1.00
½Cr Mo V – wrought and cast	500 to 600	60.3	0.80	6.0	0.80
½Cr Mo V – type IV	540 to 565	150.13	0.80	7.0	0.80
½Cr Mo V – coarse HAZ	565	301.4	0.80	100.5	0.80
1Cr Mo	450 to 600	19.9	0.84	6.0	0.84
2¼ Cr 1 Mo weld metal	540 to 565	14.6	0.67	2.8	0.67
AISI type 304 and 304H	650 to 760	35.0	1.00	7.0	1.00
AISI type 304 (service exposed)	760	99.4	0.85	49.7	0.85
AISI type 321 (wrought) inc HAZ and ageing	650	20.0	0.90	4.7	0.90
AISI type 316 and 316H (wrought, inc HAZ)	500 to 550	22.9	0.81	3.0	0.81
	625	19.6	0.89	1.9	0.89
AISI type 316 weld (as welded, stress relieved and aged)	600 to 650	56.9	0.88	10.0	0.88
AISI type 316 weld (solution treated)	550	22.9	0.81	3.0	0.81
Alloy 800H	800	80.2	0.90	25.0	0.90
Mod 9Cr steel	580 to 593	4.5	0.65	3.0	0.70
Mod 9Cr 1C-HAZ	580	19.9	0.78	10.0	0.78
2¼ Cr1 Mo	550 to 600	6.0	0.80	3.7	0.83
Aluminium alloy RR 58	150	2483.7	0.85	1500.9	0.85
Aluminium alloy 2519 — T851	135	350.8	0.90	175.42	0.90
Alloy 939	850	200.0	1.00	40.0	1.00
1Cr Mo V steel	538 to 594	14.9	0.75	4.8	0.79

Where the creep rupture ductility of the material is known, a guide to crack propagation rates may be obtained by taking q as 0.85 and deriving A from the following equation:

$$A = \frac{0.0085}{\varepsilon_f^*} \quad \text{(S.4)}$$

NOTE The creep rupture ductility value is expressed as a fraction and not a percentage.

Creep rupture ductilities for certain steels are given by the Institution of Mechanical Engineers; Creep of Steels Working Party [S.4] and the British Iron and Steel Research Association/Iron and Steel Institute [S.3].

When the creep rupture ductility is not known, a guide to propagation rates can be obtained from the following equations:

$$\dot{a}_c = 5\left[\frac{(K^p)^2}{\sigma_{ref} t_{r,ref}}\right]^{0.85} \quad \text{(S.5)}$$

where:

K^p is the elastically calculated stress intensity factor associated with primary loads in in MPa$\sqrt{}$m;

σ_{ref} is the reference stress in MPa;

$t_{r,ref}$ is the time to rupture at the reference stress in hours;
$\dot{a}_c$ is the creep crack growth rate in mmh^{-1}.

S.1.7 Creep crack initiation

Where fatigue needs be taken into account under the provisions of **9.8**, the initiation period should be ignored, unless experimental data are available for the material under the appropriate conditions (see ASTM E1457).

For situations where fatigue is insignificant, it might be possible to take account of an initiation period prior to crack extension. Creep crack initiation data may be expressed for widespread creep conditions by the relationship shown in Equation (9.10).

Where no initiation data are available, t_i is given as:

$$t_i = 0.002\ 5\left(\frac{\sigma_{ref} t_{r,ref}}{K^2}\right)^{0.85} \tag{S.6}$$

with rupture life in hours, σ_{ref} in N/mm^2 and K in $MPa\sqrt{m}$.

This equation is suitable for performing scoping calculations to determine whether initiation data need to be collected. When initiation data are available from tests performed according to ASTM E1457, t_i can be calculated from Equation (9.10).

For determining initiation periods in components, C^* can be derived from:

$$C^* = \sigma_{ref}\dot{\varepsilon}_{ref}\left(\frac{K^p}{\sigma_{ref}}\right)^2 \tag{S.7}$$

A variety of criteria may be used to define creep initiation and hence initiation time, t_i. The criteria employed should be stated. The criterion of 0.2 mm crack extension at the start as stated in ASTM E1457 is an example for correlating initiation times experimentally with respect to C* in Equation (S.7).

In order to evaluate Equation (S.7), creep rupture data are needed. Assuming that $\dot{\varepsilon}_{ref}$ can be expressed as $\varepsilon_f/t_{r,ref,}$ using a power law stress dependence, enables cracking rate to be written as:

$$\dot{a}_c = (n+1)\frac{\varepsilon_f}{\varepsilon_f^*}\frac{1}{t_{r,ref}}\left(\frac{K}{\sigma_{ref}}\right)^{2n/(n+1)}\left(\frac{r_c}{I_n^n}\right)^{1/(n+1)} \tag{S.8}$$

where it is recommended that the size of the creep damage zone is taken as r_c = 50 μm, $\varepsilon_f/\varepsilon_f^*$ = 1 for plane stress and $\varepsilon_f/\varepsilon_f^*$ = 30 for plane strain (although it might be possible to reduce this for creep ductile materials), where the values of I_n can be taken from [S.15]. Alternatively a simplified approximation to Equation (S.8) could be quoted with $n/(n + 1) = 0.85$, as is included in this annex. Conservative predictions should be obtained if lower bound rupture data are employed.

Similarly, it is possible to evaluate the initiation period from [S.16].

$$t_i = \frac{(n+1)\Delta a_i}{2\dot{a}_c} = \frac{\Delta a_i}{2}\frac{\varepsilon_f^*}{\varepsilon_f} t_{r,ref}\left(\frac{K}{\sigma_{ref}}\right)^{-2n/(n+1)}\left(\frac{r_c}{I_n^n}\right)^{-1/(n+1)} \tag{S.9}$$

Again this equation can be simplified for $n/(n + 1) = 0.85$ as in Equation (9.10). The equation is valid for $t_i > t_{red}$. For $t_i < t_{red}$, widespread creep conditions have not been achieved at the crack tip and the value of t_i calculated from Equation (S.9) should be halved to allow for $C(t)$ dominance [S.17].

 © The British Standards Institution 2019

The concept can be applied using [S.19].

$$t_i = \Delta a_i \frac{\varepsilon_f^*}{\varepsilon_f} \left(\frac{K}{\sigma_{ref}} \right)^{-2} t_{r,ref} \quad \text{(S.10)}$$

Equation (S.9) and Equation (S.10) are very similar. Equation (S.10) has been demonstrated to be satisfactory for type 316H stainless steel.

If, in practice, an assessment is marginal then experimental cracking data clearly need to be generated.

Alternative methods are available for predicting the creep crack initiation time. Further details are given in references [S.17] and [S.18].

S.2 The assessment of flaws in weldments

S.2.1 General

Many of the flaws found in high temperature plant are associated with weldments. They can arise during fabrication, PWHT and mechanical property variations. The flaws are often located in non-homogeneous material, which has a significant effect on crack growth.

Flaws in austenitic and ferritic weldments, including type IV cracking (see **S.3.2.4**), can be assessed using the methods described in this British Standard, provided that the recommendations of this annex are taken into account.

However, where cracking occurs at the interface between the austenitic weld metal and ferritic parent metal in dissimilar metal weldments, special consideration is necessary. Such weldments are excluded from the scope of this British Standard, and specialist advice should be sought when assessing them.

S.2.2 Treatment of defects in weldments

S.2.2.1 General

It is not within the scope of this annex to treat weldments in detail. Only a general description is presented here. A particular problem with weldments is the presence of residual welding stresses. Although these relax as creep strains accumulate, they can reduce creep life by initiating crack growth at shorter times and by increasing crack growth rates. Often the effect is small, particularly for stress-relieved welded joints made from creep-ductile materials. Therefore, a simple check is made here to assess whether welding residual stresses are significant. In some cases, the level of conservatism might be excessive and a more detailed procedure is described in [S.17] and [S.18]. It should, however, be recognized that, in all cases, validation for the detailed procedure is limited to specific weldment types. Finally, **S.3.2** describes some specific modes of cracking observed in high temperature weldments.

Defects in austenitic and ferritic similar metal welds and in conventional bi-material dissimilar metal welds (DMWs) can be assessed, and defects which are characterized as being fully in either the ferritic or austenitic materials adjacent to a DMW should be assessed using the R5 procedure [S.18].

Experience with the DMW crack growth procedures in reference [S.18] is currently limited to ferritic 2.25Cr1Mo to austenitic type 316 pipe or tube welds made using either austenitic or nickel-based weld metal. The procedure can, however, be used for other geometries and material combinations provided that the required data have been obtained.

Secondary stresses are assumed to relax over a redistribution period. In some cases, the secondary stresses might have completely relaxed due to creep in service at the start of the assessment period. It is, however, conservative to treat all stresses as primary and to neglect relaxation.

Allowance for an initiation time of a pre-existing defect prior to significant crack propagation is made for similar weldments under steady loading. No such period is currently assessed in reference [S.18] for DMWs; it is assumed that crack growth occurs immediately upon loading. For creep-fatigue loading, it is generally assumed that there is no initiation period.

S.2.2.2 Simplified assessment

References [S.17] and [S.18] give details of the simplified assessment. In the simplified estimate, the time for creep rupture failure and the extent of creep crack growth are estimated. It is assumed that the crack initiation time is zero.

Bulk creep damage is assessed assuming that the weld is homogeneous with the rupture properties of the weakest region. The time to failure by continuum damage mechanisms is calculated. The calculation is performed separately for each of the weldment constituents using the appropriate rupture data, but with the reference stress always defined from the homogeneous limit load. The value of t_{CD} used in the assessment is the smallest of those determined for the different regions. In order to assess creep crack growth, C^* is calculated. It is assumed that the weld is homogeneous for the purposes of calculating the reference stress. C^* is estimated with creep strain rate data of the fastest creeping region. The extent of creep crack growth rate is then obtained with this value of C^* and creep crack growth data for the region where the flaw is estimated.

S.2.2.3 Detailed assessment

References [S.17] and [S.18] give details of the detailed assessment. For the purposes of calculating the initiation time and creep crack growth, the reference stress, σ_{ref}, is calculated for the specific location of the crack. For continuum damage calculations, the reference stress is calculated for each microstructural zone. Reference stresses are different, in general, from that calculated assuming homogeneous creep properties across the joint, (see [S.17] and [S.18]). The reference stress for a given zone is generally a factor k times the corresponding homogenous cracked-body reference stress, $\sigma_{ref,hom}$, that is:

$$\sigma_{ref} = k\sigma_{ref,hom} \quad \text{(S.11)}$$

The factor k is different for the different weld zones. The source of different k values can be illustrated by considering a pipe under pressure and end load. For some stress states, such as pressure only, the maximum principal stress is approximately parallel to the fusion boundary (“hoop stress control”) and is different in the different weld zones as a result of stress redistribution; this leads to k values different from unity. For cases of “axial-stress control”, such as under high system loads where the maximum principal stress is transverse to the fusion boundary, overall stress redistribution cannot occur and $k = 1$ is more likely.

The reference stress for each constituent in a weldment is determined from a limit load calculation performed with the assumed yield stress of each region proportional to the creep rupture strength of the corresponding material for the service lifetime. The resulting limit load might differ from that of the homogeneous component due to the effects of the mis-match in plastic (creep) properties. The reference stress for each zone then follows but using the local yield stress and the mis-match limit load. The factor k is then the ratio of the resulting reference stress to the homogeneous value. Advice on the treatment of mis-match is given in Annex I and Annex P.

In general, the factor k is loading-, geometry- and material-dependent, and accounts for the elevation in stress in strong material within the weldment or, conversely, the reduction in stress in weaker materials in the weldment. This “weld redistribution factor” can be conveniently expressed as a function of the

 © The British Standards Institution 2019

ratio of weld metal/parent metal minimum creep rates for the case of a pipe-pipe butt weld under internal pressure loading.

The time to failure by continuum damage mechanisms, t_{CD}, should be calculated. The calculations should be performed separately for each of the weldment constituents using the appropriate rupture data. The value of t_{CD} is the smallest of those determined for the different regions.

S.3 Special considerations for welds

S.3.1 General

Many of the defects found in high temperature components are associated with weldments. These defects can arise during fabrication, PWHT or in service. As weldments contain wide metallurgical and mechanical property variations, the defects are often located in non-homogeneous material, which has a significant effect on crack growth.

Defects in austenitic and ferritic weldments, including type IV cracking can be assessed using the methods described in this British Standard. However, dissimilar metal weldments, where cracking occurs at the interface between the austenitic weld metal and ferritic parent metal, need special consideration. Specialist advice is contained in R5 [S.18] for assessing such weldments.

The properties of the weld metal and the HAZ are usually considerably different from those of the parent material, in terms of creep strength, crack propagation rate and fracture toughness. It is important to identify the part of the weld in which the crack is situated and then to use properties appropriate to that location.

Residual stresses in the vicinity of a weld can have a significant influence on crack propagation and failure and should be taken into account in the assessment. Typical residual stress distributions in some commonly used types of weld are provided in Annex Q and R6 [S.20]. For other configurations, in the absence of data to the contrary, it should be assumed that a tensile membrane stress of yield point magnitude is present.

Where it can be confirmed that the component has been subjected to a PWHT which reduces the residual stresses to a negligible level, they may be ignored in the assessment. It might also be possible to take credit for a reduction in residual stress when a component has been in service for a sufficiently long period at a sufficiently high temperature. R5 [S.18] provides methods for assessing this stress relaxation.

S.3.2 Plant experience

S.3.2.1 General

Weldments can fail by a number of different modes that involve creep crack growth. A basic understanding of these failure modes enables the appropriate materials properties and stresses to be identified and brought together in a procedure in order to carry out an assessment. Subclauses **S.3.2.2** to **S.3.2.5** describe some commonly encountered failure modes in pipe to pipe weldments.

S.3.2.2 Reheat cracking in ferritic weldments

In pressure vessels, etc., circumferential HAZ and transverse weld metal cracking arise during post-weld stress relief heat treatment or very early in the plant operating life. Initiation of cracking is highly dependent on the material's composition, weldment microstructure and residual stress; the last two factors depend critically on welding and heat treatment procedures. Crack growth depends on welding and heat treatment procedures and on microstructure and stress. Microstructure and stress vary initially as a function of position and

change further as a function of time and temperature as the weldment is exposed to plant conditions.

S.3.2.3 Reheat or stress-relief cracking in austenitic weldments

Stress-relief or reheat cracking similar to that described in **S.3.2.2** for ferritic steels can also occur in austenitic steels.

This brittle intergranular cracking occurs in the HAZ close to the fusion line as a result of the concentration on to grain boundaries of relaxation strains associated with stress relief, or the concentration of creep strain during extended service. This strain concentration is due to strengthening within the matrix of the grains resulting from fine precipitate dispersions on dislocation networks. The mechanism appears able to operate in service at temperatures as low as 500 °C, given sufficiently long times.

The propensity for this type of cracking is greatest in the Nb-stabilized AISI type 347 steel, but it is also encountered in the Ti-stabilized AISI type 321 steel. Dependent upon operating temperature and the level of residual or applied stress, a similar mechanism might also occur in AISI type 316 steel, particularly high carbon varieties. It is, however, less likely to occur in nitrogen-strengthened low carbon varieties, due to the greater solubility of nitrogen than carbon.

S.3.2.4 Type IV cracking in ferritic weldments

This mode of failure in pressure vessels, etc., involves the initiation and growth of circumferential creep cracks in the low temperature extremity of the HAZ adjacent to the untransformed parent material. It has been observed from times midway through the design life onwards. Axial loading over and above the nominal axial stress due to internal pressure is significant in promoting this mode of cracking.

S.3.2.5 Transverse weld metal cracking in ferritic weldments

This is the dominant mode of cracking encountered in pipe to pipe weldments subjected predominantly to internal pressure loading. Under these conditions, the weldments invariably reach or exceed their design lives, by which time the hoop strain accumulation initiates axial cracks, transverse to the weldment, in the more coarse-grained columnar regions of the weldments. This crack initiation is generally multiple, leading eventually to excessive deformation, bulging and the formation of secondary circumferential cracks in the weld metal, which result in eventual failure.

S.3.3 Structural calculations for weldments

Flaws can arise in weldments for a number of different reasons and extend by creep crack growth until they cause failure. Furthermore, creep deformation alone can lead to the initiation of discrete cracks in weldments even in the absence of pre-existing flaws. Crack growth might also involve periods of fast and slow propagation as cracking traverses regions of different microstructure. The user needs to take account of these factors in applying this standard to the assessment of pre-existing weldment flaws and growing creep cracks.

It is often sufficient to carry out a simplified analysis as described below, although in some circumstances this can be over-conservative. For a more detailed investigation, the user should refer to R5 [S.18] or seek specialist advice.

 © The British Standards Institution 2019

For fracture, bulk creep damage and crack growth, the following points should be taken into account.

a) Fracture analysis.

   1) Assume that the weldment is homogeneous.

   2) Use the yield and ultimate tensile strength of the weakest constituent of the weldment.

   3) If it can be shown that the flaw cannot propagate into another region of the weldment, use the value of K_{mat} appropriate to the region in which it is situated. If this cannot be shown, use the lowest value of K_{mat} that occurs anywhere in the weldment.

b) Analysis of bulk creep damage.

   1) Calculate σ_{ref} assuming the weldment to be homogenous.

   2) Calculate $t_{r,ref}$ for the region of the weldment with the shortest rupture life, but also check that there is adequate margin against failure, if stronger regions are present that have a low creep rupture ductility.

c) Creep crack growth analysis.

   1) Calculate C^*, assuming that the weldment is homogenous. Use the strain rate data of the fastest creeping constituent. If it can be shown that the flaw cannot propagate into another region of the weldment, use the value of $\dot{a}_c$ appropriate to the region in which it is situated. If this cannot be shown, use a value of $\dot{a}_c$ appropriate to the region with the highest crack propagation rate.

   2) In making a preliminary assessment, worst case materials data can be used in the analysis: for example, upper bound crack propagation rate and upper bound strain rates. However, excessive conservatism should not be applied – for different casts of steel to the same specification, there is an approximate proportionality between crack propagation rate and strain rate.

S.3.4 Residual stresses

A particular problem with fabrication processes such as those involving non-uniform deformation and welding is the presence of residual welding stresses. Although these relax as creep strains accumulate, they can reduce the creep life by initiating crack growth at shorter times and by increasing crack growth rates. However, the effect is often small, particularly in the case of stress-relieved welded joints made from creep ductile materials.

Residual stresses are incorporated into the calculations as described in Clause **7**.

Bibliography for Annex S

Standards publications

For dated references, only the edition cited applies. For undated references, the latest edition of the referenced document (including any amendments) applies.

ASME Boiler and Pressure Vessel Code, Section III: *Rules for construction of nuclear power plant components*

ASTM E1457, *Standard test method for measurement of creep crack growth rates in metals*

PD 6525-1, *Elevated temperature properties for steels for pressure purposes – Stress rupture properties*

Other documents

[S.1] AINSWORTH, R.A. The creep clauses of BS 7910, *In: International Journal of Pressure Vessels and Piping*, 165, August 2018, 208–213. <https://doi.org/10.1016/j.ijpvp.2018.06.014>

[S.2] RCC-MR. *Design and construction rules for mechanical components of FBR nuclear islands, as amended*. Paris: AFCEN, 1985.

[S.3] BRITISH IRON AND STEEL RESEARCH ASSOCIATION/IRON AND STEEL INSTITUTE. High-temperature properties of steels. *In: Proceedings of BISRA/ISI conference,* Eastbourne, April 4–7 1966. London: ISI, 1966.

[S.4] INSTITUTION OF MECHANICAL ENGINEERS, THE CREEP OF STEELS WORKING PARTY. *High temperature design data for ferritic pressure vessel steels*. London: Mechanical Engineering Publications Ltd, 1983. ISBN 0 85298 526 6.

[S.5] HUDDLESTON R.L, SWINDEMAN R.W. *Materials and design bases issues in ASME Code Case N-47*. Nuclear Regulatory Commission, Washington, DC (United States). Division of Engineering; Oak Ridge National Lab., TN (United States), 1993.

[S.6] NIMS STRUCTURAL MATERIALS DATASHEET [online], *Creep Data Sheet*. <http://smds.nims.go.jp/creep/index_EN.html>

[S.7] HUDSON, C.M, SEWARD, S.K. and FERRAINOLO, J.J. A compendium of sources of fracture toughness and fatigue crack growth data for metallic alloys. *In: International Journal of Fracture*. *Part 1 (1978):* 14(4), R151-R184; *Part 2 (1982):* 20(3), R57-R117; *Part 3 (1989):* 39(4), R43-R63; *Part 4 (1991)*: 48(2), R19-R43. ISSN 0376-9429.

[S.8] WATERMAN, N.A. and ASHBY, M.F. *Materials selector*. 3 Volumes. London: Elsevier, 1991. ISBN 1851666052.

[S.9] ENGINEERING SCIENCES DATA UNIT. *Fatigue crack propagation in low and medium strength low alloy steel plate, bar and forgings*. ESDU Data Sheet 81011. London: ESDU, 1981.

[S.10] HOLDSWORTH, S. R. High temperature crack growth. *In:* J. B. MARRIOTT, ed. *High temperature crack growth in steam turbine material*, EUR Report 14678, Part 3. Luxembourg: Commission of the European Communities, 1994.

[S.11] HOLLSTEIN, T., DJAVANROODI, F., WEBSTER, G.A., and HOLDSWORTH, S.R. High temperature crack growth in alloy 800H and a 1% CrMoV steel: The results of an EGF round-robin. *In: E. CZOBOLY, ed. Failure analysis theory and practice. In: Proceedings of the 7th European Conference on Fracture*. Budapest, Hungary, 1988. EMAS, UK: 1988.

[S.12] DIMOPULOS, V., NIKBIN, K.M., WEBSTER, G.A. Influence of cyclic to mean load ratio on creep/fatigue growth. In*: Metallurgical Transactions*, 1988, 19A(4), 873–880. ISSN 0360-2133.

[S.13] WINSTONE, M.R., NIKBIN, K.M. and WEBSTER, G,A. Modes of failure under creep/fatigue loading of a nickel-based superalloy. *In: Journal of Materials Science*, 1985, 20(7), 2471–2476. ISSN 0022-2461.

[S.14] NIKBIN, K.M., SMITH, D.J. and WEBSTER, G.A. Prediction of creep crack growth from uniaxial creep data. *In: Proceeding of the Royal Society London*, Series A, 1984, 396(1810), 183–197. ISSN 0080-4630.

[S.15] SHIH, C.F. *Tables of Hutchinson-Rice-Rosengren singular field quantities*. Technical Report, MRL E-147. Rhode Island: Brown University, 1983.

 © The British Standards Institution 2019

[S.16] DAVIES, C.M. Predicting creep crack initiation in austenitic and ferritic steels using the creep toughness parameter and time-dependent failure assessment diagram. *In: Fatigue and Fracture of Engineering Materials and Structures*, 2010, 33(12), 911–911. <https://onlinelibrary.wiley.com/doi/abs/10.1111/j.1460-2695.2010.01537.x>

[S.17] KOÇAK, M., WEBSTER, S., JANOSCH, J.J., AINSWORTH, R.A., and KOERS, R. *FITNET Fitness-for-Service (FFS) – Procedure (Volume 1)*. Geesthacht, Germany: GKSS Research Centre, 2008. ISBN 978-3-940923-00-4.

NOTE This document is out of print and has effectively been superseded by BS 7910:2013.

[S.18] R5 PANEL. *R5 assessment procedure for the high temperature response of structures (as amended)*. Report R5, Issue 3. Gloucester: EDF Energy, 2003.

[S.19] WEBSTER, G.A., DAVIES, C.M., SKELTON, R.P., NIKBIN, K.M. and DEAN, D.W. Determination of creep crack growth incubation periods in type 316H stainless steel. In*: Proceedings of 2nd International Conference on Creep and Fracture in High Temperature Components – Design and Life Assessment*, Zurich, April 21–23, 2009.

[S.20] R6 PANEL. *R6: Assessment of the integrity of structures containing defects*. Revision 4, as amended. Gloucester: EDF Energy, 2001.

This page deliberately left blank

Annex T (informative)

Guidance on the use of NDT with ECA

T.0 Symbols and definitions

For the purposes of this annex, the following symbols, definitions and units apply, unless otherwise indicated at the point of use.

Symbol	Definition	Units
a	Half flaw length for through-thickness flaw, flaw height for surface flaw or half height for embedded flaw	mm
B	Flux density	Tesla
c	Half flaw length for surface or embedded flaw	mm
$\pm E$	Symmetric confidence intervals for the sizing errors for UT	mm
E_1, E_2	Asymmetric confidence intervals	mm
f	Testing frequency of manual eddy current testing	Hz
R_a	Surface roughness of crack	mm
t_1, t_2	Statistics used to quantify the uncertainty of a given parameter	—
Δa	Through thickness sizing accuracy	mm
Δp	Ligament sizing accuracy	mm
$\Delta 2a$	Through-thickness sizing accuracy	mm
$\Delta 2c$	Length sizing accuracy	mm
δ	Standard penetration depth of eddy current testing	m
θ	Probability of detection (PoD) term	—
μ_r	Relative magnetic permeability	—
μ_0	Magnetic permeability of free space	H/m
σ	Conductivity of material	siemens/m
ø	Pore diameter	mm

T.1 General

The background to this annex is given in reference [T.1].

This annex is applicable when assessing planar defects or crack-like flaws that exceed the quality control acceptance criteria. It does not address local thinned areas or shape discontinuities.

The application of ECA procedures requires either the input of flaw dimensions to determine fitness-for-service, or the derivation of acceptable flaw dimensions as a condition for inferring fitness-for-service. As all inspection methods and techniques are subject to limitations with respect to their effectiveness and accuracy, it is recommended that these limitations are taken into account.

NOTE Attention is drawn to the provisos which apply to numeric values of capability given in Table T.1 to Table T.5. The capability of individual inspection methods and techniques is generally dependent on ([T.2], [T.3], [T.4], [T.5]):

- *NDT technique and procedure employed;*
- *orientation and morphology of the flaw;*
- *local geometry and access for inspection;*
- *metallurgy of the inspected region;*
- *environment (including lighting);*

- *flaw type;*
- *operator capability and training and other human factors;*
- *equipment capability.*

All techniques assume suitably trained and certified operators and well-designed procedures. For most NDT techniques, including ultrasonic testing (UT), standard Level II certification does not ensure that the operator is capable of providing measurements of through-wall size. Defect sizing qualification programmes address this capability.

Where the NDT system is subject to a qualification programme, e.g. ENIQ [T.6], DNVGL-ST-F101 [T.7] and the ASME Boiler and Pressure Vessel Code, Section V and Section XI (Mandatory Appendix VIII), the results of the qualification programme should take precedence over any specific advice given in this annex and provide the basis for the assumed reliability and any associated sizing errors. Where the normal mode of calibration is from spark eroded slots, this should be regarded as calibration data, not proof of detection or sizing capability.

The numeric values given in **T.7** are drawn from NDT test programmes carried out using various test specimens and procedures and might or might not be appropriate to specific assessments. It is the responsibility of the user to justify that the "detectable" defect sizes and sizing errors used in the assessment are appropriate.

This annex provides general guidance and the advice of NDT specialists for specific applications should be sought.

T.2 Glossary

The glossary is provided to clarify terms used elsewhere in this annex. The British Institute of NDT Yearbook [T.8] contains further information on each NDT method; references [T.9] and [T.10] give more detail.

Alternating current field measurement (ACFM) Measurement of electromagnetic fields around a flaw generated by an imposed AC field to detect and size flaws.

Alternating current potential drop (ACPD) Measurement of the change in electrical resistance across a flaw when an AC potential is applied either side of the flaw. ACPD is mostly used for sizing cracks that have been detected by other technique(s).

Automated ultrasonic testing (AUT) Generic term for the acquisition of ultrasonic data using scanners and encoders, including permanent recording of data, to determine the presence and size of flaws. For the inspection of pipeline girth welds, see also **zonal AUT**.

Certification (of personnel) Procedure used by the certification body to confirm that the **personnel qualification** requirements for a method, level and sector have been fulfilled, leading to the issuing of a certificate, according with an accredited certification scheme, e.g. as defined in BS EN ISO 9712.

Confidence interval Interval between two statistics t_1 and t_2(determined from sample values) that quantifies the uncertainty of a given parameter θ. For example, if θ is a **probability of detection** (PoD) estimated from a practical trial, then the assertion that it lies within a 90% confidence interval would be true, on average, in 90% of such trials. In this example, 90% is termed the (two-sided) confidence level.

 © The British Standards Institution 2019

Confidence limits	These define the upper and lower limits of the **confidence interval**. For example, the true PoD would, on average, lie above the estimated lower 95% confidence limit in 95% of such trials. In this example, 95% is termed the (one-sided) confidence level.
Conventional UT	This is taken to refer to both **manual UT** and **automated UT** where no specific focusing has been introduced, e.g. using flat monolithic transducer crystals.
Eddy current testing (ET)	Use of electromagnetic induction to detect the presence and dimensions of flaws in conductive materials.
Focussed phased array	Use of focal laws to adjust the beams of phased array UT probes to achieve desired focal length and focal spot size for specific purposes, e.g. volumetric examination of a weldment.
Liquid penetrant testing (PT)	Method based upon capillary action, where a low surface tension fluid penetrates into a clean and dry surface-breaking discontinuity. It can be used to locate surface-breaking flaws in any non-porous material. Dye penetrant testing uses a chemical dye (visible under white light). Fluorescent penetrant testing uses a penetrant that fluoresces under ultraviolet light and tends to be more sensitive to small flaws in components with a very smooth surface finish.
Magnetic particle inspection/testing (MPI/MT)	Use of the magnetic properties of iron oxide particles, which are usually held in suspension within a carrier fluid. The inspected (ferritic) item is saturated in a magnetic field and the flaw is detected by a concentration of the particles in the region of the magnetic flux leakage around the flaw. The particles can either be seen against a contrast paint or, in some applications, fluorescent particles are viewed under an ultraviolet light.
Manual ultrasonic testing	Detection of flaws through the transmission and detection of ultrasonic waves from a hand-held probe.
NDT method	Discipline applying a physical principle in NDT, e.g. ultrasonic testing.
NDT procedure	Written description of all essential parameters and precautions to be applied when non-destructively testing products in accordance with standard(s), code(s) and/or specification(s). This annex assumes that the NDT procedure also defines the precise steps to be followed during testing although, in practice, these detailed steps are often defined in an accompanying “NDT instruction” or “technique sheet”.
NDT system	Combination of **NDT procedure**, equipment and personnel for a specific application.
NDT technique	Specific way of utilizing an NDT method.

Personnel qualification	Demonstration of physical attributes, knowledge, skill, training and experience required to perform NDT tasks correctly, e.g. as defined in BS EN ISO 9712.
Probability of detection (PoD)	Probability that a flaw of given dimension(s) can be detected using a particular NDT system for a given application. The probability of detection should normally be quoted along with a specified **confidence limit**.
Probability of rejection (PoR)	Probability that a flaw of given severity (size) will be rejected by a particular NDT system based on the applied acceptance criteria. Detection and sizing by NDT are treated as two separate processes in this annex. For some applications, however, it is convenient to quantify the reliability of an NDT system in terms of PoR, which is a measure of the combined effect of these two processes (see reference [T.11]). In many respects PoR can be treated in the same manner as PoD. As for PoD, the PoR should normally be quoted along with a specified **confidence limit**.
Radiographic testing (RT)	Use of radiation to detect the presence of flaws on an image of the component, e.g. as captured on a film. The source of the radiation is generally either an X-ray tube or gamma rays emitted by a pellet of radioactive isotope.
Sizing error	Error associated with flaw sizing, which is normally quoted as a specified **confidence interval** or **confidence limit(s)** and should normally take into account both the random and systematic error.
Standard depth of penetration (also called skin depth)	Depth at which, under controlled conditions, an electromagnetic field (e.g. eddy currents) reaches 37% of its surface value (see **T.7.9.1**)
Time of flight diffraction (TOFD)	Accurate ultrasonic sizing technique, based on the measurement of the time taken for an ultrasonic sound wave to be diffracted from a crack tip as it travels from the transmitter to the receiver. TOFD is particularly useful for sizing through-wall height and for detection of flaws of variable orientation. Applications include weld root corrosion and screening for thick section weld flaws.
Zonal AUT	Use of specific beam angles and focal positions within the weld volume (including the fusion face) with the objective of establishing multiple go/no-go flaw detection within specific zones. This technique is commonly used for the inspection of pipeline girth welds.

T.3 Assessment of flaw tolerance using ECA

Where the purpose of the ECA is to determine the largest flaw dimensions that can be tolerated for the component to be considered fit for service and the flaw dimensions are determined by a deterministic fracture mechanics assessment, it is expected that the NDT system will be able to reliably detect flaws of these dimensions.

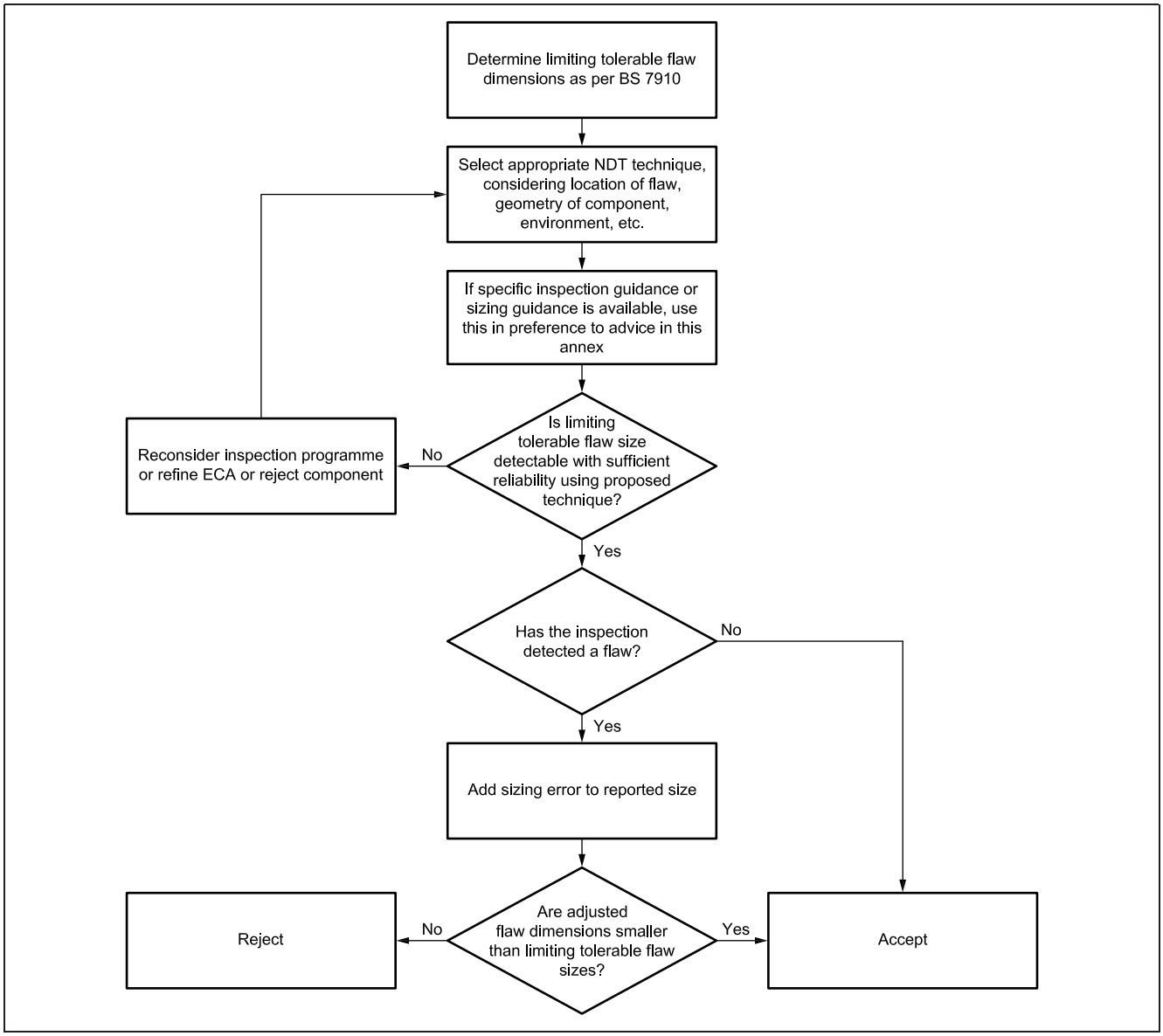
The reliability required for the inspection should reflect the risk associated with failure of the component under test, i.e. it depends on both the consequence of

failure and the probability of failure. Typical criteria for detection are given, for example, in references [T.7], [T.12] to [T.16] and ASME Boiler and Pressure Vessel Code, Section XI (Mandatory Appendix VIII). The required inspection reliability and the rigour with which it is determined should be agreed between the interested parties and documented: see ASME Boiler and Pressure Vessel Code, Section V, and references [T.6] and [T.17].

Where a flaw has been detected by NDT, the reported dimensions of the flaw should be increased by the appropriate sizing errors. If the adjusted flaw dimensions exceed the tolerable flaw size, the flaw should be rejected. This approach is illustrated in Figure T.1. An alternative (and equivalent) approach is to predetermine ECA-based acceptance criteria for reported flaw size by subtracting the flaw sizing errors from the calculated maximum tolerable flaw size.

Reliability of inspection can usually be improved if two or more complementary or repeated independent inspection techniques are used.

Figure T.1 **Assessment of flaw tolerance using ECA**

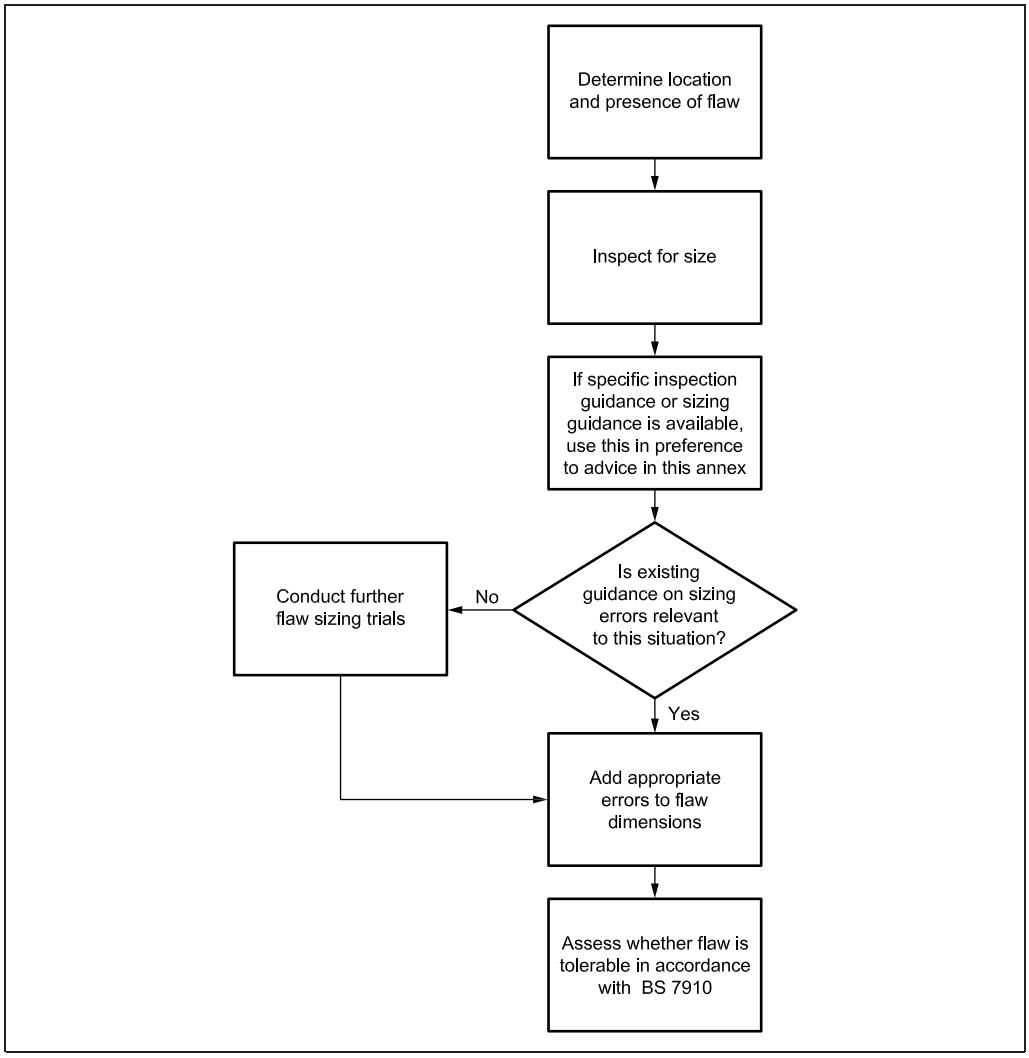


T.4 Engineering critical assessment of detected flaws

Where a flaw has been detected using NDT methods and the purpose of the assessment is to determine if a detected flaw is fit for service, the dimensions of the reference flaw used in a deterministic fracture mechanics assessment should be derived by increasing the reported flaw size by the agreed sizing errors.

Inspection for assessment is illustrated schematically in Figure T.2. This procedure may be used where a flaw fails the applicable quality acceptance criteria.

Figure T.2 **Assessment of detected flaw**



T.5 Interpretation of sizing performance data

Unless there is evidence to the contrary, a normal distribution should be assumed for the sizing errors ([T.17], [T.18]). In practice, this assumption is only valid where flaw indications are correctly identified and where the inspection procedure is applied properly. The extreme tails of the distribution are particularly sensitive to departures from normality.

Many of the sources cited in **T.7** give symmetric confidence intervals for the sizing errors of the form $\pm E$ for UT, at a two-sided confidence level of ~80% (or, equivalently, confidence limits at a one-sided 90% confidence level). In these cases, the distribution of sizing errors is taken to have zero mean. The standard deviation of the distribution is then approximately equal to $E/1.3$, where the factor of 1.3 is the tabulated value of the inverse of the cumulative standard

normal distribution function corresponding to a two-sided confidence level of ~80%.

Some sources cite asymmetric confidence intervals of the form ($+E_1$, $-E_2$). In these cases, the mean (systematic) sizing error is (E_1–E_2)/2, with a random error of $\pm(E_1+E_2)/2$ about this central value.

Care should be taken when assuming sizing errors at other confidence levels, as many of the values given in Table T.1, Table T.2 and Table T.3 were derived using a combination of review activities and engineering judgement.

T.6 Probabilistic fitness-for-service assessment

Where probabilistic based ECA methods are employed, the likelihood of a flaw being missed (i.e. 1 – PoD) or incorrectly accepted, and uncertainties in the reported size (due to sizing errors) on the estimated probabilities of failure, should be taken into account. Risk-based assessment (including the use of partial safety factors) is acceptable provided that assessment procedures are clearly documented and supported by a relevant data set of a suitable size, and an accurate description of the statistical parameters. Where a suitably relevant data set is not available, conservative limiting values should be used for the assessment, provided that the use of such values is consistent with the calculated risk. See Annex K for further guidance on probabilistic assessment.

T.7 Inspection capabilities for flaws at various locations

T.7.1 General

In general, the values given in Table T.1 to Table T.3 are derived from engineering judgement and data taken from practical trials. It is assumed that the inspection can be readily applied without hindrance with good surface conditions (including local dressing of the weld cap where appropriate). Departures from these conditions impair the detection and sizing performance for the inspection, and the effect should be assessed further in consultation with appropriate NDT specialists.

A more detailed discussion is provided for each of the inspection methods with relevant information being drawn from the references.

The following should be taken into account when referring to the values given in Table T.1, Table T.2 and Table T.3.

- Inspection capabilities refer to full penetration fine-grained isotropic welds (typical of ferritic carbon steel) in plate or pipe joints of wall thickness 10 mm to 25 mm. The tolerances and detection capabilities in Table T.1 to Table T.3 are not applicable to coarse-grained materials, e.g. stainless steel welds; inspection of such materials might require specialist advice.
- Inspection reliability assumes adequate gape (crack opening). Sizing and detection performance might be poorer if gape is tight (for RT) or if under compressive stress (all methods).

For cases not covered in this annex, refer to references given in **T.7.2** to **T.7.10**.

Table T.1 **Examples of inspection capabilities for sub-surface flaws**

Dimensions in mm

Capability	Conventional UT	Focussed phased array	Zonal AUT	TOFD	RT
Minimum size that can be reliably detected, $2a \times 2c$	3 × 15	1.5 × 10	1.5 × 10	2 × 10	1.2 Ø pore
Minimum size that can be reliably sized, $2a \times 2c$	3 × 7	2 × 7	2 × 7	2 × 7	NA [A)]
Length sizing accuracy, $\Delta 2c$	±10	±7	±7	±7	±2
Through-thickness sizing accuracy, $\Delta 2a$	4 mm under-sizing, 1 mm oversizing	±1.5	±1.5	±1.5	NA [A)]
Ligament sizing accuracy, Δp [B)]	±3	±1.5	±1.5	±1	NA [A)]
Notes	See **T.7.2**	See **T.7.3**	See **T.7.4**	See **T.7.5**	See **T.7.6**

[A)] NA = Not applicable.

[B)] Applies to through-thickness ligament sizing to component surface only; in case of the sizing of ligaments between adjacent flaws, consult an NDT specialist.

Table T.2 **Examples of inspection capabilities for back surface flaws**

Dimensions in mm

Capability	Conventional UT	Focussed phased array	Zonal AUT	TOFD	RT
Minimum size that can be reliably detected, $a \times 2c$	3 × 15	1.5 × 10	1.5 × 10	2 × 10	1.2 Ø pore
Minimum size that can be reliably sized, $a \times 2c$	3 × 7	2 × 7	2 × 7	2 × 7	NA [A)]
Length sizing accuracy, $\Delta 2c$	±10	±7	±7	±7	±2
Through-thickness sizing accuracy, Δa	±3	±1.5	±1.5	±1	NA [A)]
Notes	See **T.7.2**	See **T.7.3**	See **T.7.4**	See **T.7.5**	See **T.7.6**

NOTE All techniques except TOFD assume that the weld root is of a good standard and is regular in shape.

[A)] NA = Not applicable.

 © The British Standards Institution 2019

Table T.3 **Examples of inspection capabilities for flaws at the accessible surface**

Dimensions in unit

Capability	Conventional UT	Focussed phased array	Zonal AUT	TOFD	RT	MPI	PT	ET	ACFM
Minimum size that can be reliably detected, $a \times 2c$	3 × 15	1.5 × 10	1.5 × 10	5 × 10	1.2 Ø pore	See Table T.4	See Table T.5	3 × 15	2 × 15
Minimum size that can be reliably sized, $a \times 2c$	3 × 7	2 × 7	2 × 7	5 × 10	NA[A)]	NA [A)]	NA [A)]	NA [A)]	Equal to effective size of the sensitive area of the probe
Length sizing accuracy, $\Delta 2c$	±10	±7	±7	±7	±2	See Table T.4	±5	±5	±5
Through-thickness sizing accuracy, Δa	±3	±1.5	±1.5	±1	NA [A)]	NA [A)]	NA [A)]	NA [A)]	5 mm oversizing, 1 mm undersizing
Notes	See **T.7.2**	See **T.7.3**	See **T.7.4**	See **T.7.5**	See **T.7.6**	See **T.7.7**	See **T.7.8**	See **T.7.9**	See **T.7.10**

NOTE The flaw size which can be reliably detected generally differs from the size of the flaw that can be reliably sized, because detection and sizing (i.e. measurement of the dimensions of a flaw) are distinct processes. For conventional UT, for example, Table T.3 cites a minimum size of 3 mm × 15 mm for reliable detection, but a minimum size of 3 mm × 7 mm for reliable sizing. The PoD for 3 mm × 7 mm flaws is judged to be lower than that for 3 mm × 15 mm, but there will still be some proportion of 3 mm × 7 mm flaws that can be detected. If they are detected, then it is expected to be possible to size them reliably, i.e. the minimum size cited for reliable sizing is conditional on the flaw first being detected (flaws smaller than these are generally indistinguishable from a point source).

[A)] NA = Not applicable.

© The British Standards Institution 2019

T.7.2 Inspection capability using conventional UT

T.7.2.1 General

The following discussion, and the values given in Table T.1 to Table T.3 that relate to manual ultrasonic testing, refer to cases where the inspection is applied by well-trained and appropriately qualified personnel under good conditions. Due to the reliance on the individual operator, the results for manual ultrasonic testing are subject to human factors to a much greater degree than for automated techniques. Consequently, the inspection conditions such as access, environmental factors, time pressures, operator fatigue, etc. might all have a bearing on the reported results. Studies into the reliability of manual ultrasonic NDT, including human factors, have indicated that the performance of inspection personnel varies greatly ([T.5], [T.19], [T.20]). These studies have resulted in the UK Health and Safety Executive publishing a series of good practice guides ([T.21], [T.17]) with a view to mitigating some of these issues. Where high reliability is required it is recommended that repeat testing and/or surveillance is performed to improve the reliability of the inspection.

T.7.2.2 Detectability

The detection capability given in Table T.1 to Table T.3 is based on a capability statement produced by British Energy and BNFL Magnox for manual UT [T.22], which makes the following assumptions:

a) standard procedures are used, based on BS EN ISO 17640. Procedures generally specify 4 Mhz to 5 MHz, 0° compression wave and angled shear wave probes, supplemented by twin crystal probes where appropriate. Reporting sensitivity for shear wave probes is 20 dB more sensitive than a 3 mm side drilled-hole distance amplitude correction (DAC) curve[T.1)]. No distinction is made between the capability of manual and automated UT inspection per se, but in each case, it is assumed that there is no focussing of the beam;

b) the data are applicable to ferritic welds between 3.6 mm and 120 mm thick in plate, pipe, branches and nozzles;

c) all flaws are planar, skewed by up to 3°, and within 20° of normal incidence for at least one of the probes being used;

d) there are no restrictions to test such as geometric echoes at a similar range to the flaw signals, poor weld root profiles or counterbores.

Under these conditions, the capability statement provides high confidence in the detection of flaws larger than the following sizes:

- 3 mm through-wall ×15 mm long, for ranges (i.e. probe-to-flaw distances) up to 150 mm (this is a larger range of wall thicknesses than considered in Table T.1 to Table T.3);
- 4 mm through-wall ×15 mm long, for ranges above 150 mm.

It might be possible to detect smaller flaws than those above in certain cases, e.g. if the angle of incidence is a lot less than 20°, or if a smooth flaw forms a 90° corner with the back wall.

For in service inspection, a higher reporting sensitivity should be used than for pre-service inspection [T.23].

[T.1)] This means that a flaw response 20 dB weaker than that from a 3 mm diameter at the same depth would be recorded.

T.7.2.3 Sizing accuracy

The sizing accuracies in Table T.1 to Table T.3 are mostly based on information given in ENA TS 98/10 [T.24]. The length sizing accuracy $\Delta 2c$, however, is based on a compromise between values in [T.24] and SINTAP data [T.2]. It is assumed the back wall is smooth and of a known angle and that the flaw is sized using probe movement techniques ([T.25], [T.26]), in the full skip position (as a worst case). It is also assumed that there are no restrictions to the test such as other indications at a similar range to the flaw signals. The values given in this annex are based on a combination of experience, experiment and theory. The cited values correspond to a one-sided 90% confidence limit when considering undersizing. Automated UT is likely to be more reliable than manual UT in practice, but no attempt has been made to quantify this.

Flaw dimensions are not measurable by probe movement methods if they are smaller than the corresponding minimum measurable flaw dimensions listed in Table T.1 to Table T.3 ; such flaws exhibit a Pattern 1 echodynamic (as defined in BS EN ISO 23279). These minimum measurable sizes are again largely based on [T.24] (except that Table T.2 cites a somewhat more conservative length dimension).

Further values for sizing and positioning capabilities in more general inspection situations involving conventional UT of welds in ferritic steel components up to 125 mm in wall thickness are provided in [T.24].

T.7.2.4 Other sources of information

Other detectability information from PoD trials can be obtained from SINTAP [T.2] or [T.27] for a broader range of steel components, or NTIAC [T.4] for aerospace applications. Reference [T.28] gives results from trials of detection and sizing in ferritic plate and pipe welds between 4 mm and 12 mm thick.

For more critical applications, a specific assessment of sizing errors is recommended ([T.17], [T.24]), and it might also be necessary to increase the confidence level in such cases. For in-service inspection of nuclear power plant, for example, ASME Boiler and Pressure Vessel Code, Section XI (Mandatory Appendix VIII) requires a practical demonstration that root mean square sizing (RMS) sizing errors meet specific targets.

T.7.3 Inspection capability using focussed phased array

T.7.3.1 General

The detection and sizing capabilities given in Table T.1 to Table T.3 assume that:

a) a focussed beam is used;

b) the inspection frequency is at least 5 MHz; and

c) the beam width within the inspection volume is no greater than 3 mm in the through-wall dimension.

If the beam is unfocussed, the detection and sizing capabilities are similar to that of conventional UT.

T.7.3.2 Detectability

The detection capability given in Table T.1 to Table T.3 is based on evidence collated within specific technique qualification projects [T.29] and judgement-based modifications to ENA TS 98/10 [T.24].

T.7.3.3 Sizing

The through-wall height sizing capability is based on engineering judgement and [T.29], and represents the accuracy that can be achieved under controlled flaw sizing conditions where the operators are suitably trained and qualified for flaw sizing, using the maximum amplitude technique. If the focussed phased array inspection is required as input for more critical applications, a technical justification or capability statement should be obtained.

Focussing in the length direction is not standard practice. The length accuracy $\Delta 2c$ quoted in Table T.1 to Table T.3 is therefore similar to that quoted in [T.24] (which is itself considered more representative of conventional UT in laboratory conditions). However, if the array is focussed in the length direction the sizing capability is expected to be similar to that in the through-wall direction.

The minimum measurable sizes in Table T.1 to Table T.3 are judgement-based modifications to [T.24].

T.7.4 Inspection capability using zonal AUT

T.7.4.1 General

For girth welds in sub-sea pipelines, DNVGL-ST-F101 [T.7] recommends that the detection and sizing ability of an AUT system should be quantified by means of an agreed qualification programme. The qualification is system-specific and is valid only when all the essential variables remain nominally the same as covered by the qualification. DNVGL-ST-F101 [T.7] requires any fracture mechanics assessment to be based on the specific results from the inspection qualification. The generic guidance in Table T.1 to Table T.3 might, however, be useful for design purposes.

T.7.4.2 Detection

The detection capability given in Table T.1 to Table T.3 is based on engineering judgement and evidence collated within specific technique qualification projects ([T.30], [T.31]). The values quoted are typical of butt welds in ferritic pipelines.

Trials have, for example, demonstrated probabilities of detection of 90% for flaws with a through-wall height of 1.2 mm [T.30]. This is based on a threshold setting of 40% screen height with sensitivity based on a 3 mm flat bottomed hole set to 50% screen height.

T.7.4.3 Sizing

The through-wall height sizing capabilities are based on [T.32]. This advocates adding an allowance, typically of between 1 mm and 1.5 mm, to all through-wall sizing estimates to allow for possible undersizing. The through-thickness sizing accuracy given in Table T.1 to Table T.3 is conservatively based on the upper limit to this range. Such an allowance typically provides 90% confidence against undersizing [T.33].

Focussing in the length direction is not standard practice. The length accuracy quoted in Table T.1 to Table T.3 is therefore similar to that discussed in **T.7.3.2**. However, specific trial data should, where available, take precedence (see **T.1**).

The minimum measurable size for zonal AUT is assumed to be similar to TOFD on the basis that many AUT systems include TOFD techniques for flaw sizing.

T.7.5 Inspection capability using time of flight diffraction (TOFD)

T.7.5.1 Detection

The figures shown in Table T.1 to Table T.3 are based on expert judgement, taking account of the reliability trials by NIL ([T.34], [T.35]), the PISC II Final Report [T.36] and extensive detection information [T.37].

The relatively large size quoted for the minimum flaw size that can be reliably detected for accessible surfaces in Table T.3 is due to the near surface blind zone where the lateral wave might obscure diffracted signals. To fully assess the flaw detection capability, expert advice should be sought.

Flaw detection is based on detection of diffracted signals from the edges of the flaw. The method is relatively tolerant to signal amplitude variations but, for complex flaws or material where there are small inclusions, flaws can be confused with material noise, thus reducing flaw detection capability.

Flaws with irregular edges or closed tips provide much weaker signals than clearly defined flaw edges. In general, lower frequencies aid the detection of the flaw edges.

Further, because the technique relies upon detection of signals close to the material grain noise level, material grain structure (such as cast materials) can severely affect flaw detection capability.

T.7.5.2 Sizing

Flaw sizing depends upon resolution of the flaw edges. Hence the technique is highly dependent upon the chosen ultrasonic wavelength/frequency and material noise levels. The values for flaw sizing provided in Table T.1 to Table T.3 assume 5 MHz probes. Lower frequencies increase the sizing error.

The sizing errors quoted in Table T.1 to Table T.3 are based on engineering judgement, taking account of the NIL ([T.34], [T.35]) and PISC II reliability trials [T.36] and extensive sizing information in Section 2.3 of [T.37]. Mean length sizing errors in the NIL trials for TOFD varied from 2.5 mm undersize to 5 mm oversize.

Through-wall height sizing errors of $\pm$0.5 mm down to $\pm$0.1 mm have been reported in trials ([T.34], [T.35], [T.37], [T.38]) and supported by modelling studies [T.38]. In general, claims for flaw sizing accuracy better than quoted within Table T.1 to Table T.3 require careful study of the validation trial data. It is important that any trial data very carefully simulate the type of flaw to be detected, taking into consideration the detailed morphology of the crack tips.

The minimum measurable size for TOFD in Table T.1 and Table T.2 is assumed to be similar to focussed phased array; both techniques depend on resolving echoes diffracted from the edges of the flaw. However, the minimum measurable size at the accessible surface (Table T.3) is increased, as for detection, to reflect the near surface blind zone where the lateral wave might obscure diffracted signals.

T.7.5.3 Other sources of information

PoD information for TOFD can be found in the NIL [T.35] and PISC II trial reports [T.36], as well as the earlier DDT trials at Harwell ([T.39], [T.40]) and the ICON trials [T.41].

T.7.6 Inspection capability using radiographic testing (RT)

T.7.6.1 Detection

The detection capability in Table T.1 to Table T.3 is for an isolated gas pore and should not be used for planar flaws. It is assumed that the sensitivity is equivalent to a 0.8 mm step/hole image quality indicator (IQI). This corresponds to BS EN ISO 19232-3 image quality class A for 25 mm wall thickness (plus one IQI value to allow for possible extra unsharpness at the flaw location in the case where the IQI is on the film side of the weld). The step/hole dimension of 0.8 mm is then multiplied by 1.5, based on [T.42].

While radiography provides good detection capability for volumetric flaws such as porosity or undercut, it generally has relatively low capability when used to detect planar cracks with tight gape, especially when they are misoriented relative to the radiographic beam. Thus, the inspection capability for planar flaws is strongly influenced by the flaw gape, the angle between the flaw plane and the radiographic beam and, to a lesser extent, the penetrated thickness. If these parameters can be characterized and the IQI sensitivity is known, then the size of the smallest theoretically detectable flaw can be estimated from the Pollitt model ([T.43], [T.44]). In practice, it is difficult to estimate the gape. The Pollitt model is known to give conservative predictions in steel welds thicker than ~10 mm for flaws having a simple morphology akin to the parallel-sided slot assumed in the model. Experimental work [T.45] suggests that, whenever the Pollitt model predicts that such a flaw is detectable, then the corresponding PoD is in excess of:

- ~70% for weld thicknesses in the range 10 mm to 50 mm;
- ~90% for welds thicker than 50 mm.

T.7.6.2 Sizing

While RT is suitable for sizing flaw length, it cannot generally be used as a method for sizing through-wall height, although computed tomography (CT) and other specialized radiographic techniques are able to provide depth information using multiple radiographic exposures of a flaw from different directions [T.46].

The length tolerance given in Table T.1 to Table T.3 is judgement-based. It assumes that the flaw maintains sufficient gape along its entire length to remain visible on the radiograph; this assumption is usually valid for volumetric flaws, but might not be valid for planar cracks with tight gape (especially when they are misoriented relative to the radiographic beam).

T.7.6.3 Other sources of information

Probability of detection information (primarily for flaws in steel welds up to 25 mm thick) is summarized for RT procedures of various sensitivities in [T.27]. The NTIAC NDT capabilities handbook [T.4] gives PoD curves for many different X-ray configurations for aerospace applications. Information on procurement and conduct of radiography is given in [T.47].

T.7.7 Inspection capability using magnetic particle inspection (MPI)

T.7.7.1 Detection and sizing

The British Energy/BNFL capability statement for MPI [T.22] provides evidence for the reliable detection of surface flaws exceeding the dimensions in Table T.4.

Table T.4 **Capabilities for detection and length measurement of surface-breaking flaws by MPI**

Condition	Flaw length mm	Flaw through-wall extent mm	Length sizing accuracy mm
Machined or ground:			
– 3.2 μm R_a	5	1.5	±2
As welded:			
– with local dressing	10	2	±5
– with poor profile	20	4	±10

The capability statement makes the following assumptions:

- standard procedures based on BS EN ISO 17638 with appropriate lighting levels;
- ferritic steel with a relative permeability ≥240 at a flux density of B = 0.72 Tesla;
- flaws are surface-breaking, including those covered by thin oxide layers such as might be found in boilers. The plane of the flaw is assumed to be normal to the direction of magnetization.

The data are for a general surface finish as described; better results can be obtained from higher quality surface finishes (e.g. polished) or more sensitive procedures (e.g. higher magnetic field strength) [T.22].

MPI also has some capability (albeit more limited than that above) for the detection of sub-surface flaws with a small ligament to the accessible surface, but this capability has not been quantified.

T.7.7.2 Other sources of information

PoD data from major trials of MPI are summarized in references [T.2], [T.4] and [T.27]. The projects reviewed in [T.27] include the UCL [T.48] and ICON [T.41] trials of MPI performed underwater. Information on procurement and conduct of MPI is given in [T.49].

T.7.8 Inspection capability using liquid penetrant testing (PT)

T.7.8.1 Detection

Table T.5 gives guidance on the minimum size of linear (i.e. planar) flaws that can be detected with high confidence in practical conditions, based on references [T.50] and [T.51].

Table T.5 **Flaw detection capability for liquid penetrant testing**

Condition	Flaw length mm	Flaw through-wall extent mm
Casting	5	1.5
Machined or ground welds	5	1
As welded	20	4

The data given in Table T.5 are applicable to fluorescent or visible dye applied using standard procedures, and assume that surfaces are cleaned and descaled.

The data for castings are taken from [T.50], which assumes that the test surface is machined or ground to remove rough material [i.e. surface finish (R_a) of 1.6 μm to 6.4 μm]. A gape of at least 0.5 mm is assumed.

The data for machined or ground welds, also taken from [T.50], assume that excessive weld beads have been removed by grinding [i.e. surface finish (R_a) of 1.6 μm to 6.4 μm]. A gape of at least 0.25 mm is assumed here.

Data for the as-welded category are based on PoD trials [T.51], which did not quantify gape.

A higher detection capability for smaller flaws can be obtained by using more sensitive procedures combined with, say, 100% machining or surface grinding and cleaning [T.50].

Both [T.50] and [T.51] give extra guidance on detection capabilities for rounded flaws.

T.7.8.2 Sizing

Sizing accuracy for PT is assumed to be similar to that for MPI (see Table T.4).

T.7.8.3 Other sources of information

PoD data from major trials of PT are summarized in references [T.2], [T.4], [T.27] and [T.52]. For PoD data from as-welded surfaces, in particular, see [T.53] and [T.51]. Information on the procurement and conduct of PT is given in [T.49].

T.7.9 Inspection using manual eddy current testing (ET)

T.7.9.1 Detection

The height value of 3 mm given for detection capability in Table T.3 is based on ~80% PoD in Figure 1.3 in [T.27]. The length value of 15 mm is based on experience (signals generally reach a plateau at this length) [T.27]. It is assumed that the cap surface is in the as-welded condition, but the test surface is machined or ground to remove rough material and excessive weld beads where necessary. Where flaws are located in the parent material adjacent to the weld, detection capability is expected to be better [T.4].

Manual eddy current inspection can take many forms and the user of the inspection report should be aware of the capability of the inspection procedure. In the oil and gas industries, it is primarily aimed at the detection of fatigue

cracks in weld toes, and can work through paint coatings. Applications in the power industry include inspection for SCC, pitting corrosion, and inter-granular attack (IGA).

The performance of eddy current testing is highly dependent on the design and type of probe being deployed. As a general warning, eddy current inspection of welds is difficult and the capability of the technique to detect and size flaws depends upon the surface finish of the weld cap. Furthermore the material and in particular magnetic variations within a component can interfere with the ability to analyse the results. To alleviate these problems, special eddy current probes have been designed that reduce these effects and these probes should be used as appropriate. When used for tube testing away from welds there are fewer constraints on the technique.

For ferromagnetic materials, conventional ET is usually limited to the detection of flaws at the accessible surface. Specialized ET techniques are available with a depth capability. In non-ferromagnetic materials, however, ET also has some capability for the detection of sub-surface flaws. This capability depends on the size of the ligament to the near surface, as compared with the skin depth or "standard depth of penetration". The standard depth of penetration is defined [T.9] as:

$$\delta = (\pi f \mu_0 \mu_r \sigma)^{-0.5} \quad \text{(T.1)}$$

Under controlled conditions, the eddy current density reduces exponentially with depth, reaching 37% of its surface value at depth δ. Thus, ET is generally less sensitive to sub-surface flaws than to surface flaws.

Proof of capability should be demonstrated on realistic flaws in actual welds.

T.7.9.2 Sizing

Eddy current methods are best used only for detection. There is no evidence available for sizing of through-wall height, and length sizing capability depends on crack morphology.

The value for length sizing accuracy provided in Table T.3 is generic guidance, assuming that the sizing accuracy for ET is similar to that for MPI (Table T.4). This is judged to be an appropriate assumption only if the flaw has a simple shape. It is recommended that wherever an ET report is received, evidence of flaw detection and sizing capability is provided with that report, as appropriate.

T.7.9.3 Other sources of information

Eddy current inspection is commonly used for inspection of other metallic materials, including austenitic and duplex stainless steels and aluminium and nickel alloys. Data relating to PoD trials can be obtained from NTIAC [T.4] (aerospace applications) and SINTAP [T.2].

T.7.10 Inspection using alternating current field measurement (ACFM)

T.7.10.1 Detection

ACFM is an electromagnetic method primarily designed for inspection of fatigue cracks in ferritic welds. The values for detection capability are variable in the literature. The through-wall height value of 2 mm given in Table T.3 is based on ~80% PoD given in Figure 1.2 of [T.27]. The length value of 15 mm is based on experience of the flaw length at which ACFM signals generally approach an asymptote. It is assumed that the surface is in the as-welded condition, but that rough material/excessive weld beads are removed where necessary.

ACFM is capable of detecting and sizing flaws under paint layers (generally thicker than those possible with eddy current probes).

T.7.10.2 Sizing

The values for through-wall sizing capability (Δa) in Table T.3 are based on Figure 16.3 of [T.27]. The "characterized depths" in this figure were largely based on comparison between ACFM and ACPD measurements. ACPD is believed to systematically undersize the true through-wall size by ~10%, on average (Figure 16.1 of [T.27]). This systematic error has been taken into account in the derivation of the ACFM sizing errors in Table T.3 from Figure 16.3 of [T.27].

ACFM instruments that are currently available incorporate a specially developed look-up table that enables sizing of elliptical fatigue cracks from measurements of the AC magnetic field. The values developed in the look-up table do not include any correction to account for sizing capability. For more complex cracking (particularly multiple cracking, non-elliptical cracks, or cases of conduction across the crack faces), the sizing capability is limited.

The value for length sizing accuracy in Table T.3 assumes that it is similar to that for MPI (Table T.4). As for ET, this assumption is appropriate only if the flaw has a simple shape.

T.7.10.3 Other sources of information

The use of ACFM on stainless steel welds is subject to the same restrictions as eddy currents and evidence of the capability should be obtained for each distinct application.

Bibliography for Annex T

Standards publications

For dated references, only the edition cited applies. For undated references, the latest edition of the referenced document (including any amendments) applies.

ASME Boiler and Pressure Vessel Code, Section V: *Nondestructive examination*

ASME Boiler and Pressure Vessel Code, Section XI: *Rules for inservice inspection of nuclear power plant components*

BS EN ISO 9712, *Non-destructive testing – Qualification and certification of NDT personnel*

BS EN ISO 17638, *Non-destructive testing of welds – Magnetic particle testing*

BS EN ISO 17640, *Non-destructive testing of welds – Ultrasonic testing – Techniques, testing levels, and assessment*

BS EN ISO 19232-3, *Non-destructive testing – Image quality of radiographs – Image quality classes*

BS EN ISO 23279, *Non-destructive testing of welds – Ultrasonic testing – Characterization of discontinuities in welds*

Other documents

[T.1] SMITH, A., SCHNEIDER, C., BIRD, C. and WALL, M. Use of non-destructive testing for engineering critical assessment: background to the advice given in BS 7910:2013, *In: International Journal of Pressure Vessels and Piping*, January 2019, 169, 153–159. <https://doi.org/10.1016/j.ijpvp.2018.11.016>

[T.2] CRUTZEN, S., FRANK, F., FABBRI, L., LEMAITRE, P., SCHNEIDER, C. and VISSER, W. *Compilation of NDE effectiveness data. SINTAP Task 3.4 (Safety factors and risk) final report*. JRC, European Commission, Petten, March 1999. <http://www.eurofitnet.org/sintap_JRC_final_report.pdf>

[T.3] FØRLI, O. *Development and optimisation of NDT for practical use – Reliability of radiography and ultrasonic testing*. IIW report number IIW-V-969-91. 5e Nordiska NDT Symposiet, Esbo, Finland. Cambridge: International Institute of Welding, 1990.

[T.4] RUMMEL, W.D. and MATZKANIN, G.A. *Non-destructive evaluation (NDE) capabilities data book*. 3rd edition. NTIAC: DB-97-02. Austin, TX: Non-destructive Testing Information Analysis Centre (NTIAC), November 1997.

[T.5] McGRATH, B.A. *Programme for the assessment of NDT in industry – PANI 3*. HSE report RR617. London: HMSO, 2008. <http://www.hse.gov.uk/research/rrpdf/rr617.pdf>

[T.6] EUROPEAN COMMISSION. *European methodology for qualification of non-destructive testing – Third issue*. ENIQ report nr. 31, EUR 22906 EN, August. Luxembourg: Office for Official Publications of the European Communities, 2007. <http://publications.jrc.ec.europa.eu/repository/bitstream/JRC37908/eniq_report31.pdf>

[T.7] DNVGL-ST-F101. *Submarine pipeline systems*, October 2017. <https://www.dnvgl.com/oilgas/download/dnvgl-st-f101-submarine-pipeline-systems.html>

[T.8] BRITISH INSTITUTE OF NON-DESTRUCTIVE TESTING. *NDT Yearbook* (re-issued annually). Northampton: BINDT, 2009. ISSN 0952-2395.

[T.9] AMERICAN SOCIETY FOR NONDESTRUCTIVE TESTING. *NDT Handbook*. 3rd edition, 2010, (Volume 1–9); 2nd edition (Volume 10–11). Columbus, OH: ASNT.

[T.10] AMERICAN SOCIETY FOR METALS. *ASM Handbook*, 1989, Volume 17, Nondestructive evaluation and quality control. 9th edition. Materials Park, OH: ASM International. ISBN 10: 0-87170-023-9.

[T.11] FØRLI, O., RONOLD K.O. et al. *Guidelines for development of NDE acceptance criteria*. Nordtest NT TECHN Report 427. Espoo: Nordtest, 1999. ISSN 0283-7234.

[T.12] NATIONAL AERONAUTICS AND SPACE ADMINISTRATION. *Nondestructive evaluation requirements for fracture-critical metallic components*. NASA Technical Standard NASA-STD-5009. Washington, D.C.: NASA, 2008. <https://standards.nasa.gov/standard/nasa/nasa-std-5009>

[T.13] EUROPEAN SPACE AGENCY. *Fracture control*. ECSS Engineering Standard ECSS-E-ST-32-01C Rev.1. Noordwijk: ESA, 6 March 2009.

[T.14] US DEPARTMENT OF DEFENSE. *Standard general requirements for safe design and operation of pressurized missile and space systems*. US Dept of Air Force Military Standard MIL-STD-1522A (USAF). Washington, D.C.: US Department of Defense, 28 May 1984.

[T.15] US DEPARTMENT OF DEFENSE. *Engine structural integrity program (ENSIP)*. Military Handbook MIL-HDBK-1783A. Washington, D.C.: US Department of Defense, 22 March 1999.

[T.16] FØRLI, O. et al. *Guidelines for NDE reliability determination and description*. Nordtest NT TECHN Report 394. Espoo: Nordtest, April 1998. ISSN 0283-7234.

[T.17] HEALTH AND SAFETY EXECUTIVE. *Best practice for the procurement and conduct of non-destructive testing – Part 4: Ultrasonic sizing errors and their implication for defect assessment*. HSE Gas and Process Safety Technology Division, April 2008. <http://www.hse.gov.uk/comah/sragtech/ndt4.pdf>

[T.18] BURDEKIN, F.M. and TOWNEND, P.H. Reliability aspects of fracture on stress concentration regions in offshore structures. *In: Proceedings of the second International Symposium on Integrity of Offshore Structures*. London: Applied Science, 1981.

[T.19] MCGRATH, B.A. *Programme for the assessment of NDT in industry*. London: HSE, 1999. Available as an HSE Report on CD-ROM.

[T.20] MCGRATH B.A., WORRALL, G.M. and UDELL, C.G. *programme for the assessment of NDT in industry – PANI 2*. London: HSE, 2004. Available as an HSE Report on CD-ROM.

[T.21] HEALTH AND SAFETY EXECUTIVE. *Best practice for the procurement and conduct of non-destructive testing – Part 1: Manual ultrasonic inspection*. London: HSE, 2000. <http://www.hse.gov.uk/comah/sragtech/ndt1.pdf>

[T.22] CHAPMAN, R.K., and BOWKER, K.J. The production of capability statements for standard NDT procedures. *In: Insight*, 2001, (43)1, 36–38.

[T.23] GOUJON, N.S. and SHEPPARD, B.W.O. *Evaluation of CEN ultrasonic testing standards for in-service inspection*. London: HSE, 2005. <http://www.hse.gov.uk/research/rrpdf/rr299.pdf>

[T.24] ENERGY NETWORKS ASSOCIATION. *Manual ultrasonic testing of welds in ferritic steel sections – Part 4: Guidance on inspection capability and joint design*. Technical Specification 98-10 Part 4, Issue 1. London: ENA Ltd, November 1983.

[T.25] ENERGY NETWORKS ASSOCIATION. *Manual ultrasonic testing of welds in ferritic steel sections – Part 2: Nozzle, branch, stub and attachment welds*. Technical Specification 98-10 Part 2, Issue 1. London: ENA Ltd, 1983.

[T.26] ENERGY NETWORKS ASSOCIATION. *Manual ultrasonic testing of welds in ferritic steel sections – Part 3: Butt welds in tubes of outside diameters between 25mm and 120mm inclusive*. Technical Specification 98-10 Part 3, Issue 2. London: ENA Ltd, 1984.

[T.27] VISSER, W. POD/POS curves for non-destructive examination. *In: Offshore Technology Report 2000/018 for HSE*. London: HSE, 2002. <http://www.hse.gov.uk/research/otopdf/2000/oto00018.pdf>

[T.28] CAMPBELL, G.J., BABOROVSKY, V.M. and WOODCOCK, G.S. Capability of ultrasonic inspection of thin-section welds. *In: Proceedings of the fourth International Conference on NDE in relation to Structural Integrity for Nuclear and Pressurised Components*. December 6–8 2004, London, UK, 782–787. Luxembourg: EC. ISBN 92-79-00797-1.

[T.29] SHIPP, R., SCHNEIDER, C.R.A., BIRD, C.R. and WOOD, D.A. Independent qualification of phased array inspection of fillet welds. *In: Proceedings of the 2002 Annual British Conference on NDT*, Southport, 2002

[T.30] FØRLI, O. *Automated ultrasonic testing during offshore pipelaying: Acceptance criteria and qualification*. IIW Document V-1144-99. Cambridge: International Institute of Welding, 1999.

[T.31] RUDLIN, J.R., SCHNEIDER, C.R.A. and RAZMJOO, G.R. Reliability of inspection for root flaws in riser girth welds. *In: Proceedings of the 23rd International Conference on Offshore Mechanics and Arctic Engineering,* OMAE, Vancouver, Canada 20–25 June 2004, Paper 51523.

[T.32] MOLES, M. Defect sizing in pipeline welds: what can we really achieve? *In: Proceedings of ASME PVP Conference*, July 2004, San Diego, California.

[T.33] MORGAN, L., NOLAN, P., KIRKHAM, A. and WILKINSON, R. The use of automated ultrasonic testing (AUT) in pipeline construction. *In: Insight*, 2003, 45(11), 746–753.

[T.34] BOUMA, T., DIJKSTRA, F.H., LIEFTING, G. and STELWAGEN, U. *NIL Project; FITNESS-FOR-SERVICE, PHASE 2: Selection of NDT for FFP; Final Report for Study 1*. Document, 96-43, Dutch joint industry project, June 1996.

[T.35] STELWAGEN, U and TPB SECRETARY NDP WORKGROUP. *NIL project, non destructive testing of thin plate: final report*. Doc. No. NDP 93–40, March 1995.

[T.36] NICHOLS, R.W. and CRUTZEN, S. *Ultrasonic inspection of heavy section steel components*. PISC II final report. Barking: Elsevier Applied Science, 1988. ISBN 1-85166-155-7.

[T.37] CHARLESWORTH, J.P. and TEMPLE, J.A.G. *engineering applications of ultrasonic time-of-flight diffraction (sizing capability, detection capability*. Second edition. Baldock: Research Studies Press Ltd, 2001. ISBN 0-86380-239-7.

[T.38] TEMPLE, J. A. G. Reliable Ultrasonic Inspection in Theory and In Practice: Sizing Capability of Time of Flight Diffraction. *In: Proceedings of the 3rd European Conference on Nondestructive Testing*, Florence 15–18 October 1984.

[T.39] WATKINS, B., ERVINE, R.W. and COWBURN, K.J. The UKAEA defect detection trials (DDT paper no 1). *In: British Journal of Non-Destrustive Testing*, 1983, (25)4, 179–185.

[T.40] WATKINS, B., COWBURN, K.J., ERVINE, R.W. and LATHAM, F.G. Results Obtained from the Inspection of Test Plates 1 and 2 of the Defects Detection Trials. (DDT paper no 2). *In: British Journal of Non-Destructive Testing*, 1983, (25)4, 186–192.

[T.41] HEALTH AND SAFETY EXECUTIVE. *Intercalibration of offshore NDT (ICON)*. Offshore Technology Report OTN-96-150, Commercial in confidence. PEN/S/2736. London: HSE, August 1996.

[T.42] HALMSHAW, R. Industrial radiology – Theory and practice. Section 8.4 (1). London and New Jersey. *In: Applied Science*, 1982.

[T.43] IIW/IIS. *IIW guidance on assessment of the fitness-for-service of welded structures*. IIW/IIS Guidance document SST-1157-90. Cambridge: International Institute of Welding, 1990.

[T.44] POLLITT, C.G. Radiographic sensitivity. *In: British Journal of Non-Destructive Testing*, 1962, (4)3, 71–80.

[T.45] SCHNEIDER, C.R.A. and GEORGIOU, G.A. Radiography of thin section welds, Part 4: further modelling. *In: Insight*, 2005, (47)2.

[T.46] SOOD, S.C. NDT Flaw Depth Radiography. *In: Proceedings of the 8th International Conference on NDE in relation to Structural Integrity for Nuclear and Pressurised Components*. September 29-October 1 2010, Berlin. JRC report EUR 24824 EN-2010. Luxembourg: EC.

[T.47] HEALTH & SAFETY EXECUTIVE. *Information for the procurement and conduct of NDT – Part 3: Radiographic inspection in industry*. London: HSE, 2008. <http://www.hse.gov.uk/comah/sragtech/ndt3.pdf>

[T.48] VISSER, W., DOVER, W. L. and RUDLIN, J.R. *Review of UCL underwater inspection trials*. OTN 96 179. London: HSE, 1996.

[T.49] HEALTH & SAFETY EXECUTIVE. *Best practice for the procurement and conduct of non-destructive testing – Part 2: Magnetic particle and dye penetrant inspection*. London: HSE, 2002. <http://www.hse.gov.uk/comah/sragtech/ndt2.pdf>

[T.50] ENERGY NETWORKS ASSOCIATION. Penetrant flaw detection capability. *In: Technical Specification 98-20*, 1989, Issue 1, October. London: ENA Ltd.

[T.51] KAUPPINEN, P. and SILLANPÄÄ, J. Reliability of liquid penetrant and magnetic particle inspection. *In: Proceedings of the 10th International Conference on NDE in the Nuclear and Pressure Vessel Industries*. Espoo: Technical Research Centre of Finland, Metals Laboratory, 1990.

[T.52] RUMMEL, W.D., HARDY, G.L. and COOPER, T.D. Applications of NDE reliability to systems. *In: Metals Handbook*, Volume 17. 9th edition. Materials Park, OH: ASM International, September 1989.

[T.53] KAUPPINEN, P. and SILLANPÄÄ, J. Reliability of surface inspection methods. *In: Proceedings of the 12th World Conference on Non-Destructive Testing*. Amsterdam: Elsevier, 1989.

Annex U (informative)

Worked examples in fatigue assessment using the quality category approach

U.0 Symbols and definitions

For the purposes of this annex, the following symbols, definitions and units apply, unless otherwise indicated at the point of use.

Symbol	Definition	Units
a	Half flaw length for through-thickness flaw, flaw height for surface flaw or half height for embedded flaw	mm
$\bar{a}/B$	Effective flaw parameter used in quality categories method	—
$\bar{a}_i$	Initial value of effective flaw parameter for fatigue analysis	mm
$\bar{a}_{max}$	Maximum value of effective flaw parameter for fatigue analysis	mm
B	Section thickness in plane of flaw	mm
B'	Effective section thickness ($2a + 2p$)	mm
c	Half flaw length for surface or embedded flaw	mm
da/dN	Flaw growth rate with cycles	mm/cycle
L	Attachment length	mm
N	Fatigue life	cycles
p	Shortest distance from material surface to embedded flaw	mm
S	Reference stress range to which the graphs refer	N/mm^2
S'	Quality category reference stress range for crack growth in seawater	N/mm^2
S_i	Value of S for $\bar{a}_i$	N/mm^2
S_m	Value of S for $\bar{a}_{max}$	N/mm^2
ΔK	Stress intensity factor range	N/mm$^{3/2}$
$\Delta\sigma$	Applied stress range	N/mm^2

U.1 General

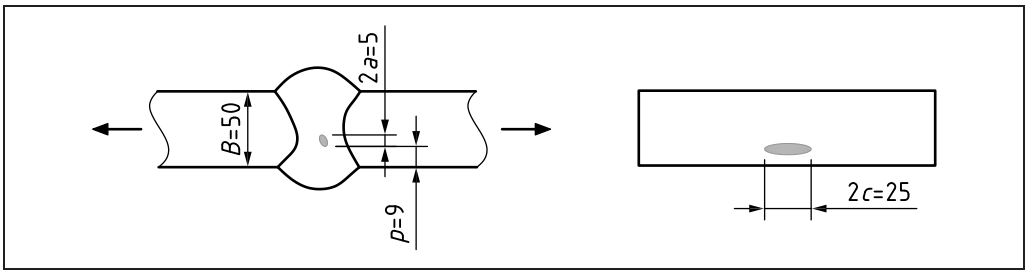
Two examples are given to illustrate the use of **8.5** for fatigue assessment of planar flaws using the quality categories.

U.2 Example 1

U.2.1 Problem

A transverse butt weld in the flange of a steel beam is found to contain an embedded flaw (see Figure U.1).

Figure U.1 **Butt weld containing embedded flaw**



There is a fillet welded cover plate further along the flange that is subjected to the same stress spectrum. A fracture assessment has established that a through-thickness fatigue crack can be tolerated in the flange without the risk of complete failure of the beam.

Determine whether the flaw is acceptable for the design life of the beam.

U.2.2 Solution

Even though the fatigue loading is not specified, the required quality category can be deduced as that corresponding to the design class of the cover plate, which is Class G in accordance with BS 7608, equivalent to Q5. Treating the flaw as a crack, the actual quality category is found from Figure U.2.

From Figure 8.4a):

- for $2a$ = 5 mm, p = 9 mm, $B' = 2a + 2p$ = 23 mm and $2c$ = 25 mm;
- $2a/B' = 0.217$; $a/2c = 0.1$, leading to $2\bar{a}/B' = 0.12$; or
- $2\bar{a} = 0.12 \times 23 = 2.76$ mm.

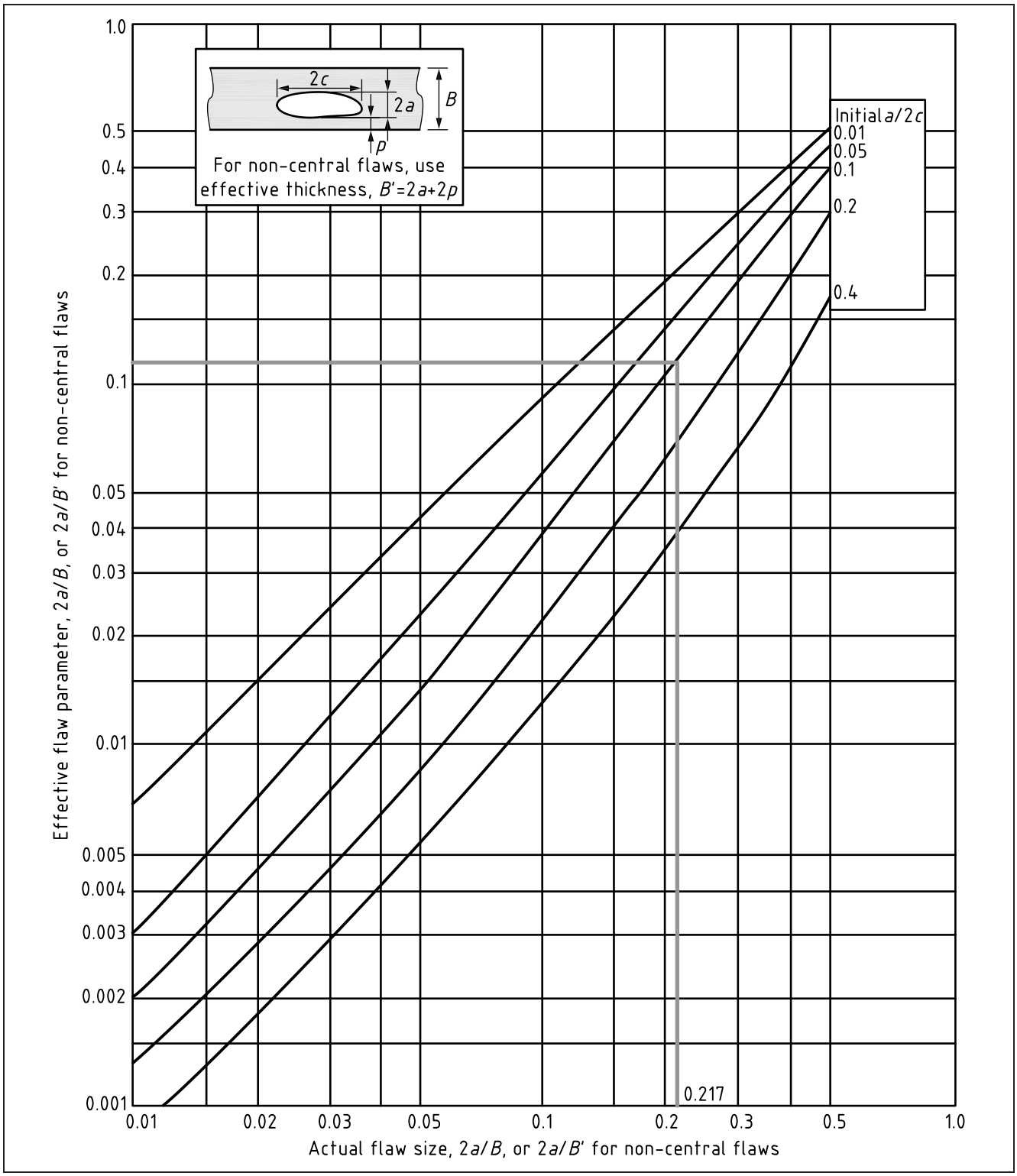
From Figure 8.4b):

- Since a through-thickness crack may be tolerated, $\bar{a}_{max} = B$, in which case $S_m = 0$. Thus, $S = S_i$ and the actual quality category is obtained directly from the graph.
- $2\bar{a}$ = 2.76 mm and B = 23 mm corresponds to a point just below the Q5 line, in which case Q5 is adopted.

The flaw is acceptable.

 © The British Standards Institution 2019

Figure U.2 **Derivation of actual quality category for a flaw**

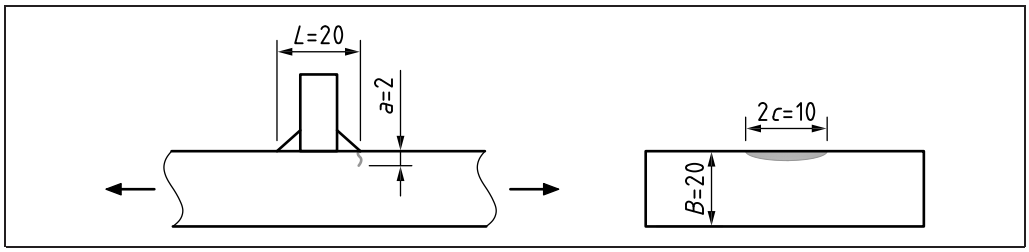


U.3 Example 2

U.3.1 Problem

A fatigue crack is discovered in service at the toe of a fillet weld in a steel plate subjected to fluctuating tension (see Figure U.3).

Figure U.3 **Fillet weld containing a surface flaw**



The weld is exposed to seawater without cathodic protection. The applied stress range is 48 N/mm^2. A fracture assessment indicates a risk of failure for a straight-fronted flaw in excess of 4 mm depth.

Estimate whether repair can be delayed for a further 200 000 cycles.

U.3.2 Solution

Referring to Figure U.4, the required quality category corresponds to the curve next above the coordinate 48 N/mm^2 and 2×10^5 cycles, that is Q10, for which the reference stress range is S = 23 N/mm^2.

Allowance should now be made for the effect of seawater on crack growth rate, as described in **8.6.4**, as the curves in Figure 8.4 to Figure 8.8 refer to crack growth in air, for which the recommended simple Paris law (from **8.2.3.5**) is given by:

$$da/dN = 5.21 \times 10^{-13}(\Delta K)^3 \quad \text{(U.1)}$$

For crack growth in seawater, the simplified law is:

$$da/dN = 2.3 \times 10^{-12}(\Delta K)^3 \quad \text{(U.2)}$$

The quality category reference stress range for crack growth in seawater, S', is therefore given by:

$$S' = S\left(\frac{5.21 \times 10^{-13}}{5.21 \times 10^{-12}}\right)^{1/3} = 0.61S \quad \text{(U.3)}$$

In the present case, S' = 23 N/mm^2, so that S = 23/0.61 = 37 N/mm^2. The corresponding required quality category is Q7.

The quality category for the flaw is obtained from Figure 8.7a) and Figure 8.7b)iii), reproduced here as Figure U.5a) and Figure U.5b).

The relevant dimensions are:

- a = 2 mm, $2c$ = 10 mm and B = 20 mm, giving a/B = 0.1 and $a/2c$ = 0.2;
- $\bar{a}_{max}$ = 5 mm and L = 20 mm, giving L/B = 1.

As L/B = 1, Figure 8.7b)iii) [Figure U.5b)] is used to deduce the quality category corresponding to growth of the equivalent flaw to the maximum tolerable size of 4 mm. The coordinate $\bar{a}_i$= 0.85 mm and B = 20 mm lies just below the Q6 curve, meaning that Q6 is the relevant quality category, giving S_i = 43 N/mm^2.

 © The British Standards Institution 2019

The coordinate $\bar{a}_{max}$= 4 mm and B = 20 mm lies just below the Q10 curve, meaning that Q10 is the relevant quality category, giving S_m = 23 N/mm^2. The reference stress range corresponding to the quality category for the flaw is then given by:

$$S = \left(S_i^3 - S_m^3\right)^{1/3} = 41\ \text{N/mm}^2 \qquad \text{(U.4)}$$

which is equivalent to Q7. Since this is also the required quality category, repair of the crack may be delayed.

Figure U.4 **Derivation of actual quality category for a flaw**

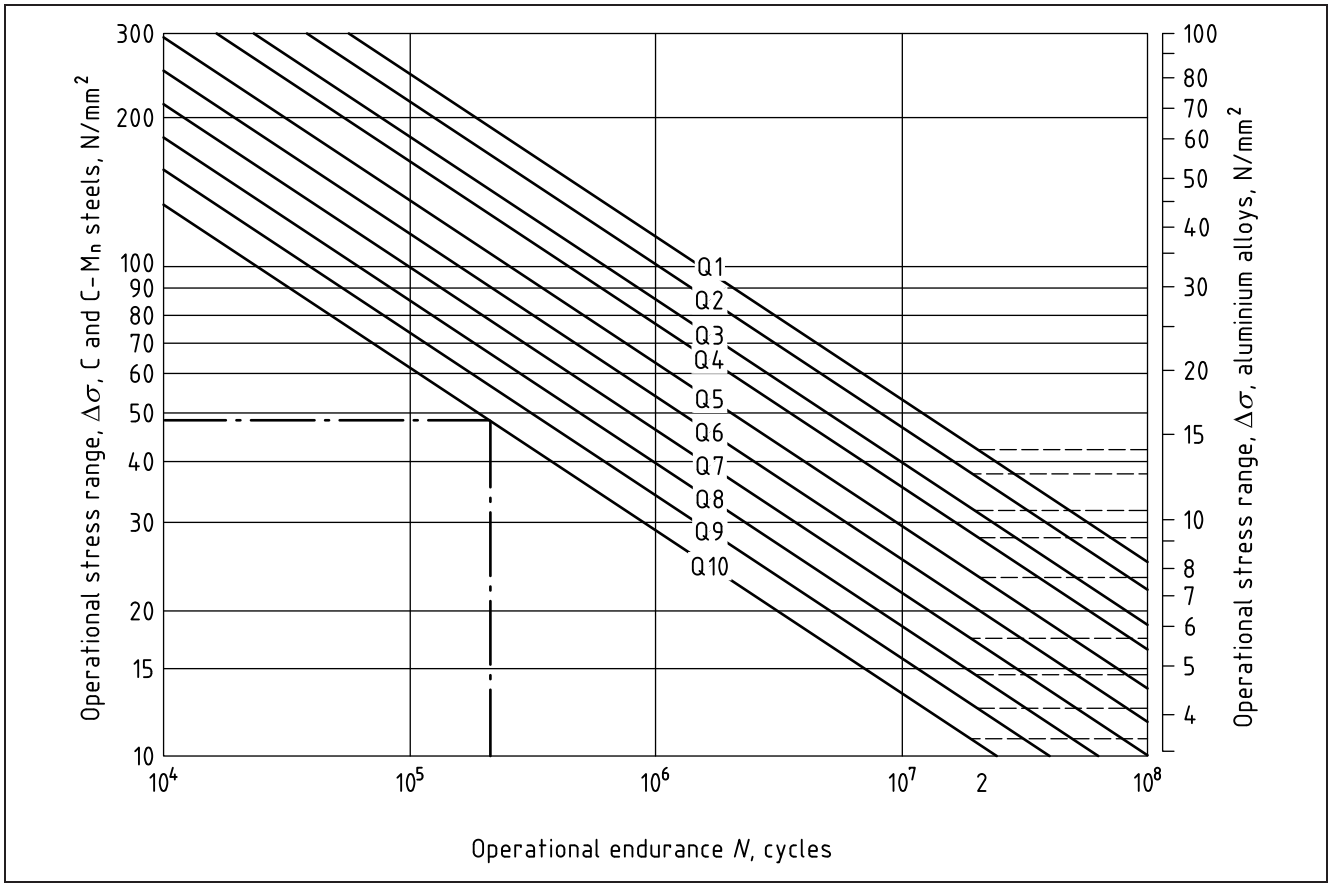
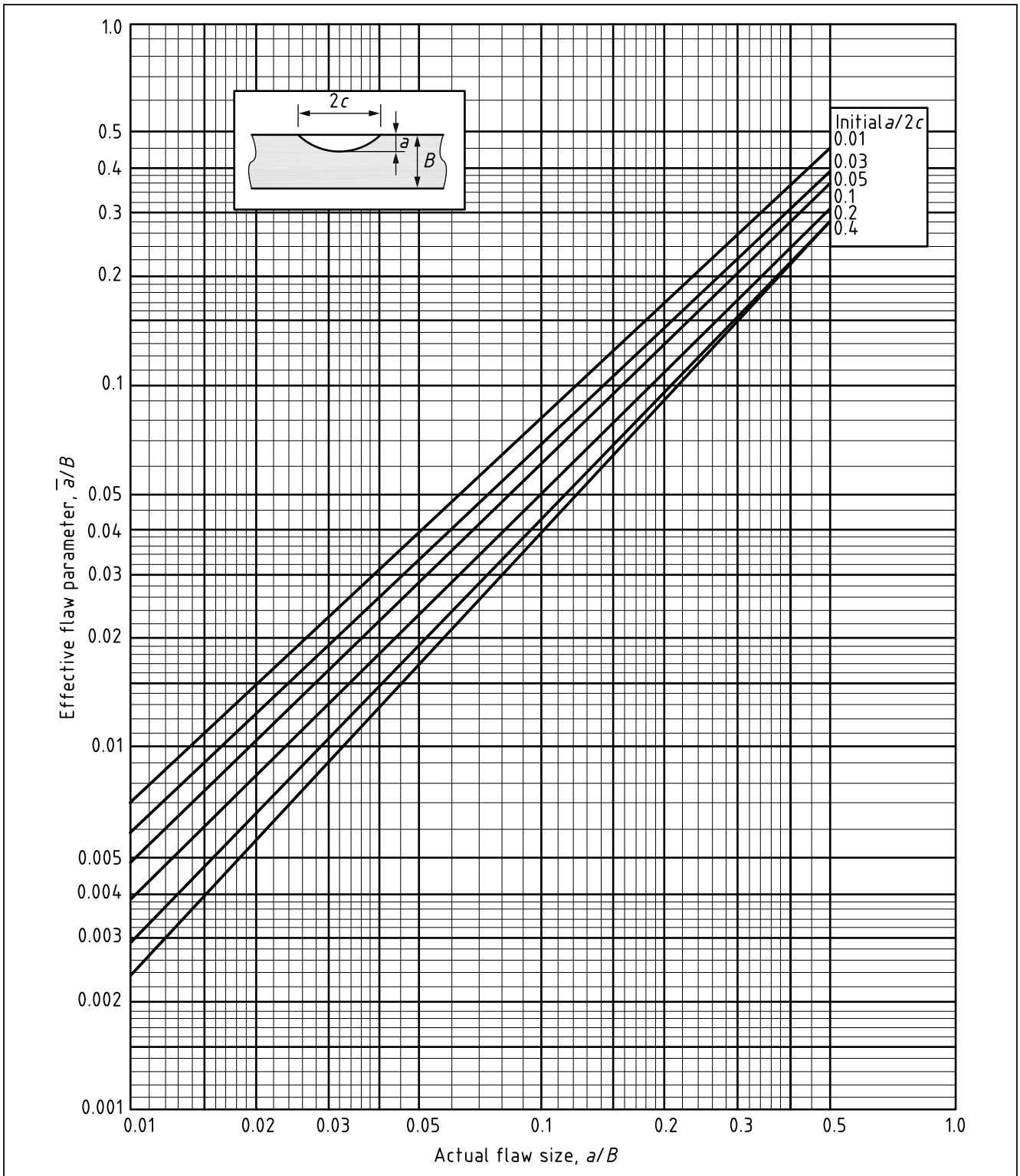


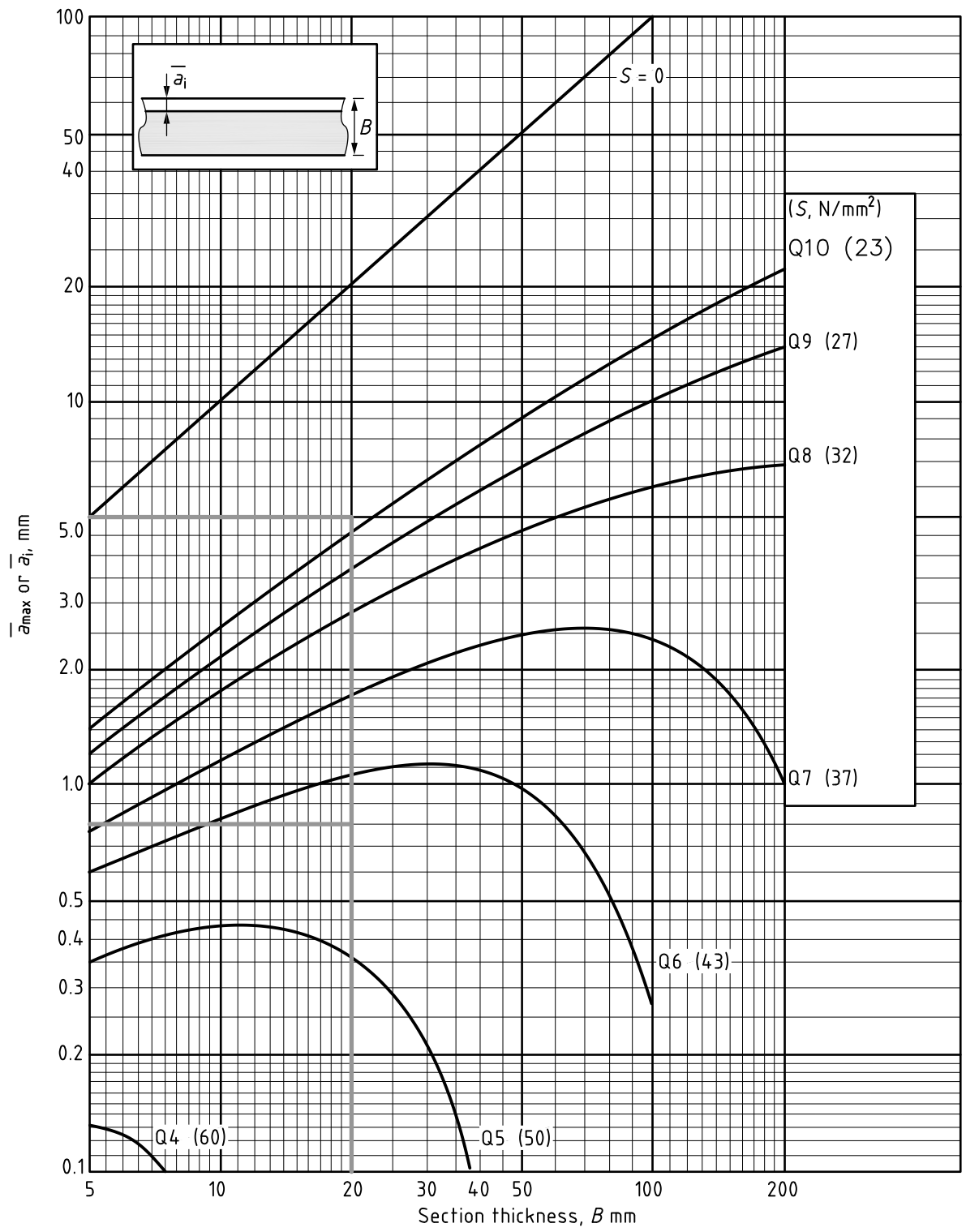
Figure U.5 **Obtaining the quality category for the flaw**



a) Obtaining the quality category for the flaw

 © The British Standards Institution 2019

Figure U.5 **Obtaining the quality category for the flaw** *(continued)*



b) Relationship between effective flaw parameter, welded joint geometry and quality category

Bibliography for Annex U

Standards publications

For dated references, only the edition cited applies. For undated references, the latest edition of the referenced document (including any amendments) applies.

BS 7608:2014+A1:2015, *Guide to fatigue design and assessment of steel products*

Other documents

There are no other references in this annex.

 © The British Standards Institution 2019

Annex V (informative)

Strain-based assessment (SBA)

V.0 Symbols and definitions

For the purposes of this annex, the following symbols, definitions and units apply, unless otherwise indicated at the point of use.

Symbol	Definition	Units
a	Flaw length [Equation (V.6)], or flaw size in general	mm
C	Coefficient in definition of R-curve [Equation (V.23)]	$N/mm^{(m+1)}$
C	Component-specific constant used in the calculation of J [Equation (V.1)]	mm
c_1, c_2	Coefficients used in the definition of the strain-based FAD	—
E	Elastic modulus	N/mm^2
J	J-integral; line or surface integral that encloses the crack front from one crack surface to the other, used to characterize the local stress-strain field around the crack tip	N/mm
J_e	Value of J determined using an elastic analysis	N/mm
J_p	Value of J determined using an a non-linear material analysis	N/mm
K	Stress intensity factor (SIF)	$N/mm^{3/2}$
K_{ep}	Total effective stress intensity factor for a linear-elastic, non-linear plastic material	$N/mm^{3/2}$
K_I^p	Stress intensity factor due to primary stress	$N/mm^{3/2}$
K_I^s	Stress intensity factor due to secondary stress	$N/mm^{3/2}$
K_{mat}	Characteristic material fracture toughness determined in terms of stress intensity factor	$N/mm^{3/2}$
K_p	SIF for non-linear materials	$N/mm^{3/2}$
K_r	Fracture ratio	—
L_r	Ratio of reference stress to yield strength (or applied load to limit load)	—
$L_{r,max}$	Maximum permitted limit of L_r	—
m	Power term in description of the R-curve	—
n	Strain-hardening exponent	—
P	Applied load	N
$P_L(a, \sigma_Y)$	Rigid plastic limit load (a function of flaw size and yield strength)	N
P_m	Membrane stress	N/mm^2
Q_r	Equivalent of L_r for strain-based assessment	—
$Q_{r,max}$	Equivalent of $L_{r,max}$ for strain-based assessment	—
$q(Q_r)$	Function defining the strain-based FAD	—
V	Plasticity correction factor	—
W	Specimen or structural width	mm
X	Factor allowing for transition from stress-based to strain-based FAL	—
Δa	Increment in a or ductile tearing	mm

(continued)

Symbol	Definition	Units
ε_f	Strain from the true stress-true strain curve when the true stress is derived from the engineering value of the material flow strength	—
ε_{nom}	Remote (nominal) strain	—
ε_{ref}	Reference strain at the reference stress σ_{ref}	—
ρ	Plasticity interaction factor	—
σ_f	Flow strength	N/mm^2
σ_{ref}	Reference stress	N/mm^2
σ_U	Tensile strength	N/mm^2
σ_U^e	Tensile strength from the engineering stress-strain curve	N/mm^2
σ_Y	Lower yield strength or 0.2% proof strength	N/mm^2
σ_Y^e	Yield strength from the engineering stress-strain curve	N/mm^2

V.1 General

The background to this annex is given in reference [V.1].

Typically, engineering structures undergo cycles of known loads, and assessments ensure that the components of the structure resist the applied load at primary stress levels that are below the material yield strength. There has been significant recent interest in the resistance of structures to higher nominal loads. Offshore pipelay, for example, is sometimes undertaken by reeling. Typical combinations of pipe and drum diameters lead to yielding of the pipe.

It has therefore been necessary to use engineering fracture mechanics to determine the flaw tolerance of welds subjected to high levels of strain. Such methods are often adopted at what might be called the design phase of a project, when the engineering team are demonstrating that the proposed structure has enough ductility to withstand the extreme loads that will be experienced. Later, it might also be necessary to consider the assessment of known flaws that have been discovered during in-service inspections.

For pipelines, the loading is often defined in terms of a change of pipeline curvature and so the load generated is dependent upon the pipeline material strength. Hence, higher strengths will lead to higher applied loads in terms of forces and moments for the same applied rotations or axial displacements. Forces and moments are primarily associated with stresses, and displacements and rotations are primarily associated with strains. It is therefore commonly assumed that loads that are defined in terms of high strains are necessarily displacement-controlled.

Annex V assumes that the baseline loading might be easily expressed as a displacement or rotation, but the system performance might display a load-controlled behaviour. This is often called elastic follow-up. It is therefore considered that strain-based calculations of component safety should be load-controlled unless proven otherwise.

Alternative methods have been developed for the strain-based assessment of flaws in girth welds in high-pressure steel pipelines. These have been reviewed in references [V.2] and [V.3]; care should be taken to ensure that any validity limits are observed, in particular where equations have been fitted to test data or analysis results. The assessment methods for strain-based loading in reference [V.4] have been successfully used for offshore pipelines. These methods are based on the stress-based procedures of Clause **7**, but due to differences in the methods and assumptions, different results might be obtained when compared

with results from the method of this annex. In particular, the derivation of nominal stress from nominal strain (and reference strain from reference stress) in this annex is based on the true stress-true strain curve. Validation work carried out to date suggests that this approach is conservative.

This annex considers applied loadings specified as a remote strain, ε_{nom}. This strain may be derived directly from an applied deformation; an example is pipeline installation by reeling where a welded pipeline is wound around a drum of known radius and the strain is defined by the drum and pipe dimensions. Alternatively, the strains may be developed by the response of a structure to imposed displacements; the strains are a function of these displacements and the materials properties. The nominal strain is usually determined using materials properties that give conservative predictions of the remote strains; typically, lower bound strength properties are used. Such lower bound properties might not give conservative assessments when subsequently used in the procedures of this annex. Materials properties giving upper bound stresses for a specified strain will usually be required for the procedures of this annex to determine tolerable flaw sizes.

This annex considers only the assessment of planar flaws under tensile applied strains. The derivation of the methods given in this annex is based on uniaxial primary stresses, but work to date suggests that the methods may be conservatively applied to cases of biaxial loading [V.5]. In some cases, other failure modes might need to be considered, for example local buckling of thin-walled sections or thin cylinders can occur under compressive remote strains; guidance is given in **10.4**, and reference [V.3] reviews predictive methods for the local buckling of high-pressure transmission pipelines.

Engineering fracture mechanics methods for the assessment of the stability of flaws under quasi-static loads are based upon the comparison of a driving force with a materials property. It is therefore important to estimate the crack tip loading and compare it to an accurately determined toughness expressed in the same way. Annex L provides an overview of the measurement of toughness, and the methods described in Clause **7** effectively compare the driving force to the toughness by use of a failure assessment diagram (FAD).

The FAD is a graph with two axes, and the assessment of the severity of loading of an individual flaw is characterized by the two coordinates of a point on the graph that represents the specific case. A failure assessment line (FAL) on the FAD is used to determine whether the specific case is safe or potentially unsafe. An assessment point that is nearer to the origin of the FAD than the FAL is safe. A point that is outside the FAL is potentially unsafe.

It is apparent, therefore, that the crack driving force is equal to the material toughness when the assessment point lies on the FAL. An introduction to the way in which the BS 7910 FAD achieves this provides a basis for the use of FADs in general and of how the FAD-based method of Clause **7** can be extended into what is known as the strain-based regime.

V.2 Materials properties for SBA

V.2.1 General

Where strains are due to thermal effects, materials properties should be measured at the appropriate temperature, or adjusted for the effects of temperature.

V.2.2 Stress-strain curve

If possible, measured stress-strain curves should be used in the procedures of this annex; see **7.1.3**. Where this is not possible, for example when deriving tolerable flaw sizes during design, conservative properties should be used.

The nominal strain is usually determined using materials properties that give conservative predictions of the remote strains; typically, lower bound strength properties are used. This is consistent with the procedures of Clause **7**. Lower bound strength properties might not give conservative assessments when subsequently used in the procedures of this annex. Materials properties giving upper bound stresses for a specified strain will usually be required for the procedures of this annex when determining tolerable flaw sizes. Alternatively, it might be appropriate to use the same strength properties both to derive the nominal strain and in the fracture assessment, but to carry out sensitivity studies covering a range of likely properties.

V.2.3 Fracture toughness

The fracture toughness used in **V.4.7** is normally the high constraint toughness as determined from testing standards using deeply-notched bend specimens such as the compact tension (CT) or single edge-notched bend (SENB) specimens (see **7.1.4** to **7.1.5**). This is assumed to represent a lower bound to the toughness for assessments. However, for conditions of low in-plane structural constraint and where the material fracture toughness at the assessment temperature exhibits a significant dependence on constraint, it is possible to take account of the increased value of toughness in the assessment. Advice on performing a constraint assessment is given in Annex N (Procedure II).

Where the assessment temperature is below the fracture toughness measurement temperature, the effects of temperature should be taken into account. If the fracture toughness moves from the upper shelf into the transition region, there can be a significant reduction in fracture toughness.

V.3 The failure assessment diagram

This subclause discusses the basis of FADs for cases where there are only primary loads.

The vertical axis of the FAD expresses the fracture ratio, K_r. Under primary loading only, it is the ratio of the applied elastic component of stress intensity factor, K, to the value of material fracture toughness expressed as a stress intensity factor, K_{mat}.

The horizontal axis of the FAD expresses the loading parameter, L_r. It is the ratio of the applied load to the limit load. The L_r parameter is dimensionless, so it can also be expressed in terms of a ratio of stresses. In terms of stress, it is the ratio of the applied reference stress, σ_{ref}, to the material yield strength, σ_Y.

The following points can be made.

- At low applied loads (low K_r, also low L_r), the crack tip driving force is approximately equal to the elastic value. The FAL therefore approaches 1.0 when L_r approaches zero.
- The net stresses on the plane of the crack approach the yield strength when L_r approaches 1.0.
- Plasticity causes the actual crack tip driving force to be higher than the elastic value, K. The difference increases with L_r. This means that the FAL reduces below unity as L_r increases.

Ainsworth [V.6] observed that the crack tip driving force given in terms of the J contour integral, J, could be expressed in terms of a component reference stress, σ_{ref}. Dimensional considerations allowed the expression to take the following form:

$$J = C\sigma_{ref}\,\varepsilon_{ref} \qquad \text{(V.1)}$$

where C is a suitable chosen component dimension and ε_{ref} is the strain

determined at σ_{ref} based upon the material stress-strain curve.It was therefore possible to express the ratio of the linear elastic value, J_e, to the non-linear value, J_p, as follows:

$$\frac{J_e}{J_p} = \frac{C_e}{C_p}\frac{\sigma_{ref}^2}{E\sigma_{ref}\varepsilon_{ref}} \quad \text{(V.2)}$$

where C_e and C_p are the linear elastic and non-linear deformation versions, respectively, of the component dimension for Equation (V.1). The elastic modulus is given by E. Ainsworth proposed that a suitable choice of the reference stress could be selected whereby $C_e = C_p$, and so Equation (V.2) could be re-expressed as follows:

$$\frac{J_e}{J_p} = \frac{\sigma_{ref}}{E\varepsilon_{ref}} \quad \text{(V.3)}$$

This was of great advantage in 1984 when Ainsworth published his result, because it meant that the non-linear component of the crack tip loading could be determined from the stress-strain curve and the elastic value of the crack tip loading. At that time, there were plenty of published solutions for the elastic loading of cracks, but elastic-plastic analyses of components were less common because of the limited availability of computer software and hardware.

Equation (V.3) can be expressed in terms of stress intensity factors for linear elastic and non-linear materials (K and K_p respectively) as follows:

$$\frac{K}{K_p} = \left(\frac{E\varepsilon_{ref}}{L_r\sigma_Y}\right)^{-0.5} \quad \text{(V.4)}$$

Here, the respective stress intensity factors have been assumed to be proportional to the square root of the J contour integral and the reference stress has been expressed in terms of L_r and the material yield strength, σ_Y.

The right-hand side of Equation (V.4) is the first term of the Option 2 FAD given in **7.3.4**, Equation (7.34). The term K_p in Equation (V.4) is the stress intensity factor for solely non-linear deformation. A proper FAD requires the denominator of the left-hand side of Equation (V.4) to be K_{ep}, which is the total effective stress intensity factor for a linear-elastic, non-linear plastic material. This is achieved by adding a term to the equation as follows:

$$\frac{K}{K_{ep}} = \left(\frac{E\varepsilon_{ref}}{L_r\sigma_Y} + \frac{L_r^3\sigma_Y}{2E\varepsilon_{ref}}\right)^{-0.5} \quad \text{(V.5)}$$

The right-hand side of Equation (V.5) is the same as the right-hand side of the Option 2 FAL given in **7.3.4**, Equation (7.34). In other words, the FAL represents a plot of the ratio of the elastic to the elastic-plastic stress intensity factors. A critical condition is expected when the applied, elastic-plastic stress intensity factor is equal to the material toughness expressed as a stress intensity factor, K_{mat}.

Criticality is represented by the following expression:

$$\frac{K}{K_{mat}} = \left(\frac{E\varepsilon_{ref}}{L_r\sigma_Y} + \frac{L_r^3\sigma_Y}{2E\varepsilon_{ref}}\right)^{-0.5} \quad \text{(V.6)}$$

Some published finite element analysis (FEA) results, however, have shown that the effective elastic-plastic driving force derived from Equation (V.5) is insufficient when load levels cause reference strains that are greater than the material yield strain (e.g. reference [V.7]). It is therefore important to re-examine the basis of the Option 2 FAL using the notes presented above. Recently, it has been found that the assumption that $C_e = C_p$ might not be accurate. Three publications ([V.7], [V.8] and [V.9]) considered the non-linear behaviour of components that deform according to a Ramberg-Osgood law [see Equation (7.4) in **7.1.3.5**].

It was found that some cases exist where Equation (V.3) should be replaced by:

$$\frac{J_e}{J_p} = \frac{(n+1)}{2n}\frac{\sigma_{ref}}{E\varepsilon_{ref}} \tag{V.7}$$

In the limit of low hardening materials (large n), therefore, Equation (V.7) becomes:

$$\frac{J_e}{J_p} = \frac{1}{2}\frac{\sigma_{ref}}{E\varepsilon_{ref}} \tag{V.8}$$

However, Equation (V.7) becomes Equation (V.3) for the trivial case of elastic deformation when n is unity. This means that, in some cases, the FAD represented by Equation (7.34) [repeated as Equation (V.6) above] might be non-conservative when the applied strains are large and when the material has low levels of hardening. The Option 2 FAD, however, is conservative when the applied strains are below the material yield strain.

A modification of Equation (V.7) has been proposed [V.9] as follows:

$$\frac{J_e}{J_p} = \frac{\sigma_{ref}}{XE\varepsilon_{ref}} \tag{V.9}$$

where the factor X provides a transition from sub-yield behaviour at low L_r to a conservative expression at values of L_r beyond unity, as shown in Equation (V.10):

$$X = \frac{1}{2}\{3 + \tanh[c_1(L_r - c_2)]\} \tag{V.10}$$

The use of X gives rise to a small change to the Option 2 material-specific FAD when applied to components that experience nominal strain levels that are beyond the material yield strain. The high strain regime FAD is given by the following expression combined with Equation (V.10) for X:

$$\frac{K}{K_{ep}} = \left(\frac{XE\varepsilon_{ref}}{L_r\sigma_Y} + \frac{L_r^3\sigma_Y}{2E\varepsilon_{ref}}\right)^{-0.5} \tag{V.11}$$

A new horizontal axis parameter, Q_r, is proposed. The FAD of Equation (V.11) is then given by:

$$q(Q_r) = \left(\frac{XQ_r}{L_r} + \frac{L_r^3}{2Q_r}\right)^{-0.5} \tag{V.12}$$

where Q_r is given by the following expression and the expression for L_r is unchanged:

$$Q_r = \frac{E\varepsilon_{ref}}{\sigma_Y} \tag{V.13}$$

It is unnecessary to change any other aspect of the fitness-for-service (FFS) methods proposed in Clause **7**. It is therefore possible to use the methods described in Clause **7** together with Equations (V.10), (V.12) and (V.13) to safely conduct FFS assessments where the applied strains are greater than the material yield strain. An overview of what this means is given in **V.4.**

This preamble has shown that it is possible to overcome some of the non-conservatisms that can occur when the methods of Clause **7** are used in the high strain regime by a modest change to the material-specific FAD. This means that the methods proposed in this annex are similar to the methods described in Clause **7**. However, the current annex recommends that the effective applied load on the structure is inferred from upper bound properties. This is a change from the recommendation given in **7.1.3.2**.

 © The British Standards Institution 2019

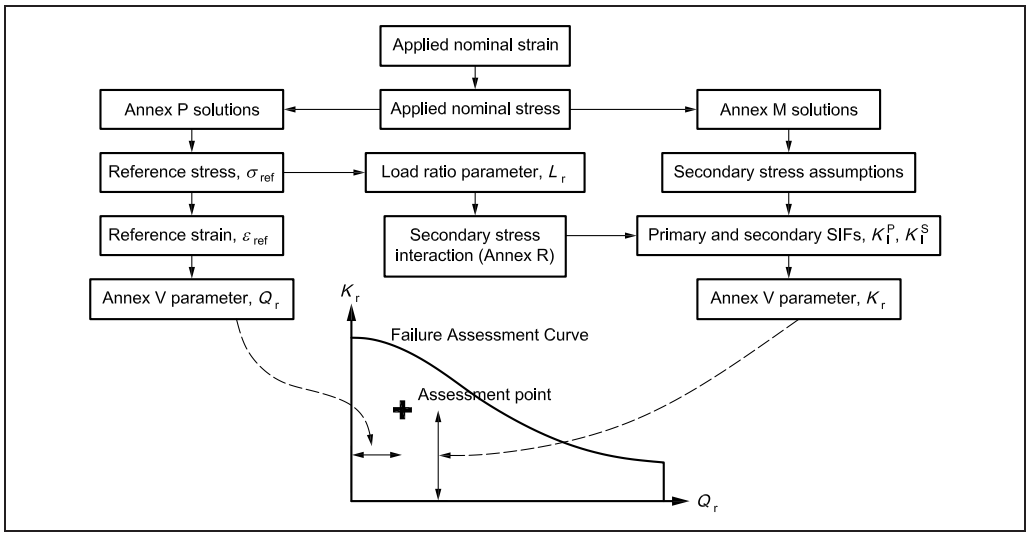
V.4 Overview of method

V.4.1 General outline

The SBA method, summarized in Figure V.1, uses an assessment line given by the equation of a curve, $K_r = q(Q_r)$, and a cut-off value of Q_r equal to $Q_{r,max}$. If the calculated assessment point (Q_r, K_r) lies within the area bounded by the axes, the assessment line and the vertical line corresponding to $Q_{r,max}$, the flaw is acceptable; if it lies on or outside the line, the flaw is unacceptable.

The assessment route includes an argument based on initiation of crack growth and the case of stable tearing under increasing load, where the material and temperature are such that a ductile tearing mechanism might occur. For ductile crack growth, the value of toughness used as a measure of initiation typically corresponds to 0.2 mm of crack extension, including blunting, in accordance with the fracture toughness testing standard used (see **7.1.4** to **7.1.5**), so ductile tearing assessment should not be performed for crack growth below that figure.

Figure V.1 **Flowchart for a strain-based assessment (SBA) using the methods of Annex V**



V.4.2 Load ratio, L_r

The load ratio, L_r, is determined from the primary loads acting on the component using the following expression:

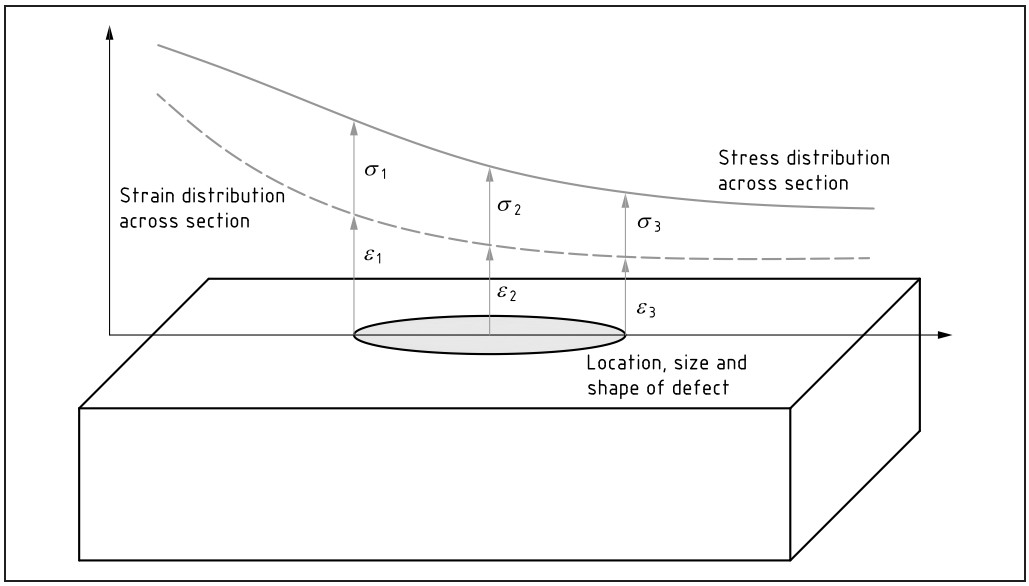
$$L_r = \frac{P}{P_L(a,\sigma_Y)} = \frac{\sigma_{ref}}{\sigma_Y} \quad \text{(V.14)}$$

The value of L_r could therefore be determined as the ratio of the applied load to the collapse load for the structure. However, it is also possible to determine L_r from the nominal strain distribution at the location of the flaw being assessed as shown in Figure V.2. It is possible that there might be a distribution of strain across the location of the flaw. This distribution of strain can be used to determine the stress at that location using the material tensile stress-strain curve. It is assumed that the appropriate stress-strain curve is given by the following equation:

$$\sigma(\varepsilon) = f(\varepsilon) \quad \text{(V.15)}$$

Therefore, the stress at location 1 (σ_1) is given by $f(\varepsilon_1)$, etc., as shown in Figure V.2. The uncracked membrane and bending stress distributions at the location of the crack can then be determined using the methods shown in Figure 7.2 and the reference stress can be determined using the appropriate equation of Annex P. Clearly, this operation is conservative when the material upper bound stress-strain curve is used.

Figure V.2 **Distribution of stress and strain across the location of the flaw being assessed from an uncracked stress analysis**



It can often be sufficient to define the loading in terms of a nominal strain, ε_{nom}, which is representative of the strain in the vicinity of the flaw. This nominal strain can be converted to the membrane stress, P_m, acting on the flaw that is equal to $f(\varepsilon_{nom})$ as shown in **V.4.3**.

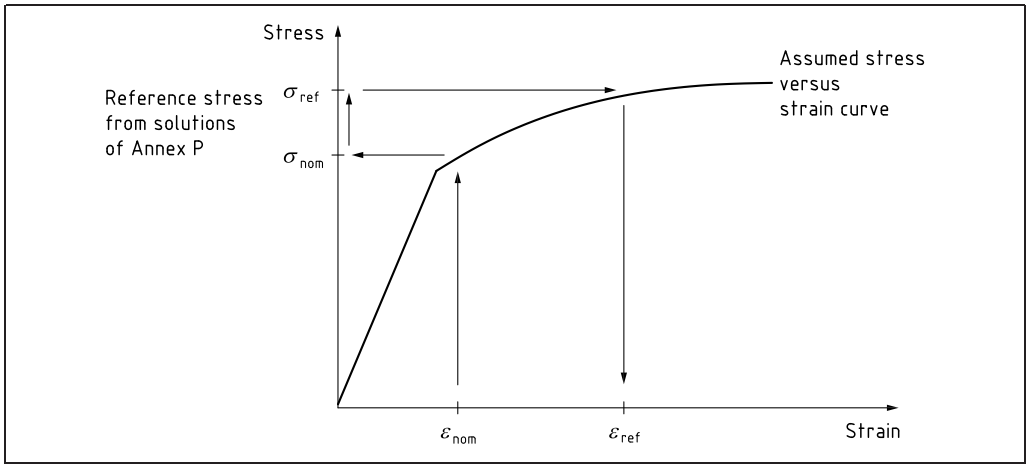
V.4.3 Load ratio, Q_r

The load ratio, Q_r, is determined from the primary loads acting on the component using the following expression:

$$Q_r = \frac{E\varepsilon_{ref}}{\sigma_Y} \tag{V.16}$$

where the reference strain, ε_{ref}, is the value of strain from the stress-strain curve when the stress is equal to the reference stress σ_{ref} (see **V.5.2** and Figure V.3).

Figure V.3 **Derivation of the reference stress, σ_{ref}, and the reference strain, ε_{ref}, from the applied nominal strain, ε_{nom}, and the material true stress-true strain curve**



 © The British Standards Institution 2019

V.4.4 High strain FAD transition factor, *X*

A high strain FAD transition factor, *X*, is needed for SBA. This is given in the following equation:

$$X = \frac{1}{2}\{3 + \tanh[c_1(L_r - c_2)]\} \quad \text{(V.17)}$$

Values of 30.0 for c_1 and 1.0 for c_2 have been found to be suitable. Other values can be used if they are supported by a suitably wide-ranging finite element analysis study.

V.4.5 Strain-based assessment failure assessment line (SBA FAL)

The SBA FAL is given by the following equation:

$$q(Q_r) = \left(\frac{XQ_r}{L_r} + \frac{L_r^3}{2Q_r}\right)^{-0.5} \quad \text{(V.18)}$$

V.4.6 Cut-off value of Q_r

The cut-off value of value of the loading parameter is given by $Q_r = Q_{r,max}$, where:

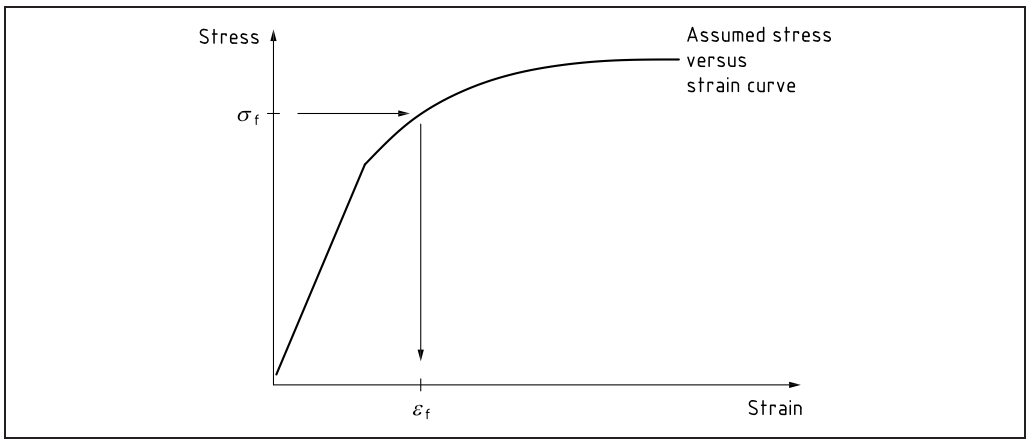
$$Q_{r,max} = \frac{E\varepsilon_f}{\sigma_Y} \quad \text{(V.19)}$$

where ε_f is the strain determined from the material true stress-true strain curve at a stress equal to the flow strength, σ_f. With σ_y^e (engineering yield strength) and σ_u^e (engineering tensile strength), the engineering flow strength is given by:

$$\sigma_f^e = \frac{\sigma_Y^e + \sigma_U^e}{2} \quad \text{(V.20)}$$

The normal conversions should be used to determine the true flow strength, σ_f, and then this is used to get the true flow strain as shown in Figure V.4.

Figure V.4 **Derivation of the flow strain, ε_f, from the material flow strength, σ_f, using the true stress-true strain curve**



V.4.7 Fracture ratio K_r

The fracture ratio, K_r, is determined by either Equation (V.21) or Equation (V.22):

$$K_r = \frac{K_I^p + VK_I^s}{K_{mat}} \quad \text{(V.21)}$$

$$K_r = \frac{K_I^p + K_I^s}{K_{mat}} + \rho \quad \text{(V.22)}$$

The terms V and ρ are defined in Annex R as functions of both the primary and secondary loads and account for plasticity interaction effects. If K_I^s is negative then K_I^s, V and ρ should be set to zero.

The fracture toughness used in Equation (V.21) and Equation (V.22) is normally the high constraint toughness as determined from testing standards using deeply-notched bend specimens such as the compact tension (CT) or single edge-notched bend (SENB) specimens (see **7.1.4** to **7.1.5**). This is assumed to represent a lower bound to the toughness for assessments. However, for conditions of low in-plane structural constraint and where the material fracture toughness at the assessment temperature exhibits a significant dependence on constraint, it is possible to take account of the increased value of toughness in the assessment. Advice on performing a constraint assessment is given in Annex N (Procedure II).

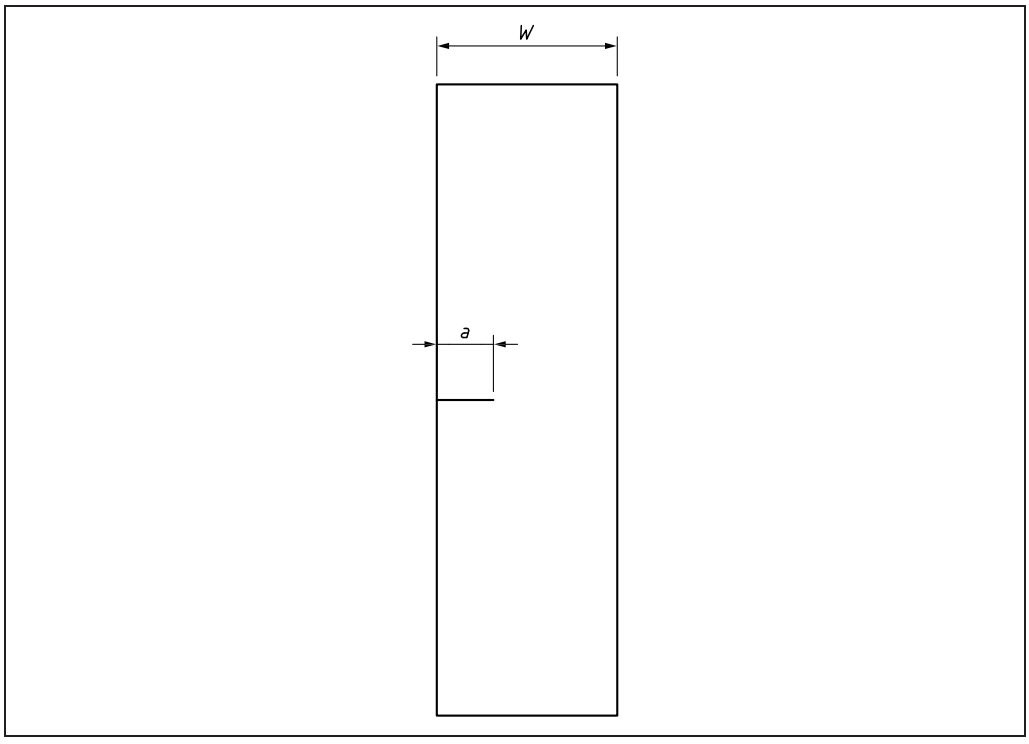
V.5 Worked example

V.5.1 Geometry

Analysis of a two-dimensional (2D) case has been undertaken of an edge flaw in a plate (Figure V.5). The details are:

- specimen width, W, equal to 18.4 mm;
- initial crack length, a, equal to 0.4 mm.

Figure V.5 **Single edge-notched tension (SENT) specimen**



V.5.2 Material

V.5.2.1 Tensile curve

A simple multilinear stress-strain curve was assumed based upon the material tested as described in reference [V.10]. The materials properties were derived from the engineering stress-strain curve as listed below:

- elastic modulus, 207 GPa;
- yield strength, 512 MPa;
- tensile strength, 597 MPa;

- strain at tensile strength, 11%;
- zero hardening after the tensile strength.

V.5.2.2 *R*-curve

The assumed *J*-*R*-curve was also based upon the parent material tested as described in reference [V.10]. The curve takes the form:

$$J = C\Delta a^{m} \quad \text{(V.23)}$$

where:

- coefficient C is 1 168 (for crack growth in mm and J in N/mm);
- exponent m is 0.71.

V.5.3 Loading

V.5.3.1 Primary loading

The primary loading was assumed to generate an increasing membrane strain.

V.5.3.2 Secondary loading

The crack was assumed to experience yield magnitude membrane stress before the application of the load.

V.5.4 Results

The results of a tearing analysis are presented in Figure V.6. The figure shows the standard method adopted for tearing as follows.

a) The failure assessment line (FAL), K_r against Q_r, is plotted.

b) A load level is chosen (e.g. an applied strain of 0.1%).

c) A small amount of crack growth is adopted.

d) The strain loading parameter, Q_r, is evaluated.

e) The primary value of the applied stress intensity factor (SIF) is determined.

f) The residual stresses are evaluated.

g) The secondary value of the applied SIF is determined.

h) The plasticity interaction factor, ρ or V, is determined.

i) The material toughness is determined based upon a small amount of crack growth using Equation (V.23).

j) The fracture ratio, K_r, is evaluated.

k) An assessment point is plotted at (Q_r, K_r).

l) This process is repeated for progressively larger crack depths.

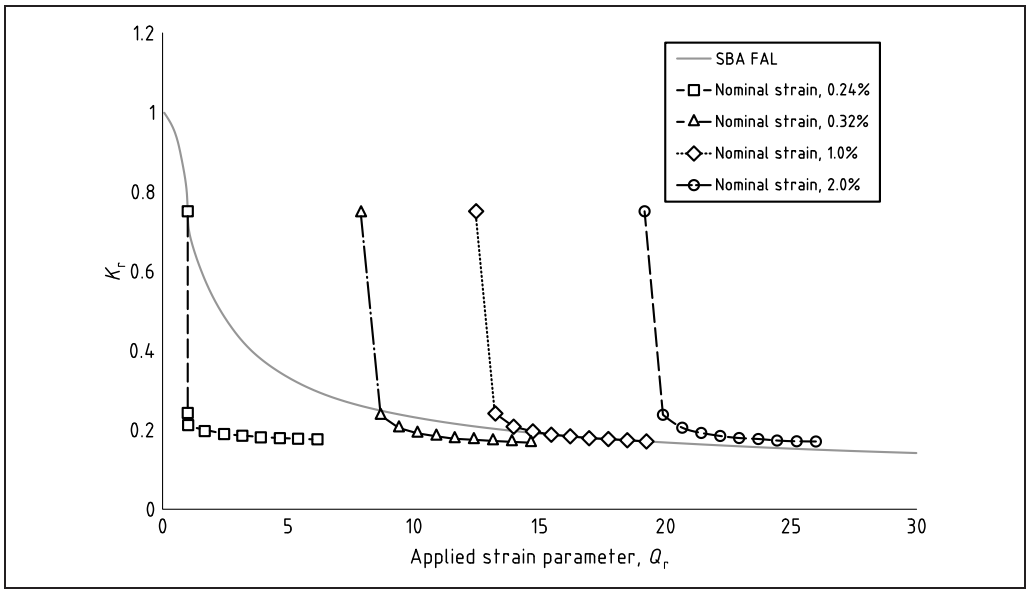
m) A line is drawn through all the assessment points for a single load level. The combination of nominal strain and initial crack is stable if the line joining the assessment points at different crack depths starts inside the FAL or passes into the FAL.

n) Further lines can be drawn until the applied load at which the tearing curve is tangential to the FAL is found. This is the maximum load that can be sustained by the cracked component.

Elements of the list above can be seen in Figure V.6. When the applied nominal strain is 0.1%, the assessment line starts and remains inside the FAL. The tearing curve starts outside the FAL but passes into the FAL when the applied strain

is 0.24% and 0.32%. It appears that the tearing curve is tangential to the FAL when the applied strain is 1.0%, so this is the lowest loading that would lead to unstable crack growth. The tearing curve evaluated when the applied nominal strain is 2.0% remains outside the FAL.

Figure V.6 **SBA FAL together with tearing lines used to determine the instability load level for a 0.4 mm deep flaw in a SENT specimen loaded in tension.**



Bibliography for Annex V

Standards publications

There are no standards references in this annex.

Other documents

[V.1] SMITH, S.D. Consideration of a proposed SBAD method for BS 7910. *In: International Journal of Pressure Vessels and Piping*, 168, December 2018, 142–147. <https://doi.org/10.1016/j.ijpvp.2018.10.001>

[V.2] WU, G. and WANG, L. An overview of strain-based fracture assessment of pipelines. *In: Proceedings of the ASME 37th International Conference on Ocean, Offshore and Arctic Engineering*. Paper OMAE2018-78685. New York: ASME: 2018.

[V.3] ANDREWS, R.M., STEPHENS, M., CARR, M. and BRÜCKNER, J. A review of strain capacity assessment methods for transmission pipelines. Paper 19. *In: Technology for Future and Ageing Pipelines*. Gent, Belgium 11–12 April 2018. Beaconsfield, UK: Tiratsoo Technical: 2018.

[V.4] DNV. *Assessment of flaws in pipeline and riser girth welds*. DNVGL-RP-F108. 2019. <https://www.dnvgl.com/oilgas/download/dnvgl-rp-f108-assessment-of-flaws-in-pipeline-and-riser-girth-welds.html>

[V.5] LEI, Y., BUDDEN, P. and AIRD, C. The effect of biaxial loading on the limit load and *J* estimate for plates with extended surface cracks. *In: 20th European Conference on Fracture (ECF20), Procedia Materials Science 3*, 2014, 667–672. <https://doi.org/10.1016/j.mspro.2014.06.110>

[V.6] AINSWORTH, R.A. The assessment of defects in structures of strain hardening material. *In: Engineering Fracture Mechanics*, 1984, 19(4), 633–642.

[V.7] JAYADEVAN, K.R., ØSTBY, E. and THAULOW, C. Fracture response of pipelines subjected to large plastic deformation under tension. *In: International Journal of Pressure Vessels and Piping,* 2004, 81, 771–783.

[V.8] BUDDEN, P. and AINSWORTH, R.A. The shape of a strain-based failure assessment diagram. *In: International Jornal of Pressure Vessels and Piping*, January 2012, 89, 59–66.

[V.9] SMITH, S.D. Development of the BS 7910 failure assessment diagram for strain based design with application to pipelines. Paper OMAE2010-83527. *In: Proceedings of the ASME 2012 31st International Conference on Ocean, Offshore and Arctic Engineering*, OMAE, 2012.

[V.10] PISARSKI, H.G., SMITH, S.D. and LONDON, T. Flaw tolerance of pipelines containing circumferential flaws subjected to axial straining and internal pressure – Tests and analyses. *In: Proceedings of the 23rd International Offshore and Polar Engineering (ISOPE)*, Anchorage, USA, 2013.

This page deliberately left blank

NO COPYING WITHOUT BSI PERMISSION EXCEPT AS PERMITTED BY COPYRIGHT LAW

British Standards Institution (BSI)

BSI is the national body responsible for preparing British Standards and other standards-related publications, information and services.

BSI is incorporated by Royal Charter. British Standards and other standardization products are published by BSI Standards Limited.

About us

We bring together business, industry, government, consumers, innovators and others to shape their combined experience and expertise into standards -based solutions.

The knowledge embodied in our standards has been carefully assembled in a dependable format and refined through our open consultation process. Organizations of all sizes and across all sectors choose standards to help them achieve their goals.

Information on standards

We can provide you with the knowledge that your organization needs to succeed. Find out more about British Standards by visiting our website at bsigroup.com/standards or contacting our Customer Services team or Knowledge Centre.

Buying standards

You can buy and download PDF versions of BSI publications, including British and adopted European and international standards, through our website at bsigroup.com/shop, where hard copies can also be purchased.

If you need international and foreign standards from other Standards Development Organizations, hard copies can be ordered from our Customer Services team.

Copyright in BSI publications

All the content in BSI publications, including British Standards, is the property of and copyrighted by BSI or some person or entity that owns copyright in the information used (such as the international standardization bodies) and has formally licensed such information to BSI for commercial publication and use.

Save for the provisions below, you may not transfer, share or disseminate any portion of the standard to any other person. You may not adapt, distribute, commercially exploit or publicly display the standard or any portion thereof in any manner whatsoever without BSI's prior written consent.

Storing and using standards

Standards purchased in soft copy format:

- A British Standard purchased in soft copy format is licensed to a sole named user for personal or internal company use only.
- The standard may be stored on more than one device provided that it is accessible by the sole named user only and that only one copy is accessed at any one time.
- A single paper copy may be printed for personal or internal company use only.

Standards purchased in hard copy format:

- A British Standard purchased in hard copy format is for personal or internal company use only.
- It may not be further reproduced – in any format – to create an additional copy. This includes scanning of the document.

If you need more than one copy of the document, or if you wish to share the document on an internal network, you can save money by choosing a subscription product (see 'Subscriptions').

Reproducing extracts

For permission to reproduce content from BSI publications contact the BSI Copyright and Licensing team.

Subscriptions

Our range of subscription services are designed to make using standards easier for you. For further information on our subscription products go to bsigroup.com/subscriptions.

With **British Standards Online (BSOL)** you'll have instant access to over 55,000 British and adopted European and international standards from your desktop. It's available 24/7 and is refreshed daily so you'll always be up to date.

You can keep in touch with standards developments and receive substantial discounts on the purchase price of standards, both in single copy and subscription format, by becoming a **BSI Subscribing Member.**

PLUS is an updating service exclusive to BSI Subscribing Members. You will automatically receive the latest hard copy of your standards when they're revised or replaced.

To find out more about becoming a BSI Subscribing Member and the benefits of membership, please visit bsigroup.com/shop.

With a **Multi-User Network Licence (MUNL)** you are able to host standards publications on your intranet. Licences can cover as few or as many users as you wish. With updates supplied as soon as they're available, you can be sure your documentation is current. For further information, email cservices@bsigroup.com.

Revisions

Our British Standards and other publications are updated by amendment or revision.

We continually improve the quality of our products and services to benefit your business. If you find an inaccuracy or ambiguity within a British Standard or other BSI publication please inform the Knowledge Centre.

Useful Contacts

Customer Services
Tel: +44 345 086 9001
Email: cservices@bsigroup.com

Subscriptions
Tel: +44 345 086 9001
Email: subscriptions@bsigroup.com

Knowledge Centre
Tel: +44 20 8996 7004
Email: knowledgecentre@bsigroup.com

Copyright & Licensing
Tel: +44 20 8996 7070
Email: copyright@bsigroup.com

BSI Group Headquarters

389 Chiswick High Road London W4 4AL UK